

UNIVERSITY OF SPLIT  
FACULTY OF ELECTRICAL ENGINEERING, MECHANICAL ENGINEERING  
AND NAVAL ARCHITECTURE

SVEUČILIŠTE U SPLITU  
FAKULTET ELEKTROTEHNIKE, STROJARSTVA I BRODOGRADNJE

**Mišo Jurčević**

**PHOTOVOLTAIC THERMAL COLLECTOR WITH  
ORGANIC PHASE CHANGE MATERIAL**

**FOTONAPONSKI TOPLINSKI KOLEKTOR S  
ORGANSKIM FAZNO-PROMJENJIVIM  
MATERIJALOM**

DOCTORAL THESIS

DOKTORSKI RAD

Split, 2024.





UNIVERSITY OF SPLIT  
FACULTY OF ELECTRICAL ENGINEERING, MECHANICAL ENGINEERING  
AND NAVAL ARCHITECTURE

SVEUČILIŠTE U SPLITU  
FAKULTET ELEKTROTEHNIKE, STROJARSTVA I BRODOGRADNJE

**Mišo Jurčević**

***Photovoltaic Thermal Collector with Organic Phase Change  
Material***

***Fotonaponski toplinski kolektor s organskim fazno-  
promjenjivim materijalom***

DOCTORAL THESIS

DOKTORSKI RAD

Split, 2024.

The research reported in this thesis was carried out at Department of Mechanical Engineering and Naval Architecture, University of Split, Faculty of Electrical Engineering, Mechanical Engineering and Naval Architecture.

Supervisor: Prof. Sandro Nižetić, PhD, FESB, University of Split, Croatia

Supervisor: Prof. Branko Klarin, PhD, FESB, University of Split, Croatia

Thesis number: xxx

---

## BIBLIOGRAPHIC INFORMATION

Keywords: renewables; solar energy; thermal energy storage; photovoltaic thermal collectors; phase change materials; nanomaterials; experimental investigation; computational fluid dynamics; economic evaluation; environmental assessment

Scientific area (znanstveno područje): Technical sciences (Tehničke znanosti)

Scientific field (znanstveno polje): Fundamental technical sciences (Temeljne tehničke znanosti)

Scientific branch (znanstvena grana): Fluid mechanics (Mehanika fluida), Thermodynamics (Termodinamika),

Institution of PhD completion: University of Split, Faculty of Electrical Engineering, Mechanical Engineering and Naval Architecture

Supervisors of the thesis: Prof. Sandro Nižetić, PhD and Prof. Branko Klarin, PhD

Number of pages: 225

Number of figures: 27

Number of tables: 11

Number of references: 123

---

Committee for assessment of doctoral thesis:

1. Assoc. Prof. Igor Pehnac, PhD, University of Split, FESB, Split, Croatia
2. Prof. Anica Trp, PhD, University of Rijeka, RITEH, Rijeka, Croatia
3. Prof. Damir Sedlar, PhD, University of Split, FESB, Split, Croatia
4. Assoc. Prof. Milan Vujanović, PhD, University of Zagreb, FSB, Zagreb, Croatia
5. Asst. Prof. Ivo Marinić-Kragić, PhD, University of Split, FESB, Split, Croatia

Committee for defense of doctoral thesis:

1. XXXX. dr.sc. XXXX Yyyyy, Institution name and City/Town
2. XXXX. dr.sc. XXXX Yyyyy, Institution name and City/Town
3. XXXX. dr.sc. XXXX Yyyyy, Institution name and City/Town
4. XXXX. dr.sc. XXXX Yyyyy, Institution name and City/Town
5. XXXX. dr.sc. XXXX Yyyyy, Institution name and City/Town

Thesis defended on: xx.month.2024.

# Photovoltaic thermal collector with organic phase change material

## Abstract:

The doctoral thesis encompasses a combined research effort presented by compiling eight papers published in distinguished scientific journals. It entails a detailed analysis of the mentioned scientific investigations and findings related to the development of the novel photovoltaic thermal (PVT) collector design, meticulously documented and presented in a coherent and systematic manner. Analysis of the state of the art in PVT collector design revealed a research gap regarding the technical solutions of conventional hybrid solar collectors, i.e., PVT collectors, leading to investigating ways to improve performances by implementing phase change materials (PCM). Phase change materials have limited thermophysical properties, so an approach to enhance properties using nanotechnology was considered. Suitable nano-enhanced phase change materials (NEPCM) for energy technologies were analyzed, based on which the research of novel NEPCMs was carried out. Thus, novel NEPCMs were subjected to thermal characteristics testing using the Transient Plane Source (TPS) method. Due to the potential toxicity of NEPCMs and high unit cost, novel hybrid phase change materials of animalistic origin were designed and subjected to thermal properties testing using the TPS method. Furthermore, the existing PVT systems with incorporated phase change materials were analyzed to determine the possible PCM implementation modalities in the novel PVT collector system. Based on this analysis, a new PVT design was conceptualized and subsequently successfully subjected to experimental field testing in Mediterranean climate circumstances. Finally, a multi-parameter numerical model of the novel PVT-PCM collector was developed and verified.

**Keywords:** renewables; solar energy; thermal energy storage; photovoltaic thermal collectors; phase change materials; nanomaterials; experimental investigation; computational fluid dynamics; economic evaluation; environmental assessment

# Fotonaponski toplinski kolektor s organskim fazno-promjenjivim materijalom

## Sažetak:

Doktorski rad obuhvaća objedinjeno istraživanje predstavljeno kompilacijom osam radova objavljenih u uglednim znanstvenim časopisima. Uključuje detaljnu analizu spomenutih znanstvenih istraživanja i rezultata koji se odnose na razvoj novog dizajna fotonaponskog toplinskog (FNT) kolektora, koji je pomno dokumentiran i predstavljen na koherentan i sustavan način. Analiza dosadašnjih znanstvenih spoznaja ustanovila je jaz u istraživanju u pogledu tehničkih rješenja konvencionalnih hibridnih solarnih kolektora, tj. FNT kolektora, što je dovelo do istraživanja načina poboljšanja performansi implementacijom fazno-promjenjivih materijala (FPM). Fazno-promjenjivi materijali imaju limitirana termofizikalna svojstva, pa je razmatran pristup poboljšanju svojstava primjenom nanotehnologije. Analizirani su prikladni nano-poboljšani fazno-promjenjivi materijali (NPFPM) za tehnologije u energetici, na temelju kojih je provedeno istraživanje novih NPFPM-ova. Stoga su novi NPFPM-ovi podvrgnuti ispitivanju toplinskih karakteristika korištenjem Transient Plain Source (TPS) metode. Zbog potencijalne toksičnosti i cijene NPFPM-ova, dizajnirani su novi fazno-promjenjivi hibridni materijali životinjskog podrijetla, koji su podvrgnuti ispitivanju toplinskih svojstava pomoću TPS metode. Nadalje, analizirani su postojeći FNT sustavi s ugrađenim fazno-promjenjivim materijalima kako bi se odredili mogući modaliteti implementacije FPM-a u novi FNT kolektorski sustav. Na temelju ove analize osmišljen je novi FNT dizajn koji je potom uspješno podvrgnut eksperimentalnom ispitivanju u okolnostima Mediteranske klime. Konačno, razvijen je i verificiran višeparametarski numerički model novog FNT-FPM kolektora.

**Ključne riječi:** obnovljivi izvori energije; solarna energija; skladište toplinske energije; fotonaponski toplinski kolektori; fazno-promjenjivi materijali; nanomaterijali; eksperimentalno istraživanje; računalna dinamika fluida; ekonomska evaluacija; okolišna evaluacija



## Acknowledgments

# Contents

|   |      |
|---|------|
| Abstract:.....  | iv   |
| Sažetak:.....   | v    |
| Acknowledgments .....   | vii  |
| Contents .....  | viii |
| List of Tables .....  | xii  |
| List of Figures.....  | xiii |
| Abbreviations.....  | xiv  |
| 1. INTRODUCTION .....   | 1    |
| 1.1. Motivation and hypothesis .....  | 1    |
| 1.2. Research methodology and scientific contributions.....                                   | 3    |
| 1.3. List of complementary papers .....   | 5    |
| 1.4. Thesis overview.....   | 6    |
| 2. GENERAL FEATURES OF PHOTOVOLTAIC THERMAL COLLECTORS.....                                   | 7    |
| 3. ANALYSIS OF SUITABLE NANO-ENHANCED PHASE CHANGE MATERIALS<br>FOR ENERGY TECHNOLOGIES ..... | 9    |
| 3.1. Practical applications of NEPCM .....  | 10   |
| 3.1.1. Thermal Energy Storage systems based on NEPCM.....                                     | 11   |
| 3.1.2. Photovoltaic solar systems and components with NEPCM.....                              | 12   |
| 3.2. Brief overview of NEPCM thermal properties .....   | 13   |
| 3.3. Critical NEPCM preparation aspects .....   | 14   |
| 3.3.1. Strategies and procedures of NEPCM preparation .....                                   | 15   |
| 3.3.2. Overview of nanomaterials toxicity and safety procedures.....                          | 16   |
| 4. INVESTIGATION OF NOVEL NANO-ENHANCED PHASE CHANGE<br>MATERIALS.....                        | 18   |
| 4.1. Employed nanocomposites preparation methodology .....                                    | 18   |
| 4.2. Thermal properties measurement methodology .....   | 19   |
| 4.3. Thermal properties of RT26 and RT28HC based NEPCMs.....                                  | 19   |
| 5. INVESTIGATION OF NOVEL HYBRID PHASE CHANGE MATERIALS.....                                  | 22   |
| 5.1. Thermal characteristics of novel hybrid phase change materials.....                      | 23   |



|        |   |    |
|--------|---|----|
| 5.2.   | Environmental implications of hybrid PCMs .....   | 26 |
| 6.     | ANALYSIS OF PVT SYSTEMS WITH INCORPORATED PHASE CHANGE MATERIALS .....  | 28 |
| 6.1.   | Overview of experimental PVT-PCM collector systems .....  | 29 |
| 6.1.1. | Implementation of phase change materials into PVT systems .....   | 29 |
| 6.1.2. | Summary of PVT-PCM design concepts .....  | 30 |
| 6.1.3. | Economic and environmental implications of PVT-PCM designs .....  | 33 |
| 6.2.   | Numerical modeling of PCMs in PVT systems .....   | 33 |
| 7.     | ANALYSIS OF NOVEL PROPOSED PVT-PCM COLLECTOR DESIGN .....   | 37 |
| 7.1.   | Concept of novel PVT-PCM collector .....  | 37 |
| 7.2.   | Experimental field research of PVT-PCM collector .....  | 39 |
| 7.2.1. | Operational regimes and performance indicators .....  | 41 |
| 7.2.2. | Assessment of collector performance at annual basis .....   | 43 |
| 7.3.   | Environmental impact and economic evaluation .....  | 44 |
| 8.     | NUMERICAL STUDY OF NOVEL PVT-PCM COLLECTOR .....  | 47 |
| 8.1.   | Experimental research of input parameters for numerical modeling .....  | 47 |
| 8.1.1. | Investigation of convective heat transfer coefficients .....  | 47 |
| 8.1.2. | Differential scanning calorimetry of pork fat PCM .....   | 51 |
| 8.2.   | Computational domains and boundary conditions .....   | 52 |
| 8.3.   | Verification of multi-parameter numerical model and discussion .....  | 54 |
| 9.     | SCIENTIFIC CONTRIBUTIONS OF PUBLICATIONS .....  | 58 |
| 9.1.   | Publication 1: Nano-enhanced phase change materials and fluids in energy applications: A review .....   | 58 |
| 9.1.1. | Publication summary .....   | 58 |
| 9.1.2. | PhD candidate contribution .....  | 58 |
| 9.2.   | Publication 2: Comprehensive analysis of preparation strategies for phase change nanocomposites and nanofluids with brief overview of safety equipment...59 |    |
| 9.2.1. | Publication summary .....   | 59 |
| 9.2.2. | PhD candidate contribution .....  | 59 |
| 9.3.   | Publication 3: Thermal constant analysis of phase change nanocomposites and discussion on selection strategies with respect to economic constraints .....   | 60 |
| 9.3.1. | Publication summary .....   | 60 |

|   |    |
|---|----|
| 9.3.2. PhD candidate contribution .....   | 60 |
| 9.4. Publication 4: Experimental investigation of novel hybrid phase change materials .....   | 61 |
| 9.4.1. Publication summary .....  | 61 |
| 9.4.2. PhD candidate contribution .....   | 61 |
| 9.5. Publication 5: Implementation of phase change materials for thermal regulation of photovoltaic thermal systems: Comprehensive analysis of design approaches.....                       | 62 |
| 9.5.1. Publication summary .....  | 62 |
| 9.5.2. PhD candidate contribution .....   | 62 |
| 9.6. Publication 6: Investigation of heat convection for photovoltaic panel towards efficient design of novel hybrid cooling approach with incorporated organic phase change material ..... | 63 |
| 9.6.1. Publication summary .....  | 63 |
| 9.6.2. PhD candidate contribution .....   | 63 |
| 9.7. Publication 7: Techno-economic and environmental evaluation of photovoltaic-thermal collector design with pork fat as phase change material .....                                      | 64 |
| 9.7.1. Publication summary .....  | 64 |
| 9.7.2. PhD candidate contribution .....   | 64 |
| 9.8. Publication 8: Towards resilient operation of photovoltaic-thermal collector with incorporated organic phase change material: Numerical and experimental investigation.....            | 65 |
| 9.8.1. Publication summary .....  | 65 |
| 9.8.2. PhD candidate contribution .....   | 65 |
| 10. CONCLUSIONS AND FUTURE DIRECTIONS .....   | 66 |
| 10.1. Summary of main conclusions .....   | 66 |
| 10.2. Future research work.....   | 69 |
| BIBLIOGRAPHY .....  | 70 |
| APPENDIX A – H.....   | 81 |
| Appendix A .....  | 81 |
| Appendix B .....  | 82 |
| Appendix C .....  | 83 |
| Appendix D .....  | 84 |

|                  |    |
|------------------|----|
| Appendix E ..... | 85 |
| Appendix F.....  | 86 |
| Appendix G.....  | 87 |
| Appendix H.....  | 88 |
| ŽIVOTOPIS.....   | 89 |
| BIOGRAPHY .....  | 91 |

## List of Tables

|   |           |
|---|-----------|
| <i>Table 4.1. Thermal characteristics of RT28HC and RT28HC-based NEPCMs [73].</i>                           | <i>20</i> |
| <i>Table 4.2. Thermal characteristics of RT26 and RT26-based NEPCMs [73].</i>                               | <i>21</i> |
| <i>Table 5.1. Thermal characteristics of pork fat and hybrid PCMs.</i>                                      | <i>26</i> |
| <i>Table 6.1. Properties of PCMs in PVT systems.</i>  | <i>30</i> |
| <i>Table 6.2. Main features and performance indicators of PVT-PCM collectors.</i>                           | <i>31</i> |
| <i>Table 6.3. Numerical approaches for phase change materials.</i>  | <i>35</i> |
| <i>Table 7.1. Energy generation and efficiency of referent PV panel and PVT-PCM collector.</i>              | <i>42</i> |
| <i>Table 7.2. Environmental footprint of PVT-PCM collector design [118].</i>                                | <i>46</i> |
| <i>Table 8.1. Experimental measurements of convection heat transfer coefficient at six positions [117].</i> | <i>50</i> |
| <i>Table 8.2. Thermophysical characteristics of solid domains [121].</i>                                    | <i>53</i> |
| <i>Table 8.3. Thermophysical characteristics of fluid domains [121].</i>                                    | <i>53</i> |

## List of Figures

|   |    |
|---|----|
| <i>Figure 1.1. Research methodology scheme</i> .....  | 4  |
| <i>Figure 2.1. Typical PVT collector design [10].</i> .....   | 8  |
| <i>Figure 3.1. Increase of research studies from 2002-2022 related to nanomaterials and prominent fields [23].</i> .....                            | 9  |
| <i>Figure 3.2. Categorization of NEPCM applications [34].</i> .....   | 11 |
| <i>Figure 3.3. Two-step NEPCM preparation approach.</i> .....   | 14 |
| <i>Figure 3.4. Flowchart illustrating the procedures and techniques for NEPCM homogenization [67].</i> .....  | 16 |
| <i>Figure 4.1. Two-step NEPCM homogenization.</i> .....   | 19 |
| <i>Figure 4.2. Graphene/NEPCM behavior in relation to thermal properties initial values (0%) of base PCMs [73].</i> .....                           | 21 |
| <i>Figure 5.1. Pork fat (lard) and hybrid PCMs [75].</i> .....  | 23 |
| <i>Figure 5.2. Impact of 5% (a), 10% (b), and 20% (c) oils volume fractions on pork fat thermal properties [75].</i> .....                          | 25 |
| <i>Figure 6.1. Three-stage selection process of latest research.</i> .....  | 29 |
| <i>Figure 7.1. Schematic layout of PVT-PCM collector [117].</i> .....   | 38 |
| <i>Figure 7.2. PVT-PCM collector with multi-block cooling [118].</i> .....  | 39 |
| <i>Figure 7.3. Experimental rig schematic [118].</i> .....  | 40 |
| <i>Figure 7.4. Free-standing referent PV panel and PVT-PCM collector [118].</i> .....   | 41 |
| <i>Figure 7.5. Front surface temperature of referent PV panel and PVT-PCM collector on September 6<sup>th</sup> [118].</i> .....                    | 43 |
| <i>Figure 7.6. Annually heat generation estimation [118].</i> .....   | 44 |
| <i>Figure 7.7. LCA flowchart connecting environmental midpoint and endpoint impacts [118].</i> .....  | 45 |
| <i>Figure 7.8. Constructive components cost share in the collector design [118].</i> .....  | 46 |
| <i>Figure 8.1. Experimental test rig layout in wind tunnel [117].</i> .....   | 48 |
| <i>Figure 8.2. Relative wind angle <math>\gamma</math> (a) and PV panel tilt angle <math>\beta</math> (b) [117].</i> .....                          | 48 |
| <i>Figure 8.3. Differential scanning calorimetry of pork fat [121].</i> .....   | 52 |
| <i>Figure 8.4. PVT-PCM collector multi-block cooling domains [121].</i> .....   | 52 |
| <i>Figure 8.5. Solar radiation in Split, Croatia, on October 26, 2021 [121].</i> .....  | 54 |
| <i>Figure 8.6. Comparison of collector and PV panel front surface temperatures with air temperature [121].</i> .....                                | 55 |
| <i>Figure 8.7. Collector back surface temperatures during the transition from passive to active mode (left) and vice versa (right) [121].</i> ..... | 56 |
| <i>Figure 8.8. Comparison of numerical and experimental temperature data for the front surface of PVT-PCM collector [121].</i> .....                | 56 |

## Abbreviations

BICPV – building-integrated concentrated photovoltaics  
CFD – computational fluid dynamics  
CHP – combined heat and power  
DSC – differential scanning calorimetry  
EVA – ethylene vinyl acetate  
1D – one-dimensional  
2D – two-dimensional  
3D – three-dimensional  
EHR – elastomeric half-mask respirator  
FEM – finite element method  
FFR – filtering facepiece respirator  
FVM – finite volume method  
HTF – heat transfer fluid  
IT – information technology  
LCA – life cycle assessment  
LCOE – levelized cost of energy  
LHTES – latent heat thermal energy storage  
NEPCM – nano-enhanced phase change material  
PCM – phase change material  
PPE – personal protective equipment  
PV – photovoltaic  
PVT – photovoltaic thermal  
SDS – safety data sheet  
STC – standard test conditions  
TES – thermal energy storage  
TPS – transient plain source  
UDF – user-defined functions

## **1. INTRODUCTION**

The doctoral thesis is prepared based on the compilation of scientific papers published in top and renowned high-impact factor journals in the field, all in the Q1 quartile. The compilation consists of eight publications, forming an integrated and cohesive whole, surpassing the impact of individual publications in the field. The thesis provides original contributions in the technical sciences area, i.e., in the field of fundamental technical sciences. The discussed topic is relevant in terms of technological progress, current geopolitical currents, and related energy policies.

### **1.1. Motivation and hypothesis**

Social imbalance, economic instability, religious, ethnic, and other turmoil are global factors shaping energy policies. States and governments, as subjects of energy policy creation, have several measures at their disposal to manipulate the energy sector landscape. In the framework of energy policies, it is necessary to consider the safety of the energy distribution system, the diversity of energy sources, and environmental aspects. Historically, energy production, distribution, and consumption mechanisms have often been instrumentalized in global and local conflicts, which has not changed to this day, as we witness in recent geopolitical confrontations. Globally, developed economies recognize the importance of the energy sector, so their ways of generating, storing and distributing energy continuously evolve following geopolitical currents and technological progress. A crucial modern state effort in energy policy is establishing efficient, dependable, and ecologically sustainable energy transfer from the production facilities to the end-users. In the ideal case, energy is produced where consumed, i.e., the time-space determinant of energy transfer is shortened as much as possible. In addition to unavoidable transport losses, large energy distribution systems require constant investment and maintenance and often represent a significant environmental hazard. Conversely, compact energy distribution systems have shorter transport routes and are typically more cost-effective by their nature. Additionally, if these systems rely on renewable energy sources, they tend to have a reduced impact on the environment and human health.

Most renewable energy sources are compatible with the spatial deficit of modern cities thanks to their compactness and cogeneration capability. Moreover, implementing modern smart technologies with renewable energy sources can significantly improve the energy efficiency of congested urban environments. Therefore, striving for flexibility and reducing energy production costs while caring for the environment is a permanent, never-ending effort that should be vertically embedded in energy policies, starting from renewable energy production facilities to consumers.

The importance of environmental and public health aspects has been recognized for decades through a series of international initiatives and agreements such as the Montreal

Protocol [1], the Kyoto Protocol [2], the Paris Agreement on climate change [3], etc. The countries that have signed the Paris Agreement have committed to limiting the increase in global average temperature within 2°C compared to pre-industrial levels, agreeing to pursue a 1.5°C increase limit. Furthermore, the agreement's framework aims to minimize the impact of human activity on the environment by reducing global greenhouse gas emissions by 43% until 2030.

Fossil energy sources undeniably contribute to the emission of toxic materials and greenhouse gases, especially CO<sub>2</sub> [4]. As much as 40% of total CO<sub>2</sub> emissions can originate from energy expenditure in buildings, which is not surprising considering that almost a third of the global energy appetite comes from this source [5]. Furthermore, 30% of global energy expenditure and 26% of total energy-associated emissions are related to buildings' operational demands [6]. More precisely, 8% of global emissions come directly from buildings, and 18% comes indirectly from generating electricity and heat consumed in that sector [6]. More than half, i.e., 55%, of the energy used in residential buildings is spent on heating, ventilation, and air conditioning, followed by lighting (17%), preparation of domestic hot water (10%), and electrical appliances (5%), etc. [7]. Thus, most energy is spent on ventilation, air temperature conditioning, and domestic hot water preparation, which conventionally require separate energy systems. However, a cogeneration approach (CHP) based on renewable energy sources can ensure dispersed clean energy production for various purposes, including residential building energy supply. Evidently, in the current decade, it is necessary to systematically carry out an accelerated energy transition towards renewable energy sources.

In the last decade, according to the annual power generated, hydropower is the most prominent among renewable energy sources, followed by wind energy, solar energy, and bioenergy [8]. However, installed photovoltaic capacities and wind energy are expected to overtake hydropower by 2024 and 2027, respectively [9].

The accelerated expansion of photovoltaic technologies results from a continuous reduction in the prices of new globally installed photovoltaic capacities. The unit price of newly installed photovoltaic capacities usually ranges from 1.5 € Wp<sup>-1</sup> to 3.5 € Wp<sup>-1</sup> [10]. The fundamental disadvantage of most photovoltaic technologies is the relatively low electrical efficiency, usually between 12% and 17% [11], while only in laboratory conditions can reach energy conversion efficiency somewhat above 20%. Obviously, most of the irradiated solar energy is wasted on enormous losses, while the rest is converted into electrical energy. Elementary logic dictates a different approach to collecting solar energy, i.e., a cogeneration approach is necessary to minimize the losses of irradiated energy.

Photovoltaic thermal (PVT) collectors represent a step forward in utilizing heat as a by-product of collecting irradiated solar energy for electric power production. Specifically, these are power-generating hybrid energy systems that convert irradiated solar energy into electricity with increased overall efficiency due to the utilization of waste heat induced in photovoltaic (PV) solar cells. In recent years, phase change materials (PCM) have been used to improve the efficiency of photovoltaic systems. In this context, PVT systems are no exception, where phase change materials are increasingly used for passive thermal management, i.e., phase change material takes on the role of a heat sink, thus creating a PVT-PCM collector. Controlled release



and storage of heat in the PCM is necessary to achieve a balance in producing electrical and thermal energy from the PVT-PCM collector. Therefore, it is essential to empirically determine all influencing parameters on the PVT-PCM system through intensive experimental research and to create prerequisites for possible improvements through extensive numerical analysis.

The doctoral thesis hypothesis are as follows:

- I. It is possible to use the Transient Plain Source technique to experimentally investigate the thermal properties of newly developed phase change materials and to apply the phase change material of organic (animalistic) origin for the thermal regulation of the photovoltaic thermal system,
- II. Using an integral experimental-numerical approach, it is possible to develop a novel concept of a photovoltaic thermal collector with a phase change material while achieving suitable performances under the circumstances of the Mediterranean climate at the location of the city of Split.

## **1.2. Research methodology and scientific contributions**

Developing a novel photovoltaic thermal collector concept is challenging due to its dual, mutually opposing thermo-electric nature. The success of this concept heavily relies on alleviating the inherent conflict between producing electricity and generating usable heat while ensuring a minimal environmental footprint. As stated above, the thermal management strategies of PVT systems increasingly include applying phase change materials as passive heat sinks. Therefore, the thermal component of the envisaged PVT collector rests on the principle of phase transition of the adequate material. The primary limiting factors for applying commercially available phase change materials in the energy sector are thermophysical characteristics and the relatively high cost. Namely, these materials have a relatively low thermal conductivity, slowing heat dissipation in energy systems.

The development and testing of a flexible, robust, and efficient PVT collector design with incorporated phase change material was carried out in three phases, Figure 1.1.

In phase 1, the ways to ameliorate energy systems by modifying the thermophysical properties of PCMs integrated with suitable nanomaterials were investigated. By reviewing the available scientific literature within Elsevier's Scopus<sup>®</sup> database, the application areas of nano-enhanced PCMs in energy-related systems were determined, considering environmental and economic aspects. Furthermore, the production methods of this type of material were investigated to produce novel phase change materials whose thermal properties are tested using the Transient Plain Source technique. Other alternative organic phase change materials, such as animal fat, were also tested using this technique. The appropriate PCM for the concept of the PVT collector was selected based on the measured thermal properties, taking into account economic and environmental aspects. Finally, in phase 1, the thermal regulation system of the collector with integrated phase change material was conceptually defined, i.e., the micro-generation passive/active unit for electricity and low-temperature thermal energy production was conceptualized.

In phase 2, the concept of the PVT collector was experimentally tested in Mediterranean climatic conditions at the Split (Croatia) location. The experimental test was carried out over a more extended period, through several months, to cover all climate circumstances, after which the system's performance could be evaluated. An economic assessment was conducted, along with an analysis of the environmental impact of the newly proposed concept.

In phase 3, in parallel with the testing of the experimental system, a numerical model of the PVT-PCM collector was developed in the Ansys Fluent software package. The developed model considers conduction, convection, and radiation along with several variable parameters such as cloud cover, air temperature, and wind speed. Through an iterative process, the numerical model was calibrated with regard to the conducted experimental research.

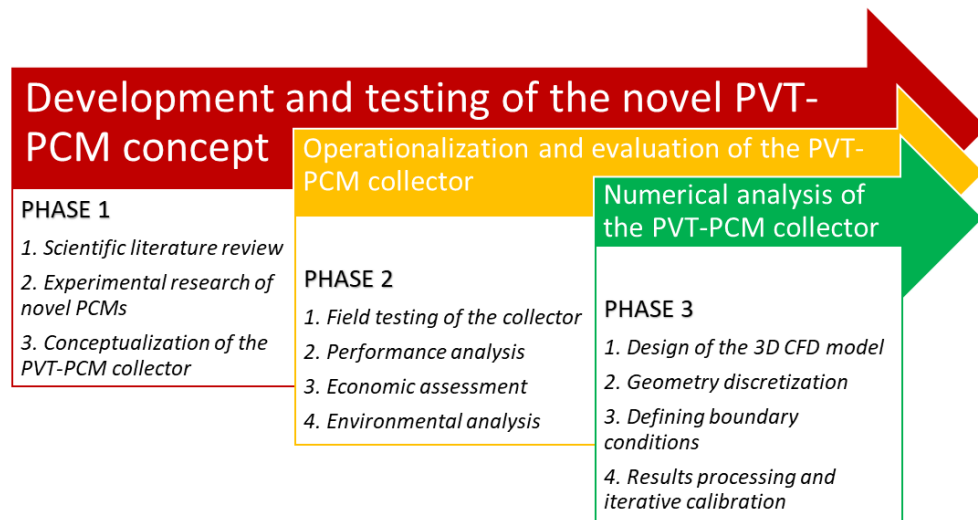


Figure 1.1. Research methodology scheme.

In general, the research contributes to the classification and understanding of the NEPCMs preparation procedures' impact on the applications in the energy field. Furthermore, the thermal properties of various phase change materials are delivered, including newly developed NEPCMs and organic PCMs. The selected PCM was implemented in the proposed and developed novel PVT concept, which was then experimentally tested in actual working conditions. The PVT concept, i.e., PVT-PCM collector, was analyzed in terms of technical performance and was further evaluated based on the economic and environmental assessment of the novel design. The numerical three-dimensional model of the proposed PVT-PCM collector was developed and calibrated iteratively based on experimental field tests. Thus, providing foundations for improving existing PVT designs or creating new ones from scratch.

The key scientific contributions of the doctoral thesis are summarized as follows:

- I. Research and thermal properties determination of novel organic phase change materials and phase change materials combined with nanomaterials.

- II. Development of the novel photovoltaic thermal collector concept design incorporating organic phase change material using experimental and numerical approaches.
- III. Comprehension of the economic and environmental aspects of the proposed photovoltaic thermal collector design.

### 1.3. List of complementary papers

The original contributions were derived from published complementary scientific papers, based on which cumulative research review, including individual and collective conclusions, was written. The published complementary papers are listed as follows:

- I. S. Nižetić, M. Jurčević, M. Arici, A.V. Arasu and G. Xie, Nano-enhanced phase change materials and fluids in energy applications: A review, *Renewable and Sustainable Energy Reviews*, 129, 109931, 2020.
- II. M. Jurčević, S. Nižetić, M. Arici and P. Ocloň, Comprehensive analysis of preparation strategies for phase change nanocomposites and nanofluids with brief overview of safety equipment, *Journal of Cleaner Production*, 274, 122963, 2020.
- III. M. Jurčević, S. Nižetić, M. Arici, A.T. Hoang, E. Giama and A. Papadopoulos, Thermal constant analysis of phase change nanocomposites and discussion on selection strategies with respect to economic constraints, *Sustainable Energy Technologies and Assessments*, 43, 100957, 2021.
- IV. M. Jurčević, S. Nižetić, D. Čoko, A.T. Hoang and A. Papadopoulos, Experimental investigation of novel hybrid phase change materials, *Clean Technologies and Environmental Policy*, 24, 201-212, 2021.
- V. S. Nižetić, M. Jurčević, D. Čoko, M. Arici and A.T. Hoang, Implementation of phase change materials for thermal regulation of photovoltaic thermal systems: Comprehensive analysis of design approaches, *Energy*, 228, 120546, 2021.
- VI. M. Jurčević, S. Nižetić, I. Marinić-Kragić, D. Čoko, M. Arici, E. Giama and A. Papadopoulos, Investigation of heat convection for photovoltaic panel towards efficient design of novel hybrid cooling approach with incorporated organic phase change material, *Sustainable Energy Technologies and Assessments*, 47, 101497, 2021.
- VII. M. Jurčević, S. Nižetić, D. Čoko, M. Arici, A.T. Hoang, E. Giama and A. Papadopoulos, Techno-economic and environmental evaluation of photovoltaic-thermal collector design with pork fat as phase change material, *Energy*, 254 (Part B), 124284, 2022.

- VIII. M. Jurčević, S. Nižetić, I. Marinić-Kragić, M. Jakić and M. Arici, Towards resilient operation of photovoltaic-thermal collector with incorporated organic phase change material: Numerical and experimental investigation, *Sustainable Energy Technologies and Assessments*, 60, 103465, 2023.

#### 1.4. Thesis overview

The motivation and objective of the thesis are elaborated in the introductory chapter, together with stated hypotheses. Furthermore, the research methodology is established, followed by original scientific contributions based on published papers. Finally, the chapter ends with a list of eight complementary papers and an overview of the doctoral thesis organization. Chapter 2 deals with the general characteristics of PVT collectors and indicates the possible directions of technology development. Chapter 3 provides an overview of the potential ways of incorporating NEPCMs into different energy technologies. It also discusses the employed preparation procedures and related issues, along with a concise examination of the relevant thermal properties. Chapters 4 and 5 cover preparation methodology and thermal properties of the newly developed nano-enhanced and hybrid phase change materials. An overview of experimental PVT-PCM collector systems and numerical approaches to PCM modeling is provided in Chapter 6. Based on the efforts described in the previous chapters, in Chapter 7, the novel PVT-PCM collector concept is introduced. Furthermore, the chapter provides results of the experimental field research, as well as environmental and economic assessments. Chapter 8 describes the numerical study of the novel PVT-PCM collector, including experimental research of input parameters necessary for numerical modeling. Moreover, this chapter discusses and justifies the verification of the developed multi-parameter numerical model of the collector. Chapter 9 summarizes published complementary scientific papers from which the doctoral thesis's original contributions are derived and isolates the PhD candidate's contributions in each publication. The conclusion chapter emphasizes research highlights and presents several possible directions for future studies. Finally, an extensive list of references and appendices concludes the thesis manuscript.

## 2. GENERAL FEATURES OF PHOTOVOLTAIC THERMAL COLLECTORS

This type of hybrid solar collector is seeing significant growth in the market compared to similar energy harvesting systems. It is preferred for its ability to better use the limited space in densely populated urban regions since it provides thermal and electric power production flexibility and reliability while saving space, i.e., combining features of traditional solar collectors with PV modules on the same surface area. Depending on the PVT design, this co-generation can substantially decrease the temperature in the PV part of the system by its thermal component-triggered heat sink effect. Generally, PVT collectors can be distinguished based on the heat transfer fluid (HTF) they use, i.e., air or liquid-based. Additionally, they can be differentiated based on their glazing, which can be covered, uncovered, or concentrated PVT layouts [10]. The operating temperature of a PVT collector is directly influenced by the type of HTF and glazing used. Regarding the PV component of the collector, monocrystalline silicon PV cells are preferred to polycrystalline PV cells due to their higher nominal electrical efficiency. However, it is important to note that this increased efficiency comes at a slightly higher purchase price. It is common for most used silicon PV technologies to experience a decrease in electrical efficiency ranging from  $0.4\% \text{ } ^\circ\text{C}^{-1}$  to  $0.5\% \text{ } ^\circ\text{C}^{-1}$  (depending on the technology) as the temperature of the cell increases [12]. Therefore, all silicon-based PVT designs experience collision between electric power production and heat generation since the thermal component inclines to higher working temperatures. Other commercially available PV technologies, such as thin film, organic solar cells, etc., are rarely used for PVT collectors, so currently, they are not relevant to the same extent as silicon-based technologies. The majority of traditional PVT collectors are designed to operate efficiently at lower hot water temperatures, generally up to  $50^\circ\text{C}$ , while concentrating PVT collectors can operate at temperatures exceeding  $80^\circ\text{C}$ . Hence, to create a well-designed PVT collector, it is essential to strike proper energy equilibrium between the electric and thermal components of the collector to achieve optimal power production for the specific consumer. The efficiency ( $\eta$ ) of a PVT collector is calculated as the sum of electrical ( $\eta_{el}$ ) and thermal efficiency ( $\eta_{th}$ ), Equation (2.1).

$$\eta = \eta_{el} + \eta_{th} \quad (2.1)$$

The effectiveness of PVT collectors in generating electricity is mainly influenced by the PV technology type, the amount of solar energy ( $G$ ), the surface area of the PVT collector ( $A_{PVT}$ ), as well as the PV cells temperature that affects both the output voltage ( $V$ ) and current ( $I$ ) as stated in Equation (2.2).

$$\eta_{el} = \frac{I \cdot V}{A_{PVT} \cdot G} \quad (2.2)$$

Calculating the thermal efficiency is slightly more intricate. Aside from the PV technology, the amount of solar energy it receives, and the size of the collector, it also relies on HTF thermal properties and mass flow rate ( $\dot{m}$ ), as seen in Equation (2.3). The specific heat capacity ( $C_p$ ) is the HTF property, while the temperature difference ( $\Delta T$ ) results from complicated interaction between the PVT collector design, HTF, and surrounding conditions.

$$\eta_{th} = \frac{\dot{m} \cdot C_p \cdot \Delta T}{A_{PVT} \cdot G} \quad (2.3)$$

Typically, a heat exchanger serves as the integrating element between the electrical and thermal components of a PVT collector. The heat exchanger of a typical PVT collector is usually attached to the rear side and consists of copper pipes fused with a copper absorber surface to form a thermal absorber, Figure 2.1. Thick thermal insulation usually shields the thermal absorber from weather conditions on its underside.

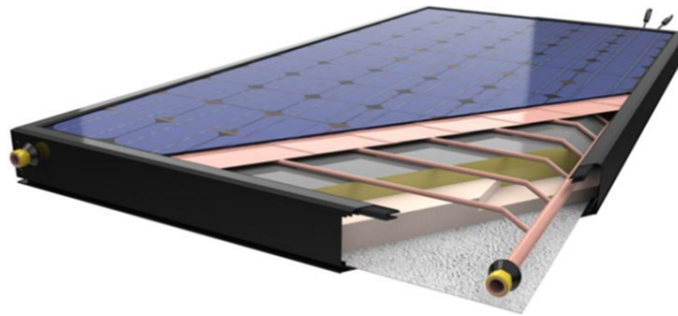


Figure 2.1. Typical PVT collector design [10].

Renowned PVT collectors commercially cost a minimum of about 300 € m<sup>-2</sup> and above, around 25% more than conventional solar collectors [13]. In comparison, classic PV systems for residential applications are priced at around 200 € m<sup>-2</sup> [10]. The high cost and consumer reluctance toward new technology may temporarily impede the widespread installation of PVT collectors. However, scientists are experimenting with various methods to control the delicate energy equilibrium of PVT collectors to produce more viable systems. One of the most notable ways to enhance the performance of PVT systems in recent and ongoing studies is through nanotechnology [14]. In order to reach their objective, they are using not only nanotechnology but also various thermal energy storage methods that incorporate different phase change materials. This is evidenced by their increasing implementation, as reported in [10].

### 3. ANALYSIS OF SUITABLE NANO-ENHANCED PHASE CHANGE MATERIALS FOR ENERGY TECHNOLOGIES

The term "nanotechnology" has been used in scientific literature since the 1970s and even earlier in some cases [14]. However, it was not until the late 1980s and early 1990s, with the advancement of microscope technology, that this field experienced significant growth. Over the past two decades, the scientific community has widely embraced this technology, especially in the realm of nanostructure materials. Nanostructures have various characteristics that can be used to describe them, such as their state, morphology, dimensions, chemical composition [15], or, similarly, the chemistry of the surface [16]. For the material to be considered a nanostructure, at least one of its dimensions must be smaller than 100 nm. A widely used classification system for nanostructures based on their geometry and dimensions is the four-level classification: 0D, 1D, 2D, and 3D. If all of the material's dimensions are on the nanoscale, it is classified as 0D. If the material has nanoscale dimensions in two directions, it is classified as 1D. A 2D classification means that only one dimension is on the nanoscale, and materials with a 3D classification do not have any dimensions on the nanoscale. Therefore, nanostructures come in different forms and shapes, such as nanoparticles (0D), quantum dots (0D), nanofibers (1D), nanorods (1D), nanowires (1D), nanosheets (2D), nanoplates (2D), complex hierarchical structures (3D), nanostructure assemblies (3D), etc. [17]. Nanostructures, also known as nanomaterials, have applications in diverse fields such as medicine [18], electronics [19], energy [20], Information Technology (IT) [21], and food safety [22]. Over the past two decades, there has been extensive research into using nanomaterials due to their immense potential for driving technological progress, Figure 3.1.

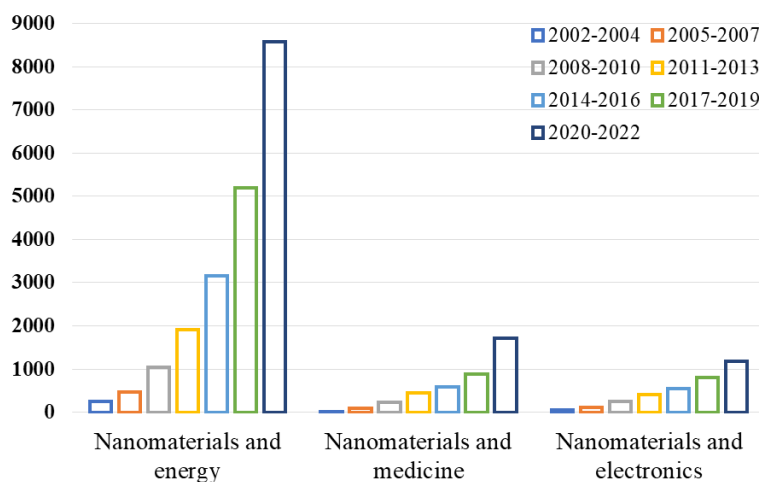


Figure 3.1. Increase of research studies from 2002-2022 related to nanomaterials and prominent fields [23].

The energy sector is particularly promising for the application of these materials due to its vast array of potential uses, including batteries [24], biofuels production [25], electromagnetic interference shielding [26], energy storage [27], solar cells [28], etc.

The insertion of nanomaterials can improve the physical properties of materials, bringing noticeable benefits and performance enhancements to various systems and processes [29]. PVT collectors are no exception, considering that nanomaterials can be found in employed heat transfer fluids [30], i.e., nanofluids, or NEPCMs [31]. Nano-enhanced phase change materials are considered a subtype of nanocomposites. According to Malhotra and Ali [32], nanocomposites are materials that have at least one nano-sized phase incorporated into a metal, ceramic, or polymer matrix. These are commonly found in the scientific literature, while other materials may also be used as a matrix [33]. The clear distinction between nanofluids and nanocomposites is not applicable due to the varying states of matter, i.e., depending on the current material phase, many nanofluids can also serve as nanocomposites and vice versa [34]. Possible examples are the creation of a nanocomposite using water [35] or a nanofluid using paraffin [36].

### **3.1. Practical applications of NEPCM**

Nanomaterials can enhance the thermal conductivity and heat-storing capacity of phase change material [37], making it an effective energy storage solution [38]. There are multiple ways to store energy, but a particularly effective method is utilizing NEPCMs for thermal energy storage (TES) systems. The fundamental idea is to store surplus or waste heat from thermal energy sources, increasing the system's efficiency [34]. Modern technology and engineering can greatly benefit from using NEPCMs, but their application is currently limited due to the high cost of these materials [34]. Nonetheless, they have the ability to absorb and release large quantities of heat when approaching the temperature at which a phase transition occurs. As a result, they are an excellent choice for a variety of thermal management applications.

Thermal management is a broader term encompassing the thermal regulation of various energy systems and other technologies to increase their overall efficiency. For example, batteries and electronics perform best within a specific temperature range. When batteries are discharging, they tend to generate heat. Electronic devices also exhibit heat generation during operation which requires an effective cooling strategy. NEPCMs provide a reliable passive cooling solution, making them an effective option for various applications, including recovering waste heat from engines [39], thermal management of lithium-ion batteries [40], battery simulators [41], and battery packs [42], cooling electronic chipsets [43] and CPUs [44], water production in solar distillers [45], water desalination [46], etc.

Based on the aforementioned, NEPCM applications can be classified into two main categories: Energy storage and Thermal management, as well as a few subcategories, Figure 3.2. In addition to other applications within the main categories, the focus of research [34] was on thermal energy storage systems and photovoltaic solar systems and components.



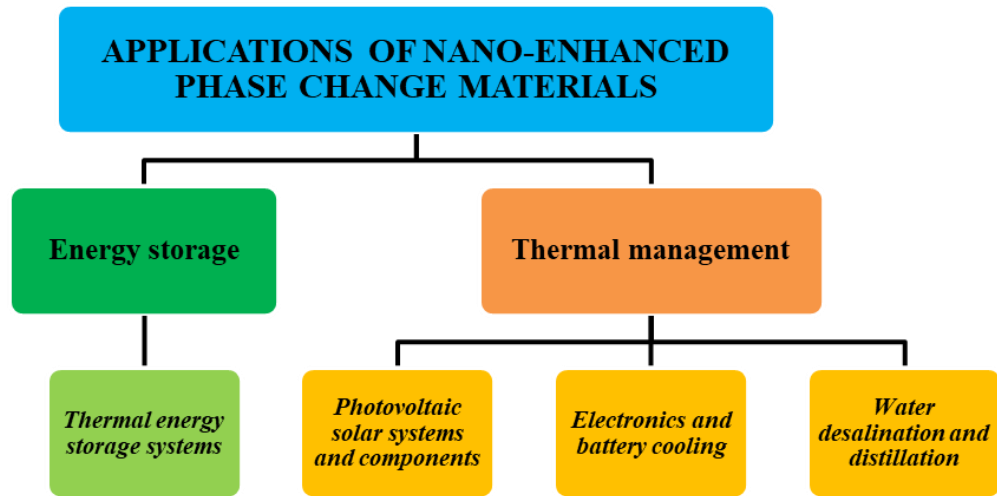


Figure 3.2. Categorization of NEPCM applications [34].

### 3.1.1. Thermal Energy Storage systems based on NEPCM

There are different approaches to accomplishing thermal energy storage, including diverse technologies and solutions [47]. Generally, there are three prominent methods [48] for storing thermal energy: chemical storage, sensible storage, and latent heat storage. Given the high-energy storage density, latent heat storage is a particularly trending topic in this context, i.e., phase change materials. Most NEPCM materials are suitable for TES applications [34]. The TES system utilizing NEPCM materials stores heat passively using the latent heat principle. These systems offer the advantage of enabling active management of the release and storage of latent heat energy due to their passive and predictable nature. The choice of appropriate NEPCM materials primarily depends on their thermal properties and exploitation conditions. The enclosure design and the storage medium's low thermal conductivity mainly restrict the thermal behavior and responsiveness of the TES unit [49]. The primary research efforts regarding NEPCM materials mainly focus on enhancing their thermal conductivity [34].

NEPCM samples (nano Cu and Paraffin) created by Lin et al. [50] exhibited a maximum growth in thermal conductivity of 46.3% (2.0 % Cu mass fraction) in comparison with pure paraffin. The nanocomposite containing 1 wt.% of Cu exhibited a 23.9% rise in thermal conductivity. This particular nanocomposite was integrated into the solar thermal energy storage system resulting in a modest 1.7% increased efficiency.

Altohamy et al. [35] carried out an experimental study on the phase transition (solidification) of water-based PCM enriched with  $\text{Al}_2\text{O}_3$  nanoparticles. The study was conducted in a spherical capsule LHTES system. Adding  $\text{Al}_2\text{O}_3$  nanoparticles to water affects the solidified mass fraction and solidification time, causing a significant decrease under certain conditions. Additionally, there was a notable increase in the speed of charging and the amount of energy stored. Research indicates that incorporating nanoparticles at a volume concentration of 2% can reduce charging time by up to 30% in comparison to using solely water.

According to Sharma et al. [51], integrating NEPCM in a flat plate solar collector TES system improved charging and discharging efficiency by 24% and 28%, respectively. A similar concept of flat plate solar collector was elaborated in research [52], where the authors determined that boosting the volume fraction of nanoparticles improves the NEPCM melting rate and thermal storage efficiency.

Shell and tube TES unit with NEPCM was numerically analyzed by Mohammad et al. [49] using the Taguchi optimization method to determine the impact of nanoparticle addition compared with optimization of geometry. Regarding the energy storage capacity, the impact of nanomaterials was not as significant as the impact of geometry. In fact, the contribution of added nanoparticles to energy storage was only around 5% to 6%, while the contribution of geometric shapes was as high as 41%. It would be incorrect to assume that this contribution ratio remains constant for all NEPCM TES system designs. However, it can be presumed that the geometry aspect will predominantly contribute to energy storage, which must be considered when designing this kind of energy system.

### **3.1.2. Photovoltaic solar systems and components with NEPCM**

Solar radiation hitting the surface of a PV cell induces electricity, while the rest of the irradiated energy is reflected, transmitted, or absorbed by the cell. The photovoltaic module experiences an increase in temperature due to its absorption of solar radiation, leading to decreased efficiency. Hence, for the sake of effectualness and economic feasibility, it is sensible to explore different approaches to the thermal regulation of photovoltaics. The advantageous thermal properties of NEPCMs could prove highly favorable in achieving this goal.

Nada and El-Nagar [53] investigated how well PCMs and NEPCMs can control the temperature of PV modules to maximize electrical efficiency, whether they are free-standing or integrated into buildings. By adding  $\text{Al}_2\text{O}_3$  nanoparticles to paraffin, the electrical efficiency of the building integrated module increased by 13.15%. In contrast, the version with pure paraffin only improved the electrical efficiency by 5.67%. Furthermore, after analyzing free-standing photovoltaics, it was determined that including PCMs or NEPCMs only increases expenses without significantly improving the thermal performance.

In study [54], researchers explored the possibility of using a combination of  $\text{Al}_2\text{O}_3$  nanoparticles and paraffin wax as a NEPCM for regulating temperature in a building-integrated PV. This approach was also analyzed for its impact on the system's effectiveness. Employment of NEPCM resulted in the PV panel's  $10.6^\circ\text{C}$  operating temperature decrease, which was then accompanied by a 13.2% increase in efficiency.

Sharma et al. [55] explored a passive thermal regulation method for building-integrated concentrated photovoltaics (BICPV), combining different techniques, including micro-fins and NEPCM (CuO nanoparticles and paraffin wax). The use of a micro-fin system along with NEPCM resulted in a notable decrease of 18.5% in temperature, equivalent to  $12.5^\circ\text{C}$ . This suggests that micro-finned surfaces and NEPCM offer superior thermal regulation.

Experimental examination [56] was conducted on a photovoltaic thermal collector that utilizes a micro-fin tube, nanofluid, and NEPCM (SiC nanoparticles) to determine its thermal efficiency and electric power production. The highest thermal efficiency reached was 77.5%. Furthermore, power production increased from 10.49 W (for the referent PV panel) to 14.5 W (for the PVT system).

Researchers are currently intensively studying photovoltaic thermal collectors with incorporated NEPCMs [14]. These investigations focus on testing various geometries and nanomaterials that could enhance the heat storage capability and temperature stability of PCMs. In turn, this could boost the performance of PVT systems.

### **3.2. Brief overview of NEPCM thermal properties**

The inclusion of nanomaterials generally impacts the thermal characteristics of base PCM. The degree to which they are affected depends on specific PCM and the quantity and type of nanomaterials added. Most research on NEPCMs mainly focuses on magnifying the thermal conductivity of PCMs. However, other characteristics such as latent heat, specific heat capacity, and melting point may also be affected [34].

In study [34], research on the NEPCMs' thermal conductivity is summarized, taking into account the type of nanomaterial and PCM used. The different kinds of nanomaterials were identified through a short explanation of their shape and size (when obtainable). The amount of nanomaterials present in the PCM is indicated by either mass or volume fraction. Typically, used nanomaterials measure less than 30 nm in size, with mass and volume fractions usually under 5%. Nanoparticles are the most common shape, but nanoplatelets, nanotubes, nanofibers, and nanosheets can also be found. In many instances the inclusion of nanomaterials in PCM led to an improvement in thermal conductivity ranging from 20% to 100%. However, there were instances where the improvement exceeded 200%, such as in study [57]. In research [58], it was found that the inclusion of Al<sub>2</sub>O<sub>3</sub> nanoparticles in paraffin resulted in a 7 to 8% decrease in thermal conductivity when compared to pure paraffin. Unfortunately, the reason for this behavior is not adequately elaborated. In general, improved thermal conductivity can lead to shorter heating, melting, and solidification times [34].

Latent heat is a crucial property in the thermal analysis of any system based on phase change materials. In most cases, introducing nanomaterials to PCMs leads to a slight reduction in latent heat, although there are a few exceptions, found in [58] and [59], where it increased.

The specific heat capacity is also an essential property to consider in the thermal analysis of any system. It is imperative to examine it more frequently in the case of NEPCMs since there is a research gap there [34]. However, some studies, among other thermal properties, have explored this particular property. Putra et al. [60] examined the thermal stability of NEPCM, which was a combination of graphene and RT22HC PCM. After adding graphene, they observed a decrease in latent heat and specific heat capacity. According to them, this decrease could be attributed to the interfacial layering of liquid, Brownian motion, and clumping of nanoparticles. A similar slight decrease in the specific heat capacity and latent heat was reported in article [61],

while in research [62] and [63], the opposite effect was achieved, i.e., an increase in the specific heat capacity was detected. According to Warzoha et al. [64], the volumetric specific heat capacity is the highest during the transition from the solid to the liquid phase. Furthermore, the authors also observed a significant difference in the thermal diffusivity of NEPCM in the solid and liquid phases, which magnifies with the increase in nanomaterial concentration and is the opposite of thermal conductivity behavior.

The phenomenon of clumping mainly limits the nanomaterials-induced altering effect of PCM thermal properties, i.e., larger fractions of nanomaterials in PCM stimulate agglomeration [34]. Agglomeration is challenging to predict, but its intensity depends on the size, mass fraction, and morphology of nanomaterials and the type, phase, and phase transition temperature of the PCM [34]. Therefore, within the NEPCM preparation strategy, it is necessary to reduce the possibility of agglomeration and to select appropriate materials to produce a nanocomposite with suitable thermal properties for particular applications.

### 3.3. Critical NEPCM preparation aspects

Preparing NEPCMs is a demanding and intricate procedure that demands strict adherence to safety standards and an extensive understanding of chemical engineering. The scientific literature reports various preparation methodologies, which, in essence, can be reduced to a one-step or two-step NEPCM preparation approach [65]. While the one-step method may be more complex and costly, the resulting NEPCM is notably more stable and less prone to agglomeration compared to that produced by the two-step method [66]. Nonetheless, most approaches are based on the two-step NEPCM preparation, which usually includes two main techniques: mechanical processing (such as stirring) and sonication, Figure 3.3.

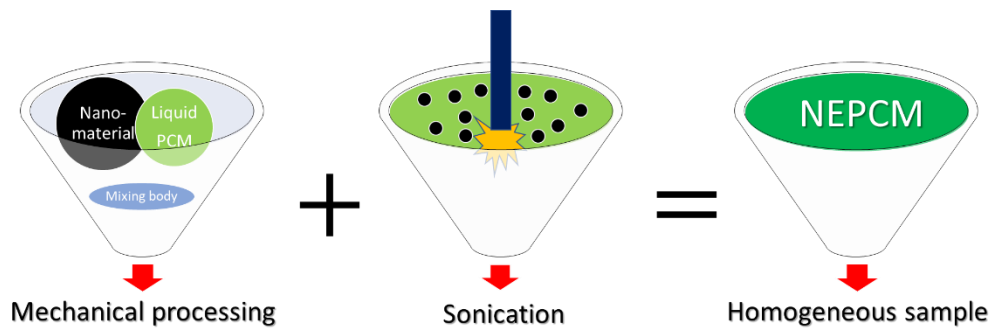


Figure 3.3. Two-step NEPCM preparation approach.

The primary objective of all preparation methodologies is to attain homogeneity of NEPCM by effectively dispersing nanomaterials and preventing agglomeration [67]. Preventing the clumping of nanomaterials is crucial to maintaining the enhancing effect of the base material. In article [67], the specific research studies that focus on the preparation procedure of nanocomposites were discussed. After selecting and reviewing research studies, it was found

that there are several methods used to create homogeneous nanocomposites. Unfortunately, the reviewed literature did not provide adequate information and details on the preparation process of the nanocomposites, making it difficult to replicate and confirm findings [67].

### **3.3.1. Strategies and procedures of NEPCM preparation**

The objective of all NEPCM preparation strategies is to obtain a uniform sample with well-distributed nanomaterials in the fluid phase of PCM. Before creating a uniform sample, it is common to prepare a heterogeneous sample through processes such as melting the base phase change material, synthesizing nanomaterials, adding surfactants in specific ratios with the nanomaterials, etc.

Preparing nanocomposite is a vast concept, and various interpretations of the starting point can be found in relevant literature [67]. Broadly, the process begins with synthesizing nanomaterials and producing base PCM. The preparation of the NEPCM in the narrow sense refers to the homogenization process. To obtain a high-quality sample with enhanced properties, it is essential to ensure that the initial preparation results in good dispersion without nanoparticle agglomerates. Adding a surfactant before the initial preparation can be beneficial to enhance the stability of samples [67]. However, there is a question regarding how this may impact the expected improvement of thermophysical properties.

A straightforward way to prepare NEPCM is by extensive mechanical mixing of the initial sample, after which a prolonged high-frequency ultrasonic treatment ends the process. The mechanical mixing process should continue until the sample is no longer visibly heterogeneous. Yet, at the nanoscale, the NEPCM will have clumps of nanomaterials that must be reduced with ultrasound. This will ensure that the nanomaterials are dispersed evenly, resulting in a uniform NEPCM material. When using ultrasound, it is important to control the temperature since the high frequency can lead to overheating, permanently damaging the base material properties. To prevent this, it is crucial to ensure sufficient sample cooling during preparation.

Selecting the appropriate processing parameters is a highly delicate procedure requiring an individual approach for each sample. Data regarding the thermophysical properties of nanomaterials and PCM is essential for determining the appropriate processing parameters to produce NEPCM with adequate characteristics.

The flowchart outlining the procedures and techniques related to NEPCM fabrication was created to systematize various homogenization approaches, Figure 3.4. The various colors in the part of the flowchart related to the homogenization of the sample represent potential homogenization procedures identified in the reviewed papers [67]. For example, in certain instances, the flowchart indicated the use of only mechanical processing or sonification with the abbreviation "w/o" meaning "without". Future research efforts can identify unused mechanical processing and sonication combinations using this flowchart to better fill the existing research gap. The diverse approaches are manifested, but more variations are possible. For example, experimenting with the potential outcomes of using a pulsating technique that combines

mechanical processing and sonication multiple times. Additionally, conducting these two processes simultaneously could also be worth considering.

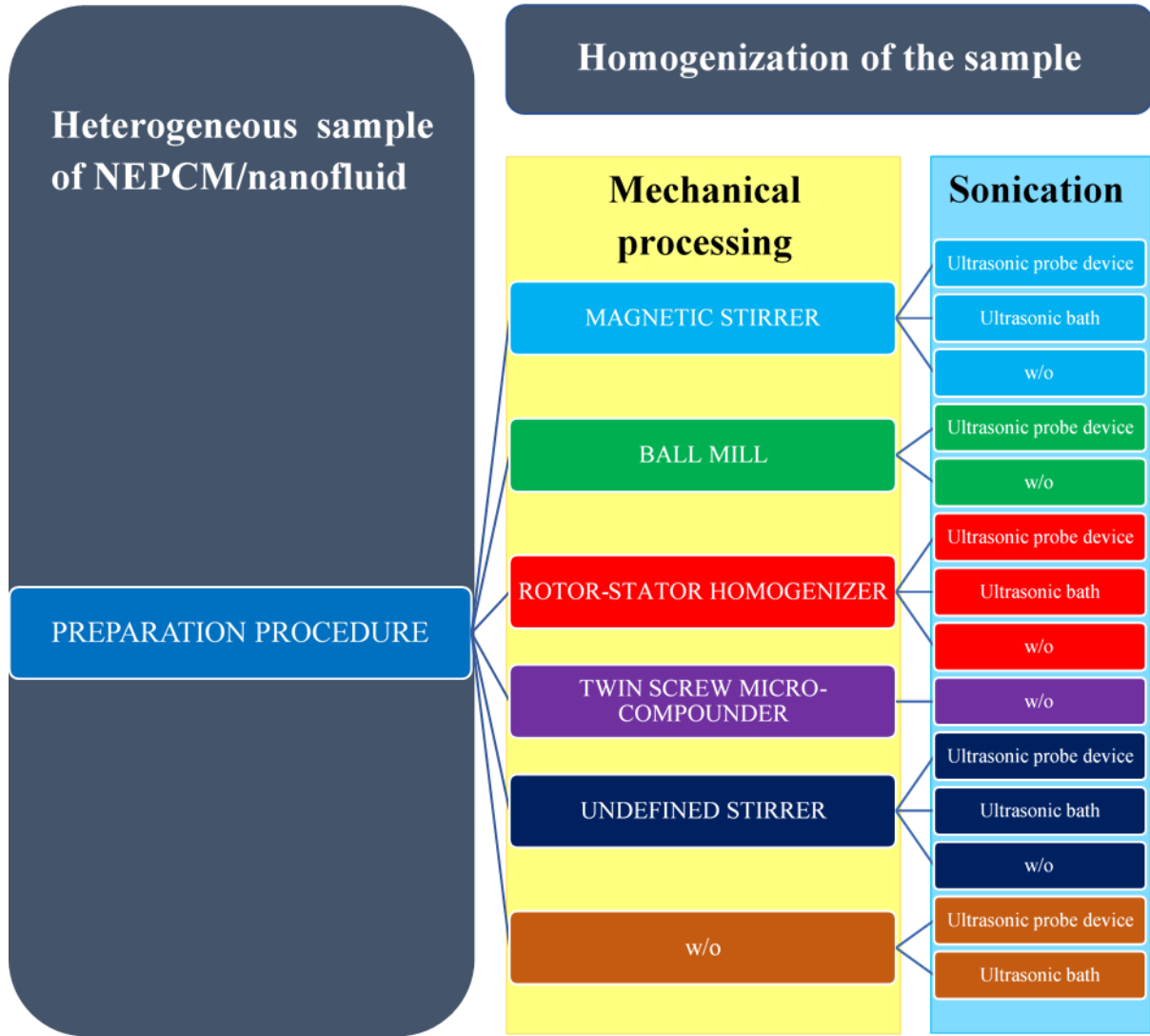


Figure 3.4. Flowchart illustrating the procedures and techniques for NEPCM homogenization [67].

### 3.3.2. Overview of nanomaterials toxicity and safety procedures

The distinguishing feature of nanomaterials is their size, which causes changes in their thermophysical properties compared to their larger-scale counterpart. This can lead to increased absorption and interaction with biological cells [68]. It is undeniable that nanomaterials have the ability to enter the human body through various means such as the respiratory system, ingestion, skin, and potentially injection [67].

As the use of nanomaterials increases, the necessary steps to evaluate their toxicity must be adequately taken. Numerous studies have reported potential toxicity issues, including

inflammation, harming the liver, kidneys, DNA, and more [69]. In investigation [70], the authors propose a proactive approach to regulating and evaluating the safety of nanomaterials. Meanwhile, in study [68], it is suggested that proactive measures should begin with thoroughly planning personal protective equipment (PPE), especially in case of workers directly in contact with nanomaterials. It is essential to include respiratory protection as a necessary component of personal protective equipment. Elastomeric half-mask respirators (EHRs) paired with filtering facepiece respirators (FFRs) are frequently utilized for safeguarding against nanomaterials. Several research studies have tested the efficiency of commonly used respirators, and it has been found that those with FFP3 and P100 filters exhibit the best performances [67]. According to research conducted by Vinches et al. [71], nanomaterials have the ability to go through specific protective clothing, including gloves. As a result, it is recommended that gloves be replaced more frequently, and laboratory coats should not be worn for extended periods or reused.

It is crucial to update nanomaterial safety data sheets (SDS) frequently and promptly in light of recent discoveries. Researchers handling nanomaterials must strictly adhere to the SDS guidelines. When working with nanomaterials in laboratories, using specialized methods and equipment is important. This can range from less expensive options such as glove bags to more costly solutions like glove boxes and powder weighing stations [67]. Still, many laboratories use traditional fume hoods as they can prevent up to 98.3% of any released nanoparticles when used correctly [72].

Before undertaking research on nanomaterials, it is advisable to conduct a health risk assessment for all staff and researchers involved. Furthermore, it is essential to implement safe work practices in line with current scientific discoveries and industry standards.

## 4. INVESTIGATION OF NOVEL NANO-ENHANCED PHASE CHANGE MATERIALS

Most studies focus on one PCM combined with one or two types of nanomaterials to produce nanocomposites. In contrast, the thermal constants investigation of eight NEPCMs involving two PCMs and four types of nanomaterials using a consistent methodology was conducted in research [73]. The RT28HC and RT26 PCMs were chosen for their organic nature, chemical stability, extended lifespan, and appropriate thermo-physical characteristics. Additionally, they possess high latent heat and a relatively small melting range. Different types of nano-powders, including silver (Ag), zinc (II) oxide (ZnO), copper (II) oxide (CuO), and graphene nanoplatelets, were selected based on their varying price ranges, sizes, and morphologies. The effects of nanomaterials types, sizes, and morphologies at constant mass fractions on specific PCMs may provide valuable insights into potential strategies and applications in different niches.

### 4.1. Employed nanocomposites preparation methodology

There are multiple pathways through which nanomaterials can enter the human body. Therefore, safety was proactively considered during the study's experimental stage, with particular attention paid to the researcher and laboratory environment. Protective equipment and procedures have been established after assessing health risks and considering safe work practices per industry standards and up-to-date scientific findings [73]. A 3M™ 6000 series elastomeric half-mask paired with FFP3 filters was utilized to preserve the respiratory system, while protective goggles were worn to shield the eyes. Safeguard measures such as wearing double-layered nitrile gloves and a 3M™ 4510 series protective suit under a disposable coat were used to minimize any potential risks to the skin. Nanomaterials were weighed and added to PCM using a professional LABCONCO XPert Nano Enclosure powder weighing station with a ULPA filter to prevent aerosols from being released to the laboratory.

To produce eight NEPCMs, base PCM samples were mixed with 0.5 wt.% of ZnO, Ag, CuO, and graphene nanomaterials. Consistent nanocomposite samples with evenly distributed nanomaterials were achieved in four phases [73]. In the first phase, 0.5% wt.% of nanomaterials were added to organic PCM to make heterogeneous nanocomposites. In the second and third phases, a two-step homogenization of NEPCM was performed to avoid agglomeration of nanomaterials, Figure 4.1. During ultrasonic homogenization the sample may experience heat generation, resulting in an increase in temperature. The samples, while homogenized, were conditioned in a thermostatic bath to stabilize the temperature. This ensures the process is carried out efficiently without causing unwanted thermophysical changes in the sample. While mechanically stirred, liquid NEPCM samples were extracted from the glass vessel and then



inserted into a two-layer PA/PE bag leading to the fourth phase, in which bags were sealed to prevent secondary exposure of the researcher to nanomaterials.

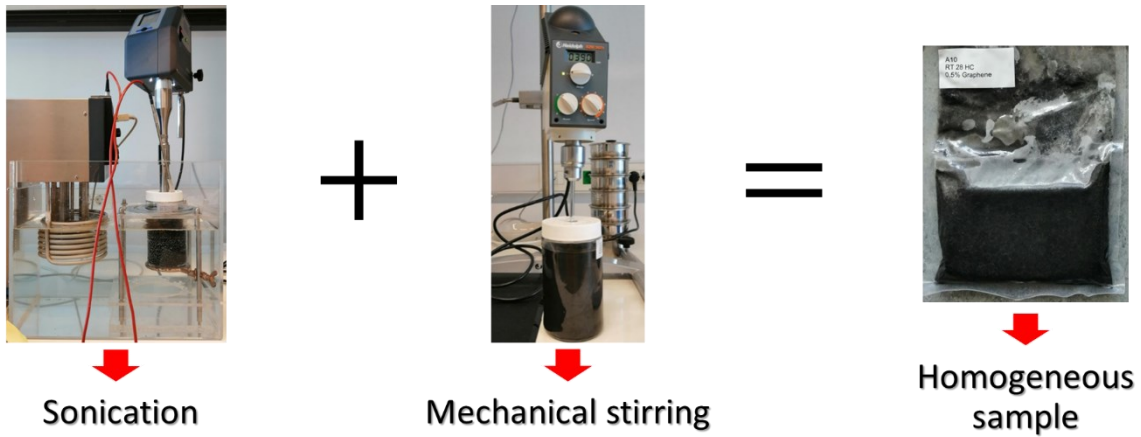


Figure 4.1. Two-step NEPCM homogenization.

## 4.2. Thermal properties measurement methodology

The non-steady-state approach based on the Transient Plane Source (TPS) technique was employed for the thermal properties' measurements of the novel NEPCMs [73]. The TPS technique utilizes a sensor that produces continuous heat, which then spreads into the measured sample. The sensor's average temperature gradually rises, depending on factors such as heating power, sensor radius, number of concentric rings, and the thermal qualities of the measured sample. According to Gustafsson [74], the sensor insulation layer can affect the accuracy of measurements, so it is recommended to disregard the first few seconds of data. Analogously, PA/PE bags can act as an extra insulation layer when taking measurements with the TPS sensor. This sealed bag method introduced in research [73] is a new approach for analyzing the thermal properties of possibly harmful substances.

Detailed descriptions of measurement procedures and specifics are available in [73]. In short, the samples were subcooled to prevent the phase transition of NEPCM from affecting the measurements. The subcooled nanocomposite samples (12°C) were tested by Hot Disk TPS 500 S device operating according to the TPS technique. A double spiral sensor protected with Kapton polyimide produced low heating power since relatively low thermal conductivity was expected. The depth of heat probing was consistently monitored by utilizing Hot Disk Thermal Constants Analyzer 7.4 Beta 24 software. The monitoring was necessary to maintain generated heat within the material's confines considering the measurement time.

## 4.3. Thermal properties of RT26 and RT28HC based NEPCMs

Thermal conductivity holds great significance when it comes to phase change materials. The mentioned thermal property directly affects the heat storage and release rate. Initial testing is necessary to determine the thermal conductivity of the base PCM. Significant variances in the

thermal conductivity of base phase change materials are possible when compared to the specifications provided by the manufacturer. For example, the deviation in the case of pure RT28HC can be as high as 44.7% [73]. Obviously, this deviation is notable; thus, caution is required when using data supplied by the manufacturer.

In most cases, NEPCMs have increased thermal conductivity compared to their base PCMs. The nanocomposites containing RT28HC exhibited a rise in thermal conductivity, with the Graphene/RT28HC NEPCM showing the most significant increase at 14.3%, Table 4.1. However, thermal conductivity may also decrease, as seen in the Graphene/RT26 nanocomposite case, Table 4.2. According to the data from Table 4.2, the CuO/RT26 NEPCM exhibits the preeminent thermal conductivity, with the ZnO/RT26 and Ag/RT26 following closely behind.

*Table 4.1. Thermal characteristics of RT28HC and RT28HC-based NEPCMs [73].*

|  | <b>RT28HC</b> | <b>CuO/<br/>RT28HC</b> | <b>ZnO/<br/>RT28HC</b> | <b>Ag/<br/>RT28HC</b> | <b>Graphene/<br/>RT28HC</b> |
|--|---------------|------------------------|------------------------|-----------------------|-----------------------------|
| <b>Thermal conductivity [W m<sup>-1</sup>K<sup>-1</sup>]</b>               | 0.362         | 0.381                  | 0.381                  | 0.376                 | 0.414                       |
| <b>Thermal diffusivity [mm<sup>2</sup> s<sup>-1</sup>]</b>                 | 0.270         | 0.266                  | 0.270                  | 0.267                 | 0.321                       |
| <b>Volumetric specific heat capacity [MJ m<sup>-3</sup>K<sup>-1</sup>]</b> | 1.342         | 1.435                  | 1.412                  | 1.414                 | 1.293                       |

The thermal diffusivity and volumetric specific heat capacity of NEPCMs were also determined in research [73]. Thermal diffusivity describes how quickly heat spreads through material from the hotter to the colder side. The product of thermal conductivity and volumetric specific heat capacity determines thermal diffusivity. Volumetric specific heat capacity is calculated by multiplying the material's density by its specific heat capacity. Adding specific nanomaterials to the PCM can either increase or decrease its thermal diffusivity. Graphene nanoplatelets most significantly impact this property when combined with certain organic PCM [73]. Specifically, they cause a decrease of 19% in RT26 thermal diffusivity, Figure 4.2. However, when combined with RT28HC, they cause an increase of 18.7%. The incorporation of graphene nanoplatelets into both RT26 and RT28HC yields contrasting outcomes, indicating divergent effects on different PCMs. Further investigation is needed to determine the precise cause and potential side effects of the peculiar interaction between nanomaterials and PCMs at a molecular level, which may be a contributing factor to this phenomenon.

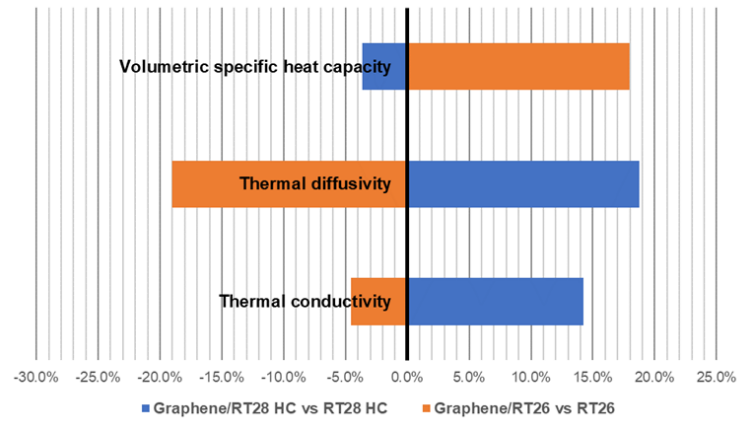


Figure 4.2. Graphene/NEPCM behavior in relation to thermal properties initial values (0%) of base PCMs [73].

The volumetric specific heat capacity indicates the heat required to alter the temperature of a material by 1 K per volume unit. For the NEPCM with RT26, the highest value of volumetric specific heat capacity was in the instance of Ag nanoparticles addition, Table 4.2. In general, RT28HC has a lower volumetric specific heat capacity than RT26, but its volumetric specific heat capacity can be increased by approximately 7% with the addition of CuO nanoparticles [73].

Table 4.2. Thermal characteristics of RT26 and RT26-based NEPCMs [73].

|  | RT26  | CuO/<br>RT26 | ZnO/<br>RT26 | Ag/<br>RT26 | Graphene/<br>RT26 |
|--|-------|--------------|--------------|-------------|-------------------|
| <b>Thermal conductivity [W m<sup>-1</sup>K<sup>-1</sup>]</b>               | 0.233 | 0.282        | 0.276        | 0.262       | 0.222             |
| <b>Thermal diffusivity [mm<sup>2</sup> s<sup>-1</sup>]</b>                 | 0.122 | 0.122        | 0.127        | 0.103       | 0.099             |
| <b>Volumetric specific heat capacity [MJ m<sup>-3</sup>K<sup>-1</sup>]</b> | 1.909 | 2.317        | 2.180        | 2.535       | 2.252             |

## 5. INVESTIGATION OF NOVEL HYBRID PHASE CHANGE MATERIALS

A range of phase change materials is used in the field of energetics, such as organic, inorganic, hygroscopic, eutectic, etc. [75]. It is important to note that most of these materials are readily available in the commercial market. However, commercially available PCMs are relatively expensive, i.e., their price ranges from 5 € kg<sup>-1</sup> to 15 € kg<sup>-1</sup> [75]. The practical and financial feasibility of systems incorporating PCM can be disputable, especially when the potential for improving efficiency and probable lifespan is limited. To enhance the economic viability of these systems, two PCM-related approaches may be taken: improving the thermal properties of existing PCMs or discovering new and more cost-effective PCMs. Improving the thermal properties of existing PCMs is a reasonable approach, but in practice, this frequently requires potentially hazardous nanomaterials. Thus, there is a significant void in the area of innovative, cost-effective, and eco-friendly phase change materials research.

In a study conducted by Nižetić et al. [76], organic PCM, i.e., pork fat, was assessed as promising for use in the passive cooling of photovoltaic systems. To evaluate its effectiveness, a numerical model was developed and employed. According to the findings, it has been established that pork fat as a PCM has comparable properties to traditional PCMs. Moreover, it has several advantages over its counterparts. Firstly, there is a significant difference in the unit costs between pork fat and the PCMs commonly available in the market. Hence, it is significantly more cost-effective, with its unit cost potentially falling below 1.0 € kg<sup>-1</sup> [76] or even less than 0.50 € kg<sup>-1</sup> [75]. Secondly, pork fat is an organic, environmentally friendly natural alternative, unlike artificially produced PCMs, which are manufactured using a range of chemicals causing the release of harmful pollutants during industrial processing and exploitation.

Based on research [76], it is evident that a significant number of resources are being dedicated to exploring new PCMs that would offer better efficiency and feasibility in terms of technology and economics. It is worth noting that economic evaluations are often overlooked in studies, which are instead primarily geared toward enhancing the effectiveness of emerging phase change materials [75].

The next step in the research undertaken was to delve into the realm of hybrid phase change materials. This area has the potential to offer a more cost-effective and ecologically sound solution. After thoroughly assessing promising findings from the research [76], pork fat was identified as a highly suitable organic PCM for the intended purpose. In addition, edible oil and waste oil from the food industry were considered potential additives to the pork fat PCM. Eventually, the goal was to produce hybrid PCMs and analyze the thermal characteristics of these innovative PCMs.

### 5.1. Thermal characteristics of novel hybrid phase change materials

An affordable and available phase change material derived from organic sources can be produced by combining sunflower and burnt oil with pork fat (lard). These particular blends are cost-effective but also exhibit environmentally friendly properties [75]. Pork fat and sunflower oil, both commercially available, were procured from a local market [75]. In addition, a restaurant chain donated burnt oil. This type of material can be commonly found in various food service establishments. To ensure homogeneity, the burnt oil samples underwent a melting process and were subsequently filtered to remove any coarse inclusions. Upon careful analysis of the available data on the melting of pork fat and close observation of its melting process, it has been ascertained that the temperature of the sample before adding oils must exceed 50°C to surpass the melting point [75]. When observed at room temperature, the pork fat appeared as a solid, with a firm and unyielding texture. In contrast, the sunflower oil was in a fluid state. The burnt oil, however, showed signs of being in a phase transitional state, with a slurry-like consistency that hinted at its ongoing metamorphosis. To create hybrid PCMs, 20%, 10%, and 5% of sunflower and waste burnt oil were added by volume to the liquid pork fat, Figure 5.1.

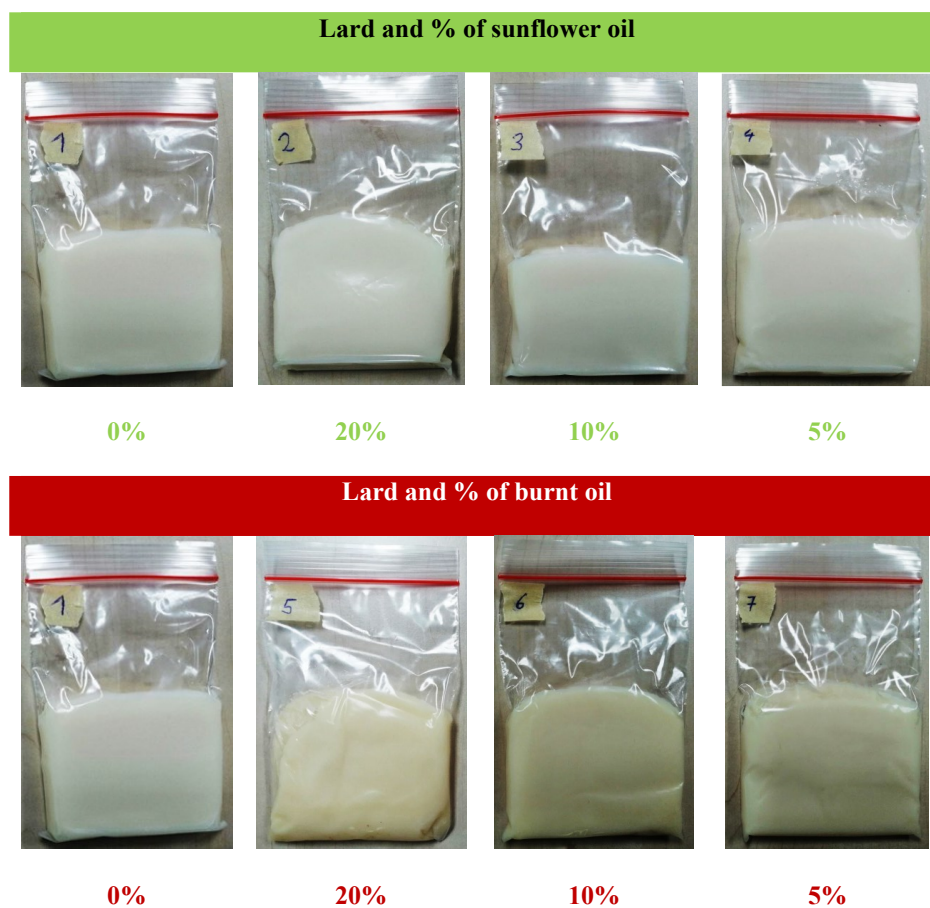
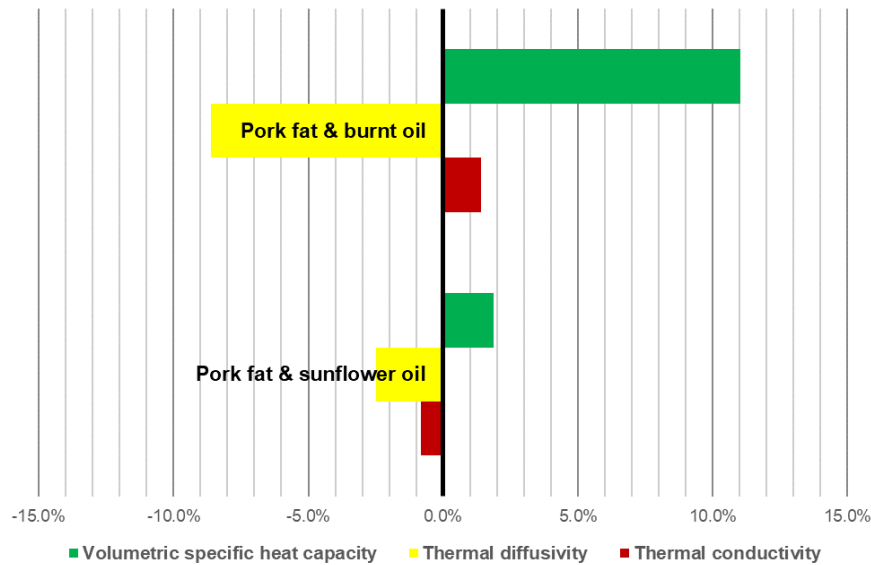
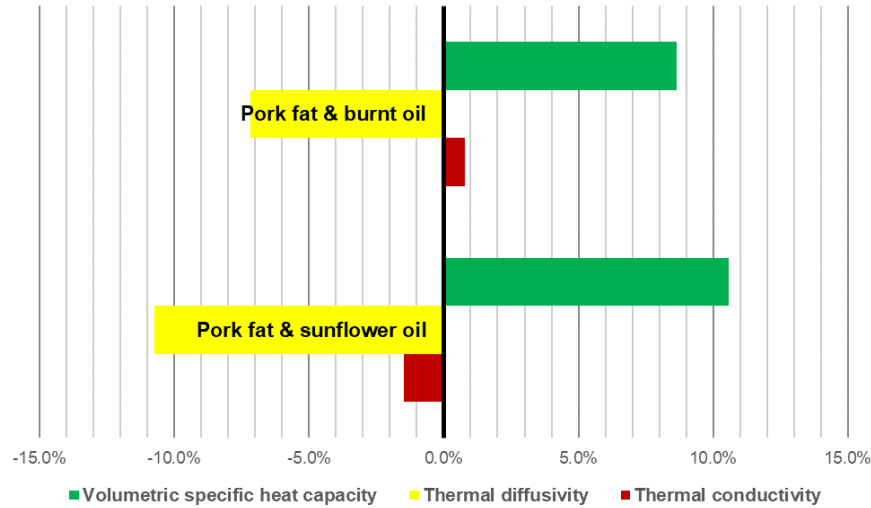


Figure 5.1. Pork fat (lard) and hybrid PCMs [75].

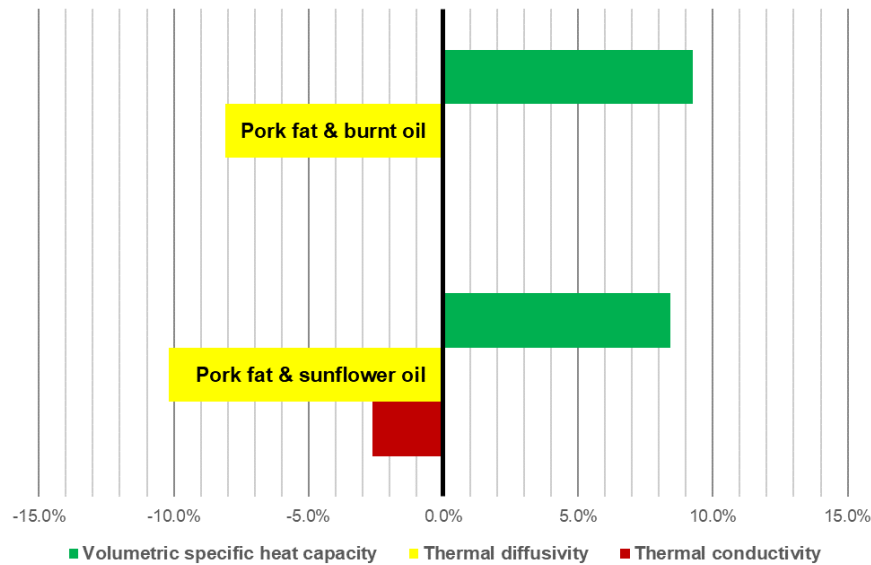
The thermal properties were determined with utmost precision by employing the non-steady-state TPS methodology, i.e., the same procedure as measurements of NEPCMs in [73]. To prevent intensive phase transitioning and sensor overheating, pork fat and hybrid PCM samples were tested at a temperature of 9°C, using a low heating power of only 20 mW. Low heating power was necessary since pork fat has relatively modest thermal conductivity. The thermal characteristics of pork fat are subject to change based on the amount of oil content. Thus, listed volume fractions of the oils significantly impact the pork fat thermal behavior. The thermal conductivity change varies between -2.6% and 1.4%, with the biggest improvement occurring when using burnt oil in a volume fraction of 5%, Figure 5.2. The thermal diffusivity reduction varies from 2.5% to nearly 11%. The most significant decrease occurs with a 20% sunflower oil volume fraction in pork fat PCM. The degree to which volumetric specific heat capacity increases can vary from around 2% to as much as 11% in the case of PCM with a 5% volume fraction of burnt oil.



(a) 5 % volume fraction



(b) 10% volume fraction



(c) 20% volume fraction

Figure 5.2. Impact of 5% (a), 10% (b), and 20% (c) oils volume fractions on pork fat thermal properties [75].

Adding sunflower oil to pork fat is not a good choice if the goal is to improve thermal conductivity. The pork fat exhibits higher thermal conductivity when compared to the hybrid PCMs containing pork fat and sunflower oil, Table 5.1. Based on the experimental findings [75], it is apparent that integrating burnt and sunflower oil into the pork fat does not produce the intended outcome in terms of thermal diffusivity, i.e., thermal diffusivity decreases. The

addition of both oils increases volumetric specific heat capacity. However, in most of the considered cases, a better effect was achieved with burnt oil. A thorough thermal analysis concluded that the optimal hybrid phase change material is a blend of pork fat and waste burnt oil (5% volume fraction). This particular mixture was found to be the most efficient in terms of its thermal performance and effectiveness since it exhibited maximum thermal conductivity ( $0.194 \text{ W m}^{-1}\text{K}^{-1}$ ) and maximum volumetric specific heat capacity ( $1.679 \text{ MJ m}^{-3}\text{K}^{-1}$ ) with a minimum amount of oil.

Table 5.1. Thermal characteristics of pork fat and hybrid PCMs.

| Vol. | PCM type      | Thermal conductivity<br>( $\text{W m}^{-1}\text{K}^{-1}$ ) | Thermal diffusivity<br>( $\text{mm}^2 \text{s}^{-1}$ ) | Volumetric specific heat<br>capacity<br>( $\text{MJ m}^{-3}\text{K}^{-1}$ ) |
|------|---------------|--|--|---|
| 0%   | Pork fat      | 0.191  | 0.127  | 1.512   |
| 5%   | Sunflower oil | 0.190  | 0.123  | 1.541   |
|      | Burnt oil     | 0.194  | 0.116  | 1.679   |
| 10%  | Sunflower oil | 0.189  | 0.113  | 1.672   |
|      | Burnt oil     | 0.193  | 0.117  | 1.643   |
| 20%  | Sunflower oil | 0.186  | 0.114  | 1.640   |
|      | Burnt oil     | 0.191  | 0.116  | 1.653   |

## 5.2. Environmental implications of hybrid PCMs

Evaluating the environmental implications of PCMs' application is a complex process that involves considering their manufacturing process and how they are incorporated into various systems [77]. The most commonly used phase change materials are paraffin waxes. However, producing these waxes requires high-energy input and involves hazardous ingredients such as formaldehyde and vinyl-chloride [75]. In the event of a fire, these substances can give off toxic fumes, thereby posing a severe threat to life. Besides, incorrect disposal of these materials can also lead to grave environmental consequences. The organic origin of pork fat and marginal toxicity of pork fat-based hybrid PCMs render them advantageous over similar materials. Nonetheless, a thorough evaluation is imperative to gauge their environmental impact throughout their life cycle. Further examination of their manufacturing logistics is needed to ascertain their overall effect.

Studies have shown that implementing cooking oil collection and reuse systems in specific regions has a substantial positive impact. If these systems were not in place, fats and oils would inevitably end up in sewerage systems, leading to an array of issues and complications [78]. Research [79] revealed that employing secondary PCMs produced from



waste cooking oils, like glycerin and fatty acids, may offer a better environmental profile when compared to paraffin-based PCMs. The analysis of these materials using LCA (Life Cycle Assessment) showed promising results in terms of sustainability. Moreover, it is noteworthy that creating PCMs from waste cooking oil results in a much lower environmental impact than other PCMs presently available in the market. This may induce positive effects on various ecological aspects like exposure to toxic materials, climate, ozone depletion, and acidification, making it a highly beneficial and sustainable option.

It is recommended to avoid using sunflower oil as the constituent in the proposed hybrid PCMs, especially if environmental factors are being considered [75]. The LCA analysis [80] determined that cultivating sunflower crops results in the most significant environmental impact compared to other crops. This is due to the substantial increase in ecological load and energy demands associated with this particular crop.

There is a literature shortage of information on the LCA of pork fat. Conducting an LCA evaluation to comprehend the environmental impact of pork fat as a PCM and to facilitate comparisons with other PCMs available in the market is essential. Such an evaluation would help assess pork fat sustainability as a PCM and aid in making informed decisions regarding its usage. Although it may be worthwhile to consider conducting pork fat and hybrid PCMs Life Cycle Assessments, it is not within the primary scope of this thesis.

## **6. ANALYSIS OF PVT SYSTEMS WITH INCORPORATED PHASE CHANGE MATERIALS**

Extensive analysis of the most recent PVT-PCM collector design solutions was necessary before embarking on a new design of these hybrid systems. By conducting such an analysis, researchers can collect valuable insights that will impact their decisions and lead to optimal design outcomes. For a comprehensive analysis it is necessary to scrutinize PVT geometries and the diverse PCM materials utilized, as well as assess the numerical modeling methods employed to investigate the phase transition phenomena of these materials. Furthermore, a thorough examination of numerical approaches is crucial to gain insight into the fundamental heat transfer mechanisms occurring before, throughout, and following the phase transition of PCMs. This analysis is essential for a comprehensive understanding of the behavior and performance of these materials. By accurately modeling the phase transition process, it becomes possible to identify any vulnerabilities in the early stages of collector development. This enables the optimization of design to enhance the system's overall efficiency.

Elsevier's Scopus® database [23] was utilized in a three-stage selection process to obtain the latest research insights. In study [10], particular PVT-PCM design configurations published between 2015 and 2020 were analyzed. Over time, the need to update and extend the research arose, so articles published between 2019 and 2022 were carefully considered, Figure 6.1. This particular time frame was chosen considering the attractiveness of the topic and to cover the current state of development of the researched subject matter. The primary selection was based on pertinent keywords and subject areas for publications produced in recent years. The initial selection process helped narrow the research, but further narrowing was needed. To achieve this, a secondary selection was made to group articles based on the main focus of the study. There were two groups established. The first group focused on experimental PVT-PCM systems. In contrast, the second group had a broader scope, including numerical approaches to PCMs in PVT systems and other engineering-related applications. In tertiary selection, publications dealing with experimental and numerical research were additionally narrowed down to gain a deeper understanding of current technology and anticipate future trends.

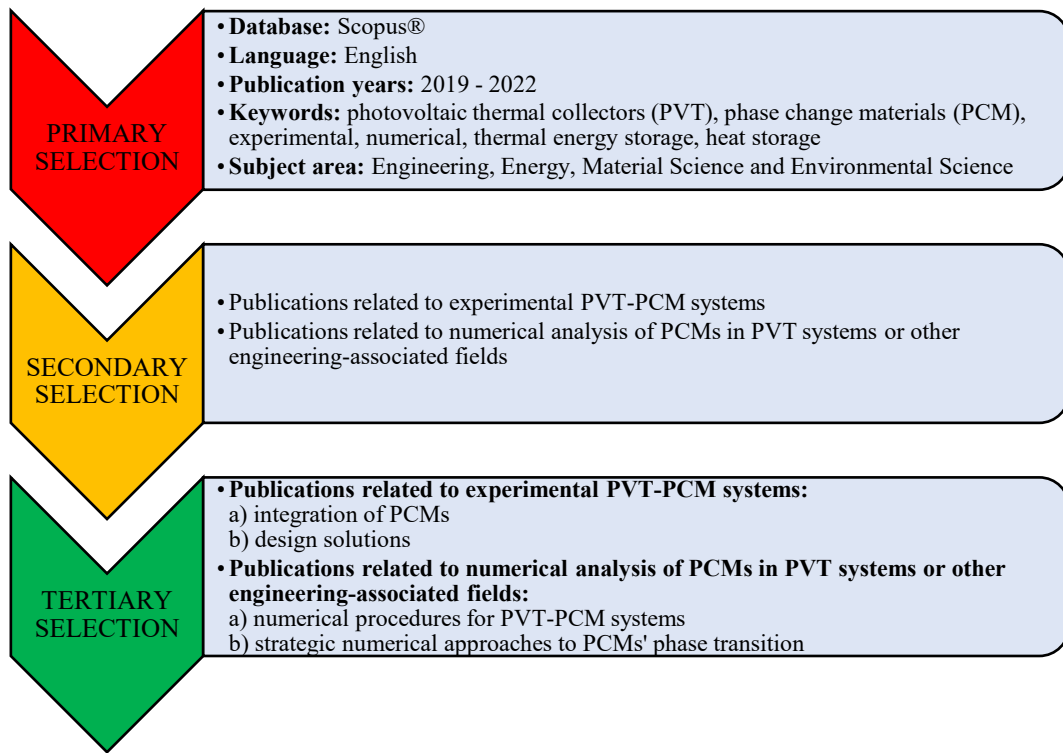


Figure 6.1. Three-stage selection process of latest research.

## 6.1. Overview of experimental PVT-PCM collector systems

### 6.1.1. Implementation of phase change materials into PVT systems

Integrating PCM and PVT systems is an efficient way to generate electricity while capturing thermal energy. This combination stabilizes the temperature of photovoltaic cells and enhances the system's overall performance while potentially prolonging the lifetime of the photovoltaic part of the system. PVT systems operate at low temperatures to balance the competing thermal and electrical efficiency natures. The PCM helps regulate the system's temperature by absorbing and releasing thermal energy, thereby maintaining a proper temperature range for the photovoltaic cells. The heat transfer process in these systems is multifaceted and intricate, making it crucial to consider the impact of PCM integration carefully. The thermal behavior of PCM is contingent upon the current external operational circumstances of the PVT collector, internal convection in PCM, its thermal inertness, and conduction within the layers of PVT collectors. The PCM thickness directly affects the collector's thermal and electrical efficiency. In particular, while a greater amount of PCM absorbs more heat, it also causes a more sluggish and costly system.

Typically, the melting of PCM materials in PVT systems occurs between 22°C and 60°C, Table 6.1. PCM materials routinely utilized are paraffin-based with relatively low thermal

conductivity, approximately  $0.2 \text{ W m}^{-1}\text{K}^{-1}$ . Latent heat ranges from  $160 \text{ kJ kg}^{-1}$  to  $250 \text{ kJ kg}^{-1}$ , while specific heat capacity varies from  $1.7 \text{ kJ kg}^{-1}\text{K}^{-1}$  to  $2.9 \text{ kJ kg}^{-1}\text{K}^{-1}$ .

*Table 6.1. Properties of PCMs in PVT systems.*

| References | PCM type                               | Melting temperature (°C) | Thermal conductivity ( $\text{W m}^{-1}\text{K}^{-1}$ ) | Latent heat ( $\text{kJ kg}^{-1}$ ) | Specific heat ( $\text{kJ kg}^{-1}\text{K}^{-1}$ ) |
|------------|--|--------------------------|---|-------------------------------------|--|
| [81]       | paraffin-coated micro-encapsulated PCM | 28                       | 0.34  | 213.5                               | 1.779  |
| [82]       | RT-35                                  | 29-36                    | 0.2   | 160                                 | 2  |
| [83]       | RT44HC-0.009%f-CNT                     | ca. 44                   | -   | 248.6505                            | -  |
| [84]       | PS-CNT foam encapsulated paraffin      | 38-47                    | 0.4   | 124.9                               | -  |
| [85]       | S21                                    | 23                       | 0.234   | 170                                 | 2.2  |
| [86]       | RT44                                   | 41-44                    | 0.2   | 168                                 | 2  |
| [87]       | RT35 HC                                | 34-36                    | 0.2   | 240                                 | 2  |
| [87]       | RT28HC                                 | 27-29                    | 0.2   | 250                                 | 2  |
| [87]       | RT25HC                                 | 22-26                    | 0.2   | 210                                 | 2  |
| [88]       | Merck 107158 (paraffin)                | 57-60                    | 0.24  | 220                                 | 2.9  |
| [89]       | PLUSICE S25                            | 25                       | 0.54  | 180                                 | 2.2  |
| [90]       | RT-35HC                                | 35                       | 0.166   | 240                                 | 2.1  |
| [91]       | A44                                    | 44                       | 0.18  | 242                                 | 2.15   |
| [92]       | Paraffin wax                           | 57                       | 0.24  | 220                                 | 2.1  |
| [93]       | RT50                                   | 50                       | 0.2   | 160                                 | 2.0  |
| [94]       | Lauric acid                            | 44-46                    | 0.19  | 228                                 | 1.7  |
| [95]       | PCM32/280                              | 32                       | 0.4   | 186                                 | -  |
| [96]       | Octadecane                             | 28                       | 0.21  | 244                                 | 1.9  |
| [97]       | Paraffin wax (Merck, 107151)           | 46-48                    | 0.24  | 220                                 | 2.9  |

### 6.1.2. Summary of PVT-PCM design concepts

A review was conducted on experimentally investigated PVT-PCM systems in different climates [10]. The review provided a summary of key performance indicators and other relevant details, including climate specifics and environmental and economic evaluations. In total, research [10] assessed seventeen distinct PVT-PCM designs. The study discovered that the effectiveness of PVT-PCM systems is significantly influenced by design and is highly responsive to the execution of PCM layer thermal regulation.

The critical design elements of individual approaches and their respective performance indicators were assessed in [10]; however, due to time passage, the findings were expanded and summarized in Table 6.2. To ensure the effectiveness of PVT-PCM designs, installing specialized heat exchangers on the rear surface of the PV panel is standard practice [10]. This helps regulate and control the PV panel's temperature, thereby maximizing its energy output and

overall performance. Poly-crystalline and mono-crystalline silicon photovoltaic cell types are frequently used in PVT-PCM collectors. This is a common occurrence, as these cell types are readily accessible and are priced affordably. Most employed PCM materials are derived from organic sources and stored in metal containers, primarily aluminum made due to accessibility and relatively lightweight. Potential parasitic heat flux from the rear of the collector to the environment and vice versa is usually prevented with an insulation layer at the backside. Water forced through pipes during the active operation of the collector is the most used coolant. Copper is widely utilized for pipes due to its exceptional thermal conductivity. The pipes are frequently shaped in a serpentine fashion, increasing the contact surface with the phase change material, and thereby enhancing heat transfer efficiency. According to research summarized in Table 6.2, it can be anticipated that the improvement of PVT-PCM collector's electrical efficiency will not be as notable as the enhancement in thermal efficiency compared to traditional PVT collectors. Based on short-term measurements, some designs demonstrated an impressive overall efficiency of more than 80%. It is worth considering, however, that the overall efficiency should be calculated annually to ensure a convincing performance assessment. The PVT-PCM collectors thermally managed by water and nano-fluids showed the highest overall efficiency improvements, while air-based PVT-PCM collectors had modest efficiency improvements. Nano-fluids enhanced both the electrical and thermal capabilities of PVT-PCM collectors. However, compared with water, the degree of improvement in performance may be insignificant in certain cases and can vary based on the specific design [10]. In general, the rise in electrical efficiency was under 20%. However, the improvement in thermal efficiency commonly fell between 30% to 70%.

*Table 6.2. Main features and performance indicators of PVT-PCM collectors.*

| Ref. | PV cell type                   | PCM type     | PCM container     | Coolant /Active cooling rig                       | Insulation    | Efficiency  |
|------|--------------------------------|--------------|-------------------|---|---------------|---|
| [85] | Copper indium gallium selenide | S21          | Metal             | Air/Straight channels                             | YES           | 37.6%-40.2% rise in overall efficiency                                    |
| [88] | Mono-Crystalline silicon       | Merck 107158 | Thin copper plate | Water-based nanofluids/<br>Straight copper pipes  | NO            | 4.2% rise in electrical and 23.5% in thermal efficiency                   |
| [89] | Mono-Crystalline silicon       | PLUSICE S25  | Aluminum          | Air/ Naturally ventilated duct                    | YES (Celotex) | 10% electrical efficiency rise and an additional 3% with fin ducting      |
| [90] | Mono-Crystalline silicon       | RT-35HC      | Aluminum sheet    | Water-based nanofluid/<br>Serpentine copper pipes | YES           | Overall efficiency increased by 14.1%, thermal efficiency was up to 45.8% |

*Chapter 6: ANALYSIS OF PVT SYSTEMS WITH INCORPORATED PHASE CHANGE MATERIALS*

|       |                          |                                     |                                |  |                               |  |
|-------|--------------------------|-------------------------------------|--------------------------------|--|-------------------------------|--|
| [91]  | Poly-Crystalline silicon | A44                                 | Aluminum bags                  | Water/ Serpentine aluminum pipes in a spiral | YES (Polyethylene)            | 83.5% overall efficiency and rise of 12.7 % in electrical efficiency                 |
| [92]  | Poly-Crystalline silicon | Paraffin wax                        | Aluminum                       | Water/ Serpentine copper pipe                | NO                            | 17.3%, 26.87% and 40.59% increase in electrical, thermal and overall efficiency      |
| [93]  | Unspecified type         | RT50                                | PAKVF4PCA metallic bags        | Water/ High-density polyethylene absorber    | YES (Rock wool)               | Up to 50% overall efficiency   |
| [93]  | Unspecified type         | C48                                 | Matchbox aluminum foil pouches | Water/ Aluminum roll-bond absorber           | YES (Rock wool)               | Up to 63% overall efficiency   |
| [98]  | Poly-Crystalline silicon | Lauric acid                         | Aluminum foil packets          | Water/ Serpentine copper pipe                | YES (Ceramic fiber paper)     | Maximum thermal and electrical efficiency of 87.72% and 11.08%                       |
| [95]  | Mono-Crystalline silicon | salt hydrate (PCM32/280)            | Polycarbonate sheet            | Air/Channel                                  | NO                            | 9% rise in electrical efficiency   |
| [97]  | Mono-Crystalline silicon | Paraffin wax (Merck, 107151)        | Acrylic glass                  | ZnO water nano-fluid/Copper pipe             | YES                           | 11.9 % improvement in electrical efficiency and maximum overall performance of 65.7% |
| [99]  | Unspecified type         | Paraffin wax with SiC nanoparticles | Galvanized steel               | SiC water nanofluid/ Serpentine copper pipes | YES (Glass wool)              | 13.7% and 72% maximum electrical and thermal efficiency                              |
| [100] | Unspecified type         | Paraffin                            | Unspecified type               | Water/ Serpentine copper pipes with plate    | YES (Corkwood)                | Overall efficiency between 46% to 63%  |
| [101] | Unspecified type         | Unspecified type                    | Unspecified type               | Air/Single channel                           | YES                           | Average thermal and electrical efficiency of about 13% and 8%                        |
| [102] | Unspecified type         | OM35+biochar                        | Plexiglass cover               | Water/ Serpentine copper pipes               | YES (Polyethylene foam sheet) | Average thermal and electrical efficiency of about 60% and 13%                       |

A marked performance enhancement in PVT-PCM collector is possible by including nanomaterials in both the PCM and the cooling water, as in study [99]. Unfortunately, a major issue with nanomaterials is their potential toxicity and environmental impact. As previously highlighted, these aspects are poorly addressed in the literature. Besides, more thorough and repeated evaluations of NEPCM thermal properties must be conducted over an extended period. Using nanomaterials to form NEPCM or in the coolant fluid (nano-fluid) requires economic justification. However, there is an evident research gap on the economic aspect of nanomaterials in PVT-PCM collectors and the economic analysis of PVT-PCM designs in general.

### 6.1.3. Economic and environmental implications of PVT-PCM designs

Based on the limited economic evaluations available, it was found that payback periods for PVT-PCM collectors ranged from 4 to 15 years [10]. It should be noted that these studies were conducted in warmer geographic regions. To showcase the magnitude of the acceptable investment for a particular PVT-PCM design in relation to the overall LCOE (Levelized Cost of Energy), a comparison was made between a PVT-PCM system and a conventional PVT system [10]. A comparison was made using the maximum allowed investment for targeted performance enhancement, which was scaled based on the € m<sup>-2</sup>. Making design changes to a conventional PVT collector to create a PVT-PCM collector would come with an extra cost per collector area, but it would also lead to an improvement in overall performance. Based on the analysis provided in [10], it is suggested to keep an investment between 36 and 120 € m<sup>-2</sup> as the upper limit for improving overall efficiency, which can result in 20% to 40% efficiency enhancement. This range can serve as a general reference point for determining the maximum investment amount that would be reasonable and appropriate. One crucial matter to consider is the search for economically feasible PCMs to guarantee the economic sustainability of PVT-PCM collector designs, as the cost of PCMs can significantly affect the overall LCOE value [10].

According to research [103], employing PCMs for the thermal management of photovoltaic panels results in a considerable environmental impact. Furthermore, the production of PVT collectors involves using different construction materials that have negative environmental footprints. The analysis of the current PVT-PCM collector designs revealed that none of the research studies considered the environmental aspects, as they were primarily focused on enhancing performance [10]. As per the findings of research [103], the incorporation of PCM holds immense significance from an environmental perspective. Based on these findings, the rationalization of PCM usage should be in focus while considering the performance goals of each PVT-PCM collector design. Ultimately, the design of the PVT-PCM collector directly affects the operational energy demand. Therefore, the collector design should aim to minimize this demand to reduce indirect adverse effects on the environment.

## 6.2. Numerical modeling of PCMs in PVT systems

Only a few publications focused on the numerical study of PV-PCM systems or, more specifically, PVT-PCM collectors. In essence, this is because of the intricate multivariable heat transfer mechanism, including various materials and phases. Through meticulous analysis of shared characteristics and evaluated numerical strategies of PCMs, the phase transition approaches across various engineering applications were systematized in Table 6.3. Typically, when it comes to the numerical analysis of phase change materials, relatively conservative options like paraffin or paraffin-based materials are commonly studied. However, it should be noted that various publications are also exploring the analysis of nano-enhanced PCMs. Numerical analysis of NEPCMs can be challenging due to the potential structural

inhomogeneity. Specifically, nanomaterials' tendency to agglomeration and sedimentation adds to the complexity of the calculations [67]. Reviewed publications fail to tackle this particular phenomenon sufficiently. In particular, the numerical investigations assume and implement the isotropy of phase change material without any discussion or exploration of this issue. The most commonly used software for numerical simulations of PCMs is the commercial Ansys Fluent simulation software, working on the finite volume method (FVM). Following that is COMSOL Multiphysics, which, on the contrary, uses the finite element method (FEM). Both 2D and 3D numerical approaches are present in the literature. Nonetheless, 3D requires more computational resources compared to 2D. The utilization of the 3D approach is a common practice among authors. However, they tend to rely on symmetric simplified geometry, which can violate the physicality of the numerical problem. Furthermore, to decrease computational cost, symmetry boundary conditions are applied to reduce the geometry domain to a much smaller size. Applying the symmetry boundary condition results in the numerical solution mirrored along the assigned domain surface. This means that any solution present on one side of the surface will be replicated on the other side as well. This may be non-physical in some cases and can result in inaccuracies, which may become apparent compared to empirical findings. The number of elements that discretize the numerical domain is determined by geometry and can range from a few thousand [104] to a couple of millions [91]. However, it is often unclear whether the cells used are 3D or 2D, as authors do not always specify. The reviewed works showed two types of simulation solution calculation: transient and steady-state. Nevertheless, the latter is not commonly used. In study [105], the steady-state solution was presented along with the transient solution. Still, in [106], only the steady-state simulation was conducted, which resulted in PCM phase transition exclusion from the consideration. Transient simulation highly depends on mesh quality, making it much more numerically demanding. The size of the time step is particularly crucial. The time step independence study helps determine the proper simulation time step, yet the authors often avoid this undemanding, time-consuming procedure. When utilizing small time steps like 0.1 seconds or 1 second, lack of time step independence study is not a vital issue. However, when working with larger time steps such as 60 seconds [107], 150 seconds [108], or 500 seconds [109], it is strongly recommended. The conventional phase transition method, which uses the enthalpy-porosity approach, is commonly utilized due to its integration in the Ansys Fluent Solidification/Melting model. The numerical procedures examined in the reviewed publications have notable differences in how they formulate heat transfer within the PCM. Most approaches focus on conduction heat transfer but often overlook the importance of convection heat transfer. When PCM is in a solid phase, conduction is the primary heat transfer mechanism. However, when it reaches the liquid phase, the convective mechanism starts to work alongside conduction. The more liquid PCM present in the domain, the stronger the impact of buoyancy forces related to convective currents. In research that explores natural convection in phase change materials, the Boussinesq approximation is commonly used instead of solving the full Navier-Stokes equations for compressible flows to determine velocity fields. The full Navier-Stokes equations are typically nonlinear. However, the Boussinesq approximation



decreases nonlinearity to some extent. As a result, it improves the stability of the simulation and increases the rate of convergence. It is essential to evaluate if the Boussinesq approximation would work for considered PCM based on the expected temperature range since it is only accurate for small density changes. Nonetheless, the research reviewed failed to justify or elaborate on the implementation of this approximation. Overall, to numerically analyze systems that involve PCMs, it is essential to properly consider all heat transfer mechanisms and modalities that contribute to simulation accuracy.

*Table 6.3. Numerical approaches for phase change materials.*

| Ref.  | PCM                            | Software                 | Geometry  | Discrete form                               | Simulation type                      | Heat transfer in PCM                      | Accentuated details   |
|-------|--------------------------------|--------------------------|---|---|--------------------------------------|---|---|
| [110] | CrodaTherm 60                  | Unspecified (FEM method) | 2D-cylinder and pipe with radial fins<br>3D-1/8 of cylinder and pipe with longitudinal fins | 143000 elements (2D)<br>71000 elements (3D) | Transient (time step is unspecified) | Conduction (convection was neglected)     | Forced convection in coolant  |
| [111] | RT25                           | ANSYS Fluent             | 3D-1/8 of cylinder and pipe with longitudinal fins  | 268500 elements                             | Transient (time step set to 0.1 s)   | Conduction and natural convection         | Natural convection (Boussinesq approximation)                                   |
| [112] | Lauric acid                    | ANSYS Fluent             | 2D-cylinder and pipes   | 16000 elements                              | Transient (time step set to 0.1 s)   | Conduction and natural convection         | Natural convection (Boussinesq approximation)                                   |
| [104] | Paraffin                       | FLUENT 16.0.             | 3D-1/4 of cylindrical tank and electric heater  | 8448 elements                               | Transient (time step set to 1 s)     | Conduction and natural convection         | Natural convection (Boussinesq approximation)                                   |
| [105] | Metallic PCMs                  | ANSYS Fluent             | 3D-1/2 of cylindrical solar receiver  | 2322019 elements                            | Transient (time step is unspecified) | Conduction (convection was not described) | Steady-state simulation was additionally conducted to analyze properties of PCM |
| [91]  | A44                            | COMSOL Multiphysics®     | 3D-PVT-PCM collector  | 1.5-7.8 million elements                    | Transient (time step is unspecified) | Conduction (convection was neglected)     | Enthalpy-based method of phase transition                                       |
| [113] | RT35HC<br>RT31<br>RT27<br>RT42 | ANSYS Fluent 19.2        | 2D-multi-layer PV-PCM window  | 15000-27000 elements                        | Transient (time step set to 1 s)     | Conduction (convection was not described) | Boussinesq approximation was used for air domain                                |

*Chapter 6: ANALYSIS OF PVT SYSTEMS WITH INCORPORATED PHASE CHANGE MATERIALS*

|       |   |                      |   |                            |  |  |   |
|-------|---|----------------------|---|----------------------------|--|--|---|
| [109] | RT28HC<br>RT35HC  | ANSYS<br>Fluent      | 2D-multi-layer<br>PV panel with<br>PCM  | Unspecified                | Transient<br>(time step set<br>to 500 s)   | Conduction<br>(convection<br>was not<br>described) | Laminar flow in liquid<br>PCM   |
| [114] | n-Octadecane<br>with<br>nanoparticles                                   | COMSOL 5.0           | 2D-multi-layer<br>PV panel with<br>PCM  | About<br>37000<br>elements | Transient<br>(time step is<br>unspecified) | Conduction<br>and natural<br>convection            | Velocity fields in<br>NEPCM were<br>obtained with Navier-<br>Stokes equations for<br>incompressible flows |
| [107] | n-Octadecane  | ANSYS<br>Fluent      | 3D-<br>thermoelectric<br>PV-PCM<br>system   | 24900<br>elements          | Transient<br>(time step set<br>to 60 s)    | Conduction<br>(convection<br>was not<br>described) | Enthalpy-porosity<br>method of phase<br>transition  |
| [115] | Paraffin wax  | ANSYS<br>Fluent 16.2 | 3D-PVT-PCM<br>collector with<br>absorber  | 6417495<br>elements        | Transient<br>(time step set<br>to 1 s)     | Conduction<br>(convection<br>was not<br>described) | Enthalpy-porosity<br>method of phase<br>transition  |
| [108] | Unspecified<br>PCM  | ANSYS<br>Fluent 16.2 | 3D-PVT-PCM<br>collector with<br>absorber  | 2.4 million<br>elements    | Transient<br>(time step set<br>to 150 s)   | Conduction<br>(convection<br>was not<br>described) | Forced convection in<br>coolant   |
| [106] | C15, C18, C22<br>Palmitic<br>acid/Capric<br>acid<br>Sodium<br>phosphate | ANSYS<br>Fluent/CFX  | PVT-PCM<br>collector with<br>sheet-and-tube<br>heat exchanger<br>(Unclear, 2D or<br>3D) | 1528960<br>elements        | Steady-state                               | Conduction<br>(convection<br>was<br>neglected)     | Pointwise software<br>was used for mesh   |
| [116] | RT28 PCM<br>with expanded<br>graphite                                   | FLUENT               | PV-PCM panel<br>(Unclear, 2D or<br>3D)  | 140895<br>elements         | Transient<br>(time step set<br>to 0.5 s)   | Conduction<br>(convection<br>was<br>neglected)     | Form-stable composite<br>PCM  |

## **7. ANALYSIS OF NOVEL PROPOSED PVT-PCM COLLECTOR DESIGN**

Conventional PV systems have a low conversion efficiency of solar irradiation into electric power. This highlights the importance of utilizing the whole solar irradiation spectral range to harness thermal gains that negatively impact electrical efficiency. Traditional PVT collector designs face a significant challenge to reconcile the conflicting natures of electrical and thermal efficiencies, i.e., improving electrical efficiency results in decreased thermal efficiency and vice versa. It is crucial to bridge the gap and to ensure the ability to balance the thermal and electric power output generated in a particular PVT collector. To address this conflict, optimizing the design of the PVT collector is essential. However, the PVT design will inevitably lean towards one aspect over the other. One potential step forward in developing these hybrid systems may be a new thermal management method for a commonly used PV panel integrated with novel PCM.

### **7.1. Concept of novel PVT-PCM collector**

As part of the doctoral thesis, nano-enhanced phase change materials [73] and hybrid phase change materials [75] based on pork fat were produced and tested. Both approaches resulted in PCMs with suitable properties for the thermal management of PVT collectors. However, pure pork fat was employed for passive thermal management of the novel hybrid PV concept [117], i.e., the PVT-PCM collector. Pork fat is an organic, environmentally acceptable PCM with suitable thermal properties comparable to nano-enhanced phase change materials. Unlike NEPCMs, pork fat is not toxic and is significantly cheaper, as mentioned earlier. Furthermore, nanomaterials tend to agglomerate, as already noted, so the long-term stability of NEPCMs is questionable [73]. Potentially, hybrid PCMs based on oil and pork fat have similar long-term stability issues, requiring further investigation [75]. Therefore, it was decided to use pure pork fat due to its suitable thermophysical characteristics, environmental implications, and reasonable natural stability over an extended period. Nonetheless, phase transition cyclic analysis of pork fat PCM should decisively determine long-term stability, which was beyond the scope of research [75].

The novel PVT concept uses pork fat PCM for passive cooling and water as the active working fluid in a recirculation system, Figure 7.1. The utilization of pork fat as a heat buffer is a novel thermal management approach to optimize the PV panel's efficiency. This technique directs the heat load toward the phase transition process instead of the temperature rise. This ultimately may result in enhanced performance and longevity of PV panels.

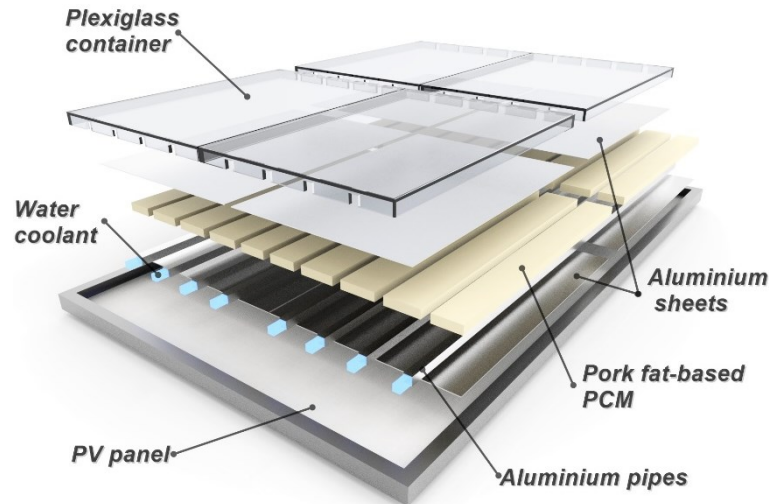


Figure 7.1. Schematic layout of PVT-PCM collector [117].

Once the latent heat capacity of PCM depletes as the pork fat melts, the control system activates the recirculation pump, allowing the active constituent to take over the cooling process. This involves incorporating an innovative thermal regulation system managing dual operation modes in order to balance the electrical and thermal output ratio. The automatic engagement of the circulation of cooling water is based on the internal temperature of the PCM, which depends on various factors such as insolation, ambient temperature, wind speed, collector geometry, etc. During active operation, water coolant is circulated through square aluminum pipes fused to aluminum sheets using epoxy adhesive for metals [118]. This integrated geometry constitutes a thermal absorber that plays a crucial role in connecting the passive and active system components. The heat stored in the pork fat is transferred to the coolant (water) through the surfaces in contact with the thermal absorber. The upper aluminium sheet of the thermal absorber is in uninterrupted contact with the rear side of the PV panel to initiate immediate cooling upon pump engagement. Thus, cooling commences right after the pump is activated, thereby preventing system inertness that may occur due to the slowness of the PCM phase transition. The active operation mode can either work on the ON/OFF principle, or it can be sustained through consistent cooling managed by valves with rotary actuators that reduce or increase the flow along the individual pipes of the absorber, as required. Properly exploiting control valves with rotary actuators can reduce potential hot spots in PV modules by allowing different flow rates through each cooling aluminum pipe.

The traditional method of utilizing a PCM to cool PV panels typically requires a single, large container fixed at the rear of the panel. However, it was observed that the method of utilizing a single large container for cooling purposes results in lower electricity generation capabilities when contrasted with the alternative approach of cooling with multiple smaller and separated containers [11]. Therefore, in article [118], a multi-block passive thermal management system based on pork fat PCM, integrated with active water cooling, was premiered in a PVT collector system. The novel PVT-PCM collector has four separate Plexiglas containers on the backside, with a total of 17.7 kg of pork fat, Figure 7.2.

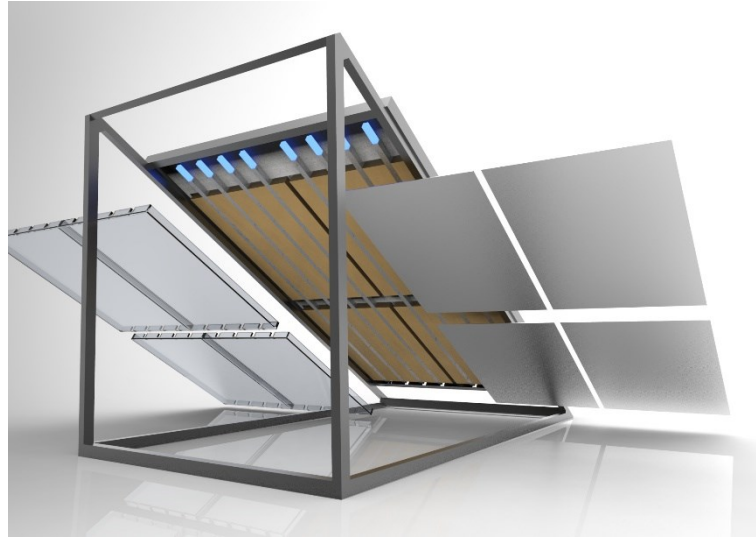


Figure 7.2. PVT-PCM collector with multi-block cooling [118].

## 7.2. Experimental field research of PVT-PCM collector

A comprehensive experimental investigation on the innovative PVT-PCM collector was carried out from August 2021 to January 2022. The experiment was conducted in the humid subtropical and Mediterranean climate on a well-sunlit roof in Split, Croatia. The research aimed to gather valuable information on the behavior and efficiency of the PVT-PCM collector under different weather conditions and other environmental factors, contributing to the advancement of renewable energy technologies. To field test the novel PVT-PCM collector in operative conditions, a purposely developed experimental set-up was harnessed, the specifics of which are described in detail in article [118]. The experimental setup for the PVT-PCM collector comprised various measuring equipment, a robust cooling system, and an installation designed to recirculate cooling water, Figure 7.3. The collector inlet manifold was placed at the bottom, effectively dividing the flow into eight separate pipes. This configuration allows for efficient distribution and management of the flow. Working water coolant flow in each pipe was individually monitored with ultrasonic flow meters. The cooling water warms through heat transfer from the collector and flows through the control valves with rotary actuators. Then, it enters the outlet manifold and departs to the heat exchanger, where it cools again and recirculates back to the inlet side. The heat exchanger was straightforward, comprising a radiator fitted with

a fan. The fan automatically turns on once the recirculation pump starts operating. It is worth noting that this heat exchanger is relatively ineffective in terms of heat transfer efficiency. Nevertheless, it proved to be robust and reliable [118]. The heat generated in the PVT-PCM collector and transferred to the cooling water was orientationally monitored using an ultrasonic calorimeter. However, thermocouples placed at pipe inlets and outlets of the collector allowed for a more detailed understanding of this heat transfer process.

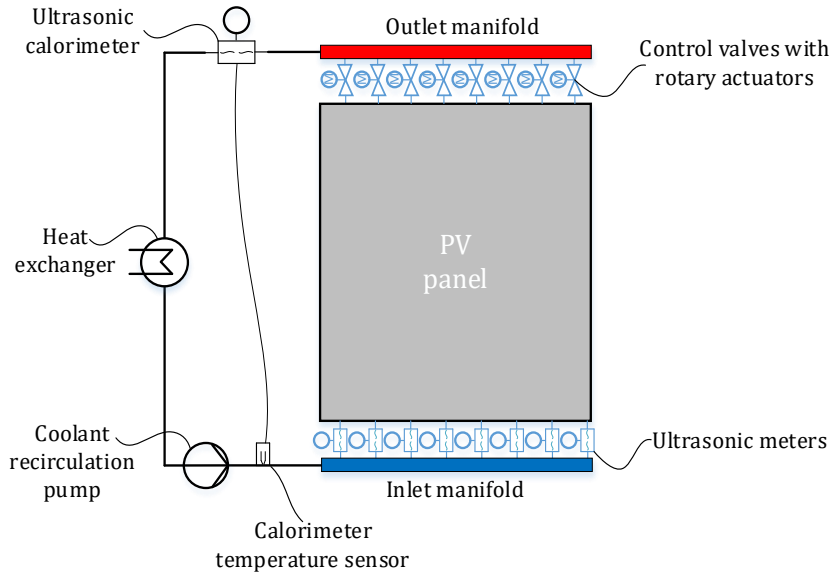


Figure 7.3. Experimental rig schematic [118].

The referent PV panel with a maximum power output of 275 Wp at Standard Test Conditions (STC) and the PVT-PCM collector were inclined at 27 degrees, with the front side oriented towards the south, Figure 7.4. The electric power generated by both systems was measured using two watt meters while connected to a fixed resistive load, monitoring the currents and voltages. A pair of resistors were employed as loads for both systems to get near the maximum power point. Measurements of temperatures were conducted on all the surfaces of the referent PV panel and PVT-PCM collector. However, the rear of the collector has a complex geometry, making it difficult to compare convincingly. Thus, temperature comparisons were limited to the front surfaces of the referent panel and collector. Thermocouples of the K-type were strategically placed on the referent PV panel's front surface, specifically on the R1, R2, and R3 positions. Correspondingly, three K-type thermocouples were positioned on the PVT-PCM collector's front surface at the C1, C2, and C3 points. A pyranometer was securely placed within the confined space between the panel and the collector to record the solar irradiance levels. In article [118], a comprehensive explanation was given regarding the equipment and measuring devices utilized.

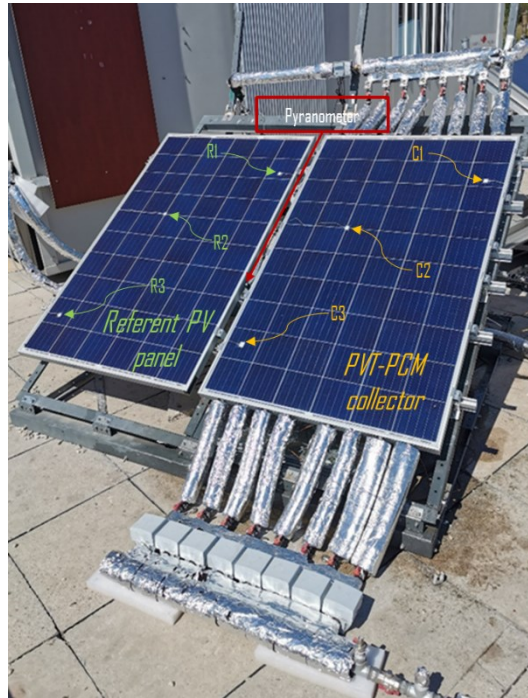


Figure 7.4. Free-standing referent PV panel and PVT-PCM collector [118].

### 7.2.1. Operational regimes and performance indicators

As previously stated, the PVT-PCM system functions in two distinct operating regimes. The primary operating mode utilizes a passive method that employs an organic PCM, specifically pork fat. This mode operates independently until a temperature of PCM reaches  $40^{\circ}\text{C}$ , at which point active water cooling is initiated. According to the data that was available during this experimental phase of research, the melting point of pork fat should be at  $41^{\circ}\text{C}$ , so due to the inertness of PCM, a buffer zone of  $1^{\circ}\text{C}$  was secured when switching to the active mode of operation [118]. However, PCMs usually exhibit melting range rather than melting point, so any data on melting point should be used cautiously. The active cooling may be initiated at a lower average PCM temperature than  $40^{\circ}\text{C}$  since the controller retrieves PCM temperature data from one point and uses it as the threshold for activating the cooling system. The active cooling process continues until the desired temperature of  $33^{\circ}\text{C}$  is attained in the pork fat. At this point, the active system is automatically turned off. Finally, the threshold temperatures can be set to different values, i.e., they can be changed with regard to ambient conditions and energy demands of consumers.

During the summer and occasionally in the fall, the active operation mode automatically engaged due to greater exposure to sunlight and increased temperatures. The performance discrepancy between the referent PV panel and the novel collector was analyzed by thoroughly examining measurement data for ten dominantly clear days in each of the six considered months. Table 7.1 summarizes the monthly values (ten days) of the generated energy and the peak efficiencies of the referent PV panel and PVT-PCM collector regarding the irradiated solar energy. The most energy by both systems was generated in August, as expected, considering

that the most solar energy was emitted that month. The peak electrical efficiency of the PV panel in August was 12%, while for the PVT-PCM collector it was 12.4%. In addition, the collector produced 45,208.7 Wh of usable heat with a peak thermal efficiency of 49.8%. The front surface temperature of the referent PV panel was up to 13.4°C higher than the temperature of the collector in August [118]. In September, lower air temperatures were recorded due to lower total insolation, so the collector generated only 24,338.1 Wh of heat. As the daily temperatures decreased in September, the electrical efficiency of both the PV panel and the collector increased compared to August. During these two months, the collector generated more electricity than the referent PV panel in addition to useful heat, resulting in a peak total efficiency of 62.2%. From October to January, the predominant operational mode was passive since the pump activation threshold temperature was not reached. In this period, the collector and the PV panel had almost identical electrical efficiency, Table 7.1. However, the collector continuously had lower peak temperatures but slightly higher mean temperatures due to the inertness of PCM [118]. During typically colder months with less sunlight, the pork fat PCM in the PVT collector will neither stimulate the overall electricity production nor downgrade it either. Overall, in sixty days during six months, the PVT-PCM collector generated 64,278.8 Wh of electricity, a modest 804.9 Wh more than the PV panel, but it also developed an additional 69,546.8 Wh of useful heat.

Table 7.1. Energy generation and efficiency of referent PV panel and PVT-PCM collector.

| Month                 | Total insolation<br>Wh m <sup>2</sup> | Total electrical energy |                 | Total heat generation<br>Wh | Peak electrical efficiency |              | Peak thermal efficiency<br>% | Peak total efficiency (PVT-PCM)<br>% |
|-----------------------|---------------------------------------|-------------------------|-----------------|-----------------------------|----------------------------|--------------|------------------------------|--------------------------------------|
|                       |                                       | Referent<br>Wh          | PVT-PCM<br>Wh   |                             | Referent<br>%              | PVT-PCM<br>% |                              |                                      |
|                       |                                       | <b>August 2021</b>      | 73,128.0        |                             | 14,136.4                   | 14,651.0     |                              |                                      |
| <b>September 2021</b> | 65,424.5                              | 13,152.4                | 13,481.7        | 24,338.1                    | 12.7                       | 12.9         | 29.8                         | 42.6                                 |
| <b>October 2021</b>   | 59,629.3                              | 12,450.5                | 12,378.6        | 0.0                         | 13.3                       | 13.2         | 0.0                          | 13.2                                 |
| <b>November 2021</b>  | 32,170.4                              | 6,103.5                 | 6,132.0         | 0.0                         | 13.4                       | 13.5         | 0.0                          | 13.5                                 |
| <b>December 2021</b>  | 36,669.7                              | 7,262.7                 | 7,256.2         | 0.0                         | 13.0                       | 12.9         | 0.0                          | 12.9                                 |
| <b>January 2022</b>   | 48,293.9                              | 10,368.4                | 10,379.3        | 0.0                         | 13.5                       | 13.5         | 0.0                          | 13.5                                 |
| <b>OVERALL</b>        | <b>315,315.8</b>                      | <b>63,473.9</b>         | <b>64,278.8</b> | <b>69,546.8</b>             |                            |              |                              |                                      |

During sunny, clear summer days with slow to moderate winds, the PVT-PCM system is expected to perform at its best [118]. An in-depth analysis of the data collected on September 6<sup>th</sup>, 2021, was carried out to understand the matter at hand comprehensively [118]. Throughout the day, there was no cloud cover and no shading. The maximum insolation was more than 1,000 W m<sup>-2</sup>. Total insolation measured 7,269.4 W m<sup>-2</sup>. Daily air temp averaged 25.6°C, humidity 38%, wind speed 6.2 km h<sup>-1</sup>. Twice during the day, the PCM exceeded the upper threshold temperature, activating the recirculation pump, thus initiating 3,351.1Wh of heat yield. Throughout the entire duration of the day, until sunset, the PVT-PCM collector consistently had a temperature below the temperature of the referent PV panel, Figure 7.5. The thermal inertia of the PCM results in a notable reduction in temperature oscillations of the collector, which is much less pronounced compared to the PV panel. During the passive operation, the PVT-PCM collector did not generate more electricity. This was due to very slight electrical efficiency



degradation of the base PV panel despite the changes in temperature of the PVT-PCM collector. Nevertheless, during the considered day, the PVT-PCM collector generated 1,492.6 Wh of electricity, surpassing the PV panel production of 1,438.8 Wh.

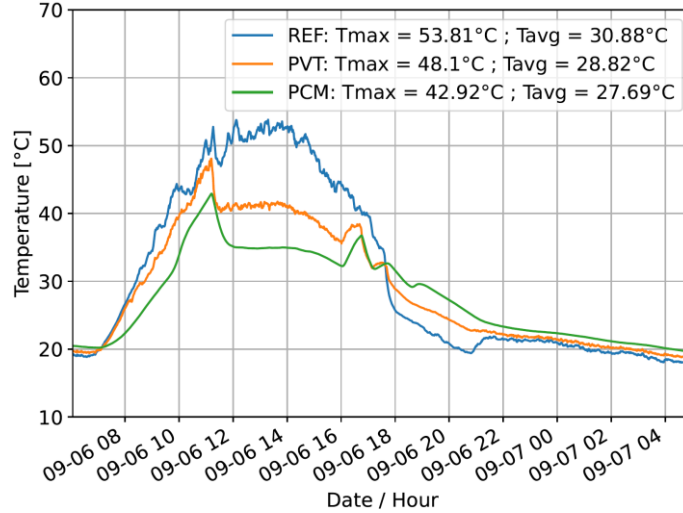


Figure 7.5. Front surface temperature of referent PV panel and PVT-PCM collector on September 6<sup>th</sup> [118].

### 7.2.2. Assessment of collector performance at annual basis

Since the experimental investigation [118] was managed over six months, it is difficult to determine the exact energy generation at a yearly level. However, based on the data collected during the six months, an estimated energy production for the entire year was calculated. In research [118], it was assessed that electricity generation primarily depends on irradiated solar energy and electrical efficiency. The efficiency of the electrical part of the PVT system depends on its electrical characteristics and how effectively heat is dissipated from the collector surfaces. This process is impacted by various environmental factors, all of which change over time. The PVGIS-SARAH2 database provided data on local solar irradiation over twelve months [118]. Since the experimental measurements were carried out over half a year, covering different seasons, it was feasible to calculate the average electrical efficiency of the PVT-PCM collector roughly. To determine the electrical efficiency of a system over a monthly period, firstly, the daily values of electrical efficiency were averaged, resulting in a single value for that precise month. Further, the monthly values were averaged to establish annual electrical efficiency. As a result, the referent PV panel and the collector de facto have the same average electrical efficiency of 12% when calculated using this method. The estimated PVT-PCM collector electrical efficiency includes the energy consumed by the recirculation pump [118]. Optimizing volume flow and selecting a more suitable pump can significantly reduce pump energy consumption and increase net electricity output. In this case, PVT-PCM collector electric power production may surpass PV panel power generation. Based on calculations in study [118], it was estimated that the PVT-PCM system installed at the test site would generate an annual electrical energy output of approximately 358 kWh, assuming an unoptimized circulation pump is used.

The amount of generated heat in PVT collectors depends on irradiated solar energy and their thermal efficiency. Thermal efficiency also depends on other environmental parameters such as ambient temperature, wind speed and direction, etc. The experimental research conducted over a couple of months was used to determine the average monthly thermal efficiency. The estimated insolation from PVGIS-SARAH2 [119] was used to determine the thermal efficiency of the PVT-PCM collector for months when experimental research was not conducted. The polynomial trendline was used to fit the functional dependence of thermal efficiency to solar radiation for the measured months [118]. This enables the extrapolation of data beyond the experimental measurement period. The minimum and maximum estimated thermal efficiency values from March to October were determined while excluding the first and last two months of the year in which the system would not reach the pump activation threshold. This decision was based on experimental measurements and estimated insolation acquired from the PVGIS-SARAH2 database. The PVT-PCM collector heat generation estimates vary greatly depending on the month, with the highest estimates occurring in July (ranging from 132 kWh to 210 kWh) and the lowest in October (ranging from 10 kWh to 32 kWh), Figure 7.6. Annually, the PVT-PCM collector considered here is expected to generate from 500 kWh to 908 kWh of usable heat, which will vary due to the weather conditions. Furthermore, the thermal efficiency will likely be between 17% and 30% [118].

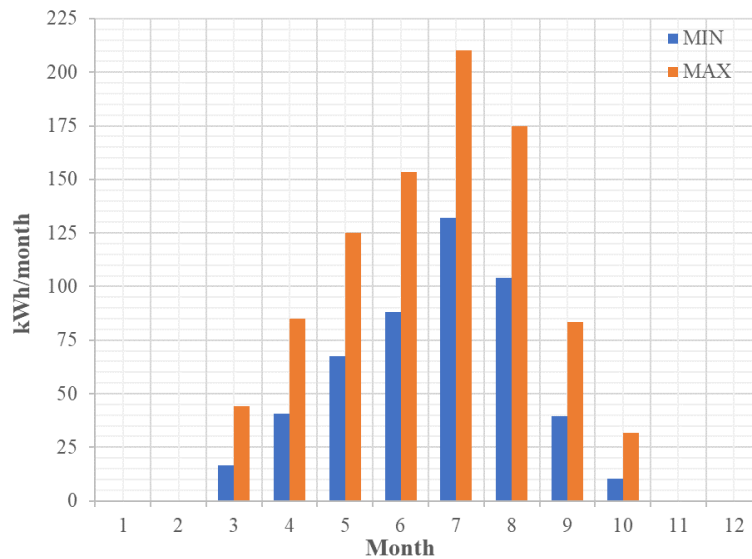


Figure 7.6. Annually heat generation estimation [118].

### 7.3. Environmental impact and economic evaluation

To better evaluate the design of the developed PVT-PCM collector, a comprehensive environmental analysis based on data from the construction phase was carried out in research [118]. The evaluation aimed to determine the potential environmental effects of the proposed energy system by Life Cycle Analysis (LCA). The LCA methodology is an extensive approach that analyzes the input of materials and energy associated with processes within a system. It then evaluates the environmental impact and provides valuable insights into the system's

sustainability. The quality of the impact assessment heavily relies on the accuracy of the data collected during the inventory phase. If the input data is unreliable, it will negatively affect the precision of the impact assessment analysis phase. The impact assessment was quantified using the EcoInvent database integrated into SimaPro<sup>®</sup> software, which is based on LCA principles [118]. During the inventory analysis phase, the software assesses the raw materials and energy inputs to determine system emissions outputs. Following the inventory phase, the subsequent phase involves assessing the environmental effects, Figure 7.7. This process is called the environmental impact assessment phase, where the outputs are associated with midpoint environmental impacts. Finally, midpoint impacts are transformed into endpoint impacts, which may manifest as damage to human health and the ecosystem or as unavailability of resources.

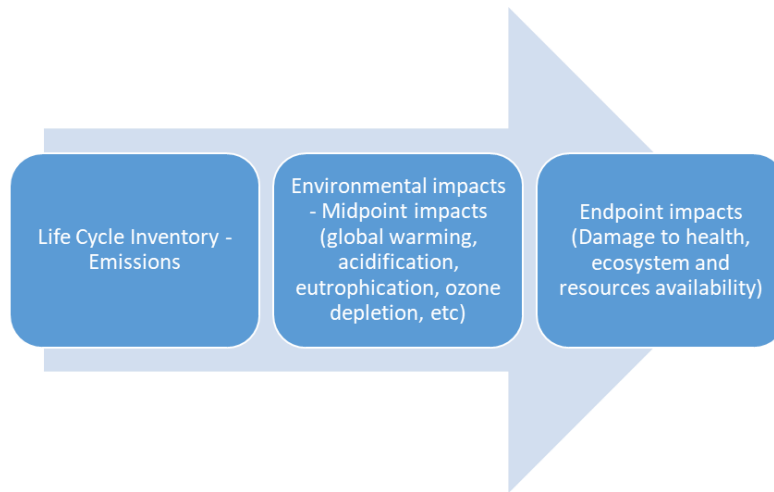


Figure 7.7. LCA flowchart connecting environmental midpoint and endpoint impacts [118].

The scope of the analysis presented in article [118] primarily centered on the design and manufacturing phase, with the evaluation of the materials utilized to produce the novel PVT-PCM system. The examined PVT-PCM collector design has a significant environmental impact related to climate change due to the materials used during the construction phase, Table 7.2. The manufacturing process of novel PVT-PCM collector involves using photovoltaic panels and aluminium, which are major contributors that affect climate change and human health. Based on the analysis, some future designs could, for example, reduce the use of aluminum to impair the environmental footprint in this regard. The collector design and manufacturing phases were well covered in the environmental analysis; however, the usage phase, which may be analyzed in the future, will help to better address environmental PVT system benefits compared with similar designs.

Table 7.2. Environmental footprint of PVT-PCM collector design [118].

| Environmental impact          | Unit                                  | PVT     |
|-------------------------------|---------------------------------------|---------|
| Carbon footprint              | kg CO <sub>2</sub> - eq               | 580.63  |
| Acidification                 | kg SO <sub>2</sub> - eq               | 33.21   |
| Eutrophication                | kg PO <sub>4</sub> - eq               | 0.3     |
| Ozone Layer Depletion         | kg CFC - eq                           | 0.00053 |
| Abiotic Depletion             | kg Sb - eq                            | 3.9     |
| Human Toxicity                | tn Db - eq                            | 8.035   |
| Photochemical Ozone Depletion | kg C <sub>2</sub> H <sub>4</sub> - eq | 1.23    |

In addition to examining the environmental impact of the proposed PVT-PCM design, it is crucial to conduct an economic assessment to ensure a comprehensive evaluation of its viability. The costs mentioned in the continuation are specifically related to the design of the prototype PVT-PCM collector. As the scale of production increases, it is reasonable to anticipate that the cost of investment per unit will decrease, resulting in a more cost-effective collector. Based on the PVT-PCM design under consideration, the estimated cost for the construction materials that were used amounts to approximately 698 € [118]. When constructing a novel PVT-PCM collector, most investment falls on Plexiglas, followed by aluminum and the base PV panel, Figure 7.8. The projected cost for the PVT-PCM collector per surface area is approximately 428 € m<sup>-2</sup>, significantly lower than the average cost of traditional PVT designs, which can exceed 600 € m<sup>-2</sup> [118]. To determine the economic implications of the collector design, the LCOE methodology was used for evaluation. Based on the performance data analysis, it was determined that the PVT-PCM collector could generate an average yearly energy output of approximately 858 kWh to 1,266 kWh, comprising both heat and electricity. Derived from the LCOE analysis and considering the specified input data, the estimated levelized energy cost would fall between 0.056 and 0.083 € kWh<sup>-1</sup> [118]. By comparison, the PVT collector design from study [120] reportedly has LCOE from 0.06 to 0.12 € kWh<sup>-1</sup>. Therefore, the novel PVT-PCM design presents a cost-effective option compared to similar designs. Moreover, the investment return time is reasonably short, at only 4 years [118].

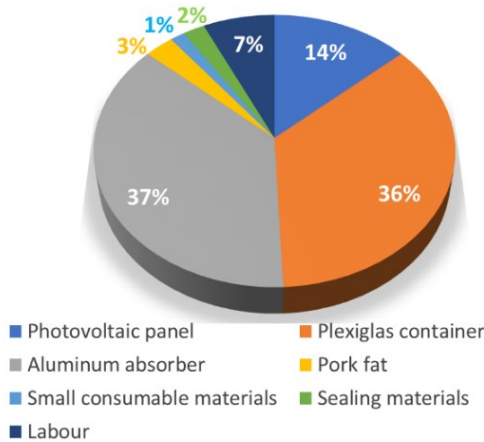


Figure 7.8. Constructive components cost share in the collector design [118].

## 8. NUMERICAL STUDY OF NOVEL PVT-PCM COLLECTOR

A comprehensive and rigorous numerical analysis of the PVT-PCM collector design, including all domains, was carried out using the transient 3D CFD method in the ANSYS Fluent software [121]. The research encompassed a range of variable boundary conditions and heat transfer processes that occur throughout the day. Volatile weather conditions spanning from sunrise to sunset were numerically analyzed to demonstrate that the CFD model can accurately and robustly simulate unexpected changes in weather or necessary sudden switches in system working regimes. The numerical study required a high level of input data precision and accuracy, ensuring reliable and trustworthy results. Therefore, to engineer a hybrid PVT-PCM system effectively, it is crucial to construct a comprehensive numerical model including a wide spectrum of significant factors that can accurately depict the underlying mechanisms of heat transfer while adequately addressing the PCM phase change phenomenon.

### 8.1. Experimental research of input parameters for numerical modeling

One of the crucial surrounding aspects that need to be numerically well managed due to its stochastic nature is the influence of wind on the convective heat transfer. Hence, the experimental setup was developed to study how the relative position of the photovoltaic panel affects the rate of convection heat transfer, specifically, the impact of wind direction and speed on the convection heat transfer coefficient from panel surfaces. Furthermore, the phase transition of pork fat PCM, which is poorly covered in the referent literature, was also experimentally examined by employing a differential scanning calorimetry (DSC) technique. As mentioned earlier, PCM phase transition usually occurs in the melting temperature range rather than in the melting point, so DSC data is indispensable for proper numerical analysis of phase change material. The numerical model accuracy of the novel PVT-PCM collector design was ensured by implementing precise input parameters obtained from conducted experiments and up-to-date literature. This guarantees that the model can be effectively utilized to enhance the collector's performance in the future.

#### 8.1.1. Investigation of convective heat transfer coefficients

A study [117] was carried out to experimentally investigate the behavior of convection heat transfer coefficients on the front and rear surfaces of a photovoltaic panel. A 50 W polycrystalline PV module with  $540 \times 670 \times 25$  mm dimensions was subjected to airflow in a wind tunnel set to three distinct average wind speeds, namely  $2.6 \text{ m s}^{-1}$ ,  $4.7 \text{ m s}^{-1}$ , and  $6.7 \text{ m s}^{-1}$ , Figure 8.1.



Figure 8.1. Experimental test rig layout in wind tunnel [117].

A detailed description of the experiment and measuring equipment, together with uncertainty analysis, is in article [117]. However, in short, the study aimed to determine the influence of wind speed ( $v$ ), relative wind angle ( $\gamma$ ), and the tilt angle of PV panel ( $\beta$ ) on the convective heat transfer, Figure 8.2. Therefore, the photovoltaic panel was strategically placed in the airstream at adjustable wind speeds and relative wind angles of  $0^\circ$ ,  $22.5^\circ$ , and  $45^\circ$ . The PV panel tilt angle was varied in three positions, i.e.,  $0^\circ$ ,  $20^\circ$ , and  $35^\circ$ .

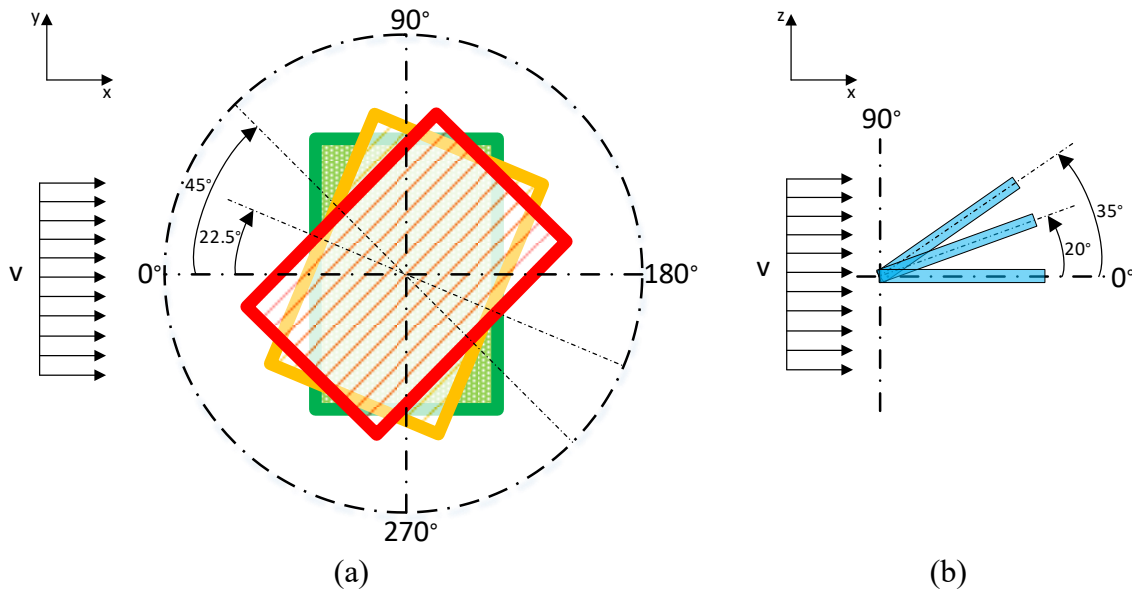


Figure 8.2. Relative wind angle  $\gamma$  (a) and PV panel tilt angle  $\beta$  (b) [117].

An indirect approach was taken to determine the convective heat transfer coefficients, which relied on the total heat flux data obtained with a heat flux sensor. The Peltier element thermoelectric effect induced the local heat flux through the PV panel, which was then measured

on the other side using the passive thermopile FHF02SC heat flux sensor. The sensor simultaneously measures heat flux and temperature and can self-calibrate using the integrated heater. Heat flux was measured in six different positions, with three positions on the front surface of the PV panel (m1, m2, m3) and three on the rear (m4, m5, m6), Figure 8.1. A consistent room temperature of around 20°C was maintained throughout the experiment. The PV panel was subjected to constant heat flux and wind speed until it reached a state of equilibrium, and measurements were taken at these steady-state conditions.

The Equation (8.1) describes the relation between the convection heat transfer coefficient and heat flux:

$$q = h(T_S - T_A), \quad (8.1)$$

where  $q$  represents the heat flux ( $\text{W m}^{-2}$ ),  $h$  is the convection heat transfer coefficient ( $\text{W m}^{-2}\text{K}^{-1}$ ),  $T_S$  is the surface temperature of the sensor (K), and  $T_A$  is the ambient air temperature (K).

To accurately determine the heat flux dissipated from the sensor's surface due to convection, it was required to deduct the portion of heat flux dissipated by radiation heat transfer. Radiation heat dissipation from the sensor surface,  $q_R$  ( $\text{W m}^{-2}$ ), was calculated from Equation (8.2):

$$q_R = \varepsilon\sigma(T_S^4 - T_W^4) \quad (8.2)$$

where the emissivity of the sensor surface is  $\varepsilon = 0.95$ ,  $T_W$  represents the cold surroundings temperature (K) and  $\sigma$  is the Stefan-Boltzmann constant [117].

Convection heat flux ( $q_C$ ) from the sensor surface was determined as the difference between induced total heat flux ( $q_T$ ) and radiation heat dissipation ( $q_R$ ), Equation (8.3):

$$q_C = q_T - q_R \quad (8.3)$$

Hence, based on experimental measurements, the convection heat transfer coefficient was analytically calculated from Equation (8.4):

$$h = \frac{q_C}{(T_S - T_A)} \quad (8.4)$$

The experiment provided the required data to thoroughly assess and analyze multiple convective cooling scenarios of the conventional PV panel. Furthermore, this data from article [117] can inherently be utilized for the analysis of PVT collectors. On average, the best convective cooling effect of the front PV panel surface was reached for 0° tilt angle  $\beta$ , while the impact of relative wind angle  $\gamma$  was less pronounced, Table 8.1. On the rear side, convection

heat transfer coefficient values tend to fluctuate due to complex geometry and local effects, so it is difficult to determine the best cooling scenario.

Table 8.1. Experimental measurements of convection heat transfer coefficient at six positions [117].

| v<br>(m s <sup>-1</sup> ) | β<br>(°) | γ<br>(°) | Convection heat transfer coefficient (W m <sup>-2</sup> K <sup>-1</sup> ) |      |      |      |      |      |
|---------------------------|----------|----------|---|------|------|------|------|------|
|                           |          |          | m1  | m2   | m3   | m4   | m5   | m6   |
| 2.6                       | 0        | 0        | 35.8  | 37.6 | 34.5 | 30.4 | 28.2 | 26.7 |
| 2.6                       | 0        | 22.5     | 35.1  | 36.1 | 33.2 | 35.0 | 26.3 | 25.7 |
| 2.6                       | 0        | 45       | 30.6  | 36.4 | 31.8 | 31.7 | 28.6 | 25.5 |
| 4.7                       | 0        | 0        | 54.1  | 56.2 | 51.1 | 46.5 | 41.3 | 41.1 |
| 4.7                       | 0        | 22.5     | 54.2  | 54.7 | 50.4 | 51.5 | 38.5 | 38.6 |
| 4.7                       | 0        | 45       | 50.8  | 56.6 | 49.2 | 47.6 | 43.8 | 39.0 |
| 6.7                       | 0        | 0        | 65.2  | 67.4 | 61.4 | 55.0 | 48.8 | 49.5 |
| 6.7                       | 0        | 22.5     | 67.1  | 67.4 | 62.1 | 61.4 | 45.7 | 46.6 |
| 6.7                       | 0        | 45       | 64.7  | 70.3 | 61.0 | 59.5 | 54.3 | 48.4 |
| 2.6                       | 20       | 0        | 32.9  | 35.7 | 33.0 | 21.8 | 29.1 | 38.1 |
| 2.6                       | 20       | 22.5     | 30.8  | 33.0 | 31.7 | 24.1 | 27.9 | 30.8 |
| 2.6                       | 20       | 45       | 28.1  | 34.1 | 31.1 | 43.4 | 33.0 | 28.2 |
| 4.7                       | 20       | 0        | 51.7  | 58.7 | 55.3 | 35.0 | 43.4 | 53.5 |
| 4.7                       | 20       | 22.5     | 49.6  | 56.8 | 53.4 | 40.5 | 41.6 | 47.3 |
| 4.7                       | 20       | 45       | 45.1  | 54.9 | 50.1 | 62.6 | 48.5 | 41.4 |
| 6.7                       | 20       | 0        | 60.9  | 69.1 | 66.6 | 43.6 | 52.5 | 64.7 |
| 6.7                       | 20       | 22.5     | 59.8  | 68.6 | 65.3 | 51.6 | 50.7 | 56.2 |
| 6.7                       | 20       | 45       | 54.9  | 66.8 | 62.0 | 76.6 | 60.0 | 51.2 |
| 2.6                       | 35       | 0        | 21.8  | 33.6 | 32.4 | 18.9 | 26.3 | 35.0 |
| 2.6                       | 35       | 22.5     | 29.4  | 33.6 | 32.8 | 18.4 | 26.2 | 30.0 |
| 2.6                       | 35       | 45       | 27.5  | 33.7 | 31.8 | 34.5 | 32.6 | 29.7 |
| 4.7                       | 35       | 0        | 46.4  | 55.0 | 53.5 | 32.0 | 41.7 | 53.3 |
| 4.7                       | 35       | 22.5     | 45.2  | 54.5 | 52.6 | 30.2 | 41.3 | 46.2 |
| 4.7                       | 35       | 45       | 41.0  | 52.7 | 49.9 | 57.8 | 48.4 | 43.4 |
| 6.7                       | 35       | 0        | 55.0  | 66.2 | 66.6 | 39.6 | 50.2 | 63.2 |
| 6.7                       | 35       | 22.5     | 53.0  | 64.2 | 63.1 | 37.7 | 49.4 | 55.6 |
| 6.7                       | 35       | 45       | 49.3  | 64.4 | 62.2 | 71.1 | 59.3 | 52.5 |

The optimal experimental conditions for field testing of the novel PVT-PCM collector can be established based on the wind tunnel experiments of convection heat transfer. However, two main issues can impact the accuracy of the convective heat transfer coefficient acquired experimentally. Firstly, the sensor thickness can cause changes to the flow field in the local area being measured. Ideally, the sensor surface should be aligned with the surface of the PV panel to minimize these effects. Secondly, the temperature field of the PV panel in actual operating circumstances is very complex [117]. Therefore, it differs from the temperature field of the locally heated PV panel in the experiment, which can limit the accuracy and applicability of the measurements. In addition to the experimental analysis, a numerical study of convection heat transfer coefficients on the front and rear surfaces of the PV panel was conducted. The average



deviation between the numerical analysis and experimental results was 12%, which indicates solid numerical forecasts of convective heat transfer coefficients [117]. However, significant deviations of the numerical results from the experimental were recorded in some areas and operating conditions, so the results of the mentioned numerical analysis should be used with caution. Nonetheless, comprehension of flow field behavior from the performed numerical analysis in conjunction with experimental measurements can be used to estimate convection heat transfer coefficients on the surfaces of novel PVT-PCM collector.

### **8.1.2. Differential scanning calorimetry of pork fat PCM**

A differential scanning calorimetry technique was employed in a controlled nitrogen atmosphere to investigate the pork fat PCM phase transition [121]. A sample of pork fat weighing around 14 mg was placed in an aluminum pan and subjected to a temperature cycle. It was heated from 0°C to 80°C, then cooled back down to 0°C, and finally reheated to 80°C, all at a controlled rate of 10°C per minute. The melting temperature was identified by analyzing the normalized DSC curves during the second heating phase, Figure 8.3. The temperature at which crystallization occurs was identified using the DSC curve from the cooling phase. The latent heat of melting was calculated by integrating the area under the endothermic peak. The latent heat of crystallization was calculated by integrating the area under the exothermic peak. The pork fat sample underwent three separate DSC analyses. Therefore, the values obtained for each parameter represent the average of the three measurements. During the second heating phase, the DSC curve displays a melting temperature range from 8.3°C to 45.2°C with a solitary endothermic peak at 34.8°C. The area under the endothermic peak was integrated to calculate the latent heat of melting, which amounts to 45.4 J g<sup>-1</sup>. During the cooling phase, the DSC curve displays a crystallization temperature range from 30.5°C to 0.3°C with triple exothermic peaks. The area under the exotherm was integrated to calculate the latent heat of crystallization, which amounts to 48.3 J g<sup>-1</sup>.

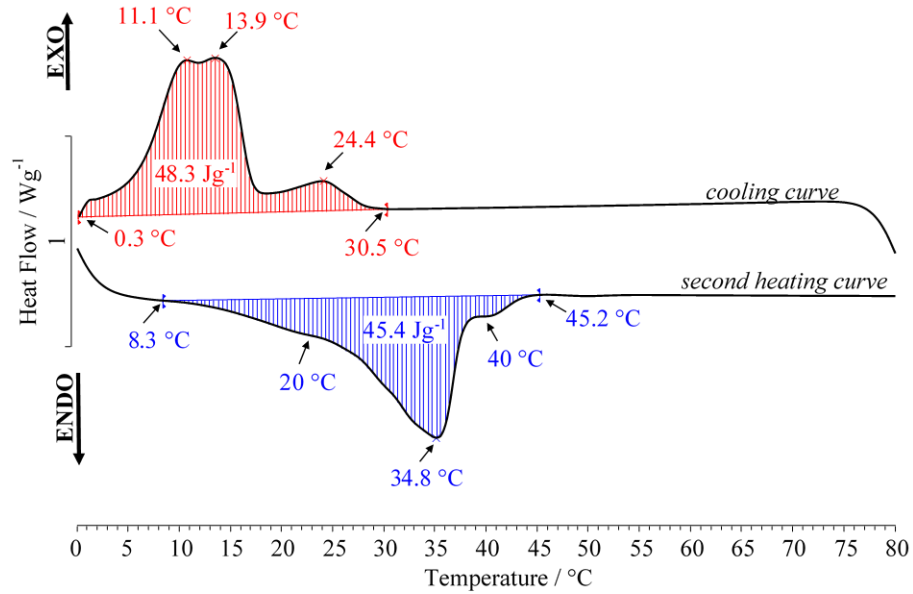


Figure 8.3. Differential scanning calorimetry of pork fat [121].

## 8.2. Computational domains and boundary conditions

The CFD simulation domains from study [121] comprised regions of both fluid and solid materials, Figure 8.4. The solid areas of the CFD model are mainly composed of PV panel assembly, including protective tempered glass, ethylene vinyl acetate (EVA) encapsulant, PV cells, tedlar back sheet, and aluminum frame. The other solid regions are part of a multi-block passive/active thermal management system made of pipes and sheets constructed from aluminium, forming a thermal absorber. The thermal absorber was covered with plexiglass to provide protection from elements while containing pork fat PCM. The fluid domains include pork fat PCM and water coolant. The atmospheric air was not modeled; instead, heat transfer from surfaces of the PVT-PCM collector was governed using convection coefficients.

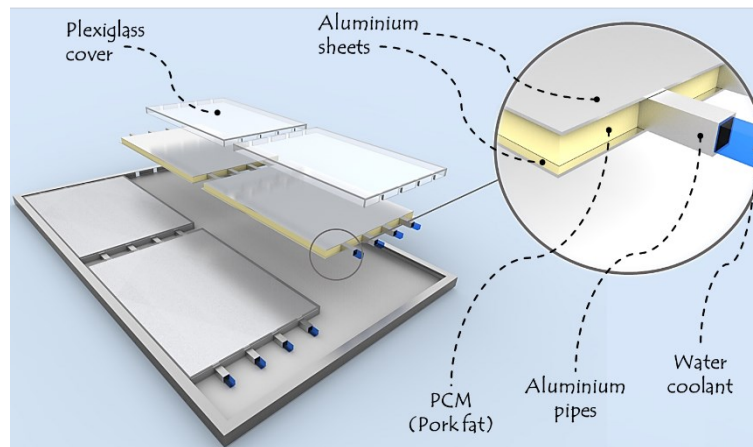


Figure 8.4. PVT-PCM collector multi-block cooling domains [121].

The thermophysical characteristics of the collector PV assembly and multi-block thermal management system components are listed in Table 8.2. The thermophysical properties of fluid domains are listed in Table 8.3. The solidus and liquidus temperatures of the pork fat PCM, i.e., melting and crystallization temperatures, as well as its latent heat, were identified based on the data derived from the differential scanning calorimetry research.

Table 8.2. Thermophysical characteristics of solid domains [121].

| Material  | Tempered glass | EVA  | PV-cell | Tedlar | Aluminium frame | Aluminium absorber | Plexiglass |
|---|----------------|------|---------|--------|-----------------|--------------------|------------|
| Density, kg m <sup>-3</sup>                             | 2515           | 960  | 2330    | 1162   | 2700            | 2719               | 1200       |
| Specific Heat, J kg <sup>-1</sup> K <sup>-1</sup>       | 820            | 2090 | 712     | 1465   | 900             | 900                | 1423       |
| Thermal Conductivity, W m <sup>-1</sup> K <sup>-1</sup> | 0.98           | 0.31 | 150     | 0.23   | 160             | 215                | 0.25       |

Table 8.3. Thermophysical characteristics of fluid domains [121].

| Material       | Density, kg m <sup>-3</sup> | Specific Heat, J kg <sup>-1</sup> K <sup>-1</sup> | Thermal Conductivity, W m <sup>-1</sup> K <sup>-1</sup> | Absolute viscosity, kg m <sup>-1</sup> s <sup>-1</sup> | Thermal expansion coefficient, K <sup>-1</sup> | Latent heat, J kg <sup>-1</sup> | Solidus Temperature, °C | Liquidus Temperature, °C |
|----------------|-----------------------------|---|---|--|--|---------------------------------|-------------------------|--------------------------|
| PCM (Pork fat) | 885<br>Boussinesq           | 2260  | 0.19  | 0.07   | 0.0007   | 45400                           | 8.3                     | 45.2                     |
| Water          | Polynomial                  | 4182  | 0.6   | 0.001003   | n/a  | n/a                             | n/a                     | n/a                      |

The 3D transient numerical analysis of the PVT-PCM collector was mainly governed by continuity, momentum, and energy equations [121]. The phase transition of PCM was numerically solved using Fluent's Solidification and Melting model based on the enthalpy-porosity approach. The natural convection in liquid PCM was simulated by employing the Boussinesq approximation, which improves the convergence rate and stability of the simulation. Furthermore, a symmetry boundary condition was established on the vertical central axis plain of the collector geometry to reduce the computational resources needed for the simulation. The surfaces of the collector that come in direct contact with the fluid regions were designated as stationary wall boundaries with no-slip conditions. A direct heat source, as in [122], was implemented in the PV cells domain to bypass solar radiation modeling, which may improve the numerical model robustness. This direct heat source was varied at every time step by user-defined functions (UDF). The heat originating from the heat source was eliminated from the front surface of the collector through a combination of convective and external radiation heat flux. The convection heat transfer coefficient is influenced by various factors, such as the wind speed, the angle at which wind hits the surface, the tilt angle of the PVT collector, and the specific geometry of the system. Based on experimental research [118] and [117], the numerical analysis considered the mentioned factors and adjusted the convection heat transfer coefficient

from the front surface every minute via UDFs. Analogously, the free stream temperature was also varied. External radiation heat flux changed every minute during clear periods of the day, with external radiation temperature managed using Swinbank's temperature model for clear sky. During pronounced cloudiness, the external radiation heat flux was neglected. On the other surfaces of the collector in the lee, the heat transfer coefficient was constant at  $12 \text{ W m}^{-2}\text{K}^{-1}$ . This constant value includes the influence of convection and radiation, which simplifies the numerical model [122]. The velocity inlet boundary condition was assigned to the PVT-PCM collector absorber inlets, while the zero-gauge pressure boundary condition was exerted at the absorber outlets. Both boundary conditions were integrated into the model through the use of user-defined functions. The used UDFs written in the C programming language were dynamically loaded in the ANSYS Fluent UDF interface.

### 8.3. Verification of multi-parameter numerical model and discussion

The numerical model was put to the test for the case of challenging weather conditions that were measured on October 26, 2021 [121]. Experimental research conducted from 6.51 AM to 6.18 PM involved unstable weather conditions such as changing wind and high levels of varying insolation due to fluctuating cloud coverage, Figure 8.5. During this autumn day, the air temperature peaked at  $20.3^\circ\text{C}$ , while the average wind speed was  $3.7 \text{ km h}^{-1}$ , with recorded occasional gusts reaching up to  $28.4 \text{ km h}^{-1}$ . The data on the selected day enabled the assessment of the model's ability to adapt to sudden variations in input parameters and suitability to simulate both operating regimes, i.e., passive and active.

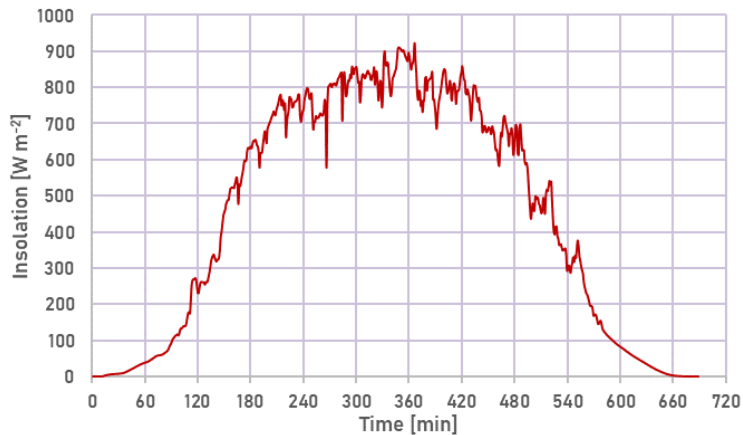


Figure 8.5. Solar radiation in Split, Croatia, on October 26, 2021 [121].

The thermal behavior of the PVT-PCM collector was analyzed numerically throughout the day, including a couple of minutes prior to sunrise and a couple of minutes after sunset. Based on the multi-point pork fat PCM temperature measurements from research [118] and the data from DSC analysis, it was determined that the PCM was in a solid state before sunrise. The initial temperature values in CFD analysis were adjusted to match experimental measurement data for the corresponding domain. It was observed from experimental measurements that the

front surfaces of the collector and the PV panel had lower temperatures than the ambient air early in the morning, Figure 8.6. This behavior results from the radiation emitted from the front glass surface to the sky [121], which is more pronounced during low-humidity nights without clouds [123]. This external radiation plays an essential role in the overall heat balance of the PVT-PCM collector for roughly two hours after sunrise while the upper layers of the atmosphere are still relatively cool. The numerical model considers this external radiation heat loss during this critical period until the atmosphere warms, resulting in significantly decreased radiation heat loss, which can then be neglected.

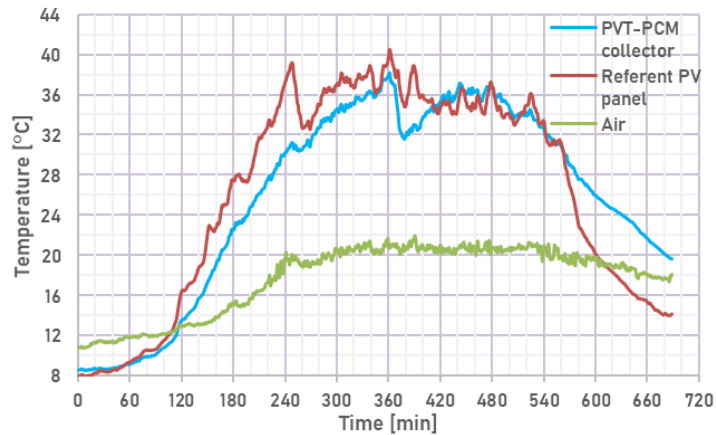


Figure 8.6. Comparison of collector and PV panel front surface temperatures with air temperature [121].

The numerical analysis proved particularly complex due to the intricate nature of the heat exchange mechanism in synergy with the phase transition of pork fat PCM [121]. The added complexity resulted from the PCM continuous phase transition during the experiment, i.e., the pork fat exhibits a phase transition from 8.3°C to 45.2°C. However, the use of passive cooling with PCM effectively reduces temperature oscillations. As a result, the PVT-PCM collector exhibits significantly less pronounced temperature oscillations than the referent PV panel, Figure 8.6. Hence, stabilizing the collector temperature with PCM could potentially extend the photovoltaic component lifetime, which may be worth investigating in the future.

Thermal processes in the PVT-PCM collector passive working regime take place at a relatively slow pace. However, a critical moment for the numerical analysis is switching operating regimes, especially the transition from passive to active mode in which heat transfer is accelerated, Figure 8.7.

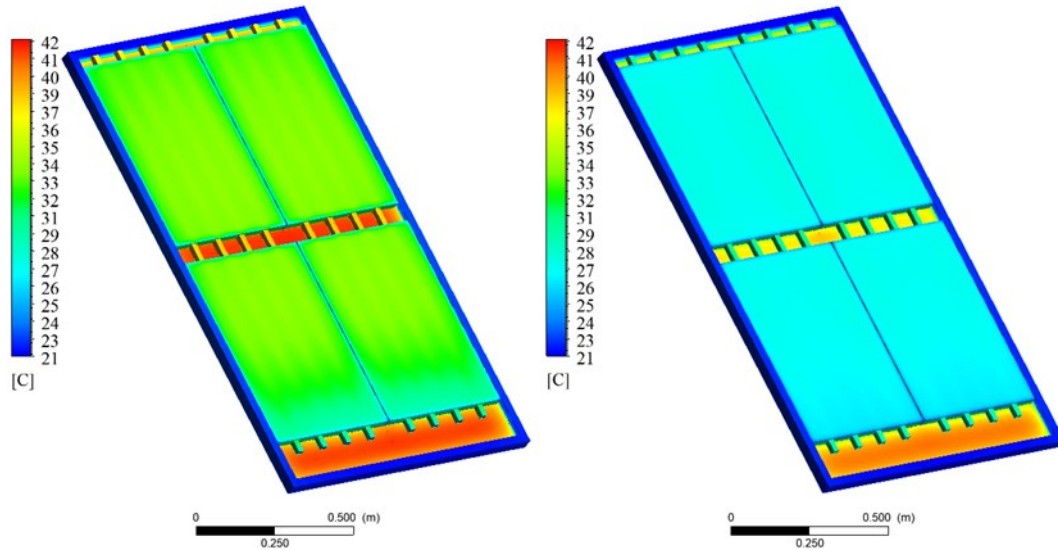


Figure 8.7. Collector back surface temperatures during the transition from passive to active mode (left) and vice versa (right) [121].

In a short period, the temperature of the PVT-PCM collector is sharply reduced, which requires the robustness of the numerical model. Therefore, achieving a high concurrence between the numerical and experimental findings was challenging. Nonetheless, the numerical analysis demonstrates an excellent agreement with the experiment in both passive and active collector operation regimes, Figure 8.8. In the early morning, the temperature difference is at its highest due to the numerical modeling of external radiation. Therefore, Swinbank's temperature model for clear sky can be substituted to ensure more accurate results by the temperate areas ISO 13790 direct temperature model [121]. Another highly critical period successfully managed by the numerical analysis occurs between the 360<sup>th</sup> and 380<sup>th</sup> minute when the collector is exposed to intensive heat transfer due to recirculation pump operation.

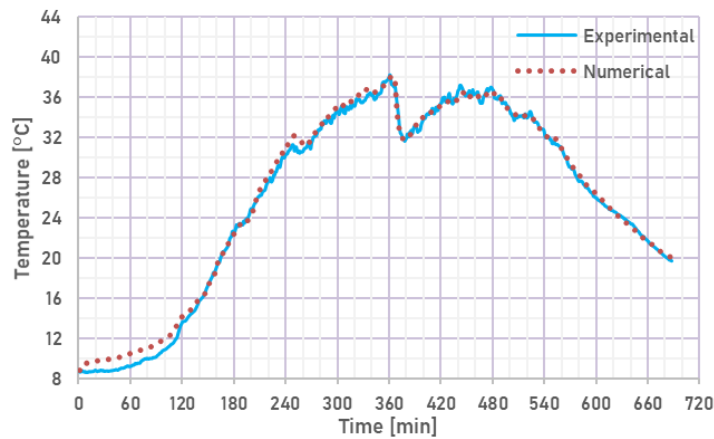


Figure 8.8. Comparison of numerical and experimental temperature data for the front surface of PVT-PCM collector [121].

The mean absolute percentage deviation from the experimental measurements for the front PVT-PCM collector surface temperature was 2.9% [121]. Furthermore, it was found that the temperature difference between the experiment and the numerical analysis for the front surface of the collector was unsubstantial, with an average discrepancy of 0.46°C. The mean absolute percentage deviation from the experimental measurements for the pork fat PCM temperature was 4.9%. The greater deviation observed in the pork fat domain may be attributed to a more intricate heat transfer, including conduction and convection with continuous phase transition. The dominant heat transfer mechanism is conduction in the beginning stages of phase transition. As the PCM liquefaction progresses, convection gains strength and eventually dominates the heat transfer, which was addressed adequately by the Boussinesq approximation in the numerical analysis.

Overall, the numerical model demonstrated exceptional robustness and accuracy, exhibiting high reliability. Furthermore, the numerical approach presented here is versatile enough to be applied across different PVT solutions and other solar technologies. Instead of relying solely on experimental investigations, the researchers can use this verified numerical model of the PVT-PCM collector as a valuable tool and data source for exploring new ideas and enhancing the current designs to create sturdier and more efficient solar systems.

## 9. SCIENTIFIC CONTRIBUTIONS OF PUBLICATIONS

### 9.1. Publication 1: Nano-enhanced phase change materials and fluids in energy applications: A review

#### 9.1.1. Publication summary

The incorporation of nano-enhanced phase change materials and nanofluids in experimental systems across various applications was reviewed. The research also delves into a detailed analysis of the nanomaterials' impact on the base materials' main thermal characteristics. The review showed that nanomaterials addition enhances some thermal properties of materials, i.e., an increase in thermal conductivity by 20% to 100% concerning the base material can be expected. However, some thermal properties, such as latent heat, can be slightly reduced, while specific heat capacity displays variable results. The review reveals that thermal energy storage and cooling systems for photovoltaics have been the most investigated applications. Nonetheless, critical data related to the preparation procedures of nano-enhanced materials are missing. Additionally, the economic and environmental assessment of nano-enhanced systems is not well covered in the reviewed publications. The literature also covers safety aspects and instructions for handling nano-enriched materials poorly. The research concludes by discussing specific issues and future nanomaterials implementation directions related to various applications.

#### 9.1.2. PhD candidate contribution

The PhD candidate participated in research on the specific applications of nanocomposites and nanofluids in experimental systems, primarily in the field of energetics. By examining the possibilities of application in the field of energetics, he noticed a lack of research in the context of phase change nanocomposites for electronics and battery cooling and for improving the efficiency of solar stills. The candidate discovered the lack of economic and environmental factors analysis in earlier studies, concluding that these aspects should be considered in future nano-enriched materials implementations. Furthermore, he analyzed, in detail, the effect of nanomaterials implementation on thermal properties. The candidate observed that the specific heat capacity property can vary in both directions depending on the complex interaction between the nanomaterial and the base material. The PhD candidate conceived the work as a potential reference guide in the field that provides valuable information for forming an integral technological approach. In collaboration with co-authors, the candidate prepared the paper manuscript for submission to the journal.



## **9.2. Publication 2: Comprehensive analysis of preparation strategies for phase change nanocomposites and nanofluids with brief overview of safety equipment**

### **9.2.1. Publication summary**

The employed preparation process strongly influences the physical properties and stability of nanocomposites and nanofluids. A meticulous preparation procedure is essential to produce consistent and reliable homogeneous samples as they are susceptible to the quality of preparation. This study analyzes various methods of preparing nano-enhanced phase change materials and nanofluids and categorizes the key parameters that impact the preparation process. Standard preparation methodologies were analyzed in detail to detect the main problems and challenges while enforcing the preparation procedures. The importance of careful planning of the preparation procedures concerning safety equipment and the toxic potential of nanomaterials was emphasized in the concise and focused overview. The research promotes the rational use of nanomaterials and the reduction of adverse environmental impacts during production and application, which can partially be achieved through a well-suited preparation technique. Furthermore, it provides practical suggestions and insights for researchers to ensure an efficient and effective preparation process for nano-enhanced materials.

### **9.2.2. PhD candidate contribution**

The PhD candidate participated in the research on the preparation methodologies of nanocomposites and nanofluids towards creating relatively homogeneous materials with stable thermophysical properties. In the study, the candidate analyzed different approaches to preparing materials enhanced with nanomaterials while categorizing the preparation methodologies regarding the process's key influencing parameters. The candidate detected the main shortcomings of existing methods and proposed methodological modifications to the preparation process. Furthermore, he also assessed the toxicity of nanomaterials while emphasizing the importance of operator safety and environmental protection from the harmful effects of nanomaterials. The candidate's effort in the research contributed to more efficient production and application of nanocomposites and nanofluids with designed thermophysical properties while rationalizing the use of nanotechnology. In collaboration with co-authors, the candidate prepared the paper manuscript for submission to the journal.

### **9.3. Publication 3: Thermal constant analysis of phase change nanocomposites and discussion on selection strategies with respect to economic constraints**

#### **9.3.1. Publication summary**

Experimental research was conducted to improve RT28HC and RT26 PCMs' thermophysical properties. These materials exhibit low thermal conductivity and reasonable other thermophysical characteristics, which were altered with four types of nanomaterials, including nanoparticles of CuO, ZnO, Ag, and graphene nanoplatelets. The preparation procedure involved four phases and was presented in detail, along with a description of the measurement methodology utilized to examine the thermal constants of novel nano-enhanced phase change materials. The experimental results demonstrated that most of the samples exhibited improvements in their thermal constants. Thermal conductivity and volumetric specific heat capacity improvement ranged between 4% and 21% and 5% to 33%, respectively. However, some thermal properties, such as in the Graphene/RT26 nanocomposite sample, showed notable degradation in certain instances. The study also discussed the strategies for selecting nanomaterials, accounting for the economic facet and experimental investigations on the thermal properties. The results indicated that it is crucial to analyze and evaluate the nanomaterials for a particular application to achieve the suitability and effectiveness of the NEPCMs. Therefore, a thorough and careful material selection process is necessary to ensure optimal performance and desired outcomes of combining nanomaterial and phase change material.

#### **9.3.2. PhD candidate contribution**

The PhD candidate participated in experimental research on phase change materials enriched with nanomaterials. He established a novel four-phase nanocomposite preparation methodology and conducted validation by measuring thermal constants. The candidate detected the importance of safety procedures and proposed an improved methodology for testing toxic materials based on the existing TPS method. The candidate prepared and tested eight newly-composed nanocomposites using the transient TPS method. Furthermore, he noticed the degradation of specific thermal properties, emphasizing the necessity of a new approach to selecting nanomaterials that should be used to design thermal properties considering the intended use. Finally, the candidate proposed a new direction for choosing a suitable nanomaterial for the formation of a nanocomposite, which includes a detailed techno-economic evaluation with regard to the cost of the material, the cost of preparation, the thermophysical properties of the nanomaterial and the expected properties of the nanocomposite in the context of a specific engineering application. In collaboration with co-authors, the candidate prepared the paper manuscript for submission to the journal.

## **9.4. Publication 4: Experimental investigation of novel hybrid phase change materials**

### **9.4.1. Publication summary**

The study investigated the engineering applications potential of hybrid phase change materials made from pork fat (lard) and edible or waste oil derived as the food processing by-product. Lard is an organic PCM readily available and has a notably lower price than traditional PCM materials. Large quantities of lard are discarded annually as it becomes nutritionally unfit for consumption. Therefore, an effort was made to find alternative uses for this natural material. The experimental study revealed that adding oils improves the thermal properties of lard, such as thermal conductivity and volumetric heat capacity, while reducing thermal diffusivity. The best-performing hybrid PCM was a mixture of lard and waste burnt oil, which showed a 1.4% improvement in thermal conductivity and an 11% amplification in volumetric specific heat capacity compared to the pure lard. The proposed hybrid phase change materials are more cost-effective, utilize waste materials, and have a reduced environmental footprint than traditional PCMs. Based on preliminary experimental results, further research should be conducted to explore the potential application of lard for engineering purposes, such as thermal energy storage applications.

### **9.4.2. PhD candidate contribution**

The PhD candidate conducted experimental testing of hybrid phase change materials as a unique combination of animal fat and edible and burnt waste oils. Using the TPS method, he tested the thermal properties of pure lard and hybrids of lard and oil. The candidate observed decreased thermal diffusivity at all oil concentrations in the lard. Furthermore, he undoubtedly proved that it is possible to manipulate the thermal properties of lard by adding oil, creating an organic hybrid material with some thermal properties at the level of commercial chemically complex phase change materials. The candidate determined the potential of newly created hybrid materials in terms of economy and environment and recognized them as an alternative to classic, often toxic, phase change materials, especially in thermal management systems. In collaboration with co-authors, the candidate prepared the paper manuscript for submission to the journal.

## **9.5. Publication 5: Implementation of phase change materials for thermal regulation of photovoltaic thermal systems: Comprehensive analysis of design approaches**

### **9.5.1. Publication summary**

This research aimed to examine various designs of photovoltaic thermal collectors that incorporate phase change materials as a method for managing thermal gains. The study analyzed the different PCMs used in PVT-PCM systems, including discussing their thermal properties. Published experimental studies in the field were reviewed, specifically concerning PVT-PCM collectors in different climates. The investigation results demonstrated that proper design features of PVT-PCM collectors can significantly enhance the overall efficiency of such systems. Specifically, various design features can usually improve electrical efficiency by less than 20%, while thermal efficiency can be improved by up to 70%. The up-to-date literature has not thoroughly addressed the economic and environmental assessment of PVT-PCM systems, which is a major flaw. However, the reported payback period for PTV-PCM system exploitation typically ranges from 4 to 15 years. The review highlighted the need for further research to improve design solutions and to holistically evaluate PVT-PCM designs, including their performance, economic viability, and environmental impact.

### **9.5.2. PhD candidate contribution**

The PhD candidate participated in research on the performance of PVT collectors that incorporate different PCMs for thermal management. He analyzed PCMs in terms of thermal properties and concrete applications in experimental PVT systems. The candidate determined that the interaction of the PCM and the concrete design is a crucial influencing parameter on the overall efficiency of the PVT-PCM system. Furthermore, he noticed that the electrical efficiency behavior is sensitive to the level of interaction between the phase change material and the rest of the system. The candidate accentuated insufficient focus on the economic and environmental aspects of PVT designs in the relevant literature. Finally, he stressed the need for a more detailed approach to the specific system elements and optimization of the PCM thickness to better understand and improve the collector performance in the PVT design life cycle context. In collaboration with co-authors, the candidate prepared the paper manuscript for submission to the journal.

## **9.6. Publication 6: Investigation of heat convection for photovoltaic panel towards efficient design of novel hybrid cooling approach with incorporated organic phase change material**

### **9.6.1. Publication summary**

The study introduces a novel concept of a PVT collector based on a free-standing PV panel upgraded with organic PCM, i.e., pork fat. This hybrid concept integrates passive and active cooling, complemented by a smart regulation system. The novel PVT concept design specifics and basic working principles were presented and elaborated. Furthermore, experimental and numerical analyses were executed to further develop the PVT-PCM experimental setup. Specifically, experimental analysis of convection heat transfer coefficients from freestanding PV panel surfaces was carried out using a wind tunnel. The PV panel convective heat transfer profile was observed for different tilt angles and relative wind angles, including varying wind speeds. Additionally, numerical analysis was performed, and a 12% average deviation was found with respect to experimental readings, indicating reasonable accuracy. The numerical analysis demonstrated that the best cooling effect was achieved at a relative wind angle of  $45^\circ$ . In comparison, the worst was obtained at approximately  $20^\circ$ , which was in line with experimental measurements. The results of this research represent valuable input data for the PVT collector empirical research. The innovative PVT collector concept has great potential to serve as an effective component in various building energy systems, particularly in applications such as air heating or hot water production.

### **9.6.2. PhD candidate contribution**

The PhD candidate proposed a conceptual solution and participated in developing a novel smart hybrid PVT collector that incorporates active water cooling with passive organic PCM-based thermal management. The candidate extensively used numerical simulations combined with an experimental approach to provide suitable input parameters necessary for the holistic numerical analysis of the novel PVT collector concept. For this purpose, he tested the convection coefficients in the wind tunnel using heat flux sensors. Through extensive use of experimental and numerical approaches, he laid the foundations for developing a robust numerical model of the hybrid PVT collector. Regarding the novel PVT collector's practical applicability, the candidate proposed implementing the concept as an integral part of the building energy system for producing electricity and domestic hot water. In collaboration with co-authors, the candidate prepared the paper manuscript for submission to the journal.

## **9.7. Publication 7: Techno-economic and environmental evaluation of photovoltaic-thermal collector design with pork fat as phase change material**

### **9.7.1. Publication summary**

The photovoltaic thermal collector with incorporated PCM was designed and tested in a Mediterranean climate. The thermal management system comprised four individual cooling blocks filled with pork fat PCM. This organic material helped to absorb excess heat and optimize the PV component cooling process. Each cooling block features straight pipes that direct working fluid (water). The PVT-PCM collector design was evaluated based on its performance, economic viability, and environmental impact. Over several months, the system's performance was closely monitored, and the results revealed an impressive maximum energy efficiency of 62.2%. According to estimates, the overall energy efficiency on an annual basis is projected to be less than 50%, indicating a significant gap between the maximum and average energy efficiency levels. The LCOE analysis revealed that the levelized energy cost from the PVT-PCM collector would be from 0.056 to 0.083 € kWh<sup>-1</sup>. According to the analysis of environmental impact, it was found that the PV panel and the utilization of aluminium were the most significant affecting factors.

### **9.7.2. PhD candidate contribution**

The PhD candidate designed and constructed a passive/active PVT collector consisting of a conventional photovoltaic panel and four cooling blocks with organic phase change material. The candidate subjected the experimental PVT collector system to field operating conditions for six months in Mediterranean climatic conditions. Moreover, he ensured continuous monitoring of all measurable parameters of the system's operation during this period. Based on the measured data, he calculated the system's efficiency and extrapolated the research results to estimate the annual performance of the collector. Also, the candidate provided input parameters for the integral evaluation of the PVT-PCM collector design with regard to technical performance and environmental and economic aspects. In collaboration with co-authors, the candidate prepared the paper manuscript for submission to the journal.

## **9.8. Publication 8: Towards resilient operation of photovoltaic-thermal collector with incorporated organic phase change material: Numerical and experimental investigation**

### **9.8.1. Publication summary**

The 3D computational fluid dynamics numerical model of a free-standing PVT-PCM collector was created in ANSYS Fluent software and was used to analyze the behavior of this newly developed collector in variable cloudiness conditions. The multi-parameter transient numerical analysis was validated with experimental measurements for cases of variable air temperature and short-term stochastic alternations in wind and cloudiness. To simulate changing weather conditions, user-defined functions were used to implement time-dependent boundary conditions. Furthermore, additional experiments were conducted using the differential scanning calorimetry technique to determine the thermal properties of organic pork fat PCM. The phase transition behavior of pork fat PCM was examined, and it was discovered that the crystal phase begins to melt at a temperature of 8.3°C, and the process continues until the sample reaches 45.2°C. The measured latent heat of melting was 45.4 J g<sup>-1</sup>. These experimental results were then integrated into a numerical model. The numerical analysis of the operating temperature showed a mean absolute percentage deviation ranging from approximately 2.9% to 4.9% when compared to the experimental data. The deviation varied based on the specific domain being considered. The results obtained from this thorough investigation can be utilized to enhance the current and future designs of PVT-PCM collectors. Or, more precisely, a verified numerical model can be employed to analyze the effect of different operational parameters on the system's behavior.

### **9.8.2. PhD candidate contribution**

The PhD candidate developed a numerical model of the PVT-PCM collector in the Ansys Fluent software package. He prepared the input parameters of the simulation and determined the material properties based on experimental research. Using numerical analysis, the candidate detected the appropriate mushy zone morphology constant of pork fat PCM, which is a crucial parameter of phase transition dynamics. Moreover, he set applicable boundary conditions, considering heat transfer mechanisms and collector domains. The candidate conducted a grid and timestep validation study to achieve an optimal numerical simulation in terms of duration and use of computing resources. Finally, he analyzed and discussed the simulation results in the context of possible numerical analysis improvements and, consequently, positive repercussions on the collector design. In collaboration with co-authors, the candidate prepared the paper manuscript for submission to the journal.

## 10. CONCLUSIONS AND FUTURE DIRECTIONS

States and governments are becoming increasingly aware of the detrimental impact that human activity is having on the planet's resources. This realization is reflected in various international protocols and agreements that address the framework for reversing negative trends and occurrences. There is a collective effort, via ongoing energy transition, to limit the usage of fossil fuels, notorious for releasing toxic materials and greenhouse gases. Legislative bodies in developed countries are actively promoting the adoption of renewable energy sources to mitigate the adverse environmental effects by implementing policies that facilitate their expansion. However, the shift towards renewables is impeded by geopolitical conflicts and tensions, but it is a crucial and necessary step en route to cleaner energy and a sustainable future. Utilizing a cogeneration strategy that relies on renewable energy sources can facilitate the production of clean energy, especially in congested urban areas. This doctoral thesis may contribute to general paradigm alternation in perceiving residential energy production and expenditure.

### 10.1. Summary of main conclusions

The thesis focuses on the novel, robust PVT-PCM collector design yielding hybrid energy from the limited surface area while providing broader research data on the NEPCMs, hybrid organic PCMs, experimental investigations, numerical analysis, etc. The main conclusions of the thesis can be summarized as follows:

- During the early stages of the collector development, there was a consideration to enhance the thermal properties of PCMs by implementing nanotechnology. Hence, an in-depth analysis of the nanomaterials' utilization in PCM-based experimental systems across various applications was conducted. The most researched applications were thermal energy storage and thermal management of photovoltaics. Also, the review revealed that the addition of nanomaterials significantly enhances the specific thermal properties of PCMs, i.e., it was observed that the thermal conductivity can be improved by up to 100% compared to the base material. Furthermore, it was noticed that specific heat capacity and latent heat are also improving by adding nanomaterials in most of the reported research papers, but at a much lower rate than the improvement in thermal conductivity. However, the research results have highlighted the fact that there is a lack of essential data related to the preparation of nano-enhanced materials. Additionally, the economic and environmental assessments of nano-enhanced systems were not well elaborated. Another issue not adequately addressed in the existing literature is the safety concerns and handling guidelines for nano-enhanced materials.
- To partially reduce the evident research gap, an analysis of strategies for preparing nanocomposites and nanofluids was carried out, considering also safety aspects. The processes involved in preparing NEPCMs were meticulously distinguished and



classified based on commonly employed preparation approaches. During the discussion, a detailed explanation was given regarding the safety equipment required when dealing with nanomaterials. Additionally, a baseline assessment was conducted to determine the level of toxicity associated with these materials. It was emphasized that well-designed NEPCM preparation procedures can significantly reduce the negative environmental impact caused by their production and usage.

- Based on the aforementioned research findings, a comprehensive study was carried out to analyze the thermal properties of novel nanocomposites, i.e., NEPCMs. The novel preparation procedure consisting of four distinct phases was elucidated alongside an elaborate explanation of the measurement methodology. The results of the measurements showed significant improvements in the thermal properties of the samples. The samples' thermal conductivity increased between 4% and 21%, while volumetric specific heat capacity increased between 5% and 33%. Furthermore, the research carefully considered nanomaterials' economic aspects and selection strategies, which was necessary before implementing NEPCMs in the PVT collector. However, this idea was not further considered due to concerns regarding the high unit cost, potential toxicity, and uncertain long-term stability of NEPCMs.
- Therefore, novel hybrid materials of animalistic origin, i.e., the combination of pork fat with burnt and sunflower oil, were experimentally tested to provide the PVT concept with alternative PCM. The pork fat was selected due to the favorable economic aspect compared to the conventional PCMs. Moreover, pork fat becomes waste material at a certain point, so the overall approach also has relevance from the circular economy aspect. The findings of the experiment suggest that incorporating oils into pork fat can enhance its thermal properties. The thermally most favorable hybrid PCM was obtained as a combination of pork fat and burnt oil. This combination resulted in 1.4% improved thermal conductivity and 11% enhanced volumetric heat capacity compared to the pure pork fat. Utilizing waste resources, the newly developed hybrid PCMs are more financially feasible and have a lower environmental footprint than traditional PCMs, as previously highlighted.
- To conceptually realize the novel PVT-PCM collector, the ways of PCM integration in PVT systems were analyzed, i.e., existing designs of PVT systems were studied. After a thorough investigation of the existing research findings on PVT-PCM systems across various climates, the experimental works revealed some crucial insights. It was found that the specifics of the PVT-PCM collector design play a vital role in overall efficiency of the system. Moreover, the usual gain in electrical efficiency is generally less than 20%, while thermal efficiency improvement could reach up to 70%; in some designs, it can go even over 70%. A lack of sufficient attention to the economic and environmental implications of the PVT-PCM systems was noted based on the current literature. However, it was found that the investment return period for PVT-PCM designs ranges from 4 to 15 years.

- Conceptually, the novel PVT system uses a hybrid thermal management technique, which utilizes both passive and active cooling approaches. The PVT system passive component comprises four cooling blocks filled with pork fat PCM. Additionally, the system incorporates a smart regulation enabling efficient heat transfer and temperature control within the system. Over several months, the PVT-PCM collector underwent systematic monitoring, during which the highest recorded overall energy efficiency was 62.2%. However, it is anticipated that the average overall energy efficiency will be less than 50% annually. According to the economic analysis, the levelized produced energy cost from the PVT-PCM collector would vary between 0.056 and 0.083 € kWh<sup>-1</sup>. The investment return period for the novel PVT-PCM collector was estimated at four years. This means that energy production costs are relatively low, making it a viable and reliable energy solution. After conducting an environmental assessment analysis of the PVT-PCM collector, it was determined that in terms of material usage, the PV panel and the aluminium parts are key factors affecting the system's environmental footprint.
- To develop a reliable and accurate numerical model of the PVT-PCM collector, a series of experiments were performed to investigate the impact of wind speed and to analyze the phase transition of pork fat PCM. The convective heat transfer coefficients of the collector surfaces were established indirectly by an experimental method that relied on the total heat flux measurements conducted with a heat flux sensor. Differential scanning calorimetry was used to characterize pork fat phase transition and to calculate the latent heat of melting necessary for numerical analysis. The latent heat of melting was estimated at 45.4 J g<sup>-1</sup>, while the melting range of pork fat was from 8.3°C to 45.2°C.
- The multi-parameter 3D CFD model was constructed to numerically assess the innovative free-standing PVT-PCM collector heat transfer in fluctuating weather conditions. The constructed numerical model considers a number of parameters that vary over time, such as clouds, air temperature, and wind. Following the validation process, the numerical model was confirmed to align with the experimental data. The collector temperature numerical forecast deviation from the actual experiment ranged from approximately 2.9% to 4.9% across the considered domains, indicating a high degree of accuracy and reliability in the model's performance.

Generally, the developed PVT-PCM collector demonstrated superior economic features and environmental viability compared to similar designs. Although the proposed design displayed a high level of thermal efficiency, its net gain in electrical efficiency was insufficient compared to the referent PV panel. The experiment utilized premium quality PV panels that experienced minimal degradation of electrical efficiency despite temperature increases. Implementing the proposed hybrid thermal management technique to the lower-grade photovoltaic panels would probably improve electrical efficiency at a higher rate. Hence, the initial investment would be reduced while further ramping up design competitiveness in relation

to existing PVT solutions. However, to avoid possible speculation, it is advised to conduct further research on this and other raised matters in the framework of this thesis.

## 10.2. Future research work

This multidisciplinary doctoral thesis tackles various engineering fields, including energy, nanotechnology, environmental and process engineering, materials, computational fluid dynamics, etc.; therefore, the possibilities of the research ramifications are diverse. The potential avenues for further exploration involve analyzing and systematizing the novel PVT-PCM collector applications in the energy sector and further experimental and numerical investigations arising from the conducted research. To elaborate further, potential directions for future work include:

- The thermal cyclic analysis of the developed PCMs' long-term stability and broader phase transition analysis using differential scanning calorimetry. These are required to fully understand the potential of the research and its implications, although significant strides in the field of phase change materials were made.
- Research of various combinations of nanomaterials and phase change materials to expand the range of NEPCM options available for multiple applications. These NEPCMs should offer enhanced thermal properties and improved performance compared to traditional PCMs, ultimately leading to more efficient and robust engineering solutions.
- Exploring different types of hybrid PCMs incorporating waste materials to identify those that could positively boost environmental aspects while reducing unit cost. By conducting techno-economic and environmental analysis of these hybrid PCMs, new ways of their use may emerge, ramping up PCM technology advancement.
- Experimental smart regulation fine-tuning of the PVT-PCM collector working regimes based on the research outcomes to increase the energy yield, i.e., optimizing the passive to active working regime shift and vice versa.
- Modifying the current design or creating an entirely new PVT-PCM collector by utilizing a verified numerical model to experiment with various PCMs, thermal absorber geometries, insulations, operating modes, and more. To ensure accuracy and avoid uncertain assumptions, it is crucial to conduct a focused investigation of single-parameter modification on the justified numerical model to isolate the singular impact on the design. This gradual approach could lead to the identification of optimal system configurations for different climates and local environments to achieve higher overall energy yield.
- To reduce environmental impact, it would be beneficial to optimize PVT-PCM collector design and focus on the reduction of raw materials, especially metals, as they are associated with the highest environmental footprints.

## BIBLIOGRAPHY

- [1] Montreal Protocol, <https://www.unep.org/ozonaction/who-we-are/about-montreal-protocol>, [Accessed, May 19, 2023].
- [2] Kyoto Protocol, [https://unfccc.int/kyoto\\_protocol](https://unfccc.int/kyoto_protocol), [Accessed, May 19, 2023].
- [3] Paris Agreement, <https://unfccc.int/process-and-meetings/the-paris-agreement>, [Accessed, May 19, 2023].
- [4] A. T. Hoang, V. V. Pham, and X. P. Nguyen, Integrating renewable sources into energy system for smart city as a sagacious strategy towards clean and sustainable process, *J Clean Prod*, 305, 127161, Jul. 2021, doi: 10.1016/j.jclepro.2021.127161.
- [5] E. Tunçbilek, M. Arıcı, M. Krajić, Y. Li, M. Jurčević, and S. Nižetić, Impact of nano-enhanced phase change material on thermal performance of building envelope and energy consumption, *Int J Energy Res*, 46, 14, 20249–20264, Nov. 2022, doi: 10.1002/er.8200.
- [6] IEA/Buildings, <https://www.iea.org/energy-system/buildings#tracking>, [Accessed, Oct. 02, 2023].
- [7] N. Hossein Motlagh, M. Mohammadrezaei, J. Hunt, and B. Zakeri, Internet of Things (IoT) and the Energy Sector, *Energies (Basel)*, 13, 2, 494, Jan. 2020, doi: 10.3390/en13020494.
- [8] IEA/Renewables Data Explorer, <https://www.iea.org/data-and-statistics/data-tools/renewables-data-explorer>, [Accessed, Oct. 03, 2023].
- [9] IEA/Renewables 2022-Analysis and forecast to 2027, <https://iea.blob.core.windows.net/assets/ada7af90-e280-46c4-a577-df2e4fb44254/Renewables2022.pdf>, [Accessed, Oct. 03, 2023].
- [10] S. Nižetić, M. Jurčević, D. Čoko, M. Arıcı, and A. T. Hoang, Implementation of phase change materials for thermal regulation of photovoltaic thermal systems: Comprehensive analysis of design approaches, *Energy*, 228, 120546, Aug. 2021, doi: 10.1016/j.energy.2021.120546.
- [11] S. Nižetić, M. Jurčević, D. Čoko, and M. Arıcı, A novel and effective passive cooling strategy for photovoltaic panel, *Renewable and Sustainable Energy Reviews*, 145, 111164, Jul. 2021, doi: 10.1016/J.RSER.2021.111164.
- [12] S. Nižetić, E. Giama, and A. M. Papadopoulos, Comprehensive analysis and general economic-environmental evaluation of cooling techniques for photovoltaic panels, Part II: Active cooling techniques, *Energy Convers Manag*, 155, 301–323, Jan. 2018, doi: 10.1016/j.enconman.2017.10.071.
- [13] SCH International Energy Agency, <https://task60.iea-shc.org/article?NewsID=214>, [Accessed, May 19, 2022].
- [14] L. Wang *et al.*, A holistic and state-of-the-art review of nanotechnology in solar cells, *Sustainable Energy Technologies and Assessments*, 54, 102864, Dec. 2022, doi: 10.1016/j.seta.2022.102864.

- [15] T. A. Saleh, Nanomaterials: Classification, properties, and environmental toxicities, *Environ Technol Innov*, 20, 101067, Nov. 2020, doi: 10.1016/j.eti.2020.101067.
- [16] P. S. Goh, K. C. Wong, and A. F. Ismail, Nanocomposite Membranes for Liquid and Gas Separations from the Perspective of Nanostructure Dimensions, *Membranes (Basel)*, 10, 10, 297, Oct. 2020, doi: 10.3390/membranes10100297.
- [17] M. Byakodi *et al.*, Emerging 0D, 1D, 2D, and 3D nanostructures for efficient point-of-care biosensing, *Biosens Bioelectron X*, 12, 100284, Dec. 2022, doi: 10.1016/j.biosx.2022.100284.
- [18] J. Li *et al.*, Development and application of nanomaterials, nanotechnology and nanomedicine for treating hematological malignancies, *J Hematol Oncol*, 16, 1, 65, Jun. 2023, doi: 10.1186/s13045-023-01460-2.
- [19] A. Shabir, S. A. Hashmi, A. A. Hor, C. M. Julien, and S. S. Islam, Long-term prospects of nano-carbon and its derivatives as anode materials for lithium-ion batteries – A review, *J Energy Storage*, 72, 108178, Nov. 2023, doi: 10.1016/j.est.2023.108178.
- [20] M. Sharma, N. Hussain, S. Mohanty, P. Puzari, and P. Deb, Robust energy storage performance enabled by the interacting interface of an epitaxial hybrid nanostructure based flexible supercapacitor, *J Energy Storage*, 72, 108345, Nov. 2023, doi: 10.1016/j.est.2023.108345.
- [21] D. Starodubtseva and O. Tikhonova, Peculiarities of Electron Wave Packet Dynamics in Planar Nanostructures in the Presence of Magnetic and Electric Fields, *Symmetry (Basel)*, 14, 10, 2215, Oct. 2022, doi: 10.3390/sym14102215.
- [22] E. Núñez-Carmona, M. Abbatangelo, D. Zappa, E. Comini, G. Sberveglieri, and V. Sberveglieri, Nanostructured MOS Sensor for the Detection, Follow up, and Threshold Pursuing of *Campylobacter Jejuni* Development in Milk Samples, *Sensors*, 20, 7, 2009, Apr. 2020, doi: 10.3390/s20072009.
- [23] Scopus, <https://www.scopus.com/search/form.uri?display=basic#basic>, [Accessed, Jul. 25, 2023].
- [24] C. Deng, S. Zhang, Z. Dong, and Y. Shang, 1D nanostructured sodium vanadium oxide as a novel anode material for aqueous sodium ion batteries, *Nano Energy*, 4, 49–55, Mar. 2014, doi: 10.1016/j.nanoen.2013.12.014.
- [25] C. Xu, M. Nasrollahzadeh, M. Sajjadi, M. Maham, R. Luque, and A. R. Puente-Santiago, Benign-by-design nature-inspired nanosystems in biofuels production and catalytic applications, *Renewable and Sustainable Energy Reviews*, 112, 195–252, Sep. 2019, doi: 10.1016/j.rser.2019.03.062.
- [26] Y. Yang, M. C. Gupta, and K. L. Dudley, Towards cost-efficient EMI shielding materials using carbon nanostructure-based nanocomposites, *Nanotechnology*, 18, 34, 345701, Aug. 2007, doi: 10.1088/0957-4484/18/34/345701.
- [27] V. K. Mariappan *et al.*, Antimonene dendritic nanostructures: Dual-functional material for high-performance energy storage and harvesting devices, *Nano Energy*, 77, 105248, Nov. 2020, doi: 10.1016/j.nanoen.2020.105248.

- [28] P. M. Rajanna, P. D. Lund, and A. G. Nasibulin, Hybrid heterojunction solar cells based on single-walled carbon nanotubes and amorphous silicon thin films, *WIREs Energy and Environment*, 11, 1, Jan. 2022, doi: 10.1002/wene.402.
- [29] L. Bacakova *et al.*, Applications of Nanocellulose/Nanocarbon Composites: Focus on Biotechnology and Medicine, *Nanomaterials*, 10, 2, 196, Jan. 2020, doi: 10.3390/nano10020196.
- [30] S. H. Bandaru, V. Becerra, S. Khanna, J. Radulovic, D. Hutchinson, and R. Khusainov, A Review of Photovoltaic Thermal (PVT) Technology for Residential Applications: Performance Indicators, Progress, and Opportunities, *Energies (Basel)*, 14, 13, 3853, Jun. 2021, doi: 10.3390/en14133853.
- [31] G. Alva, L. Liu, X. Huang, and G. Fang, Thermal energy storage materials and systems for solar energy applications, *Renewable and Sustainable Energy Reviews*, 68, 693–706, Feb. 2017, doi: 10.1016/j.rser.2016.10.021.
- [32] B. D. Malhotra and Md. A. Ali, Nanocomposite Materials, in *Nanomaterials for Biosensors*, Elsevier, 2018, 145–159. doi: 10.1016/B978-0-323-44923-6.00005-4.
- [33] M. S. Hasnain and A. K. Nayak, Nanocomposites for improved orthopedic and bone tissue engineering applications, in *Applications of Nanocomposite Materials in Orthopedics*, Elsevier, 2019, 145–177. doi: 10.1016/B978-0-12-813740-6.00008-9.
- [34] S. Nižetić, M. Jurčević, M. Arıcı, A. V. Arasu, and G. Xie, Nano-enhanced phase change materials and fluids in energy applications: A review, *Renewable and Sustainable Energy Reviews*, 129, 109931, Sep. 2020, doi: 10.1016/j.rser.2020.109931.
- [35] A. A. Altohamy, M. F. Abd Rabbo, R. Y. Sakr, and A. A. A. Attia, Effect of water based Al<sub>2</sub>O<sub>3</sub> nanoparticle PCM on cool storage performance, *Appl Therm Eng*, 84, 331–338, Jun. 2015, doi: 10.1016/j.applthermaleng.2015.03.066.
- [36] Q. Wang, W. Wei, D. Li, H. Qi, F. Wang, and M. Arıcı, Experimental investigation of thermal radiative properties of Al<sub>2</sub>O<sub>3</sub>-paraffin nanofluid, *Solar Energy*, 177, 420–426, Jan. 2019, doi: 10.1016/j.solener.2018.11.034.
- [37] M. Barthwal, A. Dhar, and S. Powar, Effect of Nanomaterial Inclusion in Phase Change Materials for Improving the Thermal Performance of Heat Storage: A Review, *ACS Appl Energy Mater*, 4, 8, 7462–7480, Aug. 2021, doi: 10.1021/acsaem.1c01268.
- [38] K. Tofani and S. Tiari, Nano-Enhanced Phase Change Materials in Latent Heat Thermal Energy Storage Systems: A Review, *Energies (Basel)*, 14, 13, 3821, Jun. 2021, doi: 10.3390/en14133821.
- [39] C. Yadav and R. R. Sahoo, Thermal analysis comparison of nano-additive PCM-based engine waste heat recovery thermal storage systems: an experimental study, *J Therm Anal Calorim*, 147, 3, 2785–2802, Feb. 2022, doi: 10.1007/s10973-021-10611-x.
- [40] A. Qaderi and F. Veysi, Investigation of a water-NEPCM cooling thermal management system for cylindrical 18650 Li-ion batteries, *Energy*, 244, 122570, Apr. 2022, doi: 10.1016/j.energy.2021.122570.

- [41] G. Karimi, M. Azizi, and A. Babapoor, Experimental study of a cylindrical lithium ion battery thermal management using phase change material composites, *J Energy Storage*, 8, 168–174, Nov. 2016, doi: 10.1016/j.est.2016.08.005.
- [42] U. N. Temel, Passive thermal management of a simulated battery pack at different climate conditions, *Appl Therm Eng*, 158, 113796, Jul. 2019, doi: 10.1016/j.applthermaleng.2019.113796.
- [43] M. Alimohammadi, Y. Aghli, E. S. Alavi, M. Sardarabadi, and M. Passandideh-Fard, Experimental investigation of the effects of using nano/phase change materials (NPCM) as coolant of electronic chipsets, under free and forced convection, *Appl Therm Eng*, 111, 271–279, Jan. 2017, doi: 10.1016/j.applthermaleng.2016.09.028.
- [44] Y. Liu *et al.*, Improvement of cooling of a high heat flux CPU by employing a cooper foam and NEPCM/water suspension, *J Energy Storage*, 55, 105682, Nov. 2022, doi: 10.1016/j.est.2022.105682.
- [45] M. T. Chaichan and H. A. Kazem, Single slope solar distillator productivity improvement using phase change material and Al<sub>2</sub>O<sub>3</sub> nanoparticle, *Solar Energy*, 164, 370–381, Apr. 2018, doi: 10.1016/J.SOLENER.2018.02.049.
- [46] D. Dsilva Winfred Rufuss, L. Suganthi, S. Iniyan, and P. A. Davies, Effects of nanoparticle-enhanced phase change material (NPCM) on solar still productivity, *J Clean Prod*, 192, 9–29, Aug. 2018, doi: 10.1016/J.JCLEPRO.2018.04.201.
- [47] G. Alva, Y. Lin, and G. Fang, An overview of thermal energy storage systems, *Energy*, 144, 341–378, Feb. 2018, doi: 10.1016/j.energy.2017.12.037.
- [48] P. Bose and V. A. Amirtham, A review on thermal conductivity enhancement of paraffinwax as latent heat energy storage material, *Renewable and Sustainable Energy Reviews*, 65, 81–100, Nov. 2016, doi: 10.1016/j.rser.2016.06.071.
- [49] M. Ghalambaz *et al.*, Melting process of the nano-enhanced phase change material (NePCM) in an optimized design of shell and tube thermal energy storage (TES): Taguchi optimization approach, *Appl Therm Eng*, 193, 116945, Jul. 2021, doi: 10.1016/j.applthermaleng.2021.116945.
- [50] S. C. Lin and H. H. Al-Kayiem, Evaluation of copper nanoparticles – Paraffin wax compositions for solar thermal energy storage, *Solar Energy*, 132, 267–278, Jul. 2016, doi: 10.1016/j.solener.2016.03.004.
- [51] H. K. Sharma, S. Kumar, S. Kumar, and S. K. Verma, Performance investigation of flat plate solar collector with nanoparticle enhanced integrated thermal energy storage system, *J Energy Storage*, 55, 105681, Nov. 2022, doi: 10.1016/j.est.2022.105681.
- [52] R. Elbahjaoui and H. El Qarnia, Performance evaluation of a solar thermal energy storage system using nanoparticle-enhanced phase change material, *Int J Hydrogen Energy*, 44, 3, 2013–2028, Jan. 2019, doi: 10.1016/j.ijhydene.2018.11.116.
- [53] S. A. Nada and D. H. El-Nagar, Possibility of using PCMs in temperature control and performance enhancements of free stand and building integrated PV modules, *Renew Energy*, 127, 630–641, Nov. 2018, doi: 10.1016/j.renene.2018.05.010.

- [54] S. A. Nada, D. H. El-Nagar, and H. M. S. Hussein, Improving the thermal regulation and efficiency enhancement of PCM-Integrated PV modules using nano particles, *Energy Convers Manag*, 166, 735–743, Jun. 2018, doi: 10.1016/j.enconman.2018.04.035.
- [55] S. Sharma, L. Micheli, W. Chang, A. A. Tahir, K. S. Reddy, and T. K. Mallick, Nano-enhanced Phase Change Material for thermal management of BICPV, *Appl Energy*, 208, 719–733, Dec. 2017, doi: 10.1016/j.apenergy.2017.09.076.
- [56] A. M. Bassam, K. Sopian, A. Ibrahim, M. F. Fauzan, A. B. Al-Aasam, and G. Y. Abusaibaa, Experimental analysis for the photovoltaic thermal collector (PVT) with nano PCM and micro-fins tube nanofluid, *Case Studies in Thermal Engineering*, 41, 102579, Jan. 2023, doi: 10.1016/j.csite.2022.102579.
- [57] S. Harish, D. Orejon, Y. Takata, and M. Kohno, Thermal conductivity enhancement of lauric acid phase change nanocomposite with graphene nanoplatelets, *Appl Therm Eng*, 80, 205–211, Apr. 2015, doi: 10.1016/J.APPLTHERMALENG.2015.01.056.
- [58] L. Colla, L. Fedele, S. Mancin, L. Danza, and O. Manca, Nano-PCMs for enhanced energy storage and passive cooling applications, *Appl Therm Eng*, 110, 584–589, Jan. 2017, doi: 10.1016/J.APPLTHERMALENG.2016.03.161.
- [59] Y. Liu and Y. Yang, Investigation of specific heat and latent heat enhancement in hydrate salt based TiO<sub>2</sub> nanofluid phase change material, *Appl Therm Eng*, 124, 533–538, Sep. 2017, doi: 10.1016/J.APPLTHERMALENG.2017.05.150.
- [60] N. Putra, M. Amin, E. A. Kosasih, R. A. Luanto, and N. A. Abdullah, Characterization of the thermal stability of RT 22 HC/graphene using a thermal cycle method based on thermoelectric methods, *Appl Therm Eng*, 124, 62–70, Sep. 2017, doi: 10.1016/J.APPLTHERMALENG.2017.06.009.
- [61] S. Ebadi, S. Humaira Tasnim, A. Abbas Aliabadi, and S. Mahmud, Geometry and nanoparticle loading effects on the bio-based nano-PCM filled cylindrical thermal energy storage system, *Appl Therm Eng*, 141, 724–740, Aug. 2018, doi: 10.1016/J.APPLTHERMALENG.2018.05.091.
- [62] M. Chieruzzi, G. F. Cerritelli, A. Miliozzi, J. M. Kenny, and L. Torre, Heat capacity of nanofluids for solar energy storage produced by dispersing oxide nanoparticles in nitrate salt mixture directly at high temperature, *Solar Energy Materials and Solar Cells*, 167, 60–69, Aug. 2017, doi: 10.1016/J.SOLMAT.2017.04.011.
- [63] Y. Liu and Y. Yang, Investigation of specific heat and latent heat enhancement in hydrate salt based TiO<sub>2</sub> nanofluid phase change material, *Appl Therm Eng*, 124, 533–538, Sep. 2017, doi: 10.1016/J.APPLTHERMALENG.2017.05.150.
- [64] R. J. Warzoha, R. M. Weigand, and A. S. Fleischer, Temperature-dependent thermal properties of a paraffin phase change material embedded with herringbone style graphite nanofibers, *Appl Energy*, 137, 716–725, Jan. 2015, doi: 10.1016/J.APENERGY.2014.03.091.
- [65] R. Reji Kumar, M. Samykano, A. K. Pandey, K. Kadirgama, and V. V. Tyagi, Phase change materials and nano-enhanced phase change materials for thermal energy storage in photovoltaic thermal systems: A futuristic approach and its technical challenges,



- Renewable and Sustainable Energy Reviews*, 133, 110341, Nov. 2020, doi: 10.1016/J.RSER.2020.110341.
- [66] M. L. G. Ho, C. S. Oon, L. L. Tan, Y. Wang, and Y. M. Hung, A review on nanofluids coupled with extended surfaces for heat transfer enhancement, *Results in Engineering*, 17, 100957, Mar. 2023, doi: 10.1016/J.RINENG.2023.100957.
- [67] M. Jurčević, S. Nižetić, M. Arıcı, and P. Ocloń, Comprehensive analysis of preparation strategies for phase change nanocomposites and nanofluids with brief overview of safety equipment, *J Clean Prod*, 274, 122963, Nov. 2020, doi: 10.1016/J.JCLEPRO.2020.122963.
- [68] T. Wu and M. Tang, Review of the effects of manufactured nanoparticles on mammalian target organs, *Journal of Applied Toxicology*, 38, 1, 25–40, Jan. 2018, doi: 10.1002/jat.3499.
- [69] W. N. Missaoui, R. D. Arnold, and B. S. Cummings, Toxicological status of nanoparticles: What we know and what we don't know, *Chem Biol Interact*, 295, 1–12, Nov. 2018, doi: 10.1016/J.CBI.2018.07.015.
- [70] A. Nel, T. Xia, L. Mädler, and N. Li, Toxic Potential of Materials at the Nanolevel, *Science (1979)*, 311, 5761, 622–627, Feb. 2006, doi: 10.1126/science.1114397.
- [71] L. Vinches, N. Testori, P. Dolez, G. Perron, K. J. Wilkinson, and S. Hallé, Experimental evaluation of the penetration of TiO<sub>2</sub> nanoparticles through protective clothing and gloves under conditions simulating occupational use, *Nanoscience Methods*, 2, 1, 1–15, Dec. 2013, doi: 10.1080/21642311.2013.771840.
- [72] A. S. Fonseca *et al.*, Particle release and control of worker exposure during laboratory-scale synthesis, handling and simulated spills of manufactured nanomaterials in fume hoods, *Journal of Nanoparticle Research*, 20, 2, 48, Feb. 2018, doi: 10.1007/s11051-018-4136-3.
- [73] M. Jurčević, S. Nižetić, M. Arıcı, A. Hoang Anh Tuan, E. Giama, and A. Papadopoulos, Thermal constant analysis of phase change nanocomposites and discussion on selection strategies with respect to economic constraints, *Sustainable Energy Technologies and Assessments*, 43, 100957, Feb. 2021, doi: 10.1016/J.SETA.2020.100957.
- [74] S. E. Gustafsson, Transient plane source techniques for thermal conductivity and thermal diffusivity measurements of solid materials, *Review of Scientific Instruments*, 62, 3, 797–804, Mar. 1991, doi: 10.1063/1.1142087.
- [75] M. Jurčević, S. Nižetić, D. Čoko, A. T. Hoang, and A. M. Papadopoulos, Experimental investigation of novel hybrid phase change materials, *Clean Technol Environ Policy*, 24, 1, 201–212, Jan. 2022, doi: 10.1007/s10098-021-02106-y.
- [76] S. Nižetić, M. Arıcı, F. Bilgin, and F. Grubišić-Čabo, Investigation of pork fat as potential novel phase change material for passive cooling applications in photovoltaics, *J Clean Prod*, 170, 1006–1016, Jan. 2018, doi: 10.1016/J.JCLEPRO.2017.09.164.
- [77] S. S. Chandel and T. Agarwal, Review of current state of research on energy storage, toxicity, health hazards and commercialization of phase changing materials, *Renewable*

- and Sustainable Energy Reviews*, 67, 581–596, Jan. 2017, doi: 10.1016/J.RSER.2016.09.070.
- [78] T. D. Tsoutsos, S. Tournaki, O. Paraíba, and S. D. Kaminaris, The Used Cooking Oil-to-biodiesel chain in Europe assessment of best practices and environmental performance, *Renewable and Sustainable Energy Reviews*, 54, 74–83, Feb. 2016, doi: 10.1016/J.RSER.2015.09.039.
- [79] C. Baldassarri, S. Sala, A. Caverzan, and M. Lamperti Tornaghi, Environmental and spatial assessment for the ecodesign of a cladding system with embedded Phase Change Materials, *Energy Build*, 156, 374–389, Dec. 2017, doi: 10.1016/J.ENBUILD.2017.09.011.
- [80] M. Dekamin, M. Barmaki, and A. kanooni, Selecting the best environmental friendly oilseed crop by using Life Cycle Assessment, water footprint and analytic hierarchy process methods, *J Clean Prod*, 198, 1239–1250, Oct. 2018, doi: 10.1016/J.JCLEPRO.2018.07.115.
- [81] Z. Fu *et al.*, Experimental investigation on the enhanced performance of a solar PVT system using micro-encapsulated PCMs, *Energy*, 228, 120509, Aug. 2021, doi: 10.1016/j.energy.2021.120509.
- [82] M. Carmona, A. Palacio Bastos, and J. D. García, Experimental evaluation of a hybrid photovoltaic and thermal solar energy collector with integrated phase change material (PVT-PCM) in comparison with a traditional photovoltaic (PV) module, *Renew Energy*, 172, 680–696, Jul. 2021, doi: 10.1016/j.renene.2021.03.022.
- [83] M. M. Islam, M. Hasanuzzaman, N. A. Rahim, A. K. Pandey, M. Rawa, and L. Kumar, Real time experimental performance investigation of a NePCM based photovoltaic thermal system: An energetic and exergetic approach, *Renew Energy*, 172, 71–87, Jul. 2021, doi: 10.1016/J.RENENE.2021.02.169.
- [84] R. Ahmadi, F. Monadinia, and M. Maleki, Passive/active photovoltaic-thermal (PVT) system implementing infiltrated phase change material (PCM) in PS-CNT foam, *Solar Energy Materials and Solar Cells*, 222, 110942, Apr. 2021, doi: 10.1016/J.SOLMAT.2020.110942.
- [85] W. Lin, Z. Ma, S. Wang, M. I. Sohel, and E. lo Cascio, Experimental investigation and two-level model-based optimisation of a solar photovoltaic thermal collector coupled with phase change material thermal energy storage, *Appl Therm Eng*, 182, 116098, Jan. 2021, doi: 10.1016/J.APPLTHERMALENG.2020.116098.
- [86] J. Song and B. Sobhani, Energy and exergy performance of an integrated desiccant cooling system with photovoltaic/thermal using phase change material and maisotsenko cooler, *J Energy Storage*, 32, 101698, Dec. 2020, doi: 10.1016/J.EST.2020.101698.
- [87] R. Tariq, J. Xamán, A. Bassam, L. J. Ricalde, and M. A. E. Soberanis, Multidimensional assessment of a photovoltaic air collector integrated phase changing material considering Mexican climatic conditions, *Energy*, 209, 118304, Oct. 2020, doi: 10.1016/J.ENERGY.2020.118304.

- [88] A. Naghdbishi, M. E. Yazdi, and G. Akbari, Experimental investigation of the effect of multi-wall carbon nanotube – Water/glycol based nanofluids on a PVT system integrated with PCM-covered collector, *Appl Therm Eng*, 178, 115556, Sep. 2020, doi: 10.1016/J.APPLTHERMALENG.2020.115556.
- [89] G. Gan and Y. Xiang, Experimental investigation of a photovoltaic thermal collector with energy storage for power generation, building heating and natural ventilation, *Renew Energy*, 150, 12–22, May 2020, doi: 10.1016/J.RENENE.2019.12.112.
- [90] A. Hassan *et al.*, Thermal management and uniform temperature regulation of photovoltaic modules using hybrid phase change materials-nanofluids system, *Renew Energy*, 145, 282–293, Jan. 2020, doi: 10.1016/J.RENENE.2019.05.130.
- [91] H. Fayaz, N. A. Rahim, M. Hasanuzzaman, R. Nasrin, and A. Rivai, Numerical and experimental investigation of the effect of operating conditions on performance of PVT and PVT-PCM, *Renew Energy*, 143, 827–841, Dec. 2019, doi: 10.1016/J.RENENE.2019.05.041.
- [92] T. Maatallah, R. Zachariah, and F. G. Al-Amri, Exergo-economic analysis of a serpentine flow type water based photovoltaic thermal system with phase change material (PVT-PCM/water), *Solar Energy*, 193, 195–204, Nov. 2019, doi: 10.1016/J.SOLENER.2019.09.063.
- [93] R. Simón-Allué, I. Guedea, R. Villén, and G. Brun, Experimental study of Phase Change Material influence on different models of Photovoltaic-Thermal collectors, *Solar Energy*, 190, 1–9, Sep. 2019, doi: 10.1016/J.SOLENER.2019.08.005.
- [94] M. S. Hossain, A. K. Pandey, J. Selvaraj, N. A. Rahim, M. M. Islam, and V. v. Tyagi, Two side serpentine flow based photovoltaic-thermal-phase change materials (PVT-PCM) system: Energy, exergy and economic analysis, *Renew Energy*, 136, 1320–1336, Jun. 2019, doi: 10.1016/J.RENENE.2018.10.097.
- [95] N. Choubineh, H. Jannesari, and A. Kasaeian, Experimental study of the effect of using phase change materials on the performance of an air-cooled photovoltaic system, *Renewable and Sustainable Energy Reviews*, 101, 103–111, Mar. 2019, doi: 10.1016/J.RSER.2018.11.001.
- [96] M. O. Lari and A. Z. Sahin, Effect of retrofitting a silver/water nanofluid-based photovoltaic/thermal (PV/T) system with a PCM-thermal battery for residential applications, *Renew Energy*, 122, 98–107, Jul. 2018, doi: 10.1016/J.RENENE.2018.01.034.
- [97] M. Hosseinzadeh, M. Sardarabadi, and M. Passandideh-Fard, Energy and exergy analysis of nanofluid based photovoltaic thermal system integrated with phase change material, *Energy*, 147, 636–647, Mar. 2018, doi: 10.1016/j.energy.2018.01.073.
- [98] M. S. Hossain, A. K. Pandey, J. Selvaraj, N. A. Rahim, M. M. Islam, and V. v. Tyagi, Two side serpentine flow based photovoltaic-thermal-phase change materials (PVT-PCM) system: Energy, exergy and economic analysis, *Renew Energy*, 136, 1320–1336, Jun. 2019, doi: 10.1016/J.RENENE.2018.10.097.

- [99] A. H. A. Al-Waeli *et al.*, Evaluation of the nanofluid and nano-PCM based photovoltaic thermal (PVT) system: An experimental study, *Energy Convers Manag*, 151, 693–708, Nov. 2017, doi: 10.1016/J.ENCONMAN.2017.09.032.
- [100] M. F. I. al Imam, R. A. Beg, M. S. Rahman, and M. Z. H. Khan, Performance of PVT solar collector with compound parabolic concentrator and phase change materials, *Energy Build*, 113, 139–144, Feb. 2016, doi: 10.1016/J.ENBUILD.2015.12.038.
- [101] W. Lin, Z. Ma, M. I. Sohel, and P. Cooper, Development and evaluation of a ceiling ventilation system enhanced by solar photovoltaic thermal collectors and phase change materials, *Energy Convers Manag*, 88, 218–230, Dec. 2014, doi: 10.1016/J.ENCONMAN.2014.08.019.
- [102] D. Das, U. Bordoloi, A. D. Kamble, H. H. Muigai, R. K. Pai, and P. Kalita, Performance investigation of a rectangular spiral flow PV/T collector with a novel form-stable composite material, *Appl Therm Eng*, 182, 116035, Jan. 2021, doi: 10.1016/J.APPLTHERMALENG.2020.116035.
- [103] S. Nižetić, A. M. Papadopoulos, and E. Giama, Comprehensive analysis and general economic-environmental evaluation of cooling techniques for photovoltaic panels, Part I: Passive cooling techniques, *Energy Convers Manag*, 149, 334–354, Oct. 2017, doi: 10.1016/J.ENCONMAN.2017.07.022.
- [104] Q. Mao, Y. Li, Y. Zhang, and C. Zhang, Numerical and Experimental Investigation on Heat Transfer Performance of a Solar Single Storage Tank, *Journal of Thermal Science*, 30, 5, 1596–1606, Sep. 2021, doi: 10.1007/s11630-021-1438-z.
- [105] M. A. Bashir, A. M. Daabo, K. P. Amber, M. S. Khan, A. Arshad, and H. Elahi, Effect of phase change materials on the short-term thermal storage in the solar receiver of dish-micro gas turbine systems: A numerical analysis, *Appl Therm Eng*, 195, 117179, Aug. 2021, doi: 10.1016/J.APPLTHERMALENG.2021.117179.
- [106] S. Mousavi, A. Kasaeian, M. B. Shafii, and M. H. Jahangir, Numerical investigation of the effects of a copper foam filled with phase change materials in a water-cooled photovoltaic/thermal system, *Energy Convers Manag*, 163, 187–195, May 2018, doi: 10.1016/J.ENCONMAN.2018.02.039.
- [107] J. Darkwa, J. Calautit, D. Du, and G. Kokogianakis, A numerical and experimental analysis of an integrated TEG-PCM power enhancement system for photovoltaic cells, *Appl Energy*, 248, 688–701, Aug. 2019, doi: 10.1016/J.APENERGY.2019.04.147.
- [108] A. Kazemian, A. Salari, A. Hakkaki-Fard, and T. Ma, Numerical investigation and parametric analysis of a photovoltaic thermal system integrated with phase change material, *Appl Energy*, 238, 734–746, Mar. 2019, doi: 10.1016/J.APENERGY.2019.01.103.
- [109] S. Aneli, R. Arena, and A. Gagliano, Numerical Simulations of a PV Module with Phase Change Material (PV-PCM) under Variable Weather Conditions, *International Journal of Heat and Technology*, 39, 2, 643–652, Apr. 2021, doi: 10.18280/ijht.390236.

- [110] G. Triscari, M. Santovito, M. Bressan, and D. Papurello, Experimental and model validation of a phase change material heat exchanger integrated into a real building, *Int J Energy Res*, 45, 12, 18222–18236, Oct. 2021, doi: 10.1002/er.7037.
- [111] M. Kirincic, A. Trp, and K. Lenic, Numerical evaluation of the latent heat thermal energy storage performance enhancement by installing longitudinal fins, *J Energy Storage*, 42, 103085, Oct. 2021, doi: 10.1016/J.EST.2021.103085.
- [112] M. S. Mahdi, H. B. Mahood, A. A. Alammar, and A. A. Khadom, Numerical investigation of PCM melting using different tube configurations in a shell and tube latent heat thermal storage unit, *Thermal Science and Engineering Progress*, 25, 101030, Oct. 2021, doi: 10.1016/J.TSEP.2021.101030.
- [113] M. M. S. Ahmed, A. Radwan, A. A. Serageldin, A. Abdeen, E. M. Abo-Zahhad, and K. Nagano, The thermal potential of a new multifunctional sliding window, *Solar Energy*, 226, 389–407, Sep. 2021, doi: 10.1016/J.SOLENER.2021.08.045.
- [114] K. Kant, A. Anand, A. Shukla, and A. Sharma, Heat transfer study of building integrated photovoltaic (BIPV) with nano-enhanced phase change materials, *J Energy Storage*, 30, 101563, Aug. 2020, doi: 10.1016/J.EST.2020.101563.
- [115] A. I. A. AL-Musawi, A. Taheri, A. Farzanehnia, M. Sardarabadi, and M. Passandideh-Fard, Numerical study of the effects of nanofluids and phase-change materials in photovoltaic thermal (PVT) systems, *J Therm Anal Calorim*, 137, 2, 623–636, Jul. 2019, doi: 10.1007/s10973-018-7972-6.
- [116] Z. Luo *et al.*, Numerical and experimental study on temperature control of solar panels with form-stable paraffin/expanded graphite composite PCM, *Energy Convers Manag*, 149, 416–423, Oct. 2017, doi: 10.1016/J.ENCONMAN.2017.07.046.
- [117] M. Jurčević *et al.*, Investigation of heat convection for photovoltaic panel towards efficient design of novel hybrid cooling approach with incorporated organic phase change material, *Sustainable Energy Technologies and Assessments*, 47, 101497, Oct. 2021, doi: 10.1016/J.SETA.2021.101497.
- [118] M. Jurčević *et al.*, Techno-economic and environmental evaluation of photovoltaic-thermal collector design with pork fat as phase change material, *Energy*, 254, 124284, Sep. 2022, doi: 10.1016/J.ENERGY.2022.124284.
- [119] PVGIS-SARAH2 database, [https://re.jrc.ec.europa.eu/pvg\\_tools/en/tools.html#PVP](https://re.jrc.ec.europa.eu/pvg_tools/en/tools.html#PVP), [Accessed, Feb. 17, 2022].
- [120] A. Ramos, M. A. Chatzopoulou, I. Guarracino, J. Freeman, and C. N. Markides, Hybrid photovoltaic-thermal solar systems for combined heating, cooling and power provision in the urban environment, *Energy Convers Manag*, 150, 838–850, Oct. 2017, doi: 10.1016/J.ENCONMAN.2017.03.024.
- [121] M. Jurčević, S. Nižetić, I. Marinić-Kragić, M. Jakić, and M. Arıcı, Towards resilient operation of photovoltaic-thermal collector with incorporated organic phase change material: Numerical and experimental investigation, *Sustainable Energy Technologies and Assessments*, 60, 103465, Dec. 2023, doi: 10.1016/J.SETA.2023.103465.

- [122] F. Grubišić-Čabo, S. Nižetić, I. Marinić Kragić, and D. Čoko, Further progress in the research of fin-based passive cooling technique for the free-standing silicon photovoltaic panels, *Int J Energy Res*, 43, 8, 3475–3495, Jun. 2019, doi: 10.1002/er.4489.
- [123] L. Evangelisti, C. Guattari, and F. Asdrubali, On the sky temperature models and their influence on buildings energy performance: A critical review, *Energy Build*, 183, 607–625, Jan. 2019, doi: 10.1016/J.ENBUILD.2018.11.037.

## APPENDIX A – H

### Appendix A

Title: Nano-enhanced phase change materials and fluids in energy applications: A review

Authors: Nižetić S., Jurčević M., Arici M., Valan Arasu A., Xie G.

Publisher: *Elsevier*

Journal: *Renewable and Sustainable Energy Reviews*

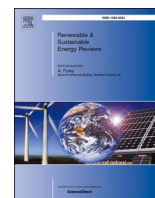
Edition, ID, year: 129, 109931, 2020.

Indexed in: Scopus, Science Citation Index Expanded, Web of Science, Current Contents, etc.

Journal Impact Factor: 14.982 Q1 (WoS and SJR-2020.)

DOI: <https://doi.org/10.1016/j.rser.2020.109931>

**Abstract:** This paper provides a review of nano-enhanced phase change materials (NEPCM) and nanofluids incorporated in experimental systems, i.e. different applications. The effect of the added nanomaterials on the main thermal properties was also discussed and analyzed in detail. According to the provided review, it was found that the addition of nanoparticles improves specific thermal properties of nano-enhanced materials. The thermal conductivity can be increased by between 20% and 100%, with respect to the base fluid. Other general thermal properties are slightly reduced such as latent heat, while for specific heat capacity the results are variable. Regarding applications, thermal energy storage systems as well as cooling systems for photovoltaics (PV-NEPCM) were investigated the most based on the existing literature. The gained results revealed that important data are missing and are related to the general preparation process of nano-enhanced materials. The economic as well as environmental evaluation of nano-enhanced systems is not covered well and addressed in the existing research findings. Safety issues and guidelines for handling nano-enhanced materials are also not properly addressed in the existing literature. Specific issues and future research directions were also discussed and linked with implementation of nanomaterials for considered applications and circumstances.



# Nano-enhanced phase change materials and fluids in energy applications: A review

Sandro Nižetić<sup>a,\*</sup>, Mišo Jurčević<sup>a</sup>, Müslüm Arıcı<sup>b</sup>, A. Valan Arasu<sup>c</sup>, Gongnan Xie<sup>d</sup>

<sup>a</sup> LTEF- Laboratory for Thermodynamics and Energy Efficiency, Faculty of Electrical Engineering, Mechanical Engineering and Naval Architecture, University of Split, Rudjera Boškovića 32, 21000, Split, Croatia

<sup>b</sup> Department of Mechanical Engineering, Faculty of Engineering, Kocaeli University, Umuttepe Campus, Kocaeli, 41380, Turkey

<sup>c</sup> Department of Mechanical Engineering, Thiagarajar College of Engineering, Madurai, 625016, Tamilnadu, India

<sup>d</sup> School of Marine Science and Technology, Northwestern Polytechnical University, Xi'an, 710072, China

## ARTICLE INFO

### Keywords:

Nanomaterials  
NEPCM  
Nanofluids  
Nanocomposites  
Applications  
Thermal properties  
Preparation  
Energy

## ABSTRACT

This paper provides a review of nano-enhanced phase change materials (NEPCM) and nanofluids incorporated in experimental systems, i.e. different applications. The effect of the added nanomaterials on the main thermal properties was also discussed and analyzed in detail. According to the provided review, it was found that the addition of nanoparticles improves specific thermal properties of nano-enhanced materials. The thermal conductivity can be increased by between 20% and 100%, with respect to the base fluid. Other general thermal properties are slightly reduced such as latent heat, while for specific heat capacity the results are variable. Regarding applications, thermal energy storage systems as well as cooling systems for photovoltaics (PV-NEPCM) were investigated the most based on the existing literature. The gained results revealed that important data are missing and are related to the general preparation process of nano-enhanced materials. The economic as well as environmental evaluation of nano-enhanced systems is not covered well and addressed in the existing research findings. Safety issues and guidelines for handling nano-enhanced materials are also not properly addressed in the existing literature. Specific issues and future research directions were also discussed and linked with implementation of nanomaterials for considered applications and circumstances.

## 1. Introduction

The application of nanomaterials has been intensively investigated in recent years since they have great potential for technical advancements, and more importantly, they provide benefits which can be linked with the implementation of nanomaterials for various purposes, [1]. Nanotechnology can be implemented in different technological fields such as IT technologies, medicine, novel materials, food safety, etc. Specifically, energy related field is one of the most interesting fields of nanotechnology, since applications of nanomaterials can lead to noticeable technological improvements in different useful engineering applications, such as production of biofuels [2], or for the cooling of the automotive radiators [3]. Nanoparticles and their applications have been widely investigated in recent years due to numerous potential implementation areas. Selected applications will be addressed in the continuation of this paper to get a deeper insight into the potential implementation area of nanotechnology. The main direction of the here

in conducted research work was focused on the energy related field.

The application of binary nanofluids for solar absorption refrigeration was reported in Ref. [4]. The investigation was focused on photo-thermal conversion efficiency in laboratory conditions with the utilization of a solar simulator. Nanoparticles in a concentration of 50 wt % lithium bromide with 50 wt% of water were considered. The results revealed that the addition of the previously specified nanoparticles can lead to the improvement of light trapping efficiency, and by that can cause an increase in the bulk temperature. The detected efficiency enhancement ranged from 4.9% to 11.9%, where it was concluded that the considered nanoparticles are suitable for solar absorption cooling applications. The potential application of nano-improved materials for thermoelectric generation was analyzed in study [5]. A nanostructured bulk alloy with added 0.1 vol% of SiC nanoparticles was considered with respect to the examination of the Seebeck and Thomson effect. The heat conduction and heat transfer loss into the surroundings were also investigated. According to the provided analysis, it was confirmed that

\* Corresponding author. University of Split, Rudjera Boškovića 32, 21000, Split, Croatia.  
E-mail address: [snizetic@fesb.hr](mailto:snizetic@fesb.hr) (S. Nižetić).



the addition of nanoparticles improved thermal efficiency in a range of 7.3%–8.7% for the considered purpose.

The experimental work related to the application of nanoparticles was addressed in Ref. [6]. The case of evacuated tube solar collector systems, with a parabolic concentrator was investigated (graphene based nanofluid was used). The graphene was selected as a nanomaterial due to its high thermal conductivity and focus of the research was to analyze the thermal efficiency of the examined solar based system. According to the experimental data, thermal efficiency of the solar collector can be improved from 31% to 76%, when compared to base fluid, and for the considered nanoparticle concentrations. The implementation of nanoparticles in photovoltaic cell applications was investigated in Ref. [7]. The focus of the work was to explore the cooling effect on photovoltaics (PV) with the usage of the compound enhancement approach and application of phase change materials (PCM). The water was enhanced with an  $\text{Al}_2\text{O}_3$ /PCM mixture with different nanoparticle concentrations. The impact of the occupation ratio in the channels was also examined. The results revealed that it was possible to achieve performance improvement in the delivered power output from the PV panel. Suitable nanoparticle concentration was detected (1 wt%) and linked with the highest improvement of power output from the PV panel.

The effect of microwaves on the  $\text{Al}_2\text{O}_3$  nanofluid was examined in Ref. [8] for the case of pool boiling. The experimental results revealed an increase in the heat transfer for the  $\text{Al}_2\text{O}_3$  nanofluid, with a highest reported heat transfer efficiency of 128%. It was also found that the increase in heat transfer efficiency causes a downward trend in the case when heat flux is increased. The effect of  $\text{SiO}_2$  and  $\text{Al}_2\text{O}_3$  nanoparticle addition in low salinity hot water was discussed in Ref. [9]. The main goal of the work was to check potential to improve heavy oil recovery. The numerical simulations revealed that it should be possible to increase the heavy oil recovery rate in a range of 2.4%–7.2% with the application of the mentioned nanoparticles, when compared to conventional water injection. It was also reported in the same study that it would be possible to improve oil recovery by about 40%. Moreover, proper optimization would allowed low energy consumption in general.

A novel thermomechanical liquid, consisted from Ni–Br-IL liquid (nickel-bromine-ionic liquid) enhanced with  $\text{VO}_2$  nanoparticles (vanadium dioxide) was proposed in Ref. [10], i.e. to form a novel nanocomposite film. The addition of nanoparticles proved the increase of ultrahigh optical properties in an amount of 27% when compared to pure  $\text{VO}_2$  film (and which is about 14.1%). The developed film could be an effective potential thermochromic material for smart window applications. Gained results could enable an efficiency improvement in high-performance buildings. An experimental investigation of mineral lubricant enriched with  $\text{TiO}_2$  nanoparticles was discussed in Ref. [11] in the case of liquefied petroleum gas refrigerant. The experimental results revealed that the addition of the previously mentioned nanoparticles in the mineral oil improved the efficiency of the refrigerator. The mean engaged power was reduced from 8% to almost 15%, i.e., depending from the concentration of the added  $\text{TiO}_2$  nanoparticles.

The addition of nanoparticles ( $\text{nSiO}_2$ ) in fatty acids was elaborated in Ref. [12] to create a potential effective NEPCM with increased thermal conductivity which is suitable for building applications. According to the experimental results, it was confirmed that the addition of nanoparticles increases both thermal conductivity and heat capacity. The investigation also included long-term performance experiments with the application of cycling stability tests. The analysis of the PCM melting speed for latent heat thermal energy storage applications was reported in Ref. [13], where the addition of nanoparticles was also considered. The results directed that energy storage efficiency decreases with the increase of nanoparticle volume fraction. The main cause for previous is increased viscosity of the PCM and reduced energy storage capacity. An analysis of direct absorption collectors with the application of nanoparticles, with enriched nanofluid, was reported in Ref. [14]. The study was conducted with the application of CFD analysis, where the addition of specific nanoparticles caused the efficiency improvement of the

considered absorption collector by about 10%. The highest increase in collector performance was found for the case where magnetic nanofluid was assumed, with an efficiency improvement of about 30%. The application of nanoparticles (copper oxide, aluminum oxide and carbon nanotubes), with water as a base fluid was numerically provided in Ref. [15], for the case of a solar collector with absorbing pipes. The thermal performance of the solar collector was improved with the addition of nanoparticles, i.e. with respect to the base fluid (water). The highest efficiency improvement was found for volumetric fractions less than 5%, with respect to higher volumetric fractions. The addition of nanoparticles towards the improvement of biohydrogen production rates (dark fermentation method) was reported and discussed in study [16]. A review of different nanoparticles was obtained, such as silver, iron, titanium oxide, nickel, etc., where in all cases the production efficiency of the biohydrogen was improved for the assumed fermentation technique.

The potential implementation of titanium nitride (TiN) as a plasmonic nanofluid for solar thermal applications was elaborated in study [17]. The results proved that TiN based nanofluid has better performance, i.e. better photothermal conversion efficiency. The improved efficiency was noted when compared to other, conventionally used nanofluids for the considered purpose such as carbon nanotube, graphene, Au, Ag, etc. A performance analysis of GaAs based plasmonic solar cells with added nanoparticles (Ag, Au) in a numerical manner was reported in Refs. [18]. It was found that the addition of nanoparticles can improve the light absorption of GaAs based solar cells. The highest rise of optical-electrical conversion efficiency was detected for Au nanoparticles. It was noticed that with the proper optimization of nanoparticle properties, it is possible to reduce the thermalization loss and increase electrical performance.

A review related to the analysis of different factors that affect the thermal performance of solar collectors (flat plate) was discussed in Ref. [19], with an assumed application of nanofluids. The results showed that the most suitable nanoparticles from an energy and exergy point of view are carbon based nanofluids. The efficiency improvement ranged from 6.3% to 37.3% when compared to conventional nanofluids, with concentrations up to 2%. An analytical study was obtained in Ref. [20] and directed to the performance improvement of hybrid photovoltaic-thermal solar collectors. The nanoparticles were added above the PV module and on the backside of the PV panel with a PCM layer (NEPCM-nano-enhanced phase change material). The numerical study showed that the overall performance of the PV/T system was reduced around 6.7% with the addition of nanoparticles. However, in the case of optical filtration above the PV panel, the overall efficiency is improved from 6% to 12%.

Novel nano-emulsions of paraffin waxes and water were experimentally tested in Ref. [21]. Different concentrations were investigated and ranged from 2% to 10%. The stability of emulsions was investigated with long-term tests. According to the experimental results, the melting heat was reduced when compared to the base fluid, however, the thermal capacity improved up to 40%. A review paper focused on the investigation of heat transfer improvements was provided in Refs. [22]. The PCMs through metallic and carbon-based porous materials/foams were in the main focus of the review. It was found that the addition of different nanoparticles in porous materials (or foams) can improve thermal conductivity by 3 to even 500 times. Useful correlations related to thermal conductivity were also reported together with the addressed research gaps in the specific field. The addition of organic nanoparticles in the PCM materials was examined and reported in study [23] for energy storage systems. A magnetic field was also applied on the considered system and the results showed that the addition of nanoparticles in a concentration of up to 4% leads to an average decrease of solidification time in an amount of 14%. The application of the magnetic field incorporating nanoparticles turned out to be an effective solution to boost solidification in energy storage applications.

The consideration of nano-encapsulated PCM materials was

discussed in Ref. [24] as a potential effective solution for building applications. It was reported that the application of a nano-encapsulated PCM can reduce heating and cooling energy demands in residential buildings in range from 1% to about 4%. The toxicity of the proposed solution was also investigated, and no-harmful effects were detected with respect to human exposure. Previously briefly addressed research works proved significant importance of the nanotechnology in various engineering applications.

### 1.1. Preceding affined review articles

The herein presented review mostly deals with the experimental researches dealing with nano-enhanced fluid and NEPCMs. A similar endeavor was published by Amaral et al. [25]. However, they focused on experimental research studies solely dealing with the enhancements of the thermal conductivity as well as latent heat capacity of PCMs (enhanced with carbon-based nanostructures (CNs) using the encapsulation method). Rigid diversification between nanofluids and nanocomposites can be considered obsolete due to more diverse applications of nanomaterials in such a context. Many nanofluids can be used as nanocomposites and vice versa depending on the present material phase. For example, water enhanced with nanomaterials or paraffin based nanofluid [26]. Furthermore, fundamentally the preparation methodologies are complementary. The authors of some papers have already included both nanofluids and nanocomposites in their review papers. Therefore, the current contribution investigates both types of materials. A related review, for instance, Al-Kayiem et al. [27] which focuses on the investigation of thermal energy storage capabilities of PCMs, nanofluids, nanocomposites, and related nano additives. A more focused review was published by Eanest Jebasingh and Valan Arasu [28] in which they presented a comprehensive assessment of the latent heat and thermal conductivity of NEPCM materials. The focus was on the operating range from 20 °C to 37 °C, i.e. low-temperature energy storage applications. A similar approach was employed by Prabhu and Valan Arasu [29]. They published a review dealing with experimental and theoretical researches of nano-enhanced paraffin wax. The goal of the work was to investigate thermophysical properties as well as characterization and synthesis. There are very few high-quality review papers covering the preparation process, thermal properties characterization and possible applications of nanocomposites and nanofluids. One of the recent review papers was published by Dhinesh Kumar and Valan Arasu [30]. They reviewed the production of metal and metal oxides

nanofluids while providing thermophysical properties characterization. Furthermore, different application areas were discussed in detail.

Compared to the above-mentioned review articles, this review delivers a more comprehensive analysis of possible applications, while identifying possible preparation issues of both nanocomposites and nanofluids including prices of typical nanomaterials, i.e. an economic aspect. Also, more thermal properties were investigated, i.e. thermal conductivity, latent heat, specific heat, thermal diffusivity, etc. In addition, herein conducted research addresses less investigated areas, therefore, pinpointing future directions and providing possible research gap.

### 1.2. Necessity for up-to-date review

From the previously conducted overview of the latest selected research findings it was demonstrated that there is a wide spectrum of possible solutions where nanotechnology can be applied with success, especially in the energy field. According to the Scopus database and targeted keywords, there is a reasonable rise in the number of publications dealing with nanoparticles for various applications, Fig. 1, from 51,867 publications in 2016 to 63,716 publications in 2019. The highest rise interest regarding the released publications is in the period of 2016–2019 in the field of PCM enhanced materials with nanoparticles in an amount of about 158% (however, the number of publications is the lowest when compared to other targeted research topics from Fig. 1). The second highest rise in publications is in the case of energy storage applications in an amount of almost 85% from 2016 to 2019. In any case, the interest of the research community for nanotechnology applications is more than evident and progressing.

Benefits related to the addition of nanoparticles are noticeable and usually linked with the performance improvement of different considered systems or processes. However, the type and quantity of added nanoparticles are critical features, as well as preparation process. Since the potential implementation areas of nanoparticles are rather wide, this review was focused on nano-enhanced fluids (nanofluids) and NEPCM. Regarding application area, the energy field was in the focus of the review. This paper represents guidelines for researchers dealing with NEPCMs, while giving an insight into NEPCM applications in fully or close to fully operable systems and various engineering applications.

The main objective of this work was to pinpoint the fields of possible future NEPCM applications and to highlight the complexity, i.e. importance of proper NEPCM preparation procedures and to address

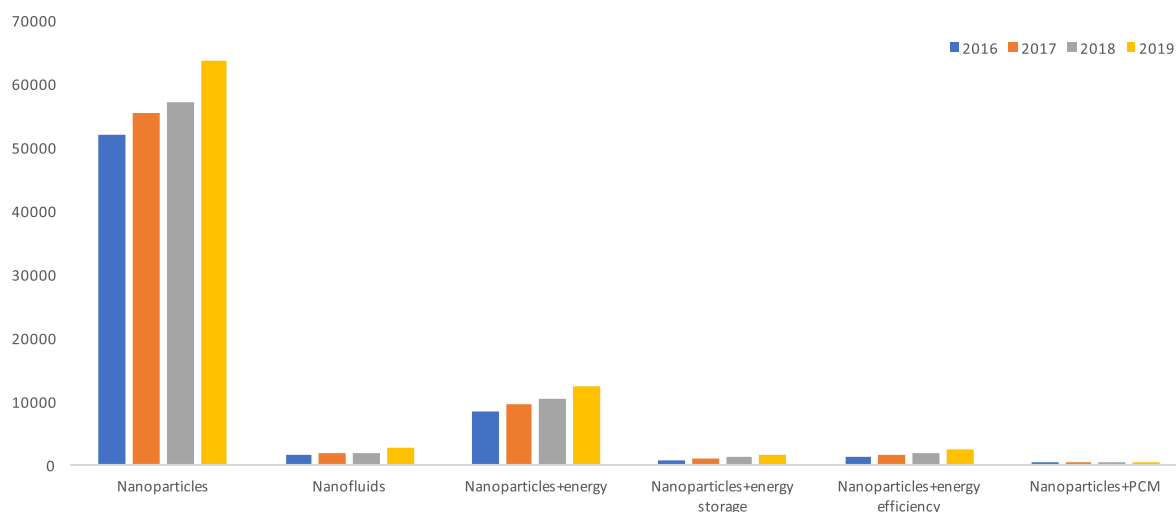


Fig. 1. Rise of research studies related to investigation of nanoparticles, [31].

achieved improvements lined with application of the nano-enhanced materials. When considering certain NEPCMs for possible applications, researchers should be aware of the NEPCM preparation challenges and expected enhancements of thermo-physical properties. This review paper could be a further contribution in the field when compared to the existing research studies.

### 1.3. Brief description of review methodology

Elsevier's Scopus database was the main source of reviewed articles, i.e. existing research findings. The primary selection was obtained with respect to the targeted keywords, Fig. 2. The subject area was limited to Energy, Engineering, Material Science and Environmental Science. The articles written in English with the year of publication being between 2015 and 2019 were selected, i.e. last six years. After the primary selection, articles dealing with NEPCMs were subjected to secondary selection where the main goal was to group the articles considering the specific fields of NEPCM application, production technologies and thermal properties, Fig. 2. The selection was done in this way because most of the articles were focused either on specific applications or on examination of specific thermal properties. Therefore, it was not possible to describe each individual article with respect to the specific NEPCM application, NEPCM preparation technology and determination of thermal properties. Instead, each article was classified with respect to the main focus of its content, i.e. with respect to the NEPCM application, the production technology and thermal properties. Depending from the specific selection criteria, some articles are addressed in multiple groups, i.e. based on the general paper content and specific research findings.

## 2. Applications of nano-enhanced phase change materials

NEPCM materials can be used in various areas of modern technology as well as engineering applications in general. The implementation of PCM-NEPCM systems is mainly limited mainly due to the relatively high cost of nanoparticles and unknown cost-benefit outcome. Nevertheless, it can be assumed that NEPCM material will find its place in a wider application in the years to come, especially when it comes to energy storage applications, [32]. Generally, it is very difficult to classify NEPCMs by application because of various potential applications and where each application is specific. The ability to absorb relatively large amounts of heat at about constant temperatures make NEPCM materials

a good choice for thermal energy storage, passive cooling, heat transfer fluids, waste heat recovery, etc. In herein conducted work, the application classification of NEPCMs was made with regard to the most common use, Fig. 3, i.e. exhaustive classification approach was applied.

### 2.1. Thermal energy storage applications

Thermal energy storage (TES) can be achieved in different ways with a whole spectrum of widely differing technologies, [33]. The basic idea is to store excess heat or the waste heat from thermal-generating sources, and there by enable the efficiency rise of the system. Also, with a small distinction, any solar thermal energy storage system is in fact a variation of the TES system. The vast majority of NEPCM materials can be used for TES. NEPCM material-based TES works on the passive storage principle of latent heat. The passivity and predictability of such systems enables the possibility for an active control of release and storage of latent heat energy which. Moreover, the smart control, can provide energy on demand. The main limiting factor is the temperature of the phase change, or more frequently, the temperature range in which the phase change occurs. Depending on the exploitation conditions, the selection of suitable NEPCM materials is mainly based on thermal properties. The main problem of all PCM materials is their weak thermal conductivity, especially in solid state. The main research efforts with NEPCM materials are primarily focused on the improvement of thermal conductivity.

The experimental work related to the thermal properties of nanocomposites, with a solar collector application, was elaborated in study [34]. For the purpose of the experimental research, the storage tank was filled with water that circulated through a solar collector with an integrated NEPCM, Fig. 4.

The results revealed that addition 1% of Cu nanoparticles to paraffin wax resulted in an increased collector efficiency of 1.7% compared to pure PCM.

Natividade et al. [6] investigated the thermal efficiency of an evacuated tube solar collector system incorporating a parabolic concentrator, Fig. 5. To create nanofluid, water was added with a multilayer graphene (MLG) in low volume fractions (0.00045% and 0.00068%) to avoid the agglomeration of nanoparticles. Unfortunately, the nanofluid preparation procedure is very superficially presented in the paper, i.e. lack of details regarding preparation parameters and the equipment used.

The efficiency (thermal) of the nanofluid enhanced solar collector

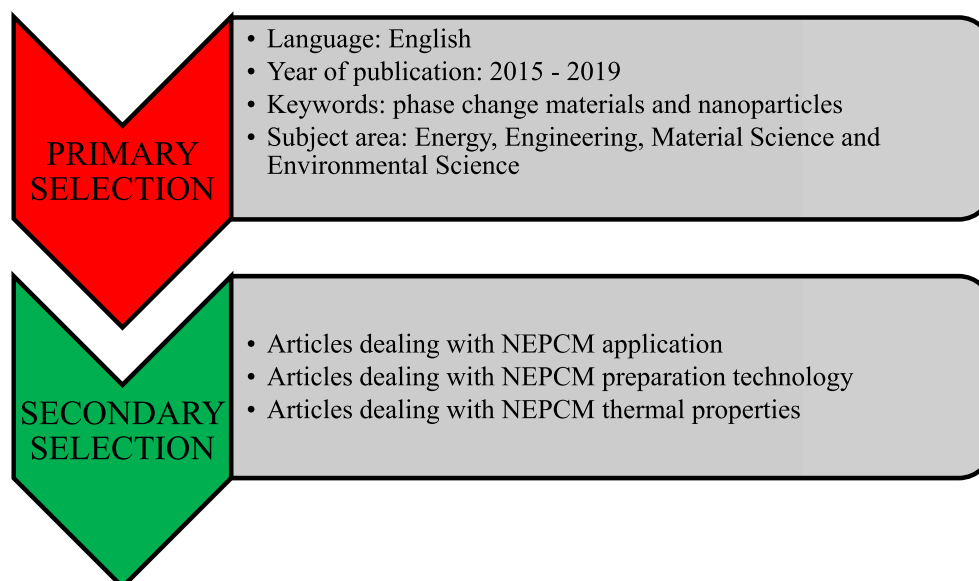


Fig. 2. Article selection procedure.

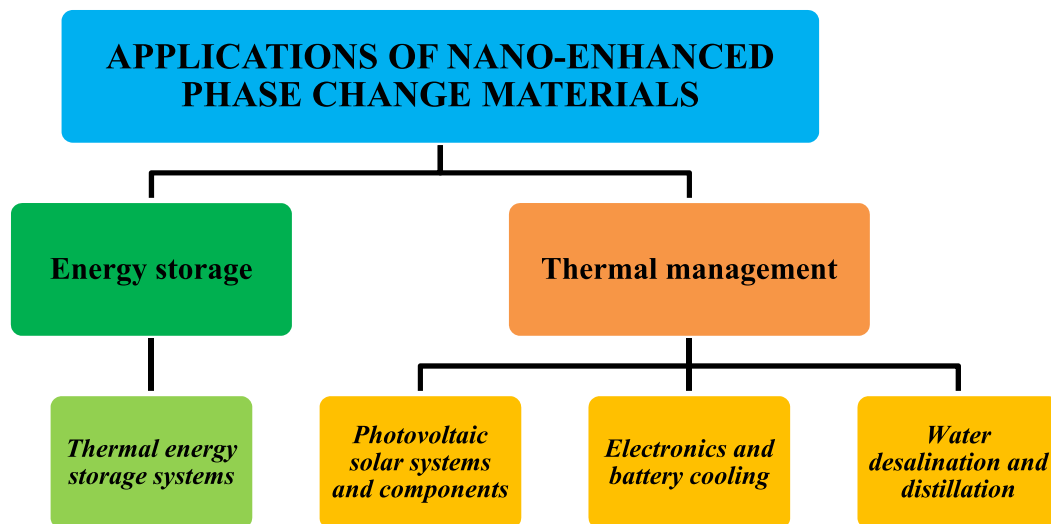


Fig. 3. Classification of NEPCM applications presented in the selected papers with respect to the general classification (Energy storage and Thermal management).

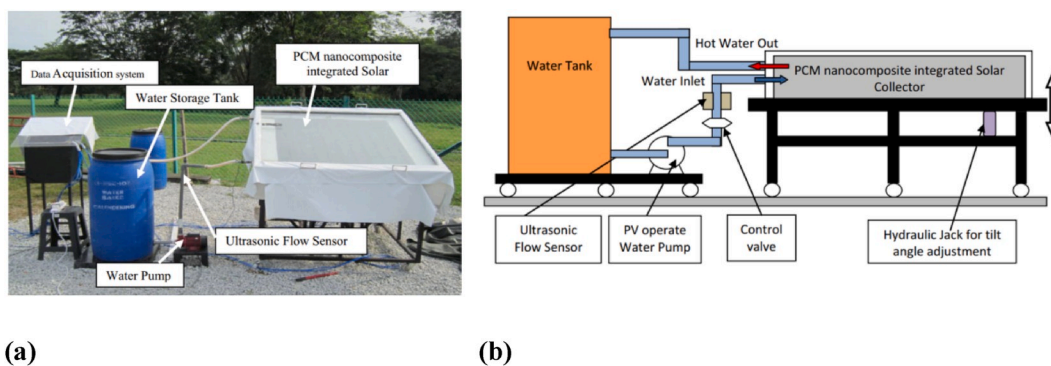


Fig. 4. Thermal energy storage solar water heater system set up (a) and schematic (b), [34].

was increased by 31% (0.00045 vol% of MLG) and 76% (0.00068 vol% of MLG) with respect to the base fluid.

Altohamy et al. [35] investigated a process of water-based nanofluid charging (which stands for solidification) in the Latent Heat Thermal Energy Storage (LHTES) system. The schematic of the experimental test rig is presented in Fig. 6.

It is reported that the addition of  $\text{Al}_2\text{O}_3$  nanoparticles in the water (PCM) has effect on the solidified mass fraction and charging time which significantly decreases for given circumstances. Furthermore, a significant improvement in the charging rate was detected and the percentage of energy stored. It is stated that, compared to pure water, the charging time can be reduced by up to 30% with a 2% volume concentration of nanoparticles.

Wilson John et al. [36] successfully recovered the heat of exhaust gas from a Diesel engine where shell and tube heat exchanger (triangular finned) was used and integrated with thermal storage tank. Storage tank had a phase change material with added  $\text{CuO}$  nanoparticles (0.01 wt%), Fig. 7. The temperature variations of the HTF were studied for different engine load regimes.

The experimental results revealed that when the engine is at full capacity, the utilized heat from the system is 4.04 kW. After testing at all loads and conditions, it was found that the achieved effectiveness of the specific heat exchanger was over 99%. It is not clearly elaborated why the efficiency was so high, therefore this result should be considered with caution.

## 2.2. Applications in photovoltaic solar systems and components

The incoming solar radiation on the surface of a photovoltaic module generates electric power, whereby the rest of the radiation is being absorbed by cell, reflected and transmitted. The absorbed solar radiation increases the temperature of the PV module and thus reduces its efficiency. In the literature, it is often stated that the increase in temperature of the PV panel causes efficiency drop by about  $0.5\%/^{\circ}\text{C}$  [37], depending on the type of photovoltaic technology. This problem is particularly prominent in building integrated photovoltaics [38], but also in the case of free-standing modules [39]. Therefore, from an aspect of efficiency and economic feasibility, it is reasonable to consider the effective strategies related to the thermal regulation of photovoltaics. The favorable thermophysical properties of NEPCMs could be of great benefit to this purpose.

Nada and El-Nagar in their work [38] investigated the efficiency of using PCM and NEPCM materials for the thermal regulation of free standing and building integrated PV modules. The authors emphasize that the electrical efficiency of the photovoltaic module is defined as the ratio of power output and incoming solar radiation by the module. According to the experimental results, it was found that for building integrated modules, the addition of a pure PCM (paraffin wax, RUBITHERM® RT55) and a PCM enhanced with 2% of  $\text{Al}_2\text{O}_3$  nanoparticles. The daily efficiency was increased from 15.01% to 15.94% (around, 5.67%) for PCMs and from 15.01% to 17.15% (around 13.15%) for NEPCMs. In the case of free stand photovoltaics, it was concluded that the addition of PCMs or NEPCMs creates additional costs without

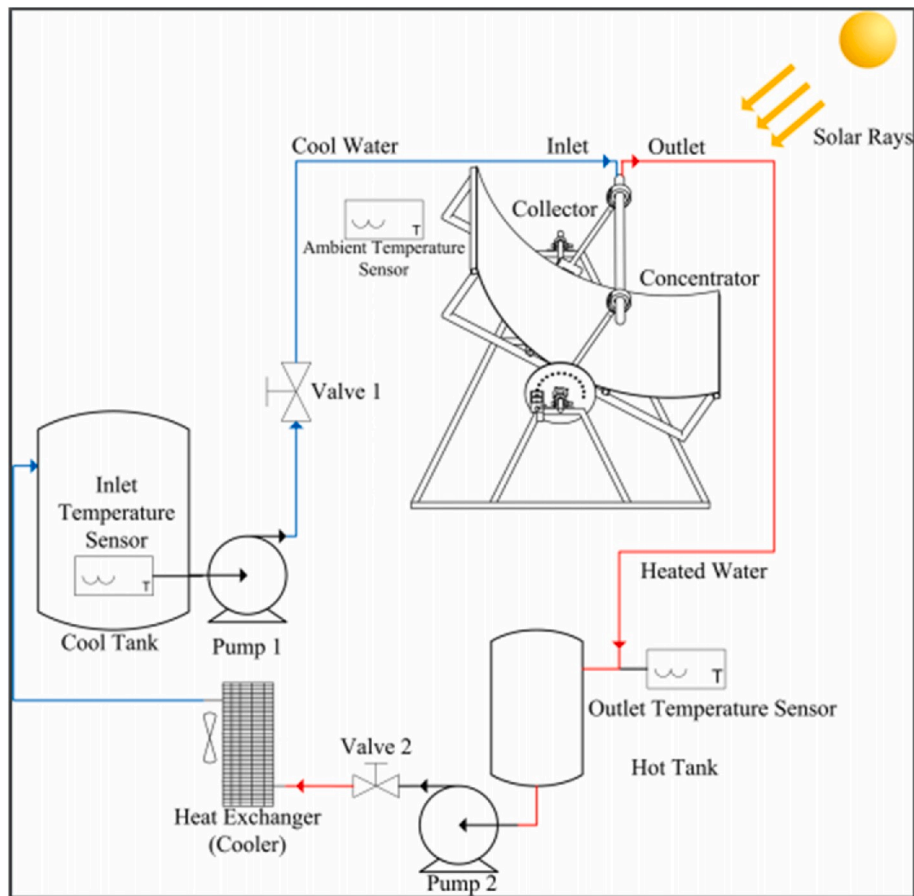


Fig. 5. Thermal energy storage solar water heater system set up, [6].

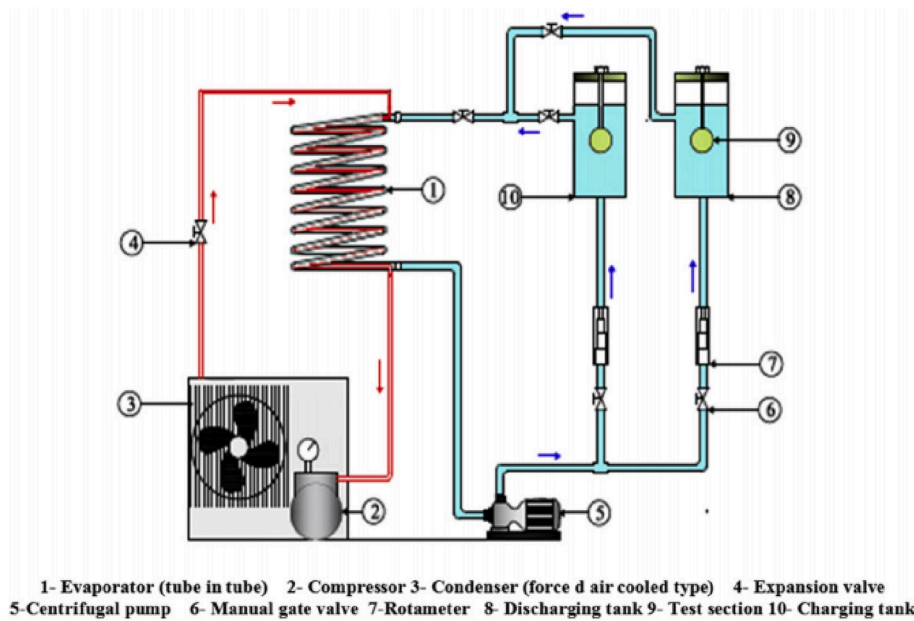


Fig. 6. Experimental test rig layout, [35].

any gains in the thermal performance as opposed to building integrated PV modules (significant gains were detected). There is no clear cost analysis based on which one can claim that it is not worth to add a PCM or NEPCM.

Nada et al. [40] examined the possibility of thermal regulation for a

PV-building integrated system with a nano-enhanced PCM (2% of  $Al_2O_3$  nanoparticles and paraffin wax, Rubitherm RT55) as well as the impact on the system efficiency. At the location of Giza, Egypt, the PV modules were experimentally tested with the PCM and NEPCM on the backside, Fig. 8.



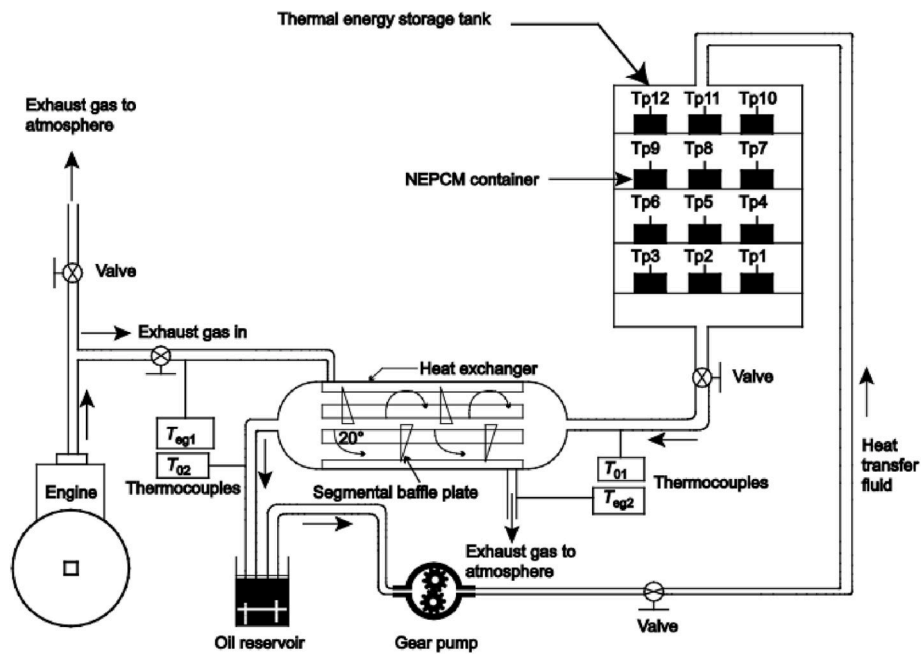


Fig. 7. Schematic of tested experimental setup, [36].



Fig. 8. Experimental setup layout, [40].

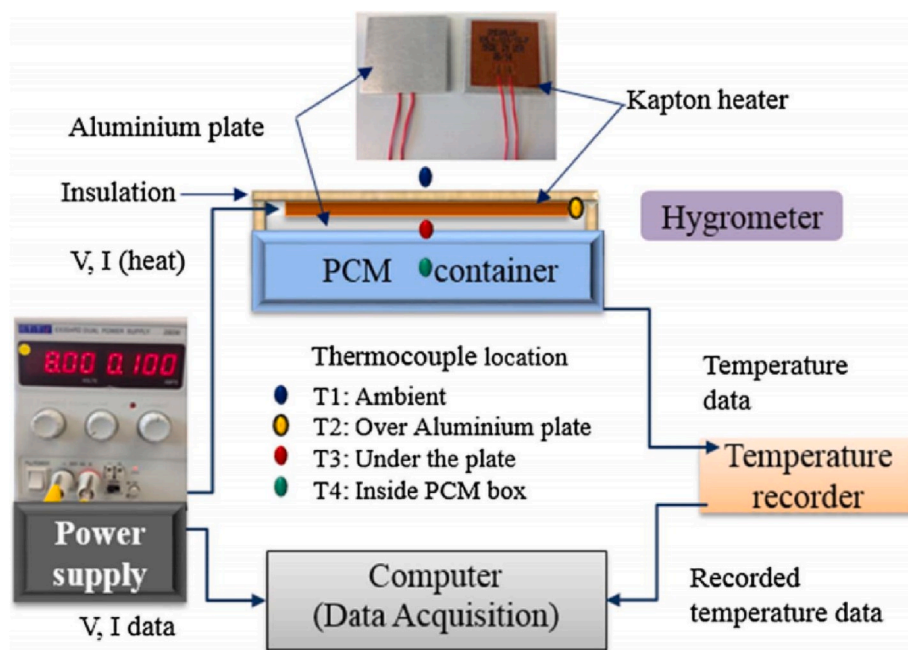


Fig. 9. Experimental system layout with thermocouple locations, [41].

One module was passively cooled with a container filled with a pure PCM, the second module was passively cooled with an NEPCM filled tank, and the third, i.e. reference one (non-cooled), was directly integrated with the building wall simulator. The results showed that the PCM or NEPCM on the back of the building integrated PV, cause the reduction of the PV panel operating temperature. The pure PCM caused a PV module temperature reduction of about 8.1 °C, with an efficiency increase of 5.7%. The addition of the NEPCM caused reduction of the PV panel operating temperature in amount of 10.6 °C, followed with an efficiency increase of 13.2%.

Sharma et al. [41] investigated a combined passive cooling solution for Building-Integrated Concentrated Photovoltaics (BICPV). To mimic the temperature profile of a BICPV (electrical heaters were used), a scaled-down system was designed and manufactured, Fig. 9. The previously mentioned work presents a novelty in terms of thermal regulation in photovoltaics. The presented scaled-down BICPV system incorporates passive cooling that combines micro-fins and a PCM (organic paraffin wax, Rubitherm RT42) or NEPCM (CuO nanoparticles, 0.5 wt%).

It was stated that in an un-finned system, the PCM lowered the average temperature at the center of the examined system (Fig. 9) by 9.6 °C (13.9%) and the NEPCM by 11.2 °C (16.2%). Furthermore, the micro-fin system reduced the temperature by 10.7 °C (15.9%) with the PCM and by 12.5 °C (18.5%) with the NEPCM, indicating better thermal regulation with micro-finned surfaces when compared to un-finned surfaces. These results must be considered with caution since they are based on the system that mimics a BICPV system.

Salem et al. [7] conducted an experimental investigation of the PV panel performance enhanced with aluminium channels located beneath the module. The channels were filled with cooling water and/or a mixture of calcium chloride hexahydrate ( $\text{CaCl}_2\text{H}_{12}\text{O}_6$ ) and  $\text{Al}_2\text{O}_3$  nanoparticles (0.25 wt%, 0.5 wt%, 0.75 wt%, 1 wt%), Fig. 10.

An average PV cell operating temperature drop of 14.5 °C was recorded for  $\lambda_{\text{PCM}} = 25\%$  (1 wt% loading of  $\text{Al}_2\text{O}_3$  nanoparticles) and 75% water (0.25 L/min). When the water flow was increased to 1 L/min, the average temperature drop was 16.6 °C resulting in a 37.1% increase in the average electrical efficiency when compared to the reference PV cell.

### 2.3. Electronics and battery cooling application

Batteries and electronic equipment usually have a temperature range in which their characteristics are good and stable. During discharge, most batteries are producing significant amounts of heat. Generally, electronic equipment often has a problem with generating heat that needs to be removed with an adequate cooling strategy that is economically feasible and effective. Passive or active cooling with NEPCMs offers a robust solution for the previously mentioned applications.

Karimi et al. [42] obtained an experimental study related to the thermal management of a cylindrical lithium ion battery by using PCM composites. Three types of nanoparticles (Cu, Ag and  $\text{Fe}_3\text{O}_4$ ), with 2 wt % as the base concentration and metal matrix were used (a paraffin mixture was used as the PCM). The heat generation in a typical Li-ion battery was simulated with the fabricated battery-like simulator, Fig. 11.

The metal matrix reduced the temperature in the metal container by about 70%, while the PCM enhanced system, with Cu nanoparticles, reduced the temperature in the container by about 60%. The Ag and  $\text{Fe}_3\text{O}_4$  nanoparticles in the PCM cooling configuration reduced the temperature in the container by about 50%. It was concluded that best performance was achieved with Ag nanoparticles when compared with other composites containing nanoparticles. It is not entirely clear what this conclusion is based on since in some aspects other nanocomposites had similar or even better results.

Temel in Ref. [43] investigated passive thermal management capabilities of RT-44 paraffin wax and NEPCM based on RT-44 and carbon-based nanoparticles (GNP) (3 wt%, 5 wt%, 7 wt%) in simulated battery pack at different climate conditions. Instead of Lithium-ion cells, electric heaters were used in the simulated battery pack for safety reasons, Fig. 12.

The downside of this approach is the presumption that battery emits constant heat during discharge, i.e. the operating temperature and the state of charge effects on the Lithium-ion battery heat dissipation were neglected. The usage of the nanocomposite with 7 wt% of GNP at the highest discharge rate (3.90 W) and surrounding temperature (30 °C) resulted in the 1.96 (compared to pure RT-44) and 7.9 (compared to natural convection) times longer effective thermal protection duration.

Alimohammadi et al. [44] examined the efficiency improvement of a cooling system for an electronic chipset that was based on the

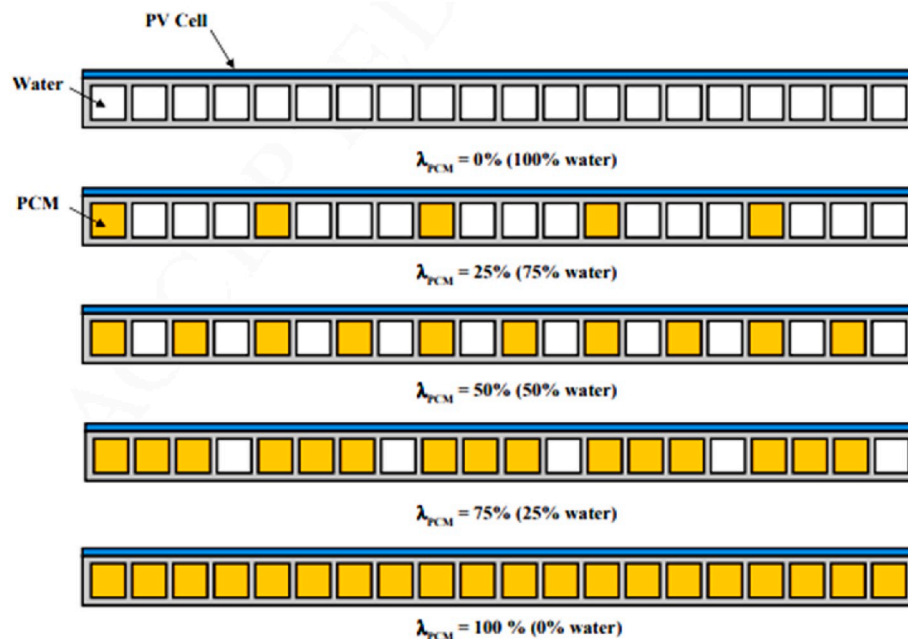


Fig. 10. Layout of channels occupied with water and/or NEPCM, [7].

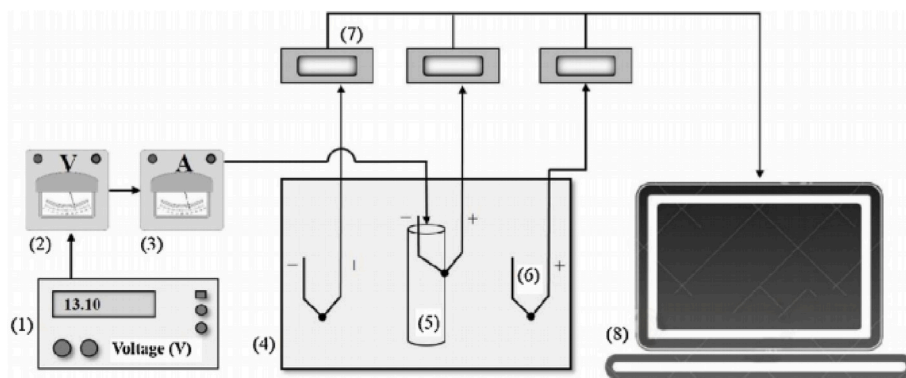


Fig. 11. Data acquisition system and experimental test rig layout (power source (1), Voltmeter (2), Ampermeter (3), container (4), battery module (5), thermocouples (6), temperature indicator (7), system of data acquisition (8), [42].



Fig. 12. Experimental layout of the simulated battery pack, [43].

application of NEPCM materials. In the reported research, an inorganic salt-hydrate type  $\text{Mn}(\text{NO}_3)_2$  was used as the PCM, whereby 1 wt%  $\text{Fe}_3\text{O}_4$  nanoparticles were dispersed in the PCM. The research was obtained for different scenarios including both free and forced convection. Three electronic chipset cooling systems were tested; a simple heat-sink (HS), a heat-sink with a phase change material (HS/PCM) and a heat-sink with an NEPCM (HS/NEPCM). They contributed to lower power consumption by 4.33%, 8.83% and 7.33% for each electronic chipset. Furthermore, the results showed that the use of the PCM and NEPCM caused a chipset temperature reduction of 14 °C and 10.5 °C when compared to a simple heat-sink for both free as well as forced convection.

Krishna et al. in their study [45] investigated the heat pipe thermal performance for electronic cooling applications. An NEPCM material was used as an energy storage medium around the adiabatic region of the heat pipe, Fig. 13. The NEPCM was based on Tricosane with the addition of  $\text{Al}_2\text{O}_3$  nanoparticles (0.5 vol%, 1 vol%, 2 vol%). The focus of the tests was to obtain temperature distributions (charge, discharge as well as simultaneous charge/discharge period for the condenser, evaporator and PCM).

The authors claimed that the use of an NEPCM caused the evaporator temperature drop by 25.75%, which made it possible to save fan power by 53% compared to the traditional heat pipe version. In addition, it was found that the NEPCM can store about 30% of energy delivered at the evaporator, thus reducing the fan load as well as power consumption.

#### 2.4. Water desalination and distillation

Our planet has limited drinking water resources, so wastewater

treatment or desalination must be imposed as a logical solution to bridge water supply issues [46]. Commonly, technologies that offer such solutions are either too expensive or have too low production capacities to have wider application [47]. Therefore, the focus should be directed to the efficiency increase of existing solutions or development of more costly, but more productive concepts, which will make sense from a cost-benefit aspect.

Chaichana and Kazem studied the influence of an NEPCM (combination of paraffin wax and  $\text{Al}_2\text{O}_3$  nanoparticles, from 0.5 wt% to 3 wt%) on the productivity of a simple solar distiller [48], Fig. 14, where three solar distillers were tested. The first one was without any modifications; the second was paraffin wax and the third one combined paraffin wax with the added nanoparticles.

The main issue of solar distillation is the inability to work after sunset, the authors state that the PCM prolonged the production period by up to 3 h after sunset. The daily distillation yield was improved to 10.38%. The NEPCM yielded even better results in the amount of 60.53%. The simple distillery daily production was 2.32 l/m<sup>2</sup>, while the NEPCM distiller had 3.708 l/m<sup>2</sup> per day.

Dsilva Winfred Rufuss et al. [49] examined the performance of solar stills with a PCM and NEPCM. The solar still is a well-known method for desalinating water by utilization of solar energy. Four solar stills were tested, one with pure paraffin and others with a combination of paraffin and 0.3 wt% of nanoparticles ( $\text{TiO}_2$ , CuO and GO), Fig. 15.

The solar still with a pure PCM produced 3.92 l/m<sup>2</sup> on daily basis, while the NEPCM based solar stills with  $\text{TiO}_2$ , CuO and GO produced 4.94 l/m<sup>2</sup>, 5.28 l/m<sup>2</sup> and 3.66 l/m<sup>2</sup>. Compared to a conventional still, the rise in system performance was 23.0%, 39.3%, 43.2% and 18.0%.



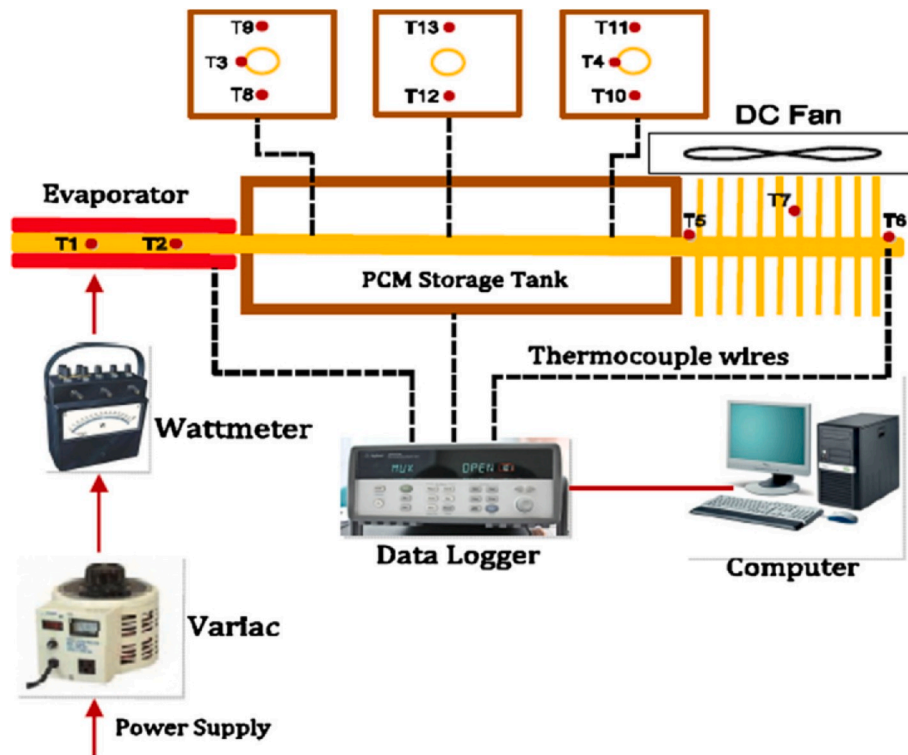


Fig. 13. Heat pipe/PCM module system scheme, [45].

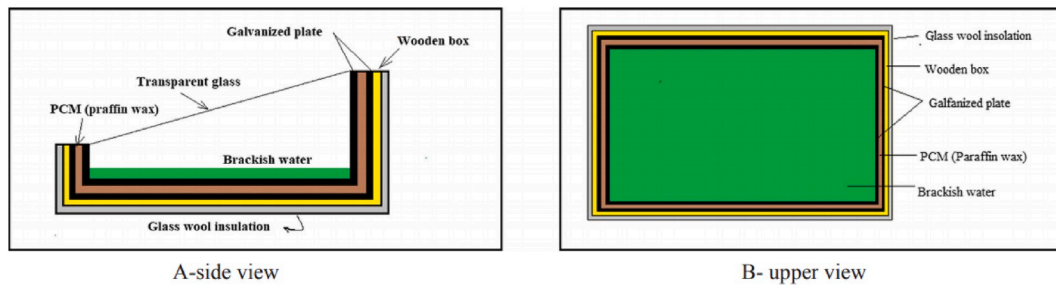


Fig. 14. Schematic diagram of distiller parts with PCM, [48].

The economic analysis directed that the cost expressed per liter of water is the lowest for the solar still based on the NEPCM with CuO nanoparticles (only costs \$ 0.026 per liter).

## 2.5. Summary of NEPCM applications

The application of nano-enhanced PCMs in specific systems, processes and components is a relatively new research area. Therefore, an arbitrary classification was made with respect to the selected research works and their technical application area of NEPCMs.

The most NEPCMs, particularly nanocomposites, can be utilized in thermal energy storage applications. In this respect, NEPCMs can be used in solar collector systems [6,34], cool storage systems [35], for engine exhaust gas heat recovery [36], etc. Furthermore, NEPCM materials are used for the thermal management of photovoltaic systems, such as in the case of the free-standing photovoltaics [38], PCM integrated PV panels [40], thermal management of the building integrated PVs [41], direct water cooling of PVs [7], but also for cooling of the electronic chipsets [44], heat pipe cooling for electronics [45] and battery cooling of lithium-ion batteries [42] or in general battery packs in different climates [43]. Due to the growing lack of potable water, the application of NEPCMs can significantly improve the efficiency of solar

desalination systems [49] and solar distillers [48]. Generally, there are very few areas of a concrete application of NEPCMs in fully operable systems, Fig. 16.

The NEPCM based thermal energy storage includes a variety of possible applications such as solar collector systems, engine waste heat recovery, cold thermal energy storage, etc. Therefore, future research should be focused on improving the efficiency of existing systems and finding possible new applications in other systems. Previously mentioned actions may result in an efficiency surplus from efficient thermal management. In a world that seeks the electrification of transport, the development of efficient battery systems is one of the main priorities. Consequently, significant breakthroughs can be expected in researches focusing on the use of NEPCM materials for thermal management of batteries. NEPCM materials may help with better heat extraction from the photovoltaic systems especially considering their relatively low overall efficiency, hence more efforts in this direction can be expected. Significant improvement of photovoltaic energy conversion efficiency is very demanding to achieve, thus each effort that can improve performance is valuable. In this respect, NEPCM materials can make a significant contribution especially because they can be used in both passive and active cooling of PV systems. Unfortunately, very few papers are concerned with the implementation of NEPCM materials for

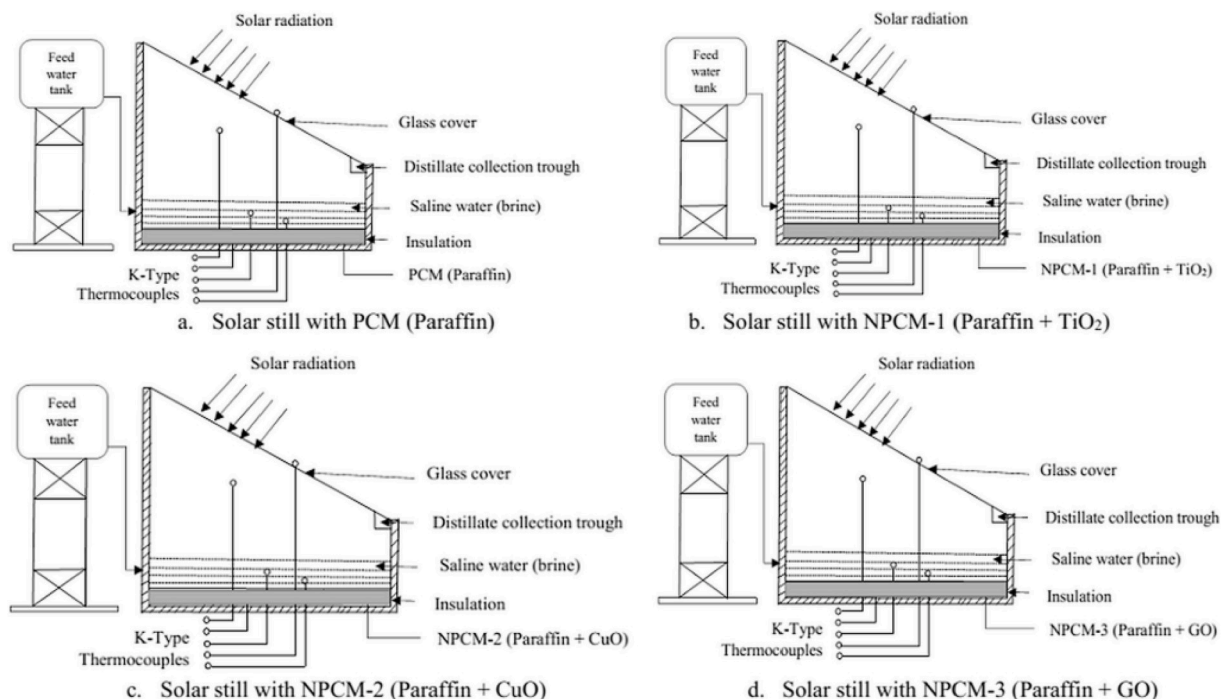


Fig. 15. Schematic diagram of tested solar stills, [49].

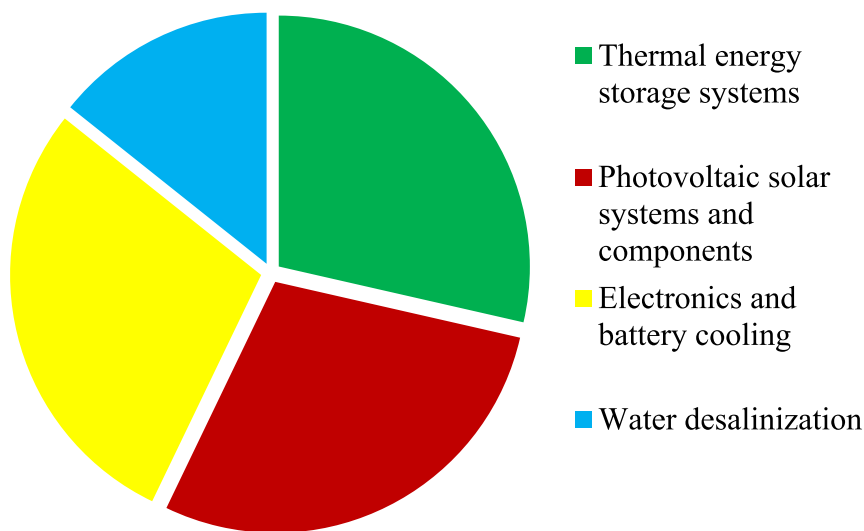


Fig. 16. Areas of NEPCM application in reviewed studies.

water desalination systems, which is a curiosity when considering the growing lack of potable water. Furthermore, these materials could be used to improve the efficiency of wastewater treatment systems. The development of nanotechnology is rapidly progressing, so we can expect a more significant and more diverse application of nano-enhanced PCM materials in the near future.

### 3. Brief overview of NEPCM preparation technology

The preparation process of an NEPCM is demanding due to general

complex physical nature of nanomaterials. The variety of different NEPCM preparation methodologies can be found in the existing literature. Mixing the PCM with nanomaterials is a very demanding operation that requires good preparation, precision and high safety standards. In the existing literature that deals with application of NEPCMs, three main groups of NEPCM materials can be found, i.e. nano-composites, nano-fluids and microencapsulated PCMs with nanomaterials. The preparation of microencapsulated PCMs will not be considered in this paper as it is above the scope of the herein covered research. The preparation of process is relatively complex problem that requires good knowledge of

chemical engineering. Nanocomposites and nanofluids are less demanding regarding the general preparation process and due to that they are more present in general applications.

### 3.1. Preparation of nanofluids

Nanofluids are often used as a heat transfer fluid (HTF) due to their suitable viscosity while many nanofluids can also be used as PCM materials. Various solutions can be used for the previous purpose where the most common are water-based nanofluids.

Altahamy et al. [35] discussed the effect of a water-based NEPCM on cool storage performance. Nanoparticles of gamma alumina ( $\gamma$ - $\text{Al}_2\text{O}_3$ ) were mixed with water in 0.5%, 1.0%, 1.5% and 2.0% volume fractions. The mixing was done by ultrasonication at a temperature of 30 °C for 90 min. The mixing device was not specified as well as mixing frequency. Shao et al. [50] investigated the solidification behaviors of hybrid nanofluids containing  $\text{TiO}_2$  nanotubes (TiNTs) and nanoplatelets (TiNPs). Hybrid nanofluids with different TiNP percentages (0%–100%) at the similar and different total  $\text{TiO}_2$  mass fractions (0.1%, 0.2%, 0.3%) were prepared. The nanofluid was based on deionized water that was mixed for 30 min with nanomaterials. The first with a magnetic stirrer (S22-2 device) and then with an ultrasonic cleaner (KQ3200DE device). It is not clear whether the 30-min period refers to a magnetic stirrer or an ultrasonic cleaner, nor does it indicate at which temperature, revolutions and frequency the mixing was performed. Liu and Yang in Ref. [51] investigated Titania based nanoparticles ( $\text{TiO}_2$ -P25) dispersed in inorganic hydrated salt PCMs (disodium hydrogen phosphate dodecahydrate ( $\text{Na}_2\text{HPO}_4 \cdot 12\text{H}_2\text{O}$ ) and sodium carbonate decahydrate ( $\text{Na}_2\text{CO}_3 \cdot 10\text{H}_2\text{O}$ ). The solution with a mass ratio 60:40. The mass fractions of the  $\text{TiO}_2$  nanoparticles were 0.1%, 0.3% and 0.5%, respectively. In the first step, the solution was placed in a beaker in a thermostated water bath (kept at 55 °C). Then, the NEPCM was stirred for 2 h at 1500 rpm and finally ultrasonicated for 30 min (with a mixing power of 120 W). Munyalo et al. [52] investigated the latent heat in the fusion of nanofluid-based phase change materials. An aqueous solution of 24 wt%  $\text{BaCl}_2 \cdot 2\text{H}_2\text{O}$  was used as a base for two nanofluids in which two types of nanomaterials were added. Nanoparticles of MgO and multi-walled carbon nanotubes (MWCNT) were added to the solutions with a mass fraction of 0.2%, 0.4%, 0.6%, 0.8% and 1.0%, Fig. 17. Both solutions were initially mixed for 30 min with a magnetic stirrer (HJ-6A device), followed by 45 min of ultrasonication (the working time was 5 s and stop time was 10 s) at a temperature of 50 °C. The authors did not specify which type of ultrasonic vibrator was used nor at what frequency. Furthermore, it was not stated at which number of revolutions and temperatures the stirrer was used.

Wang et al. [26] investigated the thermal radiative properties of  $\text{Al}_2\text{O}_3$  paraffin-based nanofluid.  $\text{Al}_2\text{O}_3$  nanoparticles (0.001, 0.005 and 0.01 vol%) were added to the liquid paraffin and dispersed using 30 min of magnetic stirring and 1.5 h of ultrasonication. Used devices and other parameters were not specified. Also, the CTAB surfactant was used as a dispersing agent to avoid possible agglomeration of nanoparticles.



Fig. 17. Multi-walled carbon nanotubes (MWCNT) nanofluids, [52].

### 3.2. Preparation of nanocomposites

NEPCM nanocomposites are most commonly based on paraffin wax to which nanomaterials of different morphologies are added. However, many other organic and inorganic PCM materials can also be found in the existing research findings.

Warzoha et al. [53] investigated the temperature dependence of thermal properties in an NEPCM based on paraffin and herringbone style graphite nanofibers with volume fractions of 0.05%, 0.1%, 0.2%, 0.3%, 0.4%, 2.8%, 5.8%, 8.5% and 11.4%. A hot plate with a constant temperature was used to melt the PCM at a temperature of 80 °C. To disperse the nanofibers in the PCM, a sonicator was used for 2 h at a frequency of 32 Hz. It was not reported which device was used for the sonication.

Nourani et al. [54] developed a new NEPCM material that was formed by dispersing  $\text{Al}_2\text{O}_3$  nanoparticles (mass fraction: 2.5%, 5.0%, 7.5%, 10.0%) in paraffin wax using a surfactant, Fig. 18. The nanoparticles were mixed for 1 h with the PCM using a magnetic stirrer and a vacuum pump (VDE 0530, KNF NEUBERGER), 600 mmHg vacuum. After that, ultrasonic vibration (1200 M, SONICA, Italy) was used for 2 h, with these parameters: 80 W, 50 kHz. During the mixing process, petroleum ether was added as the solvent to maintain the liquid phase (after mixing the solvent was removed by heating the mixture).

Motahar et al. [55] conducted an experimental study on the solidification of n-octadecane PCM enhanced with nanoparticles of Titanium (IV) oxide ( $\text{TiO}_2$ ) with mass fractions of 1.0%, 2.0% and 4.0%. The blend was first subjected to mechanical stirring and then an ultrasonic bath (VWR, USC2100D, Germany) was used for 15 min, 40 °C. The mixing parameters were not specified in the previously addressed study.

Wang et al. [56] investigated the impact of graphite nanoparticles (mass fraction: 0.05%, 0.1%) on the photothermal performance and thermal properties of water/paraffin emulsion, Fig. 19. To disperse the nanoparticles, a rotor-stator homogenizer (FJ200-SH) was used for 5 min at 12,000 rpm. The authors did not indicate at which temperature the homogenization of the mixture was performed.

Chieruzzi et al. [57] discussed the influence of mixing parameters on the thermal characteristics of NEPCMs. The nanoparticles of  $\text{SiO}_2$  and  $\text{Al}_2\text{O}_3$  with a mass fraction of 1.0% were combined with a nitrate salt mixture (60 wt%  $\text{NaNO}_3$  and 40 wt%  $\text{KNO}_3$ ). A twin-screw micro-compounder device (DSM Xplore, Model 2005) was used for mixing the NEPCM directly at high temperatures. Two combinations of different parameters were studied; 100 rpm for 15 min and 200 rpm for 30 min. It was found that the combination of 200 rpm and 30 min overall showed to be the best mixing strategy.

Ebadi et al. [58] dispersed CuO nanoparticles (mass fraction: 0.1%,

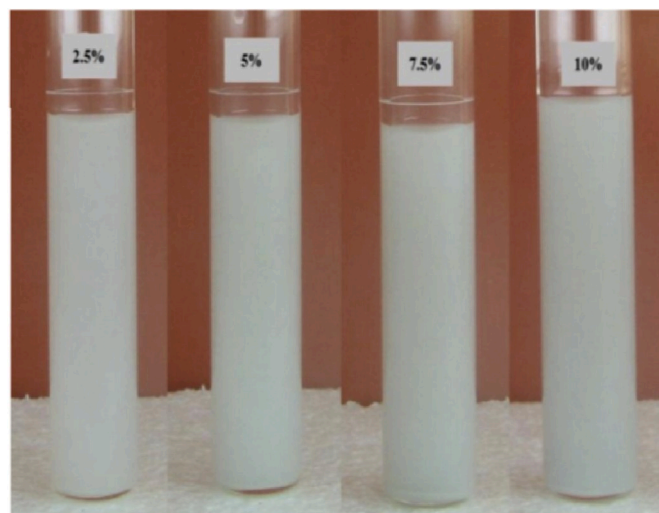


Fig. 18. Sedimentation examples of NEPCMs after 48 h, [54].



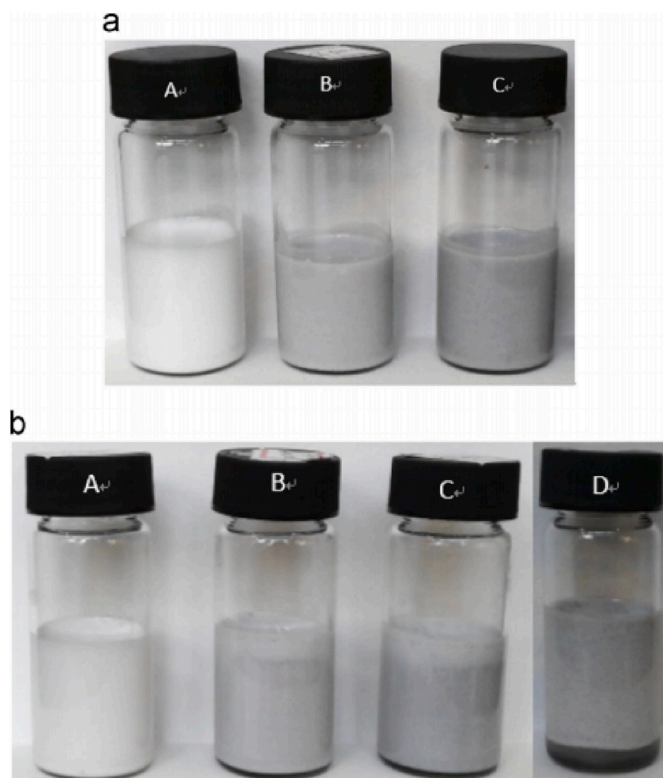


Fig. 19. (a) Emulsions before 7 days of storage and (b) Emulsions after 7 days of storage (D-after 300 heating/cooling cycles), [56].

1%) in coconut oil and examined the melting process as well as thermal properties of the nanocomposites. To achieve an adequate dispersion of the nanoparticles, a magnetic stirrer (SP88854100 device) was used for 12 h at a temperature of 60 °C. After that preparation was followed by 30 min of sonication with the Q500 (Qsonica) sonicator. The temperature and frequency of the sonication and the rpm for the magnetic stirrer were not reported.

Salyan and Suresh in Refs. [59] conducted experimental research on the effect of CuO nanoparticles (mass fraction: 0.1%, 0.2%, 0.5%) on the thermal properties of D-Mannitol ( $C_4H_{14}O_6$ ). In order to properly disperse the nanoparticles in the PCM, a low energy ball mill was used for 2.5 h at 250 rpm. Then, an ultrasonic vibrator (Make: Lark Instruments) was used at a frequency of 40 kHz, not specified at which temperature and time period.

Praveen and Suresh [60] investigated the heat transfer performance of an NEPCM based on neopentyl glycol (NPG) and CuO nanoparticles (mass fraction: 0.5%, 1.0%, 3.0%), Fig. 20. The NPG samples with the nanoparticles were prepared using a low energy ball mill (0.5HP/230V/50Hz/300 rpm, Make: VB Ceramics) at 200 rpm for a period of 120 min, followed by a probe type sonicator (Make: Lark Industries) for 10 min at 40 kHz. Unfortunately, the sample temperatures for the duration of the preparation were not specified.

### 3.3. Summary of NEPCM preparation techniques

In most of the examined research reports, the process of preparation is inadequately described. Often, important details are missing such as the physical properties of the sample, volume or mass of the sample, mixing parameters, the specifications of the equipment used, etc. These parameters and details are critical for the preparation process and could be useful for other researchers who are dealing with this subject. It is often not specified exactly which device was used (model, manufacturer, etc.) and for what period. Furthermore, it is often not declared at what number of revolutions a stirrer was used or at which frequency

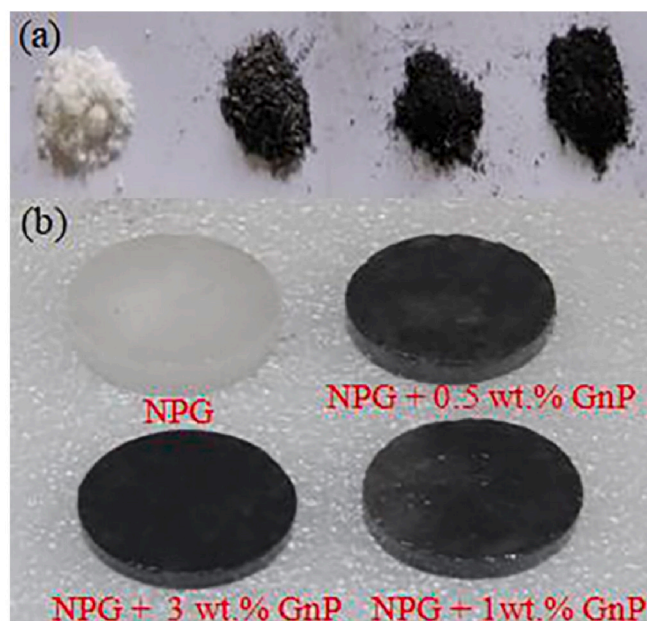


Fig. 20. (a) Powder form of NEPCM samples (b) NEPCM samples with different mass fraction of CuO nanoparticles, [60].

sonication was performed. The sample temperature during mixing should be monitored and ultimately stated in the paper. The amount of PCMs (primarily mass if possible, if not, volume) and nanomaterials (wt. % or vol%) in NEPCMs should be clearly stated because the mixing parameters directly depend on it. When dealing with nanomaterials, operator safety must be the priority, so it is necessary to have adequate protective equipment. It should be noted that an article [61] reviewed the research findings focused on preparation process where size, as well as shape of nanoparticles were examined with respect to the characterization and stability. The main research findings showed that different parameters affect thermo-physical characteristics of nanofluids and mixing process. Mainly size and shape of nanoparticles are critical, together with sonication (mixing) procedure. It was also found that size and shape are mostly dependent from the synthesis process of the nanoparticle. The stability of the nanofluids is highly affected by surface charge and which is linked with sonication preparation. Finally, it can be highlighted that mixing process and synthesis of nanoparticle are the most critical parameters that strongly affect thermal as well as physical properties of nanofluid and their stability. It would be very useful and important if future articles cover more details on the NEPCM preparation itself, including a brief description of the safety procedures.

## 4. General thermal properties of NEPCMs and nanofluids

The addition of nanomaterials affects the thermal properties of the base PCM material in general, to what extent depends on the amount and type of added nanomaterials. The main limiting factor of most PCM materials is rather weak thermal conductivity. Therefore, thermal conductivity is the most prominent material physical property in all existing research studies dealing with NEPCM materials. In addition to the thermal conductivity, significant changes in other properties such as specific heat capacity, latent heat, melting point ( $T_m$ ), etc. may also occur.

### 4.1. Overview of thermal properties

Harish et al. [62] reported that the thermal conductivity of a lauric acid based PCM ( $T_m = 44$  °C) increased with the percentage of graphene nanoplatelets (5–10 nm) in the PCM. A maximum increase of about 230% was detected for an NEPCM with 1 vol% of graphene

nanoplatelets. Warzoha et al. [53] found that the latent heat in a fusion of organic paraffin ( $T_m = 56\text{ }^\circ\text{C}$ ) decreases with the percentage of herringbone graphite nanofibers (HGNF) (2–100 nm). The latent heat of fusion in the pure paraffin PCM was 271.6 J/g, while the latent heat of fusion in the NEPCM with 11.4 vol% of graphite nanofibers was 242.7 J/g. The thermal conductivity as well as thermal diffusivity increases with the increase in volume fraction of the HGNF, Fig. 21.

Sharma et al. [63] prepared an NEPCM based on palmitic acid ( $T_m = 60\text{--}62\text{ }^\circ\text{C}$ ) and nanoparticles of  $\text{TiO}_2$  (21 nm). The authors state increase in the mass fraction of nanoparticles causes the NEPCM thermal conductivity to increase. A maximum increase in thermal conductivity of about 80% was recorded for 5 wt% loading of nanoparticles. For the same concentration of nanoparticles, there was a 15.5% decrease of latent heat of fusion with respect to the pure PCM.

Nourani et al. [54] modified the paraffin ( $T_m = 54\text{--}58\text{ }^\circ\text{C}$ ) with different mass fractions of  $\text{Al}_2\text{O}_3$  nanoparticles (10–20 nm). The mass fraction increase of nanoparticles results in the latent heat decrease as it is shown in Fig. 22, based on data from the paper [54]. The authors in the article claim that the character of the relationship between effective thermal conductivity and increasing  $\text{Al}_2\text{O}_3$  mass fraction is nonlinear, both for solid and the liquid phase. The enhancement ratio of the effective thermal conductivity was 31% in the solid phase and 13% in the liquid phase for the NEPCM with 10.0 wt% of  $\text{Al}_2\text{O}_3$  nanoparticles. A reduction of 27% regarding the heating and melting times was also detected for the same concentration of nanoparticles in the PCM.

Lin et al. [34] examined the thermal properties of nanocomposites based on paraffin wax and nanoparticles of Cu (20 nm). From the results presented in this paper, it was found that increasing the percentage of the nanoparticles in the PCM increases thermal conductivity. However, the addition of nanoparticles decreases the latent heat as presented in Fig. 23 which was generated based on the data from paper [34]. The largest increase in thermal conductivity of 46.3% was achieved by 2 wt % of nanoparticles.

Altohamy et al. [35] experimentally investigated a water based nanofluid with  $\text{Al}_2\text{O}_3$  nanoparticles (50 nm). The reduction in solidification time was about 30% at  $\text{Al}_2\text{O}_3$  2 vol% concentration when compared with pure water.

Colla et al. in Ref. [64] added  $\text{Al}_2\text{O}_3$  (10 nm) and Carbon Black (CB) (15–20 nm) nanoparticles in two paraffin waxes (RUBITHERM®RT20,  $T_m = 20\text{ }^\circ\text{C}$  and RUBITHERM® RT25,  $T_m = 25\text{ }^\circ\text{C}$ ). The authors claim that the addition of 1 wt%  $\text{Al}_2\text{O}_3$  nanoparticles causes a degradation of thermal conductivity in both PCMs by 7–8%, while 1 wt% of Carbon

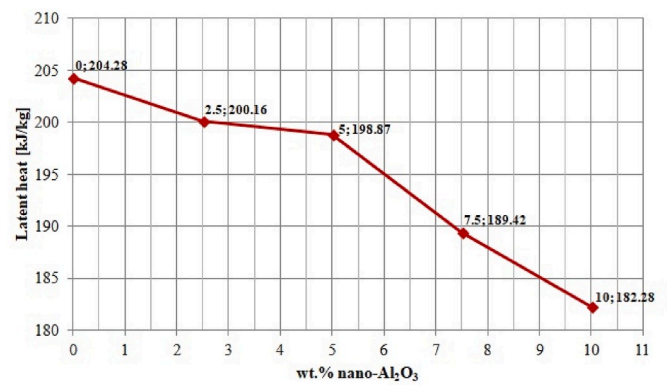


Fig. 22. Latent heat of pure paraffin and nanocomposites.

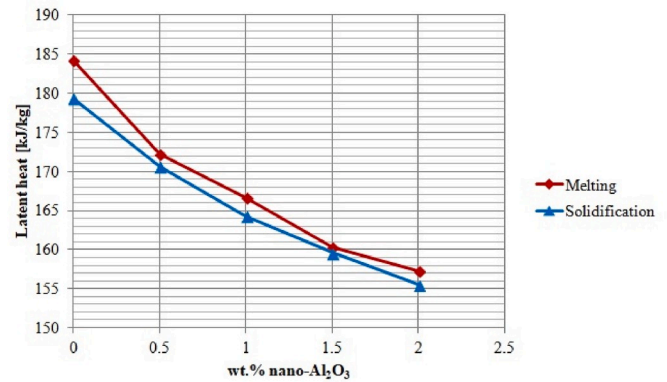
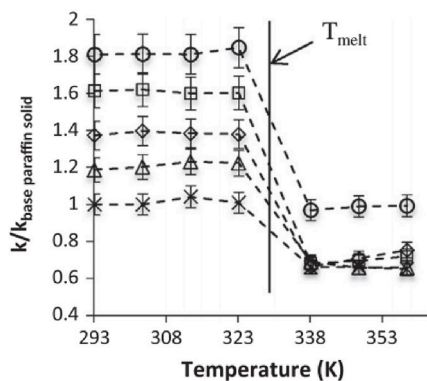


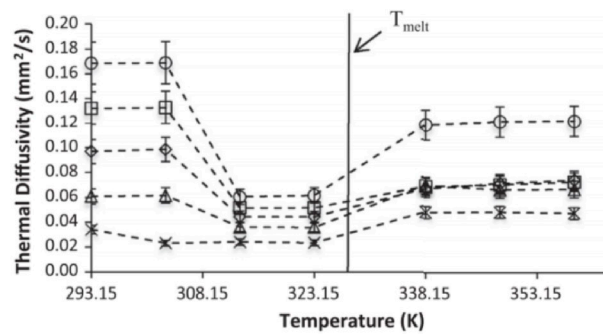
Fig. 23. Solidification/melting latent heat of pure paraffin and nanocomposites.

Black nanoparticles increases thermal conductivity by more than 25%. When the  $\text{Al}_2\text{O}_3$  nanoparticles were added to the RT20, the improvement of the latent heat was 10.8%, while in the case of CB nanoparticles the improvement was only 3.4%, Table 1. The addition of CB nanoparticles to RT25 caused the penalization of the latent heat by 11.6%, Table 1 (based on data from Ref. [64]).



- x-- Base Paraffin --△-- 2.8% HGNF
- ◇-- 5.8% HGNF --□-- 8.5% HGNF
- 11.4% HGNF

(a)



- x-- Base Paraffin --△-- 2.8% HGNF --◇-- 5.8% HGNF
- 8.5% HGNF --○-- 11.4% HGNF

(b)

Fig. 21. (a) Thermal conductivity of HGNF/PCM nanocomposites (b) Thermal diffusivity of HGNF/PCM nanocomposites, [53].

**Table 1**

Latent heat of pure paraffin waxes and nanocomposites.

| NEPCM                                | wt.% of nanomaterials | Latent heat [kJ/kg] | Variation (%) |
|--------------------------------------|-----------------------|---------------------|---------------|
| RT20                                 | 0                     | 117.782             | 0             |
| Al <sub>2</sub> O <sub>3</sub> /RT20 | 1                     | 130.495             | +11           |
| CB/RT20                              | 1                     | 121.815             | +3            |
| RT25                                 | 0                     | 133.522             | 0             |
| Al <sub>2</sub> O <sub>3</sub> /RT25 | 1                     | 134.184             | +1            |
| CB/RT25                              | 1                     | 117.998             | -12           |

Wang et al. [56] examined the thermal conductivity and photo-thermal conversion performance of emulsion, based on paraffin ( $T_m = 58\text{--}60\text{ }^\circ\text{C}$ ) and water, enhanced with graphite nanoparticles (<30 nm). The rise in thermal conductivity of 20% was perceived for an NEPCM containing 0.1 wt% of graphite when compared to the base PCM. It was also indicated in the same study that the specific heat of the tested emulsions decreased as the graphite nanoparticles mass fraction increased, Fig. 24.

Chieruzzi et al. [57] produced a nanofluid based on a nitrate salt mixture of 60 wt% NaNO<sub>3</sub> and 40 wt% KNO<sub>3</sub>,  $T_m = 220\text{ }^\circ\text{C}$ . In order to create the NEPCM, SiO<sub>2</sub> (7 nm), Al<sub>2</sub>O<sub>3</sub> (13 nm) and a mixture of SiO<sub>2</sub>/Al<sub>2</sub>O<sub>3</sub> (2–200 nm) nanoparticles (1% mass fraction) were added to the nitrate salt mixtures. The best results were achieved for the nanofluid with 1 wt% of SiO<sub>2</sub>/Al<sub>2</sub>O<sub>3</sub> nanoparticles. The specific heat in the solid phase was improved by 52.1% and in the liquid phase by 18.6%. The stored heat was increased by 13.5% compared with the pure PCM. Wang et al. [65] prepared a stable OP10E ( $T_m = 8\text{--}10\text{ }^\circ\text{C}$ ) and water emulsion which was enhanced by the addition of graphite nanoparticles (<30 nm). The authors claim that the supercooling effect of the emulsion can be eliminated by adding graphite nanoparticles in mass fraction greater than 2%. Furthermore, it was stated that the addition of graphite nanoparticles to the OP10E/water emulsion did not affect the latent heat. In the same study, it was found that 2 wt% of graphite nanoparticles resulted in a thermal conductivity increase of 88.9%. Shao et al. [50] experimented with a nanofluid based on deionized water and dispersed hybrid nanoparticles of TiO<sub>2</sub>, i.e. nanotubes (TiNT, 9–10 nm) and nanoplatelets (TiTP, 50–80 nm). The nanofluid with 0.1 wt% of TiO<sub>2</sub> (25% TiNPs) had the largest improvement in thermal conductivity by 22.30%, compared with deionized water. The effect of the super-cooling degree of hybrid nanofluid was reduced by up to  $4.97 \pm 0.2\text{ }^\circ\text{C}$  and  $5.27 \pm 0.2\text{ }^\circ\text{C}$ , when compared to ordinary nanofluid. The freezing time for hybrid nanofluid was reduced by up to 54.91% (compared with TiNT nanofluid) and 56.42% (compared with TiNP nanofluid). Bahiraei et al. [66] experimentally and numerically explored

the properties of three NEPCMs based on paraffin wax ( $T_m = 60\text{ }^\circ\text{C}$ ) and carbon-based nanomaterials (carbon nanofibers, graphene nanoplatelets and graphite nanopowder). According to the findings the highest thermal conductivity improvement of 1100% was obtained by adding 10 wt% of graphite nanopowder to the paraffin wax. Usually, the improvement of thermal conductivity is not nearly as large, so this result should be taken with certain caution. Sami and Etesami [67] investigated the thermal properties of an NEPCM based on the paraffin ( $T_m = 54\text{--}58\text{ }^\circ\text{C}$ ) and nanoparticles of TiO<sub>2</sub> (5–20 nm). Thermal conductivity was increased by 47.85% when 2 wt% of TiO<sub>2</sub> nanoparticles was added. No significant changes were observed in the melting temperature as well as latent heat after thermal cycling, Table 2. Table 2 was formed based on the selected data from paper [67].

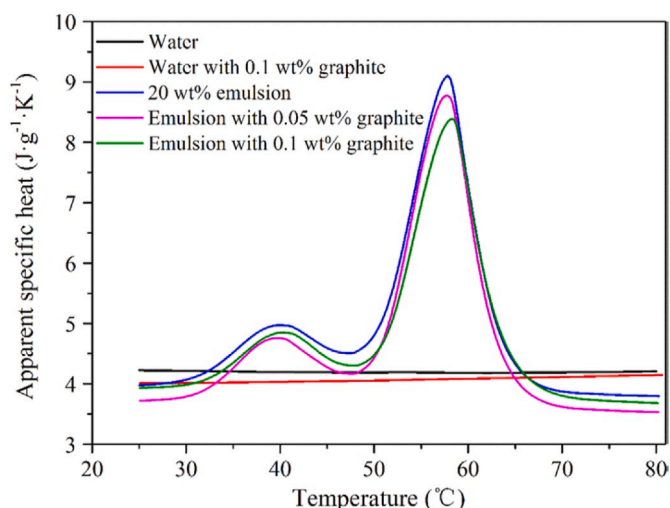
Ebadi et al. [58] enhanced coconut oil ( $T_m = 24\text{ }^\circ\text{C}$ ) with nanoparticles of CuO (<50 nm) to create bio-based NEPCMs. A nanocomposite with 1 wt% of nanoparticles had 7.5% higher thermal conductivity than the base PCM while the specific heat as well as latent heat of fusion decreased by 0.75% and 8.2%. Barreneche et al. [68] experimentally determined that the morphology of nanomaterials, e.g. spherical carbon black nanoparticles, CB (10 nm), multi-walled carbon nanotubes, MWCNT (9.5 nm), graphene oxide nanosheets, GO (2 nm), significantly affects the thermal conductivity and sub-cooling effect. However, it does not affect the phase change enthalpy of the water. The thermal conductivity of CB/H<sub>2</sub>O, MWCNT/H<sub>2</sub>O and GO/H<sub>2</sub>O NEPCM in the solid phase increased by 8%, 14% and 7% for 0.1 wt% of nanomaterials, Table 3 (based on data from Ref. [68]).

Harikrishnan et al. [69] investigated the thermal properties of myristic acid PCM ( $T_m = 52\text{ }^\circ\text{C}$ ) enhanced with SiO<sub>2</sub>nanospheres (52 nm). The highest improvement of PCM thermal conductivity was 87.27% and was achieved for 1.0 wt% of SiO<sub>2</sub> nanospheres. Liu and Yang [51] enhanced the thermal properties of inorganic hydrate salt with TiO<sub>2</sub>-P25 nanoparticles (21 nm). The specific heat was improved by 83.5% in the solid phase and 15.1% in the liquid phase by adding 0.3 wt% of nanoparticles. Furthermore, the latent heat was increased by 6.4%. Munyalo et al. [52] prepared Barium Chloride Dehydrate solutions in which nanoparticles of MgO (40 nm) and multi-walled carbon nanotubes (MWCNT) (5–20 nm) were added. The authors state that a 7% reduction of latent heat was detected for 1 wt% MWCNT enhanced fluid and 5.2% reduction for 1 wt% MgO enhanced fluid. Salyan and Suresh [59] investigated the thermal properties of D-Mannitol ( $T_m = 165\text{--}169\text{ }^\circ\text{C}$ ) enhanced with nanoparticles of CuO (10–40 nm). The addition of 0.5 wt% of CuO nanoparticles to the PCM resulted in a 25% rise in thermal conductivity. The addition of CuO nanoparticles resulted in a mostly slight decrease in the latent heat of D-Mannitol, Fig. 25 (based on data from Ref. [59]).

Mayilvelnathan and Valan Arasu [70] experimentally found the thermal conductivity of pure erythritol PCM (laser flash method was used), i.e. erythritol with 0.1% GNP, 0.5% GNP and 1% GNP (Graphene nanoparticles) before as well as after thermal cycling periods. The thermal conductivity of pure erythritol was 0.733 W/mK, while erythritol with a 0.1, 0.5 and 1 wt% GNP, the thermal conductivity was increased to 1.074, 1.095 and 1.122 W/mK. The thermal conductivity was 0.692, 0.899, 0.921, and 1.020 W/mK for pure erythritol without and with 0.1, 0.5 and 1 wt% GNP respectively (data gained after 100 thermal cycles).

Putra et al. [71] examined the thermal properties of NEPCMs based on Rubitherm® paraffin wax, RT22 HC ( $T_m = 22\text{ }^\circ\text{C}$ ) and graphene nanoplatelets (<2 nm). The thermal conductivity of the PCM was increased by 89.6% as a result of adding 0.3 wt% of graphene. More on the thermal properties of the RT22 HC/graphene NEPCM are listed in Table 4 which is based on data from Refs. [71].

Yadav et al. [72] prepared nanocomposites based on magnesium chloride hexahydrate (MCH) ( $T_m = 115\text{--}118\text{ }^\circ\text{C}$ ) and nano-graphite particles (NG). The nanocomposite (0.5 wt% of NG) had an improvement in thermal conductivity of 308% and an increase in the melting as well as solidification rate of 22% and 75% with respect to the pure PCM.

**Fig. 24.** Apparent specific heat vs temperature, [56].



**Table 2**  
Latent heat and melting temperature of pure paraffin and nanocomposites after thermal cycles.

| NEPCM                          | wt.% of nanomaterials | Melting temp. [°C] |          |          | Latent heat [J/g] |          |          |
|--------------------------------|-----------------------|--------------------|----------|----------|-------------------|----------|----------|
|                                |                       | Cycle 0            | Cycle 40 | Cycle 80 | Cycle 0           | Cycle 40 | Cycle 80 |
| Paraffin                       | 0                     | 58.9               | 57.92    | 56.31    | 137.8             | 136.61   | 135.61   |
| TiO <sub>2</sub> /Paraffin     | 3                     | 60.64              | 60.2     | 58.34    | 136.4             | 135.3    | 134.71   |
| TiO <sub>2</sub> +SSL/paraffin | 3                     | 56                 | 55.34    | 54.82    | 167               | 166.55   | 166.05   |

**Table 3**  
Properties of water-based NEPCMs enhanced with 0.1 wt% of nanomaterials, [68].

| Nanomaterial type | Size [nm] | Phase change enthalpy [kJ/kg] | Subcooling reduction [°C] | Thermal conductivity increment (solid) [%] |
|-------------------|-----------|-------------------------------|---------------------------|--|
| CB                | 100       | 291                           | 5                         | 7.6  |
| MWCNT             | 35        | 290                           | 2.5                       | 13.9                                       |
| GO                | 110       | 308                           | 4                         | 6.8  |

Águila V et al. [73] conducted research on the effect of CuO nanoparticle concentration and impact of temperature on thermal viscosity and conductivity of Octadecane ( $T_m = 28-30$  °C). The highest reported average increase in thermal conductivity for a CuO concentration of 10% w/v was 8.2%. Dsilva Winfred Rufuss et al. [49] added three types of nanoparticles to paraffin. Nanoparticles of titanium dioxide (TiO<sub>2</sub>), copper oxide (CuO) as well as graphene oxide (GO) were added in a mass fraction of 0.3% to create different NEPCMs. Their thermal conductivity was improved by 25.0%, 28.8% and 101% when compared to pure paraffin. Praveen and Suresh [60] carried out an experimental research of heat transfer performance regarding neopentyl glycol ( $T_m = 126$  °C) enhanced with nanoparticles of CuO (30–50 nm). A thermal storage and release performance test was performed. The loading of 3 wt% of CuO nanoparticles reduced the storage time by 33.8%. The thermal conductivity of the pure PCM increased by factor of 4.08 with the addition of CuO nanoparticles in the 3% mass fraction.

#### 4.2. Summary and discussion of enhanced thermal properties

The vast majority of reviewed papers are focused on thermal conductivity enhancement as direct effect of nanomaterial addition to phase change materials. Therefore, Table 5 represents an overview of the highest improvement of thermal conductivity with respect to the type of nanomaterials and type of PCM. The types of nanomaterials were

characterized by a brief description of morphology and size (if available), while the quantity of nanomaterials in the PCM is given by mass or volume fraction. Furthermore, if it was available in the considered research studies, the melting point of the PCM was provided on the list. In most research works, a noticeable improvement in thermal conductivity was reported with the addition of nanomaterials to the base PCM. The only exception was study [64] where the addition of Al<sub>2</sub>O<sub>3</sub> nanoparticles to paraffin caused 7–8% lower thermal conductivity compared with pure paraffin. There is no clear explanation of this phenomenon in mentioned study [64]. Generally, due to the improved thermal conductivity of nanocomposites and nanofluids, a reduction in heating, melting and solidification times can be expected. In most studies, the addition of nanomaterials causes a slight decrease in the latent heat, except in work [64] related to the passive cooling application and in the work [51] for the case of the hydrate salts, where an increase of 10.8% and 6.4% were reported, while in study [65] the addition of the graphite nanoparticles to OP10E/water emulsion did not affect the latent heat. The increase of latent heat can be explained by the theory of chemical with a constant chemical composition [51]. The nanocomposites had lower specific heat compared to the base PCM as for example in the case of the improvement of the photo-thermal performance [56], PCM filled

**Table 4**  
Thermal properties of RT22 HC/graphene nanocomposites.

| Mass fraction [wt.%] | Latent heat of fusion [J/g] | Latent heat of solidification [J/g] | Melting point [°C] | Freezing point [°C] | Specific heat capacity [J/g°C] |
|----------------------|-----------------------------|-------------------------------------|--------------------|---------------------|--------------------------------|
| 0                    | 163.31                      | 169.02                              | 25.37              | 19.11               | 2.1                            |
| 0.05                 | 161.43                      | 168.68                              | 24.72              | 19.80               | 1.944                          |
| 0.10                 | 160.95                      | 165.56                              | 24.55              | 19.85               | 1.860                          |
| 0.15                 | 155.47                      | 164.53                              | 25.33              | 18.96               | 1.692                          |
| 0.20                 | 155.37                      | 163.98                              | 24.27              | 19.93               | 1.548                          |
| 0.25                 | 155.20                      | 163.90                              | 25.25              | 18.91               | 1.512                          |
| 0.30                 | 155.98                      | 162.44                              | 24.84              | 19.24               | 1.332                          |

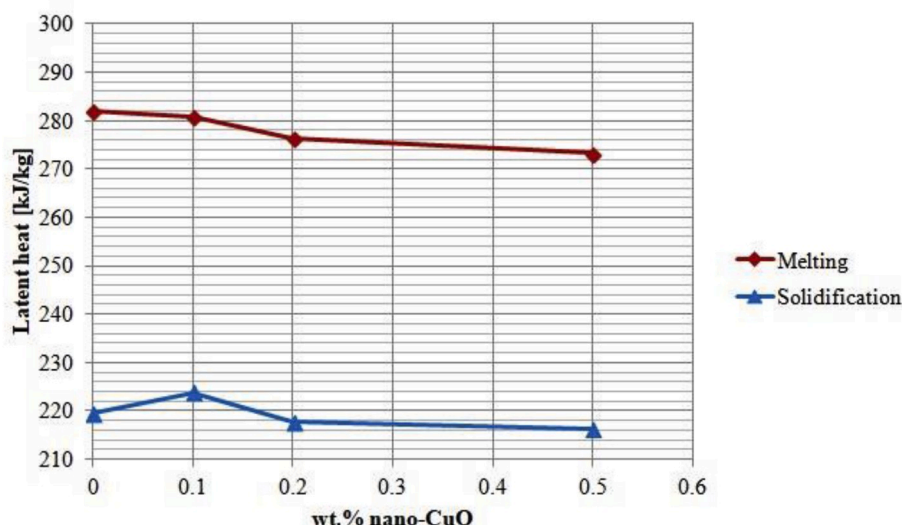


Fig. 25. Latent heat of pure D-Mannitol and D-Mannitol/CuO.

**Table 5**  
Highest enhancement of thermal conductivity with respect to type of nano-materials and type of PCM.

| Reference | PCM and melting temperature  | Nanomaterial  | Largest increase in thermal conductivity of base PCM with addition of nanomaterials  |
|-----------|--|---|--|
| [62]      | n-Dodecanoic acid (Lauric acid); $T_m = 44$ °C   | Liquid phase exfoliated multilayer graphene nanoplatelets (MLG); 5–10 nm; Volume fraction: 0.1%, 0.25%, 0.5%, 0.75%, 1%   | Maximum thermal conductivity enhancement of ~230% for graphene addition of 1 vol%.   |
| [53]      | Organic Paraffin (IGI 1230A); $T_m = 56$ °C  | Herringbone graphite nanofibers (HGNEF); 2–100 nm; Volume fraction: 0.05%, 0.1%, 0.2%, 0.3%, 0.4%, 2.8%, 5.8%, 8.5%, 11.4%  | The highest increase in thermal conductivity was achieved by 11.4 vol % of graphite nanofibers, which is particularly evident in the solid phase, Fig. 21.                               |
| [63]      | Palmitic acid; $T_m = 60$ –62 °C   | Nanoparticles of titanium dioxide ( $TiO_2$ ); 21nm; Mass fraction: 0.5%, 1.0%, 3.0%, 5.0%  | Increase in thermal conductivity of about 80% for $TiO_2$ loading of 5 wt%.  |
| [54]      | Paraffin; $T_m = 54$ –58 °C  | Nanoparticles of $Al_2O_3$ ; 10–20 nm; Mass fraction: 2.5%, 5.0%, 7.5%, 10.0%)  | The addition of 10.0 wt% of $Al_2O_3$ nanoparticles resulted in a 31% increase of the effective thermal conductivity in the solid phase and 13% in the liquid phase.                     |
| [34]      | Paraffin wax   | Nanoparticles of Cu; 20 nm; Mass fraction: 0.5%, 1.0%, 1.5%, 2.0%   | Thermal conductivity increase of 46.3% was achieved by 2 wt% of nanoparticles.   |
| [64]      | Paraffin (RUBITHERM® RT20); $T_m = 20$ °C<br>Paraffin (RUBITHERM® RT25); $T_m = 25$ °C | A) Nanoparticles of $Al_2O_3$ ; 10 nm; Mass fraction: 1.0%<br>B) Nanoparticles of Carbon black (CB); 15–20 nm; Mass fraction: 1.0%  | $Al_2O_3$ nanoparticles caused a decrease in thermal conductivity for both PCMs. Carbon Black nanoparticles (1 wt%) improved thermal conductivity by 35% and 24% for RT20 and RT25 PCMs. |
| [56]      | Paraffin ( $T_m = 58$ –60 °C) and water emulsion                                       | Graphite nanoparticles; <30 nm; Mass fraction: 0.05%, 0.1%,   | A 20% increase in thermal conductivity for the PCM containing 0.1 wt% of graphite nanoparticles.   |
| [65]      | OP10E ( $T_m = 8$ –10 °C) and water emulsion   | Graphite nanoparticles; <30 nm; Mass fraction: 0.25%, 0.5%, 1.0%, 2.0%, 4%  | Increase in the thermal conductivity of 88.9% for 2 wt% loading of graphite nanoparticles.   |
| [50]      | Deionized water  | $TiO_2$ nanotubes (TiNTs); 9–10 nm<br>$TiO_2$ nanoplatelets (TiNPs); 50–80 nm;<br>Hybrid nanofluids (with TiNTs and TiNPs). Various TiNP percentages from 0%, 25%, 50%, 75%, to 100% and at the same as well as different total | When compared with deionized water, the thermal conductivity of the hybrid nanofluid (0.1 wt% of $TiO_2$ with 25% of TiNPs) was improved by 22.30%.                                      |

**Table 5 (continued)**

| Reference | PCM and melting temperature                               | Nanomaterial   | Largest increase in thermal conductivity of base PCM with addition of nanomaterials  |
|-----------|---|--|--|
| [66]      | Paraffin wax; $T_m = 60$ °C                               | $TiO_2$ mass fractions (0.1, 0.2, 0.3%).<br>Carbon nanofiber, graphene nanoplatelets, graphite nanopowder; Mass fraction: 2.5%, 5.0%, 7.5% and 10%                       | Thermal conductivity improvement of 1100% by adding 10 wt% of graphite nanopowder to paraffin was reported.                              |
| [67]      | Paraffin; $T_m = 54$ –58 °C                               | Nanoparticles of $TiO_2$ ; 5–20 nm; Mass fraction: 0.5%, 0.7%, 1.0%, 2.0%, 3.0%, 4.0%  | Thermal conductivity was increased by 47.85% when 2 wt% of $TiO_2$ nanoparticles were added.   |
| [58]      | Coconut oil; $T_m = 24$ °C                                | Nanoparticles of CuO; <50 nm; Mass fraction: 0.1%, 1%  | The addition of 1 wt % of nanoparticles resulted in a 7.5% higher thermal conductivity.  |
| [68]      | Water   | Spherical carbon black nanoparticles, CB (10 nm), Multi-walled carbon nanotubes, MWCNT (9.5 nm), Graphene oxide nanosheets, GO (2 nm); Mass fraction: 0.01%, 0.05%, 0.1% | The thermal conductivity of the PCM in the solid phase increased by 14% with the addition of 0.1 wt% of multi-walled carbon nanotubes.   |
| [69]      | Myristic acid [ $CH_3(CH_2)_{12}COOH$ ]; $T_m = 52$ °C    | $SiO_2$ nanospheres; 52 nm; Mass fraction: 0.2%, 0.5%, 0.8% and 1.0%   | Thermal conductivity enhancement of 87.27% was achieved for 1.0 wt % of $SiO_2$ nanospheres.   |
| [59]      | D-Mannitol ( $C_4H_{14}O_6$ ); $T_m = 165$ –169 °C        | Nanoparticles of CuO; 10–40 nm; Mass fraction: 0.1%, 0.2%, 0.5%  | 0.5 wt% of nanoparticles resulted in 25% increase in thermal conductivity.   |
| [71]      | Paraffin wax RT22 HC (RUBITHERM®); $T_m = 22$ °C          | Graphene nanoplatelets; <2 nm; Mass fraction: 0.05%, 0.10%, 0.15%, 0.20%, 0.25%, 0.30%   | The thermal conductivity was increased by 89.6% for graphene loading of 0.3 wt%.   |
| [72]      | Magnesium chloride hexahydrate (MCH); $T_m = 115$ –118 °C | Nano-graphite particles (NG); Mass fractions: 0.1%, 0.2%, 0.3%, 0.4%, 0.5%   | Improvement in thermal conductivity of 308% with 0.5 wt% loading of NG.  |
| [73]      | Octadecane (organic PCM); $T_m = 28$ –30 °C               | Nanoparticles of CuO; 75 nm; weight/volume: 2.5%, 5.0%, 10.0%  | At a temperature of 40 °C for a 10% weight/volume nanoparticle concentration, an increase in thermal conductivity of 9.32% was achieved. |
| [49]      | Paraffin  | Titanium dioxide ( $TiO_2$ ), copper oxide (CuO) and graphene oxide (GO) nanoparticles; Mass fraction: 0.3%  | Thermal conductivity was improved by 25.0%, 28.8% and 101% for nanoparticles mass fraction of 0.3% when compared to pure paraffin.       |
| [60]      | Neopentyl glycol; $T_m = 126$ °C                          | Nanoparticles of CuO; 30–50 nm; Mass   | The thermal conductivity increased by factor   |

(continued on next page)



Table 5 (continued)

| Reference | PCM and melting temperature | Nanomaterial               | Largest increase in thermal conductivity of base PCM with addition of nanomaterials |
|-----------|-----------------------------|----------------------------|---|
|           |                             | fraction: 0.5%, 1.0%, 3.0% | of 4.08 with 3 wt% loading of CuO nanoparticles.                                    |

cylinder [71] and in thermoelectric applications [58]. On contrary, in the work [57] that was focused on the nitrate salt mixture or in the work [51] (hydrate salt) the specific heat was higher with respect to the base PCM.

Apart from afore-mentioned research works, very few studies addressed the results for specific heat. Adding nanomaterials to PCMs can modify numerous other thermophysical properties, such as: increase of thermal diffusivity for case of the paraffin PCMs [53], elimination in the case of PCM emulsions [65], reduction in case of the hybrid nano-fluids [50] or water as PCM [68].

Usually, the expected improvement of thermal conductivity is in a range of 20%–100%, but there are examples of even higher improvements reported. For instance in the case of the lauric acid phase change nanocomposite with graphene nanoplatelets [62], carbon-based PCM [66] or magnesium chloride hexahydrate PCM composites [72], Table 5. Generally, it can be concluded that an increase in the mass or volume fraction of nanomaterials in PCMs increases the thermal conductivity. This may be misleading since there is a limit to the amount of nanomaterials in the PCM, i.e. nanomaterials in larger fractions tend to agglomerate. Agglomeration may lead to the decrease or the increase of thermal conductivity [74]. It is hard to predict when agglomeration would occur since it depends on many parameters such as the mass or volume fraction, size and morphology of nanomaterials, etc. Furthermore, the type, phase and temperature of PCM may also have a significant influence on this phenomenon.

## 5. Typical unit cost of nanoparticles

The production of nanomaterials is a relatively complex and expensive process which requires highly trained staff, hence resulting in a costly final product. The final price depends on many factors. Initially it is determined by type, purity and size of nanomaterials. Four offers for nanopowders of CuO, ZnO, Ag and Graphene (nanoplatelets) were acquired from four suppliers and summarized in Table 6. Offer No.1 and No.2 come from suppliers based in the European Union, while offers No.3 and No.4 were from the USA suppliers. The used currency is the euro and the price refers to 1 g of nanoparticles.

The cheapest were the nanoparticles of ZnO with an average price of 0.49 EUR/g, while the most expensive were the Ag nanoparticles with an average price of 7 EUR/g. The average value of prices can be misleading because of the large range; therefore, every offer has to be individually assessed. The highest unit price is for nanoparticles dispersions and that is currently not available for all nanomaterials. The prices in Table 6 represent guide prices, therefore, need to be treated accordingly.

Table 6  
Unit cost of powder nanomaterials.

|          | Offer No.1 |           |       | Offer No.2 |         |       | Offer No.3 |          |       | Offer No.4 |          |       |
|----------|------------|-----------|-------|------------|---------|-------|------------|----------|-------|------------|----------|-------|
|          | Purity     | Size      | EUR/g | Purity     | Size    | EUR/g | Purity     | Size     | EUR/g | Purity     | Size     | EUR/g |
| CuO      | 99.9%      | 40–80 nm  | 0.48  | /          | /       | 2.91  | 99.0%      | <100 nm  | 1.32  | 99%        | 40 nm    | 0.33  |
| ZnO      | 99.9%      | 90–210 nm | 0.50  | /          | /       | 0.23  | 99.0%      | <100 nm  | 1.06  | 99.8%      | 200 nm   | 0.18  |
| Ag       | 99.5%      | 35 nm     | 4.08  | /          | <100 nm | 17.67 | 99.0%      | <100 nm  | 4.17  | 99.9%      | 20–30 nm | 2.09  |
| Graphene | 99.5%      | 11–15 nm  | 0.52  | /          | /       | 0.89  | 99.0%      | 10–15 nm | 4.19  | /          | 11–15 nm | 0.88  |

## 6. Conclusions and future directions

This paper was focused on examination of existing research findings related to nano-enhanced fluid and NPCMs. The main focus of the study was directed to specific applications, thermal properties and finally to the specific general issues that occur during the preparation of nano-enhanced systems. According to the analyzed existing research findings several general conclusions could be highlighted, as well as useful directions and recommendations in the field. Regarding applications, it was found that most NEPCM applications were related to the improvement of thermal energy storage systems. Mainly, works were directed to the solar collector systems, cooling storage systems, engine exhaust gas heat recovery and PV-PCM cooling configurations. The less investigated areas are related to applications in electronics, cooling of batteries and solar distillers. The more research efforts should be directed in that sense to secure further advancements. It was also found that used base materials for nanocomposites were materials on a paraffin base mostly and for nano-fluids it was water as the base fluid.

With respect to the improvements in thermal properties the highest detected increase was found in the case of thermal conductivity in a range of about 20%–100%, with respect to the base material. In some studies, improvement in thermal conductivity was even higher. However, just a few papers have dealt with the examination of specific heat capacity. Moreover, the results for the heat capacity are rather different, i.e. with noticeable variations. In specific studies, heat capacity was increased and in some cases, was decreased by the addition of nanoparticles. In the majority of research studies, a slight decrease of latent heat was found where roots for that needs to be further investigated. In general, it is demanding to define which nanoparticles are the most suitable from the performance point of the view, since analyzed systems are usually not comparable. Mainly due to different base material, different nanoparticles, nanoparticle sizes, concentrations, etc. The preparation process associated with nanoparticles addition is also rather different for each examined research study. The preparation strategy strongly affects the quality of the sample and accuracy in the case of the measurements. Besides the above addressed main thermal properties of nano-enhanced systems, the addition of nanomaterials also affects other different thermo-physical properties. In previous sense the main impact is related to the thermal diffusivity (usually increase), reduction of super-cooling effect, improvement of photo-thermal conversion performance, etc.

According to the herein addressed references it was found that the preparation process of nano-enhanced systems was poorly and inadequately described in the existing literature. Usually, crucial preparation details are missing and that are important for quality experimental work and sample preparation. For instance, the general properties of the base and enriched sample are missing (such as mass and volume of the sample), mixing parameters, mixing technology (used equipment), description of safety procedures, etc. It was found that one of the main challenges related to the preparation of nano-enhanced systems is to investigate the agglomeration point, since numerous factors are affecting it. The highest impact to the agglomeration has mass or volume fraction, size and morphology of nanomaterials. Moreover, interesting finding is one that agglomeration point is directly linked with the possible increase or decrease of specific thermal properties and stability of the nanofluids. One of the major drawbacks found in the existing

literature is linked with the economic aspect, environmental impact and safety issue associated with usage of nanomaterials as hazardous matters. The economic aspect was not sufficiently addressed in the existing works and the focus was more directed to the performance improvement in general. Economy is a critical feature for all engineering systems, so from that point of view, the future studies should also contain the necessary economic evaluation. The environmental impact of nanomaterials was out of the focus in the existing research studies and which is extremely important. The rise in the potential engineering applications of nanomaterials requires careful environmental evaluation which should be mandatory. Safety procedures related to the handling of the nanomaterials, or procedures during the specific experimental works were not elaborated. The safety procedures should be thoroughly described as important guidelines to ensure secure working environment for researchers. Thus share of the knowledge in that sense is vital. Overall, the conducted review indicated necessity for more intense research activity in this dynamic and progressing research field. An integral PEE (Performance-Economy-Environmental Suitability) concept should be applied in the future research works associated with nanomaterials, with necessity for clear and accurate description of the specific preparation procedures.

### Acknowledgments

This work was funded by the Croatian science foundation (Research project: Smart and hybrid cooling techniques for siliceous photovoltaic panels-IP-01-2018-2814, Croatia).

### References

- gov Nano. Benefits and applications. <https://nano.gov/you/nanotechnology-benefits>. [Accessed 8 June 2019].
- Xu C, Nasrollahzadeh M, Sajjadi M, Maham M, Luque R, Puente-Santiago AR. Benign-by-design nature-inspired nanosystems in biofuels production and catalytic applications. *Renew Sustain Energy Rev* 2019;112:112–95.
- Said Z, El Haj Assad M, Hachicha AA, Bellos E, Abdelkareem MA, Alazaizeh DZ, Yousef BAA. Enhancing the performance of automotive radiators using nanofluids. *Renew Sustain Energy Rev*; 112:183:194.
- Nourafkan E, Asachi M, Jin H, Wen D, Ahmed W. Stability and photo-thermal conversion performance of binary nanofluids for solar absorption refrigeration systems. *Renew Energy* 2019;140:264–73.
- Raihan Mohammad Siddique A, Kratz F, Mahmud S, Van Heyst B. Energy conversion by nanomaterial-based trapezoidal-shaped leg of thermoelectric generator considering convection heat transfer effect. *J Energy Resour Technol* 2019;141(8). <https://doi.org/10.1115/1.4042644>. Article number 082001.
- Natividade PSG, de Moraes Moura G, Avallone E, Bandarra Filho EP, Gelamo RV, Gonçalves JCDSI. Experimental analysis applied to an evacuated tube solar collector equipped with parabolic concentrator using multilayer graphene-based nanofluids. *Renew Energy* 2019;138:876–90.
- Salem MR, Elsayed MM, Abd-Elaziz AA, Elshazly KM. Performance enhancement of the photovoltaic cells using Al<sub>2</sub>O<sub>3</sub>/PCM mixture and/or water cooling-techniques. *Renew Energy* 2019;138:876–90.
- Shen G, Ma L, Zhang S, Zhang S, An L. Effect of ultrasonic waves on heat transfer in Al<sub>2</sub>O<sub>3</sub>nanofluid under natural convection and pool boiling. *Int J Heat Mass Tran* 2019;138:516–23.
- Ding Y, Zheng S, Meng X, Yang D. Low salinity hot water injection with addition of nanoparticles for enhancing heavy oil recovery. *Trans. of the ASME J Energy Resour Technol* 2019;141(7). <https://doi.org/10.1115/1.40132-MS>. Article number 072904.
- Chen Y, Zhu J, Ma H, Chen L, Li R, Jin P. VO<sub>2</sub>/Nickel-bromine-ionic liquid composite film for thermochromic application. *Sol Energy Mater Sol Cell* 2019; 196:124–30.
- Adelekan DS, Ohunakin OS, Gill J, Atayero AA, Diarra CD, Asuzu EA. Experimental performance of a safe charge of LPG refrigerant enhanced with varying concentrations of TiO<sub>2</sub>nano-lubricant in a domestic refrigerator. *J Therm Anal Calorim* 2019;136(6):2439–48.
- Martín M, Villalba A, Inés Fernández A, Barreneche C. Development of new nano-enhanced phase change materials (NEPCM) to improve energy efficiency in buildings: lab-scale characterization. *Energy Build* 2019;192:75–83.
- Ren Q, Xu H, Luo Z. PCM charging process accelerated with combination of optimized triangle fins and nanoparticles. *Int J Therm Sci* 2019;140:466–79.
- Balakin BV, Zhdaneev OV, Kosinska A, Kutsenko KV. Direct absorption solar collector with magnetic nanofluid: CFD model and parametric analysis. *Renew Energy* 2019;136:23–32.
- Bonab HB, Javani N. Investigation and optimization of solar volumetric absorption systems using nanoparticles. *Sol Energy Mater Sol Cell* 2019;194:229–34.
- Kumar G, Mathimani T, Rene ER, Pugazhendhi A. Application of nanotechnology in dark fermentation for enhanced biohydrogen production using inorganic nanoparticles. *Int J Hydrogen Energy* 2019;44(26):13106–13.
- Wang L, Zhu G, Wang M, Yu W, Zeng J, Yu X, Xi H, Li Q. Dual plasmonic Au/TiNnanofluids for efficient solar photothermal conversion. *Sol Energy* 2019;184: 240–8.
- Zhang JJ, Qu ZG, Maharjan A. Numerical investigation of coupled optical-electrical-thermal processes for plasmonic solar cells at various angles of incident irradiance. *Energy* 2019;174:110–21.
- Zayed ME, Zhao J, Du Y, Kabeel AE, Shalaby SM. Factors affecting the thermal performance of the flat plate solar collector using nanofluids: a review. *Sol Energy* 2019;182:382–96.
- Abdelrazik AS, Al-Sulaiman FA, Saidur R, Ben-Mansour R. Evaluation of the effects of optical filtration and nanoPCM on the performance of a hybrid photovoltaic-thermal solar collector. *Energy Convers Manag* 2019;195:139–56.
- Agresti F, Fedele L, Rossi S, Cabaleiro D, Bobbo S, Ischia G, Barison S. Nano-encapsulated PCM emulsions prepared by a solvent-assisted method for solar applications. *Sol Energy Mater Sol Cell* 2019;194:268–75.
- Rehman T-U, Ali HM, Janjua MM, Sajjad U, Yan W-M. A critical review on heat transfer augmentation of phase change materials embedded with porous materials/foams. *Int J Heat Mass Tran* 2019;135:649–73.
- Sheikholeslami M, Mahian O. Enhancement of PCM solidification using inorganic nanoparticles and an external magnetic field with application in energy storage systems. *J Clean Prod* 2019;215:963–77.
- De Matteis V, Cannavale A, Martellotta F, Rinaldi R, Calcagnile P, Ferrari F, Ayr U, Fiorito F. Nano-encapsulation of phase change materials: from design to thermal performance, simulations and toxicological assessment. *Energy Build* 2019; 188–189:1–11.
- Amaral C, Vicente R, Marques PAAP, Barros-Timmons A. Phase change materials and carbon nanostructures for thermal energy storage: a literature review. *Renew Sustain Energy Rev* 2017;79:1212–28.
- Wang Q, Wei W, Li D, Qi H, Wang F, Arıcı M. Experimental investigation of thermal radiative properties of Al<sub>2</sub>O<sub>3</sub>-paraffin nanofluid. *Sol Energy* 2019;177:420–6.
- Al-Kayiem HH, Lin SC, Lukmon A. Review on nanomaterials for thermal energy storage technologies. *Nanosci Nanotechnol - Asia* 2013;3(1):60–71.
- EanestJebasingh B, ValanArasu A. A comprehensive review on latent heat and thermal conductivity of nanoparticle dispersed phase change material for low-temperature applications. *Energy Storage Materials* 2020;24:52–74.
- Prabhu B, ValanArasu A. A review on thermal conductivity enhancement of paraffinwax as latent heat energy storage material. *Renew Sustain Energy Rev* 2016;64:81–100.
- Dhinesh Kumar D, ValanArasu A. A review on preparation, characterization, properties and applications of nanofluids. *Renew Sustain Energy Rev* 2016;60: 21–40.
- Scopus.com. <https://www.scopus.com/>. [Accessed 20 May 2019].
- Khan MMA, Ibrahim NI, Mahbubul IM, Muhammad, Ali H, Saidur R, Al-Sulaiman FA. Evaluation of solar collector designs with integrated latent heat thermal energy storage: a review. *Sol Energy* 2018;166:334–50.
- Alva G, Lin Y, Fang G. An overview of thermal energy storage systems. *Energy* 2018;144:341–78.
- Lin SC, Al-Kayiem HH. Evaluation of copper nanoparticles - paraffin wax compositions for solar thermal energy storage. *Sol Energy*; 132:267-278.
- Altohamy AA, AbdRabbo MF, Sakr RY, Attia AAA. Effect of water based Al<sub>2</sub>O<sub>3</sub> nanoparticle PCM on cool storage performance. *Appl Therm Eng* 2015;84:331–8.
- Wilson John MR, Singh AK, Singh AK, Ganapathy Subramanian LR. Waste heat recovery from diesel engine using custom designed heat exchanger and thermal storage system with nanoenhanced phase change material. *Therm Sci* 2017;21: 715–27.
- Hasan A, McCormack SJ, Huang MJ, Norton B. Evaluation of phase change materials for thermal regulation enhancement of building integrated photovoltaics. *Sol Energy* 2010;84:1601–12.
- Nada SA, El-Nagar DH. Possibility of using PCMs in temperature control and performance enhancements of free stand and building integrated PV modules. *Renew Energy* 2018;127:630–41.
- Nizetić S, Arıcı M, Bilgin F, Grubisić-Čabo F. Investigation of pork fat as potential novel phase change material for passive cooling applications in photovoltaics. *J Clean Prod* 2018;170:1006–16.
- Nada SA, El-Nagar DH, Hussein HMS. Improving the thermal regulation and efficiency enhancement of PCM-Integrated PV modules using nano particles. *Energy Convers Manag* 2018;166:735–43.
- Sharma S, Micheli L, Chang W, Tahir AA, Reddy KS, Mallick TK. Nano-enhanced phase change material for thermal management of BICPV. *Appl Energy* 2017;208: 719–33.
- Karimi G, Azizi M, Babapoor A. Experimental study of a cylindrical lithium ion battery thermal management using phase change material composites. *Journal of Energy Storage* 2016; 8:168-174.
- Temel UN. Passive thermal management of a simulated battery pack at different climate conditions. *Appl Therm Eng* 2019;158:113796.
- Alimohammadi M, Aghli Y, Alavi ES, Sardarabadi M, Passandideh-Fard M. Experimental investigation of the effects of using nano/phase change materials (NPCM) as coolant of electronic chipsets, under free and forced convection. *Appl Therm Eng*; 111:271-279.
- Krishna Jogi, Kishore PS, Brusly Solomon A. Heat pipe with nano enhanced-PCM for electronic cooling application. *Exp Therm Fluid Sci* 2017;81:84–92.

- [46] AlaeiShahmirzadi MA, Hosseini SS, Luo J, Ortiz I. Significance, evolution and recent advances in adsorption technology, materials and processes for desalination, water softening and salt removal. *J Environ Manag* 2018;215:324–44.
- [47] Rizzo L, Malato S, Antakyali D, Beretsou VG, Dolić MB, Gernjak W, Heath E, Ivancev-Tumbas I, Karaolia P, Lado Ribeiro AR, Mascolo G, McArdell CS, Schaar H, Silva AMT, Fatta-Kassinos D. Consolidated vs new advanced treatment methods for the removal of contaminants of emerging concern from urban wastewater. *Sci Total Environ* 2019;655:986–1008.
- [48] Chaichan MT, Kazem HA. Single slope solar distillator productivity improvement using phase changematerial and Al<sub>2</sub>O<sub>3</sub> nanoparticle. *Sol Energy* 2018;164:370–81.
- [49] Dsilva Winfred Rufuss D, Suganthi L, Iniyan S, Davies PA. Effects of nanoparticle-enhanced phase change material (NPCM) on solar still productivity. *J Clean Prod* 2018;192:9–29.
- [50] Shao X-F, Mo S-P, Chen Y, Yin T, Yang Z, Jia L-S, Cheng Z-D. Solidification behavior of hybrid TiO<sub>2</sub>nanofluids containing nanotubes and nanoplatelets for cold thermal energy storage. *Appl Therm Eng*; 117:427-436.
- [51] Liu Y, Yang Y. Investigation of specific heat and latent heat enhancement in hydrate salt based TiO<sub>2</sub>nanofluid phase change material. *Appl Therm Eng* 2017; 124:533–8.
- [52] Munyalo JM, Zhang X, Li Y, Chen Y, Xu X. Latent heat of fusion prediction for nanofluid based phase change material. *Appl Therm Eng* 2018;130:1590–7.
- [53] Warzoha RJ, Weigand RM, Fleischer AS. Temperature-dependent thermal properties of a paraffin phase change material embedded with herringbone style graphite nanofibers. *Appl Energy* 2015;137:716–25.
- [54] Nourani M, Hamdami N, Keramat J, Moheb A, Shahedi M. Thermal behavior of paraffin-nano-Al<sub>2</sub>O<sub>3</sub>stabilized by sodium stearylactylate as a stable phase change material with high thermal conductivity. *Renew Energy* 2016;88:474–82.
- [55] Motahar S, Alemrajabi AA, Khodabandeh R. Experimental study on solidification process of a phase change material containing TiO<sub>2</sub>nanoparticles for thermal energy storage. *Energy Convers Manag* 2017;138:162–70.
- [56] Wang F, Liu J, Fang X, Zhang Z. Graphite nanoparticles-dispersed paraffin/water emulsion with enhanced thermal-physical property and photo-thermal performance. *Sol Energy Mater Sol Cell* 2016;147:101–7.
- [57] Chieruzzi M, Cerritelli GF, Miliozzi A, Kenny JM, Torre L. Heat capacity of nanofluids for solar energy storage produced by dispersing oxide nanoparticles in nitrate salt mixture directly at high temperature. *Sol Energy Mater Sol Cell* 2017; 167:60–9.
- [58] Ebadi S, HumairaTasnim S, Abbas Aliabadi A, Mahmud S. Geometry and nanoparticle loading effects on the bio-based nano-PCM filled cylindrical thermal energy storage system. *Appl Therm Eng* 2018;141:724–40.
- [59] Salyan S, Suresh S. Study of thermo-physical properties and cycling stability of D-Mannitol-copper oxide nanocomposites as phase change materials. *Journal of Energy Storage* 2018;15:245–55.
- [60] Praveen B, Suresh S. Experimental study on heat transfer performance of neopentyl glycol/CuO composite solid-solid PCM in TES based heat sink. *Engineering Science and Technology, an International Journal* 2018;21:1086–94.
- [61] Khan I, Arasu V. Review of influence of nanoparticle synthesis and geometrical parameters on thermophysical properties and stability of nanofluids. *Thermal Science and Engineering Progress* 2019;11:334–64.
- [62] Harish S, Orejon D, Takata Y, Kohno M. Thermal conductivity enhancement of lauric acid phase change nanocomposite with graphene nanoplatelets. *Appl Therm Eng* 2015;80:205–11.
- [63] Sharma RK, Ganesan P, Tyagi VV, Metselaar HSC, Sandaran SC. Thermal properties and heat storage analysis of palmitic acid-TiO<sub>2</sub>composite as nano-enhanced organic phase change material (NEOPCM). *Appl Therm Eng* 2016;99:1254–62.
- [64] Colla L, Fedele L, Mancin S, Danza L, Manca O. Nano-PCMs for enhanced energy storage and passive cooling applications. *Appl Therm Eng* 2017;110:584–9.
- [65] Wang F, Zhang C, Liu J, Fang X, Zhang Z. Highly stable graphite nanoparticle-dispersed phase change emulsions with little supercooling and high thermal conductivity for cold energy storage. *Appl Energy* 2017;188:97–106.
- [66] Bahiraei F, Fartaj A, Nazri G-A. Experimental and numerical investigation on the performance of carbon-based nanoenhanced phase change materials for thermal management applications. *Energy Convers Manag* 2017;153:115–28.
- [67] Sami S, Etesami N. Improving thermal characteristics and stability of phase change material containing TiO<sub>2</sub>nanoparticlesafter thermal cycles for energy storage. *Appl Therm Eng* 2017;124:346–52.
- [68] Barreneche C, Mondragon R, Ventura-Espinosa D, Mata J, Cabeza LF, Fernández AI, Enrique Julia J. Influence of nanoparticle morphology and its dispersion ability regarding thermal properties of water used as phase change material. *Appl Therm Eng* 2018;128:121–6.
- [69] Harikrishnan S, Imran Hussain S, Devaraju A, Sivasamy P, Kalaiselvam S. Improved performance of a newly prepared nano-enhanced phase change material for solar energy storage. *J Mech Sci Technol* 2017;31(10):4903–10.
- [70] Mayilvelnathana V, Arasu V. Characterisation and thermophysical properties of graphene nanoparticles dispersed erythritol PCM for medium temperature thermal energy storage applications. *Thermochim Acta* 2019;676:94–103.
- [71] Putra N, Amn M, Kosasih EA, Luanto RA, Abdullah NA. Characterization of the thermal stability of RT 22 HC/graphene using a thermal cycle method based on thermoelectric methods. *Appl Therm Eng* 2017;124:62–70.
- [72] Yadav A, Barman B, Kardam A, Narayanan SS, Verma A, Jain VK. Thermal properties of nano-graphite-embedded magnesium chloride hexahydrate phase change composites. *Energy Environ* 2017;28(7):651. <https://doi.org/10.1177/0958305X17721475>.
- [73] Águila VB, Vasco DA, Galvez PP, Zapata PA. Effect of temperature and CuO-nanoparticle concentration on the thermal conductivity and viscosity of an organic phase-change material. *Int J Heat Mass Tran* 2018;120:1009–19.
- [74] Machrafi H, Lebon G, Iorio S. Effect of volume-fraction dependent agglomeration of nanoparticles on the thermal conductivity of nanocomposites: applications to epoxy resins, filled by SiO<sub>2</sub>, AlN and MgO nanoparticles. *Compos Sci Technol* 2016; 130:78–87.

## Appendix B

Title: Comprehensive analysis of preparation strategies for phase change nanocomposites and nanofluids with brief overview of safety equipment

Authors: Jurčević M., Nižetić S., Arici M., Oclon P.

Publisher: *Elsevier*

Journal: *Journal of Cleaner Production*

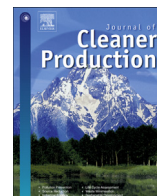
Edition, ID, year: 274, 122963, 2020.

Indexed in: Scopus, Science Citation Index Expanded, INSPEC, etc.

Journal Impact Factor: 9.297 Q1 (WoS and SJR-2020.)

DOI: <https://doi.org/10.1016/j.jclepro.2020.122963>

**Abstract:** The preparation process of the nanocomposites and nanofluids strongly affects their general physical properties and stability in general. They are very sensitive with respect to the quality of the preparation process which should be obtained carefully to produce quality and reliable homogeneous samples. This paper provides a useful analysis in different preparation procedures with the focus on the nanoenhanced phase change materials (NEPCM) and fluids (nanofluids) due to their wide application areas. The preparation processes were identified and categorized together with the key parameters that have an important impact on the preparation process in general. The main problems and issues during the preparation process were discussed and elaborated in detail, gained by a detailed analysis of commonly applied preparation procedures. Since the preparation process of both nanofluids and nanocomposites should be carefully planned regarding the working safety, an overview of the safety equipment was provided as well as an assessment of the toxic potential of nanomaterials. Quality and well obtained preparation process can contribute to the rational utilization of the nanomaterials, and by that, it could reduce negative environmental footprints released from production as well as application of the nanomaterials. The main research findings of this paper provide useful guidelines for researchers dealing with the preparation of nano-enhanced fluids and phase change materials that should be helpful to get insights directed to the complexity of the preparation process and ensure an efficient preparation process.



# Comprehensive analysis of preparation strategies for phase change nanocomposites and nanofluids with brief overview of safety equipment

Mišo Jurčević<sup>a</sup>, Sandro Nižetić<sup>a,\*</sup>, Müslüm Arıcı<sup>b</sup>, Paweł Ocioń<sup>c</sup>

<sup>a</sup> ITEF- Laboratory for Thermodynamics and Energy Efficiency, Faculty of Electrical Engineering, Mechanical Engineering and Naval Architecture, University of Split, Rudjera Boskovića 32, 21000, Split, Croatia

<sup>b</sup> Department of Mechanical Engineering, Faculty of Engineering, Kocaeli University, Umuttepe Campus, Kocaeli, 41001, Turkey

<sup>c</sup> Energy Department, Faculty of Environmental and Energy Engineering, Cracow University of Technology, Al. Jana Pawła II 37, 31-864, Kraków, Poland

## ARTICLE INFO

### Article history:

Received 8 May 2020

Received in revised form

5 June 2020

Accepted 18 June 2020

Available online 18 July 2020

Handling editor: Prof. Jiri Jaromir Klemes

### Keywords:

Preparation technique

Nanocomposites

Nano-enhanced phase change materials

Nanofluids

Nanomaterials

Safety

## ABSTRACT

The preparation process of the nanocomposites and nanofluids strongly affects their general physical properties and stability in general. They are very sensitive with respect to the quality of the preparation process which should be obtained carefully to produce quality and reliable homogeneous samples. This paper provides a useful analysis in different preparation procedures with the focus on the nano-enhanced phase change materials (NEPCM) and fluids (nanofluids) due to their wide application areas. The preparation processes were identified and categorized together with the key parameters that have an important impact on the preparation process in general. The main problems and issues during the preparation process were discussed and elaborated in detail, gained by a detailed analysis of commonly applied preparation procedures. Since the preparation process of both nanofluids and nanocomposites should be carefully planned regarding the working safety, an overview of the safety equipment was provided as well as an assessment of the toxic potential of the nanomaterials. Quality and well obtained preparation process can contribute to the rational utilization of the nanomaterials, and by that, it could reduce negative environmental footprints released from production as well as application of the nanomaterials. The main research findings of this paper provide useful guidelines for researchers dealing with the preparation of nano-enhanced fluids and phase change materials that should be helpful to get insights directed to the complexity of the preparation process and ensure an efficient preparation process.

© 2020 Elsevier Ltd. All rights reserved.

## 1. Introduction

The implementation of nanomaterials in specific areas has been intensively investigated in recent years since there are numerous benefits that can lead to important technological advances (Bhagyaraj et al., 2018). There are several main fields involved in application of nanomaterials and currently, the most investigated areas are in the field of new materials (or improvement of the specific properties of materials in various engineering applications), energy field (Nižetić et al., 2020), as well as information technology (IT) applications in general. If the research works in the last three years are analyzed, in the major areas where

nanomaterials could be applied, it is clear that the research field related development of the new nano-enhanced materials is the most progressing one, with more than 4000 papers per year on average, Fig. 1.

It can also be seen in Fig. 1 that there is a rise in published research works in almost all categories where it is clear that the least investigated area is related to environmental protection (i.e. the possibility of nanomaterial implementation for environmental protection purposes). On the other side, one of the major issues working with nanoparticles is safety and the general examination of the nanoparticle impact on the environment as well as on the staff operating with them (Stuttgen et al., 2019).

The preparation techniques involving nanoparticles are demanding where the quality and procedure of the preparation process can have a strong impact on the result, i.e. the nano-enhanced material (systems) general properties. For instance, the

\* Corresponding author. University of Split, Rudjera Boškovića 32, 21000, Split, Croatia.

E-mail address: [snizetic@fesb.hr](mailto:snizetic@fesb.hr) (S. Nižetić).



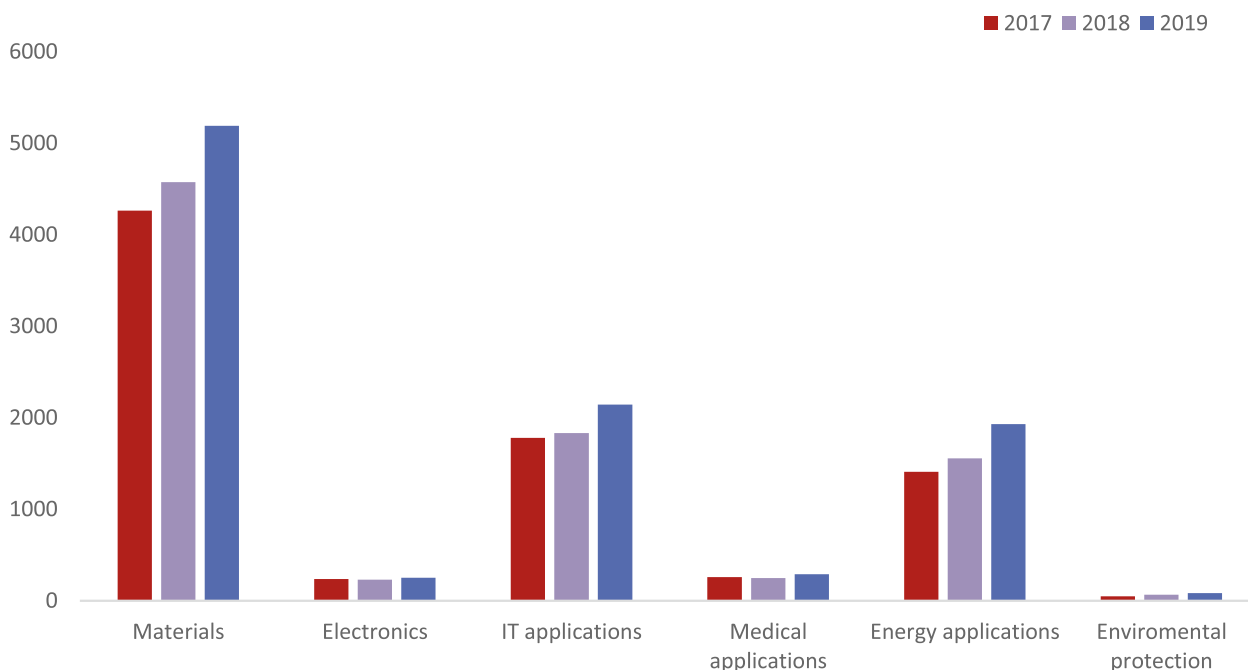


Fig. 1. General application areas of nanomaterials with respect to number of published research papers in Scopus database (2019).

preparation of nano-enhanced fluids or nano-enhanced phase change materials (NEPCM) (Arici et al., 2020) is very sensitive and preparation procedure can drastically affect the accuracy of measurements (for instance thermal conductivity, heat capacity, latent heat, etc.). The long-term properties as well as stability of nanofluids is also affected by the preparation procedure. In most cases, nanoparticles are added in the liquid phase of a specific matter and then the mixing procedure is applied (ultrasonic, mechanical mixing, etc.). The three main problems associated with the implementation of nanoparticles that usually occur are agglomeration, sedimentation and finally, as already mentioned, questionable long-term stability. The usual problem with nanoparticles and their addition into the fluids is the agglomeration issue (Totzauer et al., 2019), i.e. it is hard to achieve a consistent and equal dispersion of the nanoparticles within the specific fluids (samples that need to be investigated, i.e. measured). To prevent the agglomeration effect, different surfactants (Choudhary et al., 2020) are added to enable the equal dispersion of nanomaterials within the fluid or phase change material (PCM). The sedimentation of nanoparticles is also an issue that usually occurs during the preparation of the measured samples (Triques et al., 2020). In general, the preparation techniques can be different, depending if there are nanofluids or nanocomposites in question, but even in that case, the preparation techniques are methodologically almost the same in a sense. The preparation of nanocomposites is also demanding (Hári and Pukánszky, 2011), and has a significant impact on the material properties such as mechanical strength, stiffness, thermal stability, electrical and the optical properties of nanocomposite materials or other properties such as deflection temperature or inherent flammability, etc. The preparation procedures are different, and they vary from the specific type of nanocomposite such as, in situ polymerization, solution mixing, melt compounding and others. The most challenging issue regarding nanocomposite preparation processes is efficient dispersion as well as homogeneity and finally

the long-term properties of these materials.

In the existing literature, it is hard to find research studies that were mainly focused on the analysis of specific preparation techniques, it is especially hard to find recent review articles that address preparation techniques in a more general manner in order to establish a systematical approach and help researchers understand the insights and importance of the preparation procedure for the specific case. For instance, in review paper (Devendiran et al., 2016), the preparation, characterization and general properties of the nano-fluids were discussed and elaborated. Various techniques, as well as application areas, were examined and the review was mainly focused on the preparation of metal nanofluids as well as metal oxides and hybrid nanofluids. The heat transfer properties, i.e. thermal and chemical properties were also discussed. Study (Wei et al., 2020) deals with the preparation issue of molten salt nanofluid, where different concentrations of MgO nanoparticles were examined. Different thermal properties were measured and the most promising nanofluid was one with a concentration of 5 wt % MgO, mainly for thermal storage applications to enhance heat transfer. The preparation process was relatively well described and mainly consisted of mechanical mixing. The effect of the ultrasonic mixing duration and surfactant was reported in (Afzal et al., 2019) for the case of ZnO and CuO nano-fluids. Several experiments were conducted where the impact of the ultrasonic duration, with respect to the different surfactants was examined. It was found that with the addition of surfactant, the ultra-sonication time was increased from 2 h to 6 h. The stability of nanofluids was improved; however, some physical properties were the same, while others were significantly changed. A comprehensive review related to the sonication effect on the thermal properties, stability and heat transfer characteristics of the nanofluids was discussed in (Asadi et al., 2019a). Studies related to the sonification of nanofluids were analyzed and the usual methods to characterize dispersion. The review revealed that an increase in the ultrasonication time, as

well as power, causes an improvement in the thermal conductivity and heat transfer properties. In some cases, the increase of ultrasonic time and power caused disturbed stability and thermophysical properties, which depends on the type of specific nanofluid. Finally, the authors reported that ultrasonic probe instruments are more efficacious than ultrasonic bath instruments. The optimal sonification time on the thermal conductivity and consistency of water-formed nanofluids (MWCNT-multi-walled carbon nanotubes) was investigated in study (Asadi et al., 2019b). The samples were prepared considering different concentrations and different sonification period varied from about 10 min to maximal 80 min. An experimental result clearly showed that the sonification time has a slight impact on thermal conductivity of the considered nanofluid, and 60 min was found as an optimal sonification time since in these circumstances the thermal conductivity was the highest. Study (Betancur et al., 2019) investigated the interaction of nanoparticles and surfactants in nanofluids. Three different methodologies for the addition of surfactants were examined in order to evaluate the interaction. It was found that the type of added nanoparticle affects the absorbed amount of surfactant and by that also affects the interaction between them. A detailed review focused on graphene-based nanofluids was reported in (Bahiraie et al., 2019), where the main challenges, as well as future research directions in that matter, were discussed. The preparation techniques were also reported, analyzed and discussed in detail, especially the stability improvement as well as the application of different surfactants and their general impact in specific applications. The preparation and characterization of nanofluids for the purpose of engine cooling was elaborated in (Kumar and Subudhi, 2019). A synthesis of nanofluids was provided with respect to the engine coolant, together with a heat transfer analysis. Different suggestions and directions in the field were proposed leading towards better the performance of the cooling systems with the application of nanofluids. A detailed analysis of oil-based nanofluids was reported in (Asadi et al., 2019c) and it mainly focused on the physical properties (viscosity, density, specific heat, etc.) of oil-based nanofluids, with respect to nanoparticle size and concentration. Useful correlations from the literature were gathered and compiled, which are related to the general features of the oil-formed nanofluids. The review related to the influence of nanoparticle synthesis and morphology on the thermal characteristics and consistency of nanofluids was provided in (Khan et al., 2019). The provided review brings forward a discussion and analysis regarding the main parameters that affect the thermal properties and that are important for effective preparation and the stability of the nanofluids. When analyzing the above briefly discussed recent works it can be clearly noted that the preparation process (procedures) were not well discussed. Moreover, in most of the studies it is hard to compile all mixing parameters since data not available.

The preparation process is usually discussed and presented in a limited manner, i.e. strongly focused on within the specific research investigation, i.e. where the addition of nanoparticles was considered. Therefore, a more general approach is missing and that could be helpful as a starting point when considering the preparation of nanofluids. Moreover, the preparation techniques in some studies were weakly discussed, i.e. the preparation procedure was not sufficiently clear, or the general circumstances were not elaborated well, thus in those cases, it is hard to fully understand the preparation procedure. When analyzing existing research findings, it was found that there is a necessity for review papers being mainly directed towards the general preparation process, i.e. preparation techniques of nanofluids and nanocomposites enriched with nanoparticles. Additionally, the preparation process should be followed by high-standard procedures regarding working safety due to the toxic potential of the nanoparticles, which is usually not

addressed in the existing literature. The three most prominent types of NEPCMs are nanocomposites, nanofluids, and micro-encapsulated PCMs. The production of nanocomposites and nanofluids is less demanding compared with microencapsulated PCMs, therefore, this paper focuses on nanocomposites and nanofluids due to a more present general application. Furthermore, micro-encapsulated PCMs are left out of this research due to a relatively complex preparation methodology that demands specific knowledge in the field of chemical engineering, and it was above the main scope of this paper.

The main focus of herein presented work was to analyze and discuss in detail specific preparation techniques for the case of nanofluids and nano-enhanced phase change materials in order to provide useful insights into the key parameters of the preparation process. The main novelties are reflected through identified, categorized and summarized preparation techniques. Moreover, the main issues and general problems related to the preparation process were detected and discussed, which serve as a useful foundation for researchers dealing with nanotechnology and which would be a helpful guideline for an efficient preparation process in general. Finally, an overview of the safety equipment was also provided, together with a discussion on the general toxic potential of nanoparticles as an important aspect when dealing with nanotechnology.

## 2. Brief description of review methodology

The existing research findings were obtained from Elsevier's Scopus database. The two-step selection was conducted with respect to the targeted keywords and limited subject area, Fig. 2. The subject area refers to the main categories of the investigation. The selected articles were published in English and limited to the last five years, i.e., range 2015–2019. After the primary selection, the articles were thoroughly reviewed with all articles not dealing with nanocomposites or nanofluids excluded. The secondary selection finished with excluding all articles without experimental investigations.

The focus was placed on papers dealing with experimental research to conceivably detect specific preparation techniques and influential parameters on the results of specific approaches. Based on the analysis of such research, facts can be more clearly determined and quantified, which is a good starting point for future research.

## 3. Preparation strategies

The preparation of NEPCM materials is a seemingly simple process of dispersing nanomaterials in the base PCM. In real circumstances, it is a demanding and complex process requiring high safety standards and a solid knowledge of chemical engineering. There is a variety of preparation methodologies reported in the literature most of which can be reduced to some sort of mechanical or magnetic stirring combined with an ultrasonication procedure. The main goal of all methodologies is to achieve a NEPCM homogeneity with well-dispersed nanomaterials while avoiding agglomeration. It is important to avoid the agglomeration of nanomaterials since it annuls the enhancement effect on the base material, (Choudhary et al., 2020). The aggregation of nanoparticles is even possible after sonication, (Devendiran et al., 2016). Commonly, nanocomposites are based on paraffin wax enhanced with nanomaterials of different morphologies and sizes. However, there is a large variety of other organic and inorganic PCM materials used for this purpose with more materials reported in recent research findings, (Nizetić et al., 2018). Some nanofluids can be utilized as a PCM material and/or heat transfer fluid (HTF) with

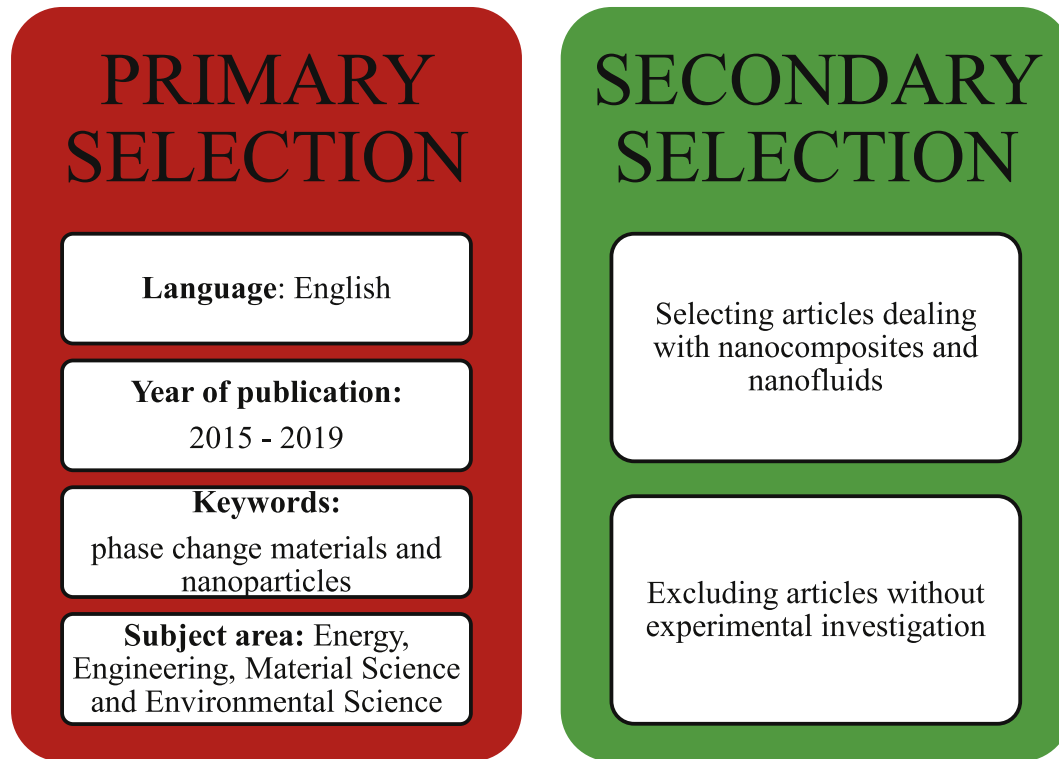


Fig. 2. General review methodology.

water being the most common base material.

### 3.1. Nanocomposites

Selected research studies are discussed in upcoming sections of the paper, where the main focus was directed towards a specific preparation procedure that involves nanocomposites. Critical features are also addressed and given the end of this chapter as a summary. Harish et al. (2015) analyzed thermal conductivity of a nanocomposite formed on lauric acid ( $T_m = 44\text{ }^\circ\text{C}$ ) and multilayer graphene nanoplatelets (MLG). Before dispersing in the lauric acid, MLG nanoplatelets (5–10 nm) were subjected to the initial preparation described in (Harish et al., 2015). In order to disperse MLG (from 0.1 vol% to maximal 1 vol%) in the lauric acid, the magnetic stirrer was used for about 30 min at uniform temperature of  $100\text{ }^\circ\text{C}$  and 250 rpm. Furthermore, samples were processed with ultrasonic processor (Hielscher GmbH, UP-400S) for a duration of 30 min at 50% amplification. The paper lacks a more precise description of the sample size, and a mass fraction of nanomaterials would be a better choice than volume fraction as some PCMs may have significant volume expansion.

Warzoha et al. (2015) analyzed the thermal properties of organic paraffin ( $T_m = 56\text{ }^\circ\text{C}$ ) enhanced with herringbone graphite nanofibers (HGNF) (2–100 nm, from 0.05 vol% to maximal 11.4 vol%). A better approach would be to use a mass fraction rather than volume fraction. After the paraffin was melted, HGNF were added, and then the nanocomposite was sonicated at 32 Hz for 2 h. It was not stated what type of device was used for sonication, nor the temperature at which sonication was performed.

Sharma et al. (2016) carried out an analysis of heat storage and thermal characteristics of palmitic acid (PA) ( $T_m = 60\text{--}62\text{ }^\circ\text{C}$ ) enhanced with  $\text{TiO}_2$  nanoparticles (21 nm, from 0.5 wt% to maximal 5.0 wt%). The nanoparticles and the PCM were mixed with ultrasonic vibrator (VCX 500, SONICS) using specific frequency of 40 kHz

and  $75\text{ }^\circ\text{C}$ , Fig. 3. The residing time was dependent on the amount of nanoparticles, i.e. 30 (0.5 wt%), 35 (1.0 wt%), 45 (3.0 wt%) and 60 (5.0 wt%) minutes. Sodium dodecylbenzene sulfonate (SDBS) was used as a surfactant (ratio 1:1 wt% of  $\text{TiO}_2$ ). Unfortunately, no details and key reasons, other than the ratio and general purpose of surfactants, were specified for the surfactant addition process.

Nourani et al. (2016) analyzed the improvement of paraffin thermal properties ( $T_m = 54\text{--}58\text{ }^\circ\text{C}$ ) with the addition of  $\text{Al}_2\text{O}_3$  nanoparticles (10–20 nm, concentration from 2.5 wt% to maximal 10.0 wt%). Sodium stearoyl lactylate (SSL) in a ratio of 1:3.5 wt% to  $\text{Al}_2\text{O}_3$  was used as a surfactant. The surfactant addition process should be further elaborated to provide additional insight into the preparation technology thus ensuring repeatability of the experiment. One hour of initial stirring was performed with a magnetic stirrer in combination with vacuum pump (VDE 0530, KNF NEUBERGER) to avoid the formation of air bubbles. In addition to this limited description of mixing, other influential parameters should be clearly stated, in particular, the angular velocity (or rpm), temperature, precise sample size, etc. Finally, the sample was exposed to ultrasonic vibration (1200 M, SONICA), power 80 W and frequency of 50 kHz in duration of about 2 h.

Lin and Al-Kayiem (2016) made an evaluation of a Cu/Paraffin nanocomposite application for solar thermal energy storage. The base PCM material is not described in detail which is a significant shortcoming. The nanoparticles of Cu (20 nm) were added to paraffin in different mass fractions (concentration from 0.5 wt% to not more than 2.0 wt%) and dispersed for 2 h with the ultrasonication device (heating and vibration feature) at  $70\text{ }^\circ\text{C}$ . The authors did not clearly specify the used device, and the preparation parameters are scant.

Colla et al. (2017) experimentally investigated two commercial paraffin waxes (RUBITHERM® RT20 ( $T_m = 20\text{ }^\circ\text{C}$ ) and RT25 ( $T_m = 25\text{ }^\circ\text{C}$ )) enhanced with nanoparticles of  $\text{Al}_2\text{O}_3$  (10 nm) and carbon black (CB) (15–20 nm) in a 1% mass fraction (four



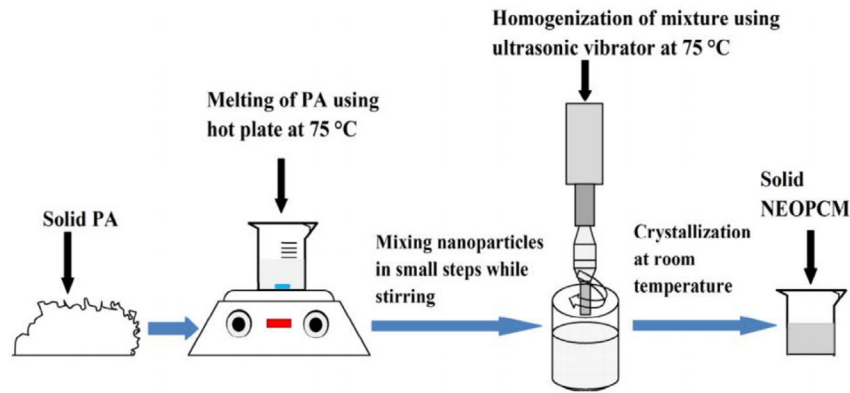


Fig. 3. The procedure of PA/TiO<sub>2</sub> nanocomposite preparation, (Sharma et al., 2016).

nanocomposites were prepared). Al<sub>2</sub>O<sub>3</sub>/RT20 and Al<sub>2</sub>O<sub>3</sub>/RT25 nanocomposites were prepared in two steps. Initially, they were subjected to 20 min of mechanical stirring at 600 rpm and then underwent ultrasonication with a probe sonicator (Hielscher UP200s) and flooded in the thermostatic bath for 150 min at 30 °C. A useful piece of information would be to compare the sample temperature and the thermostatic bath temperature over 150 min which could be used to evaluate the efficiency of the cooling process. In the case of CB/RT20 and CB/RT25 nanocomposites were subjected to mixing in the oil bath in duration of 30 min. Details of the mixing process are missing, especially in terms of the parameters used.

Singh et al. (2017) checked the solar thermal energy storage capabilities of Myo-inositol PCMs ( $T_m = 222\text{--}227\text{ °C}$ ) enhanced with nanoparticles of Al<sub>2</sub>O<sub>3</sub> (40–50 nm, 1.0 wt%, 2.0 wt%, 3.0 wt%) and CuO (40–50 nm, concentration from 1.0 wt% to maximal 3.0 wt%). The samples are prepared using a low energy ball mill for 2 h at 200 rpm. The description of the preparation is mostly inadequate and uninformative, lacking most of the details regarding the procedures and parameters used.

Motahar et al. (2017) examined the solidification process of an n-octadecane ( $T_m = 28\text{ °C}$ ) modified with nanoparticles of TiO<sub>2</sub> (concentration from 1.0 wt% to maximal 4.0 wt%). Before it was mechanically stirred, the NEPCM was liquefied and degassed using vacuum conditions. The final step in the preparation was sonication in an ultrasonic bath (VWR, USC2100D, Germany) for 15 min at 40 °C. Achieving vacuum conditions should be more clearly elaborated as well as the mechanical mixing and sonication parameters.

Babapoor and Karimi (2015) conducted measurements of thermal properties and a thermal storage investigation of nanocomposites based on paraffin and nanoparticles of Al<sub>2</sub>O<sub>3</sub> (20 nm), Fe<sub>2</sub>O<sub>3</sub> (20 nm), SiO<sub>2</sub> (11–14 nm), ZnO (>50 nm) in various mass fractions (ranging from 2.0 wt% to not more than 8.0 wt%). Before the preparation of the nanocomposites, paraffin wax ( $T_m = 53\text{--}57\text{ °C}$ ) was melted and blended with the liquid paraffin. The division of nanoparticles within the paraffin was performed with magnetic stirrer in duration of about 75 min, and after that sample was subjected to sonication (ultrasonic bath, Ultrasonic Cleaner Soner 203H, Laftech, Australia). Unfortunately, most of the parameters of mechanical mixing and sonication were not adequately specified, such as rpm, frequency, temperature, etc.

Wang et al. (2016) dispersed graphite nanoparticles (<30 nm, 0.05 wt%, 0.1 wt%) in a paraffin ( $T_m = 58\text{--}60\text{ °C}$ ) and water emulsion applying homogenizer (rotor-stator specific setup, model FJ200-SH) for 5 min at 12000 rpm. The examination of the thermophysical properties and photothermal performance of a paraffin/water nanocomposite were carried out. Another possible

application for this NEPCM might be as a heat transfer fluid but in the form of nanofluid.

Karimi et al. (2016) conducted investigation related to the thermal management issue of lithium-ion battery, based on a paraffin mixture (paraffin wax ( $T_m = 39\text{--}45\text{ °C}$ ) and liquid paraffin) enhanced with nanoparticles of Ag (80–100 nm, 2 wt%), Cu (70 nm, 2 wt%) and Fe<sub>3</sub>O<sub>4</sub> (20–30 nm, 2 wt%). The nanocomposite was prepared using a sonication (sonication bath, Ultrasonic Cleaner Soner 203H) for 2 h at the temperature exceeding melting temperature. The sonication process was not properly explained, i.e. key parameters such as frequency, sample size, exact temperature, etc. are missing.

Babapoor et al. (2016) analyzed thermal features of a nanocomposite during the solidification process. The liquid (40 wt%) and solid ( $T_m = 53\text{--}57\text{ °C}$ , 60 wt%) paraffin mixture was prepared using an ultrasonic mixing (ultrasonic bath, Ultrasonic Cleaner Soner 203H) for 45 min. Then, different nanocomposites were created by adding nanoparticles of Al<sub>2</sub>O<sub>3</sub> (20 nm), Fe<sub>2</sub>O<sub>3</sub> (20 nm), SiO<sub>2</sub> (11 nm), SiO<sub>2</sub> (20 nm), ZnO (>50 nm) in various mass fractions (concentrations from 2.0 wt% to maximal 8.0 wt%) which were finally dispersed with a magnetic stirrer for 75 min. Aside from the apparent lack of key parameters related to the preparation of NEPCM, the paper presents a slightly different approach in which only magnetic mixing was used to disperse the nanoparticles. The reason for this unique approach was not clearly stated.

Bahiraie et al. (2017) investigated the capabilities of the paraffin wax ( $T_m = 60\text{ °C}$ ) based nanocomposite for thermal management both on numerical and experimental way. The melted paraffin was enhanced with carbon nanofibers, graphene nanoplatelets and graphite nanopowder in a mass fraction from 2.5 wt% to not more than 10 wt%. A good dispersion of nanomaterials was provided with intensive 30 min stirring and 2 h of sonication at about 90 °C. Although the concrete details of the preparation are typically lacking, the paper has incorporated both a numerical and an experimental approach which is an added value of the work.

Alimohammadi et al. (2017) conducted an experimental investigation of electronic chipsets cooling based on nanocomposites. An inorganic salt-hydrate, Mn(NO<sub>3</sub>)<sub>2</sub> was used as a PCM which was enhanced with nanoparticles of Fe<sub>3</sub>O<sub>4</sub> (<40 nm, 1.0 wt%). The chemical precipitation method was used in the nanoparticle producing process. Four hours of mixing was performed with an ultrasonic machine (Wise-Clean, WUC-D10H) at 60 °C. The chemical precipitation method as well as ultrasonic processing were not well elaborated which is a pity because it is a slightly different approach than in other works.

Sami and Etesami (2017) enhanced the thermal properties of paraffin ( $T_m = 54\text{--}58\text{ °C}$ ) by adding nanoparticles of TiO<sub>2</sub>

(5–20 nm, concentrations from 0.5 wt% to 4.0 wt%). A good distribution of nanoparticles in the paraffin was achieved with a magnetic stirrer and an ultrasonic processor (Hielscher UP400s). However, precise details related to stirring and ultrasonic processing are undoubtedly missing. Sodium stearoyl lactylate (SSL) surfactant was used in a mass ratio of 1:4 for SSL/TiO<sub>2</sub>. The addition of the SSL surfactant should be described in more detail because it is an important factor that affects the properties of NEPCM.

Ebadi et al. (2018) explored an effect of the nanoparticle loading with respect to the thermal properties of the coconut oil (PCM with  $T_m = 24\text{ }^\circ\text{C}$ ). Nanoparticles of CuO (<50 nm, 0.1 wt%, 1 wt%) were dispersed in the PCM using a magnetic stirrer (SP88854100, Thermo Scientific) in duration of 12 h at 60 °C. The mixing process was completed with 30 min sonication (model: Q500, manufacturer: Qsonica). A very common approach is utilized in the research, which includes a magnetic stirrer typically followed by sonication, but some parameters are not specified (eg. frequency, rpm, etc.). It is also not clear why the stirring lasted as long as 12 h.

Nada et al. (2018) investigated the effect of Al<sub>2</sub>O<sub>3</sub> nanoparticle (<20 nm) dispersion (2%) in paraffin wax (RUBITHERM®, RT55,  $T_m = 51\text{--}57\text{ }^\circ\text{C}$ ) on thermal management as well as efficiency of the PV panels. The mixing was carried out with a mechanical stirrer. Unfortunately, the exact mixing parameters are not specified in the paper.

Harikrishnan et al. (2017) analyzed the performance of the solar thermal storage of a NEPCM, based on myristic acid (CH<sub>3</sub>(CH<sub>2</sub>)<sub>12</sub>COOH,  $T_m = 52\text{ }^\circ\text{C}$ ) enhanced with SiO<sub>2</sub> nanospheres (52 nm, concentration from 0.2 wt% to maximal 1.0 wt%). To prepare nanoparticles before mixing, sodium dodecylbenzene sulfonate (SDBS) was employed as a surfactant. An ultrasonication technique was used to mix the nanoparticles. A frequency of 40 kHz was used for all the samples but with different residence times, 45 min–60 min, with concentrations ranging from 0.2 wt% to 1.0 wt%. The ultrasonication technique is decently described, but still, the apparent lack of exact sample size and scarcity of sample temperature monitoring during the preparation process can be noticed.

Wilson John et al. (2017) created a paraffin-based nanocomposite enhanced with CuO nanoparticles (0.01 wt%) for diesel engine waste heat management. The nanocomposite was created using magnetic stirrer in duration of 30 min at 60 °C. Finally, the mixture was subjected to ultrasonic vibration for 3 h. In addition to the lack of preparation parameters, the specific devices that were used are also missing. Therefore, it is impossible for other researchers to repeat the experiment.

Chaichana and Kazem (2018) studied the improvement of solar distillator productivity enhanced with paraffin ( $T_m = 45\text{ }^\circ\text{C}$ ) based nanocomposite. Nanoparticles of Al<sub>2</sub>O<sub>3</sub> (30–60 nm, concentration from 0.5 wt% to 3.0 wt%) were added to the paraffin wax and dispersed by employing ultrasonic shaker (TELSONIC ULTRASONICS CT-12) for 4 h. The NEPCM preparation process is insufficiently elaborated by the authors and as such cannot be scientifically verified in any possible way.

Salyan and Suresh (2018) investigated the thermophysical properties and cycling stability (Fig. 4) of D-Mannitol (C<sub>4</sub>H<sub>14</sub>O<sub>6</sub>) ( $T_m = 165\text{--}169\text{ }^\circ\text{C}$ ) upgraded with nanoparticles of CuO (10–40 nm, concentration from 0.1 wt% to 0.5 wt%). The nanocomposite was prepared using a low energy ball mill (three stainless steel balls were applied into the rotating sample holder) for 2.5 h at 250 rpm followed by an ultrasonic vibrator (Lark Instruments, frequency of 40 kHz). The paper contains some important preparation parameters but still lacks basic information such as sample size (volume or mass of base PCM).

Putra et al. (2017) explored the thermal stability of RUBITHERM® paraffin wax RT22 HC ( $T_m = 22\text{ }^\circ\text{C}$ ) enhanced with graphene nanoplatelets (2 nm, concentrations from 0.05 wt% to

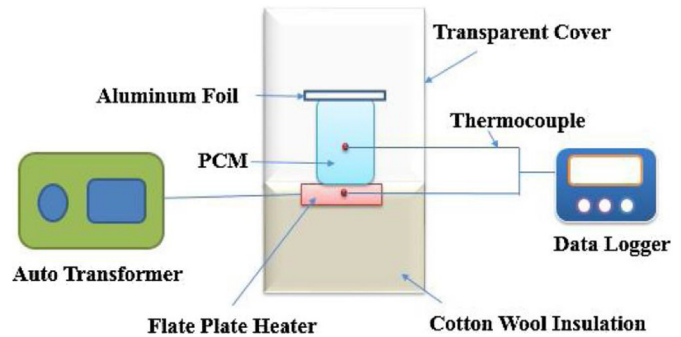


Fig. 4. Schematics of thermal cycling equipment, (Salyan and Suresh, 2018).

0.30 wt%). The proper dispersion of nanoplatelets was ensured with mixing in a beaker, stirring and 3 h of sonication (40 Hz) at 45 °C, Fig. 5. Sonication apart from the nonspecified device was decently described, however, the mixing in a beaker and stirring remains vague as well as the sample size of the base PCM.

Yadav et al. (2017) experimentally researched the thermal properties of Magnesium chloride hexahydrate (MCH) ( $T_m = 115\text{--}118\text{ }^\circ\text{C}$ ) improved with nano-graphite particles (NG) (concentration from 0.1 wt% to 0.5 wt%) using ultrasonic bath in duration of 30 min. The MCH was preheated to 130 °C. The specific ultrasonic bath device is not listed as well as other significant process parameters such as frequency, sample size, or sample temperature during the process itself which is a pity because those are valuable information for researchers.

Pahamli et al. (2017) performed the experimental characterization of a NEPCM based on RUBITHERM® RT50 paraffin ( $T_m = 51\text{ }^\circ\text{C}$ ) and nanoparticles of CuO (2.0 wt%, 4.0 wt%) which were dispersed using an ultrasonic system for 30–40 min. The paper has a general description of nanoparticle dispersion in PCM which is unacceptable especially in the context of the considerable complexity of the preparation of NEPCM materials.

Disilva Winfred Rufuss et al. (2018) analyzed the impact of adding different nanomaterials such as titanium dioxide, (TiO<sub>2</sub>), graphene oxide (GO) and finally copper oxide (CuO) to paraffin PCMs in order to improve solar still productivity. A 0.3 wt% of different nanoparticles was dispersed using sonication (40 kHz) for 40 min on temperature about 10 °C that was over the PCM melting temperature. Sodium dodecylbenzene sulfonate (SDBS) surfactant with a mass ratio to nanoparticles of 1:1 was used to improve the dispersion. More details regarding surfactant addition and base PCM sample properties are lacking but sonication was decently described apart from the unspecified device and base PCM sample mass.

Bashar and Siddiqui (2018) experimentally studied the time-dependent melting and heat transfer process of NEPCMs based on Polyfin paraffin wax ( $T_m = 55\text{ }^\circ\text{C}$ ) upgraded with 0.1 wt% of Al<sub>2</sub>O<sub>3</sub> nanoparticles (20 nm), Ag nanoparticles (30–50 nm), CuO nanoparticles (40 nm) and Multi-walled carbon nanotubes (MWCNT) (40–60 nm). The nanoparticles and nanotubes were mixed with pellets of paraffin, melted and continuously stirred for 72 h on a temperature ranging from 65 to 75 °C. The preparation process described in the paper is too general and factually vague.

Praveen and Suresh (2018) experimentally researched the heat transfer capabilities of Neopentyl glycol ( $T_m = 126\text{ }^\circ\text{C}$ ) enhanced with nanoparticles of CuO (30–50 nm, concentrations from 0.5 wt% to 3.0 wt%). The ball mill (low energy, VB Ceramics) was used for 120 min at 200 rpm followed by a sonicator (probe-type, Lark Industries) which was used for 10 min at 40 kHz. In fact, the description of preparation is well-grounded, but it is not clear

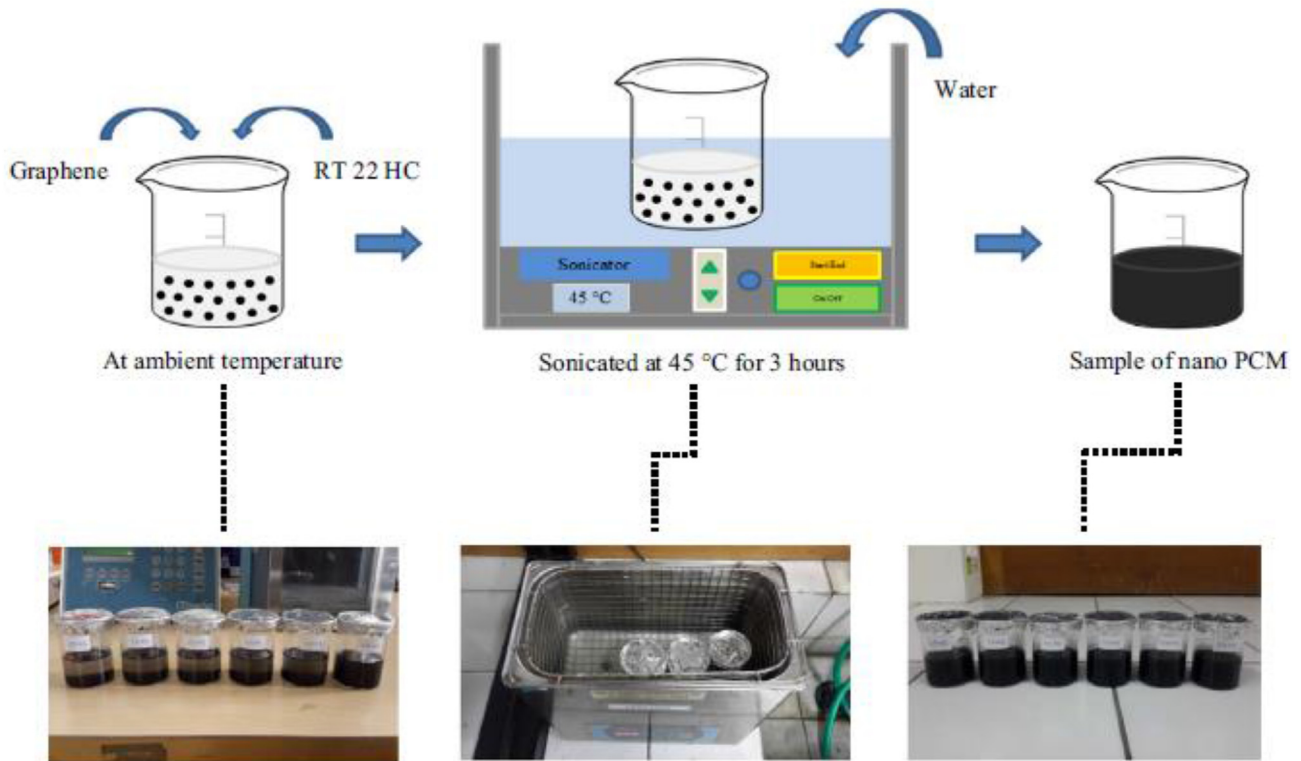


Fig. 5. NEPCM synthesis process, (Putra et al., 2017).

enough what the sample size of the base PCM is, so it is difficult to put used parameters into the proper perspective.

Jogi Krishna et al. (2017) studied the capabilities of Tricosane ( $T_m = 47\text{ °C}$ ) enhanced with nanoparticles of  $\text{Al}_2\text{O}_3$  (50 nm, from 0.5 vol% to 2.0 vol%) as an energy storage possibility in electronic applications (cooling). Homogeneity of the samples was ensured by employing an ultrasonic homogenizer (UP400S) for 30 min. The process of homogenization is too generally and inadequately described in the paper.

Sharma et al. (2017) explored the potential of thermal management of Building-Integrated Concentrated Photovoltaics (BICPV) using RUBITHERM® RT42 paraffin wax ( $T_m = 38\text{--}43\text{ °C}$ ) and nanoparticles of  $\text{CuO}$  (60 nm, 0.5 wt%). The sample was prepared with a Hilsonic® ultra-sonicator device. The duration of this procedure was 24 h. Very little attention was given to the preparation of the NEPCM in the paper, so a significant lack of reliable data in this context is noticeable.

He et al. (2019) conducted an examination and thermal characterization of myristic acid (MA) ( $T_m = 54\text{--}55\text{ °C}$ ) enhanced with graphene nanoplatelets (GNPs) (3–10 nm, from 1 wt% to 3 wt%), (MWCNTs) (<8 nm, 1 wt%, 2 wt%, 3 wt%) and nano-graphites (NG) (<40 nm, from 1 wt% to 3 wt%). The nanocomposites were prepared using the two-step method, Fig. 6. First, the samples were blended for 30 min with a magnetic stirrer and the samples underwent 1 h of ultrasonic vibration after that. With the notable exception of the scheme, there are too few details in the paper that specifically talk about the preparation of NEPCM material, i.e. the parameters of stirring and ultrasonic vibration are missing.

Temel (2019) analyzed the thermal management (passive option) of the battery pack enhanced with a nanocomposite based on RUBITHERM® paraffin wax RT 44 ( $T_m = 41\text{--}44\text{ °C}$ ) and graphene nanoplatelets (GNP) (6–8 nm, 3 wt%, 5 wt%, 7 wt%). The samples

were produced using an ultrasonic mixing device (Sonics & Materials INC, USA) for 30 min at 750 W. Data on the sample size of the base PCM would be valuable, but unfortunately, it is not explicitly stated in the paper.

Sivasamy et al. (2019) explored energy storage (thermal) capabilities of the myristic acid ( $T_m = 57\text{--}59\text{ °C}$ ) enhanced with nanoparticles of Ag (5.8 nm, concentrations from 0.1 wt% to 0.3 wt%). A stable dispersion of nanoparticles was ensured with sodium dodecylbenzene sulfonate (SDBS) surfactant and 50 min of sonication procedure. The process of surfactant addition and sonication is insufficiently described for deeper analyzes in this regard.

Venkitaraj and Suresh (2019) analyzed the thermal degradation of a NEPCM based on pentaerythritol (PE) ( $T_m = 255\text{--}259\text{ °C}$ ) and  $\text{Al}_2\text{O}_3$  nanoparticles (40–50 nm, 0.1 wt%, 1 wt%). The NEPCM was homogenized with ball mill (low energy, VB Ceramics) for 90 min at 200 rpm. The sample size is not clearly specified, so it is difficult to objectively assess the suitability of the parameters used.

Wang et al. (2019) investigated the influence of  $\text{Al}_2\text{O}_3$  nanoparticles (10–30 nm, 0.001 vol%, 0.005 vol%, 0.01 vol%) on thermal radiative features of paraffin ( $T_m = 18\text{ °C}$ ). The nanofluid was produced by the two-step approach and, mechanical agitation, sonication, and dispersants (CTAB powders) are applied for the dispersibility of mixture. Nanoparticles were mixed with the liquid paraffin in a beaker and CTAB were added. A magnetic stirring apparatus was employed to stir the mixture for 30 min, which is followed by 90 min of ultrasonication. The magnetic stirring apparatus and parameters are unknown as well as ultrasonication apparatus and parameters. This is a set of data that must be available to other researchers and in this aspect, the paper is unquestionably deficient.



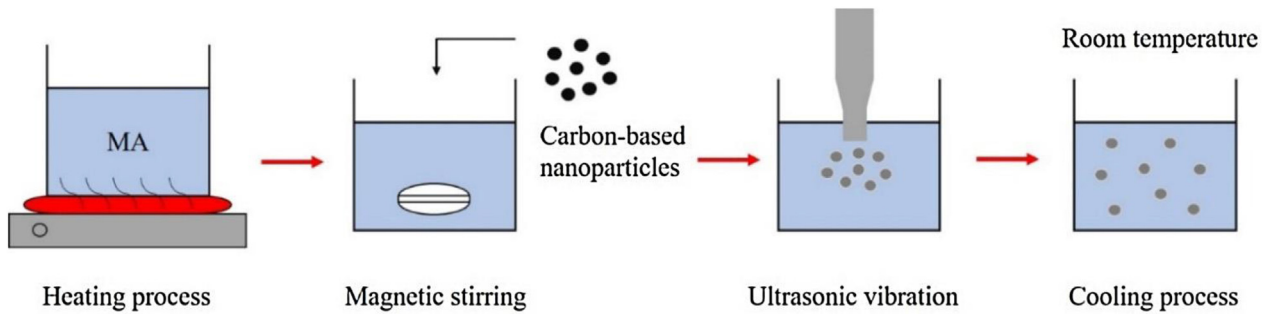


Fig. 6. Process of sample preparation, (He et al., 2019).

### 3.2. Summary of nanocomposite preparation strategies and discussion on critical aspects

Based on the previously reviewed and selected research studies, there is a variety of techniques that are used to produce homogeneous nanocomposites, most of which can be classified into two basic mixing techniques which are some type of mechanical processing (stirring) and sonication, Table 1. Table 1 summarizes the practical details of nanocomposite preparation where w/o abbreviation, meaning “without”, refers to processes and process parameters that have not been used or specifically emphasized in the paper.

Generally, in all the selected papers, the process of nanocomposite preparation is not sufficiently described in order to be repeatable. The base of each nanocomposite is a specific PCM with certain thermophysical properties which must be clearly stated in the paper and which unfortunately is often not the case. The minimum information on PCMs is the melting point temperature which was stated in most of the considered papers with exceptions of papers (Lin and Al-Kayiem, 2016), (Wilson John et al., 2017), (Dsilva Winfred Rufuss et al., 2018), dealing with paraffin, and (Alimohammadi et al., 2017) dealing with salt-hydrate. The thermophysical properties of nanomaterials represent valuable data for the aspects of the mixing approach and expected nanocomposite properties. In addition to that, the morphology, size and amount of nanoparticles are a piece of indispensable information necessary to adequately describe nanomaterials. Unfortunately, in most of the papers, some of these data are missing and which might be helpful for future researches dealing with this research topic. The authors of some papers were using volume fractions to describe the amount of multilayer graphene nanoplatelets (Harish et al., 2015), herringbone graphite nanofibers (Warzoha et al., 2015) and nanoparticles of  $\text{Al}_2\text{O}_3$  (Jogi Krishna et al., 2017), while in paper (Nada et al., 2018) it is not entirely clear whether the authors used volume or mass fraction to describe the amount of  $\text{Al}_2\text{O}_3$  nanoparticles. In other papers, the mass fraction was used which was a far better choice since PCM volume changes with the temperature resulting in insufficient repeatability of experiments. Also, the PCM mass (or at least volume) should be stated because convenient mixing parameters depend on it. Basically, all the considered papers lack clarity regarding the size of samples or they totally omit this data which is unfortunate since it represents a basic set of information which can be essential for future researches. If researchers have access to the necessary equipment, the temperature of samples during mixing should be monitored and recorded. Other mixing parameters such as the number of revolutions regarding stirrers, sonication frequency, and duration of these processes were not often specified, while in papers (Sami and Etesami, 2017), (Nada et al., 2018) they are completely omitted. Furthermore, the exact model of devices, as well as other used equipment, represents

valuable information for interested parties.

### 3.3. Preparation of nanofluids

The specific preparation procedure is analyzed and discussed in upcoming sections of the paper and focused on preparation strategies for nanofluids. The critical aspects, as well as issues linked with preparation, are elaborated at the end of this section as a summary section.

Altohamy et al. (2015) investigated effect of the nano-fluid on cool storage performance. A water and  $\gamma\text{-Al}_2\text{O}_3$  nanoparticles (50 nm, concentrations from 0.5 vol% to 2.0 vol%) based nanofluid was created with 90 min of ultrasonication at 30 °C. In addition to the data on the duration and temperature of ultrasonication, it is necessary to specify the frequency or power, which is not the case. Furthermore, the volume fraction of nanoparticles was used although the mass fraction would be a much better choice as the effect of fluid thermal expansion is avoided.

Chieruzzi et al. (2017) created a nanofluid based on a nitrate salt mixture ( $T_m = 220$  °C, concretion 60 wt%  $\text{NaNO}_3$  with also 40 wt%  $\text{KNO}_3$ ), with nanoparticles of  $\text{SiO}_2$  (7 nm, 1 wt%),  $\text{Al}_2\text{O}_3$  (13 nm, 1 wt%),  $\text{SiO}_2/\text{Al}_2\text{O}_3$  (2–200 nm, 1 wt%). The mixing process was performed directly at high temperatures, thereby eradicating the water evaporation procedure. In order to disperse the nanoparticles, the DSM Xplore micro-compounder (twin-screw, Geleen, Model, 2005) was used at 100 rpm (in duration of 15 min) and 200 rpm (in duration of 30 min), Fig. 7. The authors did not clearly specify the sample size of the base fluid to which the nanoparticles were added, which leaves room for speculation.

Wang et al. (2017) explored the thermophysical features of the 30 wt% OP10E ( $T_m = 8\text{--}10$  °C) and water emulsion enhanced with graphite nanoparticles (<30 nm, from 0.25 wt% to 4 wt%). The nanofluid was prepared in a time of 3 min with a rotor-stator homogenizer at 8000 rpm and 25 °C. More practical details about the rotor-stator homogenizer would help to better understand the process with mandatory data on the amount of base fluid to which the nanoparticles are added.

Attia et al. (2016) compared the performance of a cool storage system based on an HTF and NEPCM. The nanofluid was prepared by adding  $\gamma\text{-Al}_2\text{O}_3$  nanoparticles (50 nm, from 0.25 vol% to 1.0 vol%) to water. The mixing was performed in an ethylene glycol bath using ultra-sonication for a period of 90 min (with constant temperature of 30 °C). Mass fraction would be a much better choice, but the main problem is the lack of ultrasonication parameters and data on the amount of base fluid.

Shao et al. (2017) observed the solidification behavior and cold thermal energy storage capabilities of deionized water enhanced with  $\text{TiO}_2$  nanotubes (TiNT) (9–10 nm),  $\text{TiO}_2$  nanoplatelets (TiNP) (50–80 nm) and their hybrid (with TiNP percentages of 0%, 25%, 50%, 75%, 100%) at the same as well as different total  $\text{TiO}_2$  mass

**Table 1**  
Nanocomposite preparation technology with respect to type of nanomaterials and type of PCM.

| Reference                  | PCM   | Nanomaterial   | Mechanical processing                                       | Parameters of mechanical processing | Sonication  | Parameters of sonication  | Accentuated details  |
|----------------------------|---|--|---|-------------------------------------|---|---|--|
| Harish et al. (2015)       | n-Dodecanoic acid (Lauric acid)<br>$T_m = 44\text{ }^\circ\text{C}$   | Multilayer graphene nanoplatelets (Liquid phase exfoliated, MLG); 5–10 nm<br>Volume fraction: 0.1%, 0.25%, 0.5%, 0.75%, 1%   | magnetic stirrer  | 250 rpm, 30 min, 100 °C             | ultrasonic mixing (Hielscher GmbH, model UP-400S with H3) | 50% amplification, 30 min   | Preparation of MLG before mixing with PCM  |
| Warzoha et al. (2015)      | Organic Paraffin (IG1230A)<br>$T_m = 56\text{ }^\circ\text{C}$  | Herringbone graphite nanofibers (HGNF); 2–100 nm<br>Volume fraction: 0.05%, 0.1%, 0.2%, 0.3%, 0.4%, 2.8%, 5.8%, 8.5%, 11.4%  | w/o   | w/o                                 | sonicator   | 32 Hz, 2 h  | Initially, the PCM was liquefied using a constant temperature hot plate (353 K).                                     |
| Sharma et al. (2016)       | Palmitic acid<br>$T_m = 60\text{--}62\text{ }^\circ\text{C}$  | Nanoparticles of titanium dioxide ( $\text{TiO}_2$ ); 21 nm<br>Mass fraction: 0.5%, 1.0%, 3.0%, 5.0%   | w/o   | w/o                                 | ultrasonic vibrator (VCX 500, SONICS)                     | 40 kHz, 75 °C; The residing time was set as 30(0.5 wt%), 35(1.0 wt%), 45(3.0 wt%), 60(5.0 wt%) minutes. | Surfactant: Sodium dodecylbenzene sulfonate, ratio 1:1 wt% ( $\text{TiO}_2$ )  |
| Nourani et al. (2016)      | Paraffin<br>$T_m = 54\text{--}58\text{ }^\circ\text{C}$   | Nanoparticles of $\text{Al}_2\text{O}_3$ ; 10–20 nm<br>Mass fraction: 2.5%, 5.0%, 7.5%, 10.0%  | magnetic stirrer and a vacuum pump (VDE 0530, KNF)          | 1 h, 600 mmHg vacuum                | ultrasonic vibration (1200 M, SONICA, Italy)              | 80 W, 50 kHz, 2 h   | Surfactant: Sodium stearoyl lactylate (SSL) in the ratio 1:3.5 wt% of $\text{Al}_2\text{O}_3$                        |
| Lin and Al-Kayiem (2016)   | Paraffin wax  | Nanoparticles of Cu; 20 nm<br>Mass fraction: 0.5%, 1.0%, 1.5%, 2.0%  | w/o   | w/o                                 | ultrasonication device (heating and vibration feature)    | 4 h, 70 °C  | w/o  |
| Colla et al. (2017)        | Paraffin (RUBITHERM® RT20);<br>$T_m = 20\text{ }^\circ\text{C}$ Paraffin (RUBITHERM® RT25);<br>$T_m = 25\text{ }^\circ\text{C}$ | A) Nanoparticles of $\text{Al}_2\text{O}_3$ ; 10 nm<br>Mass fraction: 1.0% B) Nanoparticles of Carbon black (CB); 15–20 nm<br>Mass fraction: 1.0%  | A) mechanically stirred B) stirring in an oil bath          | A) 600 rpm, 20 min<br>B) 30 min     | A) probe sonicator (Hielscher UP200s)                     | thermostatic bath set at 30 °C, 150 min   | w/o  |
| Singh et al. (2017)        | Myo-Inositol (MI)<br>$T_m = 222\text{--}227\text{ }^\circ\text{C}$  | Nanoparticles of $\text{Al}_2\text{O}_3$ and CuO; 40–50 nm<br>Mass fraction: 1.0%, 2.0%, 3.0%  | ball mill (low energy with the three stainless steel balls) | 200 rpm, 2 h                        | w/o   | w/o   | w/o  |
| Motahar et al. (2017)      | n-octadecane<br>$T_m = 28\text{ }^\circ\text{C}$  | Nanoparticles of Titanium (IV) oxide ( $\text{TiO}_2$ )<br>Mass fraction: 1.0%, 2.0%, 4.0%   | mechanical stirrer  | w/o                                 | ultrasonic bath ((VWR, USC2100D, Germany)                 | 15 min, 40 °C   | Initially PCM was melted and degassed under vacuum conditions  |
| Babapoor and Karimi (2015) | Liquid paraffin Solid paraffin;<br>$T_m = 53\text{--}57\text{ }^\circ\text{C}$  | Nanoparticles of $\text{Al}_2\text{O}_3$ (20 nm), $\text{Fe}_2\text{O}_3$ (20 nm), $\text{SiO}_2$ (11–14 nm), $\text{ZnO}$ (>50 nm)<br>Mass fraction: 2.0%, 4.0%, 6.0%, 8.0%                       | magnetic stirrer  | 75 min                              | sonication bath, (Ultrasonic Cleaner Soner 203H)          | uniform temperature over the melting temperature (paraffin mixture)                                     | Solid paraffin was melted and mixed with the liquid paraffin.  |
| Wang et al. (2016)         | Paraffin ( $T_m = 58\text{--}60\text{ }^\circ\text{C}$ ) and water emulsion   | Graphite nanoparticles; <30 nm<br>Mass fraction: 0.05%, 0.1%   | rotor-stator homogenizer (model FJ200-SH)                   | 12,000 rpm, 5 min                   | w/o   | w/o   | Initially paraffin/water emulsion was prepared   |
| Karimi et al. (2016)       | Paraffin mixture<br>$T_m = 39\text{--}45\text{ }^\circ\text{C}$   | Nanoparticles of Ag (80–100 nm), Cu (70 nm), $\text{Fe}_3\text{O}_4$ (20–30 nm)<br>Mass fraction: 2.0%   | w/o   | w/o                                 | sonication bath, (Ultrasonic Cleaner Soner 203H)          | 2 h, on the temperature that was higher than the melting temperature                                    | Solid paraffin was warmed above the melting temperature. After that mixing with liquid paraffin.                     |
| Babapoor et al. (2016)     | Liquid paraffin Solid paraffin<br>$T_m = 53\text{--}57\text{ }^\circ\text{C}$   | Nanoparticles of $\text{Al}_2\text{O}_3$ (20 nm), $\text{Fe}_2\text{O}_3$ (20 nm), $\text{SiO}_2$ (11 nm), $\text{ZnO}$ (>50 nm), $\text{SiO}_2$ (20 nm),<br>Mass fraction: 2.0%, 4.0%, 6.0%, 8.0% | magnetic stirrer  | 75 min                              | w/o   | w/o   | Solid paraffin warmed up to a temperature over melting point and blended (in a sonicator bath) with liquid paraffin. |
| Bahiraeei et al. (2017)    | Paraffin wax<br>$T_m = 60\text{ }^\circ\text{C}$  | Graphene nanoplatelets, Carbon nanofiber, graphite nanopowder<br>Fraction (mass): 2.5%, 5.0%, 7.5% and 10%   | intensively stirred   | 30 min                              | sonicated   | at about 90 °C, 2 h   | w/o  |
| Alimohammadi et al. (2017) |   |  | w/o   | w/o                                 |   | 4 h, 60 °C  |  |

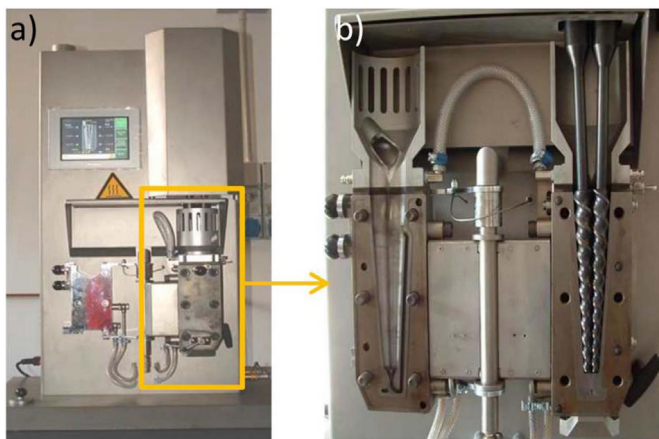
(continued on next page)

Table 1 (continued)

| Reference                           | PCM   | Nanomaterial  | Mechanical processing   | Parameters of mechanical processing | Sonication   | Parameters of sonication   | Accentuated details  |
|-------------------------------------|---|---|---|-------------------------------------|--|--|--|
| Sami and Etesami (2017)             | salt-hydrate (inorganic), Mn(NO <sub>3</sub> ) <sub>2</sub> Paraffin<br>T <sub>m</sub> = 54–58 °C | Nanoparticles of Fe <sub>3</sub> O <sub>4</sub> ; <40 nm<br>Mass fraction: 1.0%<br>Nanoparticles of TiO <sub>2</sub> ; 5–20 nm<br>Mass fraction: 0.5%, 0.7%, 1.0%, 2.0%, 3.0%, 4.0% | magnetic stirrer  | w/o                                 | ultrasonic device (model, WUC-D10H) ultrasonic mixing (Hielscher up 400 s) | w/o  | Nanoparticles producing process: the chemical precipitation method<br>Surfactant: Sodium stearoyl lactylate, mass ratio of 1:4, for SSL/TiO <sub>2</sub> |
| Ebadi et al. (2018)                 | Coconut oil<br>T <sub>m</sub> = 24 °C   | Nanoparticles of CuO; <50 nm<br>Mass fraction: 0.1%, 1%   | magnetic stirrer (model: SP88854100, manufacturer: Thermo Scientific) | 12h, 60 °C                          | sonicator (model: Q500, manufacturer: Qsonica)                             | 30 min   | w/o  |
| Nada et al. (2018)                  | Paraffin wax RT55 (RUBITHERM®)<br>T <sub>m</sub> = 51–57 °C                                       | Nanoparticles of Al <sub>2</sub> O <sub>3</sub> ; <20 nm<br>Fraction: 2%  | mechanical stirrer  | w/o                                 | w/o  | w/o  | w/o  |
| Harikrishnan et al. (2017)          | Myristic acid [CH <sub>3</sub> (CH <sub>2</sub> ) <sub>12</sub> COOH]<br>T <sub>m</sub> = 52 °C   | SiO <sub>2</sub> nanospheres; 52 nm<br>Mass fraction: 0.2%, 0.5%, 0.8% and 1.0%   | w/o   | w/o                                 | ultrasonication technique  | 40 kHz, estimated residence times were 45(0.2%), 50(0.5%), 55(0.8%) and 60(1.0%) min | Preparation of nanoparticles before mixing with PCM<br>Surfactant: Sodium dodecylbenzene sulfonate (SDBS)  |
| Wilson John et al. (2017)           | Paraffin wax  | Nanoparticles of CuO<br>Mass fraction: 0.01%  | magnetic stirrer  | 30 min, 60 °C                       | ultrasonic vibrator  | 3 h  | w/o  |
| Chaichan and Kazem (2018)           | Paraffin wax<br>T <sub>m</sub> = 45 °C  | Nanoparticles of Al <sub>2</sub> O <sub>3</sub> ; 30–60 nm<br>Mass fraction: 0.5%, 1.0%, 2.0%, 3.0%   | w/o   | w/o                                 | ultrasonic shaker (TELSONIC ULTRASONICS CT-12)                             | 4 h  | w/o  |
| Salyan et al. (2018)                | D-Mannitol (C <sub>4</sub> H <sub>14</sub> O <sub>6</sub> )<br>T <sub>m</sub> = 165–169 °C        | Nanoparticles of CuO; 10–40 nm<br>Mass fraction: 0.1%, 0.2%, 0.5%   | ball mill (low energy, three stainless steel balls)                   | 250 rpm, 2.5 h                      | ultrasonic vibrator (Lark Instruments)                                     | 40 kHz   | w/o  |
| Putra et al. (2017)                 | Paraffin wax RT22 HC(RUBITHERM®)<br>T <sub>m</sub> = 22 °C  | Graphene nanoplatelets; <2 nm<br>Mass fraction: 0.05%, 0.10%, 0.15%, 0.20%, 0.25%, 0.30%  | 1. mixed in a beaker 2. stirred                                       | w/o                                 | sonicated  | 40 Hz, 3 h, 45 °C  | w/o  |
| Yadav et al. (2017)                 | Magnesium chloride hexahydrate (MCH)<br>T <sub>m</sub> = 115–118 °C                               | Nano-graphite particles (NG)<br>Mass fraction: 0.1%, 0.2%, 0.3%, 0.4%, 0.5%   | w/o   | w/o                                 | ultrasonic bath  | 30 min   | MCH was heated to 130 °C before mixing   |
| Pahamli et al. (2017)               | Paraffin RT50 (RUBITHERM®)<br>T <sub>m</sub> = 51 °C  | Nanoparticles of CuO<br>Mass fraction: 2.0%, 4.0%   | w/o   | w/o                                 | ultrasonic system  | 30–45 min  | Before mixing, PCM was heated tortuously   |
| Dsilva Winfred Rufuss et al. (2018) | Paraffin  | Titanium dioxide (TiO <sub>2</sub> ), graphene oxide (GO), copper oxide (CuO)<br>Mass fraction: 0.3%  | w/o   | w/o                                 | sonication   | 40 kHz, 40 min, 10 °C over the PCM melting point                                     | Surfactant: Sodium dodecylbenzene sulfonate (SDBS) with the mass ratio to nanoparticles of 1:1   |
| Bashar and Siddiqui (2018)          | Paraffin wax (known as Polyfin)<br>T <sub>m</sub> = 55 °C   | Nanoparticles of Al <sub>2</sub> O <sub>3</sub> (20 nm), Ag (30–50 nm), CuO (40 nm) and MWCNT (size from 40 to 60 nm)<br>Mass fraction: 1.0%  | continuously stirred  | 72 h, 65–75 °C                      | w/o  | w/o  | Nanoparticles were mixed with solid PCM pellets. The mixture was heated and melted on a hot plate.   |
| Praveen and Suresh (2018)           | Neopentyl glycol<br>T <sub>m</sub> = 126 °C   | Nanoparticles of CuO; 30–50 nm<br>Mass fraction: 0.5%, 1.0%, 3.0%   | VB Ceramics ball mill (low energy, 0.5HP/230)                         | 200 rpm, 120 min                    | probe type sonicator (Lark Industries, India)                              | 40 kHz, 10 min   | w/o  |
| Jogi Krishna et al. (2017)          | Tricosane<br>T <sub>m</sub> = 47 °C   | Nanoparticles of Al <sub>2</sub> O <sub>3</sub> ; 50 nm<br>Volume fraction: 0.5%, 1.0%, 2.0%  | w/o   | w/o                                 | ultrasonic homogenizer (UP400S)  | 30 min   | w/o  |
| Sharma et al. (2017)                | Paraffin RT42(RUBITHERM®)<br>T <sub>m</sub> = 38–43 °C  | Nanoparticles of CuO; 60 nm<br>Mass fraction: 0.5%  | w/o   | w/o                                 | ultra-sonicator machine (Hilsonic®)  | 24 h   | w/o  |
| He et al. (2019)                    | myristic acid (MA)<br>T <sub>m</sub> = 54–55 °C   | graphene nanoplatelets (GNPs) (3–10 nm), MWCNTs, (<8 nm) with nano-graphite (NG) (<40 nm)<br>Mass fraction: 1%, 2%, 3%  | magnetic stirring   | 30 min                              | ultrasonic vibration   | 1h   | w/o  |

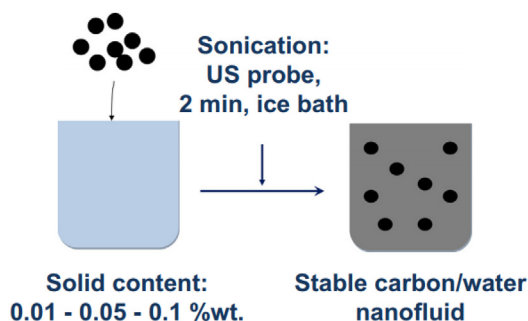
**Table 1** (continued)

| Reference                    | PCM  | Nanomaterial  | Mechanical processing                          | Parameters of mechanical processing | Sonication   | Parameters of sonication | Accentuated details                                |
|------------------------------|--|---|--|-------------------------------------|--|--------------------------|--|
| Temel (2019)                 | Paraffin wax RT 44 (RUBITHERM®)<br>$T_m = 41-44\text{ }^\circ\text{C}$ | Graphene nanoplatelets (GNP); 6–8 nm<br>Mass fraction: 3%, 5%, 7%                 | w/o  | w/o                                 | ultrasonic mixing device (Sonics & Materials INC, USA) | 750 W, 30 min            | w/o  |
| Sivasamy et al. (2019)       | Myristic acid<br>$T_m = 57-59\text{ }^\circ\text{C}$                   | Nanoparticles of Ag; 5.8 nm<br>Mass fraction: 0.1%, 0.2%, 0.3%                    | w/o  | w/o                                 | sonication   | 50 min                   | Surfactant: Sodium dodecylbenzene sulfonate (SDBS) |
| Venkitaraj and Suresh (2019) | pentaerythritol (PE)<br>$T_m = 255-259\text{ }^\circ\text{C}$          | Al <sub>2</sub> O <sub>3</sub> nanoparticles; 40–50 nm<br>Mass fraction: 0.1%, 1% | VB Ceramics ball mill (low energy, 0.5 HP/230) | 200 rpm, 90 min                     | w/o  | w/o                      | w/o  |

**Fig. 7.** Twin-screw micro-compounder (a) and recirculating channel with screws (b), (Chieruzzi et al., 2017).

fractions (from 0.1 wt% to 0.3 wt%). The hydrothermal method was utilized for the synthesis of TiNT and TiNP. The nanofluid mixing was performed with the magnetic stirrer (S22-2m Shanghai Siyue Instrument Company) and after that with the KQ3200DE cleaner (ultrasonic, Kunshan of Jiangsu Equipment) in duration of 30 min. Data on the duration of the process are useful, but it is insufficient for a quality description of the preparation. Much more precise detail is needed to provide enough valuable information for other researchers.

Barreneche et al. (2018) analyzed the impact of various nanoparticle morphologies on the thermal properties of water. A various mass fraction (from 0.01 wt% to 0.1 wt%) of spherical carbon black

**Fig. 8.** Nanofluid preparation procedure, (Barreneche et al., 2018).

nanoparticles (CB) (10 nm), multi-walled carbon nanotubes (MWCNT) (9.5 nm), graphene oxide nanosheets (GO) (2 nm) were added to water and dispersed using an ultrasound probe in an ice bath for a time period of 2 min at low input energy (15%), Fig. 8. The sample size and a defined ultrasound probe device would significantly contribute to the understanding of the process, but the authors did not provide this data explicitly enough.

Liu and Yang (2017) explored the improvement of latent and specific heat regarding the inorganic hydrate salt ( $\text{Na}_2\text{HPO}_4 \cdot 12\text{H}_2\text{O}$  and  $\text{Na}_2\text{CO}_3 \cdot 10\text{H}_2\text{O}$ ; the mass ratio was 60:40) enhanced with titanium nanoparticles ( $\text{TiO}_2\text{-P25}$ ) (21 nm, from 0.1 wt% to 0.5 wt%). The solution enhanced with nanoparticles was stirred for about 2 h at 1500 rpm and after ultrasonicated for 30 min with a power of 120 W. Most of the important data is clearly stated, but the sample size, as well as the devices used, are missing.

Munyalo et al. (2018) deal with the fusion prediction of nanofluid latent heat. The nanofluids were created by adding nanoparticles of MgO (40 nm, from 0.2 wt% to 1.0 wt%) and MWCNT (5–20 nm, from 0.2 wt% to 1.0 wt%) to a 24 wt% aqueous solution of  $\text{BaCl}_2 \cdot 2\text{H}_2\text{O}$ . In order to disperse the nanomaterials, the HJ-6A magnetic stirrer (West Jintan Zhengrong Experiment Equipment Company) was used in duration of 30 min, and then the samples were ultrasonicated in duration of 45 min at temperature of  $50\text{ }^\circ\text{C}$ , with working and stop times of 5 s and 10 s. The stirring rpm and ultrasound frequency are a set of valuable data that are not clearly stated in this paper.

Águila et al. (2018) explored thermal conductivity and viscosity of the nanofluid based on organic octadecane PCM ( $T_m = 28-30\text{ }^\circ\text{C}$ ) and nanoparticles of CuO (75 nm, w/v: 2.5%, 5.0%, 10.0%). The nanofluid was prepared in two steps, firstly, the sample was stirred and after that, it underwent sonotrode MS-3 (ultrasonic horn), with the agitator (Hielscher UP50H) for 1h (amplitude of  $180\text{ }\mu\text{m}$  at  $30\text{ }^\circ\text{C}$ ). The stirring was not well described which is a pity since in this paper the preparation of nanofluid was performed slightly different than in other researches. This potential difference could be better judged if all the key parameters influencing the homogenization of the sample were listed.

Mo et al. (2016) analyzed the subzero thermal energy storage capabilities of an aqueous ethylene glycol solution (12 vol%, 22 vol%, and 34 vol% EG solutions) enhanced with nanoparticles of  $\text{TiO}_2$  (10–40 nm, 0.1 wt%, 0.4 wt%). The homogeneity of the nanofluids was ensured with 5 min of stirring followed by 30 min of ultrasonication (KQ3200DE, Kunshan Ultrasonic Instrument Co., Ltd., China). Homogenization parameters, as in many other papers, are not clearly stated, which is a severe problem for future researches. It is necessary to generously provide all relevant data related to the preparation process because the final properties of the nanofluid directly depend on it.



### 3.4. Summary of nanofluid preparation strategies and discussion on critical aspects

The technology of nanofluid preparation does not differ from the preparation of nanocomposites since there is no clear definition of what is one or the other, i.e. it more or less depends on the possible application claimed by the researchers. Therefore, everything that was previously said about the nanocomposite preparation procedure reporting flaws also applies to the nanofluids. Compared with nanocomposites, one small distinction in the description of nanofluids might be the easiness of providing data about melting temperatures, i.e. it is much harder for authors to provide data about the melting point of solutions since they have to measure it by themselves. The available details on the materials and methodology of nanofluid preparation reported in the considered papers are summarized and presented in Table 2, followed by all important general preparation data.

### 3.5. Categorization and identification of preparation techniques

All preparation techniques aim to achieve a homogeneous sample with good dispersion of nanomaterials in the base fluid or phase change material. There are apparently big differences in preparation techniques, but in the basis, the methodology itself is the same. The preparation of a homogeneous sample is often preceded by some basic preparation of a heterogeneous sample, e.g., melting of the base PCM, synthesis of nanomaterials, preparation of a base fluid solution, addition of a surfactant in a certain ratio with nanomaterials, etc. Thus, the preparation of nanocomposites and nanofluids is a rather broad concept and therefore different interpretations of the beginning of the process can be found in different papers. In a broader sense, preparation begins with the synthesis of nanomaterials and the preparation of a base material (PCM or fluid), since their properties crucially affect the thermophysical characteristics of nanocomposites and nanofluids. Therefore, the process of homogenization, as preparation in the narrow sense, which is common to all reviewed papers, is particularly emphasized in Fig. 9.

The majority of homogenization approaches include mechanical processing accompanied by a sonication procedure, Fig. 9. The different color schemes in Fig. 9 represent possible homogenization approaches observed in the reviewed papers. Based on this flowchart, future researchers can detect unused combinations of mechanical mixing and sonication. For example, the twin-screw micro-compounder was not in any of the reviewed papers combined with sonication, or a ball mill was not combined with an ultrasonic bath. In terms of mechanical processing, magnetic stirring and ball mills are most commonly used. Rotor-stator homogenizers and twin-screw micro compounders are used less frequently. Often, in the reviewed papers the mechanical processing is stated as mechanical mixing but without specifying the device, therefore, in Fig. 9 these cases are classified under undefined stirrer. The sonification is usually performed with an ultrasonic probe device or, more rarely, in an ultrasonic bath. Furthermore, in some cases, only mechanical processing or sonication was used, therefore, w/o abbreviation, meaning "without", was used on the flowchart.

The diversity of approaches is evident, so further researches are needed in this regard. It would be interesting to see the results of a pulsating approach in which mechanical mixing with sonication would be combined multiple times. Furthermore, simultaneous mechanical mixing and sonication could be a good idea.

### 3.6. Main issues related to preparation procedure

The main challenge in the preparation of nanocomposites and nanofluids is how to achieve homogeneous samples that are stable over a longer period. This problem is particularly pronounced for phase-change nanocomposites because in their application there is generally no dynamic component that would provide mixing after initial preparation. Therefore, when the phase change occurs, nanomaterials are released, which if not well dispersed can agglomerate and ultimately sediment at the bottom. For nanofluids, this is less emphasized because they are most commonly used in some sort of recirculation systems (Natividade et al., 2019), and therefore, the homogenous mixing might be achieved easier. Thus, the stability of the sample depends directly on the quality of the initial preparation. A good quality sample with improved properties cannot be expected unless good dispersion without nanoparticle agglomerates is achieved in the initial preparation. One of the simpler methods of preparation is the extended period of intensive mechanical mixing of the initial heterogeneous sample followed by a long high-frequency ultrasonic processing. The primary role of mechanical mixing is to initially homogenize the heterogeneous sample. Globally, mechanical mixing should last until the sample basically ceases to be heterogeneous. At the macro level, the sample is homogenized when the additive particles are uniformly dispersed in PCM. Further researches are needed to clearly define what is considered uniform in this context. Therefore, it cannot be explicitly determined which approach to mechanical mixing is better or worse. However, at the nano level, the sample will contain agglomerates of nanoparticles that must be broken down by ultrasound to ensure relatively well-dispersed nanoparticles and consequently homogeneous NEPCM material. The high frequency of ultrasound can cause the temperature of the sample to rise, which can permanently degrade the properties of the base material, so it is necessary to ensure adequate cooling of the sample during preparation. Choosing the right preparation parameters is a very complex process that requires an individual approach to each sample. The further improvement of sample stability can be achieved by the addition of surfactant before initial preparation, but the question is how this will affect the desired improvement in the thermophysical properties. In this respect, there is a significant research gap that should be addressed more thoroughly in future researches.

## 4. Toxic potential of nanomaterials and brief overview of safety equipment

The major flaw of all the above-considered articles is the fact that none of them reported any safety procedures that were employed to provide a safe working environment for researchers which raises concerns for their health. Without any doubt, nanomaterials can penetrate the human body with respiratory deposition, ingestion, injection and skin penetration, (Wu and Tang, 2017), (Ellenbecker and Tsai, 2015). The researches assessing the toxicity of nanomaterials were not properly followed with the increasing rise in nanomaterial applications. However, the potential toxicity such as inflammation, liver damage, kidney damage, DNA damage, etc. was reported in many researches (Missaoui et al., 2018). The dominant characteristic of nanomaterials is their size which is a source of modified thermophysical properties compared to the bulk materials. Furthermore, the physicochemical characteristics of nanomaterials could be modified compared to the corresponding bulk materials which may result in easier uptake and significantly increased interaction with biological tissues. This may lead to



**Table 2**  
Nanofluid preparation technology with respect to type of nanomaterials and type of PCM.

| Reference                | PCM/fluid   | Nanomaterial   | Mechanical processing   | Parameters of mechanical processing                     | Sonication   | Parameters of sonication                                    | Accentuated details   |
|--------------------------|---|--|---|---|--|---|---|
| Altohamy et al. (2015)   | Water   | Nanoparticles of gammaalumina ( $\gamma - \text{Al}_2\text{O}_3$ ); 50 nm<br>Volume fraction: 0.5%, 1.0%, 1.5%, 2.0%   | w/o   | w/o   | ultra-sonication   | 90 min, 30 °C   | w/o   |
| Chieruzzi et al. (2017)  | Salt mixture-nitrate (concentration 60 wt% $\text{NaNO}_3$ with 40 wt% $\text{KNO}_3$ )<br>$T_m = 220$ °C   | Nanoparticles of $\text{SiO}_2$ (7 nm), $\text{Al}_2\text{O}_3$ (13 nm), $\text{SiO}_2/\text{Al}_2\text{O}_3$ (2–200 nm) Mass fraction: 1.0%   | DSM Xplore micro-compounder (twin screw, 2005 Geleen)               | 100 rpm (duration 15 min) and 200 rpm (duration 30 min) | w/o  | w/o   | The salt mixture was prepared by melting.   |
| Wang et al. (2017)       | OP10E ( $T_m = 8-10$ °C) and water emulsion   | Graphite nanoparticles; <30 nm<br>Mass fraction: 0.25%, 0.5%, 1.0%, 2.0%, 4%   | rotor-stator homogenizer  | 8000 rpm, 3 min, 25 °C                                  | w/o  | w/o   | Initially OP10E/water emulsion was prepared   |
| Attia et al. (2016)      | Water   | Nanoparticles of gammaalumina ( $\gamma - \text{Al}_2\text{O}_3$ ); 50 nm<br>Volume fraction: 0.25%, 0.5%, 0.75%, 1.0%   | w/o   | w/o   | ultra-sonication   | 90 min in an EG bath, 30 °C                                 | w/o   |
| Shao et al. (2017)       | Deionized water   | $\text{TiO}_2$ nanotubes (TiNTs); 9–10 nm<br>$\text{TiO}_2$ nanoplatelets (TiNPs); 50–80 nm<br>Hybrid nanofluids (with TiNT and TiNP) various TiNP ratios (from 0% to 100%) with also constant or various overall $\text{TiO}_2$ mass fractions (0.1%–0.3%). | magnetic stirrer (S22–2 Shanghai Siyue Instrument Company)          | w/o   | KQ3200DE cleaner-ultrasonic, (Kunshan of Jiangsu Equipment)  | 30 min  | Synthesis of TiNTs and TiNPs with hydrothermal method   |
| Barreneche et al. (2018) | Water   | Spherical carbon black nanoparticles, CB (10 nm), Multi-walled carbon nanotubes, MWCNT (9.5 nm), Graphene oxide nanosheets, GO (2 nm)<br>Mass fraction: 0.01%, 0.05%, 0.1%   | w/o   | w/o   | sonication (ultrasound probe)                                | input low energy (15%), with ice bath for 2 min             | Initially, CB and MWCNT were oxidized during magnetic stirring with hydrogen peroxide at 120 °C |
| Liu and Yang (2017)      | Disodium hydrogen phosphate dodecahydrate ( $\text{Na}_2\text{HPO}_4 \cdot 12\text{H}_2\text{O}$ , purity > 99%) with sodium carbonate (decahydrate) ( $\text{Na}_2\text{CO}_3 \cdot 10\text{H}_2\text{O}$ , AR); The mass ratio is 60:40 | $\text{TiO}_2$ -P25 nanoparticles, with 80% of anatase and 20% of the rutile; 21 nm<br>Mass fraction: 0.1%, 0.3%, 0.5%   | stirred   | 1500 rpm, 2 h   | ultrasonicated   | 120 W, 30 min   | The solution was prepared before mixing with nanoparticles                                      |
| Munyalo et al. (2018)    | $\text{BaCl}_2 \cdot 2\text{H}_2\text{O}$ (dissolvment in the deionized water). Final product is aqueous solution with 24 wt% $\text{BaCl}_2 \cdot 2\text{H}_2\text{O}$ .   | A) Nanoparticles of $\text{MgO}$ ; 40 nm<br>Mass fraction: 0.2%, 0.4%, 0.6%, 0.8%, 1.0%<br>B) Multi-walled carbon nanotubes (MWCNT); 5–20 nm<br>Mass fraction: 0.2%, 0.4%, 0.6%, 0.8%, 1.0%  | HJ-6A magnetic stirrer (West Jintan Zhengrong Experiment Equipment) | 30 min  | ultrasonicated   | 45 min, 50 °C, operation time (5 s) and brake period (10 s) | w/o   |
| Águila et al. (2018)     | Octadecane (organic PCM)<br>$T_m = 28-30$ °C  | Nanoparticles of $\text{CuO}$ ; 75 nm w/v: 2.5%, 5.0%, 10.0%   | w/ stirred  | w/o   | horn (ultrasonic, sonotrode MS-3, agitator)                  | amplitude of 180 $\mu\text{m}$ , 1 h, 30 °C                 | Preparation of nanoparticles before mixing with PCM   |
| Mo et al. (2016)         | Aqueous ethylene glycol solution (12, 22, and 34 vol% EG solutions)   | Nanoparticles of $\text{TiO}_2$ ; 10–40 nm<br>Mass fraction: 0.1%, 0.4%  | stirred   | 5 min   | ultrasonicated with KQ3200DE (Kunshan Ultrasonic Instrument) | 30 min  | w/o   |

oxidative stress, pulmonary inflammation, and distal organ involvement, (Nel et al., 2006).

The issues emphasized in the previously mentioned researches impose the importance of protective actions in order to achieve the safe manufacturing and handling of nanomaterials. The authors of the investigation (Nel et al., 2006) call for a proactive approach in regulatory and safety evaluations of nanomaterials, while in (Wu and Tang, 2017) it is suggested that proactive actions should start from workers exposed to nanomaterials, i.e. the necessity of rigorous planning of personal protective equipment (PPE).

Respiratory protection should be an indispensable part of PPE.

The elastomeric half-mask respirators (EHRs) with filtering face-piece respirators (FFRs) are commonly used for protection against nanoparticles, (Vo et al., 2015). In the USA, the performance criteria are defined by the National Institute for Occupational Safety and Health (NIOSH) (NIOSH-Approved Respirators, 2020) while for EU it is defined by the European Norm (EN) (European standards for respiratory protection, 2020). The effectiveness of the commonly used respirators was tested in several reported researches with the best performances associated with P100 and FFP3 filters, (Vo et al., 2015), (Shaffer and Rengasamy, 2009), (Rengasamy et al., 2009). The paper (Vo et al., 2015) deals with the effectiveness of respirators

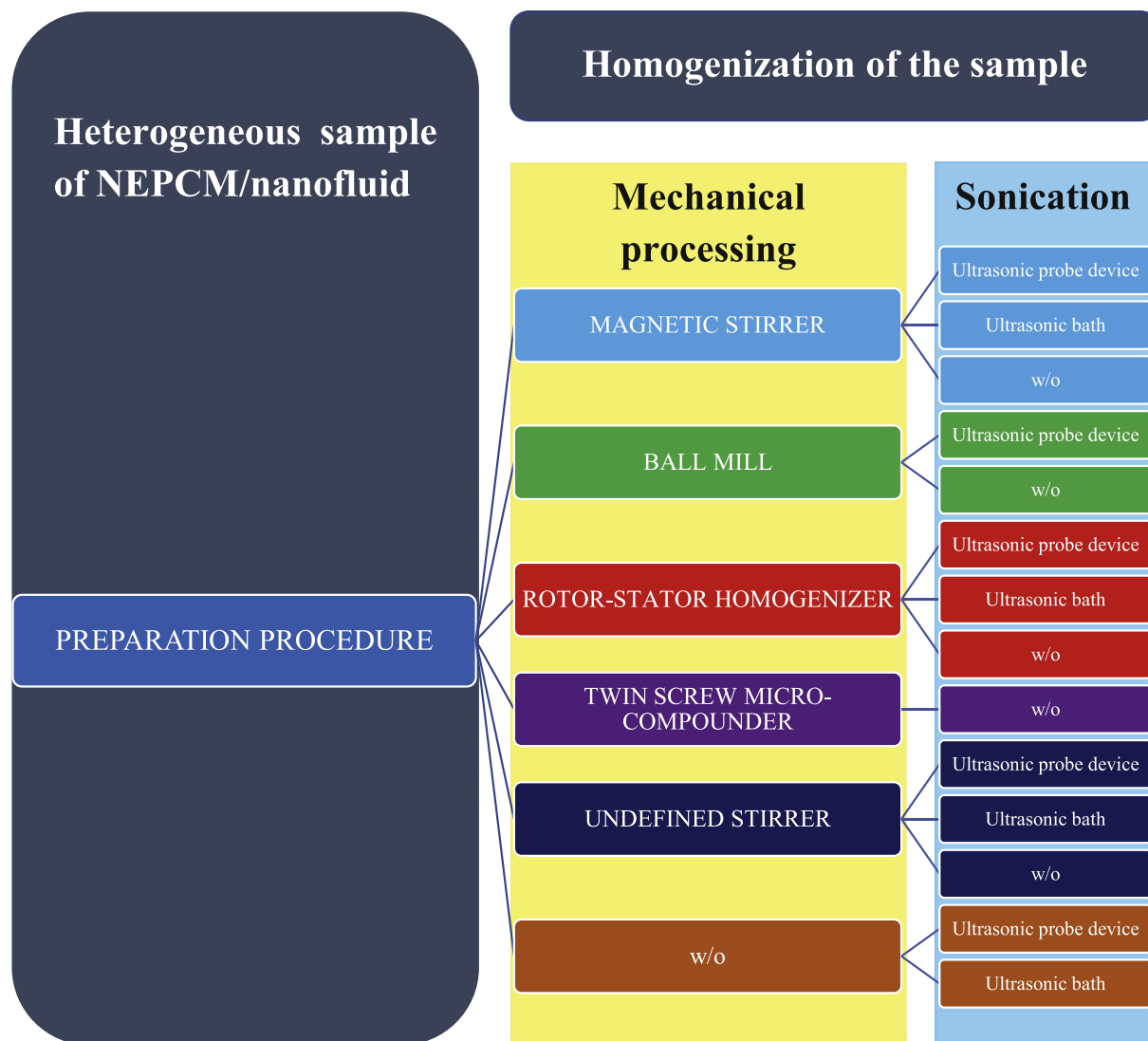


Fig. 9. Flowchart of preparation procedures and techniques.

against nanoparticles in simulated work activities, and in the paper (Shaffer and Rengasamy, 2009) a review of respiratory protection regarding airborne nanoparticles was made. In the paper (Rengasamy et al., 2009) filtration capabilities of facepiece respirators approved by NIOSH were explored.

Research (Vinches et al., 2013) proved that nanoparticles can penetrate some types of protective clothing and gloves; therefore, it is suggested to replace disposable gloves more frequently, while laboratory coats should not be reused or used for too long.

Nanomaterial safety data sheets (SDS) should be mandatorily updated more frequently in accordance with recent discoveries without any administrative delay. The SDS must be followed by workers and researchers dealing with nanomaterials.

When handling nanomaterials in laboratories, there are a few methods and devices used such as glove bags, glove boxes, Powder Weighing Stations and fume hoods. The glove bag is a cheap and robust solution, but the big issue is the lack of working space, while glove boxes and Powder Weighing Stations are more expensive solutions. Powder Weighing Stations are good solutions if they have a HEPA filter or some other filtration system that removes particles from the air stream. Filtered air can be ducted out of the laboratory

or can be recirculated. Fume hoods are usually used as equipment, but they are not the best, for reducing particle exposure in laboratories. In the past few years, researches assessing the capabilities of conventional fume hoods to control worker exposure during laboratory handling of nanomaterials are emerging. Fonseca et al. (2018) investigated worker exposure to nanomaterials while handling nanomaterials in fume hoods. They simulated the spills of nanomaterials and inhalation exposure during normal handling and synthesis of TiO<sub>2</sub>, ZnO and CuO nanoparticles. It was reported that a fully functional fume hood with an appropriate sash height (from 0.3 to 0.5 m) and face velocity (0.1–0.4 ms<sup>-1</sup>) can prevent 98.3% of released particles. During normal handling, packaging, and synthesis of the considered nanoparticles, the authors did not detect nanoparticle release in the laboratory air. The spill incidents are associated in rare cases with usually nanoparticles escaping the fume hood.

Future researches dealing with nanomaterials should start with a health risk assessment for researchers and other working staff. In addition to that, safe work practices should be enforced in accordance with norms and recent scientific discoveries.

## 5. Conclusions with discussion on future directions in field

This review paper has analyzed, discussed and examined preparation techniques mainly focused on nanofluids and nanocomposites. It is important to address that only papers directly or indirectly involved in the preparation of nanocomposites, or nanofluids and containing experimental investigations were considered. Preparation procedures are demanding and very sensitive with a strong impact on the result, i.e. prepared sample. Based on the carefully conducted review of the existing research findings, further conclusions and observations can be highlighted:

- In most of the research studies, the preparation approach was not adequately reported. Usually, specific data related to the preparation process is omitted such as, the exact quantity of used materials (both base material and nanomaterial), the thermophysical properties of the base material and nanomaterials, which are particularly important because the parameters of preparation depend directly on them,
- A general preparation procedure can be divided into the mechanical processing of a sample that is later followed by sonication (most of the preparation approaches are done in that manner). These processes, in the reviewed papers, are very poorly described and often lack information such as the number of revolutions of a stirrer, sonication frequency, duration, sample temperature, the exact model of used devices, etc.,
- The initial preparation is essential to achieve the expected improvements in thermophysical properties. A prerequisite for improvement is a homogeneous sample with well-dispersed nanoparticles in the base material,
- The quality of the preparation process strongly affects the thermophysical properties of the nano-enhanced materials as well as their long-term stability,
- The main issues related to the preparation procedure are agglomeration and sedimentation, i.e. proper and efficient dispersion of the nanomaterials with the proper size, nano-size respectively. The preparation needs to be carefully and properly obtained to avoid the previously mentioned unfavorable effects since they can reduce or nullify the desired positive effects of adding nanomaterials.
- An important aspect of proper preparation is the selection of appropriate parameters to annul the agglomeration of the nanoparticles and ultimately sedimentation. The addition of surfactants is important in that sense, i.e. to enable the more efficient homogenization of the sample and to reduce surface tension between incompatible substances,
- The selection of the specific mixing parameters (mechanical mixing and sonication) are also key features to enable quality samples. Particularly noteworthy is the duration and frequency of sonication, which is crucial in achieving a homogeneous sample while avoiding the permanent degradation of the properties of the base material due to increased temperature,
- Future research studies should be far more informative regarding the preparation process and the parameters used. It is necessary to provide all known information with respect to the thermophysical features of the base materials as well as the exact amount used in the sample preparation. Furthermore, information on the nanomaterials used, such as morphology, size, and quantity, should also be provided. When it comes to the amount of nanoparticles in the base material, a mass fraction is a much better choice than volume fraction because it is not temperature-dependent, so future researches should strive for such a description,
- The step further should be directed to the investigations of the unused combinations of mechanical mixing and sonication

since there are rather different possible mixing approaches. In that sense systematization would be a crucial one to avoid discrepancy in preparation strategies, i.e. to ensure consistency.

- The pulsating approach should be further investigated as a sequential combination of mechanical processing and sonication. Moreover, simultaneous mechanical mixing and sonication should be also analyzed in future research works.
- The pretreatment (basic preparation) should be also classified and systematized to detect other specific influential parameters that can affect repeatability and quality.
- Medical research has undoubtedly confirmed the toxicity of some nanomaterials, so any future research dealing with nanomaterials should start with a health risk assessment for researchers and other working staff. Nanomaterials should be handled with extreme caution, in accordance with the latest safety standards and recent scientific discoveries. This paper provided basic guidance on the safety aspect of working with nanomaterials during the preparation of nanocomposites and nanofluids. However, general standards (guidelines) should be prepared and implemented for all beneficiaries that deal with nanomaterials to enable minimal protection conditions,
- When working with nanomaterials, it is necessary to use personal protective equipment (PPE) in accordance with safety data sheets (SDS), with respiratory protection being indispensable. Respirators with P100 and FFP3 filters have proved to be the best so far, but it is important to note that new researches are being carried out continuously, so it is advisable to keep up with them in order to find the right solution,
- When it comes to protecting lab space from contamination, there are several solutions such as glove bags, glove boxes, Powder Weighing Stations and fume hoods. Each has some advantages and disadvantages, but most often protects the lab space well, however, environmental protection is a different story. Namely, glove bags and classic fume hoods do not have nanoparticle filtration systems, so they are a poor solution in this respect. Glove boxes and Powder Weighing Stations with a good filtration system can provide adequate protection regarding laboratory space and external environment but this comes at a higher cost.

### CRedit authorship contribution statement

**Mišo Jurčević:** Conceptualization, Methodology, Formal analysis, Software, Visualization, Writing - original draft. **Sandro Nizetić:** Conceptualization, Methodology, Formal analysis, Writing - original draft, Supervision, Writing - review & editing. **Müslüm Arıcı:** Formal analysis, Writing - original draft, Supervision, Writing - review & editing. **Paweł Ocioń:** Formal analysis, Writing - original draft, Supervision, Writing - review & editing.

### Declaration of competing interest

We wish to confirm that there are no known conflicts of interest associated with this publication in Renewable & Sustainable Energy Reviews Journal (**Comprehensive analysis of preparation strategies for phase change nanocomposites and nanofluids with brief overview of safety equipment**) and there has been no significant financial support for this work that could have influenced its outcome.

### Acknowledgments

This work was funded by the Croatian science foundation (Research project: Smart and hybrid cooling techniques for

siliceous photovoltaic panels-IP-01-2018-2814, Croatia).

## References

- Afzal, A., Khan, S.A., Ahamed Saleel, C., 2019. Role of ultrasonication duration and surfactant on characteristics of ZnO and CuO nanofluids. *Mater. Res. Express* 6 (11), 1150d8. <https://doi.org/10.1088/2053-1591/ab5013>.
- Águila, V.B., Vasco, D.A., Galvez, P.P., Zapata, P.A., 2018. Effect of temperature and CuO nanoparticle concentration on the thermal conductivity and viscosity of an organic phase change material. *Int. J. Heat Mass Tran.* 120, 1009–1019. <https://doi.org/10.1016/j.ijheatmasstransfer.2017.12.106>.
- Alimohammadi, M., Aghli, Y., Alavi, E.S., Sardarabadi, M., Passandideh-Fard, M., 2017. Experimental investigation of the effects of using nano/phase change materials (NPCM) as coolant of electronic chipsets, under free and forced convection. *Appl. Therm. Eng.* 111, 271–279. <https://doi.org/10.1016/j.applthermaleng.2016.09.028>.
- Altohamy, A.A., Abd Rabbo, M.F., Sakr, R.Y., Attia, A.A.A., 2015. Effect of water based Al<sub>2</sub>O<sub>3</sub> nanoparticle PCM on cool storage performance. *Appl. Therm. Eng.* 84, 331–338. <https://doi.org/10.1016/j.applthermaleng.2015.03.066>.
- Arci, M., Bilgin, F., Nižetić, S., Karabay, H., 2020. PCM integrated to external building walls: an optimization study on maximum activation of latent heat. *Appl. Therm. Eng.* 165, 114560. <https://doi.org/10.1016/j.applthermaleng.2019.114560>.
- Asadi, A., Aberoumand, S., Moradikazerouni, A., Pourfattah, F., Żyła, G., Estellé, P., Mahian, O., Wongwises, S., Nguyen, H.M., Arabkoohsar, A., 2019c. Recent advances in preparation methods and thermophysical properties of oil-based nanofluids: a state-of-the-art review. *Powder Technol.* 352, 209–226. <https://doi.org/10.1016/j.powtec.2019.04.054>.
- Asadi, A., Alarifi, I.M., Ali, V., Nguyen, H.M., 2019b. An experimental investigation on the effects of ultrasonication time on stability and thermal conductivity of MWCNT-water nanofluid: finding the optimum ultrasonication time. *Ultrason. Sonochem.* 58, 104639. <https://doi.org/10.1016/j.ultsonch.2019.104639>.
- Asadi, A., Pourfattah, F., Miklós Szilágyi, I., Afrand, M., Żyła, G., Seon Ahn, H., Wongwises, S., Minh Nguyen, H., Arabkoohsar, A., Mahian, O., 2019a. Effect of sonication characteristics on stability, thermophysical properties, and heat transfer of nanofluids: a comprehensive review. *Ultrason. Sonochem.* 58, 104701. <https://doi.org/10.1016/j.ultsonch.2019.104701>.
- Attia, A.A.A., Altohamy, A.A., Abd Rabbo, M.F., Sakr, R.Y., 2016. Comparative study on Al<sub>2</sub>O<sub>3</sub> nanoparticle addition on cool storage system performance. *Appl. Therm. Eng.* 94, 449–457. <https://doi.org/10.1016/j.applthermaleng.2015.10.142>.
- Babapoor, A., Karimi, G., 2015. Thermal properties measurement and heat storage analysis of paraffinnanoparticles composites phase change material: comparison and optimization. *Appl. Therm. Eng.* 90, 945–951. <https://doi.org/10.1016/j.applthermaleng.2015.07.083>.
- Babapoor, A., Karimi, G., Sabbaghi, S., 2016. Thermal characteristic of nano-composite phase change materials during solidification process. *Journal of Energy Storage* 7, 74–81. <https://doi.org/10.1016/j.est.2016.05.006>.
- Bahiraie, F., Fartaj, A., Nazri, G.-A., 2017. Experimental and numerical investigation on the performance of carbon-based nanoenhanced phase change materials for thermal management applications. *Energy Convers. Manag.* 153, 115–128. <https://doi.org/10.1016/j.enconman.2017.09.065>.
- Bahiraie, M., Heshmatian, S., 2019. Graphene family nanofluids: a critical review and future research directions. *Energy Convers. Manag.* 196, 1222–1256. <https://doi.org/10.1016/j.enconman.2019.06.076>.
- Barreneche, C., Mondragon, R., Ventura-Espinosa, D., Mata, J., Cabeza, L.F., Fernández, A.I., Enrique Julia, J., 2018. Influence of nanoparticle morphology and its dispersion ability regarding thermal properties of water used as phase change material. *Appl. Therm. Eng.* 128, 121–126. <https://doi.org/10.1016/j.applthermaleng.2017.09.014>.
- Bashar, M., Siddiqui, K., 2018. Experimental investigation of transient melting and heat transfer behavior of nanoparticle-enriched PCM in a rectangular enclosure. *Journal of Energy Storage* 18, 485–497. <https://doi.org/10.1016/j.est.2018.06.006>.
- Betancur, S., Giraldo, L.J., Carrasco-Marín, F., Riazi, M., Manrique, E.J., Quintero, H., García, H.A., Franco-Ariza, C.A., Cortés, F.B., 2019. Importance of the nanofluid preparation for ultra-low interfacial tension in enhanced oil recovery based on surfactant-nanoparticle-brine system interaction. *ACS Omega* Open Access 4 (14), 16171–16180. <https://doi.org/10.1021/acsomega.9b02372>.
- Bhagyaraj, S.M., Oluwafemi, O.S., Kalarikkal, N., Thomas, S., 2018. Applications of Nanomaterials, Advances and Key Technologies, first ed., p. 490
- Chaichan, M.T., Kazem, H.A., 2018. Single slope solar distillator productivity improvement using phase change material and Al<sub>2</sub>O<sub>3</sub> nanoparticle. *Sol. Energy* 164, 370–381. <https://doi.org/10.1016/j.solener.2018.02.049>.
- Chieruzzi, M., Cerritelli, G.F., Miliuzzi, A., Kenny, J.M., Torre, L., 2017. Heat capacity of nanofluids for solar energy storage produced by dispersing oxide nanoparticles in nitrate salt mixture directly at high temperature. *Sol. Energy Mater. Sol. Cell.* 167, 60–69. <https://doi.org/10.1016/j.solmat.2017.04.011>.
- Choudhary, S., Sachdeva, A., Kumar, P., 2020. Investigation of the stability of MgO nanofluid and its effect on the thermal performance of flat plate solar collector. *Renew. Energy* 147, 1801–1814. <https://doi.org/10.1016/j.renene.2019.09.126>.
- Colla, L., Fedele, L., Mancin, S., Danza, L., Manca, O., 2017. Nano-PCMs for enhanced energy storage and passive cooling applications. *Appl. Therm. Eng.* 110, 584–589. <https://doi.org/10.1016/j.applthermaleng.2016.03.161>.
- Devendiran, D.K., Valan Arasu, A., 2016. A review on preparation, characterization, properties and applications of nanofluids. *Renew. Sustain. Energy Rev.* 60, 21–40. <https://doi.org/10.1016/j.rser.2016.01.055>.
- Dsilva Winfred Rufuss, D., Suganthi, L., Iniyan, S., Davies, P.A., 2018. Effects of nanoparticle enhanced phase change material (NPCM) on solar still productivity. *J. Clean. Prod.* 192, 9–29. <https://doi.org/10.1016/j.jclepro.2018.04.201>.
- Ebadi, S., Humaira Tasnim, S., Abbas Aliabadi, A., Mahmud, S., 2018. Geometry and nanoparticle loading effects on the bio-based nano-PCM filled cylindrical thermal energy storage system. *Appl. Therm. Eng.* 141, 724–740. <https://doi.org/10.1016/j.applthermaleng.2018.05.091>.
- Ellenbecker, M.J., Tsai, C.S.-J., 2015. Exposure Assessment and Safety Considerations for Working with Engineered Nanoparticles. John Wiley & Sons, Inc. <https://doi.org/10.1002/9781118998694>.
- European standards for respiratory protection. [https://sg.vwr.com/cms/industrial\\_safety\\_european\\_standards\\_for\\_respiratory\\_protection](https://sg.vwr.com/cms/industrial_safety_european_standards_for_respiratory_protection) accessed 26 May 2020.
- Fonseca, A.S., Kuijpers, E., Kling, K.I., Levin, M., Koivisto, A.J., Nielsen, S.H., Fransman, W., Fedutik, Y., Jensen, K.A., Koponen, I.K., 2018. Particle release and control of worker exposure during laboratory-scale synthesis, handling and simulated spills of manufactured nanomaterials in fume hoods. *J. Nanoparticle Res.* 20, 48. <https://doi.org/10.1007/s11051-018-4136-3>.
- Hári, J., Pukánszky, B., 2011. 8 - Nanocomposites: Preparation, Structure, and Properties. *Applied Plastics Engineering Handbook*, pp. 109–142.
- Harikrishnan, S., Imran Hussain, S., Devaraju, A., Sivasamy, P., Kalaiselvam, S., 2017. Improved performance of a newly prepared nano-enhanced phase change material for solar energy storage. *J. Mech. Sci. Technol.* 31 (10), 4903–4910. <https://doi.org/10.1007/s12206-017-0938-y>.
- Harish, S., Orejon, D., Takata, Y., Kohno, M., 2015. Thermal conductivity enhancement of lauric acid phase change nanocomposite with graphene nanoplatelets. *Appl. Therm. Eng.* 80, 205–211. <https://doi.org/10.1016/j.applthermaleng.2015.01.056>.
- He, M., Yang, L., Lin, W., Chen, J., Mao, X., Ma, Z., 2019. Preparation, thermal characterization and examination of phase change materials (PCMs) enhanced by carbon-based nanoparticles for solar thermal energy storage. *Journal of Energy Storage* 25, 100874. <https://doi.org/10.1016/j.est.2019.100874>.
- Krishna, Jogi, Kishore, P.S., Brusly Solomon, A., 2017. Heat pipe with nano enhanced-PCM for electronic cooling application. *Exp. Therm. Fluid Sci.* 81, 84–92. <https://doi.org/10.1016/j.expthermflusci.2016.10.014>.
- Karimi, G., Azizi, M., Babapoor, A., 2016. Experimental study of a cylindrical lithium ion battery thermal management using phase change material composites. *Journal of Energy Storage* 8, 168–174. <https://doi.org/10.1016/j.est.2016.08.005>.
- Khan, A.I., Valan Arasu, A., 2019. A review of influence of nanoparticle synthesis and geometrical parameters on thermophysical properties and stability of nanofluids. *Thermal Science and Engineering Progress* 11, 334–364. <https://doi.org/10.1016/j.tsep.2019.04.010>.
- Kumar, A., Subudhi, S., 2019. Preparation, characterization and heat transfer analysis of nanofluids used for engine cooling. *Appl. Therm. Eng.* 160, 114092. <https://doi.org/10.1016/j.applthermaleng.2019.114092>.
- Lin, S.C., Al-Kayiem, H.H., 2016. Evaluation of copper nanoparticles - paraffin wax compositions for solar thermal energy storage. *Sol. Energy* 132, 267–278. <https://doi.org/10.1016/j.solener.2016.03.004>.
- Liu, Y., Yang, Y., 2017. Investigation of specific heat and latent heat enhancement in hydrate salt based TiO<sub>2</sub> nanofluid phase change material. *Appl. Therm. Eng.* 124, 533–538. <https://doi.org/10.1016/j.applthermaleng.2017.05.150>.
- Missaoui, W.N., Arnold, R.D., Cummings, B.S., 2018. Toxicological status of nanoparticles: what we know and what we don't know. *Chem. Biol. Interact.* 295, 1–12. <https://doi.org/10.1016/j.cbi.2018.07.015>.
- Mo, S., Zhu, K., Yin, T., Chen, Y., Cheng, Z., 2016. Phase change characteristics of ethylene glycol solution-based nanofluids for subzero thermal energy storage. *Int. J. Energy Res.* 41, 81–91. <https://doi.org/10.1002/er.3599>.
- Motahar, S., Alemrajabi, A.A., Khodabandeh, R., 2017. Experimental study on solidification process of a phase change material containing TiO<sub>2</sub> nanoparticles for thermal energy storage. *Energy Convers. Manag.* 138, 162–170. <https://doi.org/10.1016/j.enconman.2017.01.051>.
- Munyalo, J.M., Zhang, X., Li, Y., Chen, Y., Xu, X., 2018. Latent heat of fusion prediction for nanofluid based phase change material. *Appl. Therm. Eng.* 130, 1590–1597. <https://doi.org/10.1016/j.applthermaleng.2017.11.101>.
- Nada, S.A., El-Nagar, D.H., Hussein, H.M.S., 2018. Improving the thermal regulation and efficiency enhancement of PCM-Integrated PV modules using nano particles. *Energy Convers. Manag.* 166, 735–743. <https://doi.org/10.1016/j.enconman.2018.04.035>.
- Natividade, P.S.G., de Moraes Moura, G., Avallone, E., Bandarra Filho, E.P., Gelamo, R.V., Gonçalves, J.C.D.S.I., 2019. Experimental analysis applied to an evacuated tube solar collector equipped with parabolic concentrator using multilayer graphene-based nanofluids. *Renew. Energy* 138, 152–160. <https://doi.org/10.1016/j.renene.2019.01.091>.
- Nel, A., Xia, T., Mädlar, L., Li, N., 2006. Toxic potential of materials at the nanolevel. *Science* 311, 622–627. <https://doi.org/10.1126/science.1114397>.
- Niosh-Approved Respirators. The national personal protective technology laboratory (NPPTL). [https://www.cdc.gov/niosh/npptl/topics/respirators/disp\\_part/respsource1quest2.html#classified](https://www.cdc.gov/niosh/npptl/topics/respirators/disp_part/respsource1quest2.html#classified) accessed 26 May 2020.
- Nižetić, S., Arici, M., Bilgin, F., Grubišić-Cabo, F., 2018. Investigation of pork fat as potential novel phase change material for passive cooling applications in photovoltaics. *J. Clean. Prod.* 170, 1006–1016. <https://doi.org/10.1016/j.jclepro.2017.09.164>.
- Nižetić, S., Jurčević, M., Arici, M., Valan Arasu, A., Xie, G., 2020. Nano-enhanced phase change materials and fluids in energy applications: a review. *Renew. Sustain. Energy Rev.* 129, 109931. <https://doi.org/10.1016/j.rser.2020.109931>.
- Nourani, M., Hamdami, N., Keramat, J., Moheb, A., Shahedi, M., 2016. Thermal behavior of paraffinnano-Al<sub>2</sub>O<sub>3</sub> stabilized by sodium stearoyl lactylate as a

- stable phase change material with high thermal conductivity. *Renew. Energy* 88, 474–482. <https://doi.org/10.1016/j.renene.2015.11.043>.
- Pahamli, Y., Hosseini, M.J., Ranjbar, A.A., Bahrampoury, R., 2017. Effect of nanoparticle dispersion and inclination angle on melting of PCM in a shell and tube heat exchanger. *Journal of the Taiwan Institute of Chemical Engineers* 81, 316–334. <https://doi.org/10.1016/j.jtice.2017.09.044>.
- Praveen, B., Suresh, S., 2018. Experimental study on heat transfer performance of neopentyl glycol/CuO composite solid-solid PCM in TES based heat sink. *Engineering Science and Technology, an International Journal* 21, 1086–1094. <https://doi.org/10.1016/j.jestch.2018.07.010>.
- Putra, N., Amin, M., Kosasih, E.A., Luanto, R.A., Abdullah, N.A., 2017. Characterization of the thermal stability of RT 22 HC/graphene using a thermal cycle method based on thermoelectric methods. *Appl. Therm. Eng.* 124, 62–70. <https://doi.org/10.1016/j.applthermaleng.2017.06.009>.
- Rengasamy, S., Eimer, B.C., Shaffer, R.E., 2009. Comparison of nanoparticle filtration performance of NIOSH-approved and CE-marked particulate filtering facepiece respirators. *Ann. Occup. Hyg.* 53, 117–128. <https://doi.org/10.1093/annhyg/men086>.
- Salyan, S., Suresh, S., 2018. Study of thermo-physical properties and cycling stability of DMannitol-copper oxide nanocomposites as phase change materials. *Journal of Energy Storage* 15, 245–255. <https://doi.org/10.1016/j.est.2017.10.013>.
- Sami, S., Etesami, N., 2017. Improving thermal characteristics and stability of phase change material containing TiO<sub>2</sub> nanoparticles after thermal cycles for energy storage. *Appl. Therm. Eng.* 124, 346–352. <https://doi.org/10.1016/j.applthermaleng.2017.06.023>.
- Scopus database. <https://www.scopus.com/search/form.uri?display=basic> accessed 11 December 2019.
- Shaffer, R.E., Rengasamy, S., 2009. Respiratory protection against airborne nanoparticles: a review. *J. Nanoparticle Res.* 11, 1661–1672. <https://doi.org/10.1007/s11051-009-9649-3>.
- Shao, X.-F., Mo, S.-P., Chen, Y., Yin, T., Yang, Z., Jia, L.-S., Cheng, Z.-D., 2017. Solidification behavior of hybrid TiO<sub>2</sub> nanofluids containing nanotubes and nanoplatelets for cold thermal energy storage. *Appl. Therm. Eng.* 117, 427–436. <https://doi.org/10.1016/j.applthermaleng.2017.02.045>.
- Sharma, R.K., Ganesan, P., Tyagi, V.V., Metselaar, H.S.C., Sandaran, S.C., 2016. Thermal properties and heat storage analysis of palmitic acid-TiO<sub>2</sub> composite as nano-enhanced organic phase change material (NEOPCM). *Appl. Therm. Eng.* 99, 1254–1262. <https://doi.org/10.1016/j.applthermaleng.2016.01.130>.
- Sharma, S., Micheli, L., Chang, W., Tahir, A.A., Reddy, K.S., Mallick, T.K., 2017. Nano-enhanced phase change material for thermal management of BICPV. *Appl. Energy* 208, 719–733. <https://doi.org/10.1016/j.apenergy.2017.09.076>.
- Singh, D.K., Suresh, S., Singh, H., Rose, B.A.J., Tassou, S., Anantharaman, N., 2017. Myo-inositol based nano-PCM for solar thermal energy storage. *Appl. Therm. Eng.* 110, 564–572. <https://doi.org/10.1016/j.applthermaleng.2016.08.202>.
- Sivasamy, P., Harikrishnan, S., Imran Hussain, S., Kalaiselvam, S., Ganesh Babu, L., 2019. Improved thermal characteristics of Ag nanoparticles dispersed myristic acid as composite for low temperature thermal energy storage. *Mater. Res. Express* 6, 085066. <https://doi.org/10.1088/2053-1591/ab20ba>.
- Stuttgen, V., Giffney, H.E., Anandan, A., Alabdali, A., Twarog, C., Belhout, S.A., O'Loughlin, M., Podhorska, L., Delaney, C., Geoghegan, N., McFadden, J., Alhadhrami, N.A., Fleming, A., Phadke, S., Yadav, R., Fattah, S., McCartney, F., Alsharif, S.A., McCaul, J., Singh, K., Erikandath, S., O'Meara, F., Wychowanec, J.K., Cutrona, M.B., MacMaster, G., Reynolds, A.L., Gaines, S., Hogg, B., Farrelly, M., D'Alton, M., Coulahan, P., Bhattacharjee, S., 2019. The UCD nanosafety workshop (03 December 2018): towards developing a consensus on safe handling of nanomaterials within the Irish university labs and beyond—a report. *Nanotoxicology* 13 (6), 717–732. <https://doi.org/10.1080/17435390.2019.1621402>.
- Temel, U.N., 2019. Passive thermal management of a simulated battery pack at different climate conditions. *Appl. Therm. Eng.* 158, 113796. <https://doi.org/10.1016/j.applthermaleng.2019.113796>.
- Totzauer, P., Kudelcik, J., Hornak, J., Michal, O., Trnka, P., Mentlik, V., 2019. Analysis of particle size distribution and other parameters of nanoparticles in natural ester oil. *Proceedings - IEEE International Conference on Dielectric Liquids* 8796658. <https://doi.org/10.1109/ICDL.2019.8796658>.
- Triques, C.C., Fagundes-Klen, M.R., Suzuki, P.Y.R., Mateus, G.A.P., Wernke, G., Bergamasco, R., Rodrigues, M.L.F., 2020. Influence evaluation of the functionalization of magnetic nanoparticles with a natural extract coagulant in the primary treatment of a dairy cleaning-in-place wastewater. *J. Clean. Prod.* 243, 118634. <https://doi.org/10.1016/j.jclepro.2019.118634>.
- Venkataraj, K.P., Suresh, S., 2019. Experimental thermal degradation analysis of pentaerythritol with alumina nano additives for thermal energy storage application. *Journal of Energy Storage* 22, 8–16. <https://doi.org/10.1016/j.est.2019.01.017>.
- Vinches, L., Testori, N., Dolez, P., Perron, G., Wilkinson, K.J., Hallé, S., 2013. Experimental evaluation of the penetration of TiO<sub>2</sub> nanoparticles through protective clothing and gloves under conditions simulating occupational use. *Nanoscience Methods* 2, 1–15. <https://doi.org/10.1080/21642311.2013.771840>.
- Vo, E., Zhuang, Z., Horvatin, M., Liu, Y., He, X., Rengasamy, S., 2015. Respirator performance against nanoparticles under simulated workplace activities. *Ann. Occup. Hyg.* 59 (8), 1012–1021. <https://doi.org/10.1093/annhyg/mev042>.
- Wang, F., Liu, J., Fang, X., Zhang, Z., 2016. Graphite nanoparticles-dispersed paraffin/water emulsion with enhanced thermal-physical property and photo-thermal performance. *Sol. Energy Mater. Sol. Cell.* 147, 101–107. <https://doi.org/10.1016/j.solmat.2015.12.013>.
- Wang, F., Zhang, C., Liu, J., Fang, X., Zhang, Z., 2017. Highly stable graphite nanoparticle-dispersed phase change emulsions with little supercooling and high thermal conductivity for cold energy storage. *Appl. Energy* 188, 97–106. <https://doi.org/10.1016/j.apenergy.2016.11.122>.
- Wang, Q., Wei, W., Li, D., Qi, H., Wang, F., Arici, M., 2019. Experimental investigation of thermal radiative properties of Al<sub>2</sub>O<sub>3</sub>-paraffin nanofluid. *Sol. Energy* 177, 420–426. <https://doi.org/10.1016/j.solener.2018.11.034>.
- Warzoha, R.J., Weigand, R.M., Fleischer, A.S., 2015. Temperature-dependent thermal properties of a paraffin phase change material embedded with herringbone style graphite nanofibers. *Appl. Energy* 137, 716–725. <https://doi.org/10.1016/j.apenergy.2014.03.091>.
- Wei, X., Yin, Y., Qin, B., Wang, W., Ding, J., Lu, J., 2020. Preparation and enhanced thermal conductivity of molten salt nanofluids with nearly unaltered viscosity. *Renew. Energy* 145, 2435–2444. <https://doi.org/10.1016/j.renene.2019.04.153>.
- Wilson John, M.R., Singh, A.K., Singh, A.K., Ganapathy Subramanian, L.R., 2017. Waste heat recovery from diesel engine using custom designed heat exchanger and thermal storage system with nanoenhanced phase change material. *Therm. Sci.* 21, 715–727. <https://doi.org/10.2298/TSCI160426264W>.
- Wu, T., Tang, M., 2017. Review of the effects of manufactured nanoparticles on mammalian target organs. *J. Appl. Toxicol.* 38, 25–40. <https://doi.org/10.1002/jat.3499>.
- Yadav, A., Barman, B., Kardam, A., Narayanan, S.S., Verma, A., Jain, V.K., 2017. Thermal properties of nano-graphite-embedded magnesium chloride hexahydrate phase change composites. *Energy Environ.* 28 (7), 651. <https://doi.org/10.1177/0958305X17721475>.



## Appendix C

Title: Thermal constant analysis of phase change nanocomposites and discussion on selection strategies with respect to economic constraints

Authors: Jurčević M., Nižetić S., Arici M., Hoang A.T., Giama E., Papadopoulos A.

Publisher: *Elsevier*

Journal: *Sustainable Energy Technologies and Assessments*

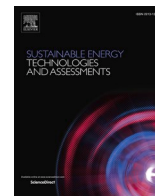
Edition, ID, year: 43, 100957, 2021.

Indexed in: Scopus, Science Citation Index Expanded, INSPEC

Journal Impact Factor: 7.632 Q1 (WoS and SJR-2021.)

DOI: <https://doi.org/10.1016/j.seta.2020.100957>

**Abstract:** This paper reports an experimental investigation focused on nano-enhanced phase change materials (NEPCM). Two different types of phase change materials (RT28 HC and RT26) with relatively low thermal conductivity and reasonable volumetric specific heat capacity were utilized as the base for NEPCMs with four types of nanoparticles (CuO, ZnO, Ag, and graphene). The novel four-phase preparation procedure was thoroughly presented together with a description of the measurement technology which was used for the examination of NEPCM thermal constants. The experimental results revealed that in most cases the thermal constants of samples were improved, such as thermal conductivity and volumetric specific heat capacity in a range of about 4% to 21% and 5% to 33%, respectively. In some cases, significant degradation of certain thermal constants was detected, such as in the case of the Graphene/RT26 nanocomposite. The possible nanomaterial selection strategies also discussed taking into account the economic aspects and experimental results related to the thermal constants. The results revealed that the selection of nanomaterials should be carefully considered with respect to the specific application since it is possible to manipulate the thermo-physical properties of the NEPCM as a unique combination of nanomaterial and PCM.



## Thermal constant analysis of phase change nanocomposites and discussion on selection strategies with respect to economic constraints

Mišo Jurčević<sup>a</sup>, Sandro Nizetić<sup>a,\*</sup>, Müslüm Arıcı<sup>b</sup>, A. Hoang Anh Tuan<sup>c</sup>, Effrosyni Giama<sup>d</sup>, Agis Papadopoulos<sup>d</sup>

<sup>a</sup> LTEF- Laboratory for Thermodynamics and Energy Efficiency, Faculty of Electrical Engineering, Mechanical Engineering and Naval Architecture, University of Split, Rudjera Boškovića 32, 21000 Split, Croatia

<sup>b</sup> Department of Mechanical Engineering, Faculty of Engineering, Kocaeli University, Umuttepe Campus, Kocaeli 41001, Turkey

<sup>c</sup> Ho Chi Minh City University of Technology, Hồ Chí Minh, Viet Nam

<sup>d</sup> Process Equipment Design Laboratory, Department of Mechanical Engineering, Aristotle University of Thessaloniki, Postal Address: GR-54124, Thessaloniki, Greece

### ARTICLE INFO

#### Keywords:

Nanocomposites  
Thermal properties  
Experimental analysis  
NEPCM  
Selection strategies  
Economic constraints

### ABSTRACT

This paper reports an experimental investigation focused on nano-enhanced phase change materials (NEPCM). Two different types of phase change materials (RT28 HC and RT26) with relatively low thermal conductivity and reasonable volumetric specific heat capacity were utilized as the base for NEPCMs with four types of nanoparticles (CuO, ZnO, Ag, and graphene). The novel four-phase preparation procedure was thoroughly presented together with a description of the measurement technology which was used for the examination of NEPCM thermal constants. The experimental results revealed that in most cases the thermal constants of samples were improved, such as thermal conductivity and volumetric specific heat capacity in a range of about 4% to 21% and 5% to 33%, respectively. In some cases, significant degradation of certain thermal constants was detected, such as in the case of the Graphene/RT26 nanocomposite. The possible nanomaterial selection strategies also discussed taking into account the economic aspects and experimental results related to the thermal constants. The results revealed that the selection of nanomaterials should be carefully considered with respect to the specific application since it is possible to manipulate the thermo-physical properties of the NEPCM as a unique combination of nanomaterial and PCM.

### Introduction

The implementation of nanomaterials has become attractive since recent research findings have demonstrated significant potential in the technological progress of various daily applications [1]. Engineering applications are one of the most challenging nanomaterial implementation fields, especially in an energy-related area [2]. Current research efforts are directed at the investigation of various nanomaterials in the formation of nanocomposites to suit various applications. The particular interest of the research community is focused on nano-enhanced phase change materials (NEPCM) [3], towards an improvement of the general thermal properties. Namely, PCMs are interesting as suitable thermal energy storage materials with a wide application potential [4]. On the other hand, the addition of nanomaterials allows for new possibilities in the further improvement of thermal characteristics via NEPCM configurations. The main current

issue with PCM materials is the relatively high unit cost as well as demanding thermal management of the PCM layer in specific technical applications. The addition of nanomaterials could contribute to a more efficient thermal regulation of the PCM layer. Different nanomaterials have been investigated in recent years, i.e. specific combinations with base materials in order to check their behavior and thermal properties [5]. Targeted manipulation of different PCMs mixed with various nanoparticles can produce combinations where it is possible to set targeted thermal properties of the NEPCM. Preparation procedures for nano-enhanced systems are very important; they require proper equipment, knowledge, and adherence to safety standards [6]. The preparation process has a strong impact on the thermal properties, stability, and quality of the sample, thus preparation procedures should be strictly defined and followed in order to secure quality and repeatability. Since the focus of this work is directed and limited to nano-enhanced PCMs, i.e. to phase change nanocomposites, the latest research findings will be

\* Corresponding author.

E-mail address: [snizetic@fesb.hr](mailto:snizetic@fesb.hr) (S. Nizetić).

<https://doi.org/10.1016/j.seta.2020.100957>

Received 12 August 2020; Received in revised form 10 November 2020; Accepted 2 December 2020

2213-1388/© 2020 Elsevier Ltd. All rights reserved.

briefly discussed in the upcoming sections of the paper.

Lignin-fatty acid hybrid nanocapsules were considered [7] for the case of thermal storage applications. Hybrid nanocapsules were produced from lignin nanoparticles and fatty acid (40 wt%) as PCMs. The produced nanocapsules were exposed to a cyclic investigation (290 heating-cooling cycles). The results showed that the produced capsules improved heat transfer characteristics which make them suitable for possible thermal energy storage applications. Hybrid nanocomposites as a combination of cement mortar and copper-titanic ( $\text{Cu-TiO}_2$ ) nanoparticles were investigated in study [8]. The main goal was to produce a building construction material with improved thermal properties. Based on the experimental data, an improvement of thermal conductivity was noted with a good thermal storage potential (190–195 J/g) during the phase change. The combination of disintegrated bacterial cellulose nanofibers mixed with graphene and a PCM (paraffin) was investigated in study [9]. The PCM was exposed to a special chemical treatment to form a foam-like structure. The addition of graphene improved the stability of the produced foams and improved energy storage capacity. However, thermal conductivity was reduced, thus the produced hybrid structure turned out to be a thermal insulator, which allows for different potential applications in engineering. The stability of  $\text{TiO}_2$ -Ag nanocomposites was investigated in [10] with paraffin as the base PCM. The main goal was to raise the efficiency of solar thermal systems. However, the preparation process involved a preparation with and without surfactants to explore their impact on the sample. A suitable nanoparticle mass concentration as well as a specific type of surfactant was found. The addition of the surfactant secured a uniform dispersion of the nanoparticles and improved stability as well as the thermal properties, which made the investigated combination suitable for energy storage materials regarding solar thermal applications. Three different types of  $\text{Al}_2\text{O}_3$  nanocomposites were analyzed in [11] for a thermal energy storage application with paraffin wax as the base PCM. An improvement in thermal energy storage was detected and an economic evaluation was conducted in order to confirm the economic effectiveness. The economic evaluation showed that a cost-benefit option would be a 1 wt% nanocomposite of  $\text{Al}_2\text{O}_3$  nanoparticles. Simulations on molecular dynamics were reported in study [12] where a nanocomposite made of graphene was considered (maximal concentration of 7.0 wt%) and a PCM (paraffin). The microscopic distribution and structure of the components were visualized, which influence the mechanical and thermal properties under various temperatures. The provided work enabled a better understanding of complex interactions on a molecular level that includes molecular and phonon transport. A novel inorganic nanomaterial (MXene) was used with paraffin wax in order to investigate the thermal properties of the produced nanocomposite [13]. The experimental results indicated an improvement in all thermal constants (heat capacity and thermal conductivity). Maximal improvement in specific heat capacity was found to be 43% with 0.3 wt% of MXene, while the highest increase in thermal conductivity was found in the amount of 16% at 0.3 wt% of MXene in the selected PCM. The proposed nanocomposite was found to be suitable for energy storage. The fabrication of a PCM nanocomposite was addressed in [14] where n-heptadecane was considered as the PCM with added  $\text{SiO}_2$  nanoparticles. The produced nanocomposite showed exceptional cycling reliability together with an improvement in thermal conductivity. The main application of the investigated nanocomposite would be in energy storage applications for building facilities. A specific design and construction of mesoporous silica/n-ecoisane PCM nanocomposites were discussed in [15]. The main objective of the work was to produce a more advanced nano-encapsulated PCM in order to improve thermal performance when compared to the existing, i.e. traditional nano-encapsulated PCM. The results showed excellent thermal performance, good thermal storage capability, and reasonable phase-change reliability. The produced novel nano-encapsulated PCM showed shorter heat-charging time, however, longer heat discharging time. Suitable applications would be in cases of fast temperature regulation purposes, i.e. in cases of precise thermal

management. High-performance PCM composites were investigated in study [16] where graphite sheets and nano-platelets were added into the paraffin wax as the base PCM. The experimental results revealed high thermal conductivity and efficient phase change behavior. The produced nanocomposite could be suitable for thermal energy harvesting applications. A carbon nanomaterial was added into carbonate salts (PCM) to investigate the effect of a nanomaterial addition on behavior and heat storage characteristics [17]. The addition of a carbon nanomaterial enabled improvement in thermal conductivity as well as heat storage capacity. However, in some cases, the heat storage capacity was decreased due to an increased melting temperature, as a direct consequence of the nanomaterial addition. Novel nanocomposites, made of pentadecane (PCM) and two nanomaterials (diatomite and sepiolite), were elaborated in study [18]. The melting temperature and latent heat capacity were detected for the proposed nanocomposites. Thermal stability, reliability, and thermal conductivity were investigated, and the results directed that both proposed composites have a reasonable potential for thermal storage applications. The thermal behavior of the polyethylene glycol PCM with added carbon nanotubes was investigated in study [19]. The addition of carbon nanotubes slightly decreased the melting temperature as well as latent heat. Excellent form stability was achieved, and the conducted tests showed that the thermal storage properties had improved. Thermal energy storage capabilities and thermal characteristics of acetamide enhanced with nanographite (NG) were investigated in [20]. An improvement in thermal conductivity was observed without significant variation in the melting point. The nanocomposite with 0.4 wt% of nanographite had a noteworthy 48% shorter melting time and 47% shorter solidification time. The phase change properties of Sorbitol-Au nanocomposites were elaborated in study [21]. Special attention was given to the examination of crystallization processes and their impact on the formation of different crystal phases. The addition of gold nanoparticles (0.002 wt%) causes a minor increase in thermal conductivity and heat capacity. However, there is a significant increase in the latent heat of the sorbitol, i.e. in some cases with a factor of 2.0. The addition of gold has a potentially strong impact on the thermal conductivity of the base PCM. Wei et al. [22] examined paraffin-based nanocomposites enhanced with copper nanoparticles (CN) and multi-walled carbon nanotubes (MWCNT). When compared to pure paraffin CN-paraffin nanocomposite with 1 wt% of copper nanoparticles had a thermal conductivity improvement of 22.3% while MWCNT-paraffin nanocomposite with 1 wt% MWCNT had an 18.9% improvement. Hybrid CN-MWCNT-paraffin nanocomposite had lower thermal conductivity than pure paraffin. In this case, a more significant tendency to agglomeration and sedimentation was observed. The phenomenon of thermal conductivity reduction is not sufficiently elaborated, but it is undoubtedly detected. An experimental, as well as numerical, investigation of paraffin wax-carbon nanocomposites, was reported in work [23]. Three types of carbon-based nanomaterials were investigated in order to check thermal properties. The investigation directed improvement in thermal conductivity but with decreased heat transfer rate in the liquid phase, caused by the presence of nanomaterials. It was also found that the addition of the nano-additives can improve heat conduction in the solid phase with minor detected degradation of latent heat. The main finding of the work is the detected direct interaction between a thermal conductivity improvement and an increase in the viscosity which degrades the natural convection, which could be used for the optimization of nanocomposites.

When taking recent researches into account, a few important observations could be noted and briefly addressed, Table 1.

In the majority of recent research works, paraffin was used as the base PCM, which is mainly due to the general flexibility related to the preparation of NEPCM, i.e. it easily melts by simple heating. Furthermore, the selection of nanomaterials is quite scattered where it is clear that the main focus is to investigate the different combinations of nanomaterials as much as possible and their effect on the base PCMs. The majority of studies are usually focused on one specific nanomaterial



**Table 1**

Overview of recent works related to PCM nanocomposites.

| Ref. | Type of used PCM    | Applied nanomaterial                 | Economic evaluation | Environmental evaluation | Special remark                                 |
|------|---------------------|--------------------------------------|---------------------|--------------------------|--|
| [7]  | fatty acid          | Lignin                               | Non                 | Non                      | Cyclic evaluation, improved heat transfer      |
| [8]  | cement mortar       | Coper-Titania                        | Non                 | Non                      | Improved thermal conductivity                  |
| [9]  | Parraffin           | cellulose nanofibers, graphene oxide | Non                 | Non                      | PCM produced in form of foam                   |
| [10] | Parraffin           | Titania-silver                       | Non                 | Non                      | Improved stability, cyclic evaluation          |
| [11] | Parraffin           | Alumina oxide                        | Yes                 | Non                      | Increase in absorbed thermal energy            |
| [12] | Parraffin           | Graphene                             | Non                 | Non                      | Numerical investigation                        |
| [13] | Parraffin           | MXene nanoparticles                  | Non                 | Non                      | Improvement in thermal constants               |
| [14] | n-heptadecane       | Silicon dioxide                      | Non                 | Non                      | Detected efficient thermal cycling reliability |
| [15] | n-eicosane          | Silica                               | Non                 | Non                      | Suitable for precise thermal management        |
| [16] | Parraffin           | graphite nanoplatelets               | Non                 | Non                      | High thermal conductivity                      |
| [17] | carbonate salts     | carbon                               | Non                 | Non                      | More intense variation of melting temperature  |
| [18] | pentadecane         | diatomite, sepiolite                 | Non                 | Non                      | Thermal stability investigated                 |
| [19] | polyethylene glycol | carbon                               | Non                 | Non                      | Improved form-stability                        |
| [21] | D-sorbitol          | gold                                 | Non                 | Non                      | High increase in thermal conductivity          |
| [23] | Parraffin           | carbon                               | Non                 | Non                      | Various carbon-based nanomaterials             |

as well as the base material, i.e. it is hard to find studies that investigated several different nanomaterials by comparing them. There is also a major research gap in the lack of analysis related to the economic or environmental evaluation of the specific nanocomposites in the given circumstances. Only one of the above-addressed studies discussed economic aspects and detected a cost-benefit case, [11] (even in that study, costs for a more demanding preparation procedure were not discussed since an increased quantity of nanoparticles requires a more demanding and expensive preparation procedure).

The main objective of this work was to experimentally investigate the thermal constants of several nanocomposites made of four different nanomaterials with two base PCM materials. The study of several nanomaterials in the herein conducted experimental work provides a useful basis for a comparison and difference analysis between the applied nanomaterials as well as base PCMs. Most of the other researches focus on a single PCM combined with a certain type of nanomaterial while in this paper eight nanocomposites were prepared similarly by embracing uniform methodology. The insights into possible strategies and niches of applications can be gained by examining the impact of diverse nanomaterials, in terms of type, size, morphology, and ultimately cost, on selected PCMs. In this context, a vast variety of types, sizes, morphologies, and numerous mass fractions of nanomaterials can be used to design nanocomposites with a respect to specific applications. Special notice was also devoted to the elaboration of the preparation procedure as well as a specific measurement technique with a novel safety approach. Finally, the added value of the work is the conducted analysis of nanomaterial selection strategies with respect to economic constraints, which is a useful novelty of the work.

## Experimental approach

### Selected materials

In order to form eight nanocomposites, appropriate PCM materials, and four various types of nanomaterials were procured. Commercially available RT28 HC and RT26 organic PCM materials were supplied from Rubitherm® Technologies GmbH, Berlin, Germany [24]. The aforementioned materials were selected for their organic origin, chemical inertness, long life and suitable thermo-physical properties, primarily, latent heat and relatively narrow melting point range. According to the manufacturer's technical datasheet [24], the RT28 HC has a melting/congealing area in a range of 27–29 °C with the RT26 range being 25–26 °C. Furthermore, the RT26 has a slightly higher maximal operation temperature (60 °C) when compared to RT28 HC (50 °C).

Nano-powders of copper (II) oxide (CuO), zinc (II) oxide (ZnO) and silver (Ag), as well as graphene nanoplatelets, were procured from IoLiTec GmbH, Heilbronn, Germany [25], Table 2. These nanomaterials were chosen because of their different price range, morphology, and

**Table 2**

Size and purity of selected nanomaterials.

| Material type          | Size      | Purity |
|------------------------|-----------|--------|
| Copper(II)oxide powder | 40–80 nm  | 99.9%  |
| Zinc(II)oxide powder   | 90–210 nm | 99.9%  |
| Silver powder          | 35 nm     | 99.5%  |
| Graphene platelets     | 11–15 nm  | 99.5%  |

size. Furthermore, for these nanomaterials, and in particular Ag and graphene, a significant research gap was observed in the context of nanocomposites based on organic PCM materials.

### Safety procedures and used equipment

Nanomaterials undoubtedly have a toxic potential [26], so it is necessary to protect researchers and other staff from unnecessary exposure. There are several ways in which nanomaterials can penetrate the human body, e.g. the respiratory system, skin, ingestion, or injection [27,28]. Therefore, in the experimental part of the research, the safety of researchers was proactively approached, taking into account the protection of the environment. Based on the health risk assessment and safe work practices with regard to standards and recent scientific discoveries, protective equipment and procedures were defined [6].

Adequate personal protective equipment (PPE) is the first line of defense against nanomaterials. In this regard, an elastomeric half-mask (3 M™ 6000 series) with a filtering face-piece respirator (FFP3 filters) was used to protect the respiratory system. Laboratory goggles were used to protect the eyes, while double nitrile gloves, a 3 M™ 4510 series protective suit, and disposable coats were used to protect the skin.

The weighing and preparation of nanomaterials were performed in a LABCONCO XPert Nano Enclosure powder weighing station to protect the laboratory space from aerosols, Fig. 1.

Furthermore, this device has a ULPA filter that ensures the nanoparticles do not escape into the environment. It is important to mention that the powder nanoparticles used in the study were at no time exposed to open air outside the powder weighing station. The prepared NEPCM samples were sealed in special two-layer PA/PE (Polyamide/Polyethylene) bags, which provide additional protection against secondary exposure to nanoparticles, Fig. 2.

### NEPCM preparation methodology

In total, eight samples of nanocomposites were prepared, with four samples based on RT28 HC and the other four samples based on RT26 organic PCMs. In order to form different NEPCMs, 0.5 wt% of CuO, ZnO, Ag and graphene nanoparticles were added to base the PCM samples. Nanoparticles, in this context, have a negative tendency to agglomerate,



Fig. 1. LABCONCO XPert Nano Enclosure powder weighing station.



Fig. 2. Example of Graphene/RT28 HC sample in two-layer PA/PE bags.

which can be avoided with proper preparation. Furthermore, higher concentrations of nanoparticles complicate the preparation and increase the possibility of agglomeration [6]. Higher nanomaterial concentrations of 0.5 wt% can frequently be found in the literature [2], but this complicates and prolongs the preparation process. Also, given the relatively large number of nanomaterials (CuO, ZnO, Ag, graphene) and two PCMs (RT26 and RT28 HC), a concentration of 0.5 wt% was chosen as a representative and conservative approach for parallel comparison. The key problem was how to produce a homogenous nanocomposite sample with well-dispersed nanomaterials while evading agglomeration. Therefore, the preparation of nanocomposites prior to thermal constant

measurements was carried out through four phases.

In phase 1, heterogeneous nanocomposite samples were produced by adding 0.5 wt% of nanoparticles in the base PCM. A quantity of 400 g of CuO/RT26 nanocomposite was prepared by weighing 398 g of melted RT26 PCM and 2 g (0.5 wt%) of CuO nanoparticles on a precision balance after which the nanoparticles were added to the molten PCM. The weighing was performed with a KERN EW620-3NM precision balance inside the LABCONCO XPert Nano Enclosure at ca. 0.3 m/s face velocity to avoid the possible aerosolization of nanoparticles and protect the operator from possible contamination. The same procedure was repeated for other nanocomposites. In phase 2, the samples were homogenized to break down the nanoparticle agglomerates and ensure an efficient dispersion. A Hielscher UP400St probe device was used to homogenize the NEPCM samples, Fig. 3. For all the samples, homogenization with ultrasound lasted 30 min with a power of 400 W and with an ultrasound amplitude of about 30%. Ultrasonic homogenization causes heat generation within the sample, leading to an increase in the sample temperature. If the sample temperature exceeds the maximum operation temperature of 50 °C for the RT28 HC and 60 °C for the RT26, there is a possibility of permanent PCM property degradation as already highlighted in section 2.1. Due to the previous reason, it is necessary to ensure the cooling of the sample during ultrasonic homogenization. Therefore, during homogenization, the samples were cooled in a thermostatic bath in order to regulate temperatures Fig. 3.

During homogenization with ultrasound, the thermostatic water bath was set at 33 °C. A specific temperature was selected as a conservative approach to ensure for the PCM to completely melt. Furthermore, during the half-hour ultrasound treatment, the water bath temperature and the sample temperature were monitored so that the latter did not exceed the maximum operation temperature of the base PCM. As can be seen in Fig. 4, the temperature of all NEPCMs did not exceed the maximum operation temperature of 50 °C/60 °C.

In phase 3, the ultrasonically homogenized samples were further mixed with a Heidolph RZR 2021 mechanical mixer at 390 rpm, Fig. 5. During the mechanical stirring, 200 ml of each sample was taken from the vessel and injected into special two-layer PA/PE bags, i.e. a 200 ml sample was injected into two bags, each containing 100 ml of the sample. The previous process was repeated for all eight NEPCM samples. For comparability, but without mixing or homogenization, the molten base PCMs were also injected into the bags in the same volumes.

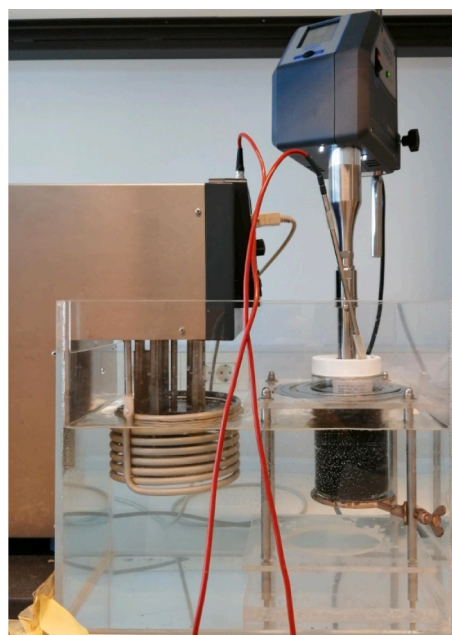


Fig. 3. Sample during ultrasound homogenization in thermostatic water bath.

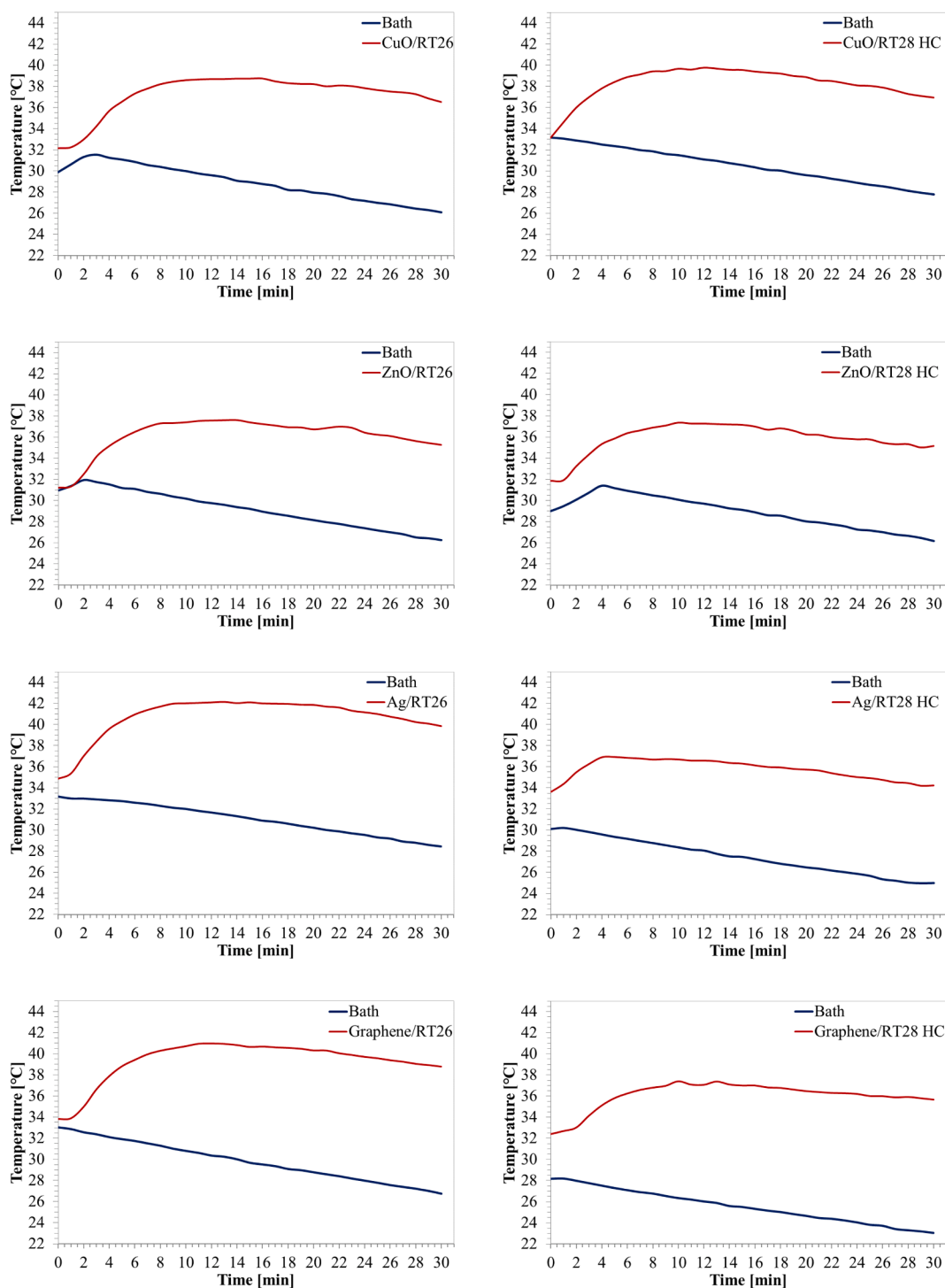


Fig. 4. Temperatures of cooling water bath and NEPCMs during ultrasonic homogenization.

In phase 4, PA/PE bags were sealed to ensure operator safety and prepare samples for the measurement of thermal constants, Fig. 2. Furthermore, the bags were inserted between two vertical surfaces to give a flat surface along the wall of the bag during solidification. The samples prepared in this way were suitable for the measurement of thermal constants with a thermal analyzer.

#### Thermal constant measurement methodology

There are several methods for the measurement of thermal constants that can generally be divided into steady-state methods and non-steady-

state methods. In this work, one of the non-steady-state methods, namely the Transient Plane Source (TPS) technique was used for measuring the thermal constants of the NEPCMs. The TPS technique is a widespread method, which was developed by Gustafson [29], for the measurement of thermal properties regarding specific materials. The TPS method relies on the sensor that generates constant heat that diffuses into the sample. The mean temperature of the sensor increases over time depending on the heating power, the radius of the sensor, the number of sensor concentric rings and the thermal properties of the sample material, [30]. By measuring the temperature function of the sensor, thermal conductivity and thermal diffusivity can be estimated. In





Fig. 5. Mechanical stirring of NEPCM.

real circumstances, the samples are not infinite or ideal, thus Gustaffson [29] suggested that due to the insulation layer on the sensor, the first few seconds of measurement should be ignored. Similarly, measurements can also be made through PA/PE bags which may be considered as an additional insulation layer on the sensor. The previous approach represents the novelty in the context of analyzing the thermal properties of potentially toxic materials.

Bohač et al. [31] improved the accuracy of the method by calculating the optimal time period for measurement using coefficient sensitivity analysis and difference analysis. In this research work [32], thermal contact A and time correction  $t_c$  parameters were included which helped to describe the necessary period for the heating of the sensor. All these efforts led to the publication of an international standard for the TPS method in 2008 [33].

The measurements for this work were performed with a Hot Disk TPS 500 S device (Thermtest Inc.) Fig. 6. This device operates on the principles of the TPS technique similar to ISO 22007-2 standard [34]. This Hot Disk thermal properties analyzer uses a sensor in the form of a double spiral.

The Hot Disk Sensor is both a heat source and a resistance thermometer that measures temperature rise over time. The sensor is usually about 10  $\mu\text{m}$  thick with a double nickel spiral. The helix is protected with a layer of polyimide called Kapton which can be used in a temperature range of  $-269\text{ }^\circ\text{C}$  to  $400\text{ }^\circ\text{C}$ , [35]. Using different sensors, it is possible to

measure the thermal conductivity of a material in a range of 0.005 W/mK to 1800 W/mK. Hot Disk Thermal Constants Analyzer 7.4 Beta 24 software was used to measure and process data.

To avoid phase transition, all samples were subcooled and measurements were made at  $12\text{ }^\circ\text{C}$ . A Kapton sensor 5465 was used at relatively low output power (30 mW) due to the low expected thermal conductivity of measured materials. It is very important to set adequate heating power so that the sensor does not overheat and to avoid permanent damage of the sensor. The measurement parameters were iteratively tuned using Hot Disk Thermal Constants Analyzer 7.4 Beta 24 software, taking care that the heating power of the sensor was relatively small so that the sensor would not be damaged as a result of an overheat. The heat probing depth was monitored using the abovementioned software and kept between borders of material with low heating power, and measurement time. The measurement parameters and details are summarized in Table 3.

#### Uncertainty analysis

Measurements on standard materials ranging from polystyrene to aluminum show that the accuracy over the entire thermal conductivity range is within  $\pm 5\%$  and the reproducibility is within  $\pm 2\%$  for Hot Disk TPS500 S [34,36]. To determine the general accuracy of the measurement and its influence on the temperature measurement, the uncertainty of measurements was calculated based on the Eq. (1), [37]. The temperature measurement ring included the T-type thermocouples coupled with PICO TC-08 data logger, [38]. According to [39] declared uncertainty for T-type thermocouples is  $\pm 0.5\text{ }^\circ\text{C}$  ( $\Delta U_t$ ) while for the PICO TC-08 data logger it equals  $\pm 0.5\text{ }^\circ\text{C}$  ( $\Delta U_{tc}$ ).

$$\Delta U = \pm \sqrt{\Delta U_t^2 + \Delta U_{tc}^2} \quad (1)$$

When the aforementioned input data are taken into account, the overall uncertainty of the temperature measurement is  $\pm 0.71\text{ }^\circ\text{C}$ .

## Results and discussion

#### Thermal conductivity of nanocomposites

Thermal conductivity is a very important parameter in the context of phase change materials. Namely, the rate of heat storage and release directly depend on this property. Therefore, the thermal conductivity of

Table 3  
Measurement parameters.

| Sensor type              | Kapton 5465 (3.189 mm radius) |
|--------------------------|-------------------------------|
| Heating power            | 30 mW                         |
| Measurement time         | 40 s                          |
| Sample temperature       | $12\text{ }^\circ\text{C}$    |
| Minimum sample thickness | 10 mm                         |

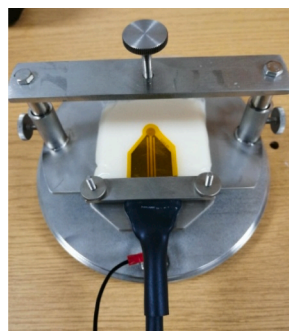


Fig. 6. Hot Disk TPS 500 S and sample holder with sensor.

the base PCMs was initially tested. Specific and noticeable deviations were observed in relation to the data from the manufacturer's datasheet. In particular, according to the manufacturer's datasheet, the thermal conductivity of the RT26 and RT28 HC organic PCMs is 0.2 W/mK. Measurements showed a thermal conductivity of 0.233 W/mK in the case of pure RT26 and 0.362 W/mK in the case of pure RT28 HC. In the case of the RT26 PCM, the deviation was within reasonable limits but in the case of the RT28 HC PCM, the deviation was as much as 44.7%. The previous leads to the conclusion that the data provided in the manufacturer's datasheet can only be used for orientation purposes, and even this is questionable given the difference in the measured data from the datasheet.

The results of the thermal conductivity measurements regarding the prepared nanocomposites are generally in line with expectations with the exception of Graphene/RT26 nanocomposite. Specifically, unlike the others, Graphene/RT26 nanocomposite had a slightly lower thermal conductivity than the basic RT26 PCM, Fig. 7. A possible cause could be the still unexplored interaction of graphene with the RT26 PCM at a molecular level. Of all the RT26-based nanocomposites, the CuO/RT26 had the highest thermal conductivity, followed by the ZnO/RT26 and Ag/RT26. To conclude, by adding 0.5 wt% of CuO, ZnO, and Ag nanoparticles in the RT26, the thermal conductivity increased by 21.3, 18.6, and 12.3% while with the addition of graphene, the thermal conductivity decreased by 4.6%.

All the RT28 HC-based nanocomposites had an increase in thermal conductivity compared to the pure RT28 HC, Fig. 8. In the case of Graphene/RT28 HC, the increase in thermal conductivity was 14.3% while in the other NEPCMs, the improvements were significantly lower, i.e. 5.1, 5.3, and 3.9% for the CuO/RT28 HC, ZnO/RT28 HC and Ag/RT28 HC.

Rare studies deal with the same nanomaterials and PCMs but in principle, it is possible to compare the results with the same nanomaterials and different PCMs. For example, in the case of nanocomposites with CuO nanoparticles, the improvement in thermal conductivity is consistent with previous studies such as [40], where the addition of 1 wt% of CuO nanoparticles to coconut oil caused an increase in thermal conductivity of about 7.5%. Moreover, in study [41] the addition of 0.3 wt% of CuO nanoparticles to paraffin caused 28.8% higher thermal conductivity. Graphene nanoplatelets in terms of thermal conductivity did not produce results at the level of work [42] where the addition of 0.3 wt% of graphene nanoplatelets in an RT22 HC PCM caused an increase of as much as 89.6%. In the specific case of ZnO nanoparticles, it is possible to achieve a higher improvement in thermal conductivity with a raised mass fraction of nanoparticles in paraffin, i.e. the addition of 2 wt% of ZnO nanoparticles to paraffin increased thermal conductivity for about 30% [43]. Ag nanoparticles are somewhat less well investigated in other researches, so a possible comparison would be unreliable.

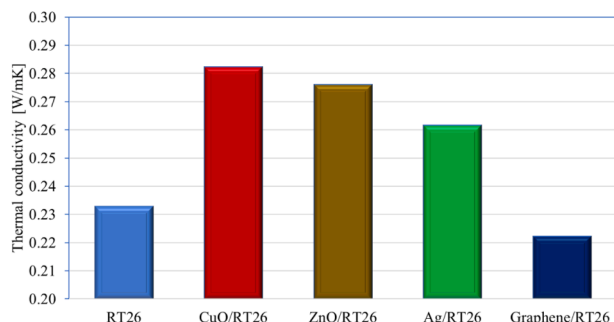


Fig. 7. Thermal conductivity of pure RT26 and RT26 based nanocomposites.

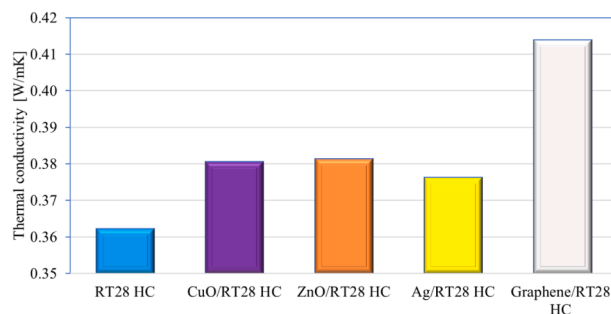


Fig. 8. Thermal conductivity of pure RT28 HC and RT28 HC based nanocomposites.

#### Thermal diffusivity of nanocomposites

Thermal diffusivity represents the ratio of thermal conductivity to volumetric specific heat capacity where volumetric specific heat capacity is the product of density as well as specific heat capacity. The thermal diffusivity of the RT26 and RT28 HC was measured, and it was found to be 0.122 mm<sup>2</sup>/s and 0.270 mm<sup>2</sup>/s, respectively.

Most nanocomposites based on RT26 had a decrease in thermal diffusivity, Fig. 9, i.e. 15.4% (Ag/RT26), 19% (Graphene/RT26) while in the case of CuO/RT26, the decrease was an insignificant 0.2%. The nanocomposite with ZnO nanoparticles had a 3.9% higher thermal diffusivity than the base RT26 PCM.

The diversified behavior of the thermal diffusivity of nanocomposites with respect to the base RT28 HC PCM is noticeable, Fig. 10. Namely, in the case of the ZnO/RT28 HC nanocomposite, the thermal diffusivity was unchanged; the CuO/RT28 HC and Ag/RT28 HC had a decrease of 1.5% and 1.3%, while in the case of Graphene/RT28 HC, there was a noticeable increase of 18.7%. However, with the notable exception of a nanocomposite with graphene nanoplatelets, the change in thermal diffusivity compared to the base PCM is not that significant.

In Figs. 9 and 10 it can be observed that only the addition of ZnO nanoparticles to base PCMs causes a favorable outcome in both cases in terms of thermal diffusivity which is consistent with [43], i.e. in this work, the highest increase in the thermal diffusivity of paraffin was obtained by the addition of ZnO nanoparticles. Other than [43] there is no significant number of published papers that deal with paraffin-based nanocomposites that contain reliable data on thermal diffusivity and also volumetric specific heat capacity. Therefore, it is not possible to provide a credible comparison for specific experimental nanocomposites in the context of the nanomaterials used (CuO, ZnO, Ag and graphene). In this sense, there is a considerable research gap in the existing literature.

#### Volumetric specific heat capacity

The indicator which presents the relationship between thermal

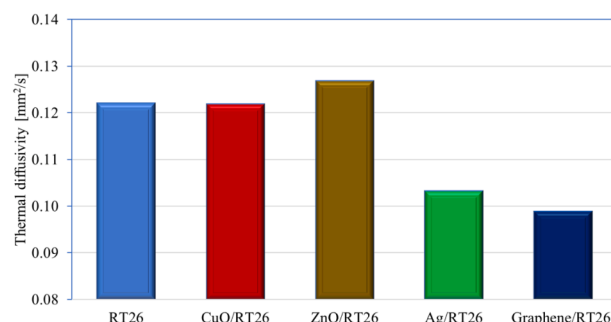


Fig. 9. Thermal diffusivity of pure RT26 and RT26 based nanocomposites.

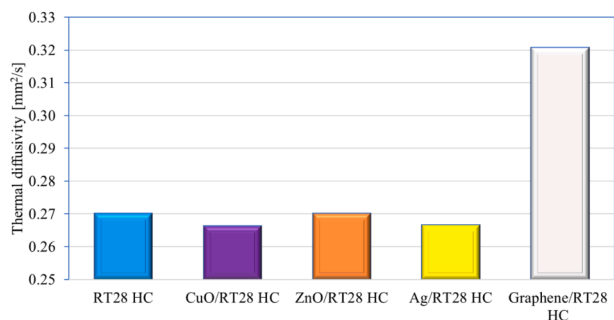


Fig. 10. Thermal diffusivity of pure RT28 HC and RT28 HC based nanocomposites.

energy and material temperature can be “per unit of volume” or “per unit of mass”. “The type” used depends on which is more appropriate in the particular engineering application. As stated before, volumetric specific heat capacity is the product of the sample volume density as well as specific heat capacity per unit of mass. It represents the amount of heat necessary to change the temperature of the sample by 1 K per unit volume. Based on the volumetric specific heat capacity value, the heat storage capability of each nanocomposite can be evaluated and compared. The detected volumetric specific heat capacity of pure RT26 was 1.909 MJ/m<sup>3</sup>K and all nanocomposites had an increase in this property when compared to this PCM, Fig. 11. Specifically, CuO/RT26, ZnO/RT26, Ag/RT26, and Graphene/RT26 nanocomposites had an increase in the volumetric specific heat capacity of 21.4, 14.2, 32.8 and 18%, respectively.

Similar behavior was observed in nanocomposites based on RT28 HC except for nanocomposites with graphene nanoplatelets in which a decrease in volumetric specific heat capacity was detected, Fig. 12. The pure RT28 HC had a volumetric specific heat capacity of 1.342 MJ/m<sup>3</sup>K while CuO/RT28 HC, ZnO/RT28 HC, and Ag/RT28 HC had 6.9, 5.2 and 5.3% larger volumetric specific heat capacity. Graphene/RT28 HC had a 3.6% reduction in volumetric specific heat capacity compared to pure RT28 HC. A similar effect was reported in [40], i.e. a coconut oil-based nanocomposite with 1 wt% of CuO nanoparticles had a specific heat reduction of 0.75% compared to a pure PCM.

It is clear that very few papers contain specific heat capacity [2] measurements, so volumetric specific heat capacity measurements represent valuable results in this context. Furthermore, knowing the volumetric specific heat capacity, it is relatively easy to calculate specific heat capacity, but this was not done to avoid the error of density measurement.

Summary of thermal constant measurements

In the case of RT26-based nanocomposites, the highest thermal conductivity was achieved with a 0.5 wt% addition of CuO

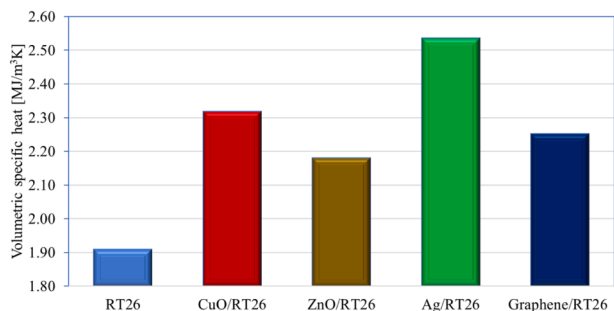


Fig. 11. Volumetric specific heat capacity of pure RT26 and RT26 based nanocomposites.

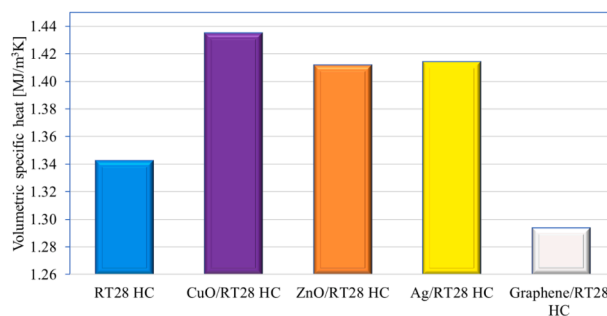


Fig. 12. Volumetric specific heat capacity of pure RT28 HC and RT28 HC based nanocomposites.

nanoparticles, Table 4. The highest thermal diffusivity was achieved with a 0.5 wt% addition of ZnO nanoparticles, but the improvement was not significant compared to the base PCM. Volumetric specific heat capacity was highest in the case of a nanocomposite with 0.5 wt% of Ag nanoparticles.

For the RT28 HC-based nanocomposites, the highest thermal conductivity and diffusivity was obtained by the addition of 0.5 wt% graphene, Table 5. Volumetric specific heat capacity was highest in the case of a nanocomposite with 0.5 wt% of CuO nanoparticles.

Possible nanocomposite selection strategies and economic evaluation

There are various ways to select a suitable phase change nanocomposite regarding the specific engineering problem. According to [2], the leading areas of NEPCM applications are thermal energy storage, photovoltaic solar systems, electronics, specific components, battery thermal management, and water desalination. The fields of possible applications are very wide, and it is difficult to make a clear distinction as to which nanocomposites are acceptable or unacceptable for a particular purpose. Therefore, it is necessary to conduct a techno-economic analysis in the context of the specific application in order to justify the application of the nanomaterials. The primary economic parameter is the price of nanomaterials because it is generally significantly higher than the unit retail price of a PCM. For the majority of the commercially available PCM units, the price ranges from about 5.0 €/kg to 10 €/kg on average [24], while for nanoparticles it ranges from about 0.2 €/g to 4.2 €/g [2], depending on the specific type of nanomaterial. In Table 6, orientation prices are listed for the nanomaterials used in the herein presented experimental work and were acquired from four suppliers. Significant discrepancies in the prices exist depending on the specific supplier. For instance, ZnO nanoparticles are the cheapest on the market, while Ag nanoparticles are the most expensive. The cost of nanocomposite preparation is not significant if the necessary equipment, like an ultrasound device or mechanical mixer, is available but this aspect should also be further investigated and quantified.

In addition to the specific price, the key parameter of the techno-economic analysis represents the improvement of the nanocomposite thermal properties compared to the base PCM. The quality of the preparation process has a notable influence on the thermo-physical properties as well as the long-term stability of the nanocomposites,

Table 4 Thermal properties of pure RT26 and RT26 based nanocomposites.

|   | RT26  | CuO/RT26 | ZnO/RT26 | Ag/RT26 | Graphene/RT26 |
|---|-------|----------|----------|---------|---------------|
| Thermal conductivity [W/mK]                             | 0.233 | 0.282    | 0.276    | 0.262   | 0.222         |
| Thermal diffusivity [mm <sup>2</sup> /s]                | 0.122 | 0.122    | 0.127    | 0.103   | 0.099         |
| Volumetric specific heat capacity [MJ/m <sup>3</sup> K] | 1.909 | 2.317    | 2.180    | 2.535   | 2.252         |

**Table 5**  
Thermal properties of pure RT28 HC and RT28 HC based nanocomposites.

|   | RT28 HC | CuO/RT28 HC | ZnO/RT28 HC | Ag/RT28 HC | Graphene/RT28 HC |
|---|---------|-------------|-------------|------------|------------------|
| Thermal conductivity [W/mK]                             | 0.362   | 0.381       | 0.381       | 0.376      | 0.414            |
| Thermal diffusivity [mm <sup>2</sup> /s]                | 0.270   | 0.266       | 0.270       | 0.267      | 0.321            |
| Volumetric specific heat capacity [MJ/m <sup>3</sup> K] | 1.342   | 1.435       | 1.412       | 1.414      | 1.293            |

Globally, the highest measured thermal conductivity and diffusivity was in the case of the Graphene/RT28 HC nanocomposite while the volumetric specific heat capacity was the highest for the CuO/RT28 HC nanocomposite.

[6]. As follows, the preparation methodology directly affects the properties of the nanocomposites and therefore the results should always be evaluated in the context of the applied methodology. The preparation methodology in this paper was consistent for all eight nanocomposites, thus it is possible to comparatively evaluate the change in thermal properties of the base PCMs. From Figs. 13–16, the 0% line represents the initial values of the thermal properties regarding the base PCM from which certain property changes are relatively in a positive or negative direction. Therefore, it is possible to compare the improvement or deterioration of particular properties depending on the base PCM. For example, the CuO nanoparticles produce a more significant effect on the thermal properties of the RT26 PCM than on the RT28 HC PCM, Fig. 13. However, CuO nanoparticles exert an evident effect on all the three thermal characteristics of the RT28 HC while the effect on the thermal diffusivity of the RT26 is negligible.

Similarly, ZnO nanoparticles cause a more considerable impact on the thermal properties of the RT26 than on the properties of the RT28 HC, with no effect on the thermal diffusivity of the RT28 HC Fig. 14.

Furthermore, Ag nanoparticles modified the thermal properties of both PCMs, but more pronounced for the RT26. In the case of Ag/RT26 nanocomposites, the diametrically opposite behavior of thermal diffusivity is much more noticeable compared to the other two properties Fig. 15.

The addition of graphene nanoplatelets in the RT26 and RT28 HC causes completely opposite results when compared to each other Fig. 16. Namely, in the specific case of the RT26, the volumetric specific heat capacity increased while the thermal conductivity and diffusivity decreased. In the case of the RT28 HC, a counter effect was achieved. A similar behavior such as the Graphene/RT26 nanocomposite was reported by Colla et al. [44] where the thermal conductivity of the RT20 PCM was reduced by 8% when 1 wt% of Al<sub>2</sub>O<sub>3</sub> nanoparticles were added to the base PCM. In the same work, the thermal conductivity of the RT25 PCM reduced by 7%. Furthermore, it was reported in the same work that the latent heat increased by 11% in the case of the RT20 and 1% when RT25 was considered.

A possible cause for this phenomenon is the specific interaction of nanoparticles and PCMs at a molecular level which requires further research to explicitly determine the precise cause and side effects. It is evident that nanomaterials in unique combinations with certain PCMs can be used to manipulate thermo-physical properties in the desired direction, i.e. towards an improvement or reduction of certain properties. This fact should be taken into account when producing and selecting appropriate nanocomposites for the desired application. Undoubtedly, further comprehensive research is required to determine how a particular nanomaterial affects the properties of different PCMs.

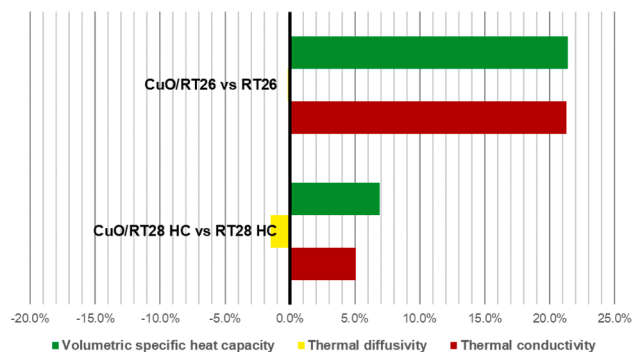


**Fig. 13.** Improvement/deterioration of CuO nanocomposite thermal properties compared to base PCMs.

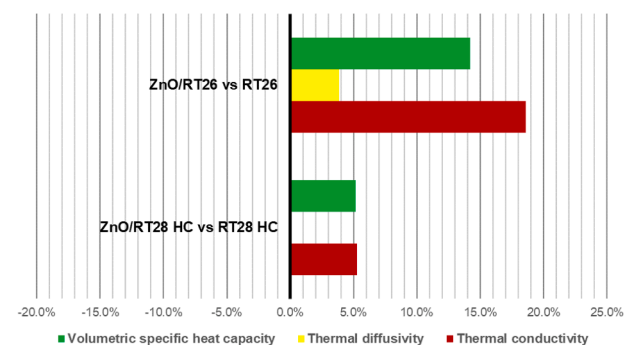


**Fig. 14.** Improvement/deterioration of ZnO nanocomposite thermal properties compared to base PCMs.

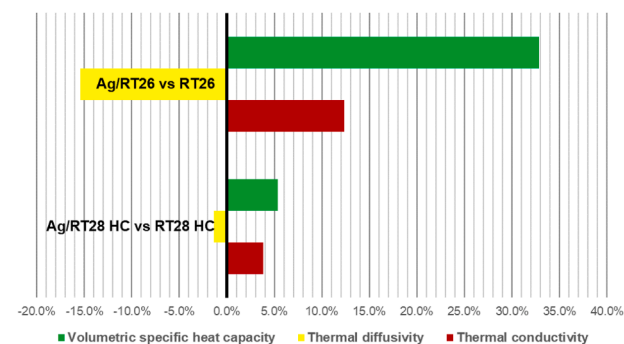


**Fig. 15.** Improvement/deterioration of Ag nanocomposite thermal properties compared to base PCMs.

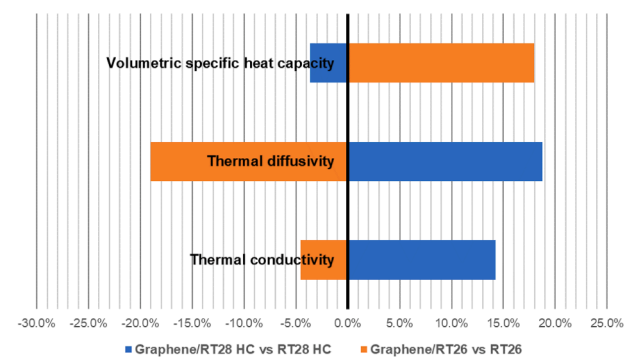


**Fig. 16.** Improvement/deterioration of graphene nanocomposite thermal properties compared to base PCMs.



**Table 6**  
The unit cost of used nanomaterials [2].

|          | Offer No. 1 |           |      | Offer No. 2 |         |       | Offer No. 3 |          |      | Offer No. 4 |          |      |
|----------|-------------|-----------|------|-------------|---------|-------|-------------|----------|------|-------------|----------|------|
|          | Purity      | Size      | €/g  | Purity      | Size    | €/g   | Purity      | Size     | €/g  | Purity      | Size     | €/g  |
| CuO      | 99.9%       | 40–80 nm  | 0.48 | /           | /       | 2.91  | 99.0%       | <100 nm  | 1.32 | 99%         | 40 nm    | 0.33 |
| ZnO      | 99.9%       | 90–210 nm | 0.50 | /           | /       | 0.23  | 99.0%       | <100 nm  | 1.06 | 99.8%       | 200 nm   | 0.18 |
| Ag       | 99.5%       | 35 nm     | 4.08 | /           | <100 nm | 17.67 | 99.0%       | <100 nm  | 4.17 | 99.9%       | 20–30 nm | 2.09 |
| Graphene | 99.5%       | 11–15 nm  | 0.52 | /           | /       | 0.89  | 99.0%       | 10–15 nm | 4.19 | /           | 11–15 nm | 0.88 |

## Conclusions

In this work, several nanocomposites were experimentally investigated with the main goal being to determine the general thermal constants and compare the main differences between the specific nanocomposites. For that purpose, four nanomaterials (CuO, ZnO, Ag, and graphene) and two base PCMs were selected (RT26 and RT28 HC). Based on the conducted experimental work, further observations could be highlighted as follows:

- The non-steady-state method, i.e. Transient Plane Source technique, was used for measuring the thermal constants of nanocomposites and it was found that the addition of nanomaterials in RT26 and RT28 HC significantly affects the thermal properties of these PCMs. The most significant rise in the thermal conductivity of 21.3% was achieved with the addition of CuO (0.5 wt%) nanoparticles in the RT26 PCM. Volumetric specific heat capacity was maximally raised by 32.8% in the case of the Ag/RT26 PCM; however, in this case, a worth mentioning reduction in thermal diffusivity of 15.4% was detected compared with the pure RT26. A significant improvement, i.e. 18.7%, in thermal diffusivity was only achieved in the case of the Graphene/RT28 HC nanocomposite,
- In the case of nanocomposites with graphene nanoplatelets, opposite behavior was detected, regarding the expected values of the thermal constants, i.e. when different PCMs are considered. To detect the possible cause for previous phenomena, the specific interaction on the molecular level of nanomaterials and PCMs should be investigated, and which is part of the future research work,
- A key point of the preparation process is ultrasonic homogenization which ensures a homogeneous sample without nanomaterial agglomerates. During this process, it is necessary to control the temperature of the examined sample and, if necessary, provide cooling to ensure that the maximum operation temperature is not exceeded,
- Unquestionably, nanomaterials have a certain toxic potential, so it is necessary to proactively approach the planning of safety procedures and use adequate protective equipment. In this context, a certain novelty in the measurement of thermal constants was introduced, i.e. two-layer PA/PE bags were used to protect the operator from secondary exposure to nanomaterials during the measurement of thermal constants,
- Regarding the selection strategies, a detailed techno-economic evaluation is necessary in the case of the nano-enhanced materials, taking into account the preparation cost, material cost, properties of nanomaterials, and finally nanocomposite characteristics for specific engineering application. Therefore, an integral approach should be provided when considering nano-enhanced systems.

## CRedit authorship contribution statement

**Mišo Jurčević:** Conceptualization, Methodology, Software. **Sandro Nizetić:** Conceptualization, Methodology, Supervision. **Müslüm Arıcı:** Supervision. **A. Hoang Anh Tuan:** Supervision. **Effrosyni Giama:** Supervision. **Agis Papadopoulos:** Supervision.

## Declaration of Competing Interest

The authors declare that they have no known competing financial interests or personal relationships that could have appeared to influence the work reported in this paper.

## Acknowledgement

This work was funded by the Croatian Science Foundation (Research project: Smart and hybrid cooling techniques for siliceous photovoltaic panels-IP-01-2018-2814).

## References

- [1] National Nanotechnology Initiative, <https://www.nano.gov/you/nanotechnology-benefits> [accessed 24 June 24 2020].
- [2] Nizetić S, Jurčević M, Arıcı M, Arasu AV, Xie G. Nano-enhanced phase change materials and fluids in energy applications: A review. *Renew Sustain Energy Rev* 2020;129:109931. <https://doi.org/10.1016/j.rser.2020.109931>.
- [3] Ghoghaei MS, Mahmoudian A, Mohammadi O, Shafii MB, Jafari Mosleh H, Zandieh M, et al. A review on the applications of micro-/nano-encapsulated phase change material slurry in heat transfer and thermal storage systems. *J Therm Anal Calorim* 2020. <https://doi.org/10.1007/s10973-020-09697-6>.
- [4] Arıcı M, Bilgin F, Nizetić S, Karabay H. PCM integrated to external building walls: An optimization study on maximum activation of latent heat. *Appl Therm Eng* 2020;165:114560. <https://doi.org/10.1016/j.applthermaleng.2019.114560>.
- [5] Qin G, Wang X, Wan X, Chen D, Qiu Bo. Nanotubes TiO<sub>2</sub> supported Pt catalyst for selective electrocatalytic oxidation of glycerol to glyceric acid. *Energy Sources Part A* 2020;42(17):2120–9. <https://doi.org/10.1080/15567036.2019.1607930>.
- [6] Jurčević M, Nizetić S, Arıcı M, Ocloń P. Comprehensive analysis of preparation strategies for phase change nanocomposites and nanofluids with brief overview of safety equipment. *J Cleaner Prod* 2020;274:122963. <https://doi.org/10.1016/j.jclepro.2020.122963>.
- [7] Sipponen MH, Henn A, Penttilä P, Österberg M. Lignin-fatty acid hybrid nanocapsules for scalable thermal energy storage in phase-change materials. *Chem Eng J* 2020;393:124711. <https://doi.org/10.1016/j.cej.2020.124711>.
- [8] Parameshwaran R, Kumar GN, Ram VV. Experimental analysis of hybrid nanocomposite-phase change material embedded cement mortar for thermal energy storage. *J Build Eng* 2020;30:101297. <https://doi.org/10.1016/j.job.2020.101297>.
- [9] Pinto SC, Silva NHCS, Pinto RJB, Freire CSR, Duarte I, Vicente R, Vesenjak M, Marques PAAP. Multifunctional hybrid structures made of open-cell aluminum foam impregnated with cellulose/graphene nanocomposites. *Carbohydr Polym* 2020;238:116197. <https://doi.org/10.1016/j.carbpol.2020.116197>.
- [10] Prabhu B, Valan Arasu A. Stability analysis of TiO<sub>2</sub>-Ag nanocomposite particles dispersed paraffin wax as energy storage material for solar thermal systems. *Renewable Energy* 2020;152:358–67. <https://doi.org/10.1016/j.renene.2020.01.043>.
- [11] Bahari M, Najafi B, Babapoor A. Evaluation of  $\alpha$ -AL2O<sub>3</sub>-PW nanocomposites for thermal energy storage in the agro-products solar dryer. *J Storage Mater* 2020;28:101181. <https://doi.org/10.1016/j.est.2019.101181>.
- [12] Zhang M, Wang C, Luo A, Liu Z, Zhang X. Molecular dynamics simulation on the thermophysical of paraffin/EVA/graphene nanocomposites as phase change materials. *Appl Therm Eng* 2020;166:114639. <https://doi.org/10.1016/j.applthermaleng.2019.114639>.
- [13] Aslfattahi N, Saidur R, Arifuzzaman A, Sadri R, Bimbo N, Sabri MFM, Maughan PA, Bouscarrat L, Dawson RJ, Said SM, Goh BT, Sidik NAC. Experimental investigation of energy storage properties and thermal conductivity of a novel organic phase change material/MXene as a new class of nanocomposites. *J Storage Mater* 2020;27:101115. <https://doi.org/10.1016/j.est.2019.101115>.
- [14] Ranjbar SG, Roudini G, Barahue F. Fabrication and characterization of phase change material-SiO<sub>2</sub> nanocomposite for thermal energy storage in buildings. *J Storage Mater* 2020;27:101168. <https://doi.org/10.1016/j.est.2019.101168>.
- [15] Liu H, Niu J, Wang X, Wu D. Design and construction of mesoporous silica/n-eicosane phase-change nanocomposites for supercooling depression and heat transfer enhancement. *Energy* 2019;188:116075. <https://doi.org/10.1016/j.energy.2019.116075>.
- [16] Wu Si, Li T, Tong Z, Chao J, Zhai T, Xu J, Yan T, Wu M, Xu Z, Bao H, Deng T, Wang R. High-performance thermally conductive phase change composites by



- large-size oriented graphite sheets for scalable thermal energy harvesting. *Adv. Mater.* 2019;31(49):1905099. <https://doi.org/10.1002/adma.201905099>.
- [17] Tao YB, Liu YK, He YL. Effect of carbon nanomaterial on latent heat storage performance of carbonate salts in horizontal concentric tube. *Energy* 2019;185: 994–1004. <https://doi.org/10.1016/j.energy.2019.07.106>.
- [18] Konuklu Y, Ersoy O, Erzin F. Development of pentadecane/diatomite and pentadecane/sepiolite nanocomposites fabricated by different compounding methods for thermal energy storage. *Int J Energy Res* 2019;43(12):6510–20. <https://doi.org/10.1002/er.4534>.
- [19] Wang C, Chen Ke, Huang J, Cai Z, Hu Z, Wang T. Thermal behavior of polyethylene glycol based phase change materials for thermal energy storage with multiwall carbon nanotubes additives. *Energy* 2019;180:873–80. <https://doi.org/10.1016/j.energy.2019.05.163>.
- [20] A. Yadav A. Verma P.K. Bhatnagar V.K. Jain V. Kumar Enhanced thermal characteristics of NG based acetamide composites. *International Journal of Innovative Technology and Exploring Engineering*. 8 10 2019 pp. 4227–4231. <https://doi.org/10.35940/ijitee.j9944.0881019>.
- [21] Liu X, Marbut C, Huitink D, Feng G, Fleischer AS. Influence of crystalline polymorphism on the phase change properties of sorbitol-Au nanocomposites. *Mater Today Energy* 2019;12:379–88. <https://doi.org/10.1016/j.mtener.2019.03.007>.
- [22] Li W, Dong Y, Wang J, Zhang Y, Zhang Xu, Liu X. Experimental study on enhanced heat transfer of nanocomposite phase change materials. *Phase Trans* 2019;92(3): 285–301. <https://doi.org/10.1080/01411594.2019.1574010>.
- [23] Bahiraei F, Fartaj A, Nazri G-A. Experimental and numerical investigation on the performance of carbon-based nanoenhanced phase change materials for thermal management applications. *Energy Convers Manage* 2017;153:115–28. <https://doi.org/10.1016/j.enconman.2017.09.065>.
- [24] Rubitherm® Technologies GmbH, <https://www.rubitherm.eu/en/index.php/productcategory/organische-pcm-rt>, [accessed 27 June 2020].
- [25] IoLiTec GmbH, <https://iolitec.de/>, [accessed 27 June 2020].
- [26] Missaoui WN, Arnold RD, Cummings BS. Toxicological status of nanoparticles: What we know and what we don't know. *Chem Biol Interact* 2018;295:1–12. <https://doi.org/10.1016/j.cbi.2018.07.015>.
- [27] Wu T, Tang M. Review of the effects of manufactured nanoparticles on mammalian target organs. *J Appl Toxicol* 2018;38(1):25–40. <https://doi.org/10.1002/jat.3499>.
- [28] Ellenbecker MJ, Tsai CS-J. Exposure assessment and safety considerations for working with engineered nanoparticles, John Wiley & Sons, Inc.; 2015. <https://doi.org/10.1002/9781118998694>.
- [29] Gustafsson SE. Transient plane source techniques for thermal conductivity and thermal diffusivity measurements of solid materials. *Rev Sci Instrum* 1991;62: 797–804.
- [30] Krupa P, Malinaric S. Using the transient plane source method for measuring thermal parameters of electroceramics. *Int J Mech Mech Eng* 2014;8(5).
- [31] Bohac V, Gustavsson MK, Kubičar L, Gustafsson SE. Parameter estimations for measurements of thermal transport properties with the hot disk thermal constants analyzer. *Rev Sci Instrum* 2000;71:15–9. <https://doi.org/10.1063/1.1150635>.
- [32] Gustavsson MK, Gustafsson SE. On power variation in self-heated thermal sensors. *Thermal Conductivity* 27. DEStech Publ Inc 2003;27:338–46.
- [33] Transient plane heat source (hot disc) method, <https://www.iso.org/standard/40683.html> [accessed 1 July 2020].
- [34] Hot Disk®, <https://www.hotdiskinstruments.com/products-services/instruments/tps-500/>, [accessed 28 June 2020].
- [35] Kapton Polyimide Characteristics, <https://dielectricmfg.com/knowledge-base/kapton/>, [accessed 1 July 2020].
- [36] T. Log S.E. Gustafsson Transient plane source (TPS) technique for measuring thermal transport properties of building materials *Fire and Materials* 1995;19: 43–49. <https://doi.org/10.1002/fam.810190107>.
- [37] Jurčević M, Penga Ž, Klarin B, Nizetić S. Numerical analysis and experimental validation of heat transfer during solidification of phase change material in a large domain. *J Storage Mater* 2020;30:101543. <https://doi.org/10.1016/j.est.2020.101543>.
- [38] Pico Technology, <https://www.picotech.com/data-logger/tc-08/usb-tc-08-accessories>, [accessed 18 April 2020].
- [39] PSE, <https://www.pico-technology-deutschland.de/Thermocouple-Type-T-R5-x-50mm-Waterproof-Stainless-Steel-Tip-3m-Lead-60C-to-200C>, [accessed 18 April 2020].
- [40] Ebadi S, Tasnim SH, Aliabadi AA, Mahmud S. Geometry and nanoparticle loading effects on the bio-based nano-PCM filled cylindrical thermal energy storage system. *Appl Therm Eng* 2018;141:724–40. <https://doi.org/10.1016/j.applthermaleng.2018.05.091>.
- [41] D. Dsilva Winfred Rufuss L. Suganthi S. Iniyan P.A. Davies Effects of nanoparticle-enhanced phase change material (NPCM) on solar still productivity *Journal of Cleaner Production* 2018;192:9–29. [10.1016/j.jclepro.2018.04.201](https://doi.org/10.1016/j.jclepro.2018.04.201).
- [42] Putra N, Amn M, Kosasih EA, Luanto RA, Abdullah NA. Characterization of the thermal stability of RT 22 HC/graphene using a thermal cycle method based on thermoelectric methods. *Appl Therm Eng* 2017;124:62–70. <https://doi.org/10.1016/j.applthermaleng.2017.06.009>.
- [43] Babapoor A, Karimi G. Thermal properties measurement and heat storage analysis of paraffin nanoparticles composites phase change material: Comparison and optimization. *Appl Therm Eng* 2015;90:945–51. <https://doi.org/10.1016/j.applthermaleng.2015.07.083>.
- [44] Colla L, Fedele L, Mancin S, Danza L, Manca O. Nano-PCMs for enhanced energy storage and passive cooling applications. *Appl Therm Eng* 2017;110:584–9. <https://doi.org/10.1016/j.applthermaleng.2016.03.161>.

## Appendix D

Title: Experimental investigation of novel hybrid phase change materials

Authors: Jurčević M., Nižetić S., Čoko D., Hoang A.T., Papadopoulos A.

Publisher: *Springer Nature*

Journal: *Clean Technologies and Environmental Policy*

Edition, pages, year: 21, 201-212, 2022.

Indexed in: Scopus, Science Citation Index Expanded, INSPEC, Current Contents, etc.

Journal Impact Factor: 4.7 Q2 (WoS-2022.), Q1 (SJR-2022.)

DOI: <https://doi.org/10.1007/s10098-021-02106-y>

**Abstract:** The novel potential of hybrid phase change materials (PCM) as a mix of animal fat, specifically pork fat (lard), with edible and waste oil from the food processing industry was investigated in this paper. Lard is a relatively accessible phase change material of organic origin, with a significantly lower unit price when compared to conventional PCM materials (wholesale price of lard can be less than 0.50 €/kg). On an annual basis, a large amount of lard is thrown away because it has become inedible from a nutritional point of view. Experimental results directed that the addition of oils can improve the thermal constants of lard such as thermal conductivity, volumetric heat capacity, with the thermal diffusivity being reduced. The best result was achieved for a hybrid PCM as a combination of pork fat and waste burnt oil as the thermal conductivity was improved by 1.4% and the volumetric heat capacity by 11% with respect to the base PCM, i.e., pork fat (lard). The novel proposed hybrid PCMs are more economically viable, enabling the utilization of waste resources, and securing less environmental impact when compared to conventional PCMs as organic materials. The possible application of lard should be further investigated for specific engineering applications, such as thermal energy storage.



# Experimental investigation of novel hybrid phase change materials

Mišo Jurčević<sup>1</sup> · Sandro Nižetić<sup>1</sup> · Duje Čoko<sup>2</sup> · Anh Tuan Hoang<sup>3</sup> · Agis M. Papadopoulos<sup>4</sup>

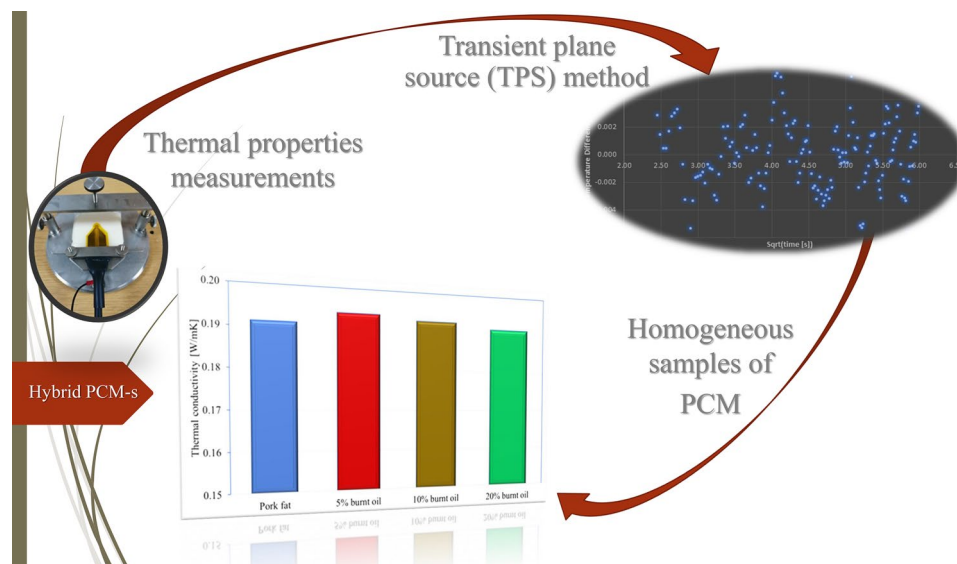
Received: 28 December 2020 / Accepted: 27 April 2021

© The Author(s), under exclusive licence to Springer-Verlag GmbH Germany, part of Springer Nature 2021

## Abstract

The novel potential of hybrid phase change materials (PCM) as a mix of animal fat, specifically pork fat (lard), with edible and waste oil from the food processing industry was investigated in this paper. Lard is a relatively accessible phase change material of organic origin, with a significantly lower unit price when compared to conventional PCM materials (wholesale price of lard can be less than 0.50 €/kg). On an annual basis, a large amount of lard is thrown away because it has become inedible from a nutritional point of view. Experimental results directed that the addition of oils can improve the thermal constants of lard such as thermal conductivity, volumetric heat capacity, with the thermal diffusivity being reduced. The best result was achieved for a hybrid PCM as a combination of pork fat and waste burnt oil as the thermal conductivity was improved by 1.4% and the volumetric heat capacity by 11% with respect to the base PCM, i.e., pork fat (lard). The novel proposed hybrid PCMs are more economically viable, enabling the utilization of waste resources, and securing less environmental impact when compared to conventional PCMs as organic materials. The possible application of lard should be further investigated for specific engineering applications, such as thermal energy storage.

## Graphic abstract



**Keywords** Phase change materials · Lard · Waste edible oil · Thermal constants · Thermal energy storage · Hybrid PCM · Thermal properties

✉ Sandro Nižetić  
snizetic@fesb.hr

Extended author information available on the last page of the article

## Introduction

Phase change materials (PCM) are often used for thermal management purposes in various engineering applications, processes, and systems. Two major implementation areas are related to the energy storage and thermal management of systems or components, (Ikutegbe and Farid 2020). More specifically, many studies have analyzed PCM-based thermal energy storage systems (Hu et al. 2021) in different implementation areas such as buildings (Yu et al. 2021), and in particular office buildings (Konstantinou et al. 2019), or for instance the specific components of energy systems (Das et al. 2021). The main role of the PCMs in thermal energy storage systems (TES) is to ensure an efficient store of waste heat from engineering equipment that releases excessive heat and enable thermal storage in more compact vessels or over longer periods of time (Kyriaki et al. 2020). A second and quite wide application area of the PCM is directed to the thermal management of systems, components, or devices. For instance, the PCM is utilized for the thermal management of photovoltaic (PV) panels (Nižetić et al. 2017) to improve the performance and durability of PV systems. Particularly, solar concentration photovoltaic systems (CPV) are suitable for the application of PCMs for efficient thermal regulation of relatively high operating temperatures, (Omara et al. 2020). The thermal management of electronics and especially batteries (Jiang et al. 2020) is also a relatively wide implementation area for PCMs. Water desalination and distillation systems are also investigated concerning the possible utilization of PCMs, (Mousa et al. 2019). In the last four years, there has been a noticeable rising trend in the number of published research works related to the analysis of PCMs in energy-related areas, in the amount of 26%, for the period 2017–2020, (Scopus® 2020). One can hence conclude that an interest in PCMs exists and is certainly rising, with different application areas being analyzed.

In general, different types of PCMs can be divided into organic, solid, hygroscopic, and eutectic. The main physical features of the PCM are related to average thermal properties such as specific heat, latent heat of fusion, thermal conductivity, and melting (solid to liquid transition) temperature. The selection of a specific PCM depends on the exact engineering application where the most important parameters are the melting temperature and latent heat of fusion. The usual range of the main physical properties related to the most used PCMs in engineering applications is presented in Table 1, (Nižetić et al. 2020). The values from Table 1 are approximate, in order to understand the range; however, exact data strongly depend on the specific type of PCM material. The usual range of the melting

**Table 1** Usual range of main PCM thermal properties

| Specific property of PCM        | Usual range |
|---------------------------------|-------------|
| Specific heat capacity (kJ/kgK) | 1.1–2.5     |
| Thermal conductivity (W/mK)     | 0.2–0.6     |
| Latent heat of fusion (kJ/kg)   | 100–250     |
| Melting temperature (°C)        | 17–70       |

temperature is from around 20 °C up to 70 °C as most PCM materials are sensitive to high working temperatures concerning the degradation of the properties. Latent fusion heat ranges from about 100 kJ/kg up to 250 kJ/kg, and PCMs with higher values of latent fusion heat are generally used with more expensive materials.

One of the major drawbacks related to the PCM is the relatively high unit cost that usually ranges from 5 €/kg up to 15 €/kg, (Rubitherm® Technologies GmbH 2020). The techno-economic viability of PCM-based systems can be questionable, especially in circumstances when performance improvement is expressed as limited regarding efficiency increases and useful lifetime. For instance, in the case of passively cooled PV panels with a PCM (PV-PCM cooling systems), the economic viability is critical, (Arıcı et al. 2018). The approach to improve the economic suitability of the PCM is either to improve thermal properties, i.e., to achieve the better performance of PCM-based systems or to discover novel and more economically suitable PCMs. The improvement of the PCM can be ensured by the addition of nanomaterials (NPCM), where according to latest research, significant improvements can be ensured regarding thermal constants, (Nižetić et al. 2020), particularly thermal conductivity. The critical feature of the NPCM is the preparation procedure that has a strong impact on the long-term stability and thermal properties of nano-enhanced PCMs, (Jurčević et al. 2020a). The problem with nanomaterials is also relatively high unit costs and toxicity, which requires a careful design approach and high safety standards.

An important issue related to PCMs is the long-term stability of specific PCMs, which usually requires sufficient cyclic testing (thermal cycling), to determine the cycling impact on performance regarding the specific considered applications via Fourier-transform infrared spectroscopy, (Dhamodharan and Bakthavatsalam 2020). The investigation of novel, more affordable, and durable PCMs is one of the possible solutions and is precisely in the direction of ongoing research work. A novel composite PCM material (aluminum substrate) was discussed in (Cheng et al. 2021), where an anodizing surface treatment was provided to produce an encapsulated PCM with 1-tetrapropanol as the base material. The results indicated a significant improvement in thermal conductivity (rise of 560%) when compared to pure tetrapropanol. The thermal properties showed excellent

stability after 400 cycles with good stability even for temperatures over 140 °C. The results revealed that the novel produced nano-encapsulated PCMs are suitable as excellent energy storage materials. The economic aspect of the novel produced PCM was not discussed, which is a critical feature. Pork fat was considered as a novel potential PCM material in (Nižetić et al. 2018), where a numerical model was developed and tested for a PV-PCM passive cooling system. The results revealed that pork fat has a similar impact on performance improvement when compared to conventional PCMs, with several advantages. The first advantage is a significantly lower unit cost for the pork fat, which according to the authors of the mentioned study could go below 1.0 €/kg. The second advantage is the environmental suitability of the pork fat as it is a natural PCM, not produced in an artificial manner by various chemicals in industrial conditions, which cause the release of different pollutants. The main open issue with pork fat could be its long-term stability, which should be thoroughly investigated with thermal cycling. A novel bio-based composite PCM was reported in (Hu et al. 2021), which was made with reduced graphene-oxide (1 wt% to 5 wt%) and spent ground coffee. The improvement of the thermal conductivity was not large, but the leakage-proof performance of the PCM was significantly improved. The provided experimental tests and cycling experiments showed excellent thermal and chemical stability regarding the novel proposed PCM. A novel composite PCM was proposed in (Wu et al. 2020) as a combination of capric acid and paraffin. The produced PCM showed suitability for seasonal thermal energy storage applications, but the economy of the considered approach was not discussed. A flexible composite PCM was proposed and examined in Huang et al. (2021) as a suitable material for the thermal regulation of batteries. The novel PCM was assembled as a combination of paraffin, styrene butadiene, and aluminum nitride. A complex experimental investigation showed that the proposed PCM is suitable for the thermal management of batteries as it considerably improved the performance of batteries. The proposed material could also be suitable for thermal energy storage applications. Taking ongoing research activity into account, it is clear that considerable efforts are being directed to the investigation of novel PCMs, which would be more efficient and suitable from a techno-economic point of view. It also needs to be highlighted that economic evaluations are usually omitted, i.e., studies are more focused on the performance improvement of novel PCMs. As already mentioned, the economic aspect of PCMs is a critical feature that requires careful attention. In that sense, the main motivation for the herein conducted research was directed to the experimental investigation of hybrid PCMs, which could be more economically viable and environmentally suitable. Pork fat (lard) was selected as the base PCM as it is an organic and cheap PCM with a suitable melting temperature. Waste oil

(burnt oil) from the food industry was taken into account for the addition to the base PCM together with edible oil (sunflower). The main goal of this work was directed to the experimental evaluation of the thermal characteristics regarding hybrid phase change materials consisting of lard, waste edible oils as potentially novel organic PCMs.

## Experimental approach

### Description of measurement technique

Thermal constant measurements were carefully performed using the non-steady-state transient plane source (TPS) method. The TPS method is generally accepted for the measurement of thermal constants and is precisely defined by the ISO 22,007–2 standard. The standard method was developed by Gustaffson (1991) and improved by Boháč et al. (2000). For direct measurements based on this method, a sensor containing a heater is used to provide a constant source of heat that penetrates the measured sample. Depending on the diameter of the sensor, the general properties of the measured material, number of concentric rings, and input heat, the average temperature of the sensor rises. Based on the temperature function, thermal constants can be accurately estimated, i.e., thermal conductivity and thermal diffusivity (Krupa and Malinaric 2014). Since the measured samples are not ideal and are often limited in volume, Gustaffson (1991) suggested that the first few seconds of direct measurement should be discarded due to the existence of insulation on the sensor. With this in mind, the measurements for the specific purposes of this paper were performed through polyethylene (PE) bags containing the samples, Fig. 1a. In this way, the potential contamination of the samples is avoided and the need to clean the sensor after the measurement is eliminated. A Hot Disk TPS 500 S device was used, Fig. 1b, which measures thermal conductivity in a range of 0.005 W/mK to 1800 W/mK and works on a principle similar to the TPS method described in ISO 22,007–2, (Hot Disk® 2020).

The sensor 5465 of this device (Fig. 1a), 10 µm in thickness, has the shape of a double spiral and is insulated with Kapton insulation, which can withstand temperatures ranging from –269 °C to 400 °C (Kapton Polyimide Characteristics 2020).

The testing of pork fat-based samples was performed at 9 °C to evade phase transitioning and with low heating power, only 20 mW, in order to avoid sensor overheating due to the relatively low thermal conductivity of the samples. The key parameters from Table 2 were generated iteratively using Hot Disk Thermal Constants Analyzer 7.4 (Beta 24 software), allowing for adequate probing depths without overheating the sophisticated sensor.



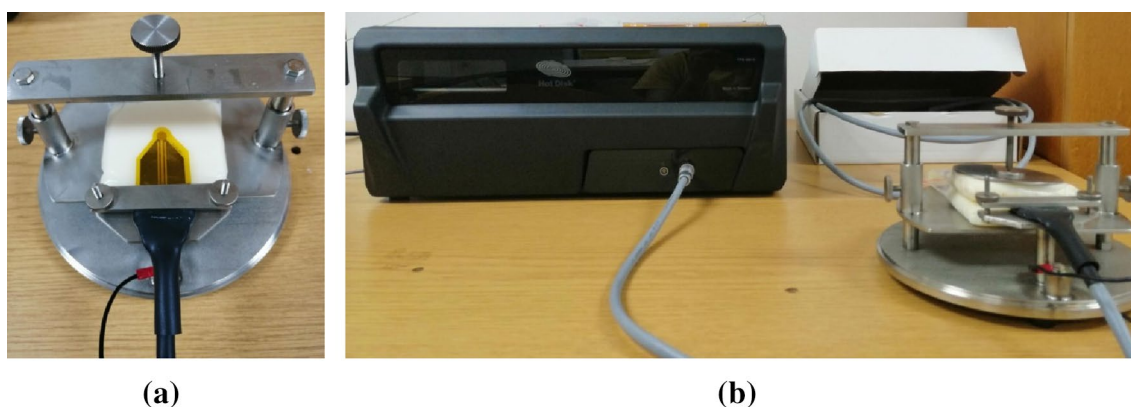


**Fig. 1** **a** 5465 sensor and sample in PE bags, **b** Hot Disk TPS 500 S device and holder for sample

**Table 2** Initial input parameters for Hot Disk device

|                          |                                     |
|--------------------------|-------------------------------------|
| Sensor type              | Kapton 5465<br>(3.189 mm<br>radius) |
| Heating power            | 20 mW                               |
| Measurement time         | 40 s                                |
| Sample temperature       | 9 °C                                |
| Minimum sample thickness | 10 mm                               |

The measurement quality is easily judged based on the software calculation of mean deviation data, which is acceptable if less than  $10^{-4}$  K (very small measurement noise). If the mean deviation is large, this will be reflected in the residual graph. The residual graph represents the difference between the measurement data and “fitted” data. Ideally, residuals should be randomly scattered around the horizontal line, Fig. 2.

The points on the depicted residual graph are randomly scattered; therefore, successful measurements and accurate calculations are subsequently yielded.

Fluctuations in the initial part of the residual graph can often be detected, which are a result of contact between the sensor surface and sample. The appearance of random irregularities may indicate the inhomogeneity of the sample material and possibly cavities.

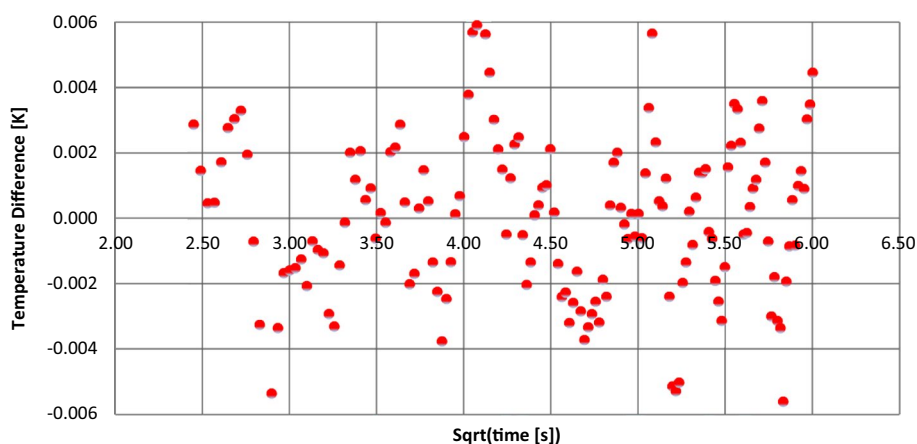
### Uncertainty of measurements

The Hot Disk TPS500 S device has a thermal conductivity accuracy of  $\pm 5\%$  and reproducibility of  $\pm 2\%$  for materials of various thermal conductivities such as aluminum or polystyrene, Hot Disk® (2020), Log and Gustafsson (1995). The influence regarding the accuracy of temperature measurements, i.e., measurement uncertainty, was calculated with Eq. (1), (Jurčević et al. 2020b).

$$\Delta U = \pm \sqrt{\Delta U_t^2 + \Delta U_{tc}^2} \quad (1)$$

A T-type thermocouple and PICO TC-08 data logger were used to measure the sample temperature, (Pico Technology 2020). The measurement uncertainty of the T-type thermocouples is  $\pm 0.5$  °C ( $\Delta U_t$ ), and  $\pm 0.5$  °C ( $\Delta U_{tc}$ ) for the

**Fig. 2** Residual graph for relatively homogeneous sample of lard



specified data logger. The total measurement uncertainty is  $\pm 0.71$  °C.

### Sample preparation and examined samples

Commercially available pork fat (lard) and sunflower oil were procured at a local market, while the burnt oil was donated by a restaurant chain. This type of burnt oil can be commonly found in other foodservice facilities. The burnt oil samples were melted and filtered from coarse inclusions to ensure a homogeneous material. A thermal conductivity of 0.18 W/mK was measured regarding the burnt oil, which is very close to the expected conductivity of lard. Namely, during the thermal food processing of animal origin, fat is released into the oil. Therefore, a relatively good thermal and chemical compatibility between the lard and burnt oil can be expected in principle. However, to explicitly confirm this, additional chemical interaction studies regarding phase change materials of related origin are needed. Sunflower oil and burnt oil in combination with lard form a relatively cheap and widely available organic phase change material, which is environmentally friendly. At room temperature, the tested lard was in a solid phase, while the sunflower oil was in a liquid phase. The burnt oil was in a transitional “slurry” phase, Fig. 3.

To form a hybrid PCM material, the lard was melted on a hot plate with a maximum sample temperature ranging from 51 to 56 °C. The sample temperature was continuously monitored with T-type thermocouples. Each lard sample typically depends on the animal species, body position, processing technology, and it is necessary to further investigate the level of these effects on the thermophysical properties of this material. Based on the available data regarding



**Fig. 3** Waste burnt oil at room temperature

the melting point of the lard (Engineering ToolBox 2020) and on direct visual observation during the melting, it was determined that a required sample temperature above 50 °C is necessary to exceed the melting point of the lard. Hybrid PCMs, 150 mL each, numbered 2, 3, and 4 were formed by adding 20%, 10%, and 5% of sunflower oil in volume to the melted lard. Furthermore, hybrid PCMs, 150 mL each (amount sufficient to form a representative sample for the TPS method-based tests), 5, 6, and 7 were produced by the same methodology, but contain 20%, 10%, and 5% of waste burnt oil in volume, Table 3. The sample listed with number 1 refers to pure lard with no oil. Volume fractions of over 20% proved to be problematic due to the formation of an oil layer on the lard surface. Possibly, this problem might be solved with emulsifiers, but consequently, this may raise the production costs of the materials with questionable effects on the thermophysical properties.

Samples 1 to 7 were carefully poured into PE bags and sealed as shown in, Fig. 4. For hybrid samples up to 20% of oil, there is no significant separation of applied oil from lard even after multiple phase changes. The samples seem to be relatively stable even after several months, but this should be further confirmed and quantified after cyclic testing.

### Results and discussion

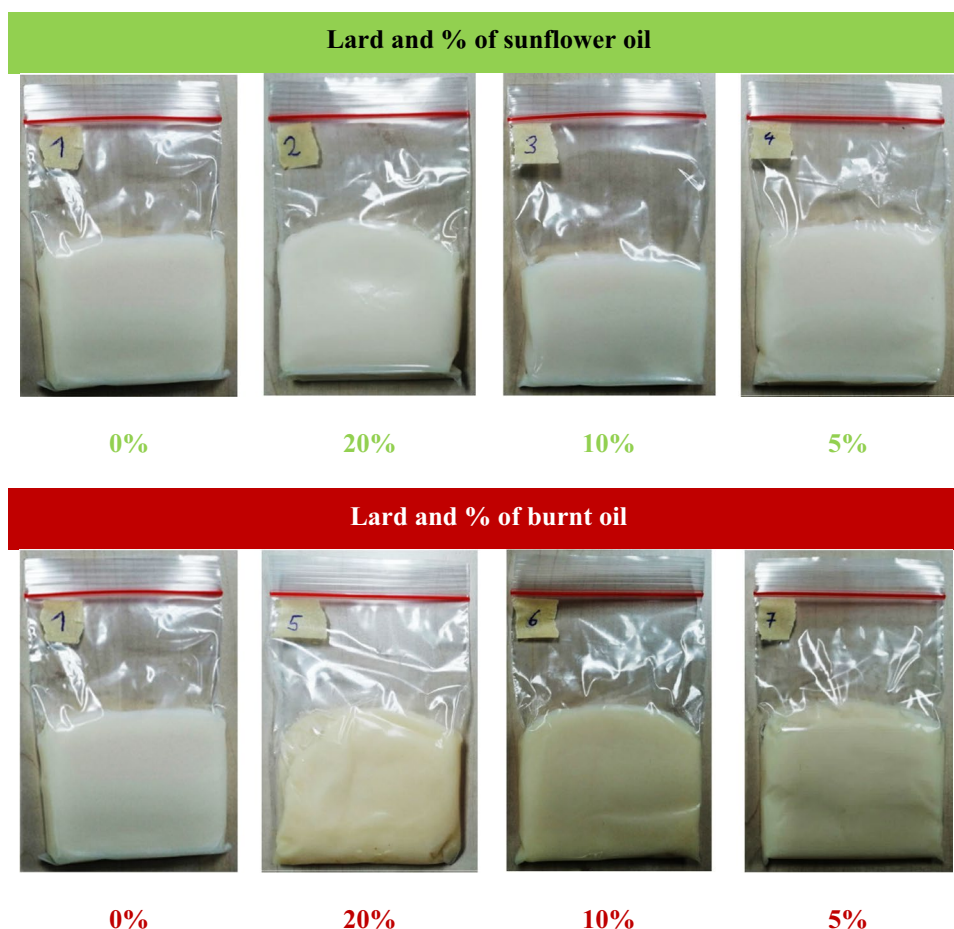
The addition of burnt oil and sunflower oil to pork fat as an organic PCM causes an impact on the thermal characteristics of the produced hybrid PCMs. The comparison of the specific results for thermal constants (volumetric specific heat capacity, thermal diffusivity, and thermal conductivity) is presented in Fig. 5, depending on the specific volume fractions, which range from 5 to 20%. Figure 5 reveals that the addition of burnt or sunflower oil into the pork fat improves the volumetric specific capacity, and it reduces thermal diffusivity in all cases. The improvement in the volumetric specific heat capacity ranges from about 2% to 11% with respect to the base PCM. The reduction in thermal diffusivity ranges

**Table 3** Numeration of samples and volume fractions

| Sample number | Lard (mL) | Sunflower oil (mL) | Sunflower oil (%) | Burnt oil (mL) | Burnt oil (%) |
|---------------|-----------|--------------------|-------------------|----------------|---------------|
| 1             | 150       | 0                  | 0                 | 0              | 0             |
| 2             | 120       | 30                 | 20                | 0              | 0             |
| 3             | 135       | 15                 | 10                | 0              | 0             |
| 4             | 142.5     | 7.5                | 5                 | 0              | 0             |
| 5             | 120       | 0                  | 0                 | 30             | 20            |
| 6             | 135       | 0                  | 0                 | 15             | 10            |
| 7             | 142.5     | 0                  | 0                 | 7.5            | 5             |



**Fig. 4** Pure lard and hybrid PCM samples



from 2.5% to almost 11% and is the largest for the highest volume fraction. Thermal conductivity is improved regarding burnt oil for volume fractions of 5% (Fig. 5a) and 10% (Fig. 5b), while for the highest volume fraction of 20% (Fig. 5c), there is no improvement in thermal conductivity. The improvement in thermal conductivity ranges from 0.8 to 1.4%, while degradation in the case of sunflower oil ranges from 0.8 to 2.6% and is the highest for a volume fraction of 20%. The specific numbers for experimentally determined thermal constants are presented in Table 4. The addition of burnt oil into the pork fat makes sense as thermal constants are improved and waste burnt oil could further improve the economy of the proposed hybrid PCMs. The waste burnt oil could be utilized in a useful manner with the proposed approach; however, the volume fraction should be from 5% up to 10% to achieve the best result in thermal constants.

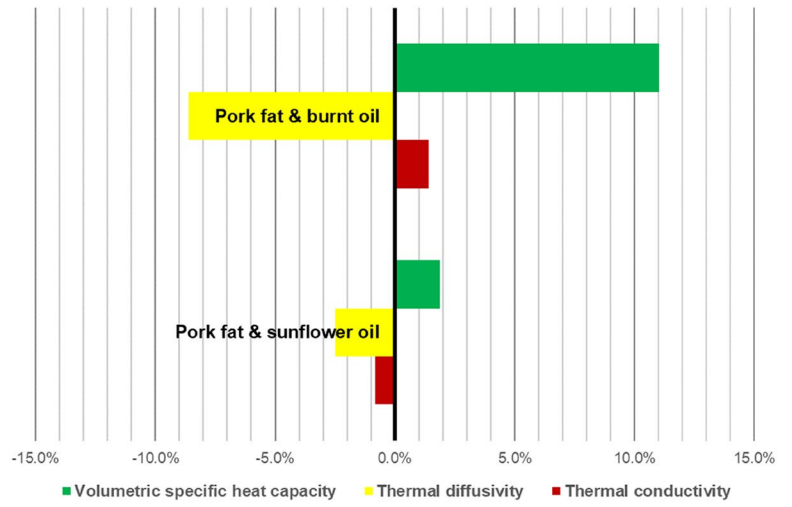
The addition of edible sunflower oil into the pork fat is not as effective as the addition of waste burnt oil, Table 4 The investigation was obtained in order to check the difference between pure oil and oil (waste) after thermal treatment, where it is clear that the advantage should be directed to the combination of pork fat mixed with

burnt oil. The highest improvement was in the case of the hybrid PCM pork fat & burnt oil, while the lowest improvement was in thermal conductivity (about 1%), and highest in the case of volumetric specific heat capacity in the amount of 9.3%. The only constant that was reduced in all cases was thermal diffusivity by about 7.8% on average, when compared to the base PCM (pork fat).

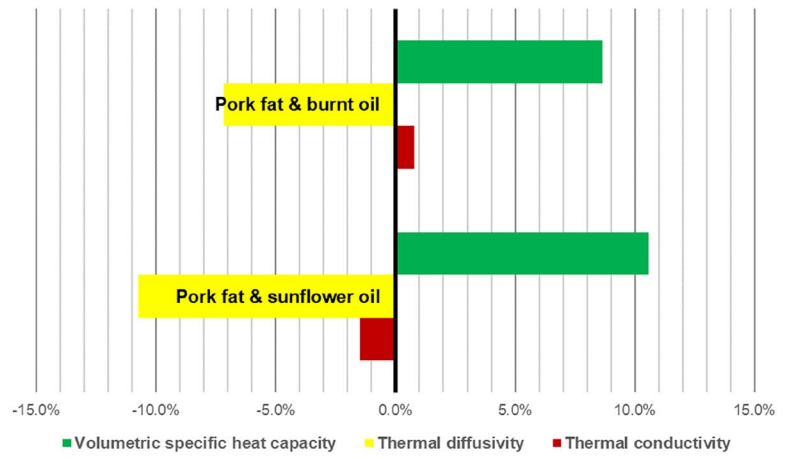
### Thermal conductivity

The thermal conductivity of the examined hybrid PCMs is presented in Fig. 6, where it is clear that the highest improvement was reached in the case of burnt oil with a volume fraction of 5%. Therefore, the suitable volume fraction of burnt oil should range somewhat from 5% up to 10% as already highlighted. The addition of sunflower oil into the pork fat does not make sense as the thermal conductivity of the pork fat is higher for all volume fractions when compared to the hybrid PCM, i.e., pork fat & sunflower oil.

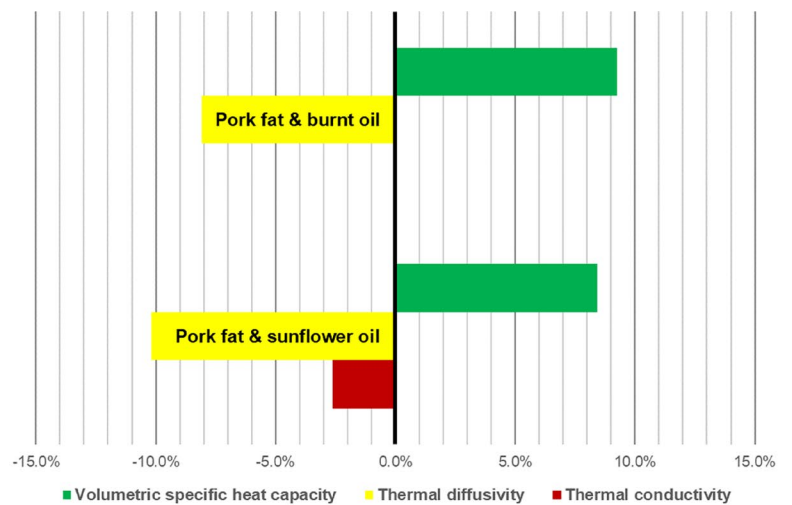
**Fig. 5** Thermal constants for hybrid PCMs (pork fat & burnt oil and pork fat & sunflower oil)



**(a)** Volume fraction 5 %



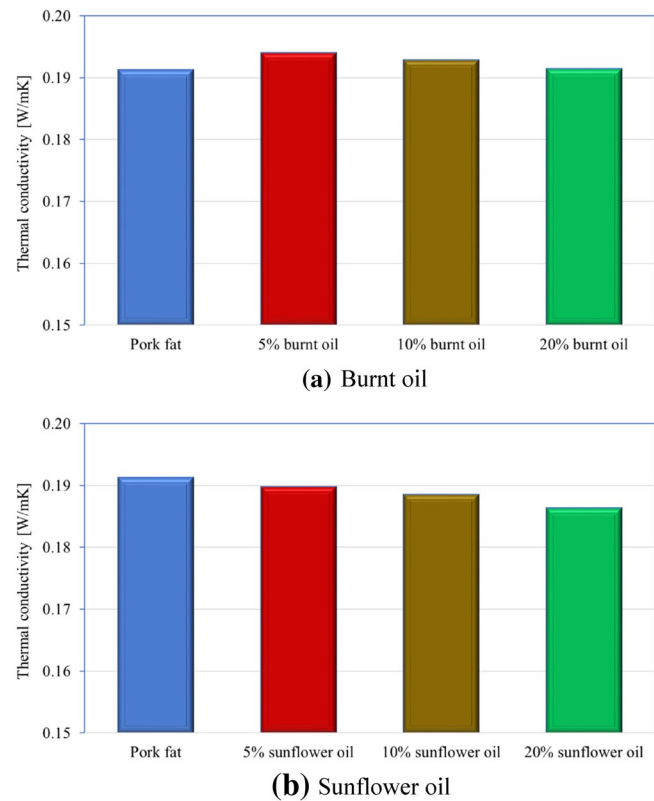
**(b)** Volume fraction 10%



**(c)** Volume fraction 20%

**Table 4** Thermal constants for investigated hybrid PCM

| Vol | PCM type      | Thermal conductivity (W/mK) | Thermal diffusivity (mm <sup>2</sup> /s) | Volumetric specific heat capacity (MJ/m <sup>3</sup> K) |
|-----|---------------|-----------------------------|--|---|
| 5%  | Pork fat      | 0.191                       | 0.127                                    | 1.512   |
|     | Sunflower oil | 0.186                       | 0.114                                    | 1.640   |
|     | Burnt oil     | 0.191                       | 0.116                                    | 1.653   |
| 10% | Pork fat      | 0.191                       | 0.127                                    | 1.512   |
|     | Sunflower oil | 0.189                       | 0.113                                    | 1.672   |
|     | Burnt oil     | 0.193                       | 0.117                                    | 1.643   |
| 20% | Pork fat      | 0.191                       | 0.127                                    | 1.512   |
|     | Sunflower oil | 0.186                       | 0.114                                    | 1.640   |
|     | Burnt oil     | 0.191                       | 0.116                                    | 1.653   |

**Fig. 6** Thermal conductivity

### Thermal diffusivity

The experimental results for thermal diffusivity are presented in Fig. 7, where it is clear that the addition of both burnt and edible sunflower oil into the pork fat as the base PCM is not effective. The thermal diffusivity degrades and the highest degradation is monitored for the hybrid PCM pork fat & sunflower oil, but more significantly for volume fractions higher than 5%, Fig. 7b. If thermal diffusivity needs to be reduced for the specific hybrid PCM, then the addition of the herein considered oils is effective for this specific case.

### Volumetric specific heat capacity

The final experimentally analyzed thermal constant was volumetric specific heat capacity, and the results are presented in Fig. 8. The best results were achieved for the pork fat & burnt oil hybrid PCM with a volume fraction of 5%, Fig. 8a. The lowest improvement of the volumetric specific heat capacity is for the case of sunflower oil, Fig. 8b. It is obvious that the addition of sunflower oil is not as suitable as in the case of burnt oil.

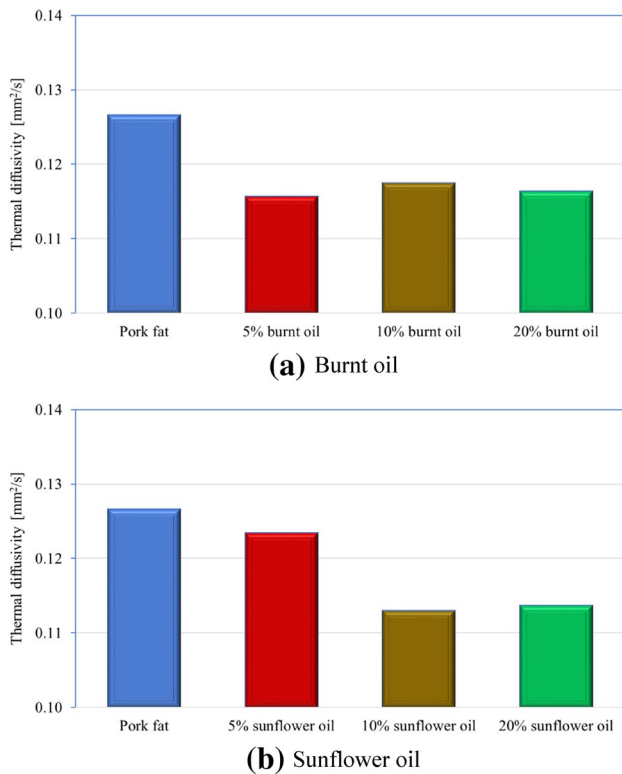


Fig. 7 Thermal diffusivity

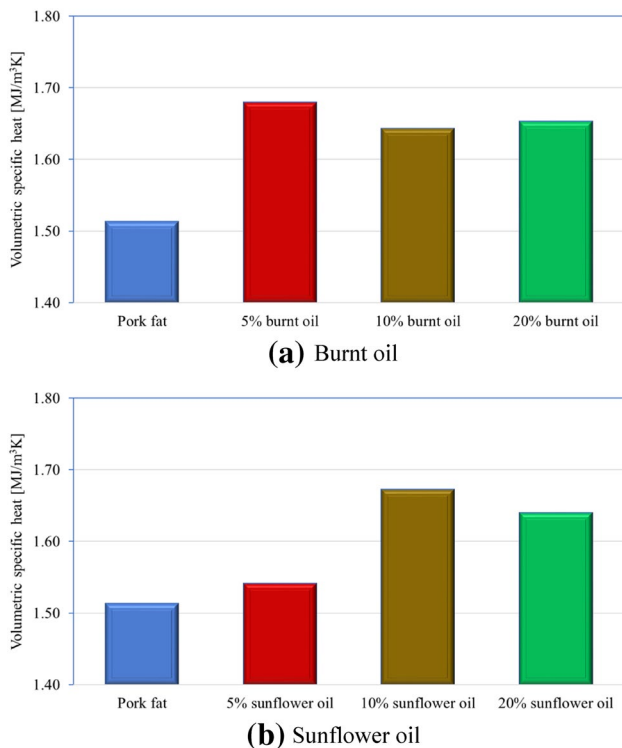


Fig. 8 Volumetric specific heat capacity

## Environmental and economic implications

PCMs based on lard and edible oils, as considered in this study, are ideally suited for a thermal storage application, encapsulated in the plasterboards used in building envelopes, for the passive cooling of PVs or low-temperature hot water storage, in the form of encapsulated spheres in hot water storage and buffer tanks, as they operate effectively in temperatures ranging between 30 and 45 °C, yet they cannot be applied above 50 °C (Kyriaki et al. 2018). The environmental assessment of PCMs is not a straightforward exercise, as it depends on their production on the one hand and on how they are incorporated in the components on the other hand where they are applied, as this determines their end-of-life treatment to a great extent (Chandel and Agarwal 2017). In all the aforementioned applications, dismantling and appropriate disposal is fairly easy; hence, one has to focus on the environmental impact when producing PCMs. The most widely used PCMs for such applications are paraffin waxes which on the one hand are quite energy-intensive to produce and contain ingredients such as vinyl-chloride and formaldehyde on the other hand, which can be hazardous when emitting vapors, in the case of fires or if inappropriately disposed of. Pork fat and edible oil wastes do not present these features; hence, they have a significant advantage. In order to evaluate their life cycle impact, a detailed analysis is needed which will be part of further research work in this matter, since the impact depends on the logistics of lards and edible oil wastes to a great extent. In regions where collection and reuse systems have been applied, it has been proven that they are of positive impact, as fats and oils would otherwise end up in sewerage systems with all the respective implications. It was also shown that economies of scale are of importance since these determine both the environmental and economic feasibility of the approach, (Tsoutsos et al. 2016). The relevant research findings related to the LCA (life cycle assessment) of the secondary PCM materials produced from waste cooling oils (such as glycerine and fatty acids), indicated potential of those products as more environmentally suitable materials, when compared with the paraffin based PCMs, (Baldassarri, et al. 2017). In the same work, the comparative assessment showed (i.e., the percentage of environmental impact expressed in %) that PCMs derived from waste cooking oil (Glycerine and Fatty Acid) have got much less environmental impact (climate change, human toxicity, ozone depletion, acidification, etc.) in comparison with market available PCMs. For instance, the climate change impact is around 11% for glycerine made from waste cooking oil, while market glycerine has got the same impact 100%. Moreover, the

human toxicity effect is less than 10% for glycerine from waste cooking oil, while the same factor is over 70% for the market glycerine, (Baldassarri et al. 2017). Previous findings in the mentioned research work are important since they indicate potential use of PCMs derived from waste cooking oils as more environmentally acceptable PCMs. The LCA analysis related to the production of the sunflower crop was provided in the study (Dekamin et al. 2018), where LCA for sunflower was compared with other seed crops such as soybean and canola oilseed. The results showed that the highest environmental impact is in the case of the sunflower production due to higher environmental load and more intense energy demands when compared with other mentioned crops. Previously specified data indicates that sunflower oil should be avoided as one of the components in the herein proposed hybrid PCMs when environmental aspect is being considered. Regarding the pork fat production, there are no available data for the LCA analysis in the existing literature; however, they are available data in the literature and related to the LCA methodology applied to the production of the pork meat (or specific pork products) in general (Bonou et al. 2020). The LCA evaluation should be conducted for the pork fat in order to be able to understand the overall environmental impact of the pork fat as PCM and to be able to compare it with other market available PCMs. More research efforts should be provided in that direction. Finally, to be able to determine the environmental impact of the novel herein proposed hybrid PCMs, the LCA analysis needs to be obtained and which was above the main scope of this work, but it would be part of the future research work.

With respect to the economic feasibility, one can notice that the typical price of market available PCMs ranges from about 5 €/kg up to 15 €/kg, (Rubitherm® Technologies GmbH, 2020). The typical wholesale price of pork fat is below 0.50 €/kg, (Alibaba.com 2020). The difference between the unit costs of pork fat and typical market available PCMs is quite significant. The addition of burnt oil enables the removal of waste so that it can further be used, i.e., waste as a resource that is used to improve the thermal effectiveness of the hybrid PCM. The addition of burnt oil into the base PCM reduces the quantity of the PCM, which finally affects the overall economy. The volume fraction of the added burnt waste oil defines the final unit cost of the hybrid PCM. The question to be asked is what in particular should be produced, i.e., what are the targeted thermal constants of the hybrid PCM. In any case, a reduction in the unit cost of the hybrid PCM (pork fat with burnt waste oil) is expected, i.e., the unit cost of the hybrid PCM is expected to be lower when compared to the unit cost of the pork fat-based PCM.

## Conclusions

This paper elaborates the experimental investigation of novel proposed hybrid PCMs as a combination of pork fat as the base PCM and burnt waste oil and sunflower oil. Pork fat is a largely accessible organic PCM that is thrown in large amounts as it becomes inedible after a certain period of time. Burnt oil from the food industry is also widely available and could be utilized; thus, the combination of pork fat and burnt oil could be turned into a useful novel hybrid PCM. The experimental work focused on the determination of the main thermal constants with respect to a specific volume fraction of added oils (burnt oil and sunflower oil), which ranged from 5 to 20%. The results revealed that the best hybrid phase change material was the combination of pork fat and waste burnt oil with respect to thermal constant improvements. The addition of waste burnt oil into the base PCM improves thermal conductivity in the amount of 1.4% and volumetric heat capacity in the amount of 11%. The best results for the thermal constants are reached for a volume fraction of 5%. Thermal diffusivity is reduced in all cases, i.e., for both added oils. The experimental results reveal that a combination of pork fat & waste burnt oil could be a good option for a novel hybrid PCM. The results of this research reveal the impact of the added oils on the thermal constants, which could be useful when producing a specific hybrid PCM with the desired thermal properties. The main limitation of this work is in its cyclic analysis (long-term stability) as well as in the investigation of the melting temperature for the produced hybrid PCMs, which is planned to be part of future research work. The presented results indicate a further possible reduction in PCM unit costs as the cost of a hybrid produced PCM (pork fat & edible oil) is lower when compared to the base PCM (pork fat), depending on the specific volume fraction. The proposed novel hybrid PCM is an organic PCM which is certainly more environmentally suitable than conventional PCMs, which are made of complex chemicals and followed with unavoidable environmental effects. To determine precise environmental impact of the novel herein proposed hybrid PCMs, the LCA analysis should be conducted as part of the future research work.

**Acknowledgements** This work was funded by the Croatian science foundation (Research project: Smart and hybrid cooling techniques for siliceous photovoltaic panels-IP-01-2018-2814).

## References

Alibaba.com (2020). <https://www.alibaba.com/showroom/pork-lard.html>. Accessed 30 Oct 2020




- Arıcı M, Bilgin F, Nižetić S, Papadopoulos AM (2018) Phase change material based cooling of photovoltaic panel: a simplified numerical model for the optimization of the phase change material layer and general economic evaluation. *J Clean Prod* 189:738–745. <https://doi.org/10.1016/j.jclepro.2018.04.057>
- Baldassarri C, Sala S, Caverzan A, Lamperti Tornaghi M (2017) Environmental and spatial assessment for the ecodesign of a cladding system with embedded Phase Change Materials. *Energy Build* 156:374–389. <https://doi.org/10.1016/j.enbuild.2017.09.011>
- Bohač V, Gustavsson MK, Kubičar L, Gustafsson SE (2000) Parameter estimations for measurements of thermal transport properties with the hot disk thermal constants analyzer. *Rev Sci Instrum* 71:15–19. <https://doi.org/10.1063/1.1150635>
- Bonou A, Colley TA, Hauschild MZ, Olsen SI, Birkved ME (2020) Life cycle assessment of Danish pork exports using different cooling technologies and comparison of upstream supply chain efficiencies between Denmark, China and Australia. *J Clean Prod* 244, Article number 118816. <https://doi.org/10.1016/j.jclepro.2019.118816>
- Chandel SS, Agarwal T (2017) Review of current state of research on energy storage, toxicity, health hazards and commercialization of phase changing materials. *Renew Sustain Energy Rev* 67:581–596. <https://doi.org/10.1016/j.rser.2016.09.070>
- Cheng F, Chen G, Lv Z, Yang C, Huang Z, Fang M, Liu Y, Wu X, Min X (2021) A novel nano-porous aluminum substrate with anodizing treatment to encapsulate 1-tetrapropanol as composite phase change materials for thermal energy utilization. *Chem Eng J* 404, Article number 124588. <https://doi.org/10.1016/j.cej.2020.124588>
- Das D, Bordoloi U, Kamble AD, Muigai HH, Pai RK, Kalita P (2021) Performance investigation of a rectangular spiral flow PV/T collector with a novel form-stable composite material. *Appl Therm Eng* 182, Article number 116035. <https://doi.org/10.1016/j.applthermaleng.2020.116035>
- Dekamin M, Barmaki M, Kanooni A (2018) Selecting the best environmental friendly oilseed crop by using Life Cycle Assessment, water footprint and analytic hierarchy process methods. *J Clean Prod* 198:1239–1250. <https://doi.org/10.1016/j.jclepro.2018.07.115>
- Dhamodharan P, Bakthavatsalam AK (2020) Experimental investigation on thermophysical properties of coconut oil and lauryl alcohol for energy recovery from cold condensate. *J Energy Storage* 31, Article number 101639. <https://doi.org/10.1016/j.est.2020.101639>
- Gustafsson SE (1991) Transient plane source techniques for thermal conductivity and thermal diffusivity measurements of solid materials. *Rev Sci Instrum* 62:797–804. <https://doi.org/10.1063/1.1142087>
- Hot Disk® (2020). <https://www.hotdiskinstruments.com/products-services/instruments/tps-500/>. Accessed 28 Sep 2020
- Huang Q, Li X, Zhang G, Deng J, Wang C (2021) Thermal management of Lithium-ion battery pack through the application of flexible form-stable composite phase change materials. *Appl Therm Eng* 183(1), Article number 116151. <https://doi.org/10.1016/j.applthermaleng.2020.116151>
- Hu X, Huang H, Hu Y, Lu X, Qin Y (2021) Novel bio-based composite phase change materials with reduced graphene oxide-functionalized spent coffee grounds for efficient solar-to-thermal energy storage. *Solar Energy Mater Solar Cells* 219, Article number 110790. <https://doi.org/10.1016/j.solmat.2020.110790>
- Ikutegbe CA, Farid MM (2020) Application of phase change material foam composites in the built environment: a critical review. *Renew Sustain Energy Rev* 131, Article number 110008. <https://doi.org/10.1016/j.rser.2020.110008>
- Jiang K, Liao G, E J, Zhang F, Chen J, Leng E (2020) Thermal management technology of power lithium-ion batteries based on the phase transition of materials: a review. *J Energy Storage* 32, Article number 101816. <https://doi.org/10.1016/j.est.2020.101816>
- Jurčević M, Nižetić S, Arıcı M, Očloň P (2020a) Comprehensive analysis of preparation strategies for phase change nanocomposites and nanofluids with brief overview of safety equipment. *J Clean Prod* 274, Article number 122963. <https://doi.org/10.1016/j.jclepro.2020.122963>
- Jurčević M, Penga Ž, Klarin B, Nižetić S (2020b) Numerical analysis and experimental validation of heat transfer during solidification of phase change material in a large domain. *J Energy Storage* 30: Article number 101543. <https://doi.org/10.1016/j.est.2020.101543>
- Kapton Polyimide Characteristics (2020). <https://dielectricmf.com/knowledge-base/kapton/>. Accessed 10 Oct 2020
- Konstantinidou CV, Lang W, Papadopoulos AM, Santamouris M (2019) Life Cycle and Life Cycle Cost implications of integrated Phase Change Materials in office buildings. *Int J Energy Res* 43(1):150–166. <https://doi.org/10.1002/er.4238>
- Krupa P, Malinaric S (2014) Using the transient plane source method for measuring thermal parameters of electroceramics. *Int J Mech Mechatron Eng* 8(5). <https://doi.org/10.5281/zenodo.1092325>
- Kyriaki E, Konstantinidou C, Giama E, Papadopoulos AM (2018) Life Cycle Analysis (LCA) and Life Cycle Cost Analysis (LCCA) of Phase Change Materials (PCM) for thermal applications: a review. *Int J Energy Res* 42(9):3068–3077. <https://doi.org/10.1002/er.3945>
- Kyriaki E, Stergiopoulos S, Papadopoulos AM (2020) Alternative storage options for solar thermal systems. *Int J Energy Res* 45(1):151–166. <https://doi.org/10.1002/er.5160>
- Log T, Gustafsson SE (1995) Transient plane source (TPS) technique for measuring thermal transport properties of building materials. *Fire Mater* 19:43–49. <https://doi.org/10.1002/fam.810190107>
- Mousa H, Naser J, Gujarathi AM, Al-Sawafi S (2019) Experimental study and analysis of solar still desalination using phase change materials. *J Energy Storage* 26, Article number 100959. <https://doi.org/10.1016/j.est.2019.100959>
- Nižetić S, Papadopoulos AM, Giama E (2017) Comprehensive analysis and general economic-environmental evaluation of cooling techniques for photovoltaic panels, part I: passive cooling techniques. *Energy Convers Manage* 149:334–354. <https://doi.org/10.1016/j.enconman.2017.07.022>
- Nižetić S, Arıcı M, Bilgin F, Grubišić-Čabro F (2018) Investigation of pork fat as potential novel phase change material for passive cooling applications in photovoltaics. *J Clean Prod* 170:1006–1016. <https://doi.org/10.1016/j.jclepro.2017.09.164>
- Nižetić S, Jurčević M, Arıcı M, Arasu AV, Xie G (2020) Nano-enhanced phase change materials and fluids in energy applications: a review. *Renew Sustain Energy Rev* 129, Article number 109931. <https://doi.org/10.1016/j.rser.2020.109931>
- Omara AAM, Abuelnuor AAA, Mohammed HA, Khiadani M (2020) Phase change materials (PCMs) for improving solar still productivity: a review. *J Therm Anal Calorim* 139:1585–1617. <https://doi.org/10.1007/s10973-019-08645-3>
- Rubitherm® Technologies GmbH (2020). <https://www.rubitherm.eu/>. Accessed 22 Oct 2020
- Scopus® (2020). <https://www.scopus.com/search/form.uri?display=basic>. Accessed 22 Oct 2020
- Pico Technology (2020) <https://www.picotech.com/data-logger/tc-08/usb-tc-08-accessories>. Accessed 18 April 2020
- Engineering ToolBox (2020) [https://www.engineeringtoolbox.com/oil-melting-point-d\\_1088.html](https://www.engineeringtoolbox.com/oil-melting-point-d_1088.html). Accessed 20 Sep 2020
- Tsoutsos TD, Tournaki S, Parafba O, Kaminaris SD (2016) The Used Cooking Oil-to-biodiesel chain in Europe assessment of best practices and environmental performance. *Renew Sustain Energy Rev* 54:74–83. <https://doi.org/10.1016/j.rser.2015.09.039>
- Wu W, Wang X, Xia M, Dou Y, Yin Z, Wang J, Lu P (2020) A novel composite PCM for seasonal thermal energy storage of solar water

heating system. *Renew Energy* 161:457–469. <https://doi.org/10.1016/j.renene.2020.06.147>

Yu G, Yang H, Yan Z, Kyeredey Ansah M (2021) A review of designs and performance of façade-based building integrated photovoltaic-thermal (BIPVT) systems. *Appl Therm Eng* 182, Article number 11608. <https://doi.org/10.1016/j.applthermaleng.2020.116081>

**Publisher's Note** Springer Nature remains neutral with regard to jurisdictional claims in published maps and institutional affiliations.

## Authors and Affiliations

Mišo Jurčević<sup>1</sup> · Sandro Nižetić<sup>1</sup>  · Duje Čoko<sup>2</sup> · Anh Tuan Hoang<sup>3</sup> · Agis M. Papadopoulos<sup>4</sup>

<sup>1</sup> LTEF-Laboratory for Thermodynamics and Energy Efficiency, Faculty of Electrical Engineering, Mechanical Engineering and Naval Architecture, University of Split, Rudjera Boskovicica 32, 21000 Split, Croatia

<sup>2</sup> Department of Electronics, Faculty of Electrical and Mechanical Engineering and Naval Architecture, University of Split, Rudjera Boskovicica 32, 21000 Split, Croatia

<sup>3</sup> Institute of Engineering, Ho Chi Minh City University of Technology (HUTECH), Ho Chi Minh City, Vietnam

<sup>4</sup> Process Equipment Design Laboratory, Dept. of Mechanical Engineering, Aristotle University, Thessaloniki, Greece



## Appendix E

Title: Implementation of phase change materials for thermal regulation of photovoltaic thermal systems: Comprehensive analysis of design approaches

Authors: Nižetić S., Jurčević M., Čoko D., Arici M., Hoang A.T.

Publisher: *Elsevier*

Journal: *Energy*

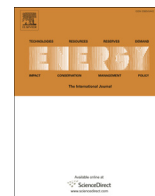
Edition, ID, year: 228, 120546, 2021.

Indexed in: Scopus, Science Citation Index Expanded, Current Contents, Web of Science, etc.

Journal Impact Factor: 8.857 Q1 (WoS and SJR-2021.)

DOI: <https://doi.org/10.1016/j.energy.2021.120546>

**Abstract:** This work was focused on the investigation of various photovoltaic thermal (PVT) solar collector designs incorporating phase change materials (PVT-PCM systems) as suitable material for thermal management. In general, the PCM materials utilized in such systems were analyzed along with a discussion regarding the main thermal properties. The experimental works were covered from existing literature and related to PVT-PCM systems in various climates. The results revealed the importance of a PVT-PCM collector design concerning the overall efficiency improvement of systems. Depending on the specific design, as well as on the specific working fluid (water, air, or nanofluids), the electrical efficiency improvement was usually less than 20%, while the improvement in thermal efficiency was usually up to 70%. The electrical efficiency improvement is especially sensitive to the specific PVT-PCM collector design. The economy of the PVT-PCM system was not addressed well in the existing literature as well as its environmental evaluation. The usual payback time of the PTV-PCM systems ranged from 4 to 15 years. The conducted review indicated the necessity for more intense research investigations related to improvements in collector designs (tube geometry and layout, novel absorbers, optimization of the PCM layer) and for an integral assessment of PVT-PCM collector designs, considering performance, economic and environmental evaluations.



# Implementation of phase change materials for thermal regulation of photovoltaic thermal systems: Comprehensive analysis of design approaches



Sandro Nižetić<sup>a,\*</sup>, Mišo Jurčević<sup>a</sup>, Duje Čoko<sup>a</sup>, Müslüm Arıcı<sup>b</sup>, Anh Tuan Hoang<sup>c</sup>

<sup>a</sup> University of Split, Rudjera Boskovicica 32, 21000, Split, Croatia

<sup>b</sup> Department of Mechanical Engineering, Faculty of Engineering, Kocaeli University, Umuttepe Campus, Kocaeli, 41001, Turkey

<sup>c</sup> Institute of Engineering, Ho Chi Minh City University of Technology (HUTECH), Ho Chi Minh City, Viet Nam

## ARTICLE INFO

### Article history:

Received 10 January 2021

Received in revised form

10 March 2021

Accepted 31 March 2021

Available online 7 April 2021

### Keywords:

Phase change materials (PCM)

Photovoltaics

Cooling

Efficiency

Solar energy

PVT-PCM

## ABSTRACT

This work was focused on the investigation of various photovoltaic thermal (PVT) solar collector designs incorporating phase change materials (PVT-PCM systems) as suitable material for thermal management. In general, the PCM materials utilized in such systems were analyzed along with a discussion regarding the main thermal properties. The experimental works were covered from existing literature and related to PVT-PCM systems in various climates. The results revealed the importance of a PVT-PCM collector design concerning the overall efficiency improvement of systems. Depending on the specific design, as well as on the specific working fluid (water, air, or nanofluids), the electrical efficiency improvement was usually less than 20%, while the improvement in thermal efficiency was usually up to 70%. The electrical efficiency improvement is especially sensitive to the specific PVT-PCM collector design. The economy of the PVT-PCM system was not addressed well in the existing literature as well as its environmental evaluation. The usual payback time of the PTV-PCM systems ranged from 4 to 15 years. The conducted review indicated the necessity for more intense research investigations related to improvements in collector designs (tube geometry and layout, novel absorbers, optimization of the PCM layer) and for an integral assessment of PVT-PCM collector designs, considering performance, economic and environmental evaluations.

© 2021 Elsevier Ltd. All rights reserved.

## 1. Introduction

The Paris climate agreement [1] indicated significant investments in renewable energy technologies to restrain CO<sub>2</sub> emissions and reduce the general negative impacts of the population on the environment, [2]. The relevance of renewable generation technologies to reach the desired climate goals is especially important in wind [3] and solar photovoltaic technologies, [4]. More specifically, photovoltaic technologies lead with respect to the overall installed global capacities since over 100 GW of newly installed PV capacities were realized in 2019 [5], with the current overall installed PV capacities reaching almost 600 GW, [6]. Moreover, the unit cost of PV systems has gradually reduced in recent years, especially regarding residential PV systems, with the

unit cost being at about 1.5 €/Wp up to 3.5 €/Wp, depending on the specific world region, Fig. 1.

Although the unit cost of PV systems has generally been reduced, there is still an issue with relatively high investment costs regarding PV systems in specific economies. The energy conversion efficiency of most used PV technologies on the market (based) is below 20%, mostly ranging from 13% to about 18%, depending on the specific technology [7] and climate circumstances, [8]. The long-term performance of PV systems [9], as well as efficiency of grids and energy storage management [10], are also identified as areas where there is space for further advancements. The end life management of PV systems (waste management and recycling in general) [11], is also a crucial and important research area that needs careful attention since there are projections for an intense cumulative growth of waste volumes caused by PV technologies, [12]. In recent years, various technical possibilities have been investigated to detect novel application areas for current PV technologies, i.e. to ensure increases in PV capacities since some regions

\* Corresponding author.

E-mail address: [snizetic@fesb.hr](mailto:snizetic@fesb.hr) (S. Nižetić).

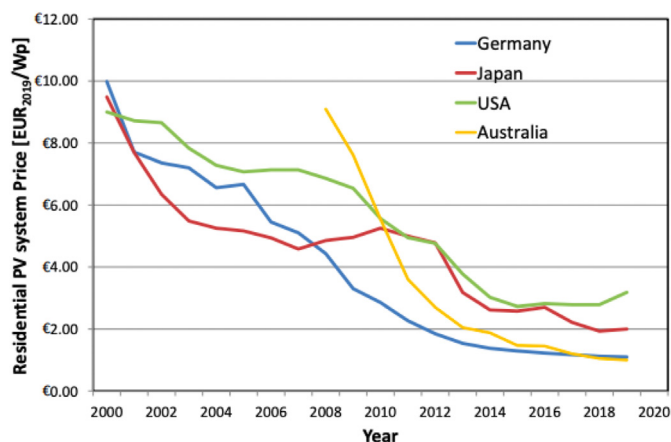


Fig. 1. Price trend regarding unit cost of residential PV systems [5].

of the world have limited land resources for the installation of PV systems. Concerning the previous, there has been a significant rise in installations of floating PV systems [13], for instance, implementation in agricultural purposes, such as agrivoltaics [14], where important benefits regarding the improvement of PV performance in these specific conditions exist. One possible way to improve the effectiveness of PV technologies when taking into account a limited surface area for installation is to implement photovoltaic-thermal (PVT) systems, [15]. The main comparative benefit of PVT systems is the simultaneous production of both electricity and thermal output per available surface area. In typical residential applications, there are usually demands for both electricity and heat, which makes PVT systems suitable for the mentioned applications, especially from a perspective of renewable energy utilization in buildings. The main issue with market present PVT technologies are the low overall installed capacities, mostly due to high unit costs per  $m^2$ , when compared with other renewable generation technologies, such as photovoltaics or solar thermal systems. PVT solar collectors are also interesting for other applications since various temperature levels of produced hot water can be reached, which opens a quite wide application area regarding PVT systems, i.e. from low-temperature systems to process heat in industrial applications. The main and most crucial part of a PVT system is the PVT collector, where the specific design affects the overall efficiency (electrical and thermal) as well as the temperature level of the produced hot water. Study [16] examined the thermal behavior of a concentrated PVT system (CPVT) which enabled the production of high-temperature hot water due to a parabolic design and ensured a solar energy concentration. The specific parabolic design through the system was elaborated with provided numerical modelling related to the heat transfer. The numerical results indicated that the electrical efficiency was improved by 38.2%, while the thermal efficiency was decreased by 8.3%. The effects of the tube length, absorber thickness, i.e. specific design parameters were thoroughly investigated. A recent study [17], discussed the specific design of a water-cooled PVT solar collector that leads to performance improvements with an economic overview analysis. The design improvement was focused on the specific construction of a heat exchanger applied on the backside surface of the PV panel. The proposed PVT collector design indicated both improvements in electrical and thermal efficiency, with a payback time of 7.4 years. A polymeric PVT collector design was proposed in work [18] and tested in laboratory conditions. A copper tube heat exchanger was mounted on the backside surface of the PV panel and fitted into a polymeric cast. The performance analysis indicated a maximal 20%

reach of thermal efficiency, however, the electrical efficiency decreased by about  $0.03\%/^{\circ}C$  (effect of polymeric material which acts as heat insulator). The use of nanomaterials in the PVT-PCM based collector designs were also investigated since heat transfer characteristics can be improved with the utilization of nanomaterials as it was indicated in review [19].

It is obvious that quite a wide range of PVT designs are possible but the most interesting designs are ones that assume the implementation of phase change materials (PCM). The main advantage of PCMs is their favorable effect on the thermal efficiency of PVT systems, but to ensure an increase in electrical efficiency, the thermal regulation of the PCM layer needs to be ensured. On the other side, the application of a PCM is demanding for modelling and the assessment of basic parameters or melting processes in general, [20]. In the previous sense, optimization related to PCM systems, such as thermal storage systems for instance Ref. [21], is key, which should also be applied in the case of PVT-PCM collectors. In recent years, different concepts of PVT-PCM collectors have been investigated, which showed different performance indicators. PVT-PCM collectors can be designed from various aspects where priorities need to be clear, i.e. the design request needs to be determined and focused on either the highest thermal efficiency or on reaching electrical efficiency improvement (or their targeted combinations).

The main goal of this work was directed to the comprehensive analysis of experimentally tested PVT-PCM collectors in order to highlight the most efficient designs, and the main features of various tested PVT-PCM designs. Based on the conducted analysis, the performance indicators were thoroughly summarized, as well as future directions in the field. It needs to be emphasized that there have already been some published review works related to PVT systems but have covered other wider aspects, while the herein presented review was more specific. For instance, the recent review work [22] was focused on PCMs as well as nano-enhanced PCMs (NPCMs) for thermal energy storage applications and PVT systems. Technical and future development trends were discussed to understand the general fundamental issues and problems. Various aspects of PCMs were analyzed in the mentioned work, the effect of NPCMs with a focus on different applications such as HVAC systems (Heating, Ventilation, and Air-Conditioning), thermal energy storage, building-integrated photovoltaics, etc. Advancements in PVT systems were discussed and analyzed, i.e. ones with and without PCMs using energy, exergy, and an exergonomic analysis, [23]. The applied approach was useful since it allowed designers to determine specific strategies to provide feasible and efficient PVT solutions. The presented work was mainly based on a thermodynamic analysis but the focus was not directed towards an experimental analysis. Review study [24] analyzed the thermo-physical properties of NPCMs used in PVT systems. The improvement in electrical and thermal efficiency was thoroughly examined for different setups, with provided performance improvements. In this review work, the focus of the investigation was narrowed to the specific designs of PVT-PCM solar collectors, which is a novelty with respect to existing research findings due to the targeted objective of the work and importance of PCMs for the considered application. Due to the general importance of PCM materials in PVT-PCM systems, there was a necessity for an in-depth analysis and the herein presented review work.

### 1.1. Review methodology

The focus of this work was to examine specific PVT-PCM designs in the last five years, i.e. period 2015–2020 Scopus® [25] database was explored with appropriate keywords directed to PVT-PCM systems (such as PVT, PCM, etc.). The experimental works mainly discussed and focused on various PVT-PCM designs in different

climates, with only few numerical studies being discussed. Basics related to PVT technologies were discussed to understand the key features and use of PCM materials in PVT-PCM systems, in order to determine the most appropriate PCMs and their expected physical properties. According to the conducted analysis, the performance features of PVT-PCM systems were thoroughly elaborated, where both environmental and economic aspects were noted.

## 2. General characteristics of PVT systems

Photovoltaic thermal systems are initially designed to ensure both electricity and thermal output, i.e. the main idea of PVT systems is to efficiently use the available solar potential in circumstances of limited surface area for the installation of solar collectors. Currently, there are only several PVT collector producers on the market, where the usual average unit cost is about 300 €/m<sup>2</sup> [26], but the unit costs can often go over 400 €/m<sup>2</sup>, depending on the specific producer. The investment cost in PVT systems is considerably higher when compared to typical PV systems, thus the techno-economic viability of PVT systems should be carefully examined. For instance, a typical roof PV system has a unit cost for residential applications of about 2.0 €/Wp (up to a 10 kWp system in nominal size, [27]), which is about 200 €/m<sup>2</sup>. The thermal part of a PVT panel can be similar in unit cost or higher when compared to the unit cost of a PV panel. A typical PVT panel consists of a conventional PV panel that is equipped with a specially designed heat exchanger, which is attached to the backside surface of the PV panel and used to collect the waste heat from the PV panel, Fig. 2, [28]. The regular design of a market available PVT panel is usually made from cast, absorber surface, glass, ribbon, and a heat exchanger made of copper tubes and thermal insulation. There are two main types of PVT collectors, which can be divided based on the working fluid, i.e. PVT air and PVT water (liquid) based collectors. Regarding glazing, there are uncovered, covered, and concentrating CPVT systems, i.e. where each mentioned glazing configuration affects the level of the PVT panel operating temperature.

Thermal power output designs from PVT systems are significantly higher than nominal electric power outputs, by a factor ranging from about 3 or even more, [28]. Regarding the temperature levels of produced hot water, PVT systems are perfectly designed to work on low operating temperatures (low-temperature applications, i.e. water temperatures below 50 °C), where mid-temperature levels are also reachable (around 50 °C), depending from the specific PVT design. There are also concentrating CPVT systems, which can reach higher operating temperature levels, i.e. over 80 °C. One of the main PVT system tasks is to ensure improvement in the electric performance of the PV panel, in the PVT configuration, when compared to an identical PV panel (referent PV panel), but not in the PVT configuration. Silicon-based photovoltaic technologies suffer from efficiency degradation due to increased working temperatures [29],

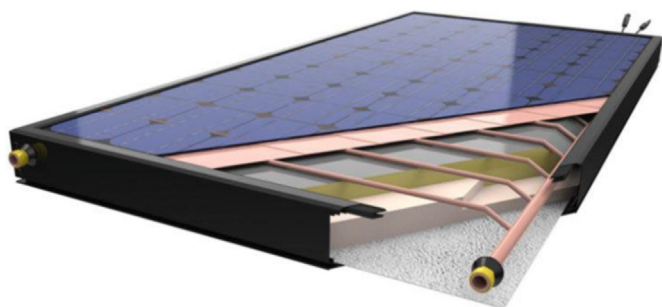


Fig. 2. Typical configuration of PVT panel [28].

there is thus an issue associated with the control of PV panel operating temperatures in the case of PVT systems. One goal is to try to reduce the lowest possible operating temperature of the PV panel (to secure improvement in electrical efficiency), while the other goal being to secure an appropriate temperature level of produced hot water, which should be at least 45 °C and above, depending from the specific requests (for instance, in cases of high hot water demands). In fact, PVT systems need to balance two opposite goals, which request a careful PVT system design and suitable match with the specific assumed application (energy demands). Due to a general request for improvement in the electrical efficiency of PV panels in PVT configurations on limited surfaces, monocrystalline silicon PV technologies are usually implemented in PVT collectors, since they have a higher energy conversion efficiency when compared to most polycrystalline PV panels. The nominal efficiency of monocrystalline PV panels in PVT systems is mostly above 15%. The cooling effect enabled in a PVT design can improve the overall electricity production from the PV panel, i.e. performance improvement of over 20% when compared to the same sized but non-cooled PV panels. The main application area of PVT systems is for residential purposes (domestic hot water), or in circumstances where there is a high hot water demand and issues linked with electric grid instability, Fig. 3. The producers of PVT systems typically provide warranties of about 10 years [28], and the main PVT collector producers originate from Europe, [30].

Moreover, the potential feature of PVT systems is to provide hot water pre-heating used for central heating systems and reduce the utilization of primary emergents, i.e. fossil fuel. There is also a potential for higher PVT system penetration in the case of countries that are requesting, or even subsidizing renewable energy sources in energy renovations, especially in the building sector (integration with heat pump systems for instance). Depending on the produced level of operating fluid PVT systems, they can also be used for process heat, but CPVT systems are assumed to be utilized in that case. There is also a reasonable potential for the utilization of PVT systems in agriculture for drying processes or desalination purposes.

## 3. Implementation of phase change materials in PVT-PCM collectors

The application of PCM materials is widely represented in various engineering applications nowadays, the focus being related to thermal energy storage issues, [31]. PVT systems are suitable for the application of PCM materials since the overtaken heat by the PCM layer can reduce the PV panel operating temperature and improve the general PV panel performance. On the other side, the overtaken heat by the PCM layer can be effectively used to generate thermal output and ensure a suitable temperature level of produced hot water. There are various types of available PCM materials, i.e. organic, inorganic, hygroscopic, etc., where the general selection depends on the specifics desired, i.e. targeted physical properties such as melting temperature, latent heat, specific heat capacity, and others. The main types and general physical characteristics of used PCMs in the case of PVT solar collectors were analyzed and summarized in Table 1 and based on the experimentally examined and tested PVT concepts.

Based on the conducted analysis related to the types of used PCM materials in PVT systems, it can be noted that various PCMs are available and can cover quite a wide melting temperature range from about 22 °C up to 60 °C, Table 2. As PVT systems are mainly designed for low-temperature applications, most of the examined PCM materials have melting temperatures below 45 °C. The thermal conductivity of the PCMs used in PVT systems is not high and ranges from 0.19 W/mK up to 0.24 W/mK. The specific heat capacity

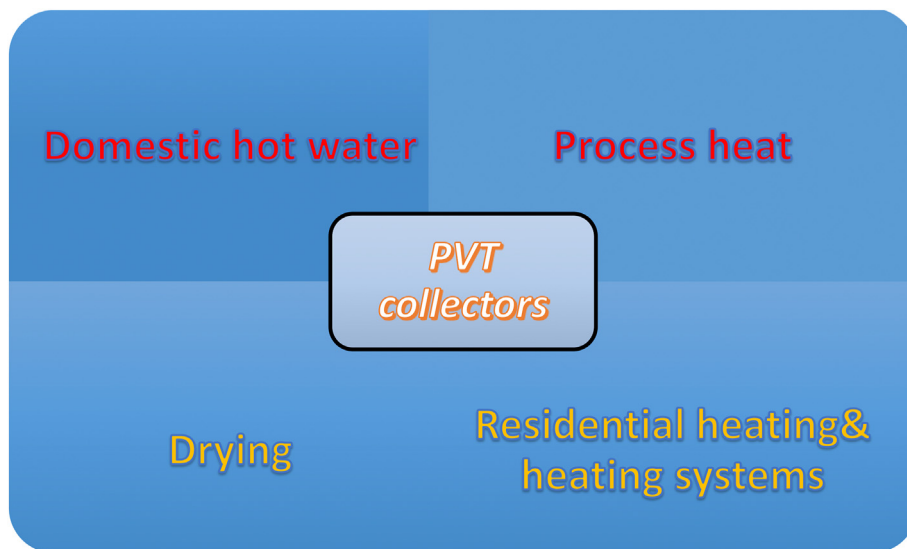


Fig. 3. Main application areas of PVT collectors.

Table 1  
Overview of used PCMs in PVT collectors.

| PCM material                 | Melting temperature (°C) | Thermal conductivity (W/mK) | Latent heat (kJ/kg) | Specific heat (kJ/kgK) | References |
|------------------------------|--------------------------|-----------------------------|---------------------|------------------------|------------|
| S21                          | 23                       | 0.234                       | 170                 | 2.2                    | [32]       |
| RT44                         | 41–44                    | 0.20                        | 168                 | 2.0                    | [33]       |
| RT35 HC                      | 34–36                    | 0.2                         | 240                 | 2.0                    | [34]       |
| RT28HC                       | 27–29                    | 0.2                         | 250                 | 2.0                    | [34]       |
| RT25HC                       | 22–26                    | 0.2                         | 210                 | 2.0                    | [34]       |
| Merck 107158 (paraffin)      | 57–60                    | 0.24                        | 220                 | 2.9                    | [35]       |
| PLUSICE S25                  | 25                       | 0.54                        | 180                 | 2.2                    | [36]       |
| RT-35HC                      | 35                       | 0.166                       | 240                 | 2.1                    | [37]       |
| A44                          | 44                       | 0.18                        | 242                 | 2.15                   | [38]       |
| Paraffin wax                 | 57                       | 0.24                        | 220                 | 2.1                    | [39]       |
| RT50                         | 50                       | 0.2                         | 160                 | 2.0                    | [40]       |
| Lauric acid                  | 44–46                    | 0.19                        | 228                 | 1.7                    | [41]       |
| PCM32/280                    | 32                       | 0.4                         | 186                 | –                      | [42]       |
| Octadecane                   | 28                       | 0.21                        | 244                 | 1.9                    | [43]       |
| Paraffin wax (Merck, 107151) | 46–48                    | 0.24                        | 220                 | 2.9                    | [44]       |

Table 2  
Typical range of main physical PCM material characteristics used in PVT-PCM collectors.

| Melting temperature (°C) | Thermal conductivity (W/mK) | Latent heat (kJ/kg) | Specific heat (kJ/kgK) |
|--------------------------|-----------------------------|---------------------|------------------------|
| 22–60                    | 0.19–0.24                   | 160–250             | 1.7–2.9                |

ranges from 1.7 kJ/kgK up to 2.9 kJ/kgK, while the latent heat ranges from 160 kJ/kg up to 250 kJ/kg. The expected range of the main physical PCM material characteristics in PVT systems is presented in Table 2.

The main problem with the PCM is its relatively high unit cost that ranges from about 5 €/kg to a maximal 15 €/kg for market available PCMs [45], however, it is usually below 10 €/kg for most PCMs. The unit cost of PCMs is increased with improved properties related to latent heat and thermal conductivity, where various types of PCMs can be produced with respect to specific requested physical properties. Besides the issue associated with high unit costs, the second problem with PCMs is their thermal management, which is usually demanding. Depending on the specific technical application, the effect of the PCM layer can be beneficial in a limited period, while in other operating circumstances, the PCM layer reduces performance, where the final effect related to performance improvement can be modest, or insignificant from a techno-

economic point of view, [46]. The thickness of the PCM layer has a direct effect on the quantity of the absorbed heat from the PV panel while later it affects the thermal management of the PV panel (removal of absorbed heat into the surroundings). A configuration with a lower PCM thickness would remove absorbed heat more efficiently to the surroundings when compared to the setup with a higher thickness of the PCM layer, for the same operating circumstances. The setup with a higher PCM thickness would be able to absorb more heat in a shorter time. Finally, the setup with a thicker PCM layer would be warmer in specific morning hours (since it absorbs heat faster), while a setup with a higher thicker PCM layer would be at a lower temperature in general in the same period of the day. Later, in periods of higher solar insolation levels, the situation would be vice versa in. Periods with higher PVT-PCM panel operating temperatures would reduce electrical performance. In the case of PVT systems, the application of a PCM material can be an issue from an overall weight aspect on specific roof surfaces, which



requires a careful design in that sense. The specific thickness of a PCM layer can be optimized with respect to certain climate circumstances and general operating conditions in order to maximize performance and reduce unit costs. In general, the application of a PCM in PVT systems should be limited to low-temperature applications, i.e. with operating temperatures up to 60 °C to secure the long-term stability of PCM physical properties. Some general requests related to PCM materials in PVT solar collectors are discussed in Table 3. The most important features of PCM materials are related to suitable thermal characteristics, stable melting points, and long-term stability. The environmental aspect associated with the utilization of PCMs should also be carefully evaluated, which unfortunately was not the case with respect to existing research findings where PCMs were considered in PVT systems.

#### 4. Analysis of design approaches for PVT-PCM collectors

PVT systems are followed by high unit costs, i.e. relatively high collector retail prices per m<sup>2</sup> as already highlighted. Concerning the previous aspect, a proper PVT solar collector design is crucial to secure the techno-economic viability of PVT systems. Specific designs of PVT solar collectors were thoroughly discussed in the upcoming sections of the paper and focused on PVT-PCM systems. The most relevant research works in recent years have been analyzed, which dealt with the experimental evaluation of specific PVT solar collector designs that involved the application of a PCM.

An air-based PVT collector with incorporated thermal energy storage (TES) was designed and experimentally tested under Australian climate conditions. The specific PVT collector design is presented in Fig. 4, where the examined system had a rotational capability (360°), [32]. The PVT collector consisted of air channels (Fig. 4b), where the air circulated as working fluid. The system was attached with a PCM TES that consisted of twelve PCM bricks, which were filled with an S21 PCM material. Regarding the specific design of the PVT collector, it is quite simple (the design procedure regarding the specific air-channel geometry was not thoroughly elaborated), as an air channel of straight geometry was used, but the main strength of the work was related to a thoroughly elaborated optimization strategy. Various variables were incorporated in the developed numerical model such as slope, flow rate, orientation and coupled with experimental readings followed by statistical analysis. The applied approach allowed for the detection of systematic improvements leading to the performance improvement of PVT-PCM systems through an optimal design. The use of air as the coolant causes less effective heat transfer, which finally affects PVT panel performance. Besides air temperature, air mass flow rates have a key role regarding the effectiveness of heat transfer and also affect operational energy. Based on the achieved experimental results, the overall efficiency of the system was improved in a range of about 37% to over 40%, with a TES capacity improvement of about 13% to almost 80%. Economic and environmental evaluations were

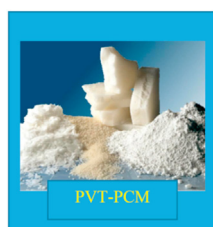
not elaborated.

An interesting concept of a PVT-PCM and water-based cooled PVT collector was discussed in work [33], where the PVT collector was an integral part of a desiccant solar cooling system. The specific design of the PVT-PCM solar collector is shown in Fig. 5, which consisted of a PV panel and a straight set of channels below it to enable water flow for the cooling of the PV panel. Below the water channels, an absorber was provided, a PCM layer (RT 44, thickness not reported), and a layer of thermal insulation. A discussion related to the selection and general design of the water flow channels was not reported. Numerical modelling was obtained for the considered energy system but with a constant water mass flow rate (sensitivity analysis should therefore be conducted).

Besides numerical modeling, the system was tested under Iranian climate operating conditions (Bandar Abbas). The results revealed that the electrical efficiency of the PV panel ranged from 13.6% to 17.7%, while the maximal thermal efficiency reached about 68%. The proposed PVT-PCM configuration showed a favorable effect on the examined solar desiccant cooling system. The economic and environmental aspects of the proposed PVT concept were not discussed. Straight channels were used instead of tubes (which is a usual setup), and which is easier for assembling where more uniform cooling could be provided when compared to a typical tube layout setup. A metal section with water channels and absorber plate is directly attached on the PCM layer, which is a good approach when ensuring an effective heat transfer between water and PCM layer. Moreover, the proposed concept allows a more flexible thermal management of the PCM layer. The pressure drop could be more intense due to the specific channel geometry and potentially cause higher operational costs.

The performance of a PVT-PCM panel was examined for Mexican climate conditions, i.e. for three cities in Mexico (Mexico City, Monterrey, and Campeche). The schematic of the specific PVT collector design is shown in Fig. 6, [34]. The PVT collector consisted of a PV panel, PCM material layer and an air channel was ensured below it and was finalized with a thermal insulation layer. Three types of PCMs were used in the obtained numerical investigation (RT35 HC, RT28HC, RT25HC). It is not clear how the specific PVT collector design was selected, there is no elaboration regarding the design approach. One of the major drawbacks is the absence of an experimental approach since the work only contains data gained by numerical modeling. An important value of the study is reflected through the examination of various types of applied PCMs which were suited for the specific examined geographical locations (climate), to reach the best possible performance of the PVT-PCM solar collector. The overall improvement in performance ranged from 20% to 24%, when compared to the case without a PCM, the best improvement being reached for Savannah climate conditions. The electrical efficiency ranged from 8% to 10.6%, while thermal efficiency ranged from 22% to 33%. With air being used as the coolant, both electrical and thermal efficiencies were not high. The

**Table 3**  
General requests for PCM materials in PVT collectors.



- Low unit cost
- High thermal properties (latent heat, thermal conductivity, specific heat capacity),
- Stable melting point,
- Environmental suitability (recycling, non-toxic),
- Efficient phase-change transition,
- Long term stability.

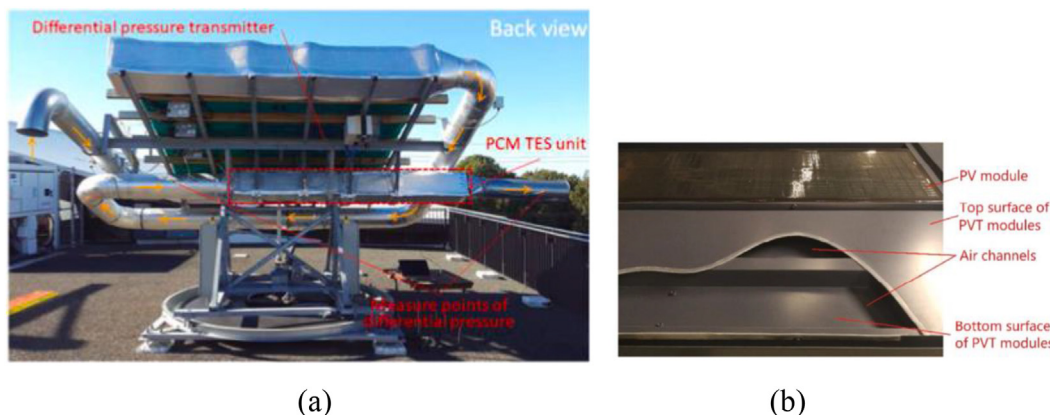


Fig. 4. Air based PVT solar collector and design details [32].

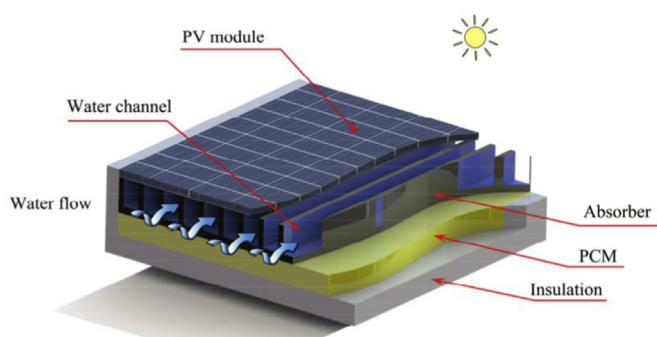


Fig. 5. PVT solar collector design with water-based cooling [33].

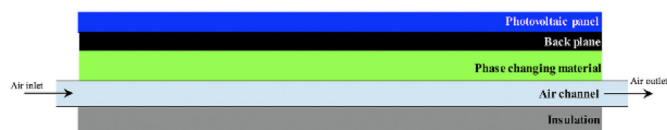


Fig. 6. Schematic of PVT air-based cooled solar panel [34].

use of air as the coolant in combination with a PCM is not an effective solution due to a weak convective heat transfer from the PCM layer to the air, which can be noticed regarding the detected rise in electrical efficiency. Although, several PCMs were used in this study, it is not clear why specific PCMs were selected since they covered limited temperature melting ranges, from 22 °C to 36 °C, i.e. in that sense a more thorough discussion is needed. An economic evaluation was obtained with the calculation of the Levelized Cost of Energy (LCOE), with a determined payback time ranging from 10 to 15 years. An environmental evaluation of the proposed PVT design was not considered.

A numerical and experimental investigation of a nano-cooled PVT-PCM solar collector was reported in work [35]. The coolant was a mixture of MWCNT nanoparticles in the base fluid (water/ethylene glycol), in two examined weight fractions (0.1 wt% and 0.2 wt%). The proposed system was experimentally tested in Iranian climate conditions (Tehran), where two panels were tested (one referent), with an energy and exergy analysis also obtained, Fig. 7a.

The specific PVT collector design is shown in Fig. 7b, which consisted of PV cells, copper plate equipped with copper tubes that were covered with a PCM material (Merck 107158). Inside the copper tubes, there was a prepared circulation of nano-fluid

(mixture of ethylene glycol, MWCNT nanoparticles with weight fractions of 0.1%–0.2%). The selection and elaboration of the proposed PVT design are missing and is unclear why the specific design solution was selected, Fig. 7b. The experimental readings showed that electrical efficiency improvements reached 4.2%, while thermal efficiency improvements were about 23.5%. The most influential parameter related to the magnitude of energy losses from the PVT panel is due to the surface temperatures of the PVT panel. A sensitivity analysis of the specific design parameters was not examined, which is beneficial for the proposed design. Moreover, economic and environmental evaluations were not reported in the obtained study although nanoparticles were used (cost and toxicity issues). The use of the nanoparticles improves heat absorption from the PV panel and generally improves the cooling performance (better heat transfer and higher specific heat capacity). In the same work, it was not discussed why specific nanoparticles in certain concentrations were selected, which is important to be discussed since they affect PVT-PCM collector performance. Higher nanoparticle weight fractions would lead to a better improvement in electrical efficiency, however, the optimum regarding nanoparticle weight fractions should be thoroughly investigated for each case (effect of specific nanomaterial being used and also taking into account that each PVT-PCM setup is different in that sense). The nanofluid preparation procedure was not well-elaborated, which strongly affects the stability and physical properties of the nanofluids in long-term.

A PVT-PCM solar panel was tested in laboratory conditions that consisted of a specific design including ducting and a PCM layer, Fig. 8. The air was the main coolant in the proposed PVT-PCM design where a PLUSICE S25 was used as the PCM material (it is not well-elaborated why the specific PCM was selected). Various thicknesses of the PCM layer were investigated (20 mm, 30 mm, and 50 mm), plus the addition of fins to improve heat transfer (typical approach in the case of PCM designs since fins boost heat transfer). The system was designed to ensure high thermal conductivity, and thermal grease was applied as a result of that. The use of thermal grease improves heat transfer efficiency but could increase unit costs, especially if thermal grease with added metal dust is used for the additional improvement of heat transfer. A rectangular air duct was incorporated behind the PCM layer, the duct being connected both to the horizontal and vertical openings to enable sufficient air circulation. The system was thermally insulated with a Celotex insulation board. The criteria for the specific selected PVT design were not discussed, i.e. the basis why this exact PVT design was selected along with air as the selected coolant (the application of the specific design to a building integrated PVT is



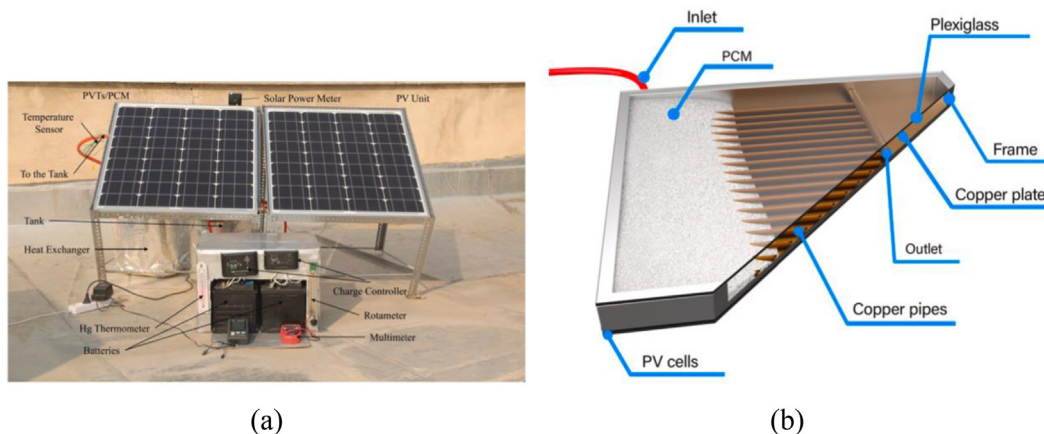


Fig. 7. Experimental setup (a) and design of PVT-PCM collector (b) [35].

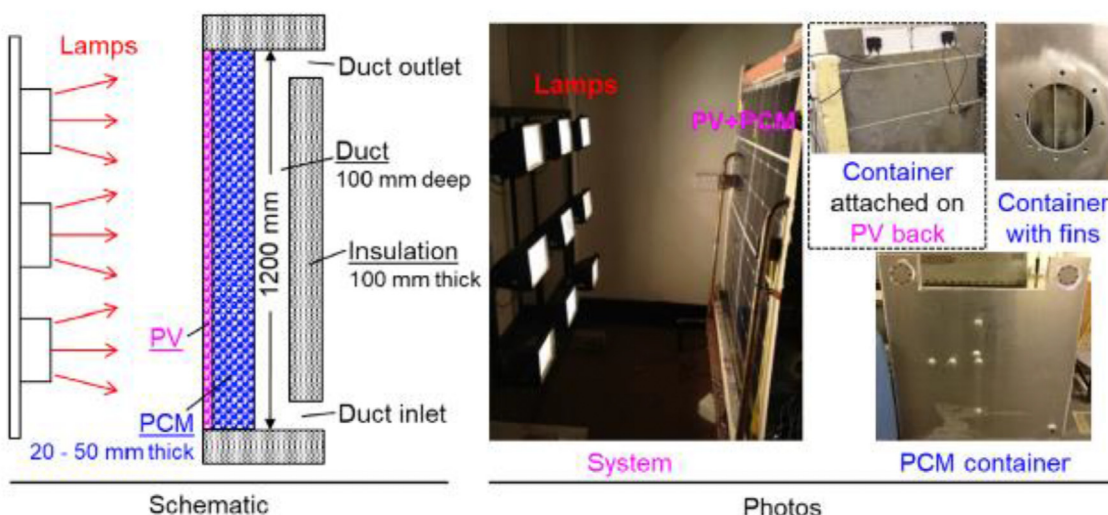


Fig. 8. Schematic of PVT-PCM panel and experimental setup [36].

assumed to be the goal). The selected design could improve the segmentization of the PCM layer (use of several smaller containers or PCM blocks rather than a solid one).

The experimental results revealed that the improvement in PV electrical performance can go up to 10%, with a secured ventilation rate of about 15 l/s. The addition of fins in the PCM layer can add up to 3% of extra improvement in electrical efficiency and around 30% of improvement in ventilation rate. The optimum capacity of the PCM layer is found to be between 20 mm and 50 mm for a PCM with a melting temperature of 25 °C. Since the results were conducted in laboratory conditions, they should be apprehended as limited. A real-field experiment is missing to determine the impact of the fluctuating surrounding environmental conditions (optimization is therefore needed). The economy of the examined configuration was not conducted in the reported work as well as the environmental evaluation.

A nano-fluid based cooling of a PVT-PCM solar collector was experimentally examined in study [37], for Pakistani climate conditions (Taxilia). Graphene was added to the base fluid (distilled water) to form nano-fluid in volume concentrations of graphene ranging from 0.05% to 0.15%. The selection of graphene (60 nm in size) was not thoroughly elaborated, although it is one of the best nanomaterials regarding improvements in thermal characteristics.

The preparation procedure was thoroughly elaborated and contained both magnetic stirring as well as sonication.

The design of the PVT collector is presented in Fig. 9 and is quite simple since a copper heat exchanger is added at the backside surface of the PV panel and filled with the PCM material (RT-35HC). Besides an actively cooled PVT-PCM collector, a passively cooled



Fig. 9. PVT-PCM solar collector [37].

PV-PCM system was also examined (PCM layer with added fins to improve heat transfer) in order to make a comparison. A referent, i.e. non-cooled PV panel was also compared with the two other previously mentioned examined configurations. The specific approach related to the design of the PVT collector was not well elaborated regarding the provided discussion how the final setup was selected and why the specific tube layout was taken. The aluminium fins were added inside the PCM layer to improve heat transfer. The experimental results revealed that the highest temperature reduction was obtained for the case of the PVT-PVM nano-cooled collector with a volume concentration of 0.1% and a water flow of 40 lit/min. The maximal improvement of the thermal efficiency was about 20.8% (when compared to water) and reached once more for a nano-fluid volume concentration of 0.1% and water flow of 40 lit/min. The improvement in electrical efficiency ranged from 10.9% to 14.1%, while the PVT system improvement in thermal efficiency ranged from 35% up to 45.8%, depending on the water flow rate, which ranged from 20 lit/min to 40 lit/min. The results indicated that the PVT-PCM system combination, with nano-fluid, ensures a better performance improvement when compared to the PV-PCM system. The same setup should be investigated with a comparison of various nanofluids in order to determine the best nanomaterial for the given purpose. A possible additional improvement could also be achieved with the addition of a nanomaterial in the PCM layer, i.e. to ensure a combination of nanomaterials in the coolant and PCM layer. The modification of the tube layout could also lead to better performance, i.e. as segment cooling for instance with a serpentine flow could be ensured, since it enables a more uniform cooling of the PV panel. The optimization of the proposed PVT-PCM collector is missing as well as economic and environmental evaluations. As the configuration was tested during several days, a long-term evaluation is needed in order to be able to get precise experimental data.

A comparison was given for PVT and PVT-PCM configurations, which were experimentally tested in laboratory conditions, [38]. The two PVT setups were tested, the first being a pure PVT and the second one being a PVT-PCM setup (PCM material, A44). In both cases, a specific serpentine heat exchanger design was considered

to provide improvement in the overall efficiency of the PVT-PCM collector, Fig. 10.

A serpentine flow configuration can improve cooling efficiency and heat absorption while leading to a higher overall efficiency of the PVT collector. The serpentine flow leads to more uniform cooling as already emphasized. The thermal paste in this configuration is used to improve heat transfer but several other improvements could be also obtained to provide a more effective PVT-PCM collector design. The tubes could be flooded in the PCM layer and not provided as PCM bricks as the heat transfer would be more effective. The serpentine flow was organized as a connected tube layout while another option could be to ensure four separate cooling sections, also with a serpentine layout. The design approach was well explained but some design aspects should be better discussed such as circumstances related to the specific selected serpentine design. Besides the laboratory examination, a numerical (CFD) model was also developed to examine the impact of various influential operating parameters. A maximal improvement in electrical efficiency was reached for the PVT-PCM configuration in the amount of 12.75%, while the highest improvement in overall efficiency for the PVT configuration was in the amount of 89.6% and 83.59% for the PVT-PCM. The PVT-PCM system has better performance with respect to electrical efficiency but lower thermal efficiency when compared to the PVT system. The proposed setup needs a long-term field experiment, i.e. experimental testing of the PVT-PCM system exposed to stochastic surrounding conditions in order to get more credible data regarding performance improvement. Economic and environmental evaluations were not obtained.

A serpentine flow-based design of in a PVT-PCM collector was discussed in work [39] and experimentally tested in Indian climate circumstances (Kottayam). The design of the collector is in its foundation simple, as a copper tube heat exchanger was applied on the backside surface of the PVT collector, which can be seen in most PVT-PCM collector designs, Fig. 11. A PCM material with a quite high melting temperature was selected, i.e. paraffin with a melting temperature of 57 °C. The overall efficiency of the PVT-PCM collector, as well as the thermal and electrical (PVT-PCM) where compared to each other and with the electrical efficiency of the PV

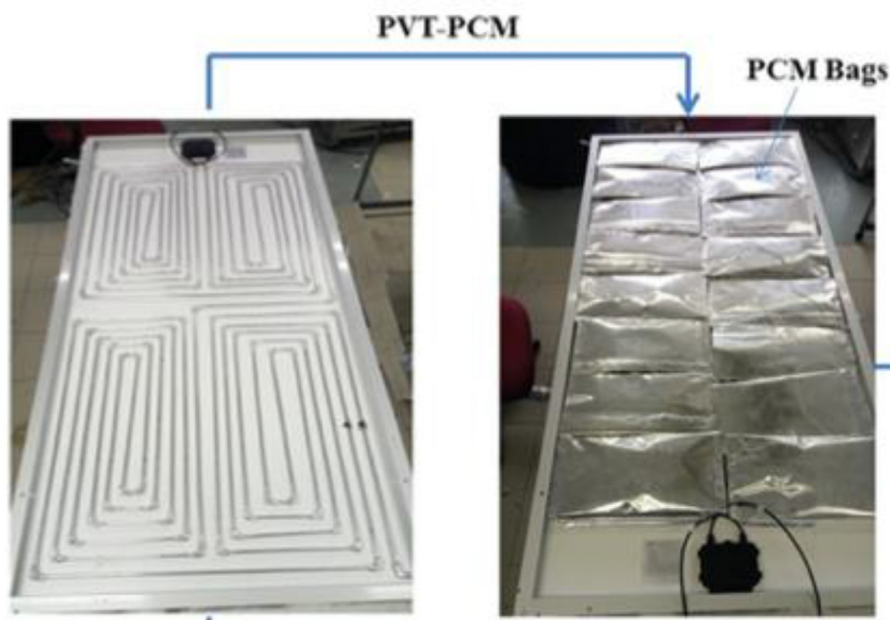


Fig. 10. Novel design of PVT-PCM collector [38].

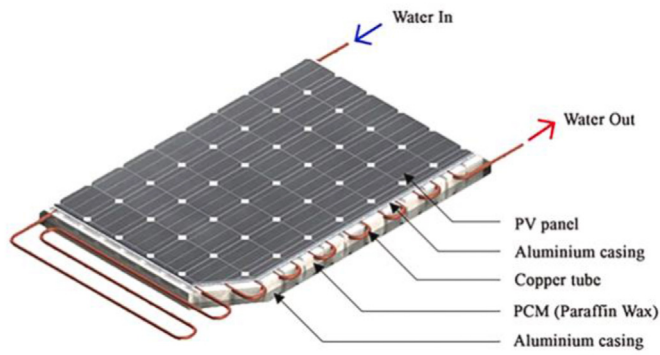


Fig. 11. Serpentine design of PVT-PCM collector [39].

panel. The PVT collector was finally equipped with thermal insulation and aluminium casing. The experimental investigation was only obtained for a few days; thus long-term performance is needed to get more credible results. Detailed reasoning and justification for the selected PVT design were not provided along with a thorough discussion of why the specific serpentine flow design was selected. The experimental work was conducted for various water flow rates and the analysis also included an exergo-economic evaluation.

The experimental results indicated an overall improvement in electrical efficiency in an amount of 17.3%, while the improvement in thermal efficiency was around 26.8%. The overall efficiency improvement of the PVT-PCM system was 40.5%, when compared to a referent PV panel of the same size. The economic analysis showed a payback time of 6 years, and the proposed PVT-PCM design has a long-term lifecycle efficiency in the amount of 27% approximately, when compared to the referent PV panel. An environmental evaluation of the system was not provided.

An experimental investigation of different PVT-PCM panel designs was reported in work [40], with the introduction of various absorbers as the main novelty. Modifications in terms of materials and specific PVT solar collector geometries were considered and compared to a referent case, i.e. sheet tube copper absorber. The glazing was also varied and experiments were conducted in periods of maximal solar irradiation levels in Spanish climate conditions (Zaragoza). Two prototypes of PVT-PCM systems were examined, the first being a polymer-based prototype, Fig. 12a, and aluminium based, Fig. 12b. The design ensured an air gap, PV panel, absorber (polymeric or aluminium roll-bond), and a PCM layer (RT50, C48) along with a thermal insulation layer. The design was well-elaborated as well as the specific constructional details. A hydraulic connection was enabled in series in order to ensure effective heat transfer in fluid flows with the fluid passing through both panels. The experimental investigation showed improvement in thermal performance in the amount of 30% for the aluminium configuration design (Fig. 12b), while the PVT-PCM collector

electrical efficiency improvement was negligible. The reason for low electrical efficiency improvement could lie in the implementation of high-quality absorbers, which caused efficient heat absorption and raised the PVT-PCM panel operating temperature, resulting in modest electrical efficiency. Therefore, the proposed design could be useful for cases when thermal performance is the priority with the electrical performance remaining the same as the one reached by the referent one, i.e. single PV panel (addition of PCM in these circumstances is questionable). The proposed concept directed to the importance of absorber designs with respect to the targeted performance improvement. In that sense, some other and alternative absorber designs could also be investigated, which would examine the balance between thermal and electrical improvement in the PVT-PCM collector performance.

Economic and environmental evaluations were not discussed for the proposed PVT-PCM configurations.

A serpentine based flow design in a PVT-PCM collector was reported in study [41], where the system was tested in Malaysian climate circumstances (Kuala Lumpur). The specific serpentine outlet of the PVT-PCM collector was presented in Fig. 13, which consisted of copper tubes mounted onto an aluminium sheet absorber filled with a PCM material (Lauric acid and Paraffin, i.e. two PCM materials were tested). In this concept, a single tube layout setup was used, but it would be more effective to divide the tube layout on several cooling loops. The PCM material was provided in the form of blocks, where close contact with a spiral copper absorber was ensured via the application of a thermally conductive paste. In general, the specific design of the PVT-PCM collector was well explained. An energy and exergy analysis was conducted along with an economic evaluation. The results revealed that the maximal reached thermal efficiency was about 87.7%, while thermal efficiency generally ranged from 75% to 85%. The maximal improvement in electrical efficiency was about 11%, while the referent PV panel had an efficiency of 9.88%, thus the maximal rise in electrical efficiency was about 11%. The economic analysis was comprehensive and detailed, which indicated a payback time of 4 years for the examined PVT-PCM system. In general, the economic analysis of the developed PVT-PCM system showed to be more economical for households than the PV system. Based on the presented results, it is not clear if a long-term performance evaluation was obtained. An environmental analysis was not obtained for the presented solution. It is also not well defined why the specific PCM materials were selected. It would also be beneficial to provide the same economic analysis for other countries in order to get a global relevance of the developed PVT-PCM collector design solution. The specific design showed the effectiveness of the proposed tube layout system since it leads to a quite high improvement regarding the thermal performance of the PV-PCM collector. The electrical performance improvement is not high, which is to be expected due to the high thermal efficiency of the PVT-PCM collector, i.e. the PVT-PCM collector is exposed to a higher operating temperatures. The proposed design in this concept should be used

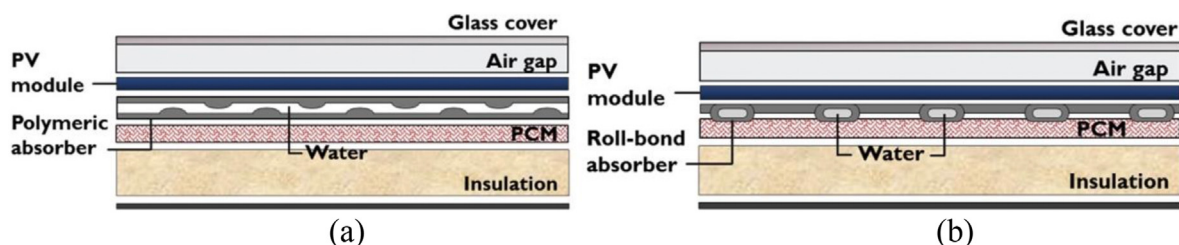


Fig. 12. Considered PVT-PCM collector designs, [40].



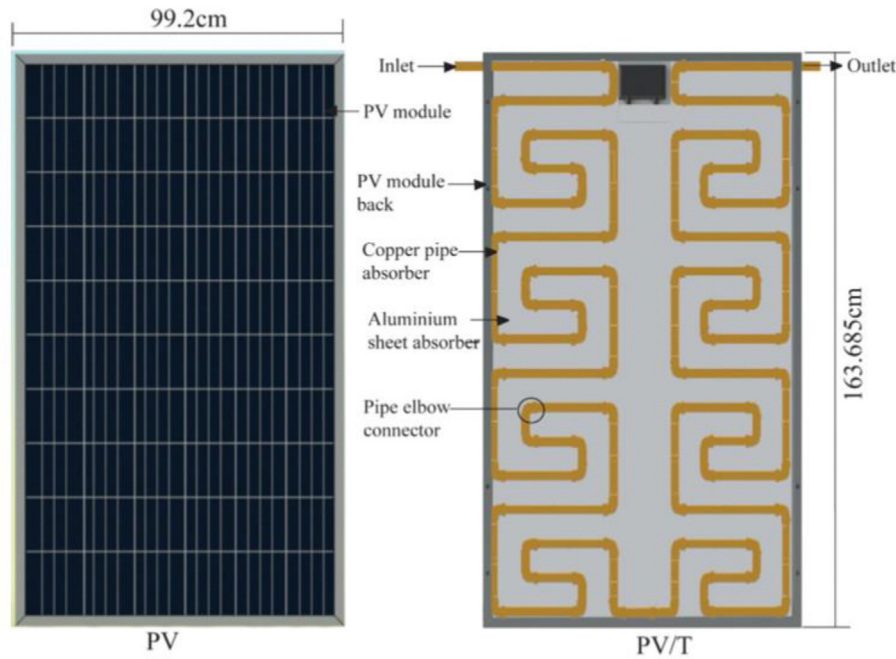


Fig. 13. Specific serpentine flow design of PVT-PCM collector [41].

for circumstances where thermal efficiency is the main target. Even though the electrical efficiency is not high in this design solution, it is still higher than the referent PV panel, which is acceptable.

An air-based PVT-PCM solar collector was experimentally analyzed for the case of a natural and forced convection in Iranian climate conditions (Tehran) [42]. The design of the PVT-PCM collector is simple; it consists of a PV panel, aluminium oxide layer, absorber plate, PCM layer (PCM32/280-salt hydrate) and air channel, Fig. 14a. The reasoning for the specific selected PVT-PCM design was not discussed in detail as well as the selection of the specific constructional details and PCM material. Experimental investigation was obtained for two months (September and October) and electrical efficiency improvement was found to be around 11% for the natural convection case and about 11.5% for the forced convection, but only when the PCM was not incorporated in the PVT collector (detail of incorporated PCM material shown in Fig. 14b). The addition of the PCM material caused an improvement in electrical efficiency by about 9% and a reduction of the PVT-PCM panel temperature ranging from 3.7 °C to 4.3 °C. The design could be improved with the addition of fins or a specific geometry that would boost the convective heat transfer from the PVT panel to the

air. Moreover, the system should also be tested for various PCMs in order to determine the most suitable PCM material. Since the work was focused on building integrated PVT collectors, the more attention in the work could also be given towards the utilization of removed heat from the PVT panel and integration to the building HVAC systems. The data related to the thermal performance of the examined PVT-PCM panel were not reported, but the effect of fan speed was examined with respect to the average increase in PVT-PCM solar collector electrical efficiency. Economic and environmental evaluations were not provided in the obtained work.

The experimental work [44] examined the case of a PVT-PCM solar collector cooled with Al<sub>2</sub>O<sub>3</sub>/water nano-fluid (weight fraction 0.2 wt%), where the results were compared with a referent PV panel and PVT panel. The experimental investigation was provided in Iranian climate conditions (Mashhad) for a period of two months (August and September). Besides the experimental approach, an energy and exergy analysis was also provided. The specific design of the PVT-PCM collector was presented in Fig. 15, i.e. a PV panel absorber was added after along with a PCM layer, which was covered by acrylic glass and a thermal insulation layer. Inside the PCM layer, copper tubes were added (12 mm in outer diameter), but

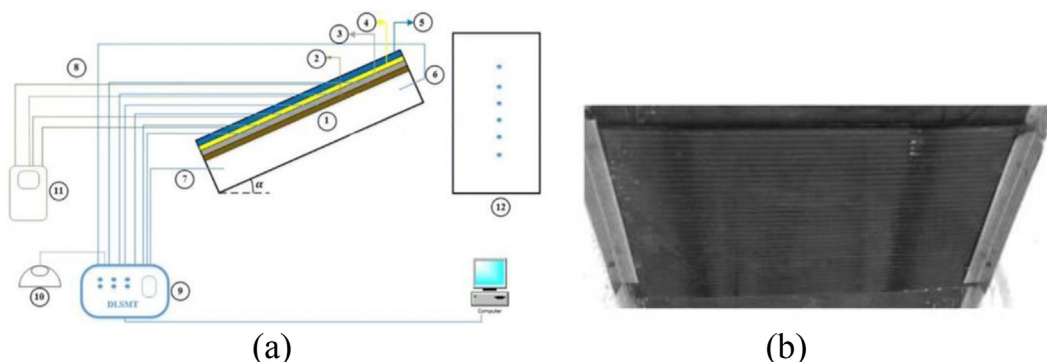


Fig. 14. Setup (a), packed PCM layer in PVT-PCM solar collector (b) [42].

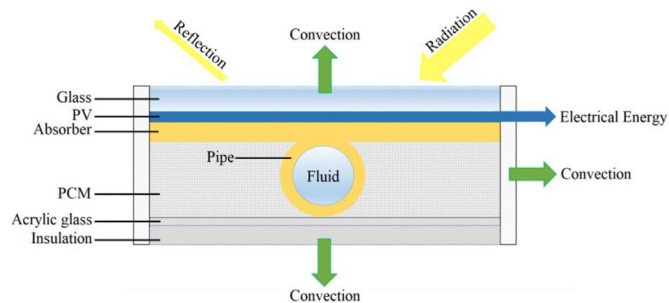
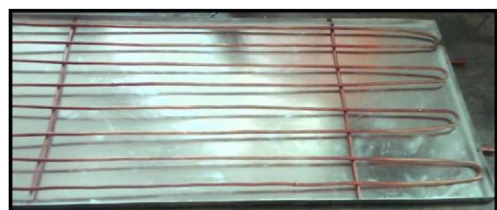


Fig. 15. PVT-PCM solar collector design with nano-fluid cooling [44].

the specific tube layout was not discussed. The PVT-PCM collector design is interesting due to the applied absorber (copper plate with tubes) and acrylic glass that was set before the thermal insulation layer, Fig. 15. The copper absorber enhances heat transfer from the PCM layer to the nano-fluid and generally enables more effective thermal regulation of the PCM layer. A step further could be the addition of a nanomaterial in the PCM layer and an experimental investigation of the overall performance. The acrylic layer was probably added to have visibility regarding the monitoring of the phase change processes, which occur in the experiment. The specific selected PVT design and its elaboration was not discussed as well as clarification on why the specific nano-fluid weight fraction was selected (it would also be interesting to see the same experiment for various nano-fluid weight fractions). The experiments were conducted for a constant mass flow rate and a sensitivity analysis is therefore missing. According to the experimental results, the average improvement in electrical efficiency was 11.8% when compared to the referent PV panel, while an improvement of about 4.5% was noticed when compared to the PVT panel. The average thermal performance was about 51.6% for the PVT-PCM collector and was 29% more efficient when compared to the PVT panel. The implementation of nano-fluids showed to have the highest PVT-PCM performance, with a highest overall performance of 65.7%. Economic and environmental evaluations were not reported in this investigation.

A PVT-PCM nano-fluid based system was proposed in Ref. [47] and examined for Malaysian climate circumstances. A SiC/water nano-fluid was considered in mass concentrations ranging from 0.1% to 4%. The examined PVT-PCM system was coupled with a water storage tank, and the specific design of the PVT-PCM solar collector was presented in Fig. 16b. The PVT-PCM collector consisted of a PV panel and silicon oil layer with a galvanized sheet. A PCM layer was added afterwards with SiC nanoparticles and a back sheet (lower sheet). The addition of the silicon layer was necessary to prevent air gaps and improve the thermal capacity of the collector. The selected tube layout was standard, already seen in other PVT-PCM collector designs. The tubes were not attached to the aluminium absorber, i.e. they were mounted on the copper stand.



(a)

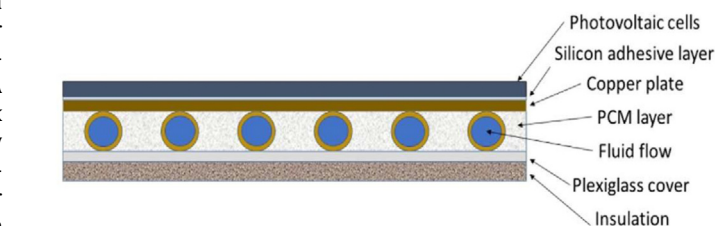
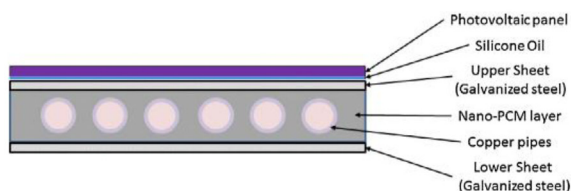


Fig. 17. PVT-PCM nano-fluid cooled collector [48].



(b)

Fig. 16. (a) Details of PVT-PCM collector design, (b) constructional layers of PVT-PCM collectors [47].

The integration of tubes with an aluminium absorber would allow for more efficient heat transfer and thermal management of the PCM layer. Regarding the specific design, it was quite simple since a PCM layer was added below the PV panel, where thermal control was established via a copper tube exchanger, Fig. 16a. The novelty regarding the other already examined setups is the added nano-material both in the PCM layer and water, which was used as the PCM layer coolant. The experimental approach compared the performances of the referent PV panel, PVT panel cooled with water, PVT-PCM panel cooled with water, and the setup that examined the PVT-PCM layer with an incorporated nanomaterial in the PCM layer and water as the coolant. The best improvement was reached for the case of the PVT-PCM collector with the application of a nano-material, i.e. electrical efficiency was raised from 7.11% (referent PV panel) to 13.7%, while thermal efficiency went from 35.4% (PVT-water cooled) to 50.5% (PVT-PCM) and finally to 72% (PVT-PCM with nanomaterials). The selected design of the PVT-PCM collector was well-elaborated, justifying the proposed concept. The addition of nanomaterials showed noticeable improvement both in the electrical and thermal performance of the PVT-PCM solar collector. Economic and environmental evaluations of the proposed nano-enhanced PVT-PCM systems are crucial, especially regarding the harmful impact of the nanomaterials. Overall, the proposed concept showed to have among the highest electrical and performance improvements with respect to other works in the existing research literature. It directs to the conclusion that the simultaneous addition of nanomaterials both in the PCM layer and in the cooling fluid could potentially ensure the highest performance improvement, but its economic aspect could be questionable. It would be interesting to examine the performance of the same PVT-PCM configuration in other climate circumstances, along with an economic evaluation. An important value of the research was the obtained comparison of the referent PV panel with other mentioned PVT configurations.

Three different experimental configurations were examined in work [48], i.e. PVT and PVT-PCM configurations, i.e. their performances were compared with a referent PV panel. A usual PVT collector was applied, as a copper tube heat exchanger was added in the PCM layer (Merck 107151), Fig. 17, to enable thermal management of the PVT collector. The design was finalized with a Plexiglas cover and thermal insulation layer. A copper plate layer

was added afterwards to the PV panel to enhance heat transfer, which also allows for more efficient temperature regulation of the PCM layer. The selection of the specific PVT collector design was not well-elaborated; i.e. the reasoning why the specific design was selected with respect to the already examined configurations. The modification of the specific tube layout could lead to the improvement of cooling performance. ZnO nanoparticles were selected due to high thermal conductivity and applied in a mass fraction of 0.2 wt% (it is not clear why the specific concentration was selected) and mixed with distilled water. A variation of the nanofluid concentration is also necessary in order to determine the optimal concentration with respect to the performance improvement and economic constrains on the other side. The stability of the nano-fluid was examined during the experimental period with density measurements, where there was no significant variation detected. Thermodynamic modeling was also obtained along with an exergy analysis. The experimental approach was obtained in Iranian climate conditions (Mashhad), in August and September. The electrical improvement of the examined PVT-PCM system was 13% when compared to the referent PV panel, while thermal efficiency was improved by 9% approximately when compared to the PVT panel. Economic and environmental evaluations of the system were not discussed, which is important as nanomaterials were implemented.

Study [49] analyzed an air-based cooled PVT-PCM collector, Fig. 18a, coupled with a compound parabolic concentrator, Fig. 18b. The specific selected collector design consisted of a PV panel and a PCM layer (paraffin) mounted in the case below it. Fins were provided inside the PCM layer to enhance heat transfer (the PCM layer was in contact with the absorber plate). The experimental investigation was obtained in December and February of 2014 for Indian climate circumstances (Bangladesh). The water flow rate was constant during the examination, which is one of the limitations and its effect should be examined. The performance analysis indicated the overall efficiency of the proposed PVT-PCM configuration, which ranged from 43% to 65%, depending on the specific day. The study did not examine the electric performance of the PVT-PCM collector, i.e. only thermal performance analyzed, which is also a limitation regarding the work (in the case of solar concentrating systems, overheating could be an issue, which reduces the electrical performance of the PV panel). Regarding the design approach, it would

be interesting to examine the addition of nanoparticles in the cooling fluid and to observe the performance improvement. Moreover, the tube layout should be modified due to higher operating temperatures as concentrator systems are in question, thus more uniform cooling is desired. The addition of a metal absorber could also ensure a more effective temperature regulation of the proposed PVT-PCM collector design. Economic and environmental evaluations were not provided.

A proposed building-integrated PVT-PCM concept was reported in study [50] as an active element for the thermal regulation of a building designed on passive architecture principles. The PVT-PCM collector was integrated into a roof (ceiling) and consisted of a PV panel, an air channel below it, then a first PCM layer, another air channel and finalized with a second PCM layer, Fig. 19. A design with two PCM layers was selected to increase the thermal mass of the ceiling (PCM material applied in the form of bricks). The exact PCM material was not specified but the data used for the simulation

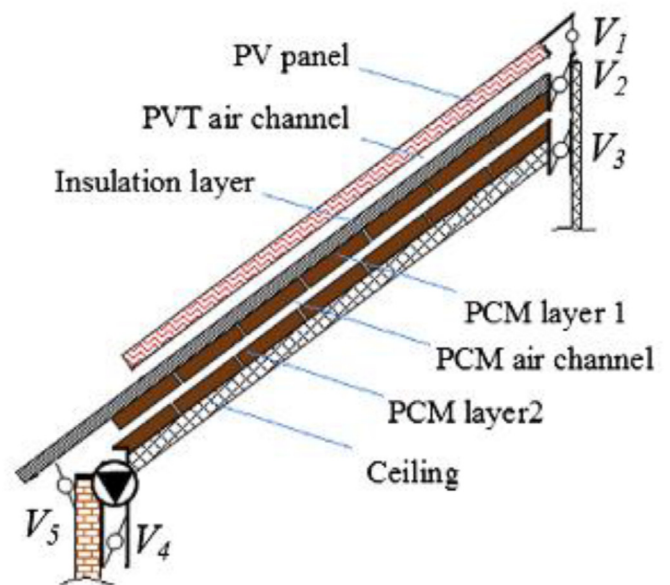


Fig. 19. Building integrated PVT-PCM collector [50].

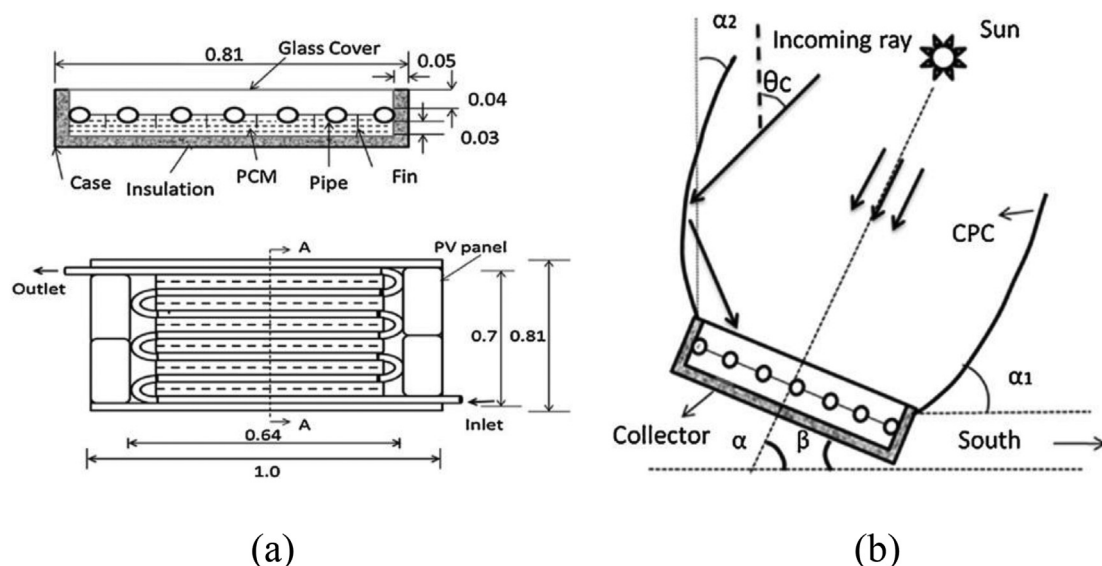


Fig. 18. Specific PVT-PCM solar collector design (a) and concentrator system (b) [49].



were related to a PCM with a latent heat of 190 kJ/kg with a melting temperature of 23 °C. The selection of the considered PCM was not well addressed in the work. The possible upgrade of the considered design should be directed to the addition of fins in the PCM layer to provide possible efficiency improvement. The integration of the proposed concept to building HVAC systems also needs to be considered to improve the energy efficiency of building energy systems. An optimization of the air channel thickness is also a critical feature for the proposed concept since it could reflect on the quantity of the utilized PCM. A simulation model was developed using a TRNSYS tool with the data being validated through available data from real field experiments (building facility in Australia, Wollongong). The performance of the PVT-PCM system was compared to a natural ventilation system. The average thermal efficiency of the PVT-PCM collector was 12.5%, while the electrical efficiency averaged about 8.31% in winter circumstances. The average thermal efficiency was 13.6%, while the average electric efficiency was 8.26%. As air was used as the coolant, there is a lower rise in the performance parameters when compared to a water coolant. The overall electricity production of the PVT-PCM panel was 17.06 kWh in winter and 34.71 kWh in summer. Economic and environmental evaluations are crucial for the proposed system as two PCM layers are used. Regarding numerical modeling, PCM layer optimization should be provided along with airflow variation to determine the behavior of the proposed system in various working regimes, i.e. to examine maximal performance benefits.

In study [51], a novel composite PMC was proposed and experimentally tested in Indian climate circumstances (Guwahati). A novel PCM material was made as a mixture of a paraffin-based PCM (OM35) and biochar utilized from derived water hyacinth. The thermal conductivity of the novel produced PCM material was around 50.5% higher when compared to the base PCM material. The specific approach of the PVT-PCM collector production is presented

in Fig. 20a, while the design of the PVT-PCM collector is shown in Fig. 20b. The PVT-PCM collector design had already been seen when compared to existing research findings, where novel details are the incorporation of a produced composite PCM and specific tube outlet, Fig. 20a. The focus of this work was mainly related to the introduction of a novel PCM composite, rather than the investigation of new design advancements. The performance analysis showed an improvement in PV panel electrical efficiency regarding the PVT-PCM configuration in the amount of 18.4%, while the average thermal efficiency ranged from 60.3% to 71.2%. The proposed configuration ensured very good improvement in electrical efficiency and excellent in thermal efficiency. With a more efficient collector design related to the absorber and specific tube layout, the performance improvement could be even higher. The novel PCM composite showed to be suitable for the considered application regarding the performance indicators. There is very few research works that have examined composite PCMs and in that sense there is a necessity for more research investigations, as composite PCMs have the potential to ensure performance improvements for a reasonable unit cost. Environmental and economic evaluations were not discussed. Collector geometry optimization is needed and the novel produced PCM composite should better suit the examined climate circumstances, and general thermal property determination is also required. The main idea of the work is inspiring, as it directed the consideration of novel composite PCMs, which are important future design options to improve PVT-PCM solar collectors.

## 5. Discussion

### 5.1. Performance indicators

Based on the conducted review related to the specific

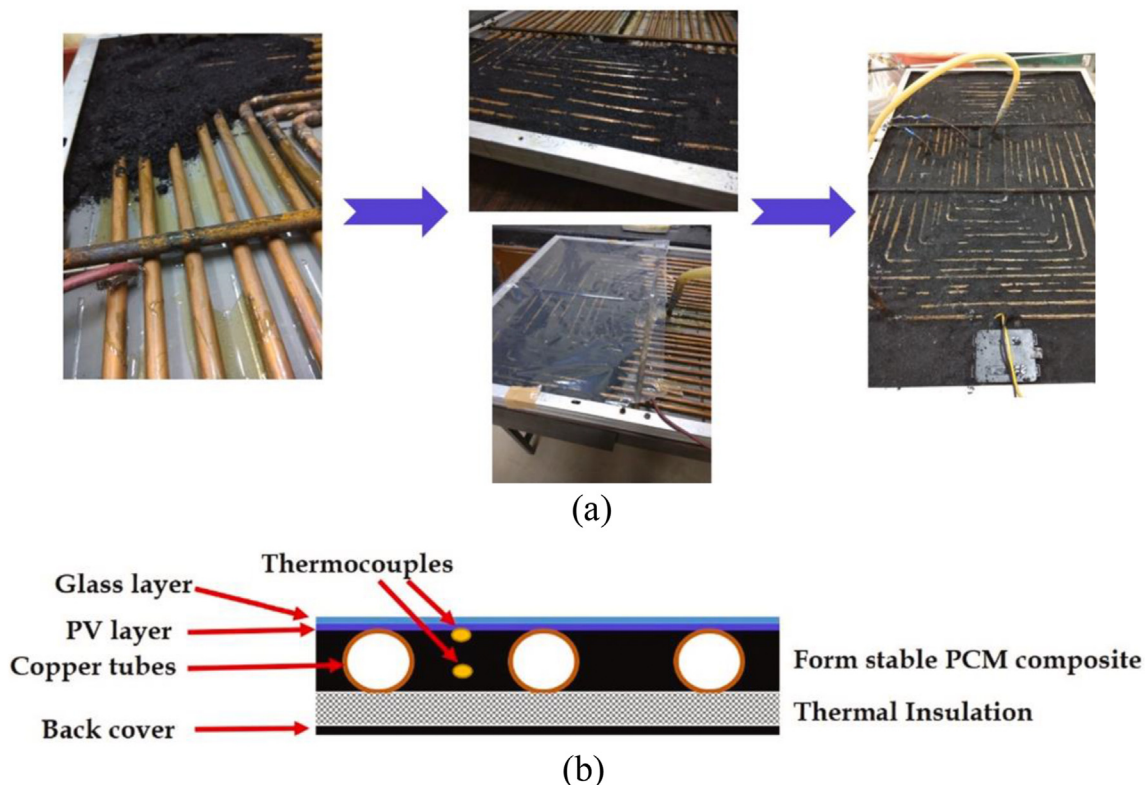


Fig. 20. Design of PVT-PCM solar collectors with incorporated PCM-biochar (a) composite, (b) PVT-PCM design [51].



examination of experimentally tested PVT-PCM systems in various climates, a summary of the main performance parameters and other details, such as specific climate or economic and environmental evaluations were presented in Table 4. Overall, seventeen specific PVT-PCM designs were analyzed, where the main results revealed that the performance of PVT-PCM systems strongly depends on certain PVT-PCM designs and is highly sensitive to how the PCM layer thermal regulation is provided. The general PVT-PCM design was mainly ensured via specific heat exchangers mounted on the backside surface of the PV panel. The heat exchangers were usually provided as a system of tubes (usually copper) in specific arrangements (straight or serpentine). In some studies, the tubes were attached to metal absorbers in order to improve the heat transfer from the PV panel to the PCM layer. The addition of absorbers allows for a more effective thermal regulation of the PCM layer. The role of the specific tube arrangement is important to ensure the uniform cooling of the PV panels. Water was mostly used as the coolant together with air or nano-fluids in the experimental investigations. The best performance improvements, i.e. overall efficiency (both in electrical and thermal efficiency) were ensured in the case of PVT-PCM collectors cooled with water and nano-fluids. The lowest performance improvements were reached in the case of air-based PVT-PCM collectors, as air has weaker thermal properties when compared to water or nanofluids. For instance, in the case of PVT-PCM collectors cooled with water or nano-fluids, the electrical efficiency improvement mostly ranged from about 4% to about 18% (when compared to referent non-cooled PV panels), i.e. the improvement in electrical efficiency was less than 20%. The improvement in thermal efficiency mostly ranged from 30% to 70%, while in some cases the maximal thermal efficiency was even greater than 80%. The lowest thermal efficiency was reached for air-based cooled PVT-PCM systems and was mainly below 40%, which is reasonable due to the low thermal properties when air is the coolant, as already highlighted. Even though, air-based PVT-PCM collectors have the lowest performance improvement, they could be effective for integration into building HVAC systems, where the energy efficiency of building heating systems could be improved in that case, and they are generally easier for maintenance.

Even if water is used as the favorable coolant with the highest expected performance improvement of the PVT-PCM collector, specific collector designs can significantly reduce the overall collector performance due to reduced electrical efficiency improvement. For instance, in the experimental work [40], the electrical efficiency improvement was negligible, while the improvement in thermal performance was about 30%. The cause for the negligible improvement in the electrical efficiency was the specific absorber design, as the use of polymer-based and aluminium-based absorbers, Fig. 12, can increase the operating temperature of the PVT collector. In these situations, the thermal output is improved, while improvement in electrical efficiency is low or could even be negative when compared to the same sized referent non-cooled PV panel. The main point of the PVT-PCM collector design is to ensure a proper balance between the targeted improvement in electrical and thermal efficiency as the PVT-PCM collector design plays a vital role in the thermal management of the PVT-PCM collector. In any case, in these situations when thermal output is mandatory, the main target should be to maintain PVT-PCM collector electrical efficiency and be somewhat similar one to the referent PV panel, but efforts should be made to ensure improvements in thermal performance.

The use of nano-fluids ensured the improvement of both electrical and thermal performance, however, the difference in performance improvement between water-based cooled PVT-PCM collectors is not significant in some cases, and varies from the

specific design. The highest improvement in PVT-PCM nano-fluid cooled collectors was reached when nano-fluid was incorporated into the PCM layer (NPCM) and in the cooling water, as reported in study [47]. The addition of nanomaterials, either in the PCM layer or in the cooling water to form nano-fluid needs to be justified economically. Unfortunately, experimental studies dealing with nanomaterial cooled PVT-PCM collectors did not consider the economic aspect linked with the use of nanomaterials in PVT-PCM collectors, where the specific selected nanomaterial concentration needs to be justified from an economic point of view. Moreover, one of the main problems with nanomaterials is their toxicity and long-term stability of thermal properties, which requires a careful cyclic investigation. A detailed description of the preparation process related to nano-fluids, or nano-enhanced PCMs (NPCM) is not well discussed in some studies, and is not fully clear why a specific nanomaterial and nanomaterial concentration was selected for specific purposes. In general, a potential exists for the implementation of nanomaterials in PVT-PCM collectors regarding performance indicators but some open issues require more attention. It was also found that there is a lack of investigations with respect to the implementation of composite PCMs. There are some recent studies that have considered composite PCMs in PVT-PCM collector designs, such as a PCM with a 15% expanded graphite as seen in study [52] or a composite PCM-foam (PS-CNT foam) [53], where the performance improvement results are promising.

Based on the conducted analysis of existing and analyzed PVT-PCM collector designs, the main constructive elements of PVT-PCM collectors have been summarized and presented in Table 5. Provided Table 5 is useful for possible consideration of the future PVT-PCM collector designs, since it clearly represents the main features of the already experimentally examined designs and with respect to the main features (such as PCM casting, the type of the PV cell, insulation, type of the tubes and tube layout geometry and finally considered coolant). In some works specific data were not specified, or it was not fully clear when checking specific design details, such as for instance the type of the specific used PV technology, type of insulation, etc. Specified data in Table 5 could be quality basis, i.e. starting point when considering novel potential designs of the PVT-PCM collectors.

Most studies were conducted in warmer climates, i.e. geographical locations with suitable solar irradiation. Colder regions are not well represented, which is due to unfavorable solar characteristics for the consideration of such PVT-PCM collector designs, but would be interesting to check their performance improvement and investigate the PVT-PCM system technical limits in colder climates.

The economic aspects of PVT-PCM systems were analyzed and discussed in few studies, as the focus of the research investigations was directed to performance improvement, rather than having evaluations regarding the economy of the proposed PVT-PCM collector designs. The few economic evaluations showed payback times ranging from 4 to 15 years, taking into account that the studies were conducted in warmer geographical locations (such as Mexico, India, Malaysia, etc.). More details regarding the economic aspects of PVT-PCM collectors will be discussed in the next section of the paper.

Environmental evaluations regarding the PVT-PCM systems are completely omitted when analyzing existing research findings. The implementation of PCMs leads to a higher environmental footprint as it was indicated in study [54] for the passive cooling of PV panels. Moreover, the implementation of nanomaterials is also associated with unavoidable environmental footprints and hazardous consequences for people (PVT system operators). The evaluation of environmental footprints regarding PVT-PCM collector designs is necessary to select less harmful designs. An additional discussion

**Table 4**  
Main performance indicators and other features of PVT-PCM collectors.

| References | Used type of PCM material              | Coolant  | Performance indicators   | Specific remarks  | Climate                                    | Economic (E)/ Environmental evaluation (EN)  |
|------------|--|--|--|---|--|--|
| [32]       | S21                                    | air  | -increase in average overall system efficiency: 37%–40%  | - PVT system + PCM TES system.<br>-simple collector design,<br>-provided optimization.  | Australia, (Wollongong)                    | E: NO<br>EN: NO                              |
| [33]       | RT44                                   | water  | -maximal electrical efficiency:17.7%<br>-maximal thermal efficiency:68.2%  | -PVT-PCM collector integrated with desiccant solar cooling system.  | Iran (Bandar Abbas)                        | E: NO<br>EN: NO                              |
| [34]       | RT35 HC<br>RT28HC<br>RT25HC            | air  | -improvement in overall performance:20%–24%<br>-electrical efficiency improvement:8%–110.6%<br>-thermal efficiency: 22%–33%.   | -only numerical investigation obtained<br>-selection of different PCMs obtained for specific locations.   | Mexico (Mexico City, Monterrey, Campeche). | E: YES (payback time: 10 –15years)<br>EN: NO |
| [35]       | Merck 107158                           | Nano-fluid: MWCNT nanoparticles + water/ ethylene glycol | -Improvement in electrical efficiency:4.2%<br>-improvement in thermal efficiency: 23.5%  | -numerical and experimental investigation obtained,<br>-weight concentration 0.1 wt% to 0.2 wt%   | Iran (Tehran)                              | E: NO<br>EN: NO                              |
| [36]       | PLUSICE S25                            | air  | -improvement in electrical efficiency:10%<br>-ventilation rate:15 l/s<br>-with fin ducting 3% extra increase in electrical efficiency and 30% in ventilation rate.   | -analysis obtained only in laboratory conditions.   | –  | E: NO<br>EN: NO                              |
| [37]       | RT-35HC                                | Nano-fluid: Graphene + distilled water                   | -lowest operating temperature of PVT panel was reached for 0.1% nano-fluid volume concentration<br>-overall PVT efficiency enhanced from 10.9% to 14.1% (highest one for nano-fluid volume concentration, 0.1%)<br>-thermal efficiency ranged from 35% up to 45.8% | -simple design<br>-optimum nano-fluid volume concentration determined,<br>-system compared with referent PV panel and PV-PCM panel<br>-experiment of several days | Pakistan (Taxilia)                         | E: NO<br>EN: NO                              |
| [38]       | A44                                    | water  | -highest overall efficiency: 89.6%(PVT)/83.5% (PVT-PCM)<br>-maximal improvement in electrical efficiency:9.2% (PVT) to 12.7% (PVT-PCM)   | -analysis obtained only in laboratory conditions<br>-numerical analysis provided  | –  | E: NO<br>EN: NO                              |
| [39]       | Paraffin wax                           | water  | -Electrical efficiency improvement: 17.3%<br>-Average thermal performance: 26.8%<br>-Overall performance improvement: 40.5%  | -Short term performance investigation   | India (Kottayam)                           | E: YES (6 year payback time)<br>EN: NO       |
| [40]       | RT50, C48                              | water  | -Thermal performance improvement:30%<br>-Electrical efficiency improvement negligible  | -various designs considered (glazing, geometry, construction, materials, PCMs)  | Spain (Zaragoza)                           | E: NO<br>EN: NO                              |
| [41]       | Lauric acid                            | water  | -maximal thermal efficiency:87.2%<br>-maximal rise in electrical efficiency: 11%   | -serpentine flow design<br>-short-term experimental investigation   | Malaysia (Kuala Lumpur)                    | E: YES (4 year payback time)<br>EN: NO       |
| [42]       | PCM32/280                              | air  | -increase in electrical efficiency: 9%   | -natural and forced convection examined,<br>-simple design<br>-data related to thermal performance not reported   | Iran (Tehran)                              | E: NO<br>EN: NO                              |
| [44]       | Paraffin wax (Merck, 107151)           | Al <sub>2</sub> O <sub>3</sub> /water nano-fluid         | -electrical efficiency improvement: 11.8%<br>-thermal efficiency: 51.6% (29% rise when compared to PVT system)<br>-maximal overall performance:65.7%   | -exergy analysis provided<br>-nano-fluid weight fraction: 0.2 wt%   | Iran (Mashhad)                             | E: NO<br>EN: NO                              |
| [47]       | Paraffin wax                           | SiC/water nanofluid                                      | -electrical efficiency improvement: 92.6% (referent PV panel, i.e. 24% to PVT-water and 11% to PVT-PCM)<br>- thermal efficiency improvement: 20.3% (PVT-water) and 42.6% (PVT-PCM)   | -mass fractions of nanomaterial: 0.1 wt% to 4.0 wt%   | Malaysia (Selangor)                        | E: NO<br>EN: NO                              |
| [48]       | Paraffin wax (Merck 107151)            | ZnO/deionized water                                      | - electrical efficiency improvement: 13%<br>-thermal efficiency improvement: 9%  | -weight nanomaterial concentration: 0.2 wt%   | Iran (Mashhad)                             | E: NO<br>EN: NO                              |
| [49]       | Paraffin                               | water  | -overall efficiency: 55%–63%<br>-thermal efficiency:40%–50%  | -numerical model developed<br>-constant water flow rate   | India (Bangladesh)                         | E: NO<br>EN: NO                              |
| [50]       | Not specified (latent heat: 190 kJ/kg, | air  | -average thermal efficiency: 12.5%<br>-average electrical efficiency: 8.31% (winter) and 8.26 (summer)   | -building integrated<br>-numerical simulation   | Australia (Wollongong)                     | E: NO<br>EN: NO                              |

(continued on next page)

Table 4 (continued)

| References | Used type of PCM material  | Coolant | Performance indicators  | Specific remarks  | Climate          | Economic (E)/ Environmental evaluation (EN) |
|------------|----------------------------|---------|---|---|------------------|---|
|            | melting temperature 23 °C) |         | -average thermal efficiency: 12.5% (winter) and 13.6% (winter)  | -winter and summer period examined  |                  |   |
| [51]       | OM35+biochar               | water   | -improvement of indoor thermal comfort (passive buildings)<br>-29% reduction in PVT panel surface temperature,<br>-electrical efficiency improvement: 18.4%<br>- thermal efficiency:60.3%–71.2% | -novel PCM composite has about 50.5% improvement in thermal conductivity with respect to base PCM | India (Guwahati) | E: NO<br>EN: NO                             |

regarding the environmental aspects of PVT-PCM collector designs was elaborated in Section 5.3.

5.2. Economic aspect

Besides the above discussed performance indicators, the key information for specific PVT-PCM designs is related to economic evaluations. Various PVT-PCM designs are linked to different initial investments and can be scaled in a specific PVT-PCM collector area (€/m<sup>2</sup>). In order to demonstrate the size of the overall allowed investment for specific PVT-PCM designs and with respect to overall LCOE (Levelized Cost of Produced Energy), the LCOE of a conventional PVT system was compared with the LCOE of a PVT-PCM system. The comparison was done from a maximal allowed amount of initial investment for specific targeted performance

improvement, scaled on a PVT collector surface €/m<sup>2</sup> (maximal in the sense that a PVT-PCM collector LCOE should be lower than the calculated LCOE of a convective PVT collector). In order to be able to provide analysis, the available data for the performance indicators were taken from real-field PVT plant installed in France (Sète) with an overall PVT collector area of 300 m<sup>2</sup>, [55]. Based on the reported performance data for PVT systems, the annual production of heat was 82,100 kWh/a, while electricity was 59,113 kWh/a, thus an overall energy production of 141,213 kWh/a (EO) was ensured, [55]. The overall investment (IC) was estimated to be about 120,000 € for the given PVT system, i.e. having a unit cost of 400 €/m<sup>2</sup>, which is an expected unit cost for PVT systems, which is based on the literature data as already discussed in Section 2. The interest rate was taken at 6% (p), an amortization period of 15 years and an annual maintenance cost of 2.0% (OM) regarding

Table 5 Main PVT-PCM collector design elements.

| References | PCM Casing                                 | PV cell type                              | Insulation                            | Tubes/Channel /Absorber                     | Coolant type   |
|------------|--|---|---------------------------------------|---|--|
| [28]       | Aluminium                                  | Mono-Crystalline silicon                  | Insulation is included (type unclear) | Straight copper pipes with pipe coupling    | Water  |
| [32]       | Metal                                      | Copper indium gallium selenide solar cell | Insulation is included (type unclear) | Straight channels                           | Fan drawn air  |
| [33]       | Unclear type                               | Mono-Crystalline silicon                  | Insulation is included (type unclear) | Straight channels                           | Water  |
| [34]       | Aluminium                                  | Poly-Crystalline silicon                  | Glass mineral wool                    | Straight channels                           | Air  |
| [35]       | Thin copper plate                          | Mono-Crystalline silicon                  | /                                     | Straight copper pipes                       | Deionized water, mixture of water/EG, MWCNT/ water and MWCNT/EG nanofluids |
| [36]       | Aluminium container                        | Mono-Crystalline silicon                  | Celotex                               | Natural ventilation duct                    | Air  |
| [37]       | Aluminium sheet container                  | Mono-Crystalline silicon                  | Insulation is included (type unclear) | Serpentine copper tubes                     | Nanofluid based on graphene nanoparticles and distilled water              |
| [38]       | Aluminium thermal collector                | Poly-Crystalline silicon                  | Polyethylene                          | Spiral serpentine aluminium pipes           | Water  |
| [39]       | Aluminium container                        | Poly-Crystalline silicon                  | No insulation                         | Serpentine copper tube                      | Water  |
| [40]       | Matchbox aluminium foil PCM pouches        | Unclear type                              | Rock wool layer                       | Aluminium roll-bond absorber                | Water  |
| [40]       | PCM in metallic bags(PAKVF4PCA)            | Unclear type                              | Rock wool layer                       | High-density polyethylene absorber          | Water  |
| [41]       | PCM in leak-proof aluminium foil packets   | Poly-Crystalline silicon                  | Ceramic fiber paper                   | Serpentine copper pipes                     | Water  |
| [44]       | Acrylic glass container                    | Mono-Crystalline silicon                  | Insulation is included (type unclear) | Serpentine copper tubing                    | 0.2 wt% ZnO/water nanofluid  |
| [47]       | Galvanized steel container                 | Unclear type                              | Glass wool                            | Serpentine copper pipes                     | SiC-water nanofluid  |
| [48]       | Copper plate and Plexiglas cover container | Mono-Crystalline silicon                  | Rigid polyurethane foam               | Copper tubes                                | ZnO/water nanofluid  |
| [49]       | Unclear type                               | Unclear type                              | Corkwood                              | Serpentine copper pipes combined with plate | Water  |
| [50]       | Unclear type                               | Unclear type                              | Insulation is included (type unclear) | Single channel                              | Air  |
| [51]       | Plexiglass back cover                      | Unclear type                              | Polyethylene foam shee                | Serpentine copper tubes                     | Water  |

initial investment. The LCOE was calculated with eq. (1) [56],

$$\text{LCOE} = \frac{\text{IC} \times \text{CRF} + \text{OM}}{\text{EO}} \quad (1)$$

where the capital recovery factor was calculated as follows,

$$\text{CRF} = \frac{(1+p)^n \cdot p}{(1+p)^n - 1} \quad (2)$$

According to the above specified input parameters, LCOE was calculated for the given case and equals 0.11 €/kW (average degradation factor for PV cell was also taken into account and equals 0.5% annually, and which is typical value). Design modifications to a convectional PVT panel to form a PVT-PCM panel would request an additional unit cost per collector area (€/m<sup>2</sup>), but on the other side it would also ensure an overall performance improvement (both electrical and thermal). In order to estimate the maximal allowed overall investment cost to modify the PVT to a PVT-PCM collector, the same LCOE framework was used. The results are presented in Table 6 with the overall efficiency improvement ranging from 20% to 40% (this range is critical as a higher performance would lead to a higher fund buffer in order to cover the requested cost for the specific design). The estimation of the maximal allowed overall investment provides an orientation figure and ranges from 36 (€/m<sup>2</sup>) to 120 (€/m<sup>2</sup>) for the given circumstances. The previous calculated numbers are estimations and are limited to the specific considered case, i.e. based on performance data from Ref. [55]. Moreover, PVT-PCM designs usually request operational energy, which also needs to be taken into account while calculating the LCOE (water or air circulation via pipeline system for instance). Since operational energy highly depends from the specific selected PVT-PCM collector design, the operational energy was excluded in this calculations due to the mentioned circumstances, which is a limitation. However, the gained data for the estimation of the unit cost per collector area are still useful as orientation and can help designers in the possible selection of specific materials and design solutions. Moreover, the amount of the allowed unit cost needs to be carefully taken into account during the design stage, where the specific design should ensure the targeted overall efficiency improvement.

The results indicated that for the considered case, the overall efficiency improvement should be at a suitable level to ensure a lower LCOE than the LCOE of a convectional PVT panel. For instance, the design of a PVT-PCM panel with a 1.5 cm thick PCM layer leads to amount of approximately 15 kg of PCM materials for an assumed PVT collector area of 1.326 m<sup>2</sup> (mass depends from the specific type of PCM material and general PVT collector dimensions). The unit cost of market available PCM materials was specified in Section 2 and if the average unit price for PCM materials is taken at about 7.0 €/kg, the cost for just the mentioned layer of PCM material equals around 105 € for the given case (79 €/m<sup>2</sup>). The herein presented results showed a strong impact of the PCM cost with respect to the LCOE value. In that sense, one of the key issues should be related to the investigation of the more economically viable PCMs to ensure the economic viability of PVT-PCM collector

designs. The review also indicated that very few studies had analyzed the economic aspect of specific PVT-PCM design solutions with a determined payback up to 15 years.

### 5.3. Environmental suitability

The production of PVT collectors is associated with the utilization of various constructional materials that cause environmental footprints. From the previous point of view, the specific design of PVT-PCM collectors should also be carefully evaluated. Unfortunately, the review of the existing PVT-PCM collector designs indicated that the environmental aspects were not evaluated in any of the herein considered research studies, as the emphasis was mainly given to performance improvement. The main constructive elements of PVT-PCM collectors are metal parts (aluminium, copper, etc.), thermal insulation and PCM material, where the exact amount of each used material depends from the specific design solution of the PVT-PCM collector. The most critical from an environmental point of view, is the use of PCM materials as it was clearly indicated in study [54]. Several cooling techniques for PV panels were evaluated in work [54] from an environmental aspect, using LCA analysis (Life Cycle Analysis). Among the evaluated cooling strategies, the PV-PCM passive cooling approach was also evaluated. The PV-PCM passive cooling concept turned out to be the worst one regarding its environmental impact, which is mainly due to the use of PCM materials, as it strongly affects global warming, acidification and eutrophication, Fig. 21.

Considering the previously mentioned findings, and taking into account that each PVT-PCM collector design is specific in a sense, the main design goal from an environmental point of view should be focused towards the minimization of PCM quantities. The focus should be directed to the optimization of PCM layers in specific climates, i.e. to find a proper balance between the performance benefit and utilized quantity of PCM materials. The second critical aspect is related to the utilization of nanomaterials in specific PVT-PCM collector designs. Nanomaterials are hazardous and highly toxic both for humans (operators) and the environment [57]. Justification regarding nanomaterial use for specific PVT-PCM collector designs should be carefully evaluated, but the goal should be to avoid the use of nanomaterials in order to reduce potential hazards. Finally, the specific PVT-PCM collector design has a direct impact on operational energy (for instance circulation pumps) where the main task in the design approach should be also to minimize the use of operational energy and by that to reduce harmful impacts to environment. The use of smart and IoT (Internet of Things) technologies could potentially ensure a more efficient use of operational energy for PVT-PCM systems.

## 6. Conclusion and future directions

Specific designs regarding photovoltaic thermal collectors were analyzed in this work, where the main direction was focused on PVT collectors with incorporated phase change materials (PVT-PCM systems). Different design concepts of PVT-PCM collectors were examined and that were experimentally tested in different climates. The results indicated the importance of the specific PVT-

**Table 6**

Maximal unit cost per collector area as function of overall efficiency improvement of PVT-PCM collector for specific case study.

| Overall efficiency improvement (%) | Allowed unit cost per collector area (€/m <sup>2</sup> ) |
|------------------------------------|--|
| 20%                                | 36   |
| 30%                                | 80   |
| 40%                                | 120  |

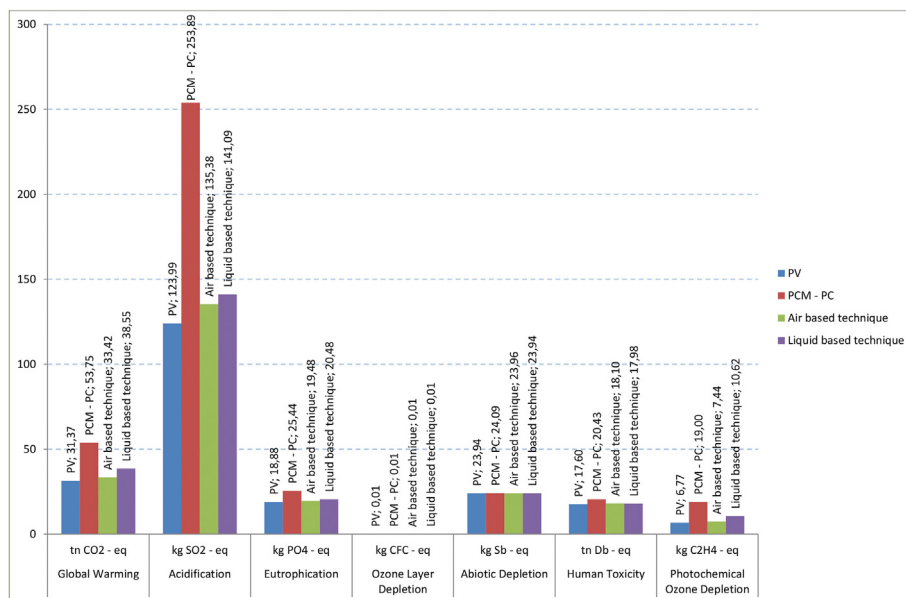


Fig. 21. Environmental evaluation of passive cooling techniques for PV panels [54].

PCM collector design and its impact on electrical and thermal performance. According to the conducted comprehensive analysis in this work, further important conclusions, as well as useful insights towards future directions in the field, are highlighted as follows:

- Depending on the specific PVT-PCM collector design and used coolant (air, water, nano-fluid), the electrical performance of the PVT-PCM collector is usually less than 20%, while improvements in thermal performance ranges mostly from 40% to 70% (in some specific cases it can go over 80%). The highest overall efficiency in PVT-PCM collectors is reached when water or nano-fluids are used as coolants and is usually over 60%, or also in the case when specially designed absorbers are considered. For air-based cooled PVT-PCM collectors, the overall efficiency is mostly lower than 40%. Even though air-based cooled PVT-PCM collectors have the lowest performance indicators, more research efforts should be directed to the integration of these collectors within HVAC systems in buildings, and by that to improve the energy efficiency of building systems,
- The performance indicators for PVT-PCM systems were not systematically compared in existing research works, which makes it difficult to correctly compare the general performance of various PVT-PCM collector designs. The improvement in electrical performance of specific PVT-PCM collector designs should be compared with a referent PV panel of the same nominal size, while thermal efficiency should be compared with a PVT panel (one without an incorporated PCM layer and cooling setup). The proposed comparison approach would allow for a precise and correct evaluation of performance improvements, concerning specific PVT collector designs, and give a fair basis for comparison in general. Future research efforts should be carefully considered along with the herein proposed comparison approach,
- The specific PVT-PCM collector designs were not well-elaborated, i.e. it is unclear why certain designs were selected and what the general motivation was for specific conceptual approaches. It indicates the necessity for more comprehensive design approaches to justify the specific determined PVT-PCM collector designs. In general, there is the necessity to

categorize and distinguish suitable collector designs with respect to different climates to detect the most effective designs that would ensure improvements both in electrical and thermal efficiency. With respect to existing research findings, more experimental investigation is needed to investigate PVT-PCM collector performances, as some geographical areas are not well covered with experiments. An important aspect of experimental investigations is to discover the performance limits of the PVT-PCM collectors in different climates and specific collector designs,

- Alternative tube geometries, as well as specific tube layouts, should also be considered in future research efforts to ensure uniform and more effective PVT-PCM collector cooling. A combination of tube geometries, tube layouts and specific absorbers could lead to important performance benefits,
- Most studies did not consider PCM layer thickness optimization for certain geographical locations, i.e., sensitivity analysis regarding certain climate conditions with respect to the optimal PCM layer thickness is necessary. The influence of supercooling as well as PCM phase separation should also be investigated more thoroughly in future research works with respect to the performance of PVT-PCM collectors. The use of microencapsulate suspensions could also be considered in PVT-PCM collector designs.
- The investigation of novel and suitable PCMs is necessary for PVT-PCM collectors to discover viable economic solutions (high unit costs of PCM materials) and PCMs with longer lifetime and proper environmental suitability as the production of PCMs leaves environmental footprints. More experimental approaches should also be conducted with composite PCMs,
- The use of nanomaterials could be beneficial for the overall efficiency of PVT-PCM systems but the key aspect is their economic suitability. Regarding existing research works, it is mostly unclear why specific nanomaterials were used in certain concentrations. The optimization of nanomaterial concentrations is necessary to check the highest possible performance improvement and finally explore the economic aspect. Due to the toxicity and environmental impacts of nanomaterials, their general application in PVT-PCM collectors needs to be further justified and which requires further investigations,



- The economic evaluations of the PVT-PCM collectors are not well covered in the existing research literature. Very few studies obtained economic analyses and revealed payback times ranging from 4 up to 15 years, but the results are limited to studies in warmer climates. An important aspect for future research work should be directed to the economic evaluation of certain PVT-PCM collector designs,
- Environmental PVT-PCM collector design evaluations are completely omitted when analyzing present research findings. It is necessary to provide environmental evaluations regarding PVT-PCM concepts to compare and discover less harmful collector designs concerning environmental footprints and rational use of resources.

### Credit roles

Sandro Nizetić; - Conceptualization, Methodology, Analysis of results, Writing, Supervision. Mišo Jurčević; - Conceptualization, Methodology, Analysis of results, Writing, Supervision and Editing, Duje Čoko - Analysis of results, Writing, Supervision and Editing, Müslüm Arıcı; - Analysis of results, Writing, Supervision and Editing, Anh Tuan Hoang- Analysis of results, Writing, Supervision and Editing.

### Declaration of competing interest

The authors declare that they have no known competing financial interests or personal relationships that could have appeared to influence the work reported in this paper.

### Acknowledgments

This work was funded by the Croatian science foundation (Research project: Smart and hybrid cooling techniques for siliceous photovoltaic panels-IP-01-2018-2814).

### References

- [1] United nations climate change. unfccc.int/process-and-meetings/the-paris-agreement/the-paris-agreement. [Accessed 14 December 2020].
- [2] Khan I, Hou F, Le HP. The impact of natural resources, energy consumption, and population growth on environmental quality: fresh evidence from the United States of America. *Sci Total Environ* 2021;754. Article number 142222.
- [3] Stephens S, Robinson BMK. The social license to operate in the onshore wind energy industry: a comparative case study of Scotland and South Africa. *Energy Pol* 2021;148. Article number 111981.
- [4] Grubišić-Cabo F, Nizetić S, Marinić Kragić I, Čoko D. Further progress in the research of fin-based passive cooling technique for the free-standing silicon photovoltaic panels. *Int J Energy Res* 2019;43(8):3475–95.
- [5] EU Commission. PV status report. 2019. [ec.europa.eu/jrc/sites/jrcsh/files/kjna29938enn\\_1.pdf](https://ec.europa.eu/jrc/sites/jrcsh/files/kjna29938enn_1.pdf). [Accessed 12 December 2020].
- [6] IRENA. [irena.org/-/media/Files/IRENA/Agency/Publication/2020/Mar/IRENA\\_RE\\_Capacity\\_Highlights\\_2020.pdf?la=en&hash=B6BDF8C3306D271327729B9F9C9AF5F1274FE30B](https://www.irena.org/-/media/Files/IRENA/Agency/Publication/2020/Mar/IRENA_RE_Capacity_Highlights_2020.pdf?la=en&hash=B6BDF8C3306D271327729B9F9C9AF5F1274FE30B). [Accessed 12 December 2020].
- [7] Photovoltaics report. [ise.fraunhofer.de/content/dam/ise/de/documents/publications/studies/Photovoltaics-Report.pdf](https://www.ise.fraunhofer.de/content/dam/ise/de/documents/publications/studies/Photovoltaics-Report.pdf). [Accessed 4 December 2020].
- [8] Marinić-Kragić I, Nizetić S, Grubišić-Cabo F, Papadopoulos AM. Analysis of flow separation effect in the case of the free-standing photovoltaic panel exposed to various operating conditions. *J Clean Prod* 2018;174:53–64.
- [9] Atsu D, Seres I, Aghaei M, Farkas I. Analysis of long-term performance and reliability of PV modules under tropical climatic conditions in sub-Saharan. *Renew Energy* 2020;162:285–95.
- [10] Saranchimeg S, Nair NKC. A novel framework for integration analysis of large-scale photovoltaic plants into weak grids. *Appl Energy* 2021;282. Article number 116141.
- [11] Nain P, Kumar A. Metal dissolution from end-of-life solar photovoltaics in real landfill leachate versus synthetic solutions: one-year study. *Waste Manag* 2020;114:351–61.
- [12] Kim Hana, Park Hun. PV waste management at the crossroads of circular economy and energy transition: the case of South Korea. *Sustainability* 2018;10(10). Article number 3565.

- [13] Sulaeman S, Brown E, Quispe-Abad R, Müller N. Floating PV system as an alternative pathway to the amazon dam underproduction. *Renew Sustain Energy Rev* 2021;135. Article number 110082.
- [14] Meitzner R, Schubert US, Hoppe H. Agrivoltaics—the perfect fit for the future of organic photovoltaics. *Advanced Energy Materials* 2020;1–7:2002551.
- [15] Herez A, El Hage H, Lemenand T, Ramadan M, Khaled M. Review on photovoltaic/thermal hybrid solar collectors: classifications, applications and new systems. *Sol Energy* 2020;207:1321–47.
- [16] Herez A, El Hage H, Lemenand T, Ramadan M, Khaled M. Parabolic trough photovoltaic/thermal hybrid system: thermal modeling and parametric analysis. *Renew Energy* 2021;165:224–36.
- [17] Daghigh Roonak, Oramipoor Hooman, Shahidian Roonak. Improving the performance and economic analysis of photovoltaic panel using copper tubular-rectangular ducted heat exchanger. *Renew Energy* 2020;156: 1076–88.
- [18] Yandri Erkata. Methods for the development and testing of polymeric hybrid photovoltaic thermal (PVT) collector for indoor experiments. *Methods (Duluth)* 2019;6:2620–35.
- [19] Xu HJ, Xing ZB, Wang FQ, Cheng ZM. Review on heat conduction, heat convection, thermal radiation and phase change heat transfer of nanofluids in porous media: fundamentals and applications. *Chem Eng Sci* 2019;195: 462–83.
- [20] Xu H, Wang Y, Han X. Analytical considerations of thermal storage and interface evolution of a PCM with/without porous media. *Int J Numer Methods Heat Fluid Flow* 2019;30(1):373–400.
- [21] Xu HJ, Zhao CY. Analytical considerations on optimization of cascaded heat transfer process for thermal storage system with principles of thermodynamic. *Renew Energy* 2019;132:826–45.
- [22] Reji Kumar R, Samykano M, Pandey AK, Kadigama K, Tyagi VV. Phase change materials and nano-enhanced phase change materials for thermal energy storage in photovoltaic thermal systems: a futuristic approach and its technical challenges. *Renew Sustain Energy Rev* 2020;133. Article number 110341.
- [23] Laghari IA, Samykano M, Pandey AK, Kadigama K, Tyagi VV. Advancements in PV-thermal systems with and without phase change materials as a sustainable energy solution: energy, exergy and exergoeconomic (3E) analytic approach. *Sustainable Energy and Fuels* 2020;4(10):4956–87.
- [24] Hemmat Esfe M, Kamyab MH, Valadkhani M. Application of nanofluids and fluids in photovoltaic thermal system: an updated review. *Sol Energy* 2020;199:796–818.
- [25] Scopus. <https://www.scopus.com/search/form.uri?display=basic>. [Accessed 25 December 2020].
- [26] SCH International Energy Agency. <https://task60.iea-shc.org/article?NewsID=214>. Accessed 27 December 2020.
- [27] Photovoltaics report. <https://www.ise.fraunhofer.de/content/dam/ise/de/documents/publications/studies/Photovoltaics-Report.pdf>. [Accessed 4 December 2020].
- [28] Convert Energy. <https://www.convertenergy.co.uk/pv-t-hybrid-solar>. [Accessed 12 December 2020].
- [29] Nizetić S, Giama E, Papadopoulos AM. Comprehensive analysis and general economic-environmental evaluation of cooling techniques for photovoltaic panels, Part II: Active cooling techniques. *Energy Convers Manag* 2018;155: 301–23.
- [30] Wrap-Up PVT. Energy systems with photovoltaic-thermal solar collectors. [https://spfc.ch/fileadmin/user\\_upload/spfc/publ/PVT\\_WrapUp\\_Final\\_EN.pdf](https://spfc.ch/fileadmin/user_upload/spfc/publ/PVT_WrapUp_Final_EN.pdf). [Accessed 6 December 2020].
- [31] Rostami S, Afrand M, Shahsavari A, Sheikholeslami M, Kalbasi R, Aghakhani S, Shadloo MS, Oztop HF. A review of melting and freezing processes of PCM/nano-PCM and their application in energy storage. *Energy* 2020;211. Article number 118698.
- [32] Lin W, M Z, Wang S, Sohel MI, Lo Cascio E. Experimental investigation and two-level model-based optimisation of a solar photovoltaic thermal collector coupled with phase change material thermal energy storage. *Appl Therm Eng* 2021;182. Article Number 116098.
- [33] Song J, Sobhani B. Energy and exergy performance of an integrated desiccant cooling system with photovoltaic/thermal using phase change material and maisotsenko cooler. *Journal of Energy Storage* 2020;32. Article Number 101698.
- [34] Tariq R, Xamán J, Bassam A, Ricalde LJ, Soberanis MAE. Multidimensional assessment of a photovoltaic air collector integrated phase changing material considering Mexican climatic conditions. *Energy* 2020;209. Article number 118304.
- [35] Naghdbishi A, Yazdi ME, Akbari G. Experimental investigation of the effect of multi-wall carbon nanotube – water/glycol based nanofluids on a PVT system integrated with PCM-covered collector. *Appl Therm Eng* 2020;178. Article number 115556.
- [36] Gan G, Xiang YV. Experimental investigation of a photovoltaic thermal collector with energy storage for power generation, building heating and natural ventilation. *Renew Energy* 2020;150:12–22.
- [37] Hassan A, Wahab A, Qasim MA, Janjua MM, Ali MA, Ali HM, Jadoon TR, Ali E, Raza A, Javaid N. Thermal management and uniform temperature regulation of photovoltaic modules using hybrid phase change materials-nanofluids system. *Renew Energy* 2020;145:282–93.
- [38] Fayaz H, Rahim NA, Hasanuzzaman M, Nasrin R, Rivai A. Numerical and experimental investigation of the effect of operating conditions on

- performance of PVT and PVT-PCM. *Renew Energy* 2019;143:827–41.
- [39] Maatallah T, Zachariah R, Al-Amri FG. Exergo-economic analysis of a serpentine flow type water based photovoltaic thermal system with phase change material (PVT-PCM/water). *Sol Energy* 2019;193:195–204.
- [40] Simón-Allué R, Guedea I, Villén R, Brun G. Experimental study of Phase Change Material influence on different models of Photovoltaic-Thermal collectors. *Sol Energy* 2019;190:1–9.
- [41] Hossain MS, Pandey AK, Selvaraj J, Rahim NA, Islam MM, Tyagi VV. Two side serpentine flow based photovoltaic-thermal-phase change materials (PVT-PCM) system: energy, exergy and economic analysis. *Renew Energy* 2019;136:1320–36.
- [42] Choubineh N, Jannesari H, Kasaiean A. Experimental study of the effect of using phase change materials on the performance of an air-cooled photovoltaic system. *Renew Sustain Energy Rev* 2019;101:103–11.
- [43] Lari MO, Sahin AZ. Effect of retrofitting a silver/water nanofluid-based photovoltaic/thermal (PV/T) system with a PCM-thermal battery for residential applications. *Renew Energy* 2018;122:98–107.
- [44] Hosseinzadeh M, Sardarabadi M, Passandideh-Fard M. Energy and exergy analysis of nanofluid based photovoltaic thermal system integrated with phase change material. *Energy* 2018;147:636–647x22.
- [45] Rubitherm® Technologies GmbH. <https://www.rubitherm.eu/>. [Accessed 6 December 2020].
- [46] Arıcı M, Bilgin F, Nizetić S, Papadopoulos AM. Phase change material based cooling of photovoltaic panel: a simplified numerical model for the optimization of the phase change material layer and general economic evaluation. *J Clean Prod* 2018;189:738–45.
- [47] Ali HA, Al-Waeli, Sopian K, Chaichan Miqdam T, Kazem HA, Ibrahima A, Mat S, Ruslan MH. Evaluation of the nanofluid and nano-PCM based photovoltaic thermal (PVT) system: an experimental study. *Energy Convers Manag* 2017;151:693–708.
- [48] Sardarabadi M, Passandideh-Fard M, Maghrebi JM, Ghazikhani M. Experimental study of using both ZnO/water nanofluid and phase change material (PCM) in photovoltaic thermal systems. *Sol Energy Mater Sol Cells* 2017;161:62–9.
- [49] Al-Imam MFI, Beg RA, Rahman MS, Khan MZH. Performance of PVT solar collector with compound parabolic concentrator and phase change materials. *Energy Build* 2015;113:139–44.
- [50] Lin Wenyue, Ma Zhenjun, Imroz Sohel M, Cooper Paul. Development and evaluation of a ceiling ventilation system enhanced by solar photovoltaic thermal collectors and phase change materials. *Energy Convers Manag* 2014;88:218–30.
- [51] Das Dudul, Bordoloi Urbashi, Akash Dilip Kamble, Harrison Hihu, Muigai, Krishna Paic Ranjith, Kalitaa Pankaj. Performance investigation of a rectangular spiral flow PV/T collector with a novel form-stable composite material. *Appl Therm Eng* 2021;182. Article number 116035.
- [52] Fu Z, Liang X, Li Y, Li L, Zhu Q. Performance improvement of a PVT system using a multilayer structural heat exchanger with PCMs. *Renew Energy* 2021;169:308–17.
- [53] Ahmadi R, Monadinia F, Maleki M. Passive/active photovoltaic-thermal (PVT) system implementing infiltrated phase change material (PCM) in PS-CNT foam. *Sol Energy Mater Sol Cell* 2021;222. Article number 110942.
- [54] Nizetić S, Papadopoulos AM, Giama E. Comprehensive analysis and general economic-environmental evaluation of cooling techniques for photovoltaic panels, Part I: passive cooling techniques. *Energy Convers Manag* 2017;149:334–54.
- [55] Solar Heat Europe. [solarheateurope.eu/2018/04/30/increasingly-popular-heat-and-power-from-the-same-roof/](https://solarheateurope.eu/2018/04/30/increasingly-popular-heat-and-power-from-the-same-roof/), [Accessed 22 February 2021].
- [56] Grubišić Cabo F, Nizetić S, Giama E, Papadopoulos A. Techno-economic and environmental evaluation of passive cooled photovoltaic systems in Mediterranean climate conditions. *Appl Therm Eng* 2020;169. Article number 114947.
- [57] Jurčević M, Nizetić S, Arıcı Mb, Octoń P. Comprehensive analysis of preparation strategies for phase change nanocomposites and nanofluids with brief overview of safety equipment. *J Clean Prod* 2020;274. Article number 122963.



## Appendix F

Title: Investigation of heat convection for photovoltaic panel towards efficient design of novel hybrid cooling approach with incorporated organic phase change material

Authors: Jurčević M., Nižetić S., Marinić Kragić I., Čoko D., Arici M., Giama E., Papadopoulos A.

Publisher: *Elsevier*

Journal: *Sustainable Energy Technologies and Assessments*

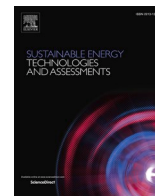
Edition, ID, year: 47, 101497, 2021.

Indexed in: Scopus, Science Citation Index Expanded, INSPEC

Journal Impact Factor: 7.632 Q1 (WoS and SJR-2021.)

DOI: <https://doi.org/10.1016/j.seta.2021.101497>

**Abstract:** A novel hybrid cooling strategy was proposed for the free-standing photovoltaic panel (PV), i.e. the design of a novel photovoltaic-thermal collector (PVT) was proposed. The hybrid cooling approach assumes both passive (PCM-Phase Change Material) and active (water) cooling approach with an incorporated smart regulation system. The design details of a novel hybrid cooling approach, i.e. novel PVT collector were elaborated in detail. Besides elaboration of the specific design approach, the experimental and numerical investigation was also carried out as a necessary step for further development of the ongoing experimental setup. Namely, the convective heat transfer coefficients were investigated by the experimental way in the wind tunnel for freestanding PV panel. The idea was also to investigate a general behaviour of the convective heat transfer profiles for various wind speeds (0 m/s to 6.7 m/s), relative wind angles (0° to 45°), and PV panel tilt angles (0° to 35°) since they strongly affect performance. The numerical analysis was conducted, and simulations were compared with experimental readings. An average deviation between the measurement and experimental data was determined to be around 12%, and which directs that the developed numerical model is reasonably accurate. Numerically, the best PV cooling effect was reached for 45° wind angle while the worst was achieved for a wind angle of about 20°. Furthermore, this phenomenon was confirmed by experimental data. The gained research outcomes in this work are important for the finalization of the experimental setup that would be enabled in the Mediterranean climate operating conditions. The proposed concept of a novel PVT collector could be suitable for building applications as an integral part of the building energy systems, i.e. for space heating or hot water preparation.



## Investigation of heat convection for photovoltaic panel towards efficient design of novel hybrid cooling approach with incorporated organic phase change material

Mišo Jurčević<sup>a</sup>, Sandro Nižetić<sup>a,\*</sup>, Ivo Marinić-Kragić<sup>a</sup>, Duje Čoko<sup>a</sup>, Müslüm Arıcı<sup>b</sup>, Effrosyni Giama<sup>c</sup>, Agis Papadopoulos<sup>c</sup>

<sup>a</sup> University of Split, FESB, Split, Croatia

<sup>b</sup> Kocaeli University, Kocaeli, Turkey

<sup>c</sup> Aristotle University of Thessaloniki, Thessaloniki, Greece

### ARTICLE INFO

#### Keywords:

Photovoltaic-thermal  
PVT  
PCM  
Solar energy  
Renewable energy  
Efficiency

### ABSTRACT

A novel hybrid cooling strategy was proposed for the free-standing photovoltaic panel (PV), i.e. the design of a novel photovoltaic-thermal collector (PVT) was proposed. The hybrid cooling approach assumes both passive (PCM-Phase Change Material) and active (water) cooling approach with an incorporated smart regulation system. The design details of a novel hybrid cooling approach, i.e. novel PVT collector were elaborated in detail. Besides elaboration of the specific design approach, the experimental and numerical investigation was also carried out as a necessary step for further development of the ongoing experimental setup. Namely, the convective heat transfer coefficients were investigated by the experimental way in the wind tunnel for free-standing PV panel. The idea was also to investigate a general behaviour of the convective heat transfer profiles for various wind speeds (0 m/s to 6.7 m/s), relative wind angles (0° to 45°), and PV panel tilt angles (0° to 35°) since they strongly affect performance. The numerical analysis was conducted, and simulations were compared with experimental readings. An average deviation between the measurement and experimental data was determined to be around 12%, and which directs that the developed numerical model is reasonably accurate. Numerically, the best PV cooling effect was reached for 45° wind angle while the worst was achieved for a wind angle of about 20°. Furthermore, this phenomenon was confirmed by experimental data. The gained research outcomes in this work are important for the finalization of the experimental setup that would be enabled in the Mediterranean climate operating conditions. The proposed concept of a novel PVT collector could be suitable for building applications as an integral part of the building energy systems, i.e. for space heating or hot water preparation.

### Introduction

The role of renewable energy technologies [1] is a key one with respect to the necessary energy transition goals [2] and the shift from fossil-based technologies towards decarbonization of convective energy systems and industries in general, [3]. Moreover, the photovoltaic [4] and wind generation technologies [5] are dominant ones regarding the new overall added installed capacities. For instance, in 2019 the solar and wind generation technologies confirm further expansion and leading position regarding newly added capacities. According to the report [6] almost 100 GW of the solar capacities and over 50 GW of the

wind capacities were added in 2019, Fig. 1, which makes their joint share of about 90% in 2019.

The use of solar energy is mainly directed to the implementation of the photovoltaic (PV) technologies that are in majority based on the silicon (c-Si) PV panels with a current market share of over 95%, [7]. The PV technologies have become more affordable, but still, they suffer from relatively low overall energy conversion efficiency that is usually below 18% in real operating conditions.

The improvement in the economic aspect, as well as further expansion of the PV systems, could be ensured via further development and more intense implementation of photovoltaic-thermal (PVT) systems,

\* Corresponding author at: University of Split, Faculty of FESB, Rudjera Boškovića 32, 21000 Split, Croatia.

E-mail address: [snizetic@fesb.hr](mailto:snizetic@fesb.hr) (S. Nižetić).

<https://doi.org/10.1016/j.seta.2021.101497>

Received 30 April 2021; Received in revised form 28 June 2021; Accepted 19 July 2021

Available online 2 August 2021

2213-1388/© 2021 Elsevier Ltd. All rights reserved.

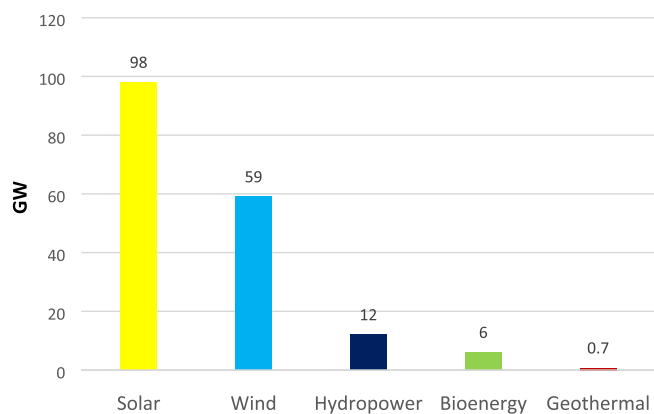


Fig. 1. Comparison of newly added renewable energy capacities in 2019, [6].

[8]. The PVT systems are capable to produce electricity and thermal power output at the usually limited available surface area, i.e. they represent in essence a kind of micro-cogeneration units, albeit in a reverse approach. One of the major problems with PV technologies currently available on the market is their performance drop linked by elevated working temperatures [9], which directly affects the economics of the PV systems. In the PVT configurations, the PV panels are being cooled achieving thereby an improvement of their performance, which usually goes up to 20% with respect to referent PV panel (non-cooled). At the same time, the removed heat is utilized in the buildings, with a thermal efficiency of the PVT systems that mostly range from 40% to 70%; however it strongly depends on the certain PVT collector solution, [10]. Namely, various design elements affect the overall efficiency of the PVT collectors and some of them will be elaborated in continuation.

As mentioned above, the design of the PVT collectors has an impact on the overall efficiency of the PVT systems where the general design of the PVT collector should be obtained with respect to certain energy demands (electric and thermal). With respect to the previous, the PVT systems are usually implemented to produce domestic hot water, [11] to meet the demand of residential buildings. Besides, the hot water preparation of the PVT systems can be also efficiently applied to support the space heating systems [12], for drying purposes [13], or even for the production of process heat in industrial applications [14]. With a request for an increase in the temperature of delivered hot water from the PVT collector, the thermal efficiency of the PVT collectors is being increased, while in these situations the improvement of the electrical performance is usually being limited (elevated operating temperatures of the PV panel). Regarding the specific energy requests, the design of the PVT collector should be carefully carried out, to ensure the proper balancing (matching) expressed by the targeted production ratio of thermal and electric output.

The main design elements of the PVT collectors are PV cell (mono or poly-crystalline silicon), casing (aluminum, steel, acrylic glass, etc.), an insulation layer (mineral wool, polyethylene foam, mineral wool, corkwood, ceramic fiber paper, etc.), tubes or channels (mostly straight or serpentine ones made of copper or aluminum), PCM layer (if it is a PVT-PCM configuration) and finally coolant (water, air, and nanofluids). According to the field experiments, the lowest performance improvement is recorded for air-cooled PVT collectors, [9], since air has weak thermal properties. Furthermore, since the efficiency of air-cooled PVTs depends on ambient air temperature, it is decreasing when it would be most needed, i.e. in warm conditions. However, air-based PVT collectors are interesting and suitable for integration in the building facilities in order to directly heat the adjacent rooms. Furthermore, the PVT designs with water and/or nanofluids are ensuring the highest increase in the overall performance improvement, since apart from better thermodynamic features, they can utilize water at temperatures significantly lower than ambient air. In the case of nanofluids, the main

problem is economic viability, since nanomaterials are expensive, and they require a careful preparation process (issue of long-term stability of nanofluids properties). Finally, there is also a problem with the toxicity of nanomaterials and that needs to be carefully considered [15].

Designs of the PVT collectors with included Phase Change Materials (PCM) are also interesting since the PCM layer is effective for the short-term thermal regulation of the PVT working temperature, based on this (limited thermal storage). However, the issue with PCM materials is problematic thermal regulation of the PCM material in the long-term (issue with thermal inertia of the PCM layer), and which has a reflection on the operational energy of the PVT-PCM collector, due to more intense circulation of the coolant and the respective energy consumption by the circulation pumps. The second problem with the implementation of the PCM is the high unit purchase cost, and which strongly affects the economic suitability of the PVT-PCM collectors. For the aforementioned reasons, the PVT-PCM collectors request careful design, proper selection of suitable PCMs (organic, composite, inorganic, etc.), and optimization of the PCM layer. The further upgrade of the PVT-PCM collectors can be ensured via the addition of various nanomaterials (SiC, Al<sub>2</sub>O<sub>3</sub>, ZnO, graphene, etc.) in the PCM layer to form nPCM composites, [16]. The implementation of the nanomaterials in the PCM material needs to be carefully provided since there could be issues with agglomeration and as already mentioned long-term stability of nPCM physical characteristics.

The tube layout, or geometry of the cooling channel, is also a vital and important part of the PVT collectors since it influences the uniformity of the cooling approach. An efficient tube layout ensures a more uniform cooling of the PVT collector which is beneficial for performance improvement. Usually, copper tubes are being used in various layouts such as straight or serpentine configurations. Serpentine configuration leads to a higher performance improvement in general, compared to the straight tube layout configuration (better cooling uniformity). Apart from the tubes, the straight channels of various geometry can be also used for thermal management of the PVT collectors. The straight channels are usually being used for the air-based PVT collectors as the most suitable design, ensuring a uniform pressure drop and a controlled airflow. Finally, the absorber design is also crucial to ensure the reasonable overall efficiency of the PVT collector where different approaches are possible such as the combination of plates with attached tubes, or special absorbers made of polymeric or aluminum roll-bond materials.

Various PVT collector designs have been recently examined and that was directed on the performance investigations in different operating, i. e. climate conditions. An experimental analysis of the PVT-PCM collector and comparison with conventional PV panel was reported in [17]. The general design of the PVT-PCM collector was made from tubes that were installed in a container filled with PCM material. The field results indicated a rise in the electrical performance of the PVT-PCM collector by 7.43%, comparing with the referent PV panel. The implementation of the PCM material ensured performance improvement, however, an economic check was not obtained to examine the economic suitability of the proposed PVT-PCM concept. The investigation of the nano-enhanced PVT system was discussed in [18] for PVT collector tested in Malaysian climate conditions. The nanomaterial was added to the PCM material and that reduced the PV panel's temperature by about 4 °C, where the temperature of the produced hot water was raised over 46 °C. Experiments were conducted for different water flow rates (ranging from 0.5 l/min to 4.0 l/min). The maximal overall energy performance of the PVT-nPCM collector was 85%. Again, the economics of the proposed system was not checked, which could be questionable due to the addition of the rather costly nanomaterials. The numerical and experimental evaluation of the PVT collector design was discussed in [19] for PVT collector cooled with air. The design solution of the PVT collector was quite basic, i.e. the straight channel was provided below the PV panel with a V-groove absorber and equipped with a layer of thermal insulation. The collector was examined in Indian climate circumstances (specifically in Ghaziabad). The electrical performance of the air-based PVT panel was

up to 10.2%, the thermal one up to 41.5%, and the overall performance was up to 52%. The developed numerical model was validated with experimental readings and showed well matching. An economic analysis of the examined PVT collector design was not provided. The plain serpentine tube and serpentine sinusoidal tube design of the PVT collector were reported in work [20], which was the main novelty of the work. The system also considered cooling with nanofluid (magnetite) with nanomaterial concentrations ranging from 0.5% to 2%. The various operating conditions were tested in laboratory circumstances for the case of the small-scaled PVT panel, together with an energetic and exergetic performance analysis. The best performance was reached for the nanofluid concentration of 2%, with overall energy efficiency ranging from about 87% to 92%, depending on the specific wavelength. The results of the mentioned study are promising but they should be provided on the large-sized PVT panel in the real operating conditions, to ensure more precise performance data as well as to examine the impact of the larger PV panel's geometry. The performance analysis of the PVT collector was provided in [21] using two different liquid working fluids along with the tested variation of the cooling channel geometry. The specific PVT collector design was obtained from the glass cover (bellow layer of the air), then PV panel and finally below the PV panel a copper absorber with attached cooling tubes was provided together with thermal insulation. The different channel geometries were examined, i.e. half-circular tube, half-square, and circular tubes. The results showed that the best tube configuration is the half-circular tube design when compared with other configurations. Two cooling fluids were examined, i.e. water and a mixture of antifreeze medium and water. The water as coolant ensured better improvement in the overall performance when compared to the mixture of water and antifreeze (60:40% mixing ratio of water and ethylene). The improvement in the thermal efficiency was about 4.5%, while electric efficiency about 1.85%. The economic aspect of the examined PVT collector design was not provided. The configuration with a full square channel should be also investigated to get a clear comparison of various channel geometries. In work [22], authors have applied a design that involves front water cooling of the PVT panel, i.e. glass and water channel below glass and PV panel. The numerical analysis was conducted in the same work together with experimental work. The performance analysis indicated improvement in the electrical efficiency from 0.8% to 1% by front water cooling, while the overall energy efficiency of the proposed PVT collector design was about 81%. The study calls for an economic evaluation in order to justify performance improvement. A novel water-based PVT collector solution was presented in the study [23]. The work was targeted on the numerical investigations and results were compared with experimental readings. The novel PVT panel design proposed a hybrid approach, where a PV panel was installed at the bottom of solar collector (direct absorption). Results based on the numerical investigations showed a significant performance improvement of a novel proposed PVT collector in comparison with other designs. The optimization of the rectangular cooling channel was also provided, together with an in-depth analysis of all influential parameters.

From a brief previous analysis of the recent research findings in this field, it is noticeable that there is still high research interest focused on the development of novel and upgraded PVT collector designs.

The main target of this work is to present a novel design of the hybrid PVT collector design with the proposed concept of the cooling approach that involves four independent containers with absorbers that were set in the layer of the PCM (pork fat, i.e. animal fat as a cheap and organic PCM). The main novelty herein is a proposal of the passive/active cooling concept (hybrid approach) ensured by section cooling of the PVT panel. The novel proposed design concept involves a smart regulation system that allows suitable balancing of the overall energy output ratio, i.e. electric/thermal output ratio. The experimental and numerical analysis was also reported in this work as a necessary basis for the development of the suitable PVT collector design. The proposed novel PVT panel design could be beneficial since it could be suitable for

efficient integration into the building energy systems in general.

### Concept of hybrid PV panel: Design approach details

The relatively low conversion efficiency of the solar irradiation into electricity by conventional PV systems indicates the need for utilization of the full irradiation spectral range, i.e. possible harvest of the thermal gains that adversely affect the electrical efficiency. In that sense, conventional PVT collector designs have a significant design issue related to the quite opposing natures of increasing electrical and thermal efficiencies achieved by specific PVT collector designs, as an improvement in the electrical efficiency leads to a reduction in thermal efficiency and vice versa. Obviously, it is necessary to bridge this gap and to ensure the possibility of the proper balancing between the thermal/electric power output produces from a specific PVT collector solution. Conventional PVT collector designs predominantly rely on air or water as a working fluid with nominal thermal power output prevailing electrical by a factor of about 3, [10]. As already previously highlighted, the main step further is a proposal of the passive/active cooling concept of a commercially available PV panel, incorporating a smart regulation system that would allow balancing the ratio between produced electrical and thermal outputs. The proposed concept can be implemented to most of the new commercially available PV panels as well as an upgrade of already existing used PV systems. The proposed hybrid PV concept is passively cooled with pork fat-based PCM, while the active component utilizes water as the suitable working fluid, Fig. 2. Pork fat is organic and widely available to be used as a phase change material that has suitable thermal properties for thermal energy storage application and with considerably lower unit costs, compared to the market available paraffin-based PCMs, [24]. In this context, the pork fat-based PCM material is placed in four separate transparent containers made of Plexiglas, enabling a visual insight into the phase transition process.

Water-cooled aluminum pipes together with aluminum sheets form four flat-plate thermal absorbers, as shown in Fig. 2. Square aluminum pipes were selected to increase the contact area with the aluminum sheets. The primary role of the absorber is to ensure the phase restitution of the pork fat after the passive component of the system fails, i.e. the reversion of the liquid PCM to the solid phase. Additionally, the upper sheet of the absorber is in direct contact with the rear surface of the PV panel to reduce the inertia of the PCM phase change, i.e. immediately after switching on the water circulation the absorber cools the back surface (PV panel), while simultaneously inducing the phase transition of the PCM. The lower aluminum sheet increases the contact surface with PCM thus accelerating the phase transition.

The hardware part of the coolant recirculation system should be very flexible in terms of flow and flow regulation to ensure and fully exploit smart regulation. Therefore, the control valves with rotary actuators are

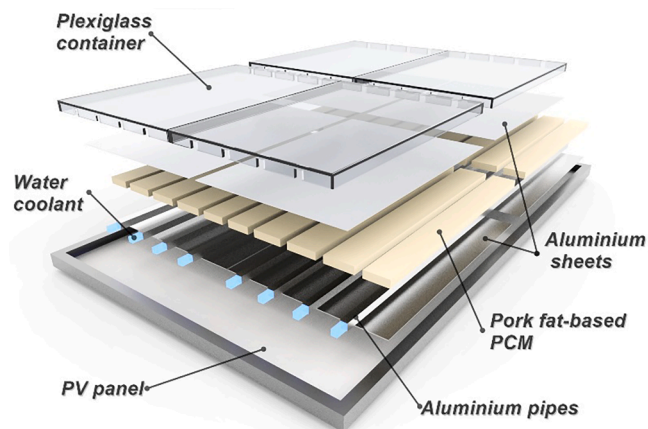


Fig. 2. Schematic cross-section of hybrid PV concept.

located at the inlets of the cooling aluminum pipes, while ultrasonic flow meters are positioned at the outlets of the pipes, Fig. 3. In addition to ultrasonic flow meters, the system also has an ultrasonic calorimeter that measures the amount of energy (heat flow) rejected to the cooling water from the hybrid PV panel.

The smart control system dynamically adjusts the cooling water circulation regarding the temperature and convection (wind speed) from the outer surfaces of the hybrid PV panel as well as the other environmental conditions and the interior temperature of the PCM. In addition to the previous parameters, an essential input represents the ratio between electrical and thermal energy output with respect to consumer requirements. The active component of the system can operate on the ON/OFF principle or, if necessary, it can provide continuous cooling with reduced flows along the pipe parallels of the absorber. By proper exploitation of control valves with rotary actuators, each cooling aluminium pipe can deliver a different flow of cooling water which ensures the possibility of reducing potential PV module hot spots. Balancing and optimization of the smart regulation system will be possible after the experimental installation becomes fully operational.

In order to develop and optimize such a complex automated hybrid PVT system, an extensive experimental and numerical approach is necessary. The analysis required to investigate the proposed cooling methods can be provided by CFD (Computational Fluid Dynamics), which includes fluid flow as well as thermal analysis. In this paper, the focal point is related to experimental investigation and numerical modeling of convective heat transfer of a commercially available conventional PV panel. At the current PVT collector development stage, this holistic approach serves as the basis for the future upgrade of the PVT collector numerical model. The field conditions adjacent to the PV panel affects the convective heat exchange from the PV panel surface to the surroundings. The PVT collector with straight water channels and conventional RT44 PCM was numerically modeled for the constant water mass flow rate, [25]. The convection heat exchange from the surface of the PV panel to the ambient, depending on the wind velocity ( $v$ ), was defined by equation (1), [25]:

$$h_{PV-a} = 2.8 + 3v \quad (1)$$

A similar approach related to the numerical modeling PVT-PCM collectors was applied in [26] where the convective/radiative heat transfer coefficient  $h_i$  is defined by Eq. (2),

$$h_i = 5.7 + 3.8V_m \quad (2)$$

where  $V_m$  is described as average wind speed.

In the work [27] the experimental and numerical research of nanofluid-based PVT system was considered where the coefficient of heat transfer from PVT top surface to ambient had a fixed value of 7.14 (the unit was not explicitly specified). The main shortage in defining the heat transfer coefficient in these works is the one-dimensional approach used to estimate the wind influence or, in some cases, the complete absence of such an analysis. The wind undoubtedly affects the heat transfer coefficient, but its local influence on this coefficient is relative with respect to the geometry, position, and tilt angle of the PV panel (or PVT collector).

Hence, it becomes clear to successfully design a hybrid PVT system, it is important to develop a numerical model that incorporates a broad range of influential parameters to correctly describe the physical mechanism of the heat transfer phenomena. One of the development points is the correct modeling of the impact of wind on the heat transfer coefficient. Therefore, the experimental setup was set to investigate the influence of the photovoltaic panel's relative position on the convection heat transfer coefficient, with respect to wind direction and wind speed. The experimental approach would ensure accurate input data for the numerical model of the herein proposed PVT collector design and which is part of the ongoing research work.

## Experimental approach

### Experimental test installation

In order to accurately define input values for numerical modeling of the PVT collector, an experimental evaluation was obtained and mainly focused on the investigation of the convective heat transfer coefficients. The 50 W polycrystalline PV module (540 × 670 × 25 mm) was exposed to an airstream in a wind tunnel at three specific wind speeds, i.e. 2.6 m/s, 4.7 m/s, and 6.7 m/s, Fig. 4a.

The convective heat transfer coefficient was indirectly determined based on the total heat flux measured using an FHF02SC sensor device, Fig. 4b. The FHF02SC is a passive thermopile heat flux sensor that has an integrated thermocouple for temperature measurements. The mentioned sensor includes a heater, so it can also serve as a source of

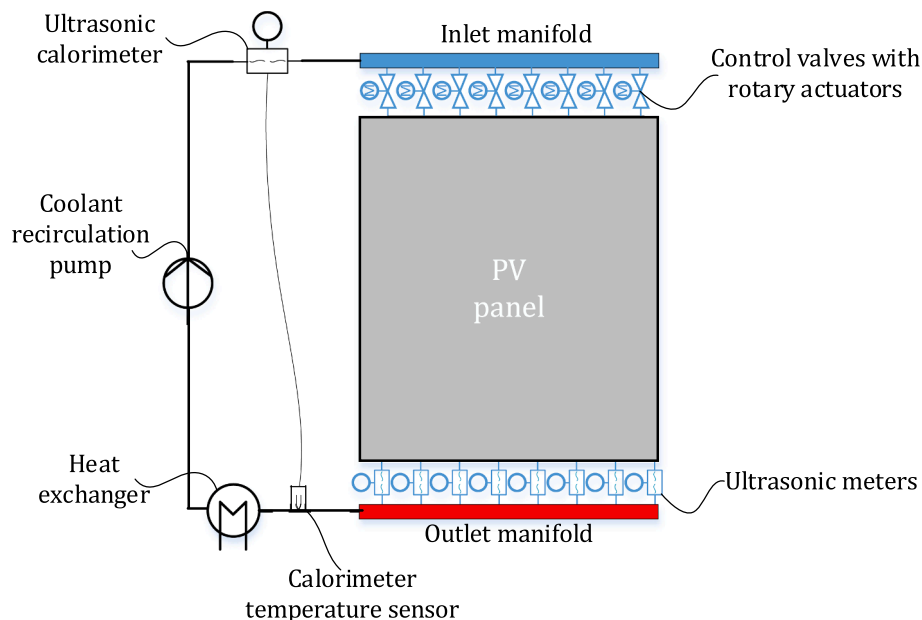


Fig. 3. Hybrid PV system schematic.



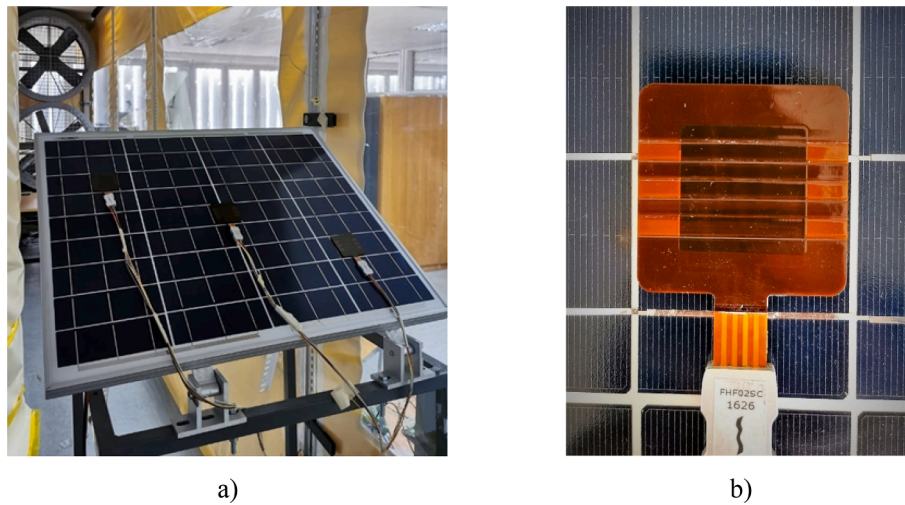


Fig. 4. a) Experimental setup in wind tunnel b) FHF02SC sensor on PV panel surface.

heat flux and has the ability to self-calibrate. The operating temperature range of the sensor is  $-40\text{ }^{\circ}\text{C}$  to  $+150\text{ }^{\circ}\text{C}$ , and the measurement range is from  $-10 \times 10^3\text{ W/m}^2$  to  $+10 \times 10^3\text{ W/m}^2$  at the temperature of  $20\text{ }^{\circ}\text{C}$  (heat sink). The sensing area of the sensor is  $9 \times 10^{-4}\text{ m}^2$ , while the passive guard area is  $16 \times 10^{-4}\text{ m}^2$ , [28]. Heat flux sensors that include surface temperature sensors were connected to a CR1000X data logger, while the air temperature was recorded with a K-type sensor connected to a PICO TC-08 data logger.

Uncertainty analysis

The declared temperature dependence of the FHF02SC sensor is  $<0.3\%/^{\circ}\text{C}$ , and the nonlinearity is  $<\pm 2\%$  ( $0-3.5 \times 10^3\text{ W/m}^2$ ), [27].

The uncertainty analysis of ambient air temperature ( $T_A$ ) measurements is determined based on Eq. (3), [29]:

$$\Delta U = \pm \sqrt{\Delta U_{tc}^2 + \Delta U_t^2} \tag{3}$$

The uncertainty (declared) of PICO TC-08 logger is  $\Delta U_{tc} = \pm 0.5\text{ }^{\circ}\text{C}$  while measurement uncertainty for K-type sensor is  $\Delta U_t = \pm 0.5\text{ }^{\circ}\text{C}$ , [30]. When the previous data are considered, the total measurement uncertainty of the ambient air temperature measurement is  $\pm 0.70\text{ }^{\circ}\text{C}$ .

Experimental research

The specific behavior of the heat transfer coefficients was investigated in the experimental circumstances on the front and rear surfaces of the photovoltaic panel with respect to the relative wind angle  $\gamma$ , tilt angle  $\beta$ , and wind speed  $v$ . The photovoltaic panel was positioned in the airstream at three wind speeds and three relative wind angles  $\gamma$ , i.e.  $0^{\circ}$ ,  $22.5^{\circ}$ , and  $45^{\circ}$ , Fig. 5a. Furthermore, the tilt angles of  $0^{\circ}$ ,  $20^{\circ}$ , and  $35^{\circ}$  were also varied, Fig. 5b. The tilt angles were selected relatively conservative for middle latitudes.

The local heat flux through the PV panel was measured using FHF02SC sensor while it was induced by the thermoelectric effect, i.e. Peltier element with dimensions of  $40 \times 40 \times 3.8\text{ mm}$  and maximum nominal capacity of  $53\text{ W}$ . Heat flux measurements were performed at a relatively constant room temperature (approx.  $20\text{ }^{\circ}\text{C}$ ) with the induced heat flux acting on the system until steady-state conditions were reached. To accurately determine the heat transfer coefficient from the front surface of the PV panel, the heat flux sensors were positioned at m1, m2 and m3 location as shown in Fig. 6a wherein the Peltier elements were carefully positioned on the opposing side to cause heat flux in the desired direction. When examining the heat transfer coefficients on the backside surface (PV panel), it is necessary to reverse the logic and position the Peltier elements on the front surface as in Fig. 6b and heat flux sensor on the opposite side at m4, m5 and m6 location.

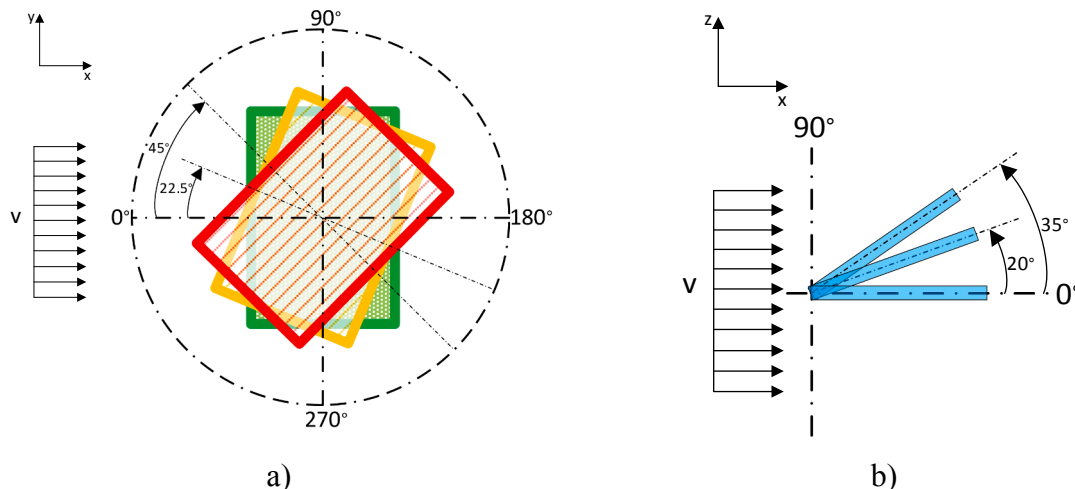


Fig. 5. a) Relative wind angle  $\gamma$  b) Tilt angle  $\beta$ .



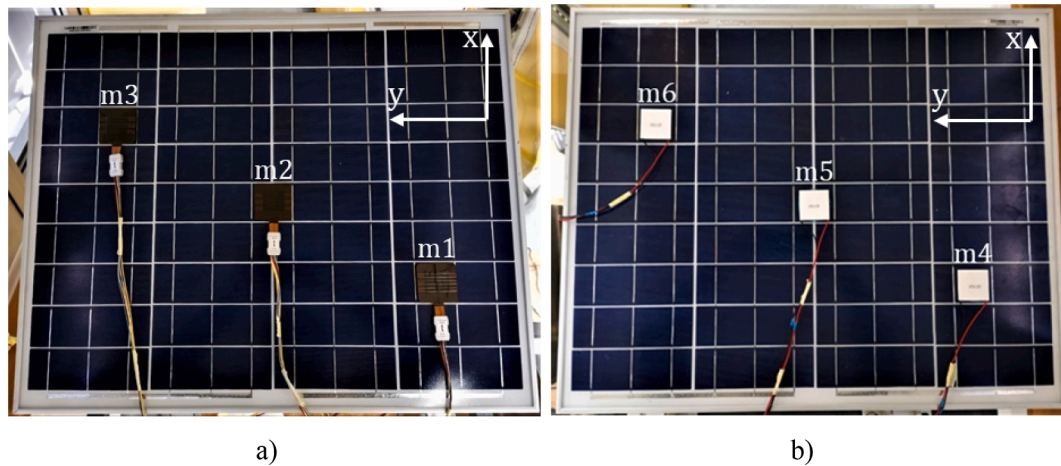


Fig. 6. a) Heat flux sensors on the front surface/Peltier elements on the rear surface b) Peltier elements on the front surface /Heat flux sensors on the rear surface.

The direct relation between heat flux and convective heat transfer coefficient is given following by expression,

$$q = h(T_S - T_A) \quad (4)$$

where  $q$  is the heat flux ( $\text{W}/\text{m}^2$ ),  $h$  heat convection coefficient ( $\text{W}/\text{m}^2\text{K}$ ), while  $T_S$  and  $T_A$  stand for the temperature of the sensor as well as surrounding air (K).

In order to obtain the exact amount of heat flux dissipated from the surface of the sensor by convection, it is necessary to eliminate the part of the heat flux dissipated by radiation. Radiation heat loss,  $q_R$  ( $\text{W}/\text{m}^2$ ), was determined based on Eq. (5):

$$q_R = \varepsilon\sigma(T_S^4 - T_W^4) \quad (5)$$

where  $\varepsilon$  represents the emissivity coefficient of the sensor surface,  $T_W$  the temperature of cold surroundings and  $\sigma$  the Stefan-Boltzmann constant. The sensor emissivity was determined using FLIR E76 24° thermal imaging camera and it is about 0.95.

Heat flux dissipated by convection,  $q_C$  ( $\text{W}/\text{m}^2$ ), from the sensor surface to the surrounding air is equal to total heat flux,  $q_T$  ( $\text{W}/\text{m}^2$ ), which is measured with the sensor, reduced by radiation heat loss, Eq. (6):

$$q_C = q_T - q_R \quad (6)$$

Finally, the convective heat transfer coefficient is determined according to Eq. (7):

$$h = \frac{q_C}{(T_S - T_A)} \quad (7)$$

## Numerical analysis

### Modeling convection heat transfer in turbulent flow conditions

In work [31], it was shown that specific wind directions exist which maximize the convective heat transfer. The results were based on computational fluid dynamics (CFD) validated by an experimental model. This ideal wind direction was shown to be independent of wind speed and solar radiation. In [32], a roof PV panel was investigated regarding convective heat losses for different mounting positions. Several variations of PV panel height and different tilt angles were tested. The tilt angle was shown to be a significant factor regarding convective heat transfer for low-wind conditions (natural convection). However, this was not the case for conditions with significant wind velocity. A similar study was performed in [33], where 3D CFD was used for a referent PV panel exposed to various wind velocities and several solar radiation cases. Together with the wind velocity and angle, in a

general case, turbulence intensity is also a significant factor for convective heat transfer. The impact of the turbulence intensity on heat transfer for a PV panel was investigated in [34]. The convective heat transfer was raised by the rise of the turbulence intensity with an additional groove element. The effects of turbulence are especially important in the current work, where the PV panel was experimentally tested in turbulent flow conditions.

Numerical analysis of PV panel exposed to different wind conditions can be performed using either steady-state or transient CFD analysis. For example, in [35], where dynamic changes in wind velocity and solar radiation are considered, transient numerical models were used. Meanwhile, steady-state conditions of radiation and wind velocity were used in [36] and [31], and the same results were obtained as in the dynamic conditions. The actual wind is always turbulent, which means that local flow features at smaller time scales are transient. The effects of turbulence are averaged in most engineering simulations by applying the Reynolds averaged Navier-Stokes (RANS) equations. A significantly more detailed approach is to use large eddy simulation (LES) models, as for example in [37] or hybrid LES-RANS models [38]. However, these models require exponentially more computational resources since both temporal and spatial resolution must be refined.

In the current paper, the steady-state RANS equations were used within the numerical model. Two most often used RANS models are  $k-\varepsilon$  and SST  $k-\omega$  [39]. In earlier numerical studies (for example [40]), the  $k-\varepsilon$  model was often used for PV panel-related modeling. In more up-to-date studies, the SST  $k-\omega$  is the most common approach. The important flow characteristic of the free-standing PV panel simulation is the flow separation, which must be modeled correctly. The SST  $k-\omega$  model is noted for its more accurate flow separation prediction [39]. Specifically related to the PV system, the SST model results were compared with the experimental flow field obtained using particle image velocimetry [41]. Related to this, the numerical model should correctly predict the convective heat transfer. Again, the SST model has shown a reasonable well relationship with experimental data in previous research [42].

The case of PV panel with relatively low surface temperature and high wind velocity are considered in this work. In these conditions, the buoyancy force can also be considered although its effects are minor. In a more general case, ideal gas law can be included in the numerical model. However, this adds unrequired complexity in the current case. Alternatively, to variable density fluid, Boussinesq approximation can be applied. This has shown good results even for more complex natural convection flows [36].

### Governing equations

The RANS equations are obtained by application of Reynolds aver-

aging on the continuity and momentum relations:

$$\rho \frac{\partial \bar{u}_j}{\partial x_j} = 0 \tag{8}$$

$$\rho \frac{\partial \bar{u}_i}{\partial t} + \rho \frac{\partial \bar{u}_i \bar{u}_j}{\partial x_j} = -\frac{\partial p}{\partial x_i} + \frac{\partial}{\partial x_j} \mu \left[ \left( \frac{\partial \bar{u}_i}{\partial x_j} + \frac{\partial \bar{u}_j}{\partial x_i} \right) - \frac{2}{3} \frac{\partial \bar{u}_k}{\partial x_k} \delta_{ij} \right] + \frac{\partial}{\partial x_j} [R_{ij}] + \rho f_i \tag{9}$$

$$R_{ij} = -\rho \bar{u}_i \bar{u}_j = \mu_t \left[ \left( \frac{\partial \bar{u}_i}{\partial x_j} + \frac{\partial \bar{u}_j}{\partial x_i} \right) - \frac{2}{3} \frac{\partial \bar{u}_k}{\partial x_k} \delta_{ij} \right] - \frac{2}{3} \rho k' \delta_{ij} \tag{10}$$

where  $\rho, p$  are the mean flow pressure and density;  $\bar{u}_i$  ( $\bar{u}_1, \bar{u}_2$  and  $\bar{u}_3$ ) are the velocity components (Cartesian) respectively; Cartesian coordinates are  $x_i$  ( $x_1, x_2$  and  $x_3$ );  $\mu$  is the molecular viscosity;  $f_i$  are the body force which includes the buoyance effects by Boussinesq approximation; the turbulence related quantities are:  $\mu_t$  - turbulent viscosity and  $k'$  - turbulence kinetic energy, which are obtained using the SST k- $\omega$  turbulence model. The energy conservation relation also has to be solved coupled with the previous equations:

$$\rho \frac{\partial e}{\partial t} + \frac{\partial}{\partial x_j} [(\rho e + p) \bar{u}_j] = \frac{\partial}{\partial x_j} \left[ (k + k_t) \frac{\partial T}{\partial x_j} \right] + S_h \tag{11}$$

where the thermal conductivity appears as:  $k$  - thermal conductivity from fluid properties and  $k_t$  - is the thermal conductivity addition caused by the flow turbulence and calculated from the SST turbulence model;  $T$  is the temperature; the enthalpy is  $h$ ; and  $e$  is total internal energy (specific), that can be determined as follows,

$$e = h - \frac{p}{\rho} + \frac{\bar{u}^2}{2} \tag{12}$$

**Computational domain**

The computational domain was obtained of a single fluid region. This region was divided into two zones: global zone and refined-mesh zone near the PV panel as shown in Fig. 7. The selected dimensions of the fluid region were based on previous research [36]. The length of the domain was  $L = 4$  m, the width was  $W = 3.6$  m, and the height was  $H = 2$  m. The PV panel was placed at a distance of 1.5 m from the inlet section, and its lowest point was at a height of 0.5 m. At the inlet section, velocity was applied uniformly and in the normal direction to the surface. On the opposite side, a pressure outlet was used with zero pressure conditions. The bottom boundary (floor) was a no-slip wall, while other surrounding air boundaries were considered a free-slip wall. The boundary condition at all PV panel surfaces is no-slip regarding flow equations ( $\mathbf{u}(\mathbf{x}) = \mathbf{0}$ )

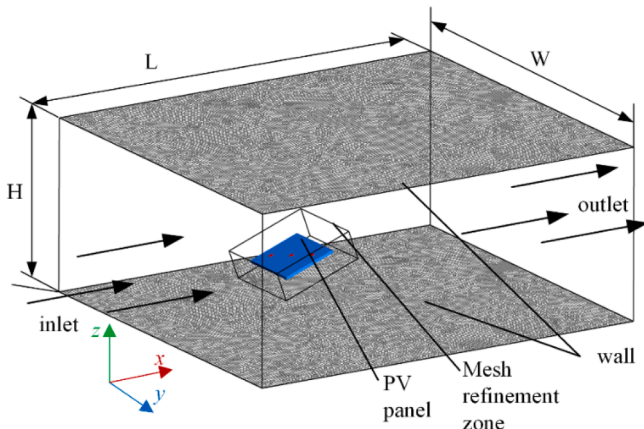


Fig. 7. The fluid domain and PV panel.

and equal temperature for fluid and solid region ( $T_{\text{fluid}}(\mathbf{x}) = T_{\text{solid}}(\mathbf{x})$ ).

For more accurate convective heat transfer modelling from PV panel to the surrounding air, the most important part of the computational domain is the near-wall region. This problem can be modelled using wall functions near the wall or by application of the turbulence model in the complete computational domain including the near-wall region. The second approach is the standard when using the SST k- $\omega$  turbulence model. This required application of a prismatic mesh layer at walls, with the first layer thickness  $y^+ \approx 1$ . An accurate numerical solution of the boundary layer is of prime importance for modelling the convection problems, but also for flow separation. Fig. 8 shows the mesh at a section surrounding the PV panel.

The solution of the numerical model was solved using ANSYS Fluent. The mesh was initially composed of tetrahedrons and converted to polyhedral mesh within the ANSYS Fluent. The energy and momentum equations were solved with a double-precision coupled solver together with a second-order upwind scheme. The all examined cases were steady

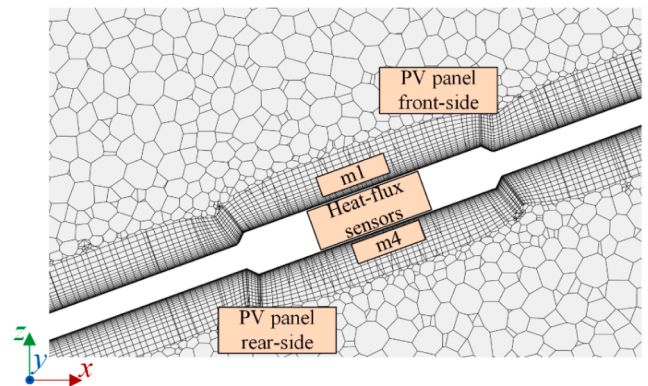
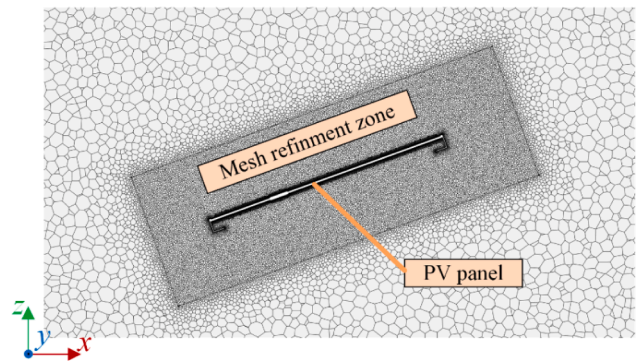
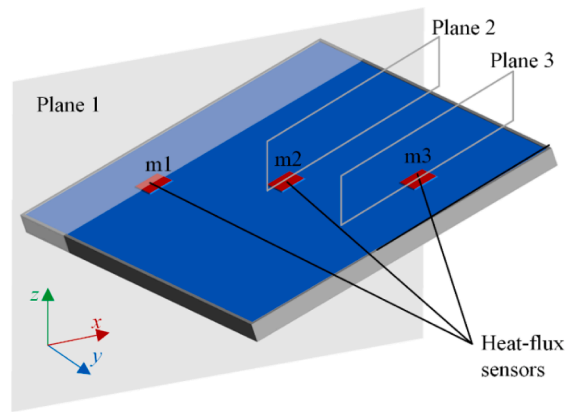


Fig. 8. Mesh in various fluid regions: the overall views, region near the PV panel and last figure the prismatic layer and which is adjacent to the PV panel wall.

state with convergence criteria targeted to  $10^{-4}$ .

**Mesh test**

A Mesh validation test was obtained for wind velocity  $v = 6.7$  m/s and heat-flux sensor temperature difference of  $7^\circ\text{C}$ . The heat flux was monitored on all 6 measurement points. The size of elements was varied so that the mesh contained from 10 to 80 million elements. The resulting heat-flux at the measurement points for different resolutions of the mesh are presented in Fig. 9. As it can be noted, the heat flux on the front side (m1-m3) converges practically from the coarsest mesh 10 M mesh. Meanwhile, the backside is more problematic. The required mesh resolution is near 80 M elements. This is due to the more complex flow on the backside, which is further discussed in the results section.

**Results and discussion**

The developed numerical model was compared and validated with obtained experimental readings from the previously elaborated approach in Section 3. The experimental and numerical results were compared and discussed in the continuation of the work.

The flow field for the case of  $v = 6.7$  m/s,  $\beta = 20^\circ$  and  $\gamma = 0^\circ$  is shown in Fig. 10. This case shows the flow field complexity even for the simplest wind angle of  $\gamma = 0^\circ$ . Regarding the top side of the PV panel, the flow is relatively simple, and it is expected that the results will correspond to the experimental. A small positive velocity gradient in the  $x$ -direction can be noted, thus a slight increase in heat convection coefficient is expected from point m1 to m3. The flow field on the lower side is much more complicated due to flow separation which occurs on the lower part of the PV panel aluminium frame. Fig. 10a shows the flow field in plane 1 (see Fig. 8). The measurement point m4 (Fig. 10a) is located in the middle of a relatively small separation zone (compared to m5, Fig. 10b). The flow details of the separation zone are in general, difficult to predict accurately using CFD. Thus, it can be expected that at this point there will be a difference when compared to the experimental data due to mentioned circumstances. The point m5 in the middle of the panel is located in the centre of the whole separation zone. The flow field is more uniform here compared to flow near m4, so more accurate predictions can be expected in that zone. The heat transfer coefficient can vary significantly over the surface, which requires measurements in several locations. Two problems affect the results obtained by measurement. First, the sensor size itself changes the flow field locally. In an ideal case, the sensor surface would be coplanar with the PV panel surface in which case these effects are minimized. The second effect is related to changes in the temperature field. Differences in the temperature field can also influence the results. To minimize the effects of differences in the temperature field, the PV panel surface would have to be heated so that the temperature field resembles the one in the actual

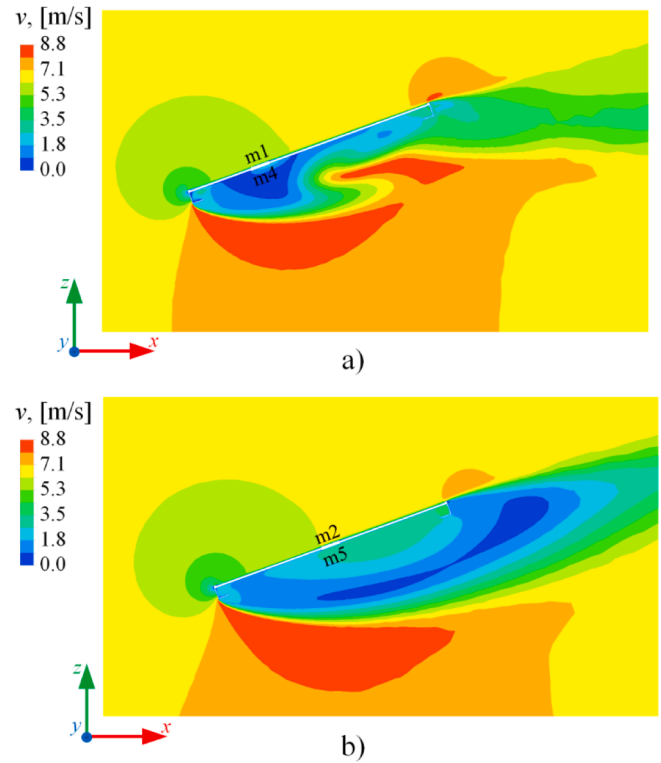


Fig. 10. Flow field for wind velocity  $v = 6.7$  m/s,  $\beta = 20^\circ$  and  $\gamma = 0^\circ$  and measurement area surface temperature  $\Delta T = 7^\circ\text{C}$  in: a) plane 1 as well as b) plane 2.

case. As it was shown in [9], the temperature field is very complex, so it is difficult to reproduce in the experiment. These effects could be analyzed numerically which can be a topic of a future study.

Similar observations to the ones presented in Fig. 10 can be made on the remaining cases with tilted panel ( $\beta = 20^\circ$  and  $\beta = 35^\circ$ ). The case with the horizontal panel is characterized by different flow field features. As shown in Fig. 11, the flow field around the horizontal panel in plane 1 (m1 and m4 section), shows relatively small but elongated flow separation regions. In this case, the PV panel frame is the main geometrical feature that influences the flow. In addition to the expected flow separation under the PV panel, a slight flow separation exists on the front side at m1 location. The separation zones are also always followed by an increase in turbulence kinetic energy. The reduced flow velocity and increased turbulence kinetic energy have opposite effects on the convective heat transfer, so it is difficult to predict the result based only on flow field observation. Detailed data for all measurement points and all cases are given in the upcoming tables, i.e. Table 1.

The relative differences between numerical and experimental results are shown in Table 2. Positive percentages indicate that the experimental data gives higher values than CFD, and negative percentages the opposite. On average, experimental results give 12% higher values. Among these, the differences smallest for the horizontal panel which gives 7% higher values on average. For tilted panel with  $\beta = 20^\circ$  and  $\beta = 35^\circ$ , the experiment overshoots by 14% and 15% respectively. The loss of accuracy of CFD in highly separated flow is predictably due to complex fluid flow conditions. As previously discussed, and based on Fig. 10, the point m4 is located in a centre of a relatively small separation zone and larger errors were expected.

The overall effect of the wind angle on the PV panel efficiency can be analyzed by observing the average heat transfer convection coefficient (average on 6 measurement points). It was numerically observed already in [31] that wind angle has a noticeable effect on the PV panel temperature, where the maximal temperature was observed at wind angle around  $20^\circ$ . A similar conclusion can be obtained in this paper, by

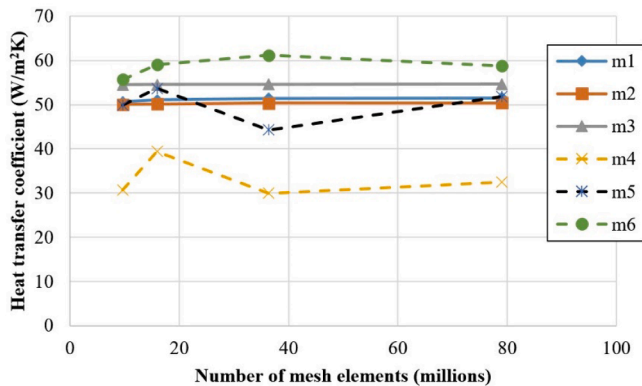


Fig. 9. Wind velocity mesh test  $v = 6.7$  m/s and heat source (equivalent)  $Q = 600$  W/m<sup>2</sup>.



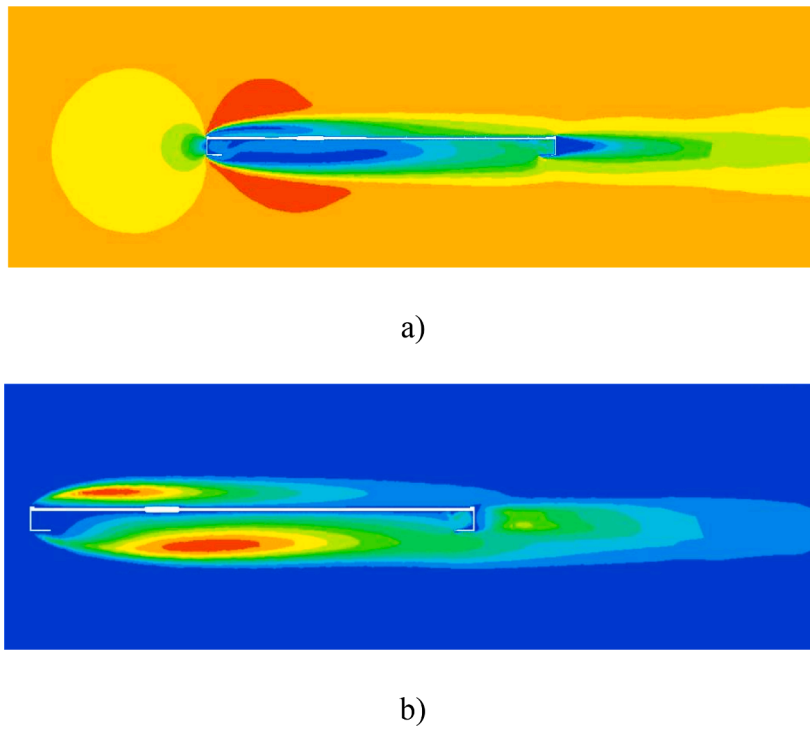


Fig. 11. Flow field for wind velocity  $v = 6.7$  m/s,  $\beta = 0^\circ$  and  $\gamma = 0^\circ$ ,  $\Delta T = 7$  °C in plane 1: a) wind velocity and b) turbulence kinetic energy.

**Table 1**  
Convective heat transfer at measurement locations m1-m6 for all case.

| v (m/s) | $\beta$ (°) | $\gamma$ (°) | Convective heat transfer, CFD-based (W/m <sup>2</sup> K) |      |      |      |      |      | Convective heat transfer, - experimental (W/m <sup>2</sup> K) |      |      |      |      |      |
|---------|-------------|--------------|--|------|------|------|------|------|---|------|------|------|------|------|
|         |             |              | m1   | m2   | m3   | m4   | m5   | m6   | m1  | m2   | m3   | m4   | m5   | m6   |
| 2.6     | 0           | 0            | 26.7   | 24.6 | 28.5 | 23.1 | 25.8 | 27.2 | 35.8  | 37.6 | 34.5 | 30.4 | 28.2 | 26.7 |
| 2.6     | 0           | 22.5         | 32.9   | 33.2 | 30.8 | 34.5 | 34.1 | 29.7 | 35.1  | 36.1 | 33.2 | 35.0 | 26.3 | 25.7 |
| 2.6     | 0           | 45           | 33.0   | 31.5 | 31.5 | 34.0 | 30.9 | 24.2 | 30.6  | 36.4 | 31.8 | 31.7 | 28.6 | 25.5 |
| 4.7     | 0           | 0            | 40.4   | 37.3 | 41.6 | 33.9 | 38.5 | 39.5 | 54.1  | 56.2 | 51.1 | 46.5 | 41.3 | 41.1 |
| 4.7     | 0           | 22.5         | 48.3   | 48.0 | 45.5 | 50.3 | 50.4 | 43.9 | 54.2  | 54.7 | 50.4 | 51.5 | 38.5 | 38.6 |
| 4.7     | 0           | 45           | 47.9   | 46.2 | 45.9 | 47.0 | 44.2 | 36.7 | 50.8  | 56.6 | 49.2 | 47.6 | 43.8 | 39.0 |
| 6.7     | 0           | 0            | 51.9   | 48.0 | 52.7 | 42.5 | 49.3 | 50.7 | 65.2  | 67.4 | 61.4 | 55.0 | 48.8 | 49.5 |
| 6.7     | 0           | 22.5         | 61.6   | 60.7 | 57.5 | 65.4 | 63.4 | 55.9 | 67.1  | 67.4 | 62.1 | 61.4 | 45.7 | 46.6 |
| 6.7     | 0           | 45           | 60.6   | 58.6 | 58.1 | 61.0 | 56.6 | 47.1 | 64.7  | 70.3 | 61.0 | 59.5 | 54.3 | 48.4 |
| 2.6     | 20          | 0            | 28.2   | 27.4 | 29.6 | 16.6 | 29.3 | 28.4 | 32.9  | 35.7 | 33.0 | 21.8 | 29.1 | 38.1 |
| 2.6     | 20          | 22.5         | 27.7   | 29.1 | 31.0 | 23.1 | 20.5 | 28.2 | 30.8  | 33.0 | 31.7 | 24.1 | 27.9 | 30.8 |
| 2.6     | 20          | 45           | 28.8   | 29.8 | 30.8 | 30.8 | 34.2 | 30.2 | 28.1  | 34.1 | 31.1 | 43.4 | 33.0 | 28.2 |
| 4.7     | 20          | 0            | 40.9   | 39.7 | 43.0 | 23.1 | 37.0 | 49.2 | 51.7  | 58.7 | 55.3 | 35.0 | 43.4 | 53.5 |
| 4.7     | 20          | 22.5         | 40.0   | 42.3 | 45.0 | 30.8 | 30.6 | 41.7 | 49.6  | 56.8 | 53.4 | 40.5 | 41.6 | 47.3 |
| 4.7     | 20          | 45           | 42.0   | 43.4 | 44.6 | 31.5 | 48.4 | 43.4 | 45.1  | 54.9 | 50.1 | 62.6 | 48.5 | 41.4 |
| 6.7     | 20          | 0            | 51.8   | 50.4 | 54.4 | 29.0 | 53.8 | 57.4 | 60.9  | 69.1 | 66.6 | 43.6 | 52.5 | 64.7 |
| 6.7     | 20          | 22.5         | 50.6   | 53.4 | 56.7 | 36.5 | 39.4 | 51.8 | 59.8  | 68.6 | 65.3 | 51.6 | 50.7 | 56.2 |
| 6.7     | 20          | 45           | 52.9   | 54.6 | 56.4 | 35.1 | 65.5 | 54.7 | 54.9  | 66.8 | 62.0 | 76.6 | 60.0 | 51.2 |
| 2.6     | 35          | 0            | 27.2   | 25.9 | 29.4 | 15.6 | 24.8 | 25.3 | 21.8  | 33.6 | 32.4 | 18.9 | 26.3 | 35.0 |
| 2.6     | 35          | 22.5         | 25.6   | 28.0 | 31.4 | 15.5 | 25.8 | 30.8 | 29.4  | 33.6 | 32.8 | 18.4 | 26.2 | 30.0 |
| 2.6     | 35          | 45           | 27.2   | 28.9 | 30.9 | 16.2 | 20.3 | 28.5 | 27.5  | 33.7 | 31.8 | 34.5 | 32.6 | 29.7 |
| 4.7     | 35          | 0            | 37.3   | 36.7 | 42.2 | 23.9 | 36.4 | 37.4 | 46.4  | 55.0 | 53.5 | 32.0 | 41.7 | 53.3 |
| 4.7     | 35          | 22.5         | 35.2   | 40.0 | 45.1 | 23.7 | 38.2 | 47.8 | 45.2  | 54.5 | 52.6 | 30.2 | 41.3 | 46.2 |
| 4.7     | 35          | 45           | 38.1   | 41.7 | 44.7 | 25.1 | 33.8 | 43.0 | 41.0  | 52.7 | 49.9 | 57.8 | 48.4 | 43.4 |
| 6.7     | 35          | 0            | 46.0   | 46.2 | 53.4 | 31.2 | 46.4 | 48.2 | 55.0  | 66.2 | 66.6 | 39.6 | 50.2 | 63.2 |
| 6.7     | 35          | 22.5         | 43.9   | 50.2 | 56.7 | 32.4 | 50.1 | 60.6 | 53.0  | 64.2 | 63.1 | 37.7 | 49.4 | 55.6 |
| 6.7     | 35          | 45           | 48.0   | 52.5 | 56.3 | 32.2 | 44.0 | 56.2 | 49.3  | 64.4 | 62.2 | 71.1 | 59.3 | 52.5 |

observing the minimum in the heat transfer coefficient near the 20° wind angle, both in the experimental and in the numerical study, as shown in Fig. 12. This indicates that the numerical model has good prediction capabilities. This applies at least regarding the relative values i.e. the minimum and the maximum values appear at the same wind angles.

**Conclusions**

A concept of a novel hybrid cooling approach for photovoltaic (PV) panel was proposed in this work, i.e. design details for the novel PVT panel used as a micro-cogeneration unit were elaborated. The main design approach was focused on hybrid cooling, i.e. combination of the passive and active cooling strategy ensured via four independent cooling containers made of plexiglass. This type of sectional cooling combined

**Table 2**  
Differences between convective heat transfer coefficient obtained by the numerical and the experimental analyses.

| $v$<br>(m/s) | $\beta$ (°) | $\gamma$ (°) | Convective heat transfer difference Exp.-CFD (%) |     |     |     |      |      |
|--------------|-------------|--------------|--|-----|-----|-----|------|------|
|              |             |              | m1   | m2  | m3  | m4  | m5   | m6   |
| 2.6          | 0           | 0            | 25%  | 35% | 17% | 24% | 8%   | -2%  |
| 2.6          | 0           | 22.5         | 6%   | 8%  | 7%  | 2%  | -23% | -14% |
| 2.6          | 0           | 45           | -7%  | 13% | 1%  | -7% | -7%  | 5%   |
| 4.7          | 0           | 0            | 25%  | 34% | 19% | 27% | 7%   | 4%   |
| 4.7          | 0           | 22.5         | 11%  | 12% | 10% | 2%  | -24% | -12% |
| 4.7          | 0           | 45           | 6%   | 18% | 7%  | 1%  | -1%  | 6%   |
| 6.7          | 0           | 0            | 20%  | 29% | 14% | 23% | -1%  | -2%  |
| 6.7          | 0           | 22.5         | 8%   | 10% | 7%  | -6% | -28% | -17% |
| 6.7          | 0           | 45           | 6%   | 17% | 5%  | -2% | -4%  | 3%   |
| 2.6          | 20          | 0            | 15%  | 24% | 10% | 30% | 16%  | 20%  |
| 2.6          | 20          | 22.5         | 10%  | 12% | 2%  | 10% | 23%  | 7%   |
| 2.6          | 20          | 45           | 0%   | 13% | 1%  | 15% | -6%  | -7%  |
| 4.7          | 20          | 0            | 23%  | 33% | 22% | 29% | 4%   | 20%  |
| 4.7          | 20          | 22.5         | 21%  | 26% | 16% | 54% | 12%  | 10%  |
| 4.7          | 20          | 45           | 8%   | 21% | 11% | 9%  | -5%  | -7%  |
| 6.7          | 20          | 0            | 17%  | 28% | 18% | 26% | 0%   | 11%  |
| 6.7          | 20          | 22.5         | 17%  | 23% | 13% | 48% | 8%   | 2%   |
| 6.7          | 20          | 45           | 5%   | 18% | 9%  | 13% | -7%  | -7%  |
| 2.6          | 35          | 0            | -19%   | 23% | 9%  | 17% | 5%   | 26%  |
| 2.6          | 35          | 22.5         | 13%  | 17% | 5%  | 9%  | -3%  | -6%  |
| 2.6          | 35          | 45           | 1%   | 14% | 3%  | 47% | 33%  | 3%   |
| 4.7          | 35          | 0            | 20%  | 33% | 21% | 24% | 12%  | 28%  |
| 4.7          | 35          | 22.5         | 22%  | 27% | 14% | 16% | 4%   | -3%  |
| 4.7          | 35          | 45           | 7%   | 21% | 10% | 57% | 30%  | 1%   |
| 6.7          | 35          | 0            | 16%  | 30% | 20% | 21% | 8%   | 24%  |
| 6.7          | 35          | 22.5         | 17%  | 22% | 10% | 14% | -1%  | -8%  |
| 6.7          | 35          | 45           | 2%   | 19% | 9%  | 55% | 26%  | -7%  |

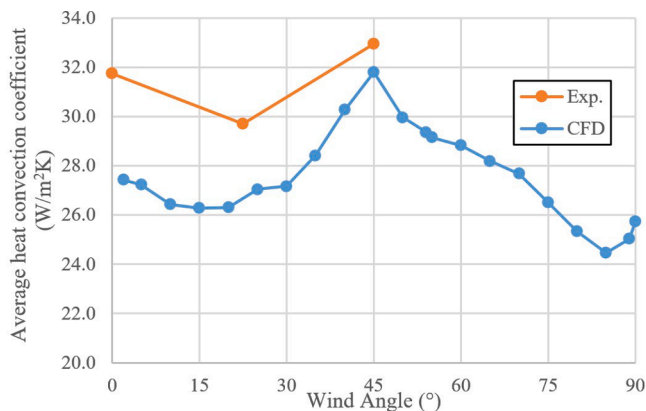


**Fig. 12.** Average heat convection coefficient for  $v = 2.6$  m/s,  $\beta = 20^\circ$ ,  $\Delta T = 7$  °C for different wind angles.

with a smart regulation system should cause greater overall system efficiency. The passive cooling component was ensured by pork fat as cheap and organic PCM, while the active cooling part was provided via a specially designed aluminum absorber, with enabled water circulation (working fluid). The assumed use of pork fat as suitable PCM is also an important aspect of the herein proposed concept since for sure it would have a favorable effect both on the economic and environmental aspects. The overall setup was followed by smart regulation to ensure proper balancing between the electric and thermal efficiency of the novel PVT panel. Besides the elaboration of the specific design, an experimental investigation of the convective heat transfer coefficients was conducted in the wind tunnel circumstances to ensure key input values for numerical modeling of the novel proposed PVT panel, and to be able to finalize the experimental setup. The experimental investigation was completed by obtained numerical analysis using CFD modeling. The PV panel was experimentally investigated for three different wind speeds (2.4 m/s, 4.7 m/s, and 6.7 m/s), relative wind attack angles (0°, 22.5° and 45°), and PV panel tilt angles (0°, 20°, and 35°). The average deviation between the numerical data and experimental readings is about 12%. In some specific operating circumstances, the deviation is higher which is associated with the specific regions of the PV panel (complex

fluid conditions and impact of specific PV panel sections), the accuracy of the developed CFD model, and finally impact of the wind tunnel geometry on the flow turbulences in general. However, the developed numerical model has got reasonable accuracy and it will be helpful to examine various operating conditions for the novel hybrid PVT panel and to finalize collector design towards an experimental prototype. The herein presented results indicated an impact of the heat convection profiles and which must be carefully considered during the design stage. It needs to be noted that this work is part of the ongoing research work related to the development of the smart and hybrid cooling approach and that would be finalized with the prototype (experimental investigation) of the herein proposed novel concept of the smart and hybrid cooling approach for PV panel. The development of the concept implies the extensive use of the CFD to achieve an optimal solution in technical and economic terms. The economic aspects of the newly developed concept will be analyzed after the prototype is operational. At this stage, herein presented research findings are necessary to determine the final design of the hybrid cooling approach. The herein proposed PVT collector solution can be coupled with the building energy systems leading towards improvement in building energy performance as well as a rise in renewable energy capacities in buildings, as part of the strategy towards Nearly Zero Energy Buildings.

#### CRedit authorship contribution statement

**Mišo Jurčević:** Conceptualization, Methodology, Software. **Sandro Nizetić:** Conceptualization, Methodology, Supervision. **Ivo Marinić-Kragić:** Conceptualization, Methodology, Software. **Duje Čoko:** Supervision. **Müslüm Arıcı:** Supervision. **Effrosyni Giama:** Supervision. **Agis Papadopoulos:** Methodology, Supervision.

#### Declaration of Competing Interest

The authors declare that they have no known competing financial interests or personal relationships that could have appeared to influence the work reported in this paper.

#### Acknowledgment

This work was granted by the Croatian Science Foundation, project IP-01-2018-2814.

#### References:

- Ninić N, Nizetić S. Elementary theory of stationary vortex columns for solar chimney power plants. *Sol Energy* 2009;83(4). <https://doi.org/10.1016/j.solener.2008.09.002>.
- Dobracev V, Matak N, Sakulin C, Kraljčić G. Multilevel governance energy planning and policy: a view on local energy initiatives. *Energy Sustain Soc* 2021. <https://doi.org/10.1186/s13705-020-00277-y>.
- Sovacool BK, Bazilian M, Griffiths S, Kim J, Foley A, Rooney D. Decarbonizing the food and beverages industry: a critical and systematic review of developments, sociotechnical systems and policy options. *Renew Sustain Energy Rev* 2021. <https://doi.org/10.1016/j.rser.2021.110856>.
- Parkunam N, Pandiyan L, Navaneethakrishnan G, Arul S, Vijayan V. Experimental analysis on passive cooling of flat photovoltaic panel with heat sink and wick structure. *Energy Sources, Part A Recover Util Environ Eff* 2020. <https://doi.org/10.1080/15567036.2019.1588429>.
- Opan M, Ünlü M, Özkale C, Çelik C, Saraç Hİ. Optimal energy production from wind and hydroelectric power plants. *Energy Sources, Part A Recover Util Environ Eff* 2019. <https://doi.org/10.1080/15567036.2018.1555626>.
- International Renewable Energy Agency n.d. <https://irena.org/publications/2020/Mar/Renewable-Capacity-Statistics-2020> (accessed May 6, 2021).
- Fraunhofer ISE n.d. <https://www.ise.fraunhofer.de/content/dam/ise/de/documents/publications/studies/Photovoltaics-Report.pdf> (accessed May 6, 2021).
- Herez A, El Hage H, Lemenand T, Ramadan M, Khaled M. Review on photovoltaic/thermal hybrid solar collectors: classifications, applications and new systems. *Sol Energy* 2020. <https://doi.org/10.1016/j.solener.2020.07.062>.
- Grubišić-Cabo F, Nizetić S, Marinić-Kragić I, Čoko D. Further progress in the research of fin-based passive cooling technique for the free-standing silicon photovoltaic panels. *Int J Energy Res* 2019;43. <https://doi.org/10.1002/er.4489>.
- Nizetić S, Jurčević M, Čoko D, Arıcı M, Hoang AT. Implementation of phase change materials for thermal regulation of photovoltaic thermal systems: comprehensive analysis of design approaches. *Energy* 2021. <https://doi.org/10.1016/j.energy.2021.120546>.
- Brottier L, Bennacer R. Thermal performance analysis of 28 PVT solar domestic hot water installations in Western Europe. *Renew Energy* 2020. <https://doi.org/10.1016/j.renene.2020.06.072>.
- Nizetić S, Papadopoulos AM, Tina GM, Rosa-Clot M. Hybrid energy scenarios for residential applications based on the heat pump split air-conditioning units for operation in the Mediterranean climate conditions. *Energy Build* 2017. <https://doi.org/10.1016/j.enbuild.2017.01.064>.
- Veeramanipriya E, Umayal SA. Performance evaluation of hybrid photovoltaic thermal (PVT) solar dryer for drying of cassava. *Sol Energy* 2021;215:240–51. <https://doi.org/10.1016/j.solener.2020.12.027>.
- Kumar L, Hasanuzzaman M, Rahim NA, Islam MM. Modeling, simulation and outdoor experimental performance analysis of a solar-assisted process heating system for industrial process heat. *Renew Energy* 2021. <https://doi.org/10.1016/j.renene.2020.09.062>.
- Nizetić S, Jurčević M, Arıcı M, Arasu AV, Xie G. Nano-enhanced phase change materials and fluids in energy applications: a review. *Renew Sustain Energy Rev* 2020. <https://doi.org/10.1016/j.rser.2020.109931>.
- Lari MO, Sahin AZ. Effect of retrofitting a silver/water nanofluid-based photovoltaic/thermal (PV/T) system with a PCM-thermal battery for residential applications. *Renew Energy* 2018. <https://doi.org/10.1016/j.renene.2018.01.034>.
- Carmona M, Palacio Bastos A, García JD. Experimental evaluation of a hybrid photovoltaic and thermal solar energy collector with integrated phase change material (PVT-PCM) in comparison with a traditional photovoltaic (PV) module. *Renew Energy* 2021. <https://doi.org/10.1016/j.renene.2021.03.022>.
- Islam MM, Hasanuzzaman M, Rahim NA, Pandey AK, Rawa M, Kumar L. Real time experimental performance investigation of a NePCM based photovoltaic thermal system: an energetic and exergetic approach. *Renew Energy* 2021. <https://doi.org/10.1016/j.renene.2021.02.169>.
- Diwania S, Siddiqui AS, Agrawal S, Kumar R. Performance assessment of PVT-air collector with V-groove absorber: a theoretical and experimental analysis. *Heat Mass Transf Und Stoffuebertragung* 2021. <https://doi.org/10.1007/s00231-020-02980-0>.
- Shahsavari A. Experimental evaluation of energy and exergy performance of a nanofluid-based photovoltaic/thermal system equipped with a sheet-and-sinusoidal serpentine tube collector. *J Clean Prod* 2021. <https://doi.org/10.1016/j.jclepro.2020.125064>.
- Hissouf M, Feddaoui M, Najim M, Charef A. Performance of a photovoltaic-thermal solar collector using two types of working fluids at different fluid channels geometry. *Renew Energy* 2020. <https://doi.org/10.1016/j.renene.2020.09.097>.
- Arefin MA, Islam MT, Zunaed M, Mostakim K. Performance analysis of a novel integrated photovoltaic-thermal system by top-surface forced circulation of water. *Clean Energy* 2020. <https://doi.org/10.1093/ce/zkaa018>.
- Ramdani H, Ould-Lahoucine C. Study on the overall energy and exergy performances of a novel water-based hybrid photovoltaic-thermal solar collector. *Energy Convers Manage* 2020. <https://doi.org/10.1016/j.enconman.2020.113238>.
- Jurčević M, Nizetić S, Arıcı M, Hoang Anh Tuan A, Giama E, Papadopoulos A. Thermal constant analysis of phase change nanocomposites and discussion on selection strategies with respect to economic constraints. *Sustain Energy Technol Assessments* 2021. <https://doi.org/10.1016/j.seta.2020.100957>.
- Song J, Sobhani B. Energy and exergy performance of an integrated desiccant cooling system with photovoltaic/thermal using phase change material and maisotsenko cooler. *J Energy Storage* 2020. <https://doi.org/10.1016/j.est.2020.101698>.
- Naghdhishi A, Yazdi ME, Akbari G. Experimental investigation of the effect of multi-wall carbon nanotube – water/glycol based nanofluids on a PVT system integrated with PCM-covered collector. *Appl Therm Eng* 2020;178:115556. <https://doi.org/10.1016/j.applthermaleng.2020.115556>.
- Nasrin R, Rahim NA, Fayaz H, Hasanuzzaman M. Water/MWCNT nanofluid based cooling system of PVT: experimental and numerical research. *Renew Energy* 2018. <https://doi.org/10.1016/j.renene.2018.01.014>.
- FHF02SC manual n.d. [https://www.hukseflux.com/uploads/product-documents/FHF02SC\\_manual\\_v2004.pdf](https://www.hukseflux.com/uploads/product-documents/FHF02SC_manual_v2004.pdf) (accessed April 27, 2021).
- Nizetić S, Ninić N, Klarin B. Analysis and feasibility of implementing solar chimney power plants in the Mediterranean region. *Energy* 2008. <https://doi.org/10.1016/j.energy.2008.05.012>.
- PICO technology n.d. <https://www.pico-technology-deutschland.de/Thermocouple-1m-PTFE-Wires-Exposed-Junction-Plug-75-to-250C> (accessed April 27, 2021).
- Nizetić S, Grubišić-Cabo F, Marinić-Kragić I, Papadopoulos AM. Experimental and numerical investigation of a backside convective cooling mechanism on photovoltaic panels. *Energy* 2016;111:211–25. <https://doi.org/10.1016/j.energy.2016.05.103>.
- Wilson MJ, Paul MC. Effect of mounting geometry on convection occurring under a photovoltaic panel and the corresponding efficiency using CFD. *Sol Energy* 2011; 85:2540–50. <https://doi.org/10.1016/j.solener.2011.07.013>.
- Zhang R, Mirzaei PA, Carmeliet J. Prediction of the surface temperature of building-integrated photovoltaics: development of a high accuracy correlation using computational fluid dynamics. *Sol Energy* 2017;147:151–63. <https://doi.org/10.1016/j.solener.2017.03.023>.
- Arianmehr I, Ting D-S-K, Ray S. Effect of a transverse groove on cooling of a surrogate photovoltaic panel. *Int J Environ Stud* 2014;1–12. <https://doi.org/10.1080/00207233.2014.967016>.



- [35] Armstrong S, Hurley WG. A thermal model for photovoltaic panels under varying atmospheric conditions. *Appl Therm Eng* 2010;30:1488–95. <https://doi.org/10.1016/j.applthermaleng.2010.03.012>.
- [36] Marinić-Kragić I, Nizetić S, Grubišić-Čabo F, Papadopoulos AM. Analysis of flow separation effect in the case of the free-standing photovoltaic panel exposed to various operating conditions. *J Clean Prod* 2018;174. <https://doi.org/10.1016/j.jclepro.2017.10.310>.
- [37] Aly AM. On the evaluation of wind loads on solar panels: the scale issue. *Sol Energy* 2016;135:423–34. <https://doi.org/10.1016/j.solener.2016.06.018>.
- [38] Peng S-H, Haase W. *Advances in Hybrid RANS-LES Modelling*. vol. 97. Berlin, Heidelberg, Heidelberg: Springer Berlin Heidelberg; 2008. DOI:10.1007/978-3-540-77815-8.
- [39] Menter F. Zonal Two Equation k-w Turbulence Models For Aerodynamic Flows. 23rd Fluid Dyn. Plasmadynamics, Lasers Conf., Reston, Virginia: American Institute of Aeronautics and Astronautics; 1993. DOI:10.2514/6.1993-2906.
- [40] Fatnassi H, Poncet C, Bazzano MM, Brun R, Bertin N. A numerical simulation of the photovoltaic greenhouse microclimate. *Sol Energy* 2015;120:575–84. <https://doi.org/10.1016/j.solener.2015.07.019>.
- [41] Jubayer CM, Siddiqui K, Hangan H. CFD analysis of convective heat transfer from ground mounted solar panels. *Sol Energy* 2016;133:556–66. <https://doi.org/10.1016/j.solener.2016.04.027>.
- [42] Brinkworth B, Cross B, Marshall R, Yang H. Thermal regulation of photovoltaic cladding. *Sol Energy* 1997;61:169–78. [https://doi.org/10.1016/S0038-092X\(97\)00044-3](https://doi.org/10.1016/S0038-092X(97)00044-3).

## Appendix G

Title: Techno-economic and environmental evaluation of photovoltaic-thermal collector design with pork fat as phase change material

Authors: Jurčević M., Nižetić S., Čoko D., Arici M., Hoang A.T., Giama E., Papadopoulos A.

Publisher: *Elsevier*

Journal: *Energy*

Edition, ID, year: 254, 124284, 2022.

Indexed in: Scopus, Science Citation Index Expanded, Current Contents, Web of Science, etc.

Journal Impact Factor: 8.9 Q1 (WoS and SJR-2022.)

DOI: <https://doi.org/10.1016/j.energy.2022.124284>

**Abstract:** This novel photovoltaic-thermal (PVT) collector work design was proposed and experimentally tested in Mediterranean climate conditions. The integral evaluation of the PVT collector design was obtained considering performance, economic and environmental aspects. The specific PVT design consisted of four cooling blocks, where each block was equipped with straight pipes (water as working fluid) and a plexiglass container filled with organic phase change material (PCM), i.e. pork fat. The system was monitored for several months where the maximum reached overall energy efficiency of the examined system was 62.2%. However, the average annual estimated overall energy efficiency is expected to be lower than 50%. The economic analysis showed that the levelized cost of overall produced energy from the PVT collector would range from 0.056 to 0.083 €/kWh. The environmental impact analysis evaluated the PVT system in terms of material use concluding that the PV panel itself, and the use of aluminium are the most critical parameters regarding the environmental impact.



# Techno-economic and environmental evaluation of photovoltaic-thermal collector design with pork fat as phase change material

Mišo Jurčević<sup>a</sup>, Sandro Nižetić<sup>b,\*</sup>, Duje Čoko<sup>a</sup>, Müslüm Arıcı<sup>b</sup>, Anh Tuan Hoang<sup>c</sup>, Effrosyni Giama<sup>d</sup>, Agis Papadopoulos<sup>d</sup>

<sup>a</sup> University of Split, FESB, Split, Croatia

<sup>b</sup> Kocaeli University, Kocaeli, Turkey

<sup>c</sup> Institute of Engineering, HUTECH University, Ho Chi Minh City, Viet Nam

<sup>d</sup> Aristotle University of Thessaloniki, Thessaloniki, Greece

## ARTICLE INFO

### Article history:

Received 18 March 2022

Received in revised form

22 April 2022

Accepted 13 May 2022

Available online 21 May 2022

### Keywords:

Photovoltaics

Phase change material (PCM)

PVT

Efficiency

Renewables

Environmental impact analysis

## ABSTRACT

This novel photovoltaic-thermal (PVT) collector work design was proposed and experimentally tested in Mediterranean climate conditions. The integral evaluation of the PVT collector design was obtained considering performance, economic and environmental aspects. The specific PVT design consisted of four cooling blocks, where each block was equipped with straight pipes (water as working fluid) and a plexiglass container filled with organic phase change material (PCM), i.e. pork fat. The system was monitored for several months where the maximum reached overall energy efficiency of the examined system was 62.2%. However, the average annual estimated overall energy efficiency is expected to be lower than 50%. The economic analysis showed that the levelized cost of overall produced energy from the PVT collector would range from 0.056 to 0.083 €/kWh. The environmental impact analysis evaluated the PVT system in terms of material use concluding that the PV panel itself, and the use of aluminium are the most critical parameters regarding the environmental impact.

© 2022 Elsevier Ltd. All rights reserved.

## 1. Introduction

The current issues with the COVID-19 pandemic clearly directed how such events can rapidly affect global energy systems [1] as well as global supply chains, indicating the importance of renewable energy technologies [2] to be able to secure sufficient energy supplies in specific circumstances. Different renewable energy technologies are available nowadays, however, solar and wind generation technologies currently lead with respect to globally installed capacities. According to the latest report by the International Energy Agency [3], despite the pandemic circumstances, photovoltaic (PV) capacities had stable growth in 2021, where almost half of the overall globally installed renewable energy capacities (around 290 GW) are related to photovoltaics, followed by wind and hydropower generation technologies, [3]. Photovoltaic technologies grow each year and in 2021 almost 160 GW of new PV capacities were estimated to be installed globally, [3]. The EU

market accounted for almost 30 GW of installed PV capacities in 2021 [4], which was a historical record, while the leading market for PVs is the Asian region. China added around 53 GW of new PV capacities in 2021 and currently is the country with the highest number of installed PV capacities globally, [5]. The general importance of PV technologies is vital when considering global energy transition goals and the necessary decarbonization of power systems. Based on the projections by IRENA [6], over 8500 GW of installed PV capacities will be necessary by 2050, Fig. 1, to reach low-carbon energy transformations.

Besides the use of PV technologies in residential or large-scale systems, there are also other application areas of PVs such as photovoltaic-thermal systems (PVT), [7]. PVT systems are important in the context of the energy transition as they represent suitable energy generation systems that can both produce electricity and heat, which are typical energy demands for building facilities. PVT collectors can be used in various applications, i.e. for the production of low-temperature heat (domestic hot water), in residential heating systems, swimming pool heating, air heating, for drying applications, and finally as process heat in industrial facilities.

\* Corresponding author. University of Split, Faculty of FESB, Rudjera Boškovića 32, 21000, Split, Croatia.

E-mail address: [snizetic@fesb.hr](mailto:snizetic@fesb.hr) (S. Nižetić).

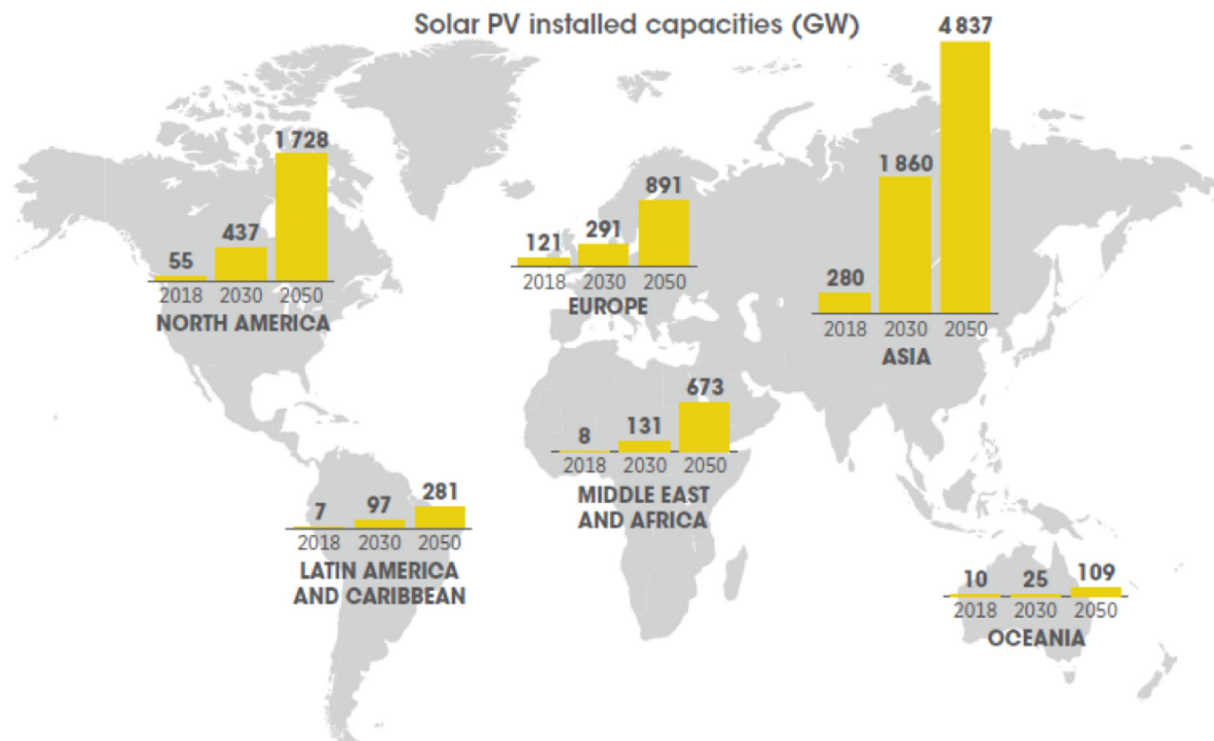


Fig. 1. Projection of installed PV capacities by IRENA [6].

Currently, there are over twenty PVT collector manufacturers in eleven countries, and production is mainly focused on liquid-based PVT collectors, i.e. (48%) uncovered flat plate collectors, (28%) covered flat plate collectors, while the rest are vacuum tubes, air-based, or concentrating PVT collectors, [8]. The EU PVT market leads regarding the overall installed area of PVT collectors, where most of the PVT capacities are installed in France and Germany, while most of the installed capacities in Asia are in China and Korea ([8] and data from 2018). The main PVT installations are directed to solar air systems, i.e. over 22,000 systems in 2018, followed by domestic hot water systems with over 1600 installations globally, [8]. The main issue with the PVT system is its relatively high unit cost, which affects the dynamic of installed capacities. Namely, when analysing data from 2018 [8], and based on real installed PVT systems in the EU, the minimal investment was about 330 €/m<sup>2</sup> of collector area, while in most cases, the investment ranged from about 600 €/m<sup>2</sup> to 900 €/m<sup>2</sup>. In some cases, the overall cost of the PVT system was over 1000 €/m<sup>2</sup>, which of course depends on specific PVT technology, application area, and finally geographical location. No matter that PVT technology is followed by a relatively high unit cost, in the context of the ongoing energy transition, PVT systems have their role. The main advantage of the PVT system is the possibility of efficient integration within more complex energy systems, considering the implementation and integration of heat pumps or even cogeneration systems.

The key feature of PVT collectors is their specific design since it affects the overall electrical as well as the thermal performance of PVT systems. Usually, the electrical performance of PVT collectors is less than 20%, while the thermal ranges in most cases from 40% up to 80%, [7]. The role of the working fluid is also critical with respect to the expected overall performance of the PVT collector. The lowest performance of PVT systems can be expected for air-based PVT collectors, while the highest performance improvement is possible in the case of water or nanofluids, which is directly linked with the

suitable thermal properties of the mentioned working fluids. Nanoparticles in addition to improving the thermal properties of PCM or coolant fluid can also be used to improve the efficiency of irradiated solar energy conversion by implementing nanofluid-based spectral splitting in concentrating PVT systems, [9]. The economic and environmental aspect of PVT designs is not covered well in the existing literature [10], i.e. the main focus was on the investigation of performance improvement. There are various designs of PVT collectors as well as PVT systems as a whole, where some recent findings will be briefly tackled in the continuation to highlight some recent research advancements in the field.

A novel PVT collector design was reported in Ref. [11], where overall twelve cooling blocks were applied on the backside surface of a PVT panel to reduce the operating temperature of the PV panel. The experiments were conducted in laboratory conditions, together with a numerical investigation. The overall improvement of the electrical efficiency was around 4.7%, while the highest electrical efficiency was about 17.7%. The highest thermal efficiency was 58.5%. The economic and environmental evaluation of the proposed PVT collector design was not carried out, which is also an important aspect that should be analysed. A specific design of a PVT collector with a cross-fined channel box was elaborated in study [12]. The PVT collector design was specific due to the design of a water flow channel that had a serpentine layout and ensured a more uniform cooling of the PV panel. The study only contained a numerical investigation, where the impact of the specific PVT collector design was examined with respect to the specific temperature distributions, as well as the collector performance in general. The developed concept requests experimental verification in order to be able to get credible results. A novel design of a PVT collector for drying green tea was presented in Ref. [13]. The PVT collector consisted of a PV, followed by a collector box equipped with a special absorber plate and DC fan units. The PVT setup recorded the highest performance of about 58.7%, with a maximum drying efficiency rate of

26.3%. The economic and environmental evaluation of the proposed design was not evaluated. Study [14] reported three different PVT collector designs involving phase change materials (PCM) as well as nanoparticles. CuO nanoparticles were used in order to enhance the thermal properties of paraffin wax. The experimental results indicated an overall exergy efficiency ranging from 10.5% to 15.4%, depending on the specific examined setup while electrical efficiency was in the range from 10% to 13.3%. Depending on the air mass flow rate the thermal efficiency ranged from 40.1% to 68.9%. The introduction of nano-enhanced PCMs boosted the electrical and thermal performance of the PVT collector. The sustainability index was also evaluated for the PVT collector setups, while the economic evaluation was not conducted. The outdoor experimental study [15] of the PVT system enhanced with SiO<sub>2</sub>/TiO<sub>2</sub> interference thin film resulted in a 4.94% improvement in overall energy efficiency, however, the estimated payback time is 17 years which is relatively long but reasonable. A PVT collector design made of fiberglass was reported in Ref. [16], which was quite simple in design. The PVT collector was assembled from a spiral tube absorber attached to the backside surface and was covered with fiberglass. Based on the experimental findings, the highest recorded thermal efficiency was almost 73%, while the electrical efficiency was 9.7% (Malaysian climate conditions). The proposed PVT collector design was more effective regarding the thermal performance rather than the electrical. The economic aspect was not discussed as well as the environmental. The economic assessment of various PVT collector designs was discussed in study [17], using the evaluation method based on energy yield per area, volume, and weight. The proposed and demonstrated method is useful in the classification and design analysis of various PVT collector designs. A novel and innovative design of a dual-purpose PVT collector was proposed in Ref. [18]. The developed PVT collector has a double pane cover instead of a single pane cover, using water passing between the panes. Metamaterial thin film was also added to the collector surface to enhance radiative cooling. The proposed design was experimentally tested and found to be suitable for integration into building HVAC systems. A water-based cooled PVT collector (serpentine pipe layout) with an integrated thermoelectric generator was proposed in Ref. [19]. Besides an experimental approach, the simulation model was also developed and validated with real field data. The proposed design ensured an improvement in electrical efficiency of about 5.7% (hourly basis). An environmental and cost analysis was also conducted. The performance analysis of three different nanofluid-based PVT collectors was analysed in Ref. [20]. Three specific tube layouts were analysed, i.e. sheet and serpentine tube collectors with sheets and grooved serpentines with a groove pitch, with two different pitch dimensions. The highest overall energy efficiency was reached for the case of grooved serpentine tube type collectors with the highest groove pitch, with an overall recorded improvement of 15%. The experimental results provided useful data for the design of novel and efficient PVT collectors. An economic and environmental evaluation of the PVT systems needs to be carried out for the proposed PVT designs in the mentioned work. An experimental and numerical analysis of crucial design parameters for PVT air-based collectors was obtained in study [21]. A comparison of numerical and experimental data was also provided with reasonable matching. The most influential parameters on performance were air flow rate as well as the air layer depth. It was found that a reduction in depth causes improvement in the thermal performance with a weak effect on the electrical performance. The economic and environmental evaluation was not conducted.

From the briefly discussed and elaborated research findings, it

can be noted that various PVT collector designs, or PVT system configurations, are still being intensively investigated. The main aim of the ongoing investigations is to find the most suitable PVT design from a performance point of view. However, it must be noted that very few studies analysed the economic and environmental aspects of the specific PVT designs, thus the main focus of future investigations should be based on the integral evaluation of the proposed PVT collector designs.

The main objective of this work was to report an integral analysis of a novel PVT collector design consisting of four independent cooling blocks filled with an organic phase change material equipped with water pipes. The integral analysis assumes performance, economic as well as environmental evaluation. The analysis was based on a several-month experimental measurement period in typical Mediterranean climate circumstances, while the annual performance was estimated based on the measured experimental data.

## 2. Description of PVT collector design and experimental approach

### 2.1. PVT-PCM collector design

Regardless of the design, the overall efficiency of all PVT collectors is the result of electrical and thermal efficiency that have contradictory natures. It is necessary to optimize the design of the PVT collector to reconcile this contradiction, but still, the design of the PVT collector will favor one or the other. Optimization can be performed iteratively with extensive use of numerical analyses in conjunction with experimental approaches. For this purpose, a new concept of a PVT collector with an incorporated organic phase change material was developed and subjected to experimental testing in Mediterranean climatic conditions. The thermal management system of the newly developed PVT-PCM collector combines passive cooling based on the phase transition of the organic material with an active refrigerant recirculation controlled by a smart regulation apparatus. The passive component of the system uses pork fat as a relatively inexpensive and widely available phase change material with appropriate thermal properties, i.e. thermal conductivity of 0.191 W/mK and volumetric specific heat capacity of 1.512 MJ/m<sup>3</sup>K, [22]. Pork fat serves as a heat buffer for the photovoltaic panel where thermal energy is expended on the phase transition rather than on temperature rise. After the latent heat capacity of the passive component is consumed, i.e. the fat is melted, the smart control system switches on the recirculation pump, and cooling is therefore taken over by the active component of the system. Water flows through eight square aluminum pipes, 20 × 20 × 2 mm, that are bonded to aluminum sheets, 658 × 448 × 2 mm, with a two-component epoxy adhesive for metals. The merged geometry forms a thermal absorber that serves as an integrative element between the passive and active components of the system since heat is transferred from the pork fat to the cooling water via the contact surfaces of the thermal absorber, Fig. 2. The upper plate of the thermal absorber is in direct contact with the back of the panel to establish cooling of the panel immediately after activating the pump, thus eliminating the inertia of the phase change. Hybrid cooling is applied to a 1640 × 992 × 40 mm polycrystalline photovoltaic panel with 60 cells nominally generating 275 Wp of peak power (P<sub>MPP</sub>) output at Standard Test Conditions (STC) with a peak power tolerance of −0/+4.9 W, [23]. The panel efficiency at STC is 16.9% with a temperature coefficient of power −0.41%/K.

The conventional approach to cooling PV panels with a PCM



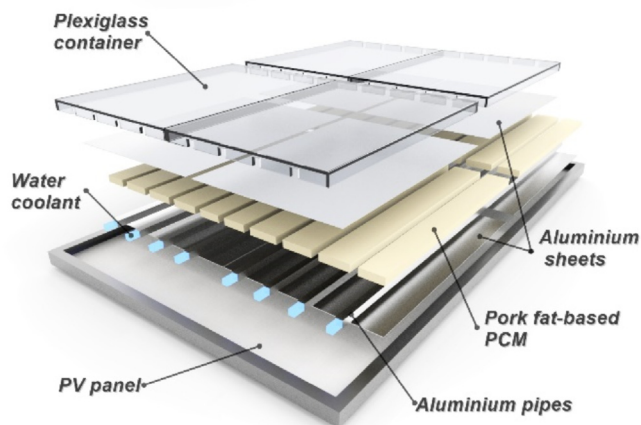


Fig. 2. Schematic cross-section of PVT-PCM collector, [24].

material generally involves one large continuous container at the back of the panel. However, this approach has proven to be weaker in terms of electricity generation compared to the concept of cooling with several smaller separated containers, [25]. Therefore, for the first time, a passive concept based on multi-block pork fat PCM combined with active cooling water recirculation was used for thermal management of the PVT collector. The new PVT-PCM collector concept, unlike the conventional approach, has four independent containers on the back, Fig. 3. Loaded Plexiglas containers, measuring  $676 \times 466 \times 30$  mm each, containing 17.7 kg of pork fat in total, form four cooling blocks.

The inlet manifold of the PVT-PCM collector is placed at the bottom where the flow is divided into eight pipes, Fig. 4. Ultrasonic flow meters are located on the pipes to individually monitor the flow in each pipe. Warm water, after the heat is transferred from the collector, passes through the control valves and outlet manifold and then enters the heat exchanger, where heat is transferred to the environment. The heat exchanger is relatively simple and consists of a convectively cooled radiator with a fan that turns on automatically after starting the recirculation pump. This heat exchanger is relatively inefficient and serves as a temporary robust solution in the experimental phase of optimizing the new PVT-PCM collector concept. Rough monitoring of the induced heat in the PVT-PCM collector delivered to the cooling water is performed with an ultrasonic calorimeter. A more detailed insight into this mechanism is

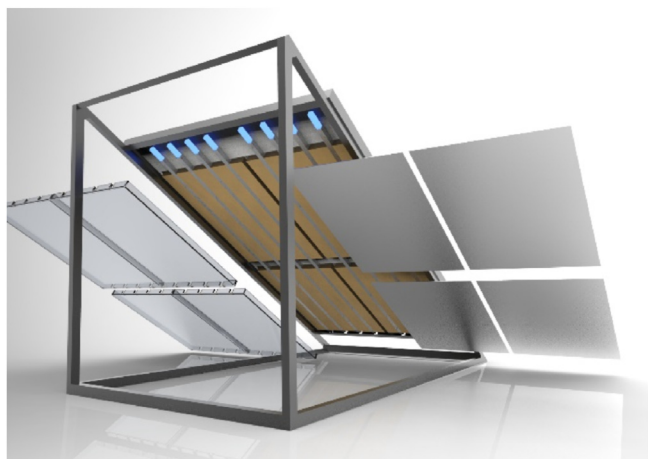


Fig. 3. PVT-PCM collector concept with four separate containers.

possible due to the thermocouples at the inlets and outlets of the aluminium pipes of the collector.

## 2.2. Experimental layout and measuring equipment

The experimental research on the novel PVT-PCM collector was conducted from August 2021 to January 2022 in the city of Split (Croatia) which has a humid subtropical and Mediterranean climate. The PVT-PCM collector and the referent polycrystalline 275 Wp PV panel were inclined at an angle of  $27^\circ$  while facing south. For both systems, the currents and voltages were measured at a fixed resistive load to determine the dissipated electric power using two YoctoWatt USB wattmeters. Two  $4.7\text{-}\Omega$  resistors rated at 1 kW were used as loads to bring both panels close to the maximum power point. Nominally, PV panels have a rated current ( $I_{MPP}$ ) of 8.5 A and rated voltage ( $V_{MPP}$ ) of 32.38 V at Standard Test Conditions (STC) with a current and voltage tolerance of  $\pm 3\%$ , [23]. K-type thermocouples were used on the surfaces of the PV panel and PVT collector, while a T-type was used for the temperature monitoring of the pork fat and water. Temperatures were measured on all surfaces of the panel and collector, but due to the geometric complexity of the rear of the PVT-PCM collector, temperatures were compared only on the front surfaces. Three K-type thermocouples (R1, R2, and R3) were positioned on the front surface of the referent PV panel, while three K-type thermocouples (C1, C2, C3) were fixed on the front surface of the PVT-PCM collector at the corresponding positions, Fig. 5. In the narrow gap between the panel and the collector, an Apogee Sp-420 pyranometer was fixed for the continuous monitoring of solar irradiance. All sensors and measuring devices of appropriate accuracy were connected to the computer for continuous data acquisition, as given in Table 1.

## 3. Operational modes and performance analysis

As mentioned earlier, the PVT-PCM system operates in two operating modes. The primary cooling system is passive based on an organic PCM, i.e. pork fat. For the first time, pork fat was used as a PCM for the thermal management of a specific energy system, which in the process of phase transition absorbs heat from the PV panel. The energy of the phase transition is transformed into the generated heat of the novel PVT setup. A passive component based on pork fat (lard) operates independently up to a temperature of  $40^\circ\text{C}$  when active water cooling is started. After the capacity of latent heat is consumed, the active component parallelly takes over the cooling of the PV panel and PCM. The industrially processed pork fat (lard) has a melting point of  $41^\circ\text{C}$ , according to very limited available data [26], so the transition of the system to active mode is fixed at  $40^\circ\text{C}$ . A temperature difference of  $1^\circ\text{C}$  between the set temperature of the active system actuation and melting point serves as a temperature buffer zone due to the thermal inertia of the PCM. The controller takes the temperature data for the threshold from one point so it is possible for active cooling to start at an average PCM temperature lower than  $40^\circ\text{C}$ . Cooling water recirculation is performed until the pork fat temperature reaches  $33^\circ\text{C}$  when it is automatically switched off. It makes no sense to further reduce the temperature since the pork fat at that particular temperature is in the solid phase. Therefore, a further recirculation would lead to unnecessary energy consumption without additional yield in terms of warm water. The measurement data for a period of six months were thoroughly analysed, focusing on ten clear and/or mostly clear days in each month to perceive the performance difference between the conventional PV panel and the novel PVT collector.



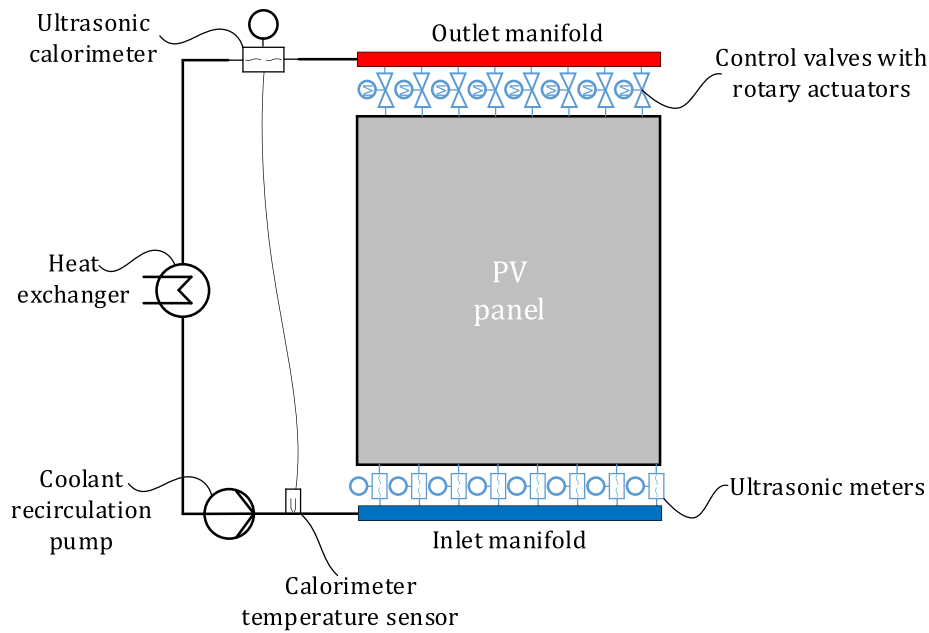


Fig. 4. Experimental test rig scheme.

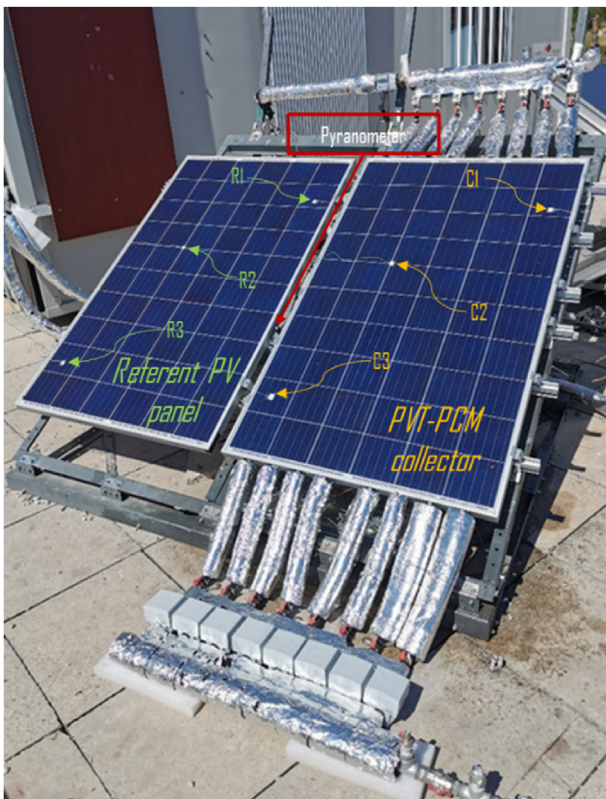


Fig. 5. Experimental layout.

Table 1  
Measurement accuracy deviation for used sensors and devices.

| Sensor/Measurement device | Measurement accuracy deviation |
|---------------------------|--------------------------------|
| <b>Wattmeter</b>          | ±1.5%                          |
| <b>Thermocouple</b>       | ±0.2%                          |
| <b>Pyranometer</b>        | <1.0%                          |

### 3.1. Active PVT-PCM system operation mode

Throughout the six-month measurement period, the active PVT-PCM system operation mode was automatically engaged at times mostly during two months. The active operation mode of the PVT-PCM system was increasingly engaged in summer, and occasionally in autumn, due to more pronounced insolation and higher temperatures. The average daily air temperature in August was 27.4 °C with a moderate average wind speed of 4.3 km/h while the average humidity was 49%. The maximum recorded air temperature in August was 38.5 °C while the maximum wind speed was 28.4 km/h. In August, the referent conventional PV panel produced 14136.4 Wh of electricity with an efficiency ranging from 11.7% to 12%, Table 2. In the same period, the PVT-PCM collector produced 14651 Wh of electricity with an electrical efficiency ranging from 12.0% to 12.4%. Furthermore, the PVT-PCM collector generated 45208.7 Wh of heat with a maximum thermal efficiency of 49.8%. The maximum total efficiency of the collector was 62.2%. The peak temperature difference between the referent PV panel (position R2) and PVT-PCM collector (position C2) was 13.4 °C.

The average daily air temperature in September was 23.2 °C with a moderate average wind speed of 4.3 km/h while the average humidity was 54%. The maximum recorded air temperature in September was 30.5 °C while the maximum wind speed was 41.4 km/h. In September the referent PV panel generated 13152.4 Wh of electricity with an electrical efficiency ranging from 11.9% to 12.7%, Table 3. In the same month, the PVT-PCM collector produced 13481.7 Wh of electrical energy with an efficiency ranging from 12.0% to 12.9%. Additionally, the PVT-PCM collector generated 24338.1 Wh of heat with a maximum thermal efficiency of 29.8%. The maximum total efficiency of the collector was 42.6%. The maximum peak temperature difference between the referent PV panel (position R2) and PVT-PCM collector (position C2) was 9.5 °C.

An increase in the electrical efficiency of the referent PV panel and PVT-PCM collector in September compared to August is evident, which was expected given the lower daily temperatures. Lower daily temperatures with weaker insolation unquestionably lead to lesser temperature degradation, hence, increased electrical

**Table 2**  
Power production and collector efficiency in August.

| Date           | Power production |                   |                |                 | Efficiency |          |         |                 | Temperature |      |         |      |
|----------------|------------------|-------------------|----------------|-----------------|------------|----------|---------|-----------------|-------------|------|---------|------|
|                | Insolation       | Electrical energy |                | Heat generation | Electrical |          | Thermal | TOTAL (PVT-PCM) | Referent    |      | PVT-PCM |      |
|                |                  | Total             | Referent       |                 | PVT-PCM    | Referent |         |                 | PVT-PCM     | Peak | Mean    | Peak |
|                | 2021             | Wh/m <sup>2</sup> | Wh             | Wh              | Wh         |          |         |                 | °C          | °C   | °C      | °C   |
| 06.08.         | 7940.0           | 1510.3            | 1552.7         | 4299.8          | 11.7%      | 12.0%    | 33.3%   | 45.3%           | 54.9        | 32.0 | 49.8    | 31.1 |
| 11.08.         | 7294.3           | 1385.3            | 1453.1         | 5676.1          | 11.7%      | 12.2%    | 47.8%   | 60.1%           | 57.8        | 36.9 | 48.1    | 34.4 |
| 12.08.         | 7404.8           | 1440.0            | 1497.3         | 5509.3          | 12.0%      | 12.4%    | 45.7%   | 58.2%           | 59.5        | 36.0 | 47.5    | 33.9 |
| 14.08.         | 7407.9           | 1419.2            | 1484.0         | 6007.2          | 11.8%      | 12.3%    | 49.8%   | 62.2%           | 62.3        | 36.9 | 48.9    | 34.2 |
| 15.08.         | 7364.3           | 1426.4            | 1484.9         | 5905.4          | 11.9%      | 12.4%    | 49.3%   | 61.7%           | 58.9        | 35.6 | 47.2    | 33.1 |
| 20.08.         | 7531.1           | 1469.7            | 1515.5         | 3633.0          | 12.0%      | 12.4%    | 29.7%   | 42.0%           | 56.2        | 32.3 | 51.6    | 30.9 |
| 21.08.         | 7165.1           | 1396.8            | 1445.4         | 3721.5          | 12.0%      | 12.4%    | 31.9%   | 44.3%           | 56.6        | 33.4 | 52.5    | 31.8 |
| 22.08.         | 7484.9           | 1445.4            | 1502.6         | 4212.2          | 11.9%      | 12.3%    | 34.6%   | 46.9%           | 58.2        | 33.0 | 50.5    | 31.2 |
| 23.08.         | 7063.0           | 1380.0            | 1423.6         | 3742.8          | 12.0%      | 12.4%    | 32.6%   | 45.0%           | 56.1        | 33.1 | 50.5    | 31.3 |
| 24.08.         | 6472.6           | 1263.3            | 1291.9         | 2501.4          | 12.0%      | 12.3%    | 23.8%   | 36.0%           | 52.2        | 32.7 | 50.1    | 32.7 |
| <b>OVERALL</b> | <b>73128.0</b>   | <b>14136.4</b>    | <b>14651.0</b> | <b>45208.7</b>  |            |          |         |                 |             |      |         |      |

**Table 3**  
Power production and collector efficiency in September.

| Date           | Power production |                   |                |                 | Efficiency |          |         |                 | Temperature |      |         |      |
|----------------|------------------|-------------------|----------------|-----------------|------------|----------|---------|-----------------|-------------|------|---------|------|
|                | Insolation       | Electrical energy |                | Heat generation | Electrical |          | Thermal | TOTAL (PVT-PCM) | Referent    |      | PVT-PCM |      |
|                |                  | Total             | Referent       |                 | PVT-PCM    | Referent |         |                 | PVT-PCM     | Peak | Mean    | Peak |
|                | 2021             | Wh/m <sup>2</sup> | Wh             | Wh              | Wh         |          |         |                 | °C          | °C   | °C      | °C   |
| 05.09.         | 6781.8           | 1362.6            | 1407.2         | 3292.6          | 12.4%      | 12.8%    | 29.8%   | 42.6%           | 57.0        | 30.3 | 47.5    | 28.3 |
| 06.09.         | 7269.4           | 1438.8            | 1492.6         | 3351.1          | 12.2%      | 12.6%    | 28.3%   | 41.0%           | 53.8        | 30.9 | 48.1    | 28.8 |
| 07.09.         | 7022.1           | 1397.7            | 1446.7         | 3163.9          | 12.2%      | 12.7%    | 27.7%   | 40.4%           | 55.1        | 29.8 | 48.2    | 28.0 |
| 08.09.         | 7083.8           | 1417.0            | 1456.6         | 2707.0          | 12.3%      | 12.6%    | 23.5%   | 36.1%           | 51.9        | 28.8 | 46.6    | 27.4 |
| 09.09.         | 6965.1           | 1414.3            | 1442.8         | 2272.5          | 12.5%      | 12.7%    | 20.1%   | 32.8%           | 50.8        | 28.9 | 47.0    | 27.8 |
| 15.09.         | 6181.3           | 1217.2            | 1255.1         | 2529.4          | 12.1%      | 12.5%    | 25.2%   | 37.6%           | 53.4        | 29.8 | 47.9    | 28.4 |
| 25.09.         | 6765.1           | 1399.4            | 1415.1         | 1565.4          | 12.7%      | 12.9%    | 14.2%   | 27.1%           | 50.3        | 26.5 | 48.6    | 26.0 |
| 26.09.         | 6019.9           | 1238.4            | 1258.0         | 1934.6          | 12.6%      | 12.8%    | 19.8%   | 32.6%           | 51.2        | 27.9 | 46.2    | 27.0 |
| 27.09.         | 4790.6           | 926.1             | 934.0          | 1077.3          | 11.9%      | 12.0%    | 13.8%   | 25.8%           | 52.0        | 26.8 | 46.5    | 26.3 |
| 28.09.         | 6545.4           | 1340.9            | 1373.6         | 2444.3          | 12.6%      | 12.9%    | 23.0%   | 35.9%           | 54.0        | 28.4 | 49.1    | 26.8 |
| <b>OVERALL</b> | <b>65424.5</b>   | <b>13152.4</b>    | <b>13481.7</b> | <b>24338.1</b>  |            |          |         |                 |             |      |         |      |

efficiency. However, the generated heat is almost twice as low with a significantly lower overall efficiency of the PVT-PCM collector. The PVT-PCM collector produced more electricity than the PV panel in these two months, and also generated heat. Even when the energy expended on the circulation is taken into account, the electrical efficiency of the PVT-PCM collector remains at the level of the PV panel and could easily surpass it by optimizing the flow and circulation pump. The circulation pump was oversized to add flexibility to the experiments.

3.2. Passive PVT-PCM system operation mode

The passive mode of operation dominated the period from October to January except for a few autumn days. October, as expected, was slightly more volatile compared to the summer months with an average air temperature of 16.4 °C and average humidity of 56%. The average wind was also slightly stronger with a speed of 6.3 km/h. The maximum recorded wind speed was 46.8 km/h while the maximum air temperature was 25.8 °C. The average temperatures of the PV panel and the PVT-PCM collector in October at positions R2 and C2 were about 10 °C lower than in September. The insolation was 59629.3 Wh/m<sup>2</sup>, which is only slightly less than in September. The referent PV panel produced 12450.5 Wh of electricity with an efficiency ranging from 12.5% to 13.3%. The PVT-PCM collector produced a similar amount of electricity with an efficiency between 12.5% and 13.2%, Table 4. In the considered days, the PCM

temperature did not reach the threshold therefore there was no generated heat to be collected.

November was significantly rainier than October, so some of the analysed days were not clear or mostly clear, thus the total insolation was significantly lower, i.e. 32170.4 Wh/m<sup>2</sup>. The average air temperature was 14.3 °C while the humidity even reached 70% on average. The wind did not deviate significantly compared to previous months with an average speed of 4.8 km/h and a maximum speed of 48.6 km/h. The average temperatures of the PV panel and PVT-PCM collector were almost constantly below 20 °C with the collector being generally slightly warmer, Table 5. However, when peak temperature is considered, the PVT-PCM collector is constantly cooler with a maximum temperature difference of 4.7 °C. The maximum electrical efficiency of the PV panel and PVT-PCM collector was 13.4% and 13.5%, respectively.

December had less rainfall than November so insolation was somewhat more pronounced with a total irradiated energy of 36669.7 Wh/m<sup>2</sup>. The average air temperature was significantly lower (9.7 °C) with a relatively high average humidity of 62% and a wind speed of 6.7 km/h. The maximum air temperature was 18.9 °C while the maximum wind speed was 53.3 km/h. As in the previous month, the PVT-PCM collector was warmer than the PV panel, but its peak temperature was constantly lower with a maximum difference of 7.7 °C, Table 6.

The electrical output of the PV panel and PVT-PCM collector is almost identical, and the same applies to their maximum electrical

**Table 4**  
Power production and collector efficiency in October.

| Date           | Power production |                   |                |                 | Efficiency |          |         |           | Temperature |      |         |      |
|----------------|------------------|-------------------|----------------|-----------------|------------|----------|---------|-----------|-------------|------|---------|------|
|                | Insolation       | Electrical energy |                | Heat generation | Electrical |          | Thermal | TOTAL     | Referent    |      | PVT-PCM |      |
|                |                  | Total             | Referent       |                 | PVT-PCM    | Referent |         |           | PVT-PCM     | Peak | Mean    | Peak |
|                | 2021             | Wh/m <sup>2</sup> | Wh             | Wh              | Wh         | Referent | PVT-PCM | (PVT-PCM) | °C          | °C   | °C      | °C   |
| 02.10.         | 6510.7           | 1335.2            | 1324.9         | /               | 12.6%      | 12.5%    | 0.0%    | 12.5%     | 47.2        | 24.3 | 47.2    | 25.6 |
| 03.10.         | 6585.1           | 1352.3            | 1342.3         | /               | 12.6%      | 12.5%    | 0.0%    | 12.5%     | 49.4        | 25.5 | 49.0    | 26.5 |
| 11.10.         | 5859.9           | 1189.2            | 1188.6         | /               | 12.5%      | 12.5%    | 0.0%    | 12.5%     | 41.5        | 19.0 | 38.6    | 19.6 |
| 12.10.         | 5321.9           | 1124.0            | 1116.4         | /               | 13.0%      | 12.9%    | 0.0%    | 12.9%     | 37.5        | 17.5 | 36.9    | 18.3 |
| 13.10.         | 6283.4           | 1354.7            | 1350.5         | /               | 13.3%      | 13.2%    | 0.0%    | 13.2%     | 40.7        | 17.3 | 39.7    | 17.8 |
| 16.10.         | 6098.1           | 1300.9            | 1293.3         | /               | 13.1%      | 13.0%    | 0.0%    | 13.0%     | 44.6        | 20.8 | 44.3    | 21.9 |
| 17.10.         | 6111.6           | 1290.4            | 1280.2         | /               | 13.0%      | 12.9%    | 0.0%    | 12.9%     | 45.1        | 20.5 | 44.0    | 21.7 |
| 18.10.         | 5688.9           | 1169.4            | 1162.2         | /               | 12.6%      | 12.6%    | 0.0%    | 12.6%     | 45.3        | 20.9 | 44.0    | 22.0 |
| 24.10.         | 6008.8           | 1254.8            | 1246.2         | /               | 12.8%      | 12.7%    | 0.0%    | 12.7%     | 43.8        | 20.3 | 41.7    | 21.5 |
| 27.10.         | 5160.9           | 1079.6            | 1074.0         | /               | 12.9%      | 12.8%    | 0.0%    | 12.8%     | 41.9        | 18.4 | 40.6    | 19.7 |
| <b>OVERALL</b> | <b>59629.3</b>   | <b>12450.5</b>    | <b>12378.6</b> | <b>0.0</b>      |            |          |         |           |             |      |         |      |

**Table 5**  
Power production and collector efficiency in November.

| Date           | Power production |                   |               |                 | Efficiency |          |         |           | Temperature |      |         |      |
|----------------|------------------|-------------------|---------------|-----------------|------------|----------|---------|-----------|-------------|------|---------|------|
|                | Insolation       | Electrical energy |               | Heat generation | Electrical |          | Thermal | TOTAL     | Referent    |      | PVT-PCM |      |
|                |                  | Total             | Referent      |                 | PVT-PCM    | Referent |         |           | PVT-PCM     | Peak | Mean    | Peak |
|                | 2021             | Wh/m <sup>2</sup> | Wh            | Wh              | Wh         | Referent | PVT-PCM | (PVT-PCM) | °C          | °C   | °C      | °C   |
| 11.11.         | 4459.3           | 924.5             | 922.5         | /               | 12.7%      | 12.7%    | 0.0%    | 12.7%     | 40.1        | 20.2 | 38.6    | 21.1 |
| 12.11.         | 2171.8           | 303.4             | 305.9         | /               | 8.6%       | 8.7%     | 0.0%    | 8.7%      | 37.1        | 17.8 | 33.1    | 18.6 |
| 13.11.         | 670.1            | 36.0              | 36.9          | /               | 3.3%       | 3.4%     | 0.0%    | 3.4%      | 23.7        | 15.2 | 23.2    | 15.8 |
| 15.11.         | 2675.4           | 396.8             | 397.6         | /               | 9.1%       | 9.1%     | 0.0%    | 9.1%      | 36.6        | 18.8 | 33.3    | 19.5 |
| 18.11.         | 1925.4           | 232.7             | 238.7         | /               | 7.4%       | 7.6%     | 0.0%    | 7.6%      | 35.3        | 14.1 | 30.7    | 14.6 |
| 19.11.         | 4311.2           | 873.3             | 877.3         | /               | 12.5%      | 12.5%    | 0.0%    | 12.5%     | 40.9        | 16.7 | 36.3    | 17.8 |
| 21.11.         | 4677.4           | 1007.6            | 1009.1        | /               | 13.2%      | 13.3%    | 0.0%    | 13.3%     | 41.8        | 18.8 | 38.5    | 19.4 |
| 24.11.         | 4411.0           | 965.0             | 970.8         | /               | 13.4%      | 13.5%    | 0.0%    | 13.5%     | 38.8        | 16.2 | 35.3    | 17.2 |
| 26.11.         | 1896.8           | 296.4             | 301.4         | /               | 9.6%       | 9.8%     | 0.0%    | 9.8%      | 33.4        | 13.9 | 29.7    | 14.6 |
| 30.11.         | 4972.0           | 1067.8            | 1072.0        | /               | 13.2%      | 13.3%    | 0.0%    | 13.3%     | 31.5        | 10.7 | 30.0    | 11.4 |
| <b>OVERALL</b> | <b>32170.4</b>   | <b>6103.5</b>     | <b>6132.0</b> | <b>0.0</b>      |            |          |         |           |             |      |         |      |

**Table 6**  
Power production and collector efficiency in December.

| Date           | Power production |                   |               |                 | Efficiency |          |         |           | Temperature |      |         |      |
|----------------|------------------|-------------------|---------------|-----------------|------------|----------|---------|-----------|-------------|------|---------|------|
|                | Insolation       | Electrical energy |               | Heat generation | Electrical |          | Thermal | TOTAL     | Referent    |      | PVT-PCM |      |
|                |                  | Total             | Referent      |                 | PVT-PCM    | Referent |         |           | PVT-PCM     | Peak | Mean    | Peak |
|                | 2021             | Wh/m <sup>2</sup> | Wh            | Wh              | Wh         | Referent | PVT-PCM | (PVT-PCM) | °C          | °C   | °C      | °C   |
| 04.12.         | 4300.9           | 893.2             | 894.6         | /               | 12.8%      | 12.8%    | 0.0%    | 12.8%     | 34.1        | 13.1 | 31.2    | 13.6 |
| 08.12.         | 2417.3           | 394.7             | 384.3         | /               | 10.0%      | 9.8%     | 0.0%    | 9.8%      | 27.4        | 11.0 | 24.7    | 11.4 |
| 10.12.         | 1469.2           | 189.2             | 192.4         | /               | 7.9%       | 8.1%     | 0.0%    | 8.1%      | 27.7        | 7.7  | 21.2    | 8.3  |
| 14.12.         | 4591.0           | 970.1             | 967.1         | /               | 13.0%      | 12.9%    | 0.0%    | 12.9%     | 31.3        | 12.2 | 30.1    | 12.6 |
| 16.12.         | 4315.0           | 866.7             | 865.3         | /               | 12.3%      | 12.3%    | 0.0%    | 12.3%     | 33.0        | 13.0 | 31.2    | 13.6 |
| 17.12.         | 4244.5           | 835.2             | 836.4         | /               | 12.1%      | 12.1%    | 0.0%    | 12.1%     | 35.7        | 12.2 | 32.2    | 12.9 |
| 19.12.         | 4464.3           | 938.5             | 938.6         | /               | 12.9%      | 12.9%    | 0.0%    | 12.9%     | 33.4        | 11.5 | 32.1    | 12.4 |
| 20.12.         | 4596.9           | 968.1             | 965.7         | /               | 12.9%      | 12.9%    | 0.0%    | 12.9%     | 32.0        | 8.8  | 29.9    | 9.6  |
| 21.12.         | 4625.3           | 969.0             | 967.8         | /               | 12.9%      | 12.9%    | 0.0%    | 12.9%     | 29.6        | 9.9  | 28.8    | 10.9 |
| 27.12.         | 1645.3           | 238.0             | 243.9         | /               | 8.9%       | 9.1%     | 0.0%    | 9.1%      | 38.2        | 13.0 | 30.4    | 13.7 |
| <b>OVERALL</b> | <b>36669.7</b>   | <b>7262.7</b>     | <b>7256.2</b> | <b>0.0</b>      |            |          |         |           |             |      |         |      |

efficiencies. January was very dry with very little rainfall so the insolation was relatively high with 48293.9 Wh/m<sup>2</sup>. The average air temperature was 8.6 °C while the maximum was 17.9 °C. It is important to emphasize that a temperature minus was also recorded in January. Humidity averaged at 51% while wind speed was 6 km/h. The maximum wind speed was 45 km/h, which was expected for this part of the year. The electrical efficiency of the PV panel and PVT-PCM collector ranged from 12.8% to 13.5% while the electrical output was almost identical, Table 7. The maximum

difference between the peak temperatures of the PVT-PCM collector and PV panel was 4.2 °C while the mean collector temperature at position C2 was consistently higher than the panel temperature at position R2.

In the passive mode, the PVT-PCM collector produced almost the same amount of electricity as the PV panel, i.e. the difference is within measurement error. The PCM reduced peak temperatures, but due to thermal inertia, the mean temperatures are slightly higher. Higher ambient temperatures and stronger insolation are

**Table 7**  
Power production and collector efficiency in January.

| Date           | Power production |                   |                |                 | Efficiency |          |         | Temperature        |          |      |         |      |
|----------------|------------------|-------------------|----------------|-----------------|------------|----------|---------|--------------------|----------|------|---------|------|
|                | Insolation       | Electrical energy |                | Heat generation | Electrical |          | Thermal | TOTAL<br>(PVT-PCM) | Referent |      | PVT-PCM |      |
|                |                  | Total             | Referent       |                 | PVT-PCM    | Referent |         |                    | PVT-PCM  | Peak | Mean    | Peak |
|                | 2022.            | Wh/m <sup>2</sup> | Wh             | Wh              | Wh         |          |         |                    | °C       | °C   | °C      | °C   |
| 01.01.         | 4446.2           | 925.2             | 926.2          | /               | 12.8%      | 12.8%    | 0.0%    | 12.8%              | 37.8     | 14.5 | 35.3    | 15.6 |
| 02.01.         | 4641.0           | 972.6             | 971.3          | /               | 12.9%      | 12.9%    | 0.0%    | 12.9%              | 39.3     | 15.5 | 37.3    | 16.6 |
| 07.01.         | 4317.4           | 907.9             | 913.0          | /               | 12.9%      | 13.0%    | 0.0%    | 13.0%              | 34.4     | 11.3 | 31.3    | 12.2 |
| 12.01.         | 4805.5           | 1047.0            | 1047.7         | /               | 13.4%      | 13.4%    | 0.0%    | 13.4%              | 25.1     | 8.1  | 25.0    | 8.7  |
| 13.01.         | 5053.5           | 1105.1            | 1105.6         | /               | 13.4%      | 13.4%    | 0.0%    | 13.4%              | 29.4     | 9.5  | 28.4    | 10.1 |
| 14.01.         | 4845.9           | 1034.2            | 1039.6         | /               | 13.1%      | 13.2%    | 0.0%    | 13.2%              | 39.3     | 14.9 | 35.1    | 15.5 |
| 15.01.         | 4985.6           | 1073.3            | 1073.4         | /               | 13.2%      | 13.2%    | 0.0%    | 13.2%              | 38.0     | 15.6 | 36.3    | 16.9 |
| 16.01.         | 5022.3           | 1077.6            | 1079.2         | /               | 13.2%      | 13.2%    | 0.0%    | 13.2%              | 36.1     | 13.3 | 35.3    | 14.6 |
| 18.01.         | 5065.8           | 1116.1            | 1113.6         | /               | 13.5%      | 13.5%    | 0.0%    | 13.5%              | 27.8     | 10.2 | 28.5    | 11.0 |
| 19.01.         | 5110.7           | 1109.4            | 1109.6         | /               | 13.3%      | 13.3%    | 0.0%    | 13.3%              | 35.2     | 11.3 | 32.3    | 12.3 |
| <b>OVERALL</b> | <b>48293.9</b>   | <b>10368.4</b>    | <b>10379.3</b> | <b>0.0</b>      |            |          |         |                    |          |      |         |      |

needed to spot the impact of the temperature degradation on the electrical efficiency. In nominally colder months with lower insolation, a PCM will not contribute to increased electricity production, but it will not degrade it either.

3.3. Analysis of system performance on typical sunny day

Comparatively, the best system performance is expected during fully sunny summer days with relatively weak or moderate winds. For this purpose, the measured data for September 6, 2021, was analysed. Total insolation of 7269.4 Wh/m<sup>2</sup> was measured with an average daily air temperature of 25.6 °C, humidity of 38%, and wind speed of 6.2 km/h. The maximum air temperature was 30 °C and the wind speed was 24.1 km/h. There was no shading or clouds throughout the day with maximum insolation of over 1000 W/m<sup>2</sup>, Fig. 6. (a). The morning temperature before sunrise of the referent PV panel (position R2) and PVT-PCM collector (position C2) was around 20 °C, with the latter being slightly warmer, Fig. 6. (b). After sunrise, the referent PV panel had a faster temperature rise while the PVT-PCM collector temperature rise was slower due to PCM (pork fat) thermal inertia. At about 11 a.m. the PCM temperature reached the threshold (40 °C) and the circulation pump switched on. The insolation was very pronounced, and the cooling system managed to reduce the PCM temperature below the lower limit of 33 °C at around 4 p.m. after which the pump switched off. The

pump had another start at around 5 p.m., but it worked quite shortly because towards the end of the day the insolation was reduced. The sunset behind the surrounding buildings was just before 6 p.m., so the insolation diagram shows a sharp drop. The influence of the PCM thermal inertia is visible after sunset since the temperature of the PVT collector in the middle of the front surface remains higher than the temperature of the referent PV panel. From sunrise to sunset, the PVT-PCM collector was constantly cooler than the referent PV panel.

The effect of lower temperatures is visible in the power generation diagram where the PVT-PCM collector produced more power in total, Fig. 7. (a). The PVT-PCM collector did not produce more electricity in the passive part of the operation due to the high efficiency of the base PV panel and low degradation of the electrical efficiency due to temperature. In the active operating mode, a total of 3351.1 Wh of heat was generated during the two pump operating periods, Fig. 7. (b).

From the temperature distribution on the front surface of the referent panel (R1, R2, R3) and collector (C1, C2, C3), it is evident that the collector is continuously colder during both active and passive operation modes, Fig. 8. Significantly fewer temperature oscillations of the collector compared to the PV panel are noticeable as a result of PCM thermal inertia. Furthermore, a jump in PV panel temperature is noticeable at position R1 in the morning and position R3 in the afternoon, probably due to reflection from the

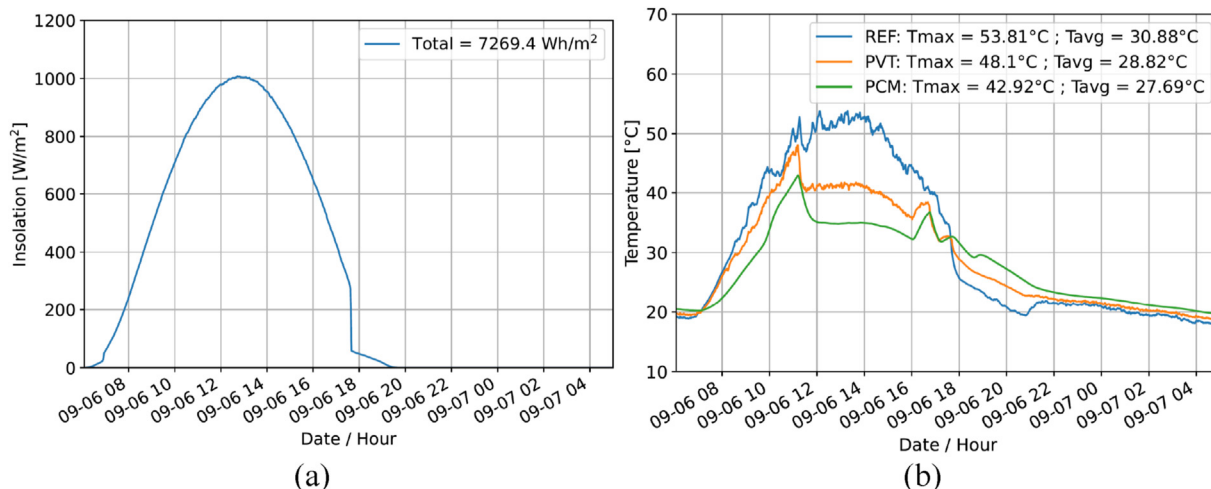


Fig. 6. (a) Insolation on September 6th, (b) Temperature of PV panel and PVT-PCM collector on September 6th.



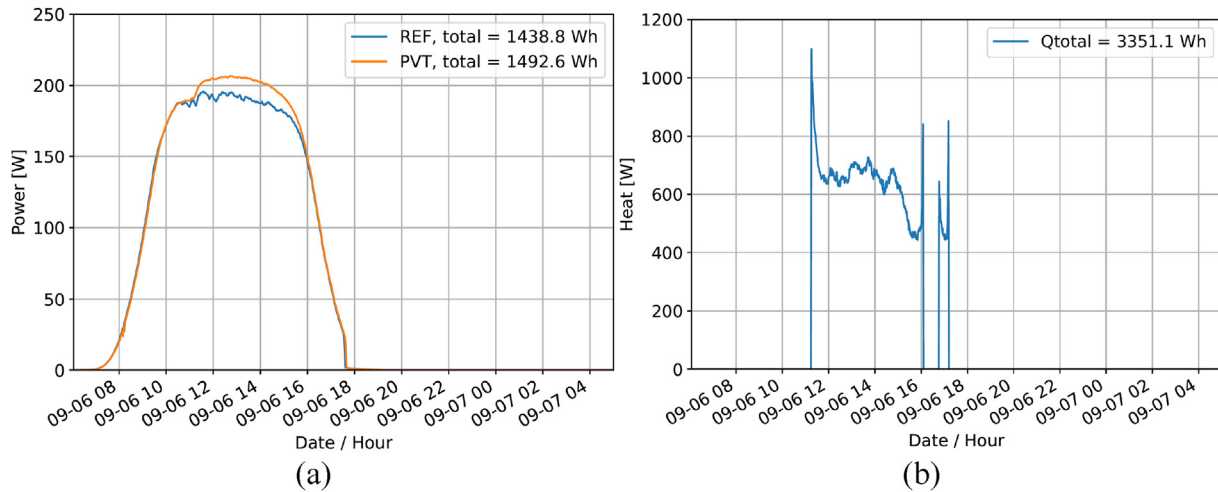


Fig. 7. (a) Electricity produced on September 6th, (b) Heat generated on September 6th.

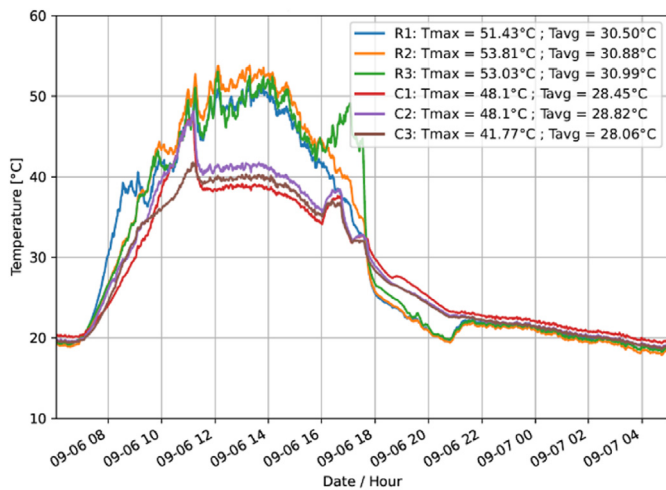


Fig. 8. Front surface temperature distribution of PV panel and PVT-PCM collector.

surrounding buildings and objects. This phenomenon was not detected on the collector, probably due to the thermal inertness of the PCM and heat sink effect.

### 3.4. Estimation of PVT-PCM collector performance at annual level

The experimental research was conducted during six months, so energy production at a yearly level can only be estimated. It is assumed that electricity production is primarily a function of radiated solar energy and electrical efficiency. Electrical efficiency depends on the electrical characteristics of the base PV panel and the rate of heat dissipation from the surfaces of the PVT-PCM collector. The heat dissipation rate depends on the ambient conditions such as air temperature, wind speed (convection coefficient), possible dirt on the surfaces of the collector (hot spot), etc. Thus, electrical efficiency is a direct result of the heat dissipation rate from the collector surfaces, i.e. directly depends on several environmental parameters that fluctuate over time. The data on local irradiated solar energy for twelve months were taken from the PVGIS-SARAH2 database, [27]. Given that the experimental measurements were carried out in a period of half a year, i.e. different

seasons, it is possible to estimate the average electrical efficiency of the system quite accurately. Firstly, the daily values of the calculated electrical efficiency were averaged to obtain the value of electrical efficiency in a particular month. Then, the obtained monthly values were averaged to determine the electrical efficiency on an annual basis. The average electrical efficiency of the PV panel and PVT-PCM collector, calculated in this way, was practically identical, i.e. 12%. It is important to emphasize that in the case of PVT-PCM collector, it represents the net amount of efficiency that includes the energy consumption of the circulation pump. To ensure system flexibility during the experiment, the pump was significantly oversized and could power a much larger system. The energy consumption of the pump could be significantly reduced with the optimization of the volume flow including a more adequate choice of a circulation pump, thus, increasing the net amount of electricity obtained. It is estimated that at the test site, the PVT-PCM system with an unoptimized circulation pump would produce about 358 kWh of electricity on an annual level.

Heat generation is a function of radiated solar energy and thermal efficiency. Similar to electrical efficiency, all ambient influence parameters (air temperature, wind, etc.) also affect the thermal efficiency of the system. The average monthly thermal efficiency was determined based on a few months of experimental research. For the months in which no experimental research was conducted, the thermal efficiency of the PVT-PCM collector was determined based on the thermal efficiency dependence on the estimated insolation (PVGIS-SARAH2), [27]. This functional dependence was fitted with a polynomial trendline for the measured months to extrapolate unknown data, Fig. 9. Hence, minimum and maximum estimated values of thermal efficiency for eight months of the year were determined.

The first two and last two months of the year were excluded from consideration because based on experimental data and expected insolation (PVGIS-SARAH2), it was estimated that the system would not reach the threshold, hence, the pump would not start in those months, Fig. 10. The highest estimated heat generation is in July, ranging from 132 kWh to 210 kWh, while the lowest is in October, ranging from 10 kWh to 32 kWh. The total estimated annual heat generation from here in the considered PVT-PCM collector will range from 500 kWh to 908 kWh depending on weather conditions. Finally, the estimated thermal efficiency at an annual level is expected to range between 17% and 30%.

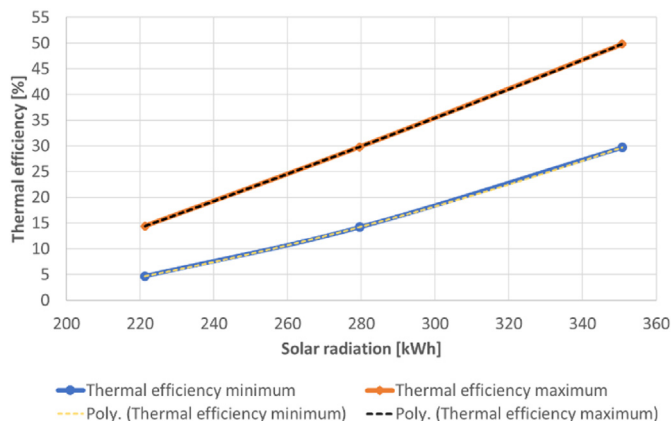


Fig. 9. Polynomial trendlines of experimental data.

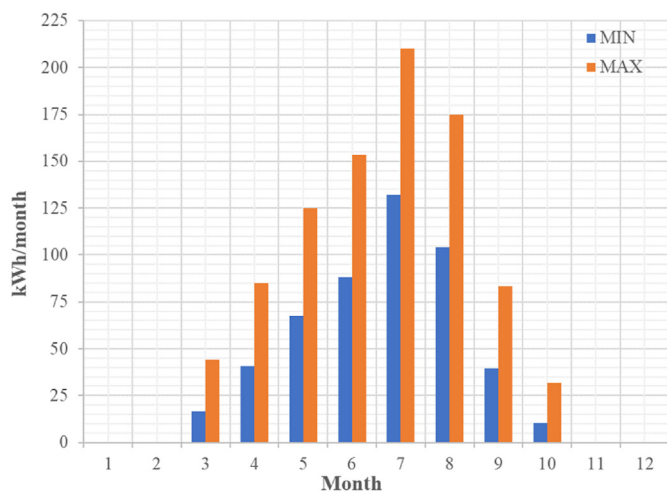


Fig. 10. Annual estimated heat generation.

#### 4. Environmental impact evaluation

In order to evaluate the newly developed PVT collector design more comprehensively, an environmental evaluation was conducted to calculate the impact of the energy system proposed in terms of environmental effect based on the construction stage. More specifically, and according to ISO 14040 series [28], supported by SimaPro Software [29], a Life Cycle Analysis approach was implemented to quantify the impact on climate change (“carbon footprint”), acidification (“acid rain”), eutrophication (“algal bloom”), photochemical oxidant creation (“summer smog”), and ozone depletion (“ozone hole”), among other aspects related to the environment. Based on LCA, the inventory stage is defined and according to detailed material input analysis, the environmental metrics are registered. The approach is better to be presented as a “cradle to gate” approach, as it is mainly focused on the design stage rather than on the use or end of life stage. The LCA approach is a methodology that evaluates the material and energy flows related to the processes which are included in the system and evaluates them in relation to environmental impact. Based on other methodologies and tools, such as Carbon Footprint Analysis, LCA provides a more complete approach to issues of environmental evaluation [30]. These impacts are present in different stages of the

production chain as well as within the life of the product [31]. The main goal of LCA is to identify those stages that harm to a greater extent the environment and suggest alternatives in order to improve the environmental profile of the system studied. The LCA approach offers a complex analysis that links actions and the system design with environmental impacts. It is a necessary action in order to introduce environmental aspects with quantified metrics to the decision-making process. The detection of improvement scenarios is possible via analysis of qualitative results, considering integration between system operation and environmental impacts, [32]. The impact assessment analysis is strongly related to the inventory stage. The reliability of the input data affects the accuracy of the impact assessment analysis stage. In order to present quantified impact assessment data, an accurate LCA-based SimaPro software was used with an embodied EcoInvent database. Normalisation and weighting factors are included, specialized to connect the input data with the impact assessment results. More detailed the LCA approach includes the inventory analysis stage where the inputs (energy and raw materials) are quantified for the system studied and the outputs (emissions) are determined based on the software used. After the inventory stage, the outputs are related to the environmental impacts (midpoint impacts), this is called the environmental impact assessment stage. After this stage, the environmental impacts are transformed into the impacts caused to the ecosystem, human health, and resources unavailability. The issue is to identify those processes in the system studied in which interpretation and improvements can be made in order to reduce energy consumption and raw materials use and consequently reduce environmental impacts (midpoint as well as endpoint). The only restriction in LCA methodology is that specialized software and database are needed for the inventory analysis as well as the impact assessment stage.

The outcomes are divided into midpoint categories based on the common mechanisms (e.g. climate change) or mostly accepted categorization (e.g. ecotoxicity) as well as endpoint impacts on human health and the ecosystem. The connection between midpoint and endpoint categories is presented in Fig. 11 showing the damage that environmental impacts can cause to humans and the ecosystem [33]. The analysis is mainly focused on the design and manufacturing stage evaluating comprehensively the material used for the production of the newly proposed experimental PVT system.

It is obvious from Table 8 that the studied PVT collector design contributes mainly to climate change impacts because of the material used in the construction stage. In some future analyses, where the usage stage will be analysed, the mentioned impact will be affected by energy consumption, however, environmental benefits will occur in comparison to other conventional systems.

The energy and environmental benefit of the system will be better defined in relation to other energy alternatives. Keeping in mind the material-oriented analysis, the material contribution to each environmental impact is evaluated and presented in Fig. 12 below.

PV panels are the most responsible for effects on human health and climate change impact. The following constructional component which mainly contributes to climate change, as well as human health, is the use of aluminium. As it is mentioned above, the SimaPro software and EcoInvent global database are applied for mid-point analysis and Impact 2002+ database for end-point analysis. The end-point analysis presents the environmental impact of the system studied in relation to human health, which is a significant criterion in the decision-making process. The results of



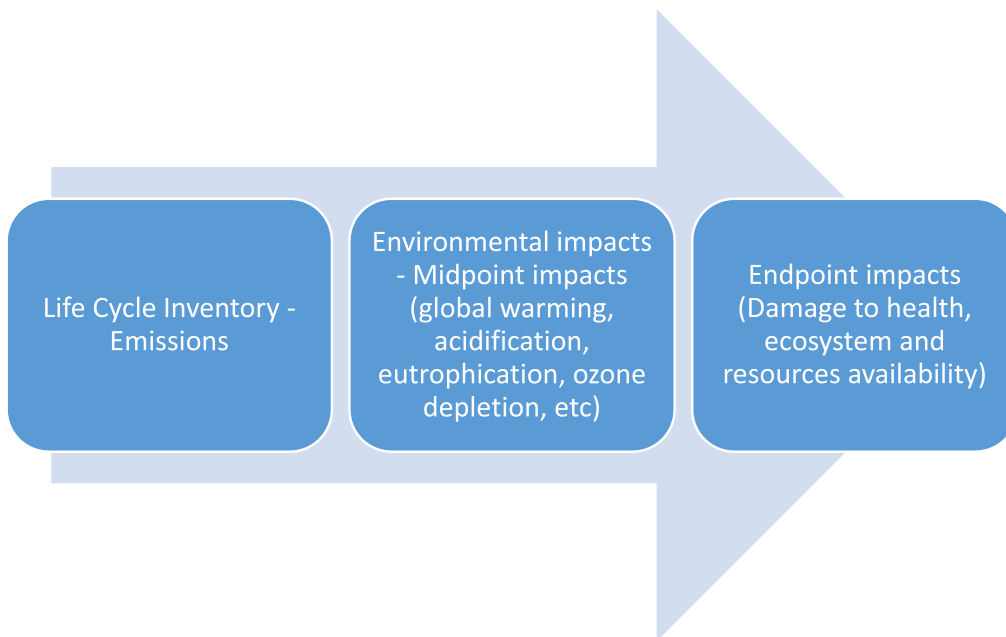


Fig. 11. Midpoint and endpoint environmental impacts in LCA based on different databases.

Table 8  
Environmental impact of PVT collector design.

| Environmental impact          | Unit         | PVT     |
|-------------------------------|--------------|---------|
| Carbon footprint              | kg CO2 - eq  | 580.63  |
| Acidification                 | kg SO2 - eq  | 33.21   |
| Eutrophication                | kg PO4 - eq  | 0.3     |
| Ozone Layer Depletion         | kg CFC - eq  | 0.00053 |
| Abiotic Depletion             | kg Sb - eq   | 3.9     |
| Human Toxicity                | tn Db - eq   | 8.035   |
| Photochemical Ozone Depletion | kg C2H4 - eq | 1.23    |

the end-point analysis in the LCA stage sum up the total environmental impact in relation to human health and ecosystem damage. Based on the “cradle to gate” analysis which focuses mainly on the construction stage and material-oriented approach, the contribution of different PVT components to human health and ecosystem equality is presented in Fig. 13. As expected from the mid-point analysis (Fig. 12), the PV panel and aluminium were detected as the components with the most significant environmental impacts.

A future study could be the possible replacement of most hazardous and environmentally unfriendly components with other

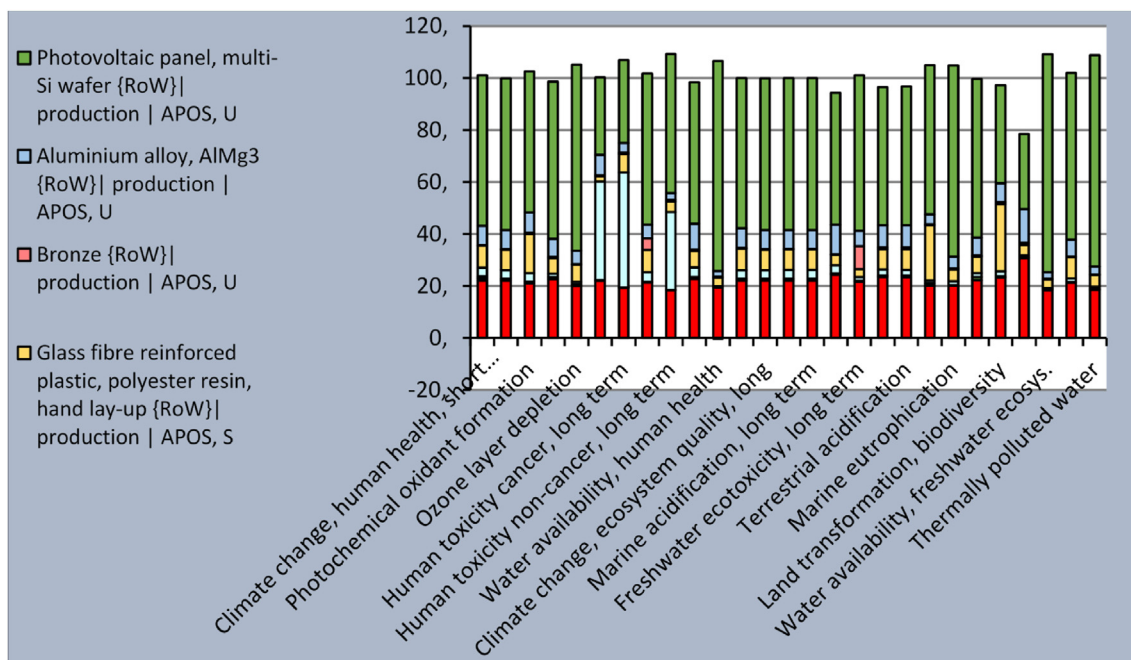


Fig. 12. Percentage contribution to environmental impact assessment of PVT components.

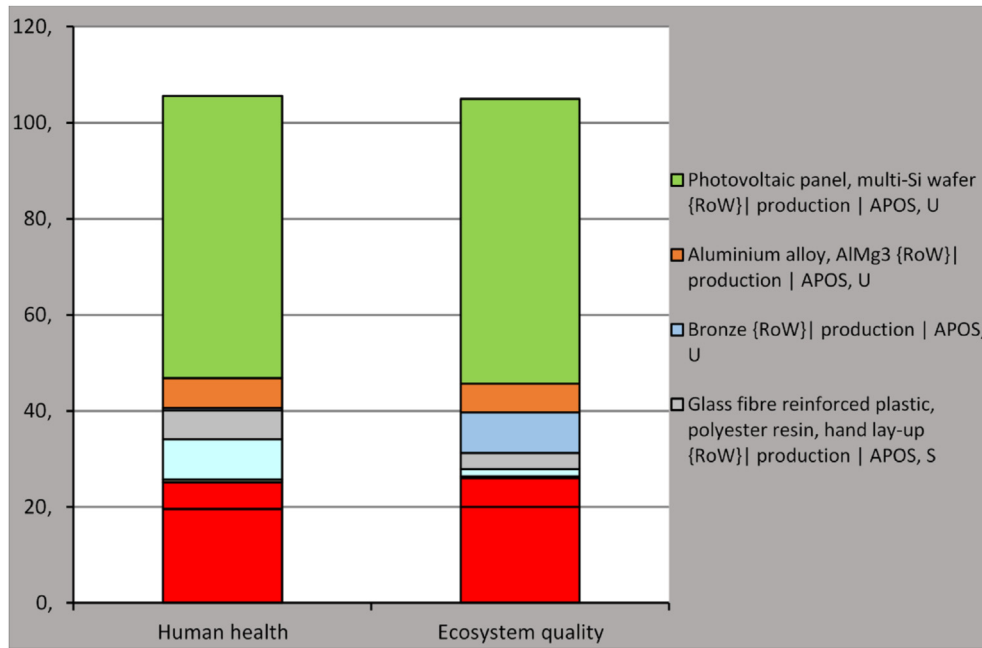


Fig. 13. End-point analysis of PVT components.

innovative, technically efficient, cost-effective design solutions with reduced environmental impact and human health effects.

5. Economic evaluation

Besides performance and environmental analysis, an economic evaluation is also necessary, in order to secure an integral evaluation of the proposed design. It needs to be emphasized that the reported costs in the continuation should be considered for the custom design of the PVT collector, i.e. for purpose of research investigations. In the case of large-scale production, it is expected that unit investment costs would be reduced, which is a quite realistic expectation. In Table 9, unit cost specifications for used construction materials with respect to the considered design of the PVT collector were provided. The highest unit cost falls to the use of Plexiglas, aluminum, and finally the PV panel with 36%, 37%, and 14%, respectively, Fig. 14. The overall expected working hours for labour are estimated to be 7 h per PVT panel, with an estimated labour cost of about 7 €/h [31], which finally leads to about 49 € of expected labour cost per PVT collector.

The overall estimated cost is about 698 €, i.e. about 428 €/m<sup>2</sup> scaled on the PVT panel surface. The overall investment cost seems reasonable when compared with existing PVT designs, where it was usually over 600 €/m<sup>2</sup>, [8].

To evaluate the economic impact, the LCOE (Levelized Cost of Energy) framework was applied with the same approach as it was obtained in the previous study [31], Eq. (1),

$$LCOE = \frac{AC}{EO} = \frac{IC \times CRF + OM}{EO} \tag{1}$$

where CRF is the capital recovery factor, EO is the average produced electricity from the PV system, kWh/y, IC is the overall investment in the PV system, € and OM operation and maintenance cost, €/year and that was calculated by the following equation,

$$CRF = \frac{(1 + p)^n \cdot p}{(1 + p)^n - 1} \tag{2}$$

Table 9 Unit cost specifications of construction materials for PVT collector.

| Construction material      | Unit cost, € |
|----------------------------|--------------|
| Photovoltaic panel         | 94           |
| Plexiglas container        | 250          |
| Aluminium absorber         | 260          |
| Pork fat                   | 20           |
| Small consumable materials | 10           |
| Sealing materials          | 15           |
| Labour                     | 49           |
| <b>Overall</b>             | <b>698</b>   |

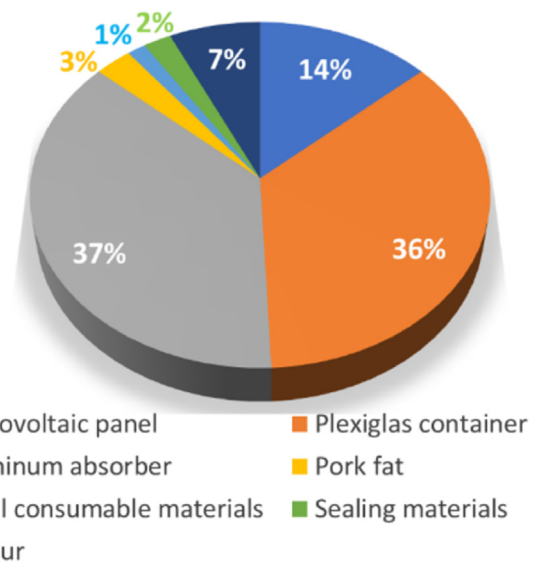


Fig. 14. Specific unit cost share of construction materials.

The interest rate was taken at 6% and an amortization period of 25 years, with an estimated annual maintenance cost of about 13 €

(2.0% of IC per year). According to the performance data, the PVT panel is expected to produce about 358 kWh of electricity on an annual level, where heat generation would range from a minimum of 500 kWh to about 908 kWh. The overall energy output from the herein considered PVT panel (electricity and heat) would range from 858 kWh to 1266 kWh per year. Taking into account the above-noted LCOE calculation framework, as well as specified input data, the expected LCOE would range from 0.056 to 0.083 €/kWh. For comparison in the study [34], it was reported that the LCOE for the air-based PVT collectors is expected to vary from 0.06 to 0.12 €/kWh. The herein PVT design values are lower, as could be expected since water is used as a working fluid.

According to the payback period of the investment, the overall initial investment cost (Table 9) has been taken into account to the profit estimated from the energy saving which is related to the expected production of about 358 kWh of electricity on an annual level and a minimum of 500 kWh of heat generation. The payback period is estimated to be about 4 years which is acceptable if we consider the lifetime of the investment.

## 6. Conclusions

In this study, a novel PVT collector design was elaborated, together with discussed performance indicators based on a several-month experimental field monitoring in typical Mediterranean climate operating circumstances. The PVT design was focused on a more flexible cooling approach by the introduction of four cooling blocks filled with an organic PCM material, i.e. pork fat, where the block was cooled with lines of straight water pipes. The second key target was the use of pork fat as a PCM for the first time in the case of the herein examined PVT configuration. The pork fat showed to be a suitable PCM material regarding general thermal properties and general behavior, however, an investigation of long-term properties is necessary to be obtained as part of future research work. Preliminary measurements of thermal properties after six months of operative application showed pork fat to be stable in terms of thermal properties. The examined configuration reached a maximum overall energy efficiency of about 62%. The average annual values for overall energy efficiency were lower and expected to range from 29% to 42% (estimation based on available measurement data). The proposed design showed reasonable thermal efficiency, however, the net improvement in electrical efficiency was negligible when compared with the referent PV panel. Therefore, the proposed design should be enhanced and improved to secure higher improvement in electrical efficiency. It needs to be noted that the operation of the circulation pump was not optimized, which certainly had an impact on the electrical efficiency in general. Moreover, high-quality PV panels were used in the experiment with a relatively low degradation of electrical efficiency due to temperature rises, which resulted in the disparity of electrical efficiency, nonetheless, a temperature difference between the referent PV panel and PVT-PCM collector existed. The collector was generally colder at peak heat loads, but an expected proportional increase in electrical efficiency was not achieved relative to the referent PV panel. The PVT system would have a significantly better effect on nominally lower quality PV panels, which would also reduce the initial investment cost due to the lower price and would affect the economy in general. The economic evaluation showed that the expected LCOE would range from 0.056 to 0.083 €/kWh, with an overall determined PVT collector design cost of about 428 €/m<sup>2</sup>. The environmental analysis directed that the most harmful impact besides the use of PV panels is due to the use of aluminum, so further designs should consider the restricted use of aluminum. The proposed PVT collector design showed reasonable performance as well as economic indicators, with the clear necessity for future

design improvements, in order to secure higher electricity yield, which would be part of future research work.

## Declaration of competing interest

The authors declare that they have no known competing financial interests or personal relationships that could have appeared to influence the work reported in this paper.

## Acknowledgments

This work was funded by the Croatian science foundation (Research project: Smart and hybrid cooling techniques for siliceous photovoltaic panels-IP-01-2018-2814).

## References

- [1] Hoang AT, Nizetić Sandro, Olcer AI, Ong HC, Chen WH, Chong CT, et al. Impacts of COVID-19 pandemic on the global energy system and the shift progress to renewable energy: opportunities, challenges, and policy implications. *Energy Pol* 2021;154:112322. <https://doi.org/10.1016/j.enpol.2021.112322>.
- [2] Gangwar P, Singh R, Tripathi RP, Singh AK. Effective solar power harnessing using a few novel solar tree designs and their performance assessment. *Energy Sources, Part A Recovery, Util Environ Eff* 2019;41:1828–37. <https://doi.org/10.1080/15567036.2018.1549162>.
- [3] [www.iea.org/reports/renewables-2021/executive-summary](http://www.iea.org/reports/renewables-2021/executive-summary); 2022.
- [4] [www.energylivenews.com/2021/12/30/european-solar-pv-capacity-jumped-34-in-2021/](http://www.energylivenews.com/2021/12/30/european-solar-pv-capacity-jumped-34-in-2021/); 2022.
- [5] [www.pv-magazine.com/2022/01/21/chinese-pv-industry-brief-china-added-53-gw-of-new-pv-capacity-in-2021/](http://www.pv-magazine.com/2022/01/21/chinese-pv-industry-brief-china-added-53-gw-of-new-pv-capacity-in-2021/); 2022.
- [6] [https://www.irena.org/-/media/Files/IRENA/Agency/Webinars/07012020\\_INSIGHTS\\_webinar\\_Wind-and-Solar.pdf?la=en&hash=BC60764A90CC2C4D80B374C1D169A47FB59C3F9D](https://www.irena.org/-/media/Files/IRENA/Agency/Webinars/07012020_INSIGHTS_webinar_Wind-and-Solar.pdf?la=en&hash=BC60764A90CC2C4D80B374C1D169A47FB59C3F9D); 2022.
- [7] Hamzat AK, Sahin AZ, Omisanya MI, Alhems LM. Advances in PV and PVT cooling technologies: a review. *Sustain Energy Technol Assessments* 2021;47:101360. <https://doi.org/10.1016/j.seta.2021.101360>.
- [8] Existing PVT systems and solutions 2022. [www.iea-shc.org/Data/Sites/1/publications/IEA-SHC-Task60-A1-Existing-PVT-Systems-and-Solutions.pdf](http://www.iea-shc.org/Data/Sites/1/publications/IEA-SHC-Task60-A1-Existing-PVT-Systems-and-Solutions.pdf). [Accessed 20 February 2022].
- [9] Huaxu L, Fuqiang W, Dong Z, Ziming C, Chuanxin Z, Bo L, et al. Experimental investigation of cost-effective ZnO nanofluid based spectral splitting CPVT system. *Energy* 2020;194:116913. <https://doi.org/10.1016/j.energy.2020.116913>.
- [10] Nizetić S, Jurčević M, Čoko D, Arıcı M, Hoang AT. Implementation of phase change materials for thermal regulation of photovoltaic thermal systems: comprehensive analysis of design approaches. *Energy* 2021;228:120546. <https://doi.org/10.1016/j.energy.2021.120546>.
- [11] Gelis K, Ozbek K, Celik AN, Ozyurt O. A novel cooler block design for photovoltaic thermal systems and performance evaluation using factorial design. *J Build Eng* 2022;48:103928. <https://doi.org/10.1016/j.jobe.2021.103928>.
- [12] Gomaa MR, Ahmed M, Rezk H. Temperature distribution modeling of PV and cooling water PV/T collectors through thin and thick cooling cross-fined channel box. *Energy Rep* 2022;8:1144–53. <https://doi.org/10.1016/j.egyr.2021.11.061>.
- [13] Gupta A, Biswas A, Das B, Reddy B v. Development and testing of novel photovoltaic-thermal collector-based solar dryer for green tea drying application. *Sol Energy* 2022;231:1072–91. <https://doi.org/10.1016/j.solener.2021.12.030>.
- [14] Selimefendigil F, Şirin C. Energy and exergy analysis of a hybrid photovoltaic/thermal-air collector modified with nano-enhanced latent heat thermal energy storage unit. *J Energy Storage* 2022;45:103467. <https://doi.org/10.1016/j.est.2021.103467>.
- [15] Liang H, Han H, Wang F, Cheng Z, Lin B, Pan Y, et al. Experimental investigation on spectral splitting of photovoltaic/thermal hybrid system with two-axis sun tracking based on SiO<sub>2</sub>/TiO<sub>2</sub> interference thin film. *Energy Convers Manag* 2019;188:230–40. <https://doi.org/10.1016/j.enconman.2019.03.060>.
- [16] Mustafa W, Fudholi A, Sopian K, Mustapha M, Ahmudiarto Y. The water based photovoltaic thermal fiberglass collector: an experimental investigation. *Int J Renew Energy Resour* 2021;11:1663–72. <https://doi.org/10.20508/ijrer.v11i4.12522.g8320>.
- [17] Sultan SM, Abdullah MZ, Hussein HM, Tso CP, Sopian K. Modified methods for assessing photovoltaic solar thermal collectors. *Case Stud Therm Eng* 2021;28:101690. <https://doi.org/10.1016/j.csite.2021.101690>.
- [18] Miao R, Hu X, Yu Y, Zhang Y, Wood M, Olson G. Experimental study of a newly developed dual-purpose solar thermal collector for heat and cold collection. *Energy Build* 2021;252:111370. <https://doi.org/10.1016/j.enbuild.2021.111370>.
- [19] Gupta A, Agrawal S, Pal Y. Performance analysis of the photovoltaic-thermo-electric system combined with serpentine type water collector. *Int J Energy Res* 2021;45:19147–64. <https://doi.org/10.1002/er.7015>.

- [20] Shahsavari A, Jha P, Arıcı M, Nizetić S, Ma Z. Energetic and exergetic performances of a nanofluid-based photovoltaic/thermal system equipped with a sheet-and-grooved serpentine tube collector: indoor experimental tests. *Sol Energy* 2021;225:918–33. <https://doi.org/10.1016/j.solener.2021.08.005>.
- [21] Baklouti I, Driss Z. Numerical and experimental study of the impact of key parameters on a PVT air collector: mass flow rate and duct depth. *J Therm Sci* 2021;30:1625–42. <https://doi.org/10.1007/s11630-020-1345-8>.
- [22] Jurčević M, Nizetić S, Čoko D, Hoang AT, Papadopoulos AM. Experimental investigation of novel hybrid phase change materials. *Clean Technol Environ Policy* 2022;24:201–12. <https://doi.org/10.1007/s10098-021-02106-y>.
- [23] [https://solvis.hr/wp-content/uploads/2019/04/LQSOLVIS-DS-EN-SV60\\_5BB-1640x992x40-255-275-20190125.pdf](https://solvis.hr/wp-content/uploads/2019/04/LQSOLVIS-DS-EN-SV60_5BB-1640x992x40-255-275-20190125.pdf); 2022.
- [24] Jurčević M, Nizetić S, Marinić-Kragić I, Čoko D, Arıcı M, Giama E, et al. Investigation of heat convection for photovoltaic panel towards efficient design of novel hybrid cooling approach with incorporated organic phase change material. *Sustain Energy Technol Assessments* 2021;47:101497. <https://doi.org/10.1016/j.seta.2021.101497>.
- [25] Nizetić S, Jurčević M, Čoko D, Arıcı M. A novel and effective passive cooling strategy for photovoltaic panel. *Renew Sustain Energy Rev* 2021;145:111164. <https://doi.org/10.1016/j.rser.2021.111164>.
- [26] [https://www.engineeringtoolbox.com/oil-melting-point-d\\_1088.html](https://www.engineeringtoolbox.com/oil-melting-point-d_1088.html); 2022.
- [27] [https://re.jrc.ec.europa.eu/pvg\\_tools/en/tools.html#PVP](https://re.jrc.ec.europa.eu/pvg_tools/en/tools.html#PVP); 2022.
- [28] ISO 14040 2006. <https://www.iso.org/standard/37456.html>. [Accessed 1 March 2022].
- [29] SimaPro Software. Life Cycle analysis software. 2006. <https://gabi.sphera.com/international/index/>. [Accessed 4 March 2022].
- [30] Energy performance of buildings. Cham: Springer International Publishing; 2016. <https://doi.org/10.1007/978-3-319-20831-2>.
- [31] Grubisić Čabo F, Nizetić S, Giama E, Papadopoulos A. Techno-economic and environmental evaluation of passive cooled photovoltaic systems in Mediterranean climate conditions. *Appl Therm Eng* 2020;169:114947. <https://doi.org/10.1016/j.applthermaleng.2020.114947>.
- [32] de Bruijn H, van Duin R, Huijbregts MAJ, Guinee JB, Gorree M, Heijungs R, et al., editors. Handbook on life cycle assessment, vol. 7. Dordrecht: Springer Netherlands; 2002. <https://doi.org/10.1007/0-306-48055-7>.
- [33] Li C, Wang N, Zhang H, Liu Q, Chai Y, Shen X, et al. Environmental impact evaluation of distributed renewable energy system based on life cycle assessment and fuzzy rough sets. *Energies* 2019;12:4214. <https://doi.org/10.3390/en12214214>.
- [34] Ramos A, Chatzopoulou MA, Guarracino I, Freeman J, Markides CN. Hybrid photovoltaic-thermal solar systems for combined heating, cooling and power provision in the urban environment. *Energy Convers Manag* 2017;150: 838–50. <https://doi.org/10.1016/j.enconman.2017.03.024>.

## Appendix H

Title: Towards resilient operation of photovoltaic-thermal collector with incorporated organic phase change material: Numerical and experimental investigation

Authors: Jurčević M., Nižetić S., Marinić-Kragić I., Jakić M., Arıcı M.

Publisher: *Elsevier*

Journal: *Sustainable Energy Technologies and Assessments*

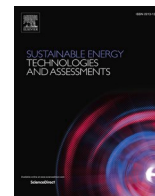
Edition, ID, year: 60, 103465, 2023.

Indexed in: Scopus, Science Citation Index Expanded, INSPEC

Journal Impact Factor: 8 Q1 (WoS and SJR-2022.)

DOI: <https://doi.org/10.1016/j.seta.2023.103465>

**Abstract:** The resilient operation of the novel free-standing photovoltaic-thermal (PVT) collector with an integrated phase change material (PCM) in variable weather conditions was examined by developing the computational fluid dynamics (CFD) 3D model to perform numerical analysis of heat transfer. The developed transient multiparameter numerical model was directly compared with experimental measurements for the case of variable cloudiness, unstable ambient temperature, and fluctuating wind. Due to volatile weather conditions, the numerical analysis included variable time-dependent boundary conditions implemented using user-defined functions (UDF). The investigation considered a novel multi-parameter numerical approach, together with novel experimental data for unconventional organic PCM. Specifically, the thermal characteristics of unconventional organic PCM, i.e., pork fat, were experimentally determined with the differential scanning calorimetry (DSC) method and embedded in the numerical model. It was found that melting of the crystal phase of pork fat PCM starts at 8.3 °C and ends at 45.2 °C with a latent heat of melting being 45.4 Jg<sup>-1</sup>. The numerical model was successfully validated with experimental data. The mean absolute percentage deviation of the operating temperature numerical forecast compared with the experiment was from about 2.9% to 4.9%, depending on the considered domain. The findings of this investigation can be used to improve the existing designs of PVT-PCM collectors. Furthermore, a validated numerical model can be used to investigate the impact of various operating parameters on the system performance to enhance the resilience aspect in the early development phase of novel designs.



## Towards resilient operation of photovoltaic-thermal collector with incorporated organic phase change material: Numerical and experimental investigation

Mišo Jurčević<sup>a</sup>, Sandro Nižetić<sup>a,\*</sup>, Ivo Marinić-Kragić<sup>a</sup>, Miće Jakić<sup>b</sup>, Müslüm Arıcı<sup>c</sup>

<sup>a</sup> University of Split, FESB, Rudjera Boškovića 32, Split 21000, Croatia

<sup>b</sup> University of Split, KTF, Rudjera Boškovića 35, Split 21000, Croatia

<sup>c</sup> Kocaeli University, Engineering Faculty, Mechanical Engineering Department, Kocaeli 41001, Türkiye

### ARTICLE INFO

#### Keywords:

Photovoltaic-thermal  
Photovoltaics  
CFD  
PCM  
Resilient operation  
Renewables  
Solar Energy

### ABSTRACT

The resilient operation of the novel free-standing photovoltaic-thermal (PVT) collector with an integrated phase change material (PCM) in variable weather conditions was examined by developing the computational fluid dynamics (CFD) 3D model to perform numerical analysis of heat transfer. The developed transient multi-parameter numerical model was directly compared with experimental measurements for the case of variable cloudiness, unstable ambient temperature, and fluctuating wind. Due to volatile weather conditions, the numerical analysis included variable time-dependent boundary conditions implemented using user-defined functions (UDF). The investigation considered a novel multi-parameter numerical approach, together with novel experimental data for unconventional organic PCM. Specifically, the thermal characteristics of unconventional organic PCM, i.e., pork fat, were experimentally determined with the differential scanning calorimetry (DSC) method and embedded in the numerical model. It was found that melting of the crystal phase of pork fat PCM starts at 8.3 °C and ends at 45.2 °C with a latent heat of melting being 45.4 Jg<sup>-1</sup>. The numerical model was successfully validated with experimental data. The mean absolute percentage deviation of the operating temperature numerical forecast compared with the experiment was from about 2.9% to 4.9%, depending on the considered domain. The findings of this investigation can be used to improve the existing designs of PVT-PCM collectors. Furthermore, a validated numerical model can be used to investigate the impact of various operating parameters on the system performance to enhance the resilience aspect in the early development phase of novel designs.

### Introduction

The recent energy-related circumstances in the European Union (EU) have just highlighted the importance of renewable energy technologies, [1]. There is a necessity for strong investments in renewable energy generation capacities to meet general targets set by Paris Agreement [2]. For instance, the EU defined a target of 32% renewable energy generation by 2023, [3]. To be able to meet mentioned and defined targets, it is vital to secure sufficient production capacities for renewables, as well as to secure sufficient quantities of key raw materials for their production. The energy conversion efficiency of renewable energy technologies is also important, and there is a constant need to improve the performance (efficiency) of market-available renewable energy generation technologies, [4]. The current overall globally installed renewable

energy capacities are mainly directed to photovoltaic (PV) and wind generation technologies. According to the IEA report for 2022, the expected global energy generation by renewables in 2027 would be around 38%, [5]. In the same report, the most significant expected rise in the global renewable generation capacities is directed to PV technologies, i.e., around 22% in the period from 2010 to 2027, which is followed by wind generation technologies in the amount of about 14% for the same period. However, fossil-based generation is still highly involved in forecasts, i.e., around 40% rise is expected in the period from 2010 to 2027. As already previously noted, the PV capacities are leading with over 260 GW of recently installed capacities in 2022, [6], while in 2023 there are predictions of over 310 GW of newly installed PV capacities. The significant rise in PV capacities will affect the overall cost of the produced electricity from the PV systems due to the expected further price drop of PV modules. The also important aspect related to the

\* Corresponding author.

E-mail address: [snizetic@fesb.hr](mailto:snizetic@fesb.hr) (S. Nižetić).

<https://doi.org/10.1016/j.seta.2023.103465>

Received 2 June 2023; Received in revised form 12 August 2023; Accepted 16 September 2023  
2213-1388/© 2023 Elsevier Ltd. All rights reserved.



**Nomenclature**

|              |  |
|--------------|--|
| $C_{mush}$   | Mushy zone morphology constant, $\text{kg m}^{-3} \text{s}^{-1}$ |
| $C_p$        | Specific heat, $\text{J kg}^{-1} \text{K}^{-1}$                  |
| $H$          | Enthalpy, $\text{J kg}^{-1}$                                     |
| $h$          | Sensible enthalpy, $\text{J kg}^{-1}$                            |
| $h_{ref}$    | Reference enthalpy, $\text{J kg}^{-1}$                           |
| $\Delta H_c$ | Latent heat of crystallization, $\text{J/g}$                     |
| $\Delta H_m$ | Latent heat of melting, $\text{J/g}$                             |
| $k$          | Thermal conductivity, $\text{W m}^{-1} \text{K}^{-1}$            |
| $L$          | Latent heat ( $\text{J kg}^{-1}$ )                               |
| $p$          | Pressure, Pa   |
| $q$          | Convective heat flux, $\text{W/m}^2$                             |
| $q_R$        | External radiation heat flux, $\text{W/m}^2$                     |
| Re           | Reynolds number  |
| $\vec{S}$    | Momentum sink term, $\text{N/m}^{-3}$                            |
| $S_e$        | Energy source term, $\text{W/m}^{-3}$                            |
| $T$          | Temperature, °C, K   |
| $T_A$        | Ambient air temperature, K                                       |
| $T_S$        | Sky temperature, K   |
| $T_W$        | Wall surface temperature, K                                      |
| $T_{pc}$     | Crystallization temperature, °C                                  |
| $T_{pm}$     | Peak temperature, °C   |
| $\vec{u}$    | Velocity, m/s  |

**Abbreviations**

|     |                                   |
|-----|-----------------------------------|
| CFD | Computational Fluid Dynamics      |
| DSC | Differential Scanning Calorimetry |
| 3D  | Three-dimensional                 |
| EVA | Ethylene Vinyl Acetate            |
| IEA | International Energy Agency       |
| PV  | Photovoltaic                      |
| PVT | Photovoltaic-thermal              |
| PCM | Phase Change Material             |
| UDF | User-defined Functions            |

**Greek symbols**

|               |  |
|---------------|--|
| $\alpha$      | Convective heat transfer coefficient, $\text{W/m}^2 \text{K}^{-1}$ |
| $\beta$       | Liquid fraction  |
| $\varepsilon$ | External emissivity coefficient                                    |
| $\rho$        | Density, $\text{kg m}^{-3}$  |
| $\sigma$      | Stefan-Boltzmann constant  |
| $\vec{\tau}$  | Stress tensor, $\text{N/m}^2$                                      |

**Subscripts**

|                 |                |
|-----------------|----------------|
| <i>Exp</i>      | Experimental   |
| <i>liquidus</i> | liquid state   |
| <i>mush</i>     | mushy zone     |
| <i>ref</i>      | reference      |
| <i>solidus</i>  | at solid state |

market available PV technologies is to reconsider other resources and applications, i.e., alternative implementation areas like green hydrogen production [7] or other implementation approaches that would secure additional land, for renewable energy generation such as floating photovoltaics [8], agrivoltaics [9], etc. The previously mentioned aspect is crucial in the case of limited land resources for the installment of PV systems. Moreover, there are other concepts where PV technologies could be utilized in useful configurations (designs) that can produce simultaneously electricity and thermal output. The most common and market-available solutions are photovoltaic thermal collectors (PVT), which can be found in different designs and configurations, [10]. The role of specific PVT collector design is crucial to be able to secure reasonable performance of the PVT system in certain climate conditions. The critical input required for each PVT design is the expected electricity and heat production ratio. Overheating the PV panel is reducing electricity yield, while on the other side producing hot water needs to be on a specific suitable temperature level. Therefore, the quality design would allow better flexibility and proper balancing between electricity yield and heat output from the PVT collector. The critical issue with PVT collectors is their relatively high unit cost which affects an overall economic aspect. Due to previously mentioned circumstances, different PVT collector designs or concepts of PVT systems have been investigated to reach the most suitable designs from a techno-economic point of view.

The numerical investigation of the concentrated photovoltaic-thermal module was obtained in work [11]. The collector design considered the use of the phase change material (PCM) type RT26, for which the analysis was done under two specific climatic zones (desert climate and typical Mediterranean climate). The results indicated that the use of PCM in the proposed collector design is effective for hot climates, while in Mediterranean climate conditions (winter period), the system does not operate effectively. The analysis was obtained only in a numerical way, therefore, experimental verification is necessary. Furthermore, economic evaluation is recommended, since PCM is being used in the design and can be a critical feature from an economic point of view. Several case studies were numerically evaluated in work [12] to determine the optimal design of the specific PVT configuration. Besides different examined PVT designs, the study also considered various

working fluids: water, CuO/water, and CNT/water nanofluid. Several operating parameters were investigated and followed by energy and exergy analysis. Based on the performance analysis, the most suitable design was a baffled PVT panel operating with CNT/water nanofluid since the overall exergy increase was 2.38%. Similarly, to the previous study, the experimental verification is missing as well as the evaluation of the economic aspect. A thermodynamic evaluation of the novel PVT collector design, coupled with a heat pump system was elaborated in [13]. The study involved the selection of the optimal working fluid for the heat pump system. The relative improvement, depending on the season, in the electrical efficiency ranged from 1.1% to 13.7% when compared to the non-cooled PV panel. According to the provided analysis, the optimal refrigerant is found to be R717 due to the highest annual energy utilization coefficient. The economy of the proposed approach was not evaluated which is a critical feature since the PVT system is coupled with the heat pump system. The numerical analysis and optimization approach was obtained in work [14] for PVT collector design with three different geometries of the thermal absorber (plain, ribbed, porous-ribbed). The nanofluid was used as a working fluid, i.e., silver/water nanofluid in concentrations up to 2%. The results revealed that the plain and ribbed absorber design is more effective than the porous-ribbed concerning the produced temperature of the hot water. It was also found that an increase in the nanoparticles concentration increases pressure drop in the pipes (up to 41%) and also affects the reduction of hot water temperature. Again, like in other previous studies, an economic evaluation is missing and this study was mainly limited to the numerical investigation. The use of micro-fins in PVT collector design in combination with nanofluid (SiC/water, 1%) as working fluid was examined in work [15]. The study was done in laboratory conditions using a solar simulator and with the secured variation of the fluid mass flow rate. The results revealed improvement in the electrical efficiency up to 9.6%, while the highest reached thermal efficiency was about 77.5%. The laboratory conditions most likely contributed to relatively high thermal efficiency. Nonetheless, other concepts, like in [16], can reach an even higher peak thermal efficiency of 85.3%. While peak efficiency is valuable information, more insightful conclusions can be drawn from average efficiency data. An investigation

of the PVT collector design in combination with water/air cooling and incorporated PCM material (thermal energy storage, i.e., heat taken from PVT panel) was reported in [17] for the case of building integrated PVT systems (BPVT). The results indicated that the overall seasonal efficiency of the system was around 39.4%, with energy-saving efficiency of 64.2%. The proposed concept demonstrated effective control of the water temperature. The economic evaluation determined a payback period of 13.1 years, while environmental analysis indicated annual maximal CO<sub>2</sub> savings of around 156 kg year<sup>-1</sup>. A design of the novel PVT collector with an embedded tank was analyzed in work [18]. The water storage tank was incorporated at the backside of the PV panel to boost thermal output from the PVT panel. The absorber was made in a serpentine geometrical design. The work was directed to the computational fluid dynamics (CFD) simulation, where numerical modeling was used to investigate the impact of different internal geometric parameters (fluid type, thickness of insulation, absorber type, material of absorber, etc.). The work is missing experimental evaluation and discussion of economic and environmental aspects related to the proposed design. The novel design of the PVT collector was proposed in [19] with a baffle-based collector and with nanofluid as a working fluid (SWCNT/water). The investigation contains both numerical and experimental evaluations of specific PVT collector design. The results of the conducted investigation indicated that the proposed baffle-based design is more efficient when compared to the straightforward collector design. The main advantage of the proposed design is the more intense heat transfer due to local vortices caused by baffles. The overall reached efficiency of a PVT collector with a baffle design is 66.4%, while for a conventional design is 63.85%. It was also noted that the use of nanofluid is not bringing any important advantage regarding the collector performance. Work is missing economic and environmental evaluation. These are key for this study since the difference in overall efficiency between examined designs is not high even though the proposed PVT collector design is more complex when compared to the conventional one. Moreover, there is the use of nanofluids which is costly and followed by potential environmental issues. Study [20] examined the PVT field (during 9 months) consisting of twenty PVT panels with a design that involved the use of PCM material. The field results were compared with laboratory testing. The use of PCM material indicated an improvement in thermal efficiency of 26% and electrical in the amount of 3%. The use of PCM is more effective in the summer period when compared to the winter period. The study did not involve an economic evaluation which is a limitation. In the same work authors indicated technical issues related to the implementation of the PCMs in examined configuration. The implementation of PCM in the PVT system is equally challenging from the numerical point of view due to the complexity of the phase transition and various influential thermal parameters. A parametric study of PCM dynamic behavior regarding variation in thermal parameters was investigated in work [21], however, it was limited to the analytical solution. In numerical investigations, the phase transition of PCM is usually taken into account using the enthalpy method [22], or the enthalpy porosity method [23], while often heat convection is neglected in the PVT system, [24]. Nevertheless, it is necessary to take into account all mechanisms of heat transfer to achieve reasonable agreement between numerical and experimental results.

Considering the latest research findings from the field it can be concluded that there are still significant research efforts related to the development of novel and more effective PVT collector designs. The development path in the design of PVT collectors generally relies on experimental ways, but the shortcuts offered by the numerical approach are often overlooked. Various PVT solutions are being investigated, however, there is a lack of investigations related to numerical aspects of PCM integration in PVT systems. Researchers usually integrate numerical and experimental approaches at an elementary level, i.e., at best, the numerical methods are used to conduct a 3D simulation of partial PVT system components, or computational domains tend to be further reduced to simple 2D geometries. Very few publications deal with the

numerical analysis of large 3D domains exposed to complex boundary conditions over a long period.

The main objective of this work is a numerical investigation of the novel proposed design of the PVT-PCM collector, to be able to analyze the influence of operating parameters on the performance of the system. The proposed design was experimentally investigated [25], so the next step was developing a full-scale numerical model, which was validated for credibility. Transient full-scale 3D CFD analysis of all PVT-PCM collector domains was performed for complex boundary conditions and heat transfer mechanisms throughout the day. The numerical analysis results were compared with experimentally obtained data, accompanied by a discussion of possible numerical model improvements and performance-related enhancements of the PVT-PCM collector design.

## Design of PVT collector and experimental approach

### *PVT-PCM design features*

The novel developed PVT collector is based on the passive phase change material multi-block cooling of free-standing Si-poly PV panels. The modular approach generates more electrical energy with significantly less material consumption, which enhances the economic and environmental aspects of the design, [26]. In article [27], a passive/active smart cooling concept of a commercial PV panel was introduced, enabling the simultaneous production of electricity and thermal energy. This concept of a hybrid PV panel, i.e., PVT-PCM collector, was thoroughly experimentally tested and described in detail in work [25]. The investigated PVT-PCM collector consists of four cooling blocks filled with industrially processed pork fat, i.e., lard. Each cooling block consists of an aluminium absorber bounded by a plexiglass cover, Fig. 1.

Maximizing the energy efficiency of systems in which PVT collectors are implemented requires overall system flexibility given the conflicting nature of the electrical and thermal efficiency of PVT collectors, i.e., if one increases, the other decreases, [25]. In some periods, there is an increased demand for electrical energy, while thermal energy is more in demand in other periods. The system flexibility can be ensured by the appropriate design of the PVT collector concerning the specific energy demand at a particular moment. A well-designed active component of the PVT system is necessary for the successful thermal energy yield and to reconcile the conflicting nature. Therefore, the developed PVT-PCM collector has active cooling implemented through aluminium pipes that are an integral part of the absorber, [25].

### *Experimental test rig and operating modes*

The experimental study was carried out, from August 2021 to January 2022, in the city of Split (Croatia), whose climate can be characterized as the Mediterranean and humid subtropical. The experimental setup was purposefully developed for evaluating the new design of the PVT collector and proved to be very reliable over several months of testing, Fig. 2. Measuring equipment, accuracy, and precise dimensions of PVT-PCM collector were elaborated in the previously published paper [25].

In order for the PVT system to be robust and efficient, the newly developed PVT collector has two operating modes, [25]. The primary operating mode is passive and is based on the organic phase change material, i.e., industrially processed pork fat. The latent heat capacity of this organic PCM is gradually depleting, thus serving as a sort of heat sink since irradiated solar energy is spent on the phase transition and not on the increase in temperature, which eventually results in a cooler PV part of the system. The secondary operating mode with active water cooling takes over when the latent heat of the PCM is mainly consumed, i.e., the recirculation pump forcing coolant ensures the solidification of the PCM with an instant decrease in the temperature of the photovoltaic part of the collector.

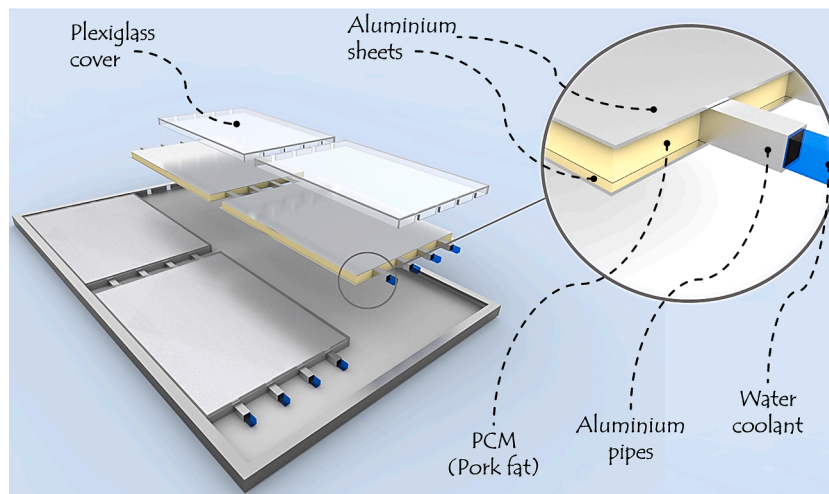


Fig. 1. Multi-block cooling of PVT-PCM collector.

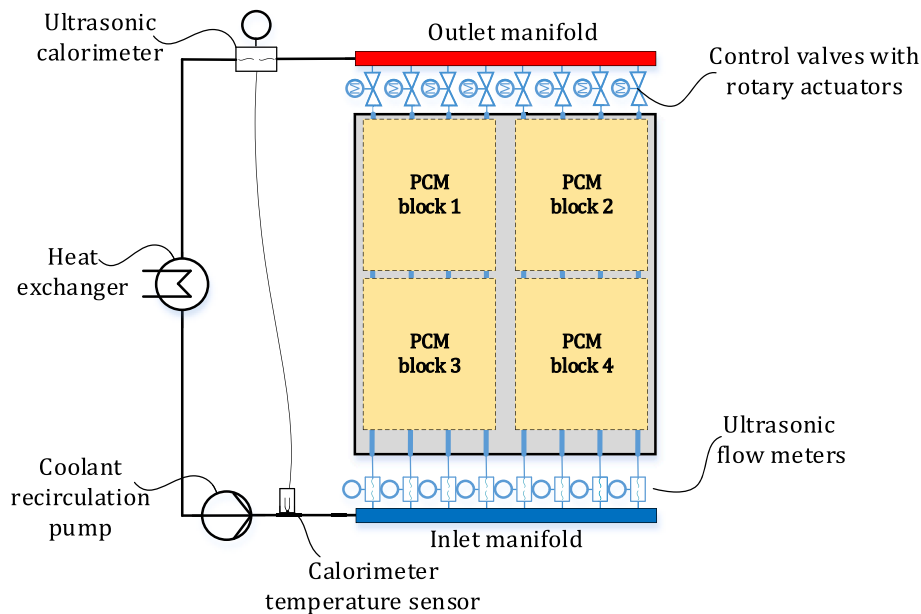


Fig. 2. Experimental test rig layout with multi-block cooled PVT collector.

Differential scanning calorimetry of pork fat

To determine the thermal characteristics of the PCM sample, differential scanning calorimetry (Mettler Toledo DSC 823e) in a nitrogen atmosphere ( $30 \text{ cm}^3 \text{ min}^{-1}$ ) was utilized. The calibration of the calorimeter was performed in the standard aluminium crucible ( $40 \mu\text{l}$ ) by using Indium as the standard calibration substance ( $156.6 \pm 0.3 \text{ }^\circ\text{C}$ ;  $28.45 \pm 0.6 \text{ J g}^{-1}$ ). After calibration, the so-called checks have been performed. The STAR<sup>e</sup> Software incorporated into DSC823e enables calibration checks and performs evaluations to verify whether the measured values of the DSC module are within the limits of permissible error. The pork fat sample of approximately 14 mg was pressed in the aluminium pan and then heated from 0 to  $80 \text{ }^\circ\text{C}$ , cooled to  $0 \text{ }^\circ\text{C}$  and reheated to  $80 \text{ }^\circ\text{C}$ , at a rate of  $10 \text{ }^\circ\text{C min}^{-1}$ , Fig. 3. The sample was kept isothermally for 5 min at 0 and  $80 \text{ }^\circ\text{C}$ , respectively. The melting point of the sample was determined from normalized DSC curves (second heating) following international standard ISO 11357-3, [28], as the peak temperature ( $T_{pm}$ ). Likewise, the crystallization temperature ( $T_{pc}$ ) was determined in the same way from DSC cooling curves according to the

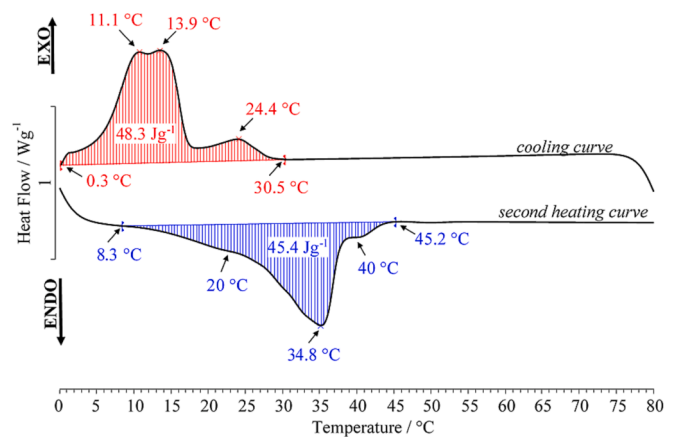


Fig. 3. Normalized DSC curve of the pork fat sample.

latter international standard. The latent heat of melting and crystallization,  $\Delta H_m$  and  $\Delta H_c$ , were determined as the areas of endothermic and exothermic peaks, respectively. According to the mentioned ISO standard, a sample should be tested in duplicate and the arithmetic mean as well as the lower and upper values reported. In this work, DSC analysis of the pork fat sample was repeated three times and the corresponding value of each parameter showed in this manuscript is the arithmetic mean of the three (3) individual measurements. The DSC heating curve (second heating) shows one endotherm, representing the melting of the crystal phase, from the left limit (8.3 °C) to the right limit (45.2 °C), with a single peak at 34.8 °C ( $T_{pm}$ ). The area under the endothermic transition, which represents the latent heat of melting of the sample, is integrated by using STAR<sup>e</sup> software and amounts to 45.4 J g<sup>-1</sup>. Besides the main endotherm, there are two distinctive “shoulders” at around 20 and 40 °C, respectively. On the other hand, the DSC cooling curve shows one exotherm which represents the crystallization from the melt during the cooling of the sample. Crystallization starts at 30.5 °C (right limit) and ends at 0.3 °C (left limit). The area under the exothermic transition is integrated and amounts to 48.3 J g<sup>-1</sup>. As in the case of endotherm, there are three distinctive peaks as follows 24.4, 13.9, and 11.1 °C. This undoubtedly proves that the sample consisted of many different fractions, each characterized by different molecular weight, length, and melting temperature.

Jiménez-Colmenero et al. [29] analyzed the melting of pork fat by DSC. They showed a melting curve with a main peak at 32 °C and a small peak at 44 °C. Likewise, they calculated the fusion enthalpy value (52.3 J g<sup>-1</sup>). Finally, the latter authors attributed these results to the glycerides with high melting points. Another study was performed by Glorieux et al. [30] in which DSC was used to analyze the two types of lard. Furthermore, they also studied the effect of animal fatty acid composition on the melting peak areas of both lard types. They concluded that the fat type significantly affected the melting peak area. The presented DSC curves in their work also consisted of multiple “shoulders” with the main peak. The latent heat of melting of the first fat sample was 47.2 J g<sup>-1</sup>, compared to the second fat sample which showed a smaller value (28.1 J g<sup>-1</sup>). Latter authors attributed these differences to stearic acid proportion and the degree of saturation, respectively, where as a consequence, a lower or higher melting peak area could be expected.

## Numerical analysis

Transient CFD simulation of heat transfer in the complex PVT collector system was performed using ANSYS Fluent software. The whole day from sunrise to sunset with volatile weather conditions was selected for the numerical analysis of the collector. The mentioned approach was selected to prove that the numerical model is valid in the case of sudden changes. Sudden changes may occur naturally or when the system switches between working regimes.

### Computational domains and material properties

The computational domains consisted of multiple fluid and solid regions. The solid regions of the model consisted primarily of PV panel layers, i.e., tempered glass, ethylene vinyl acetate (EVA), PV-cell, tedlar and aluminium frame. The thermophysical properties of PV panel layers were obtained from work [31] and are summarized in Table 1. The secondary solid regions refer to the multi-block cooling system

composed of the aluminium absorber, which consists of pipes and sheets closed with a plexiglass cover, Fig. 1.

The other domains of the PVT collector included water coolant and PCM (Pork fat) as a fluid part of the multi-block cooling system, while the surrounding air was not modeled as a domain. Heat transfer from the surfaces of the collector to the surrounding air was modeled using corresponding convection coefficients considering wind velocity. The pork fat solidus and liquidus temperatures and latent heat were determined from the DSC curve, Fig. 3, while thermal conductivity was acquired from work [32] and specific heat from source [33]. The thermophysical properties of fluid regions are summarized in Table 2.

The temperature-dependent density of water was incorporated into the model in the form of a polynomial expression, [34]. The phase transition of water was not relevant since the temperature in all domains was above its solidus/liquidus temperature. The thermal expansion coefficient appears if the buoyancy effect in the fluid is modeled using the Boussinesq approximation.

### Governing equations

The numerical analysis is based on the following equations:

Continuity equation:

$$\frac{\partial \rho}{\partial t} + \nabla \cdot (\rho \vec{u}) = 0 \quad (1)$$

Momentum equation:

$$\frac{\partial}{\partial t} (\rho \vec{u}) + \nabla \cdot (\rho \vec{u} \vec{u}) = \nabla \cdot (\vec{\tau}) - \nabla p + \rho \vec{g} + \vec{S} \quad (2)$$

The natural convection in PCM was modeled with Boussinesq approximation as an alternative to solving velocity fields with the full form Navier Stokes equations for compressible flows. This approach partially reduces the nonlinearity of Navier Stokes equations and enhances the stability and convergence of the simulation.

The phase transition of pork fat was numerically governed by Fluent's Solidification & Melting model. The Fluent's Solidification & Melting model is based on the conventional enthalpy-porosity formulation and is commonly used to simulate the phase transition of various phase change materials. In this model, the mushy zone is treated as a porous zone in which the porosity decreases as the volume fraction of the solid phase increases. Due to the reducing porosity in the mushy zone, the momentum sink term ( $\vec{S}$ ) is calculated as:

$$\vec{S} = -\frac{(1-\beta)^2}{(\beta^3 + \epsilon)} C_{mush} \vec{u} \quad (3)$$

where  $\epsilon$  is a small number necessary to prevent division by zero (e.g. 0.001, [34]).  $C_{mush}$  is a mushy zone morphology constant that defines a decrease of velocity towards zero as PCM solidifies, i.e., the higher value results in a sharper velocity decrease to zero. Conventionally, the  $C_{mush}$  constant is between 10<sup>4</sup> to 10<sup>7</sup> kg m<sup>-3</sup> s<sup>-1</sup>, [35]. Thus, it was found that the upper value of 10<sup>7</sup> kg m<sup>-3</sup> s<sup>-1</sup> well describes the lard phase transition.

The phase transition state is designated with the liquid fraction ( $\beta$ ) quantity corresponding to the fraction of the liquid phase in every cell volume of the considered domain:

**Table 1**

Thermophysical properties of solid regions.

| Material  | Tempered glass | EVA  | PV-cell | Tedlar | Aluminium frame | Aluminium absorber | Plexiglass |
|---|----------------|------|---------|--------|-----------------|--------------------|------------|
| Density, kg m <sup>-3</sup>                             | 2515           | 960  | 2330    | 1162   | 2700            | 2719               | 1200       |
| Specific Heat, J kg <sup>-1</sup> K <sup>-1</sup>       | 820            | 2090 | 712     | 1465   | 900             | 900                | 1423       |
| Thermal Conductivity, W m <sup>-1</sup> K <sup>-1</sup> | 0.98           | 0.31 | 150     | 0.23   | 160             | 215                | 0.25       |



**Table 2**  
Thermophysical properties of fluid regions.

| Material          | Density,<br>kg m <sup>-3</sup> | Specific<br>Heat,<br>J kg <sup>-1</sup> K <sup>-1</sup> | Thermal<br>Conductivity,<br>W m <sup>-1</sup> K <sup>-1</sup> | Absolute<br>viscosity,<br>kg m <sup>-1</sup> s <sup>-1</sup> | Thermal expansion<br>coefficient,<br>K <sup>-1</sup> | Latent<br>heat,<br>J kg <sup>-1</sup> | Solidus<br>Temperature,<br>°C | Liquidus<br>Temperature,<br>°C |
|-------------------|--------------------------------|---|---|--|--|---------------------------------------|-------------------------------|--------------------------------|
| PCM (Pork<br>fat) | 885<br>Boussinesq              | 2260  | 0.19  | 0.07   | 0.0007   | 45,400                                | 8.3                           | 45.2                           |
| Water             | Polynomial                     | 4182  | 0.6   | 0.001003   | n/a  | n/a                                   | n/a                           | n/a                            |

$$\beta = \begin{cases} 0 & \text{if } T < T_{\text{solidus}} \\ 1 & \text{if } T > T_{\text{liquidus}} \\ \frac{T - T_{\text{solidus}}}{T_{\text{liquidus}} - T_{\text{solidus}}} & \text{if } T_{\text{liquidus}} > T > T_{\text{solidus}} \end{cases} \quad (4)$$

Now, the latent heat content ( $\Delta H$ ) can be related to the latent heat of material ( $L$ ):

$$\Delta H = \beta L \quad (5)$$

The sensible enthalpy ( $h$ ) is added to the latent heat content ( $\Delta H$ ) to compute the enthalpy of material ( $H$ ):

$$H = h + \Delta H \quad (6)$$

$$h = h_{\text{ref}} + \int_{T_{\text{ref}}}^T c_p dT \quad (7)$$

where  $h_{\text{ref}}$  is the reference enthalpy with the corresponding reference temperature  $T_{\text{ref}}$ , while  $c_p$  is the specific heat at constant pressure.

Therefore, based on Eq. (4) to (7), the energy equation can be inscribed as:

$$\frac{\partial}{\partial t}(\rho H) + \nabla \cdot (\rho \vec{u} H) = \nabla \cdot (k \nabla T) + S_e \quad (8)$$

where  $k$  is the thermal conductivity while  $S_e$  stands for the energy source term.

The developed numerical model includes complex heat transfer mechanisms and phase transition, so it was necessary to carry out a transient simulation. The pressure–velocity coupling scheme was set as SIMPLE with the second-order implicit transient formulation. The momentum and energy equations were solved with a second-order upwind scheme, while the pressure equation used PRESTO! discretization scheme. Convergence criteria for all equations were targeted at  $10^{-4}$ , while for the energy equation, it was sharper,  $10^{-6}$ .

### Boundary conditions

The symmetry boundary condition was set along the vertical axis of the PVT-PCM collector geometry to speed up the simulation and reduce the required computational resources. Therefore, the PVT-PCM collector discretization was reduced by half. All collector surfaces in direct contact with the fluid domains were assigned as no-slip stationary wall boundaries.

### Heat source

The main external energy contribution to any PVT collector system is solar radiation. Solar radiation in photovoltaic systems manifests through electricity generation and as a heat input that paradoxically impairs electrical efficiency. A heat source approach was adopted to avoid solar radiation modeling resulting in a robust numerical model, [36]. To obtain a proper time-dependent heat source the irradiated energy of the sun was reduced by reflection losses, which are usually less than 20% but can be more due to aging and dirt. In work [36], reflection losses were reported to be 17%, where the majority refers to the silicon cell, and a lesser part refers to the polycarbonate. Furthermore, 12% of the irradiated energy, at the annual level, is converted into electricity,

[25]. However, a meteorologically variable day was analyzed, so the numerical calculation cannot be based on annual efficiency data. Instead of the average annual electrical efficiency from article [25], the electrical efficiency data for each minute were taken from the same experiment. With transmission neglected, the rest of the irradiance is transferred to heat. This variable heat input was directly given as a heat source ( $S_e$  in Eq. (8)) within the volume of PV cells' material zone, thus, changing each time step with user-defined functions.

### Heat dissipation from front surface

The generated heat from the heat source was removed from the front tempered glass surface of the PVT-PCM collector by the combined interaction of convection and external radiation. Convective heat flux in the model was defined by the convective heat transfer coefficient and free stream temperature, i.e., ambient air temperature, Eq. (9):

$$q = \alpha(T_A - T_w) \quad (9)$$

where  $q$  represents the convective heat flux ( $\text{W/m}^2$ ),  $\alpha$  is the convective heat transfer coefficient ( $\text{W/m}^2 \text{K}^{-1}$ ),  $T_w$  represents wall surface temperature (K), and  $T_A$  stands for ambient air temperature (K).

The convective heat transfer coefficient depends on wind speed, relative wind angle, PVT collector tilt angle, and geometry specifics. These parameters were taken from the experiment described in work [25]; however, wind speed and direction data were reduced to the minute level. Furthermore, the convective heat transfer coefficient for each minute was determined based on the experimental research of a conventional PV panel in a wind tunnel, while considering the impact of PVT collector tilt angle, wind angle, and wind speed, [27].

External radiation heat flux,  $q_R$  ( $\text{W/m}^2$ ), was governed by Eq. (10):

$$q_R = \varepsilon \sigma (T_S^4 - T_w^4) \quad (10)$$

where  $\varepsilon$  is the external emissivity coefficient of the front collector surface which was set at 0.9 while  $\sigma$  is the Stefan-Boltzmann constant.  $T_S$  represents the external radiation temperature (K), i.e., the temperature of the sky. The sky temperature depends on cloud cover as a result of natural meteorological conditions, although, in urban areas, atmospheric pollution can be an additional factor. A direct temperature model like Swinbank's can be applied if the sky is clear [37], Eq. (11):

$$T_S = 0.0553(T_A)^{1.5} \quad (11)$$

For clear periods of the day, the sky temperature was calculated according to Eq. (11), however, during cloudy periods it was assumed that the sky temperature was equal to the ambient air temperature, [38], i.e., external radiation was neglected. Finally, unstable parameters that change every minute such as heat transfer coefficient and free stream temperature in case of convection and external radiation temperature in case of radiation were implemented in the numerical model with user-defined functions.

### Heat dissipation from other surfaces

Other external surfaces of the PVT collector include the rear surface of the PV panel, which is made of tedlar, the aluminium frame, the plexiglass cover, and the exposed part of the aluminium absorber, i.e., pipes. These surfaces are mainly in the lee, so the convective heat transfer coefficient fluctuates much less, thus, its value can be fixed. Radiative heat transfer was not modeled analogously to the front

surface. Instead, the convective heat transfer coefficients were increased for the influence of radiation to simplify the model, [36]. The approach from paper [36] was combined with the experimental investigation from paper [27] to provide a suitable coefficient that considers wind velocity, wind direction and collector geometry to describe the heat dissipation from remaining surfaces. Based on these efforts, the heat transfer coefficient in Eq. (9) was set to be  $12 \text{ W m}^{-2}\text{K}^{-1}$ , including both convection and radiation. Free stream temperature in Eq. (9) varies from minute to minute, thus, this change was incorporated as a user-defined function.

**Inlet and outlet boundary conditions**

On one side of the aluminium pipes, a velocity inlet boundary condition was set for a uniform velocity in the normal direction relative to the surface. The flow rate in the pipes was zero except when the recirculation pump was switched on, i.e., the active mode of operation, [25]. In the active mode of operation, the flow velocity in the pipes was  $0.106 \text{ m s}^{-1}$ , thus, the Reynolds number was relatively low,  $Re = 1693$ , which means that the flow was laminar. Water temperature and flow velocity at the inlet were defined at the minute level, therefore they were incorporated into the numerical model using user-defined functions. Pressure outlet boundary condition with zero-gauge pressure was placed on the opposite side of the pipes.

**User-defined functions**

User-defined functions (UDF) were written in C programming language and compiled with the ANSYS Fluent UDF interface. Almost all of the boundary conditions were variable during the day due to the transient nature of the simulation. The required data was measured in different timesteps than the ones used in the numerical simulation, thus requiring the use of the interpolation method when the numerical timestep was unlike the one in the available experimental data. A simple linear interpolation was used for this purpose:

$$y_{CFD}(t) = y_{Exp}(t_i) + \frac{y_{Exp}(t_{i+1}) - y_{Exp}(t_i)}{t_{i+1} - t_i} (t - t_i) \tag{12}$$

where  $y_{Exp}$  is the measured parameter (temperature, pipe flow rate, insolation, etc.),  $t_i$  and  $t_{i+1}$  are the nearest time points for which the experimental data is available.

**Grid and timestep validation study**

The grid and time step validation studies for a real-time duration of 90 min were performed with identical boundary conditions as the concluding simulation. It was estimated that 90 min is sufficient considering that during that time, the numerical model of the PVT-PCM

collector was subjected to both operation regimes, and PCM alternates between both phase transition processes, i.e., liquefaction and solidification. The initialization was performed at a temperature of  $36 \text{ }^\circ\text{C}$  because the PCM, as the numerically most challenging domain, is deep in the phase transition, i.e., the DSC heating curve reaches the temperature peak at  $34.8 \text{ }^\circ\text{C}$ , Fig. 3. A grid independency study was conducted on three meshes to induce a grid-independent solution for the average temperature of PCM, Fig. 4(a). The total number of volumes per mesh ranged from 690 thousand to 24.4 million, i.e., element sizes ranged from approximately 1 mm to 4 mm. The simulation results were roughly consistent for all three meshes, but there was a noticeable deviation for the mesh with 690 thousand volumes compared to the finer meshes. Concluding simulation of the PVT-PCM collector implies the numerical analysis of the whole day with very complex boundary conditions, therefore, a mesh with 24.4 million volumes would be computationally very demanding and time-consuming. A conservative mesh of 3.7 million volumes that provides high-fidelity numerical analysis results, with a reasonable harnessing of computer resources, was selected. Globally, the given mesh was a high-quality structured hexahedral mesh with approximately 2 mm element sizes and a minimum orthogonal quality of 0.69, i.e., the average orthogonality was almost perfect, 0.99. Then, the selected mesh was subjected to a timestep study to induce a timestep-independent solution for the temperature of the PVT-PCM collector domains. Three timesteps with a relatively large mutual time discrepancy were directly compared, and no significant deviation in the results was found, Fig. 4(b). Based on the timestep analysis, the largest timestep of 60 s was chosen to save computer resources and reduce computing time. Despite changing weather conditions, a relatively large timestep of 60 s was possible due to the PVT collector’s thermal inertness and the PCM’s slow phase transition.

**Numerical model verification and discussion**

The developed numerical model was assessed based on the PVT-PCM collector experimental investigation of the operational conditions during variable cloudiness day, from 6.51 AM to 6.18 PM. An autumn day in October with a maximum air temperature of  $20.3 \text{ }^\circ\text{C}$  and maximum insolation of  $921 \text{ W m}^{-2}$  was analyzed numerically. The wind direction was volatile, with the average wind velocity being  $3.7 \text{ km h}^{-1}$  and the maximum gust of up to  $28.4 \text{ km h}^{-1}$ . October 26, 2021, was chosen to test the numerical model under demanding weather conditions, i.e., relatively high insolation, variable wind, and unstable cloud cover. This day was selected to test the model under sudden changes in input parameters due to variable cloud cover and to expose it to different operating regimes. A numerical investigation of the PVT-PCM collector was performed for the period from sunrise to sunset, i.e., a few minutes

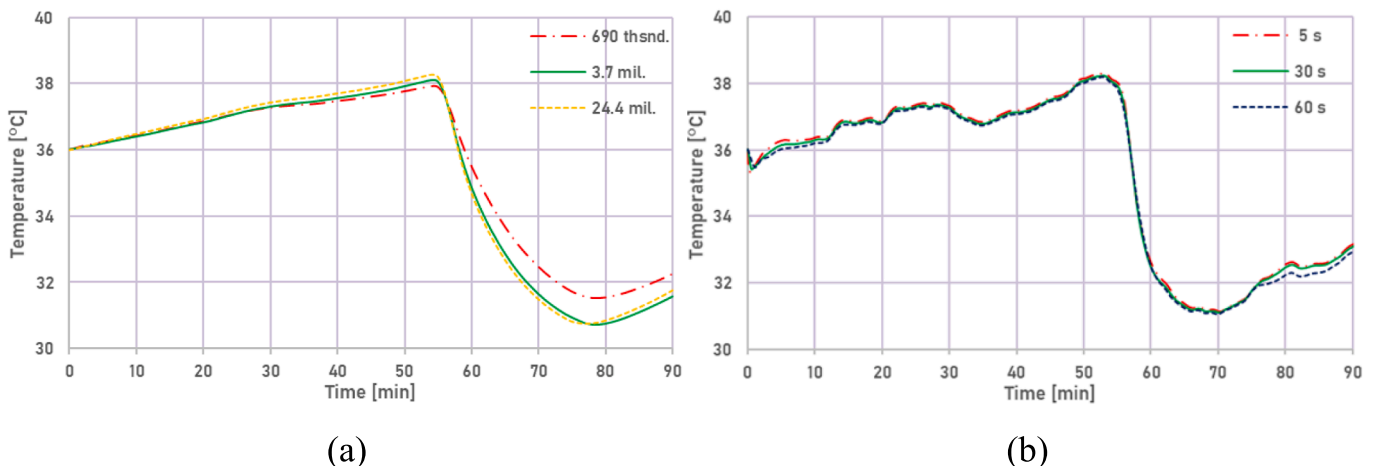


Fig. 4. Analysis of grid-independent solution (a) and timestep-independent solution (b).



before sunrise and after sunset were included in the investigation. Before sunrise, the PCM was completely solidified according to multi-point experimental measurements of PCM temperature in relation to the DSC curve, Fig. 3. Therefore, the PCM phase transition begins with sunrise. Furthermore, the initial CFD simulation temperature values were patched to the belonging domain based on the multi-point experimental measurements, [25]. Therefore, a couple of minutes before sunrise were included in the simulation to eliminate the effect of initial conditions.

The analyzed day was mostly clear for the first 120 min after sunrise, after which clear and cloudy periods alternated, Fig. 5. Occasionally, more intense cloud cover occurs between the 180th and 540th minute of the day. After the 540th minute of the day, the clouds subside, hence, the sky is clear until sunset.

According to experimental data, the front glass surfaces of the PVT-PCM collector and referent PV panel were colder early in the morning than the surrounding air, Fig. 6. This phenomenon cannot be explained with conduction and convection heat transfer mechanisms, i.e., external radiation from the front surface to the sky must also be considered. Radiative cooling of the collector and PV panel is more intense on clear nights when the humidity is low, [38]. The humidity in the early morning and during the night was about 45%. External radiation heat loss is most significant in the morning before the sun gradually warms the upper layers of the atmosphere. The numerical model includes external radiation heat loss during roughly the first two hours from sunrise until the Earth's atmosphere is not heated enough. As the atmosphere heats up, radiative heat exchange decreases since sky long-wave radiation is a function of effective sky temperature, [38]. Thus, external radiation heat loss can be partially neglected later in the day.

The challenging part of the numerical analysis was the complex heat transfer mechanism in interaction with the continuous phase transition since pork fat phase change occurs between 8.3 °C and 45.2 °C, Table 2. To buffer generated heat, the PVT system combines PCM passive cooling with active coolant recirculation driven by smart control apparatus, [25]. Passive cooling with PCM triggers a heat sink effect that dampens temperature oscillations, i.e., the PVT-PCM collector has fewer temperature oscillations than the referent PV panel, Fig. 6. During most of the day, the temperature regulation of the PVT-PCM collector is performed by the passive component of the system until the PCM temperature reaches the set threshold when the pump is activated, [25]. Thermal processes occurring during the passive mode of operation are relatively slow, so a good agreement between numerical and experimental findings is expected, Fig. 7. The greatest temperature difference is early in the morning when external radiation heat loss is significant.

Thus, to achieve better-matching results, Swinbank's direct sky temperature model could be replaced with a standard model like ISO 13790 direct model for temperate areas, [38]. But even without upgrades, the mean absolute percentage deviation of the numerical forecast in relation to the experimental values is acceptable at 2.9% for the temperature of the front surface of the collector. Overall, the average discrepancy in the temperature of the front surface of the PVT-PCM collector between experimental measurements on three positions and the numerical analysis is only 0.46 °C, with the maximum difference being 1.47 °C. The critical period for the numerical analysis roughly occurs between the 360th minute of the day when the recirculation pump activates and the 380th minute when it deactivates. The performed CFD analysis proved to be highly capable even in this numerically demanding period since it is in excellent agreement with experimental measurements.

During the active mode of operation, in addition to being mushy, the PCM alternates between processes of liquefaction and solidification. Intensive pork fat PCM solidification induced by cooling water causes a marked drop in the temperature of the PVT-PCM collector. The drop in collector temperature one minute after pump deactivation compared to one minute before activation is apparent, Fig. 8. This temperature drop ultimately results in increased electricity production while generating usable waste heat.

The mean absolute percentage deviation of the numerical forecast for the average temperature of pork fat PCM is slightly more but stands at an acceptable 4.9%. The larger deviation in the fluid PCM domain can be caused by a more complex heat transfer mechanism and experimental measurement specifics, although the trend is evidently similar, Fig. 9(a). Initially, the heat transfer mechanism is dominantly driven by conduction; however, as PCM liquifies, the convection intensifies and gradually takes over. Boussinesq approximation was used to solve convection-induced buoyancy force in pork fat PCM. Furthermore, the discrepancy between the numerical results and the experiment may be due to the positioning of the temperature sensors in the middle of the PCM cooling blocks. Positioning the sensors this way was necessary to avoid contact with the surrounding walls in the experiment. The sensors were not numerically modeled, but in reality, they partially obstruct convective flows and potentially affect heat transfer circumstances.

During the substantial part of the simulation, there was no flow in the absorber pipes, but convective flows were not absent. Polynomial expression was used for the temperature-dependent density of water, so numerical analysis includes convection impact in the water domain. The numerical forecast of water temperatures at pipes outlets is in accordance with experimental measurements throughout the morning until the pump shuts down around the 380th minute of the day, Fig. 9(b).

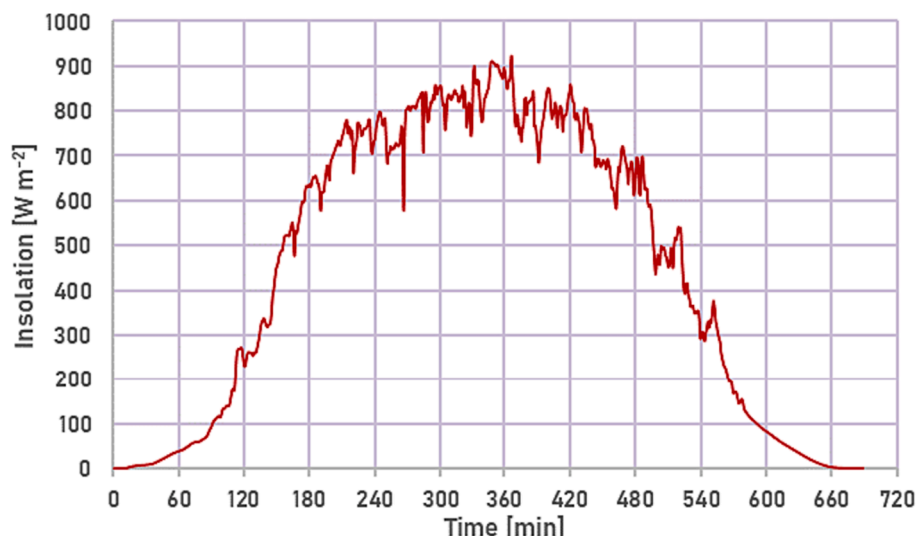


Fig. 5. Insolation on October 26, 2021, in Split (Croatia).

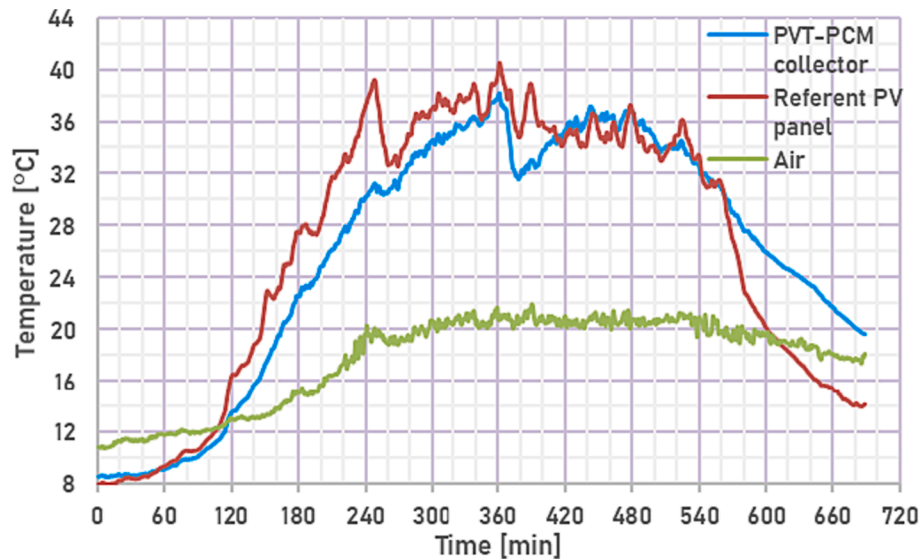


Fig. 6. Experimental data of front glass surface temperature and ambient air temperature.

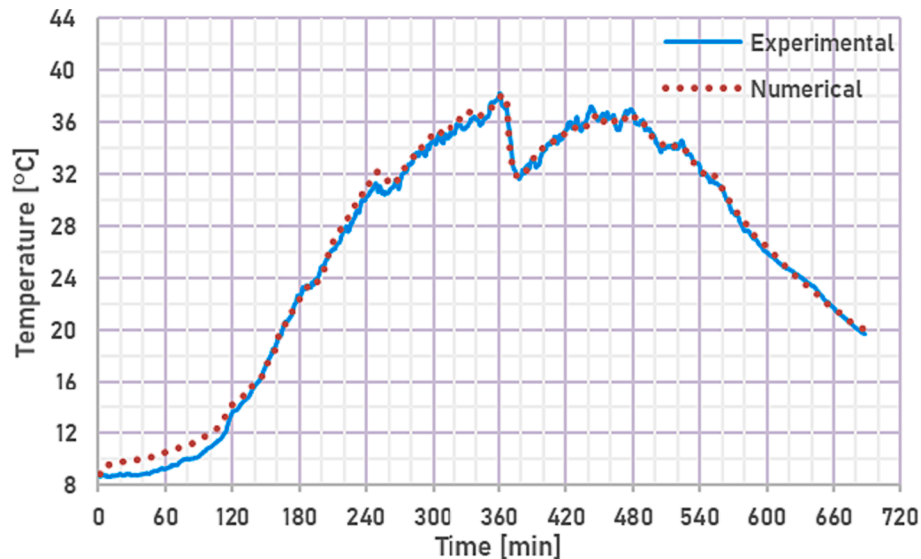


Fig. 7. PVT-PCM collector front glass surface temperature.

After that, a significant deviation appears, resulting from convective flows in the experiment. Namely, the outlet manifold was located above the PVT-PCM collector, so the cold water gradually mixes with the warmer water in the collector pipes after turning off the pump. Water subcooling in the experiment after the 380th minute could not occur in the simulation because the outlet manifold was not modeled. The outlet manifold could be modeled numerically, but this is unessential since this problem only occurs after the pump is turned off and it does not affect other domains significantly. This problem should be addressed in future experiments since it can be easily solved by adding a one-way valve on outlets or simply positioning the outlet manifold at a lower point than the outlets from the collector.

The relatively ineffective heat exchanger used in the experiment should be replaced with a heat pump providing a constant temperature of the cooling water in the inlet manifold. Therefore, the boundary conditions at the inlet would be simplified, so the UDF for inlet temperature would be redundant. Additional geometry modifications can be made to improve the thermal management of the PVT-PCM collector. Possible design modifications may include PCM with better thermal

properties, adding thermal insulation, increasing the volume of cooling water in the system, reducing the amount of PCM, etc. The impact of any possible modification should not be speculated. Rather, it should be numerically tested separately on a previously justified model. Finally, performed numerical analysis resulted in the validated model, so it is possible to achieve a balanced design solution that will not compromise electricity production while significantly improving the thermal component of the PVT system.

## Conclusions

A numerical model of the PVT-PCM collector was developed and validated based on previously published experimental research. Additionally, for the credibility of the numerical model, the thermal characteristics of industrially processed pork fat PCM were experimentally tested using the differential scanning calorimetry method. The DSC heating and cooling curves were provided from which the endothermic and exothermic transition areas were integrated. The latent heat of melting for pork fat PCM was determined to be  $45.4 \text{ J g}^{-1}$ , while the

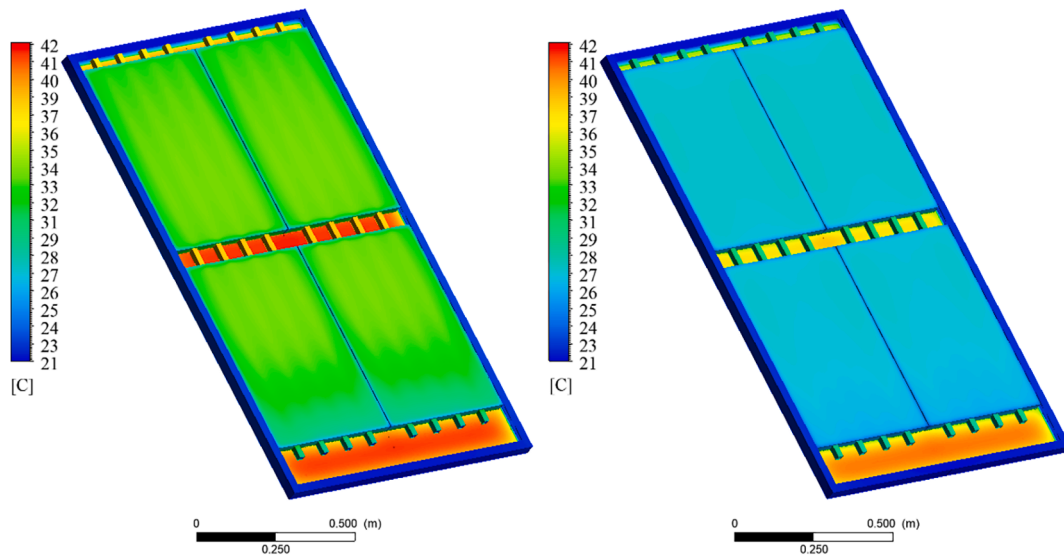


Fig. 8. PVT-PCM collector back surfaces temperatures at pump activation (a) and deactivation (b).

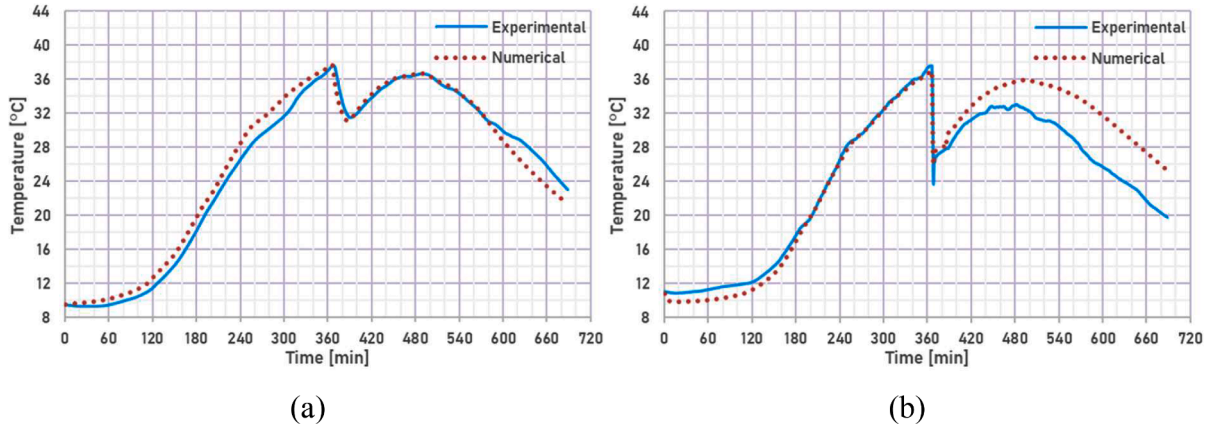


Fig. 9. Average pork fat PCM (a) and absorber pipes outlets (b) temperatures.

latent heat of crystallization amounts to  $48.3 \text{ J g}^{-1}$ . The experimentally measured data were incorporated into a 3D numerical model to simulate the PVT-PCM collector for the unconventional case of variable cloudiness day. The transient numerical analysis of a PVT collector containing relatively large domains, including a phase change material, subjected to volatile weather conditions represents an important novelty over similar publications in the field. Variable weather circumstances require variable time-dependent boundary conditions which were implemented by linear interpolation based user-defined functions. The phase transition as a time-determined process was solved with the conventional enthalpy-porosity approach. The heat transfer within PCM resulted from a complex interaction of the conduction and the convection mechanisms, which is frequently not the case in existing literature, where the impact of convection is frequently omitted. The Boussinesq approximation was used to model natural convection in PCM by inducing buoyancy force. Heat transfer from PVT-PCM collector surfaces was primarily governed by convection depending on the wind and collector geometry. However, experimental measurements detected subcooling of the collector compared to the surrounding air in the early morning as a result of external radiation to space. Hence, the numerical model included external radiation heat loss from the front collector surface for roughly the first two hours of the day. Overall, the developed numerical model proved robust and precise, given that the mean absolute percentage deviation of the numerical forecast for the front surface

temperature was 2.9% from experimental measurements. To put it in perspective, the average temperature discrepancy of the front collector surface between numerical and experimental values was just  $0.46 \text{ }^\circ\text{C}$ , while the maximum difference was  $1.47 \text{ }^\circ\text{C}$ . Even for the numerically demanding domain of phase change material, the mean absolute percentage deviation of the numerical forecast was acceptable at 4.9%. The herein-presented numerical approach can be beneficial to understand the resilience aspect and is applicable to different PVT solutions and other photovoltaic and solar-related technologies. However, it should be noted that the numerical analysis was carried out for one day under unique weather conditions. Therefore, when implementing the described numerical approach in other systems, all variable input parameters, such as convection coefficients, sky temperature, ambient air temperature, etc., should be determined for the specific case study. Furthermore, in a system containing phase change material, particular regard should be given to all aspects of the numerical analysis related to the phase transition, i.e., determining the appropriate mushy zone morphology constant as well as the thermophysical properties of the selected PCM is necessary to obtain sensible numerical results. The validated numerical model of the PVT-PCM collector, as part of future research, can be used for the investigation of a new concept or to additionally improve the existing design for a more resilient PVT system. It can be done by altering the collector geometry or testing different operating conditions and modes of operation. One of the possible future

directions in the development of sustainable PVT-PCM collectors is the numerical study of various phase change materials to obtain optimal solutions regarding exploitation, climatic conditions, environmental and economic indicators.

### CRediT authorship contribution statement

**Mišo Jurčević:** Investigation, Conceptualization, Methodology, Formal analysis, Software, Supervision. **Sandro Nizetić:** Conceptualization, Methodology, Formal analysis, Supervision. **Ivo Marinić-Kragić:** Software, Formal analysis. **Miće Jakić:** Investigation, Formal analysis. **Müslüm Arıcı:** Formal analysis, Supervision.

### Declaration of Competing Interest

The authors declare that they have no known competing financial interests or personal relationships that could have appeared to influence the work reported in this paper.

### Data availability

Data will be made available on request.

### Acknowledgments

This work was granted by the Croatian Science Foundation, project IP-01-2018-2814.

### References

- [1] Hampo CC, Ojo DO, Olatunde DE, Isioma OJ, Oni OO, Echendu AJ, et al. Life cycle assessment of renewable energy technologies in Northern Africa: A critical review. *Energy Sources Part A* 2022;44(4):10248–69.
- [2] Paris Agreement n.d. <https://unfccc.int/process-and-meetings/the-paris-agreement> (accessed February 24, 2023).
- [3] European Commission-Renewable energy n.d. [https://energy.ec.europa.eu/topics/renewable-energy\\_en](https://energy.ec.europa.eu/topics/renewable-energy_en) (accessed February 24, 2023).
- [4] Marinić-Kragić I, Nizetić S, Grubišić-Cabo F, Papadopoulos AM. Analysis of flow separation effect in the case of the free-standing photovoltaic panel exposed to various operating conditions. *J. Clean. Prod.* 2018;174:53–64. <https://doi.org/10.1016/j.jclepro.2017.10.310>.
- [5] IEA-Renewables 2022 n.d. <https://www.iea.org/reports/renewables-2022/executive-summary> (accessed February 24, 2023).
- [6] PV magazine n.d. <https://www.pv-magazine.com/2022/12/23/global-solar-capacity-additions-hit-268-gw-in-2022-says-bnef/> (accessed February 24, 2023).
- [7] Mazzeo D, Herdem MS, Matera N, Wen JZ. Green hydrogen production: Analysis for different single or combined large-scale photovoltaic and wind renewable systems. *Renew. Energy* 2022;200:360–78. <https://doi.org/10.1016/j.renene.2022.09.057>.
- [8] Essak L, Ghosh A. Floating Photovoltaics: A Review. *Clean Technologies* 2022;4: 752–69. <https://doi.org/10.3390/cleantechnol4030046>.
- [9] Williams HJ, Hashad K, Wang H, Max ZK. The potential for agrivoltaics to enhance solar farm cooling. *Appl. Energy* 2023;332:120478. <https://doi.org/10.1016/j.apenergy.2022.120478>.
- [10] Nizetić S, Jurčević M, Čoko D, Arıcı M, Hoang AT. Implementation of phase change materials for thermal regulation of photovoltaic thermal systems: Comprehensive analysis of design approaches. *Energy* 2021;228:120546. <https://doi.org/10.1016/j.energy.2021.120546>.
- [11] Rejeb O, Lamrani B, Lamba R, Kouskou T, Salameh T, Jemni A, et al. Numerical investigations of concentrated photovoltaic thermal system integrated with thermoelectric power generator and phase change material. *J Energy Storage* 2023;62:106820.
- [12] Ahmadinejad M, Moosavi R. Energy and exergy evaluation of a baffled-nanofluid-based photovoltaic thermal system (PVT). *Int. J. Heat Mass Transf.* 2023;203: 123775. <https://doi.org/10.1016/j.ijheatmasstransfer.2022.123775>.
- [13] Yang H, Wang X, Yao S. Thermodynamic analysis of a novel solar photovoltaic thermal collector coupled with switchable air source heat pump system. *Appl. Therm. Eng.* 2023;218:119410. <https://doi.org/10.1016/j.applthermaleng.2022.119410>.
- [14] Fu X, El-Rahman MA, Abdalla AN, Hasani Malekshah E, Sharifpur M. The numerical analysis and optimization of a Photovoltaic thermal collector with three different plain, ribbed, and porous-ribbed absorber tubes and a nanofluid coolant using two-phase model. *J. Taiwan Inst. Chem. Eng.* 2023;148:104725.
- [15] Bassam AM, Sopian K, Ibrahim A, Fauzan MF, Al-Aasam AB, Abusaibaa GY. Experimental analysis for the photovoltaic thermal collector (PVT) with nano PCM and micro-fins tube nanofluid. *Case Studies in Thermal Engineering* 2023;41: 102579. <https://doi.org/10.1016/j.csite.2022.102579>.
- [16] Sheikholeslami M, Khalili Z. Investigation of solar photovoltaic-thermoelectric system for building unit in presence of helical tapes and jet impingement of hybrid nanomaterial. *J. Build. Eng.* 2023;74:106871. <https://doi.org/10.1016/j.jobe.2023.106871>.
- [17] Li J, Zhang W, Xie L, Li Z, Wu X, Zhao O, et al. A hybrid photovoltaic and water/air based thermal(PVT) solar energy collector with integrated PCM for building application. *Renew. Energy* 2022;199:662–71.
- [18] Ul Abdin Z, Rachid A, Korkut TB. Design and analysis of an innovative photovoltaic-thermal collector with embedded tank. *Sol. Energy* 2022;245:290–8. <https://doi.org/10.1016/j.solener.2022.09.018>.
- [19] Ahmadinejad M, Soleimani A, Gerami A. The effects of a novel baffle-based collector on the performance of a photovoltaic/thermal system using SWCNT/ Water nanofluid. *Thermal Sci. Eng. Progr.* 2022;34:101443. <https://doi.org/10.1016/j.tsep.2022.101443>.
- [20] Simón-Allué R, Guedea I, Coca-Ortegón A, Villén R, Brun G. Performance evaluation of PVT panel with phase change material: Experimental study in lab testing and field measurement. *Sol. Energy* 2022;241:738–51. <https://doi.org/10.1016/j.solener.2022.05.035>.
- [21] Mazzeo D, Oliveti G. Parametric study and approximation of the exact analytical solution of the Stefan problem in a finite PCM layer in a steady periodic regime. *Int. Commun. Heat Mass Transfer* 2017;84:49–65. <https://doi.org/10.1016/j.icheatmasstransfer.2017.03.013>.
- [22] Bonyadi N, Sömek SK, Özalevli CC, Baker D, Tari İ. Numerical Analysis of Phase Change Material Characteristics Used in a Thermal Energy Storage Device. *Heat Transfer Eng.* 2018;39:268–76. <https://doi.org/10.1080/01457632.2017.1295741>.
- [23] Ahmed MMS, Radwan A, Serageldin AA, Abdeen A, Abo-Zahhad EM, Nagano K. The thermal potential of a new multifunctional sliding window. *Sol. Energy* 2021; 226:389–407. <https://doi.org/10.1016/j.solener.2021.08.045>.
- [24] Mousavi S, Kasaeian A, Shafii MB, Jahangir MH. Numerical investigation of the effects of a copper foam filled with phase change materials in a water-cooled photovoltaic/thermal system. *Energy Convers Manag* 2018;163:187–95. <https://doi.org/10.1016/j.enconman.2018.02.039>.
- [25] Jurčević M, Nizetić S, Čoko D, Arıcı M, Hoang AT, Giama E, et al. Techno-economic and environmental evaluation of photovoltaic-thermal collector design with pork fat as phase change material. *Energy* 2022;254:124284.
- [26] Nizetić S, Jurčević M, Čoko D, Arıcı M. A novel and effective passive cooling strategy for photovoltaic panel. *Renew. Sustain. Energy Rev.* 2021;145:111164. <https://doi.org/10.1016/j.rser.2021.111164>.
- [27] Jurčević M, Nizetić S, Marinić-Kragić I, Čoko D, Arıcı M, Giama E, et al. Investigation of heat convection for photovoltaic panel towards efficient design of novel hybrid cooling approach with incorporated organic phase change material. *Sustain. Energy Technol. Assess.* 2021;47:101497.
- [28] ISO Standard n.d. <https://www.iso.org/standard/41638.html> (accessed March 20, 2023).
- [29] Jiménez-Colmenero F, Cofrades S, Herrero AM, Fernández-Martín F, Rodríguez-Salas L, Ruiz-Capillas C. Konjac gel fat analogue for use in meat products: Comparison with pork fats. *Food Hydrocoll.* 2012;26:63–72. <https://doi.org/10.1016/j.foodhyd.2011.04.007>.
- [30] Glorieux S, Steen L, De Brabanter J, Foubert I, Fraeye I. Effect of meat type, animal fatty acid composition, and isothermal temperature on the viscoelastic properties of meat batters. *J. Food Sci.* 2018;83:1596–604. <https://doi.org/10.1111/1750-3841.14182>.
- [31] Chamkha A, Selimefendigil F. Numerical analysis for thermal performance of a photovoltaic thermal solar collector with SiO<sub>2</sub>-water nanofluid. *Appl. Sci.* 2018;8: 2223. <https://doi.org/10.3390/app8112223>.
- [32] Jurčević M, Nizetić S, Čoko D, Hoang AT, Papadopoulos AM. Experimental investigation of novel hybrid phase change materials. *Clean Techn. Environ. Policy* 2022;24:201–12. <https://doi.org/10.1007/s10098-021-02106-y>.
- [33] Engineering ToolBox-Food and Foodstuff - Specific Heat n.d. [https://www.engineeringtoolbox.com/specific-heat-capacity-food-d\\_295.html](https://www.engineeringtoolbox.com/specific-heat-capacity-food-d_295.html) (accessed March 10, 2023).
- [34] Jurčević M, Penga Ž, Klarin B, Nizetić S. Numerical analysis and experimental validation of heat transfer during solidification of phase change material in a large domain. *J Energy Storage* 2020;30:101543. <https://doi.org/10.1016/j.est.2020.101543>.
- [35] Youssef W, Ge YT, Tassou SA. CFD modelling development and experimental validation of a phase change material (PCM) heat exchanger with spiral-wired tubes. *Energy Convers Manag* 2018;157:498–510. <https://doi.org/10.1016/j.enconman.2017.12.036>.
- [36] Grubišić-Cabo F, Nizetić S, Marinić Kragić I, Čoko D. Further progress in the research of fin-based passive cooling technique for the free-standing silicon photovoltaic panels. *Int. J. Energy Res.* 2019;43:3475–95. <https://doi.org/10.1002/er.4489>.
- [37] Nowak H. The sky temperature in net radiant heat loss calculations from low-sloped roofs. *Infrared Phys.* 1989;29:231–2. [https://doi.org/10.1016/0020-0891\(89\)90055-9](https://doi.org/10.1016/0020-0891(89)90055-9).
- [38] Evangelisti L, Guattari C, Asdrubali F. On the sky temperature models and their influence on buildings energy performance: A critical review. *Energy. Buildings* 2019;183:607–25. <https://doi.org/10.1016/j.enbuild.2018.11.037>.

## ŽIVOTOPIS

Mišo Jurčević je rođen 23. rujna 1991. godine u Tomislavgradu, Bosna i Hercegovina. Osnovnoškolsko obrazovanje započinje u rodnom mjestu u Osnovnoj školi Stjepana Radića (područna škola Vinica), a završava ga u Osnovnoj školi Strožanac (Podstrana). Potom pohađa V. gimnaziju Vladimir Nator u Splitu koju uspješno završava nakon čega 2010. godine upisuje preddiplomski studij industrijskog inženjerstva na Fakultetu elektrotehnike, strojarstva i brodogradnje (FESB) u Splitu. Navedeni studij završava 2013. godine, obranom završnog rada, te stječe titulu sveučilišnog prvostupnika inženjera industrijskog inženjerstva (*univ.bacc.ing.industr.*). Na FESB-u, 2015. godine diplomira te stječe titulu magistra inženjera industrijskog inženjerstva (*mag.ing.industr.*), a potom, 2016. godine na FESB-u završava preddiplomski studij strojarstva, te stječe titulu sveučilišnog prvostupnika inženjera strojarstva (*univ.bacc.ing.mech.*). Nakon toga upisuje i diplomski studij strojarstva na FESB-u kojeg 2018. godine uspješno završava te stječe titulu magistra inženjera strojarstva (*mag.ing.mech.*). Paralelno s diplomskim studijem strojarstva radi kao vanjski suradnik u naslovnom suradničkom zvanju asistent, kolegij „Inovacije u tehnici“, na diplomskom studiju industrijskog inženjerstva na FESB-u, a potom u istom svojstvu radi i na kolegiju „Mehanika fluida“. Nadalje, u suradnji s privredom, radi kao suradnik na razvojno-istraživačkom projektu koji se bavio razvojem i istraživanjem ledenih platformi. Rad na navedenom projektu je rezultirao stručnim elaboratom o izvodljivosti „Istraživanje i razvoj plutajućih platformi“ u kojem sudjeluje kao koautor s fokusom na numeričku analizu i računalne simulacije te obradu eksperimentalno dobivenih podataka. Temeljem istraživanja i studije izvodljivosti odobren je znanstveno-istraživački CEKOM projekt P12 na kojem radi kao suradnik. Akademske godine 2018. / 2019. upisuje poslijediplomski studij strojarstva na Fakultetu elektrotehnike, strojarstva i brodogradnje pod mentorstvom prof. dr. sc. Sandra Nižetića. Od 2019. godine radi kao sveučilišni asistent pri Katedri za mehaniku fluida (FESB) na kolegijima Mehanika fluida, Mehanika fluida 1, Hidraulički strojevi, Strujanje fluida, Računalna dinamika fluida. U svojstvu suradnika radi na razvojno-istraživačkom projektu koji se bavi razvojem putničkog jedrenjaka s nultom emisijom ispušnih plinova, sufinanciran sredstvima EU. Nadalje, u svojstvu suradnika je sudjelovao u projektu „Pametne hibridne tehnike hlađenja silicijskih fotonaponskih panela (IP-01-2018-2814)“ financiranom od Hrvatske zaklade za znanost. U sklopu navedenog projekta, koji je uspješno okončan uz potpuno ispunjene ciljeve te premašena očekivanja prema vrednovanju Hrvatske zaklade za znanost, radi i na doktorskom radu. Bio je član tima koji je osvojio prvo mjesto u velikoj konkurenciji od čak 42 sveučilišta iz cijelog svijeta s projektom naziva „Customized location-based optimization of hybrid micro-grid system and analysis of possible elements“ na značajnom međunarodnom natjecanju ESTECO Academy Microgrid Design Competition (2018. / 2019.). Radio je na razvoju numeričkog simulacijskog modela aktivno hlađenog fotonaponskog panela kao dijela integriranog rješenja najučinkovitijeg i najjeftinijeg hibridnog microgrid sustava za opskrbu električnom energijom Cummins-ovog kampusa u Indiji. Navedeni uspjeh je iznimno značajan za promociju Sveučilišta u Splitu i hrvatske znanosti u cjelini. Radio je kao član lokalnog organizacijskog odbora na međunarodnim



znanstvenim skupovima SpliTech2019 (International Conference on Smart and Sustainable Technologies), SpliTech2020, SpliTech2021, SpliTech2022, SpliTech2023 te na 9<sup>th</sup> Global Conference on Global Warming (GCGW 2021) i PRES2022 (Conference on Process Integration for Energy Saving and Pollution Reduction). Recenzira radove u uglednim znanstvenim časopisima poput *Journal of Cleaner Production* (**IF: 11.1**), *Solar Energy* (**IF: 6.7**), *Energy & Buildings* (**IF: 6.7**), *International Journal of Energy Research* (**IF: 4.6**), *Thermal Analysis and Calorimetry* (**IF: 4.4**), *Energy Sources Part A: Recovery, Utilization and Environmental Effects* (**IF: 2.9**). U dosadašnjoj znanstvenoj karijeri objavio je 41 rad od kojih je 15 radova A kategorije (većina u CC bazi), 24 rada na međunarodnim znanstvenim konferencijama te 2 stručna rada. Radovi A-kategorije objavljeni su u uglednim međunarodnim časopisima s izrazito visokim faktorom odjeka (14 u Q1 kvartili i 1 u Q3 kvartili). Od ostalih aktivnosti može se istaknuti izniman interes za sport i geopolitiku. Više od 15 godina se bavi rekreativno boksom pri čemu je povremeno nastupao i kao aktivni natjecatelj.



## BIOGRAPHY

Mišo Jurčević was born on September 23, 1991, in Tomislavgrad, Bosnia and Herzegovina. He started his elementary education in his homeplace at the Stjepan Radić Elementary School (Vinica district school) and finished it at the Strožanac Elementary School (Podstrana). He then attended 5<sup>th</sup> Gymnasium "Vladimir Nazor" in Split, which he successfully completed, after which, in 2010, he enrolled in undergraduate studies in Industrial Engineering at the Faculty of Electrical Engineering, Mechanical Engineering and Naval Architecture (FESB) in Split. The aforementioned study ended in 2013, with the defense of the final thesis, and he received the academic title of University Bachelor of Industrial Engineering (*univ.bacc.ing.industr.*). In 2015, he graduated from FESB and obtained the academic title of Master of Industrial Engineering (*mag.ing.industr.*), and then, in 2016, he completed undergraduate studies in Mechanical Engineering at FESB and obtained a university bachelor's degree in Mechanical Engineering (*univ.bacc.ing.mech.*). After that, he enrolled in a graduate study in Mechanical Engineering at FESB, which he successfully completed in 2018 and obtained the academic title of Master of Mechanical Engineering (*mag.ing.mech.*). In parallel with his graduate studies in Mechanical Engineering, he worked as an external associate assistant in the graduate university study in Industrial Engineering on the "Innovations in Technics" course at FESB. Then he worked in the same capacity on the "Fluid Mechanics" course. Furthermore, in cooperation with the economy, he worked as an associate on a research project dealing with the development and research of ice platforms. The work on this project resulted in the feasibility study "*Research and development of floating platforms*", in which he participated as a co-author focusing on numerical analysis, computer simulations, and processing of experimentally obtained data. Based on research and the feasibility study, the scientific research CEKOM project P12, on which he worked as an associate, was approved. In the academic year 2018. / 2019. he enrolled in postgraduate studies in Mechanical Engineering at the Faculty of Electrical Engineering, Mechanical Engineering and Naval Architecture under the mentorship of Prof. Sandro Nižetić, PhD. Since 2019, he has been working as a university assistant at the Chair of Fluid Mechanics (FESB) on the courses Fluid Mechanics, Fluid Mechanics 1, Hydraulic Machines, Fluid Flow, and Computational Fluid Dynamics. As an associate, he worked on a research project that dealt with developing a passenger sailing ship with zero emissions, co-financed by the EU. Furthermore, as an associate, he participated in the research project "*Smart and hybrid cooling techniques for siliceous photovoltaic panels (IP-01-2018-2814)*", financed by the Croatian Science Foundation. As an integral part of the aforementioned project, which was successfully completed with fully met goals and exceeded expectations according to the evaluation of the Croatian Science Foundation, he worked on his doctoral thesis. He was a member of the team that won first place in the prestigious international competition ESTECO Academy Microgrid Design Competition (2018. / 2019.) which included participants from 42 universities from all over the world, with a project called "*Customized location-based optimization of hybrid micro-grid system and analysis of possible elements*". He worked on developing a numerical simulation model of an actively cooled photovoltaic panel

## BIOGRAPHY

---

as part of an integrated solution of the most efficient and least expensive hybrid microgrid system for the power supply of the Cummins campus in India. This success is significant for promoting the University of Split and Croatian science. He worked as a member of the local organizing committee at international scientific conferences SpliTech2019 (International Conference on Smart and Sustainable Technologies), SpliTech2020, SpliTech2021, SpliTech2022, SpliTech2023 and at the 9<sup>th</sup> Global Conference on Global Warming (GCGW 2021) and PRES2022 (Conference on Process Integration for Energy Saving and Pollution Reduction). He works as a reviewer in reputable scientific journals such as *Journal of Cleaner Production* (**IF: 11.1**), *Solar Energy* (**IF: 6.7**), *Energy & Buildings* (**IF: 6.7**), *International Journal of Energy Research* (**IF: 4.6**), *Thermal Analysis and Calorimetry* (**IF: 4.4**), *Energy Sources Part A: Recovery, Utilization and Environmental Effects* (**IF: 2.9**). In his scientific career so far, he has published 41 papers, of which 15 are category A papers (majority in the CC database), 24 are papers at international scientific conferences, and 2 are professional papers. A-category papers were published in reputable international journals with high impact factors (14 in the Q1 quartile and 1 in the Q3 quartile). Among his other activities, he has an exceptional interest in sports and geopolitics. He has been boxing recreationally for over 15 years, occasionally performing as an active competitor.